IN-PLANE SHEAR BEHAVIOUR OF FULLY GROUTED REINFORCED MASONRY SHEAR WALLS

HANY MOHAMED SEIF ELDIN

Ph.D. Thesis

in

The Department of
Building, Civil and Environmental Engineering

Presented in Partial Fulfillment of the Requirements
for the Degree of Doctor of Philosophy (Civil Engineering) at

Concordia University

Montréal, Québec, Canada

March 2016

CONCORDIA UNIVERSITY
School of Graduate Studies

This is to certify that the thesis prepared

By: Hany Mohamed Seif ElDin
Entitled: **In-Plane Shear Behaviour of Fully Grouted Reinforced Masonry Shear Walls**

and submitted in partial fulfillment of the requirements for the degree of

Doctor of Philosophy (Civil Engineering)
complies with the regulations of the university and meets the accepted standards with respect to originality and quality.

Signed by the final examining committee:

______________________________ Chair
Dr. C. W. Trueman

______________________________ External Examiner
Dr. Nigel G. Shrive

______________________________ External to Program
Dr. Rajamohan Ganesan

______________________________ Examiner
Dr. Oscar A. Pekau

______________________________ Examiner
Dr. Ashutosh Bagchi

______________________________ Thesis supervisor
Dr. Khaled Galal

Approved by

____
Dr. Fariborz Haghighat, GPD
Department of Building, Civil and Environmental Engineering

____
Dr. Amir Asif, Dean
Faculty of Engineering and Computer Science

Date 2016-03-23

ABSTRACT

In-Plane Shear Behaviour of Fully Grouted Reinforced Masonry Shear Walls

Hany Mohamed Seif ElDin, Ph.D.
Concordia University, 2016

Reinforced masonry (RM) shear walls are the key structural elements widely used to resist lateral loads in masonry buildings due to their capability to provide lateral strength, stiffness, and energy dissipation. The flexural behaviour of RM shear walls is well defined and follows the simple flexural theory of reinforced concrete structures based on plane-section assumption. On the other hand, the shear behaviour of RM shear walls in the plastic hinge region is more complex due to the interaction between the nonlinear responses of their constituent materials, namely: concrete masonry blocks, mortar, grout, and steel reinforcement. The main objective of this thesis is to evaluate the inelastic behaviour of fully grouted RM shear walls that are dominated by shear failure. The research objective was achieved by conducting experimental, numerical, and analytical studies.

The experimental work involved assessing the response of nine full-scale fully grouted rectangular RM shear walls when subjected to in-plane axial compressive stress, cyclic lateral excitations, and top moment. The main variables considered were the level of axial compressive stress, shear span to depth ratio, horizontal reinforcement ratio, anchorage end detail, and the spacing of horizontal and vertical reinforcement. The effect of the studied parameters is analyzed and presented in detail according to force-based, displacement-based, and performance-based seismic design considerations. Moreover, nonlinear finite element models were developed to simulate the behaviour of RM shear walls subjected to cyclic loading, and validated using results from the nine RM tested walls. Good agreements with the experimental load-displacement hysteretic loops were achieved in all models. In addition, a parametric study was performed to consider more variations in some of the parameters examined in the experimental work, which arrived at similar conclusions of the tested walls.

Using the results of the tested RM shear walls together with the parametric study, an equation for predicting the in-plane shear strength, V_n, of RM shear walls was proposed and verified with results of 64 RM wall tests from five sources in the literature. Statistical analysis was performed to evaluate the accuracy of the proposed equation against ten widely-used equations, including the design equations given in the Canadian Standards Association CSA S304-2014, the US Masonry Standards Joint Committee MSJC-2013, and the Standards Association of New Zealand NZS 4230:2004. The analysis shows that the proposed equation provides a sufficiently conservative and more accurate prediction for V_n than any of the other evaluated equations.

To my beloved parents

ACKNOWLEDGEMENTS

I would like to express my sincere gratitude to my supervisor, Dr. Khaled Galal, for his continued guidance, academic and financial support, encouragement, and valuable advice throughout my Masters and Ph.D. journey.

The financial support and awards from Concordia University are acknowledged and greatly appreciated, as is the donation of construction materials for the experimental work from the Canada Masonry Design Centre (CMDC) and Lafarge Canada Inc.

My dear colleagues Hossam El-Sokkary and Mohamed El-Sharawy cannot be thanked enough for their sincere supporting me throughout this project. I would like to acknowledge the contribution of my colleague Mohamed Al Butainy to complete the numerical study.

I would also like to acknowledge the technical assistance and support of Mr. Joseph Hrib and Mr. Jaime, with my experimental work. Moreover, I sincerely thank everyone who helped me during my program.

Finally, I dedicate this thesis to my parents, my wife, my son, my brothers, and my sisters for their unfailing support during my years of study. Without their love and their belief in me, I could not have completed this thesis. They deserve, and they have, all my love.

TABLE OF CONTENTS

LIST OF FIGURES

LIST OF TABLES

LIST OF EQUATIONS

LIST OF ABBREVIATIONS

AS	Australian Standard
ASCE	American Society of Civil Engineering
ASTM	American Society for Testing and Materials
ATC	Applied Technology Council
CMU	Concrete Masonry Unit
CSA	Canadian Standards Association
DBD	Displacement-Based Design
DSFM	Disturbed Stress Field Model
FBD	Force-Based Design
FE	Finite Element
FEMA	Federal Emergency Management Agency
MCFT	Modified Compression Field Theory
MSJC	Masonry Standards Joint Committee
NBCC	National Building Code of Canada
NEHRP	National Earthquake Hazards Reduction Program
NZS	New Zealand Standard
RC	Reinforced Concrete
RM	Reinforced Masonry
SDOF	Single-Degree-Of-Freedom
UBC	Uniform Building Code

LIST OF SYMBOLS

A_e = effective cross-sectional area of the wall (see Figure 2.24), mm^2

A_g = gross cross-sectional area of the wall, mm^2

A_{st} = total cross-sectional area of vertical reinforcement, mm^2

A_{sv} = cross-sectional area of horizontal reinforcement, mm^2

b_w = overall web width, which does not include flanges or projections formed by intersecting walls when calculating factored shear resistance of walls, mm

c = distance from extreme compression fiber to the neutral axis, mm

d = distance from extreme compression fiber to centroid of tension reinforcement, mm, for uniform distributed vertical reinforcement, it could be taken as the distance from extreme compression fiber to centroid of extreme tension bar

d_{eff} = reduced effective depth of wall section for the calculation of the in-plane shear resistance provided by horizontal reinforcement, V_s, mm. Shall be taken as 0.8 times the smaller between l_w and h_e (see Figure 6.3)

d_v = effective depth for shear calculations, mm

$d_v \geq 0.8 l_w$ for walls with flexural reinforcement distributed along the length

E_d = energy dissipation (see Section Figure 4.18)

E_m = modulus of elasticity of masonry, MPa

E_s = stored strain energy (see Section Figure 4.18)

f'_m = compressive strength of masonry normal to the bed joint at 28 d, MPa

f_t = flexural tensile strength of masonry (also called the modulus of rupture or the flexural bond strength), MPa

f_y = yield strength of reinforcement, MPa

f_{yh} = yield strength of horizontal reinforcement, MPa

f_{yv} = yield strength of vertical reinforcement, MPa

h_e = effective height, shall be taken as M/V, mm, where, M and V are the moment and shear at the section under consideration, respectively

h_w = total wall height, mm

k_1 = ductility related modification factor for in-plane shear resistance provided by masonry and axial compression load, V_{m+p}, (see Figure 6.4)

k_2 = ductility related modification factor for in-plane shear resistance provided by the horizontal reinforcement, V_s, (see Figure 6.4)

k_ϕ = factor concerning loading method (see Section 6.2)

l_d = development length of reinforcement bar, mm

l_w = wall length, mm

M/Vd_v = shear span to depth ratio, shall be taken as not less than 1.0 nor more than 2.0

P_d = axial compression load on the section under consideration, based on 0.9 times dead load, P_{DL}, including any axial load arising from bending in coupling beams, N, and shall not be taken greater than ($0.1\ f'_m A_g$), (see Section 6.2)

Q_{ue} = experimental peak lateral force

Q_{ye} = experimental lateral yield force, was defined at the lateral yield displacement, Δ_{ye}, on the backbone curve

R_d = ductility-related seismic force modification factor that reflects the capability of a structure to dissipate energy through inelastic behaviour

R_o = overstrength-related seismic force modification factor (see Eq. 4.3)

s = spacing of reinforcement, mm

s_h = horizontal spacing of vertical reinforcement, mm

s_v = vertical spacing of horizontal reinforcement, mm

V_i = initial shear strength, kN

V_m = in-plane shear resistance provided by masonry, kN

V_n = in-plane shear strength of RM shear walls, kN

V_p = in-plane shear resistance provided by the axial compression load, kN

V_r = residual shear strength, kN

V_s = in-plane shear resistance provided by horizontal reinforcement, kN

α = angle formed between the wall axis and the strut from the point of load application to the centre of the flexural compression zone for a cantilever wall. For a wall in double bending (pier), α is the angle between the wall axis and the line joining the centres of flexural compression at the top and bottom of the wall (see Figure 6.2)

α_w = section property reduction factor used for wall effective stiffness properties

γ_g = factor to account for partially grouted walls that are constructed of hollow or semi-solid units and is taken according to (see Section 2.4.7)

Δ = lateral displacement

Δ_{Que} = experimental lateral displacement at the peak lateral force, Q_{ue}

$\Delta_{0.8Que}$ = experimental lateral displacement defined at a drop in wall capacity to 80% of Q_{ue}

Δ_{ye} = experimental lateral yield displacement, it was taken as the average between the top lateral displacements that are corresponding to the first yield in the vertical reinforcement in each direction

ζ_{eq} = equivalent viscous damping ratio (see Eq. 4.7)

μ_{Δ} = experimental lateral displacements ductility

$\mu_{\Delta e1\%}$ = experimental lateral displacements ductility corresponding to the top drift of 1.0%

$\mu_{\Delta Que}$ = experimental lateral displacements ductility at peak force

$\mu_{\Delta 0.8Que}$ = experimental lateral displacements ductility at a drop in wall capacity to 80% of Q_{ue}

ρ = reinforcement ratio

ρ_v = total vertical reinforcement ratio = $(A_{st})_{\text{total}} / b_w d$

σ_n = axial compressive stress, MPa

ϕ = strength reduction factor for design

ϕ_m = resistance factor for masonry (according to CSA S304-14)

ϕ_s = resistance factor for steel reinforcement (according to CSA S304-14)

CHAPTER 1

INTRODUCTION

1.1 BACKGROUND

During significant earthquakes in the twentieth century, many *unreinforced* masonry structures suffered severe damage due to their limited inelastic deformation capacity (See Figure 1.1). Consequently, a coordinated research program between the U.S. and Japan was conducted at the beginning of the 1980s to investigate the seismic performance of *reinforced* masonry (RM) structures. The main goal of that research program was to build a five-story RM building that had the required inelastic deformation capacity to resist seismic loads.

http://nisee.berkeley.edu/elibrary/Image/S2381 http://nisee.berkeley.edu/elibrary/Image/S2239

Figure 1.1: Damage to masonry walls due to Alaska earthquake, March 27, 1964
Photos taken by Steinbrugge, Karl V, NISEE, *University of California, Berkeley*

The results of the research showed that providing vertical and lateral reinforcement for masonry walls enhances their inelastic behaviour under lateral loads in terms of strength and deformation. Thus, most design codes recently limit the use of unreinforced masonry shear walls to structures located in low seismic zones. On the other hand, all design standards necessitate the use of RM shear walls in medium and high seismic areas. The advancement in the design standards, along with the expansion in the masonry contractors and producers industry, led to an increase in the number of multi-story buildings constructed with reinforced masonry in the last few decades.

1.2 BEHAVIOUR AND FAILURE MECHANISMS

The behaviour of RM shear walls subjected to the combined effects of axial and lateral loads is influenced by several parameters including: the load conditions, the amount and distribution of horizontal and vertical reinforcement, the geometry of the wall, the mechanical properties of the masonry and steel, and boundary conditions. Excluding the premature lap-splice or bond failure of the reinforcement, the failure modes for RM shear walls can be summarized as: flexural failure, shear failure, and flexural/shear failure (see Figure 1.2). A brief description of each mode is presented in the following section.

1. Flexural failure

This failure mode is more common for RM shear walls with high shear span to depth ratio, M/Vd_v, accompanied by a moderate level of axial stress, σ_n. In this mode of failure, considerable horizontal cracking takes place parallel to the bed joint followed by yielding in the outermost vertical reinforcement near the bottom part of the tensile zone. As the lateral load increases, the cracks become wider and new cracks are initiated at a higher level, resulting in the formation of the plastic hinge. This type of cracking is characterized by low stiffness degradation; in addition, the yielding of the vertical reinforcement occurs at an early stage of deformation as shown in Figure 1.2a. Therefore, this failure mode is preferred in general due to its capability to achieve a high level of ductility and for the way it effectively dissipates energy. In the ultimate stages of failure, crushing of masonry in the compression zones takes place. Next, the compression reinforcement might buckle in some cases if spalling of the outer shell and grout occurs. In addition, there is the possibility of minor diagonal shear cracks. The percentage of vertical reinforcement has a major contribution in the flexural resistance mechanism compared to the lateral reinforcement.

2. Shear failure

When the principal tensile stress, σ_t, due to the combined effect of the lateral and vertical gravity loads, exceeds the tensile strength of masonry, the initiation of diagonal shear cracks takes place in masonry walls. This failure mechanism is known as a diagonal shear failure (see Figure 1.2b) and it is usually characterized for RM shear walls with a low shear span to depth ratio and light lateral reinforcement. As shown in Figure 1.2b, yielding in the vertical reinforcement occurs at the late stage of loading followed by rapid strength degradation once the wall reaches its lateral load capacity. This type of performance can be classified as more brittle and poor energy dispassion compared to the flexural failure dominated behaviour. The horizontal reinforcement ratio, distribution and anchorage detail have a major effect on the crack propagation in terms of density and width of cracks. Moreover, the level of axial compressive stress has a main influence on the orientation of cracks.

Sveinsson et al. (1985) and Voon (2007) classified the diagonal shear failure as brittle shear failure and ductile shear failure. It is important to mention that the term "ductile behaviour" usually refers to the flexural failure; instead, the shear failure mechanisms are generally known as brittle. However, the author of this thesis prefers to classify it as a brittle and moderately ductile shear failure. The brittle shear failure is usually characterized by two major diagonal cracks that causes severe deterioration in strength followed by sudden collapse. This kind of failure is more common for unreinforced or partially grouted masonry walls or RM walls with poor lateral reinforcement distribution. On the other hand, good distribution and anchorage of the transverse reinforcement along the height of RM walls replace the major diagonal cracks with sets of minor cracks. These minor cracks develop and gradually spread over the wall diagonals, as the initial diagonal cracks do not widen significantly, as the applied cyclic lateral load is increased. After large imposed lateral displacements, partial crushing occurs at the compression toe and at severely diagonally cracked portions of the wall.

Another form of shear failure is the sliding failure mechanism. This failure mode typically occurs for masonry walls that are subjected to high lateral forces accompanied by low vertical loads. That is why it is more common in low-rise masonry structures at the lower level. In some events, sliding shear failure is observed in medium-rise building where insufficient vertical reinforcement, i.e. dowel action, is provided at the base level or at upper stories where accelerations induced by earthquake ground motion are high and the gravity loads are small.

3. Flexural/shear failure.

A mixed failure mechanism could occur as shown in Figure 1.2c. A detailed discussion about the different failure mechanisms for RM walls is provided in FEMA 307 (1998).

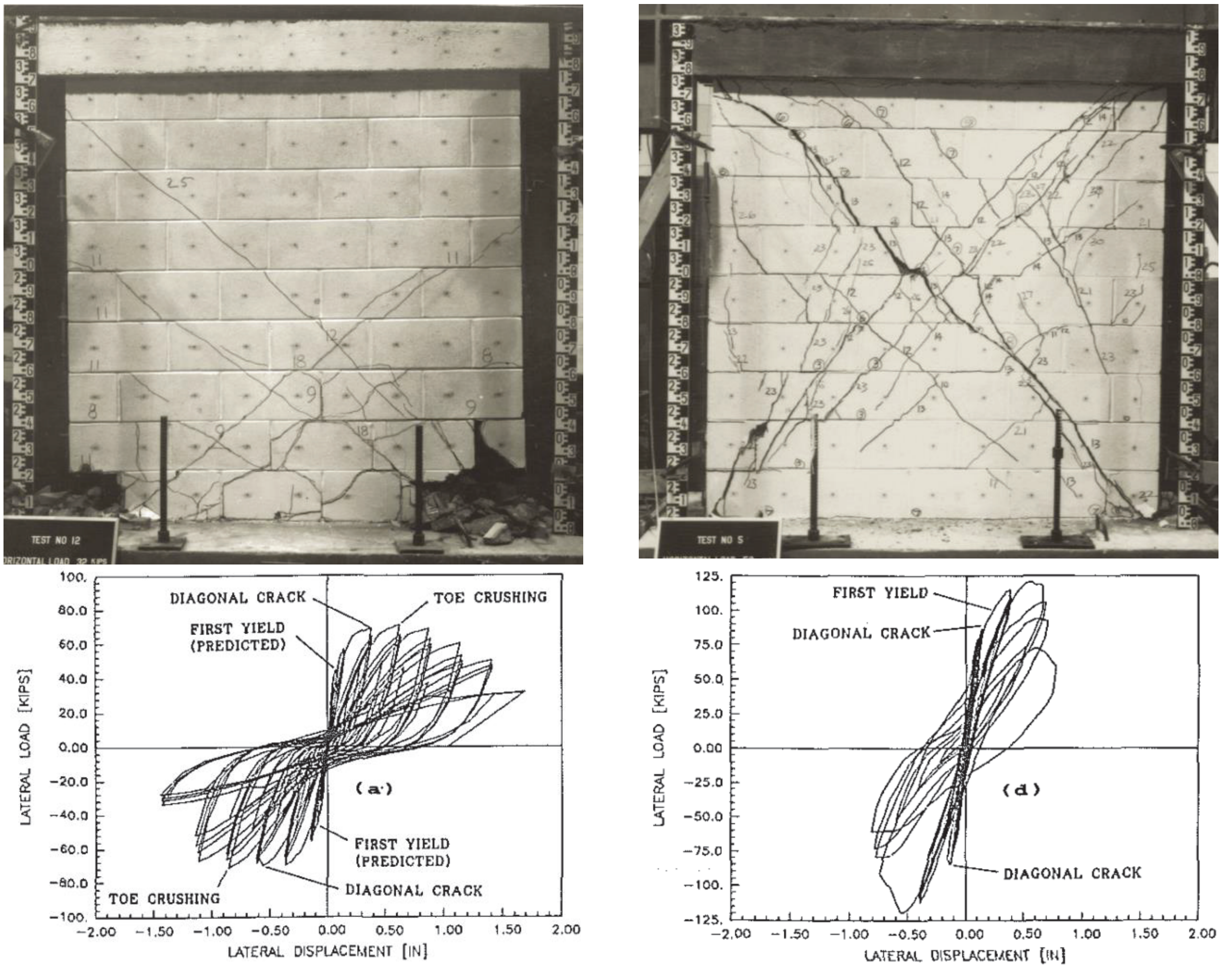

(a) Flexural failure (b) Shear failure

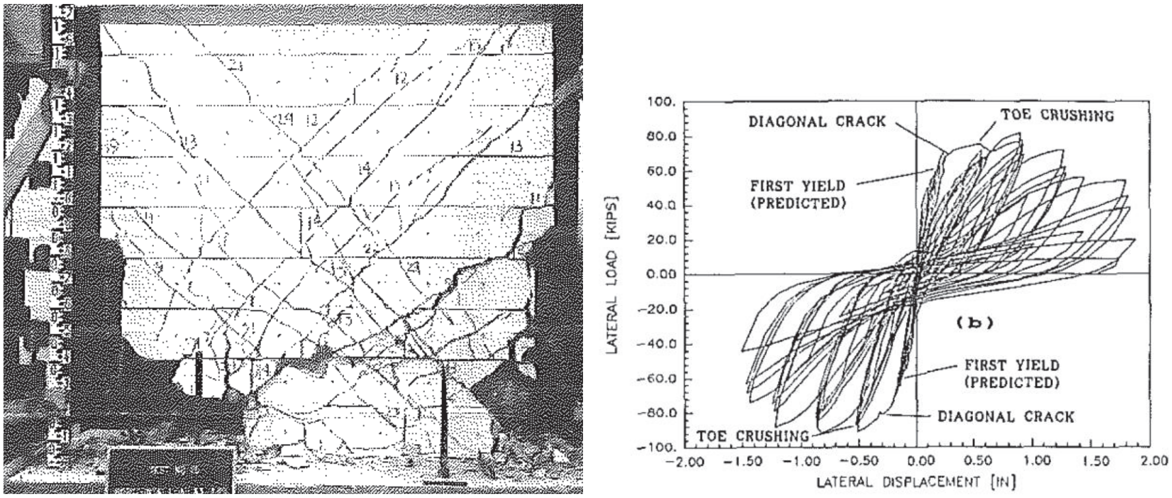

(c) Flexural/Shear failure

Figure 1.2: Different failure modes for RM shear walls (Shing et al., 1989)

Another way to define the aforementioned three failure modes can be presented based on the interaction between the flexural performance and the shear strength envelope using the model, ATC-6 (1981), presented by the Applied Technology Council (ATC). As shown in Figure 1.3, a brittle shear failure occurs when the lateral force, V, corresponding to the flexural strength is greater than the initial shear strength, V_i. However, if this lateral force is less than the residual shear strength, V_r, a ductile flexural failure is expected. Flexural/shear failure (Anderson and Priestley, 1992), or in other words, a moderately ductile failure, occurs when the lateral force corresponding to the flexural strength is between the initial and the residual shear strength.

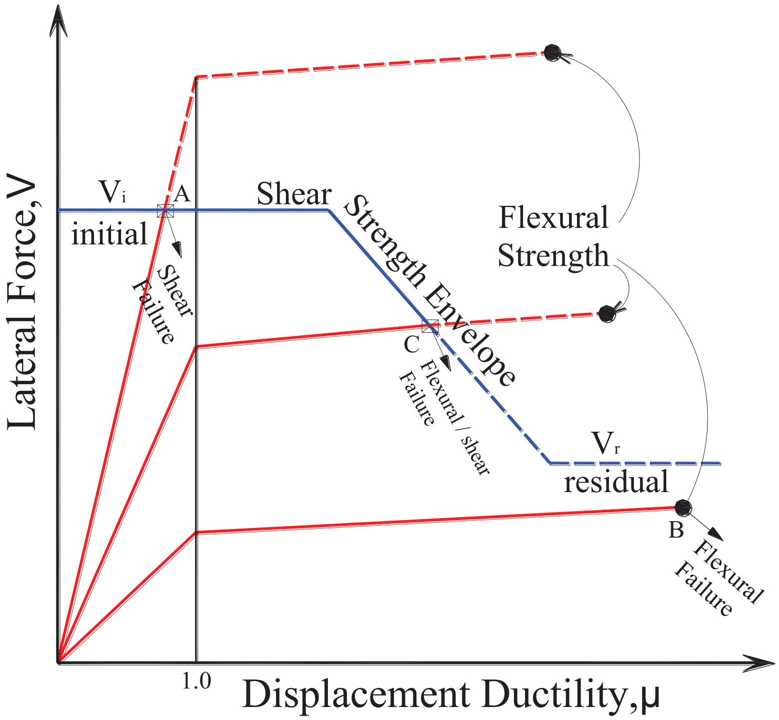

Figure 1.3: Interaction between flexural and shear performance (ATC-6 Model, 1981)

1.3 OBJECTIVE AND SCOPE OF WORK

The research work presented in this thesis is part of an ongoing research program at Concordia University that aims to investigate and enhance the seismic performance of masonry structures. Reinforced masonry (RM) shear walls are the key structural elements widely used to resist lateral loads in masonry buildings due to their capability to provide lateral strength, stiffness, and energy dissipation. The flexural behaviour of RM shear walls is well defined and follows the simple flexural theory of reinforced concrete structures based on plane-section assumption. On the other hand, the shear behaviour of RM shear walls in the plastic hinge region is more complex due to the interaction between the nonlinear responses of their constituent materials, namely: concrete masonry blocks, mortar, grout, and steel reinforcement. The main objective of this thesis is to evaluate the inelastic behaviour of fully grouted rectangular RM shear walls that are dominated by shear failure. Consequently, the performance of partially grouted, unreinforced, or masonry walls with boundary elements are beyond the scope of this research. To achieve the research objective, the main goals are to.

- Investigate experimentally the in-plane shear behaviour of RM shear walls.
- Perform numerical simulation of the inelastic performance of RM shear walls dominated by diagonal shear failure.
- Propose an accurate equation for predicting the in-plane shear strength, V_n, of RM shear walls.

According to these goals, the scope of work is defined as following:

- The experimental work involves assessing the response of nine full-scale fully grouted rectangular RM shear walls when subjected to in-plane axial compressive stress, cyclic lateral excitations, and top moment. The main variables considered are the level of axial compressive stress, shear span to depth ratio, horizontal reinforcement ratio, anchorage end detail, and the spacing of horizontal and vertical reinforcement. The work also involves analyzing the effect of the studied parameters according to force-based, displacement-based, and performance-based seismic design considerations.

- Developing nonlinear FE models to simulate the behaviour of RM shear walls subjected to cyclic loading, and validating those models using results from the nine RM tested walls. In addition, performing a mesh sensitivity analysis to evaluate the influence of mesh size on the precision of the output results, and conducting a parametric study to consider more variations in the effect of the horizontal reinforcement distribution, the level of axial compressive stress, and the wall aspect ratio on the in-plane shear behaviour of RM shear walls.
- Using the results of the tested RM shear walls along with the parametric study to propose an equation for predicting the in-plane shear strength, V_n, of RM shear walls that takes into account the adjustments in the in-plane shear resistances provided by masonry, V_m, axial compressive stress, V_p, and horizontal reinforcement, V_s, at high levels of displacement ductility. Thereafter, verifying this equation with the available experimental results from the literature, and performing a statistical analysis to evaluate the accuracy of the proposed equation against ten widely used equations, including the design equations given in the Canadian Standards Association CSA S304-2014, the US Masonry Standards Joint Committee MSJC-2013, and the Standards Association of New Zealand NZS 4230:2004.

1.4 THESIS LAYOUT

This thesis provides all the details of the experimental, numerical, and analytical work that has been conducted to achieve the research objectives, and is divided into seven chapters including this chapter. A brief description of each chapter along with their related appendices is provided in the following sections.

1.4.1 CHAPTER 2: LITERATURE SURVEY

This chapter provides a short review of the relevant literature that identifies the methodology of this research. Three main topics are covered in this chapter. A brief survey of previous experimental work on fully grouted RM walls is presented in the Section 2.2, covering the previously studied parameters and test results. One of the parameters that has considerable influence on the accuracy of the experimental results is realistic simulation of the boundary conditions and loading protocol. Section 2.3 discusses the common test setups for single/multi story masonry walls that are subjected to cyclic in-plane lateral forces, while Section 2.4 presents a selection of design equations for in-plane shear capacity, V_n, of RM shear walls. Finally, Section 2.5 provides a discussion and summary, based upon which the studied parameters for the experimental work in Chapter 3 are defined.

1.4.2 CHAPTER 3: EXPERIMENTAL WORK

A description of the experimental work is provided in this chapter. The first part of the chapter describes the studied parameters along with the test matrix and the details of the studied walls. The second part evaluates the properties of the materials used in the construction of the walls as well as the auxiliary laboratory tests, which is followed by a discussion of the test setup and instrumentation. A short overview of the testing procedure, including the loading protocol, is presented at the end of the chapter.

1.4.3 CHAPTER 4: EXPERIMENTAL RESULTS

This chapter provides a detailed discussion of the test results and observations made during the experimental testing of the nine RM shear walls in four main sections. The first section provides a summary of the measured lateral strength and displacements in addition to the lateral force-displacement hysteresis and failure modes for all walls. As an example, a detailed analysis of the results of the reference wall W-Ref, including aspects related to force-based, displacement-based, and performance-based design approaches, is given in Section 4.3. This is followed by a separate discussion on the influence of each parameter on these three different design approaches. The last section provides more discussion and proposes equations for the in-plane lateral stiffness degradation, equivalent viscous damping, and effective stiffness for seismic calculations.

1.4.4 CHAPTER 5: NUMERICAL SIMULATION

In recent years, several numerical models based on the finite element (FE) method have been developed to simulate the structural behaviour of masonry. FE analysis is a cost effective tool to predict the performance of structural elements. This chapter aims to provide a numerical model that has the capability to simulate the in-plane performance of RM shear walls dominated by diagonal shear failure. The first part of this chapter presents a brief overview of the Modified Compression Field Theory (MCFT) and the Disturbed Stress Field Model (DSFM). The second part provides a detailed discussion of the FE modeling, including the element type, materials models, and loading protocol, followed by verification of the FE modeling using the results of the tested walls in Chapter 4. The last part of this chapter discusses the result of a parametric study that was performed to consider more variations in some of the studied parameters in the experimental work.

1.4.5 CHAPTER 6: PROPOSED EQUATION FOR IN-PLANE SHEAR STRENGTH OF RM SHEAR WALLS

Using the results of the tested RM shear walls and based on the effects of the studied parameters in Chapter 4, in addition to the results of the parametric study in Chapter 5, an equation for predicting the in-plane shear strength, V_n, of RM shear walls is proposed and presented in this chapter. The proposed equation was verified with results of 64 RM wall tests from five sources in the literature. Statistical analysis was performed in Section 6.4 to evaluate the accuracy of the proposed equation against ten widely used equations, including the design equations given in the Canadian Standards Association CSA S304-2014, the US Masonry Standards Joint Committee MSJC-2013, and the Standards Association of New Zealand NZS 4230:2004. The analysis shows that the proposed equation provides a sufficiently conservative and more accurate prediction for V_n than any of the other evaluated equations. To simplify the proposed equation for design purposes, such that it can be easily handled by designers, the last section in this chapter provides some modifications in the proposed equation for codification.

1.4.6 CHAPTER 7: SUMMARY AND CONCLUSIONS

A summary of the conducted work in this research is presented in Section 7.2, while conclusions are drawn and summarized in Section 7.3 based on the study's results and findings. In the last section, recommendations are provided for future related research with the aim of improving the inelastic performance of RM buildings.

1.4.7 APPENDIX A

Appendix A provides more data related to Chapter 6. Table A.1 provides all the properties of the 73 RM walls used in the verification of the proposed equation. Moreover, the predicted in-plane shear resistances provided by masonry, V_m, axial compression load, V_p, horizontal reinforcement, V_s, and the nominal shear strength, V_n, for each wall were calculated using the proposed equation along with ten widely used equations, which are presented in Tables A.2, A.3, A.4, and A.5, respectively. A comparison between the accuracy of the eleven equations in terms of $V_{experimental}/V_{predicted}$ is given in Table A.6.

CHAPTER 2

LITERATURE SURVEY

2.1 INTRODUCTION

Three main topics are covered in this chapter. A brief survey of previous experimental work on fully grouted RM walls is presented in the Section 2.2, covering the previously studied parameters and test results. One of the parameters that has a considerable influence on the accuracy of the experimental results is the realistic simulation of the boundary conditions and loading protocol. Section 2.3 discusses the common test setups for single/multi story masonry walls that are subjected to cyclic in-plane lateral forces, while Section 2.4 presents a selection of design equations for in-plane shear capacity, V_n, of RM shear walls. Finally, Section 2.5 provides a discussion and summary, based upon which the studied parameters for the experimental work in Chapter 3 are defined.

2.2 IN-PLANE SHEAR TESTS ON MASONRY PANELS

2.2.1 U.S.-JAPAN COORDINATED PROGRAM ON MASONRY RESEARCH

During significant earthquakes in the twentieth century, many masonry structures suffered severe damage due to their limited inelastic deformation capacity. Consequently, a coordinated research program between the U.S. and Japan was conducted at the beginning of the 1980s to investigate the seismic performance of reinforced masonry structures. The main goal of the research was to build a five-story RM building that had the required inelastic deformation capacity to resist seismic loads. The primary program objectives were to:

1. Develop design criteria for reinforced masonry buildings and components.
2. Provide a comprehensive experimental database on the behaviour of masonry materials, components, and systems.
3. Develop an analytical nonlinear model for research and design purposes, including detailed analysis, system analysis, and dynamic loads determination.
4. Improve masonry fabrication procedures and sub-assemblage experimental procedures for obtaining masonry properties.

Throughout this coordinated program, many experimental studies were carried out on masonry walls under cyclic lateral loads in the U.S. and Japan. This section presents some of these studies.

2.2.1.1 Matsumura (1985, 1986, 1988)

As a part of the U.S.-Japan coordinated research program to investigate the behaviour of masonry buildings, comprehensive experimental work was carried out in Japan during the 1980s. Matsumura (1985 and 1986) tested eighty masonry panels to evaluate their in-plane shear performance. Out of the eighty walls, fifty-seven wall specimens were constructed using hollow concrete block while the rest were made of brick units. Two different types of specimens were constructed, namely: wall and beam (see Figure 2.1). A total of fifty-five full size walls type specimens with a fixed base and top free only to move horizontally were subjected to horizontal cyclic lateral load, which was applied at the middle-height, creating a double moment on the wall. In addition, twenty-five beams were laid horizontally and subjected to a vertical shear load like a deep beam. Sixteen concrete and four brick masonry walls type were fully grouted while the rest of the specimens were partially grouted. The dimensions of the walls type ranged between 1600-1800 mm height, 790-1970 mm length, and 150-190 mm thickness, while the specimens for the beam type were relatively smaller. The results of the four fully grouted brick masonry walls did not show a significant influence of the horizontal reinforcement on their shear capacity. Matsumura (1986) attributed that to inadequate grouting during construction of the walls. Consequently, these four walls were retested and the results reported in Matsumura (1988).

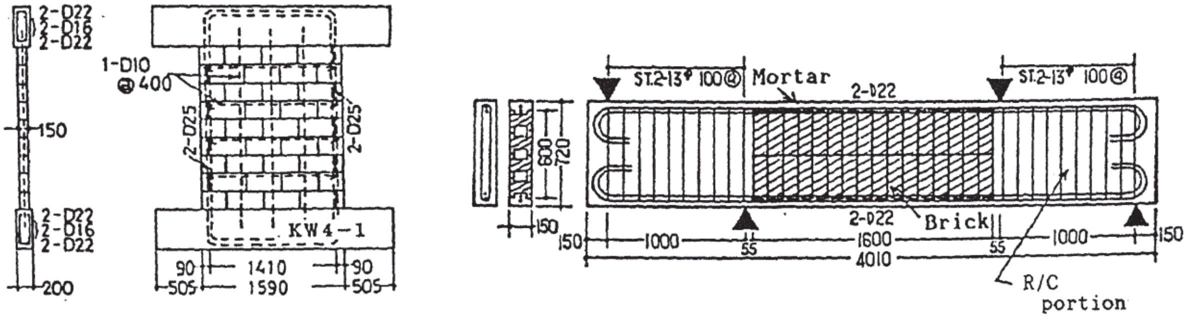

(a) Specimen for wall type loading (b) Specimen for beam type loading

Figure 2.1: Examples of tested specimens (Matsumura, 1988)

Many parameters were considered in the test matrix, such as: the masonry compressive strength, f'_m, the vertical and horizontal steel reinforcement ratios, the axial compressive stress, the grout pattern, and the wall height to the effective flexural depth ratio, *h/d*. The lateral load was applied at the middle height of the wall, thus, the effective height, h_e, is equal to *h/2*. However, it is important to mention that the author in his study considered this ratio, *h/d*, as the shear span to depth ratio.

For the twenty fully grouted masonry wall type, *h/d* varied from 1.2 to 2.57 and *M/Vd* ranged from 0.6 to 1.29. The masonry compressive strength, f'_m, ranged from 21.8 to 31.4 MPa. Moreover, the vertical and lateral reinforcement ratios varied from 0.57 to 1.3% and from 0.0 to 0.67%, respectively. Two values for axial compressive stress, σ_n, were evaluated as 0.49 and

1.96 MPa. Three failure mechanisms were observed; shear, flexural, and flexural/shear. Based on the test results, the author concluded the following:

a) The relation between shear strength, v_m, and the masonry compressive strength, f'_m, is not linear and it may be acceptable that masonry shear strength increases approximately in proportion to $\sqrt{f'_m}$.

b) Masonry shear strength increases linearly with increasing axial compressive stress, σ_n, and decreases inversely in relation to the shear span to depth ratio.

c) Providing lateral and vertical steel reinforcement increases the shear strength of masonry walls; yet it has a negligible effect before cracking.

2.2.1.2 Okamoto et al. (1987)

During 1984 and 1985, Okamoto et al. tested thirty-five masonry specimens including twenty-six walls and nine beams. The principal objective of their work was to experimentally evaluate the effect of the axial compressive stress, horizontal reinforcement ratio, splices, confining of compression zone, transverse wall, shear span to depth ratio, and the RC slab, on shear and flexural behaviour of masonry walls and beams. The twenty-six walls consisted of three RC, five clay bricks, and eighteen concrete masonry walls. All the tested masonry specimens were fully grouted and constructed in running bond with a 50% overlap per unit in alternate courses. Out of the twenty-three masonry walls, five concrete masonry blocks and three clay bricks walls were dominated by shear failure. The main variables for these walls were: aspect ratio (0.9, 1.5, and 2.25), compressive axial stress (0.0, 1.96, 3.92, and 5.88 MPa), and vertical reinforcement ratio (0.53, 0.73, and 1.0%). Instead, the horizontal reinforcement ratio, ρ_h, was not one of the investigated parameters for the masonry walls that failed in shear; all of these walls had a constant ρ_h equal to 0.17%. The conclusions obtained from the test results were as follows:

a) In general all the walls constructed with clay bricks show a higher shear strength compared to the concrete masonry walls due to their higher masonry compressive strength, f'_m.

b) Gain in shear strength by 22% and 33% was reported as the axial compressive stress, σ_n, increased from 1.96 to 3.92 and 5.88 MPa, respectively. These results show that the relation between the axial compressive stress and its contribution, V_p, toward the shear strength is not a linear relation. Instead, the rate of this contribution will decrease by increasing σ_n.

c) Increasing the wall aspect ratio from 0.9 to 1.5 and 2.25 increased the flexural deformations and decreased the shear capacity by 25% and 35%, respectively.

d) The specimens that dominated by shear failure had approximately 50% of the deformation capacity of those that failed in a flexure mode.

2.2.1.3 Kaminosono et al. (1988)

Another set of experimental tests for masonry walls were carried out by Kaminosono et al. (1988) through the U.S.-Japan coordinated earthquake research program. Twenty-two walls were tested to investigate the influence of many parameters on the seismic performance of masonry walls, including: axial compressive stress, shear span to depth ratio, amount of horizontal reinforcement, joint method of reinforcement bar, spiral reinforcement at the compressive toe of the wall, and transverse wall. The tested walls were fourteen concrete block masonry, five clay block masonry, and three reinforced concrete walls. The twenty-two walls were divided into eighteen “I”, three “T”, and one “+” shaped walls. All the walls had the same thickness of 190 mm and were tested under a double curvature deformation test setup, where the cyclic lateral load was applied at the middle height of the tested walls. The axial compressive stress and the shear span to depth ratio ranged between 0.5 to 6.0 MPa and 0.452 to 1.14, respectively, and the horizontal reinforcement ratio varied from 0.17 to 0.68 %. The authors concluded the following from the test results:

a) For the specimens that failed in shear, increasing the axial compressive stress enhanced the shear strength but decreased the deformation capacity. However, the shear span to depth ratio has an opposite influence on both shear strength and deformation capacity.
b) Increasing the horizontal reinforcement ratio and providing confinement of the compression toe by spiral reinforcement, enhances the deformation capacity for the walls failed in flexural.
c) For the walls that had a shear span to depth ratio, M/Vd_v, of less than 0.8, they reached their maximum load resistance at a drift of 0.002 radian followed by rapid strength degradation. However, the walls with M/Vd_v equal to 1.14 reached their capacity at a drift of 0.0075 radian, and the deterioration of shear strength was small until a drift of 0.014 radian.
d) The joint of reinforcing bars has a negligible influence on the deformation capacity; yet providing transverse walls increased the strength and the deformation capacity.

2.2.1.4 Research conducted at University of California at Berkeley

In the late 1970s and 80s, an extensive program of cyclic loading tests on masonry structural elements was carried out at the University of California, Berkeley. As a part of this program, ninety-three single pier tests were conducted by several researchers and the test results were published in four research reports: Hidalgo et al. (1978, 1979), Chen et al. (1978), and Sveinsson et al. (1985). Many parameters were considered in their experimental work such as: the level of bearing stress, type of masonry unit and grout, amount and anchorage of horizontal reinforcement, and distribution of vertical and lateral reinforcement. The tested walls were mainly classified based on their aspect ratio, and the result of each group was presented separately as shown in Table 2.1. In this section, more attention is given to the work carried out by Sveinsson et al. (1985), since in some of the other tests the magnitude of the axial load was changed at failure because of the load arrangement (Anderson and Priestley, 1992).

Table 2.1: Single Masonry Pier Test Program (Sveinsson et al., 1985)

Authors	Aspect ratio (H/L)	Hollow clay brick (HCBR)	Double Wythe grouted core clay brick (CBRC)	Hollow concrete block (HCBL)	Total number
Hidalgo et al. (1978)	2:1	9	5	0	14
Chen et al. (1978)	1:1	13	7	11	31
Hidalgo et al. (1979)	1:2	6	6	6	18
Sveinsson et al. (1985)	1:1	13	5	12	30

As an extension of the work done by Chen et al. (1978), Sveinsson et al. (1985) conducted cyclic in-plane shear tests on thirty fully grouted masonry walls with a height to width ratio of one. Three different types of masonry units were used: a hollow concrete block, a hollow clay brick, and a double wythe grouted core clay brick that consisted of two brick wythes and a 75 mm grouted core. The effects of four parameters were evaluated in their test series. Three of these parameters were related to the reinforcement, including the amount and anchorage of the lateral reinforcement and the distribution of the vertical reinforcement. Furthermore, the influence of the level of bearing stress was investigated. For the twenty-five walls that were constructed using hollow units (see Table 2.1), the vertical and lateral reinforcement ratios ranged between 0.17 and 0.45% and 0.1 and 0.62% from the cross-sectional area of the tested walls, respectively. Moreover, the value of the bearing stress varied from 0.7 to 3.1 MPa.

To evaluate the effect of the distribution of the vertical reinforcement, three combinations of vertical bars were used: 2 #7 (A_{st} = 774 mm^2), 4 #5 (A_{st} = 800 mm^2), and 6 #4 (A_{st} = 774 mm^2). Two of the bars were placed in the outer cells while the remainder, if applicable, were equally distributed over the remaining length. This study is one of few studies that considered the effect of the anchorage end detail of the lateral reinforcement on its contribution towards the in-plane shear strength of RM walls. Three types of horizontal bar anchorage were investigated as shown in Figure 2.2.

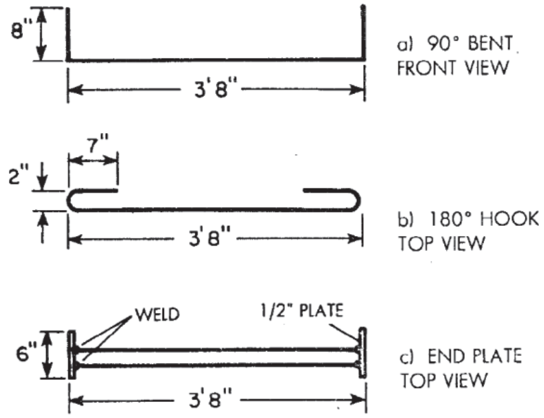

Figure 2.2: Types of anchorage of horizontal bars (Sveinsson et al., 1985)

To calculate the masonry compressive strength of the tested specimens, three short and three tall slender prisms were tested under uniaxial compression load until failure. The height to thickness ratio, *h/t*, was 2 and 5 for the short and tall prisms respectively. In general, the prisms with higher *h/t* showed less masonry compressive strength. Four different failure modes were observed during testing and were classified as: diagonal shear, shear-sliding, sliding, and flexural modes. Generally, most of the walls that were constructed using hollow clay bricks were dominated by shear-sliding or sliding failure. The pure sliding failure was observed for just two walls that were heavily reinforced in the lateral direction with a small amount of vertical reinforcement. On the other hand, out of the twelve concrete block masonry walls, ten walls exhibited diagonal shear failure and two walls were governed by flexural mode.

Sveinsson et al. (1985) defined the displacement ductility as the ratio of the maximum relative lateral displacement experienced by the tested wall before failure, δ_m, to the crack displacement, δ_{cr}, without considering the first yield point of vertical reinforcement, as shown in Figure 2.3. In addition, the failure point was not defined at a certain level of strength (e.g. at P_u or at a drop in wall capacity to 80% of P_u), however, all walls were loaded up to the first lateral displacement after the strength degradation was initiated.

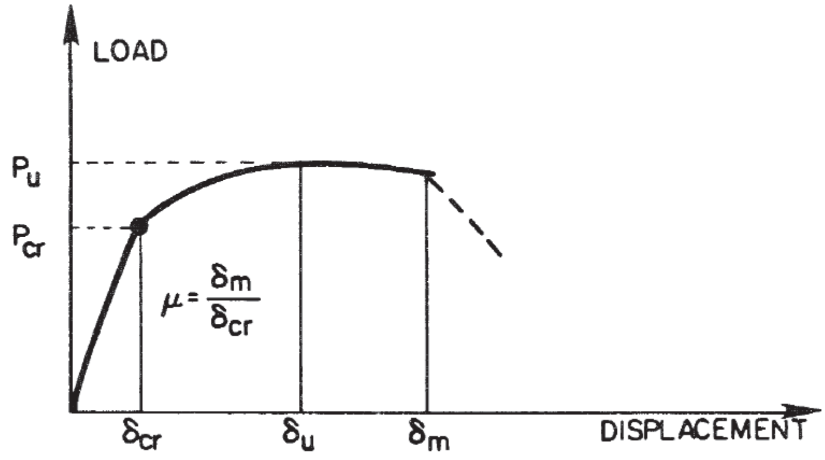

Figure 2.3: Definition of hysteresis envelope parameters (Sveinsson et al., 1985)

The test results of the thirty RM walls showed that:

a) When the horizontal reinforcement with 180° hook was doubled from 2 to 4 #5 bars, the in-plane lateral load was increased by 16%. Furthermore, the displacement ductility, δ_m/δ_{cr}, was more than double. However, when the 90° bent was used for the same reinforcement increase, the shear capacity was increased by just 4% with negligible influence on the ductility.

b) For the walls with heavy lateral reinforcement, the end plate was the most effective anchorage end detail, whereas the 90° bent was the least effective. On the other hand, where the horizontal reinforcement was light, both the 180° hook and the end plate were more effective than the 90° bent and showed similar performance. Still, it is important to mention that all three types of anchorage end details enhanced the pre-diagonal crack behaviour of the RM walls that were dominated by shear failure in terms of strength and ductility.

c) The overall effect of distributing the vertical reinforcement seems to be inconsistent. For the hollow concrete block specimens, the influence of distribution was minor. However, for the hollow clay brick walls, the effect was considerably higher.

2.2.1.5 Shing et al. (1988, 1989, 1990, 1991, 1993)

A total of twenty-two masonry walls were tested by Shing et al. 1988 at the University of Colorado as a part of the U.S. coordinated program for masonry building research (Noland 1987). The test results of this experimental work were presented and discussed in several publications. The main objective of their study was to evaluate the design equations for reinforced masonry shear walls. Of the twenty-two RM walls, sixteen were built with hollow concrete blocks and six with hollow clay bricks. All the tested specimens had the same in-plane dimensions of 1.83 m x 1.83 m with an aspect ratio of 1.0. However, the actual wall width was 143 and 137 mm for the concrete masonry and clay specimens, respectively.

The investigated parameters included amount of vertical and lateral reinforcement, magnitude of applied compression load, and type of masonry units. All the walls were fully grouted with uniformly distributed vertical and horizontal reinforcement. Different failure mechanisms were observed during the experimental study. Seven walls reached their flexural yielding capacity of the vertical reinforcement followed by crushing of masonry at the wall toes, which was classified as a flexural failure. Moreover, ten specimens exhibited a diagonal tension shear failure and the rest of the tested walls were governed by mixed flexural/shear behaviour, which was characterized by significant flexural deformations followed by toe crushing as well as diagonal and sliding shear cracks.

For the walls dominated by shear failure, the vertical and lateral reinforcement ratios ranged from 0.38 to 0.74% and 0.14 to 0.26% from the horizontal and vertical wall cross-sectional area, respectively. In addition, the value of axial compressive stress varied between 0.0, 0.69, 1.86, and 1.93 MPa. A constant spacing of 406 mm was used between the vertical and horizontal reinforcing bars. Shing et al. (1990) characterized the lateral displacement, Δ, at the top of a wall panel as the sum of four distinct mechanisms, as shown in Figure 2.4, using the following equation:

$$\varDelta = \varDelta^{SL} + \varDelta^{SH} + \varDelta^{UP} + \varDelta^{FL} \qquad \text{Eq. 2.1}$$

where:

Δ^{SL} = base sliding deformation

Δ^{SH} = overall diagonal deformation

Δ^{UP} = base uplift due to the bond slippage and elongation of the vertical steel embedded in the base footing

Δ^{FL} = flexural deformation that can be calculated from the average section curvatures along the height of the wall

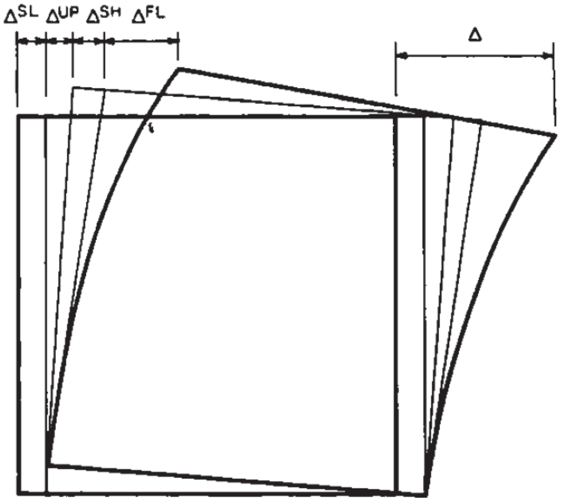

Figure 2.4: Deformation mechanisms of a wall panel (Shing et al., 1990)

Based on the experimental results, Shing et al. (1990) concluded that:

a) Clay masonry has a higher compressive strength than concrete masonry. In addition, the walls that are dominated by flexural mode exhibit a more ductile behaviour than those dominated by diagonal shear failure.

b) The simple flexural theory based on the plane-section assumption could be applied to predict the flexural strength and ductility of RM wall panel with an aspect ratio of one. However, when the shear wall is subjected to seismic loads the actual flexural strength can be slightly higher than the predicted by the flexural theory as a result of the strain hardening under cyclic loads; yet this strain hardening effect reduces as the axial stress increases.

c) Increasing the axial stress leads to more severe toe crushing. Consequently, the ductility can be significantly reduced. On the other hand, using proper confinement at the compression toe could enhance the ductility of masonry shear walls under high axial stress.

d) The compressive strength of masonry, the applied axial stress, and the vertical reinforcement ratio have a major influence on the residual strength of masonry after diagonal cracking. On the other hand, the lateral and vertical reinforcement have a slight effect on the pre-crack performance of RM shear walls.

2.2.2 VOON AND INGHAM (2006, 2007)

Voon and Ingham (2006) tested ten single-story RM shear walls to investigate their in-plane shear behaviour. The main variables being considered in their experimental work were as follows: the wall aspect ratio, type of grouting, lateral reinforcement ratio and distribution, and the level of axial compressive stress. All the tested walls were built using running bond pattern of 140 mm wide concrete masonry units. The masonry compressive strength ranged between 17.0 and 24.3 MPa. Two walls were constructed with an aspect ratio, h_w/l_w, of 2.0 and 0.6 while the rest had h_w/l_w equal to 1.0. Eight walls were fully grouted and two were partially grouted. For the two partially grouted walls, one had vertical reinforcing bars placed every 400 and the other every 800 mm, with no shear reinforcement. Only cells containing reinforcing bars were filled with grout. For the rest of walls, the horizontal reinforcement was uniformly distributed up the height of the walls and was hooked around the outermost vertical reinforcing bars using 180° standard hook. Four lateral reinforcement ratios were evaluated in their study: 0.01, 0.05, 0.06, and 0.14%. Furthermore, the axial compressive stress varied from 0.0 to 0.5 MPa.

Out of the ten walls, eight walls were dominated by diagonal tension shear, one failed by flexural/shear, and one exhibited a flexural/sliding mode of failure. The reported displacement ductility, μ_Δ, ranged from 1.33 to 2.86, where μ_Δ is the ratio between the ultimate to nominal yield lateral displacements, Δ_u, and Δ_y, respectively. It is important to mention that Voon and Ingham did not measure Δ_y at the first yield point of the vertical reinforcement; instead, they defined it as shown in Figure 2.5 according to the following equation:

$$\Delta_y = \frac{2F_n}{F_1 - F_2}\Delta_{1mm} \qquad \text{Eq. 2.2}$$

where:

F_1 = measured lateral force at lateral displacement of +1.0 mm, kN

F_2 = measured lateral force at lateral displacement of -1.0 mm, kN

F_n = the expected, calculated, nominal lateral force required to develop the wall flexural strength, kN

Δ_{1mm} = 1.0 mm

From the test results, the authors concluded the following:

a) Increasing the wall aspect ratio from 0.6 to 2.0 resulted in decreasing the lateral in-plane shear capacity by 65%. However for the same ratio, the displacement ductility increased by more than 100%.

b) When shear strength is calculated according to the net cross-sectional area of both the masonry units and grouted cells, the influence of grouting was insignificant. In addition, decreasing the spacing between the lateral reinforcement enhanced the post-cracking behaviour.

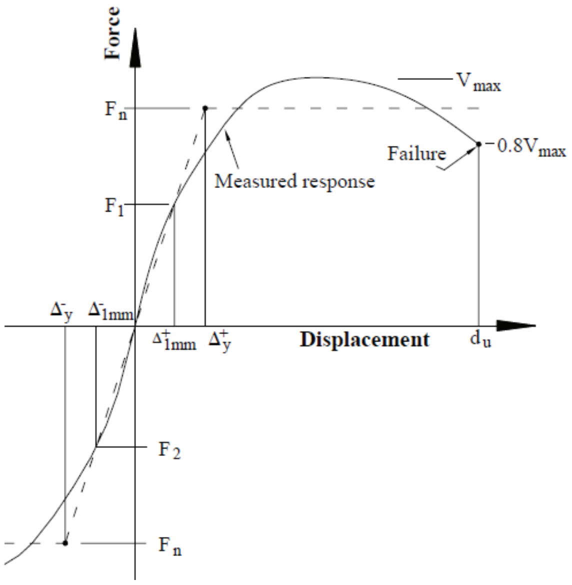

Figure 2.5: Nominal yield displacement (Voon, 2007)

2.3 TEST SETUP

Most of the existing empirical equations for in-plane shear strength of masonry walls are derived from experimental work. One of the main parameters that have a considerable influence on the accuracy of the experimental results is the realistic simulation of the boundary conditions and loading protocol. Throughout this section, most of the common test setups for single or multi-story masonry walls that are subjected to cyclic lateral forces are presented and discussed.

The shear behaviour of masonry can be investigated at the micro-level, meso-level, and macro-level, as shown in Figure 2.6 (Van Vliet, 2004). At the micro-level, the lowest level, the loads are applied on two masonry units connected by one bed joint, which is common for evaluating the bond characterization of mortar joints. The behaviour of single story high or more is considered as macro-level, while the meso-level usually refers to specimens that are relatively small, approximately 1.0 m × 1.0 m, and is generally used for shear tests by means of compression, as can be seen in Figure 2.7. In this type of shear test, the specimens are laid at angle with the loading direction; thus, the masonry is loaded by a combination of normal compression and shear stresses.

In this section, more attention is provided to the shear tests at the macro-level where the masonry wall panel with bed joints in the horizontal direction is subjected to in-plane lateral loads. There are several factors that control the suitable test setup, for example: the grout pattern, the amount and distribution of the vertical reinforcing bars, and number of stories. This section provides further discussion of the boundary conditions at the top and bottom of the tested walls; this is in addition to the way in which the cyclic lateral force is introduced.

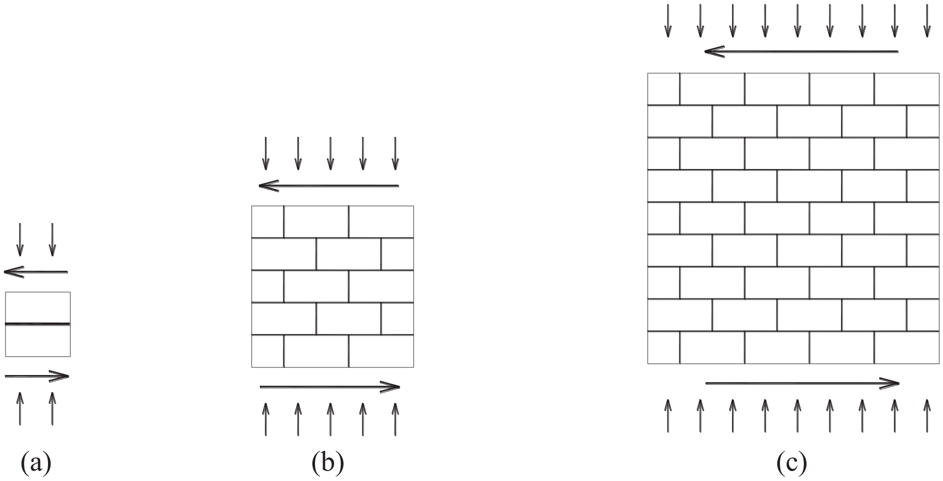

Figure 2.6: Shear tests on masonry at: (a) Micro-level; (b) Meso-level; (c) Macro-level

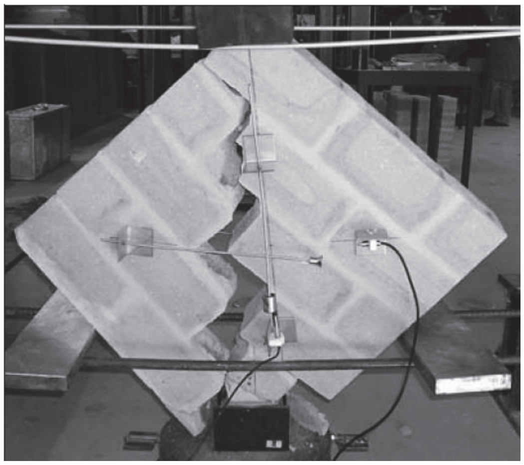

Figure 2.7: Shear tests by means of compression tests (Haach, 2009)

2.3.1 SINGLE STORY MASONRY WALL PANEL

Due to the height limitation in most structure laboratories, a high percentage of the experimental work investigating the seismic performance of masonry shear walls has been conducted on a single story wall panel. Usually this tested panel simulates the plastic hinge zone of a real multi-story masonry shear wall. Researchers have used different test-setups over the years. Based on the deformation mode of shape, the in-plane shear test on masonry shear walls can be generally classified as either a single or double curvature shear test.

2.3.1.1 Single curvature shear test

The lateral behaviour of a tested wall panel using the single curvature shear test is closer to the performance of a free cantilever wall with a fixed base and free top. There are different ways to simulate the boundary conditions of the wall panel using reinforced concrete, reinforced masonry, steel beams or even mechanical mechanisms. Some examples for different test setups from previous research are presented and discussed below.

2.3.1.1.1 Masonry wall panel with top RC loading beam

Six masonry wall specimens of size 1.83 m × 1.83 m were tested by Mosallam and Banerjee (2011) to evaluate the enhancement in their in-plane shear capacity using fibre reinforced polymer (FRP) composites. Each wall was fully grouted and was vertically reinforced with 5#6 @ 203 mm. However, no lateral reinforcement was provided to achieve shear failure. All the investigated walls were tested under a combination of constant axial stress and incremental lateral cyclic loads and each of them was constructed on a 0.45 m thick RC footing. This footing was fixed to a strong floor. To transfer the applied axial and lateral forces, a 0.2 m wide × 0.45 m high RC beam was poured over the top of each specimen as presented Figure 2.8.

The axial compressive stress was applied using four hydraulic jacks that were placed on the top of the wall and connected to load cells to monitor the magnitude of the vertical load during testing. Two steel beams were placed between the hydraulic jacks and the walls to distribute and transfer the axial load. Moreover, the top RC loading beam was horizontally clamped using two steel plates and four steel rods, and this clamping system was connected to the lateral actuator. The applied cyclic lateral loads was then transferred to the tested wall by means of bearing stress between the steel plates and the loading beam in each loading direction. Noticeably, no supports were attached to the tested wall to prevent any out-of-plane deformation if it occurred, and there is a question about the magnitude of the axial load at high levels of lateral deformation.

Haach et al. (2010) used a similar test-setup to investigate the seismic performance of eight half-scaled concrete block masonry walls as shown in Figure 2.9. The base RC beam of the tested wall was fixed to a steel beam using eight steel bolts and two adjustable clamping angles. The steel beam was then fixed to the strong floor through steel rods to avoid uplift and slippage of the wall base. The axial compression load was applied by using a vertical actuator with vertical steel cables that were anchored at the strong floor. Two steel beams were used for the distribution of the vertical load at two different levels. Unlike the test-setup by Mosallam and Banerjee (2011), a set of steel rollers was placed under the loading-distributing beam to allow relative displacement of the wall with respect to the vertical actuator.

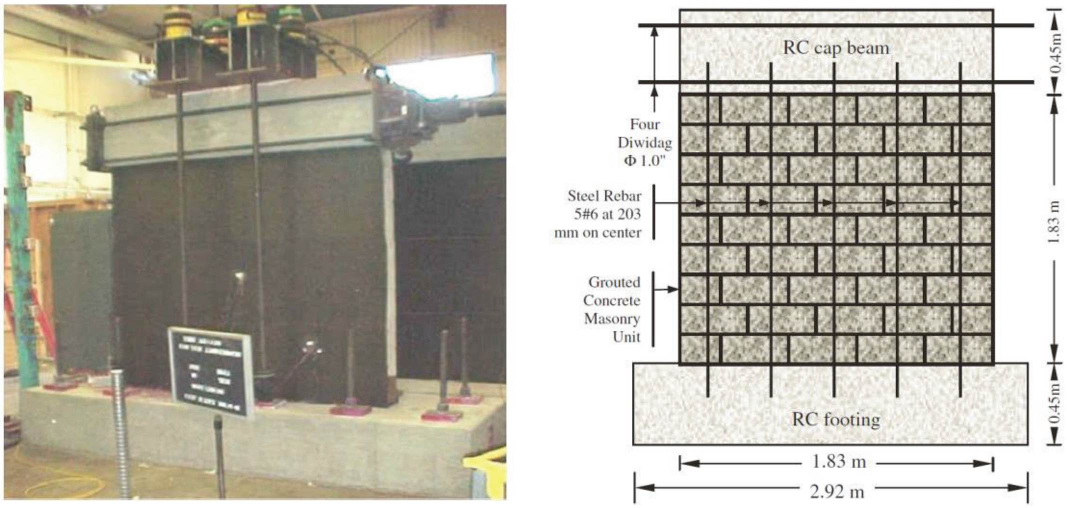

Figure 2.8: In-plane shear test setup for masonry walls with top RC loading beam (Mosallam and Banerjee, 2011)

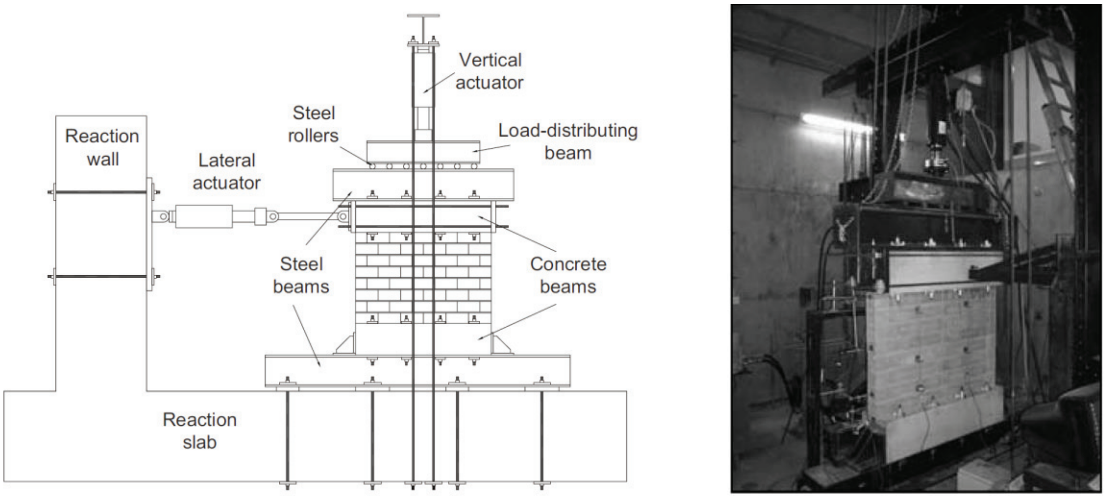

Figure 2.9: Test setup for in-plane cyclic horizontal load (Haach et al., 2010)

2.3.1.1.2 Masonry wall panel with top RM loading beam

Ingham et al. (2001), Minaie et al. (2010), ElMapruk (2010), and Nolph and ElGawady (2012) used a top RM loading beam instead of a RC beam as shown in Figure 2.10. This test setup is more common for evaluating the seismic performance of partially grouted masonry walls. In this type of masonry wall, the amount of vertical reinforcement is usually not sufficient to provide the required dowel action between the top RC beam and the tested wall.

Consequently, the lateral load is applied directly on the top of the tested wall. On the other hand, the top RM loading beam is used to transfer and distribute the vertical load over the whole length of the specimen. As presented in Figure 2.10, the vertical reinforcing bars of the wall continue to the top RM beam that is three fully grouted masonry courses high and well reinforced in the lateral direction. Similar to most of the common test setups, each wall was constructed on a RC footing and each footing then fixed to the laboratory strong floor. Furthermore, the concrete base was braced using two stiff built-up steel angles that were bolted to the strong floor. The lateral load was applied through a pair of C-channels that were bolted to the masonry specimen on each side using threaded rods and connected to the horizontal actuator. These rods were anchored and grouted in place during construction at the bottom course of the top RM loading beam. Figure 2.11 shows one of the techniques used by ElMapruk (2010) for partial grouting. As can be seen, a plastic mesh was placed below each cell to be grouted to prevent the grout from flowing to the lower cells during pouring.

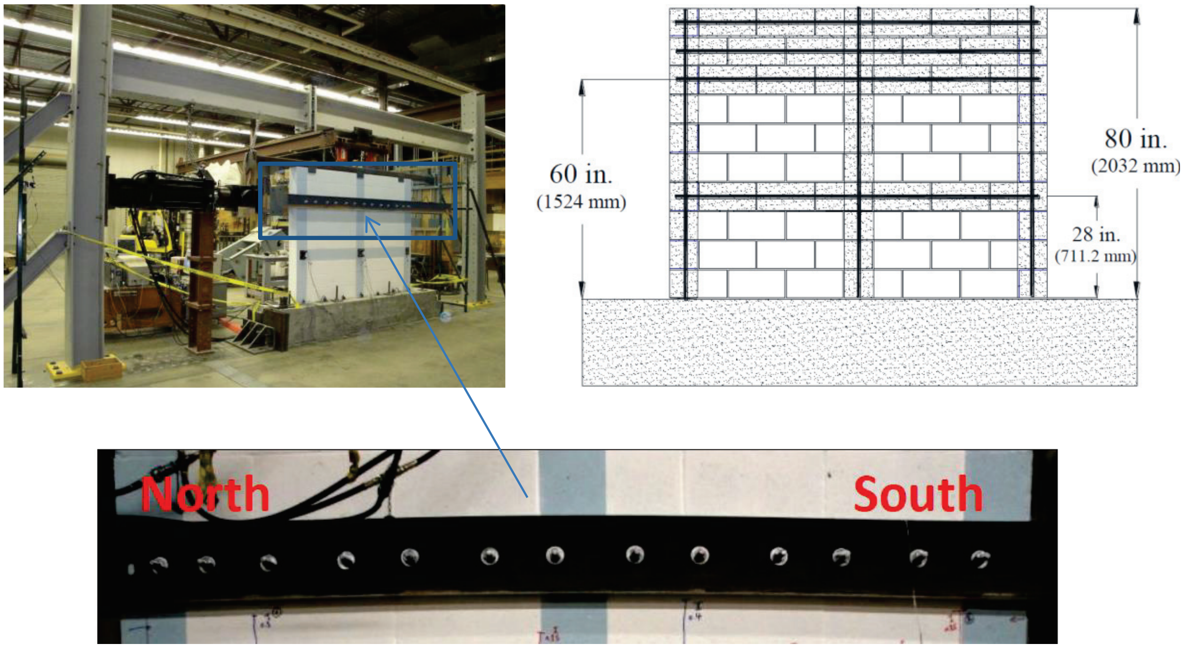

Figure 2.10: Test setup for partially grouted RM shear wall with top RM loading beam (ElMapruk, 2010)

Figure 2.11: **Construction of bond beam in partially grouted masonry wall (ElMapruk, 2010)**

2.3.1.1.3 Masonry wall panel with top steel loading beam

To investigate their in-plane shear performance, Voon and Ingham (2006) tested ten single story RM shear walls with different parameters. Of the ten walls, nine walls were constructed on a re-usable RC footing. This footing had starter bars that were drilled and tapped to accommodate the vertical reinforcement of the tested walls as presented in Figure 2.12. Furthermore, the RC footing was fixed to the laboratory floor to prevent any movement between the footing and the floor. Four walls were tested under axial compressive stress and six without. Figure 2.13 shows a typical test-setup for the specimens with axial compressive stress. The in-plane lateral displacement was introduced using a horizontality mounted hydraulic actuator that was connected to the top of the walls through a 150 x 75 steel channel section. Two parallel horizontal struts were connected to the top steel channel to prevent the test wall from moving in an out-of-plane direction.

Two pairs of high strength 23 mm diameter prestressing bars were installed to apply the axial compressive stress if applicable. As shown in Figure 2.13, a rocker beam was used to ensure equal axial force in the prestressing bars on either side of the wall. Moreover, each of the prestressed bars passed through a 1.0 kN/mm coil spring. The prestressing bars were then tensioned by tightening the nuts until the studied value of axial compressive stress was reached.

Load cells were placed between the rocker beam and the coil spring to monitor the magnitude of tension forces in the prestressing bars during testing. All the specimens were subjected to a series of in-plane lateral displacement-controlled components until failure. The failure was defined as a point on the loading curve at which the wall strength reduced to 80% of its lateral capacity in whichever direction this occurred first. Each stage of loading consisted of two repeated cycles for each target displacement increment.

Although the authors in this experimental study used the top rocker beam, coil spring, and hinge to maintain a constant vertical force during testing, it was not the way to ensure a constant value of axial compressive stress at high lateral displacement. Furthermore, using a re-usable RC footing to save time and material means that every tested wall was constructed separately with a gap in time between them. Consequently, there are some questions about the consistency of the construction materials properties.

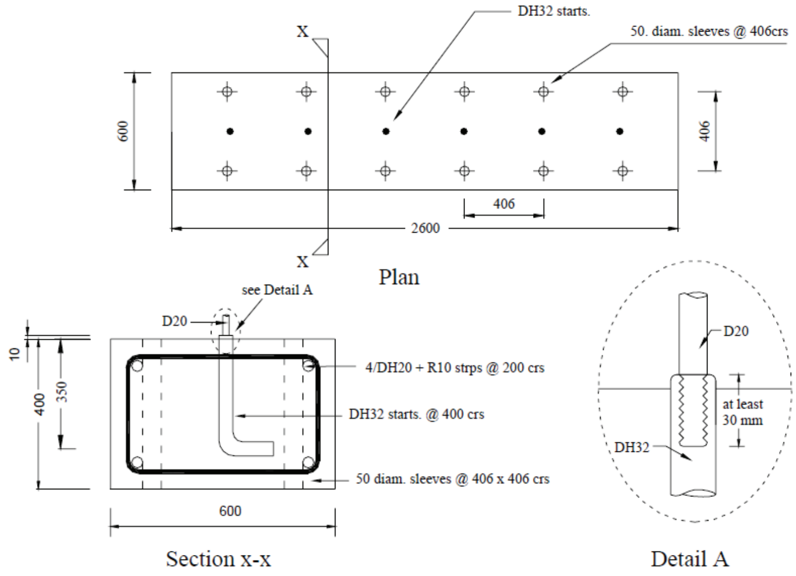

Figure 2.12: Re-usable RC footing (Voon, 2007)

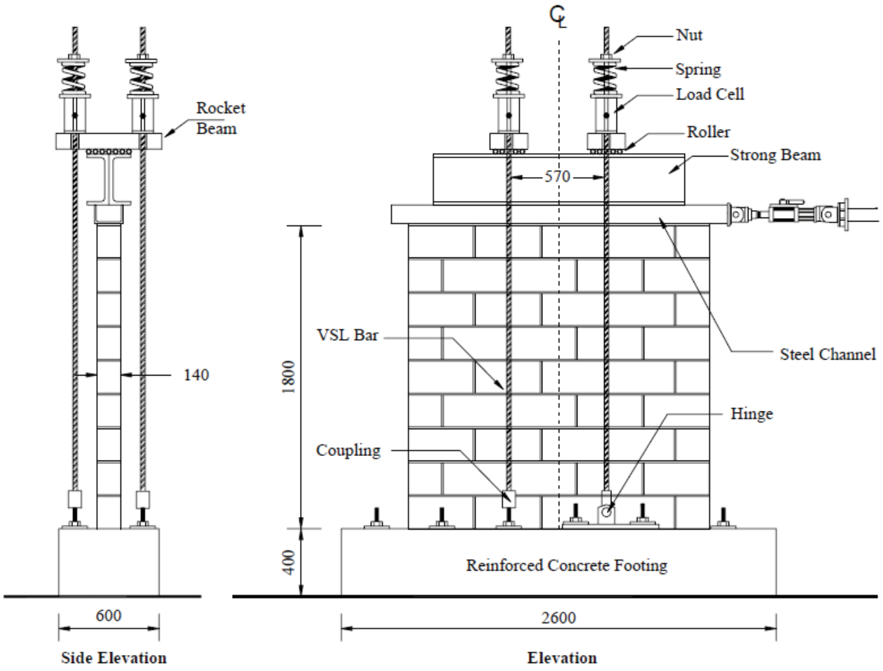

Figure 2.13: Test set-up for walls with applied axial load (Voon, 2007)

2.3.1.1.4 Masonry wall panel without bottom footing

Oan (2013) investigated the in-plane shear behaviour of partially grouted (PG) concrete masonry walls under bi-axial monotonic loading. Throughout his experimental program, a total of sixty-six concrete masonry walls were tested. All the tested walls had the same aspect ratio, h_w/l_w, of 0.875 and they were 1.6 m long by 1.4 m high. Out of the sixty-six walls, fifty-one walls were constructed with partial grouting and fifteen were ungrouted (UG). The influence of many parameters on the shear resistance of PG masonry walls was evaluated in his study such as: the percentage and type of reinforcement, level of axial compressive stress, and grouting. However, the effect of the method of construction was only studied for the UG walls.

As presented in Figure 2.14, all the tested walls were constructed without a base footing. The axial load was applied by a vertical actuator and was spread over the whole length of the wall using a double I-beam. A layer of fiberboard was placed between the distributor steel beam and the top of the wall. However, no connection was provided between the loading beam and the tested wall. To prevent the top I-beam from any lateral movement, two out-of-plane rods supported it and were bolted to the testing frame. Moreover, the lateral load was applied directly to the top of the tested wall in one direction until failure. The failure point was defined when the lateral load dropped to 90% of the maximum achieved value for the PG walls or 80% for the UG walls. A 25 kN in-plane load was applied at the bottom in the opposite direction of the top lateral actuator in addition to a bracket at the other end to prevent the wall from sliding. Furthermore, two struts and plates were attached on each side of the wall's lower course to avoid out-of-plane sliding. Moreover, the level of the applied axial compressive stresses were chosen relatively high, ranging between 2.0 to 4.0 MPa, to avoid overturning the tested specimens at high lateral loads.

The static loads were applied in two stages. In the first the stage, the vertical load was applied under force control at a rate of approximately 1.0 kN/s until the required axial load was reached. Then, the lateral load was introduced at a displacement rate of 0.1 mm/s. This test-setup is suitable for UG masonry walls where there is no dowel action of the vertical reinforcement; such that, constructing the tested walls on a bottom footing or build a top-loading beam will not be efficient.

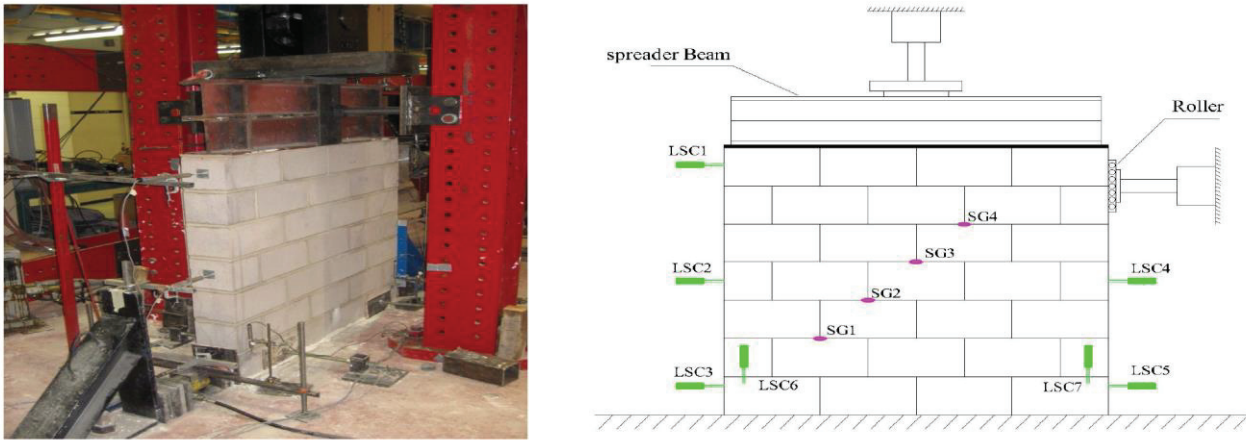

Figure 2.14: Test setup for PG masonry walls (Oan and Shrive, 2012)

A similar setup with some modifications was used by Dickie and Lissel (2011) to test twenty-two masonry shear walls under a cyclic lateral load as shown in Figure 2.15. The walls were divided into nine groups: seven groups were partially grouted, one group was fully grouted, and one group was ungrouted. Each group consisted of 2 to 4 replicates of each test wall. Instead of doweling the RM walls into RC base footing, each wall was constructed on a C-channel base beam. However, prior to building the walls, 600 mm long dowels were welded to each channel at the same location as the vertical reinforcing bars. The base beam was then bolted to the laboratory floor to simulate the fixed base of the tested wall.

The horizontal and vertical loads were transferred to the tested specimen via a stiff steel beam. A layer of mortar type S was placed between the loading beam and the top of the wall. In addition, the bottom flange of the loading beam had a welded bead pattern. Since no dowel action was provided between the tested wall and the loading beam, the lateral force was transferred through the friction connection at the interface between the loading beam and the top surface of the wall. Unlike most of the test setups that have been used to investigate the behaviour of masonry shear wall, the lateral load was applied at mid-length of the wall as can be seen in Figure 2.15. The lateral actuator was attached to two loading arms that were located on each side of the wall and connected to the loading beam using a round steel pin. This is one of the advantages of this test setup.

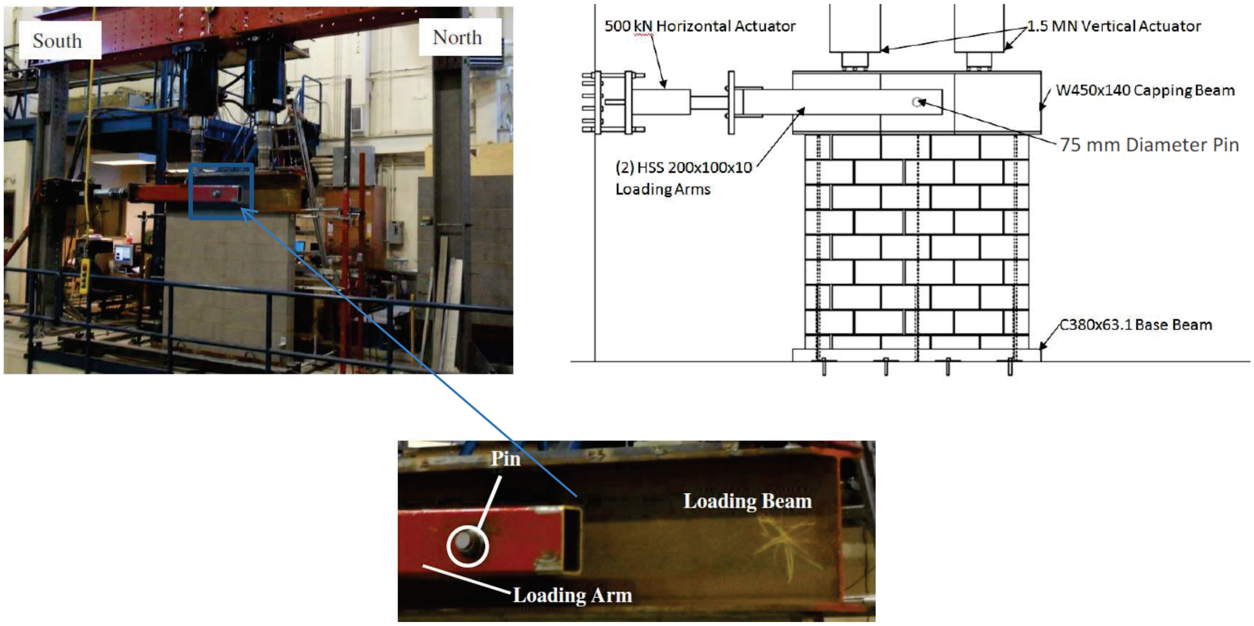

Figure 2.15: Test setup for masonry shear walls (Dickie and Lissel, 2011)

2.3.1.2 Double curvatures shear test

In this type of shear test, the tested wall specimens are subjected to an in-plane shear load that creates double curvatures at the top and bottom levels with an inflection point in-between.

2.3.1.2.1 Horizontal bed joint (wall type)

Throughout the collaborative masonry research program between the U.S. and Japan, several Japanese researchers carried out experimental work to evaluate the seismic performance of RM shear walls (Matsumura, 1985; Fujisawa et al., 1986; Okamoto et al., 1987; and Kaminosono et al., 1988). They all used a similar test setup to that shown in Figure 2.16 where all the walls were constructed with a top and bottom RC beam. Fixed boundary conditions were provided for the base footing while the top was free to move horizontally with restrained rotation. Furthermore, the lateral force was applied at the middle height producing a double curvature deformation mode of shape under a constant axial stress. Thus, the effective height, h_e, was equal to $h_w/2$.

Most of the tested walls were subjected to 4 to 5 reverse cycles lateral loads with respect to the drift angles until failure. One of the advantages of this test setup is that the tested walls could reach their nominal shear resistance, V_n, before they reach their flexural yield capacity or a bit after, with low displacement ductility because of the small effective height, h_e. However, there is a question of whether testing masonry walls under double curvatures presents the first mode of shape in a realistic seismic deformed RM shear wall. In addition, restraining the rotation of the top RC beam means that the axial stress was applied using displacement control not a load control, which could affect the value of the axial stress during testing.

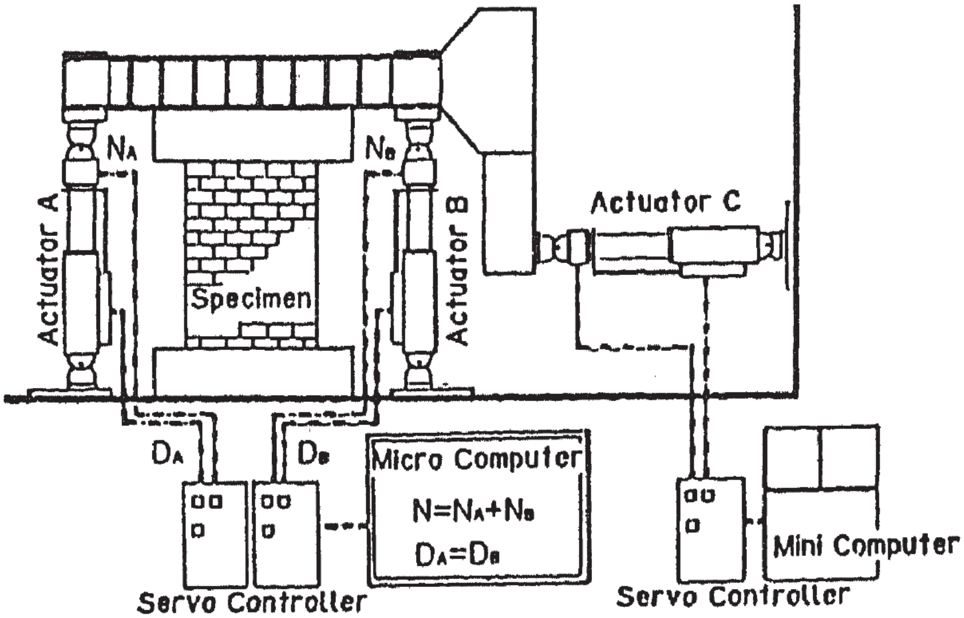

Figure 2.16: Test setup for RM wall with double curvatures (Kaminosono et al., 1988)

Sveinsson et al. (1985) used another test setup to test thirty fully grouted RM walls under cyclic lateral loads, as shown in Figure 2.17. All the tested specimens had top and bottom masonry flanges and were constructed on top of a 19.0 mm thick steel plate. In addition, a similar plate was placed on top of the walls after grouting. To provide a sufficient connection for shear transfer between the RM wall and the steel plates, both plates had openings to permit anchorage of the vertical steel reinforcement and keys that were embedded in the grout. The test setup consisted of a 6.0 m high braced reaction frame supporting a horizontal actuator in addition to a top loading beam and base footing. The footing is composed of a concrete base and a wide flange steel beam and the loading beam is fabricated from two wide flange steel beams. These top and base beams were used to simulate the action of rigid floor diaphragms in actual masonry construction. The vertical reinforcing bars of the tested specimens were anchored to both the loading beam and base footing through the steel plates, after placing a layer of hydrostone between the surfaces of the plates and the beams.

Two vertical actuators were installed to apply the axial compressive stress similar to the gravity loads experienced by masonry walls in actual structures. Moreover, they were connected to the top-loading beam and developed a couple forces moment in the opposite direction of the introduced force by the lateral actuator that produced an inflection point at the middle height and prevented any rotation of the top surface of the tested wall (see Figure 2.18). Each specimen was subjected to a series of in-plane cyclic lateral displacements with an increment of 0.5 mm until 5.0 mm, and then this increment was increased to 1.27 mm until failure. Each stage was consisted on three sinusoidal cycles at a frequency of 0.02 cycles per second.

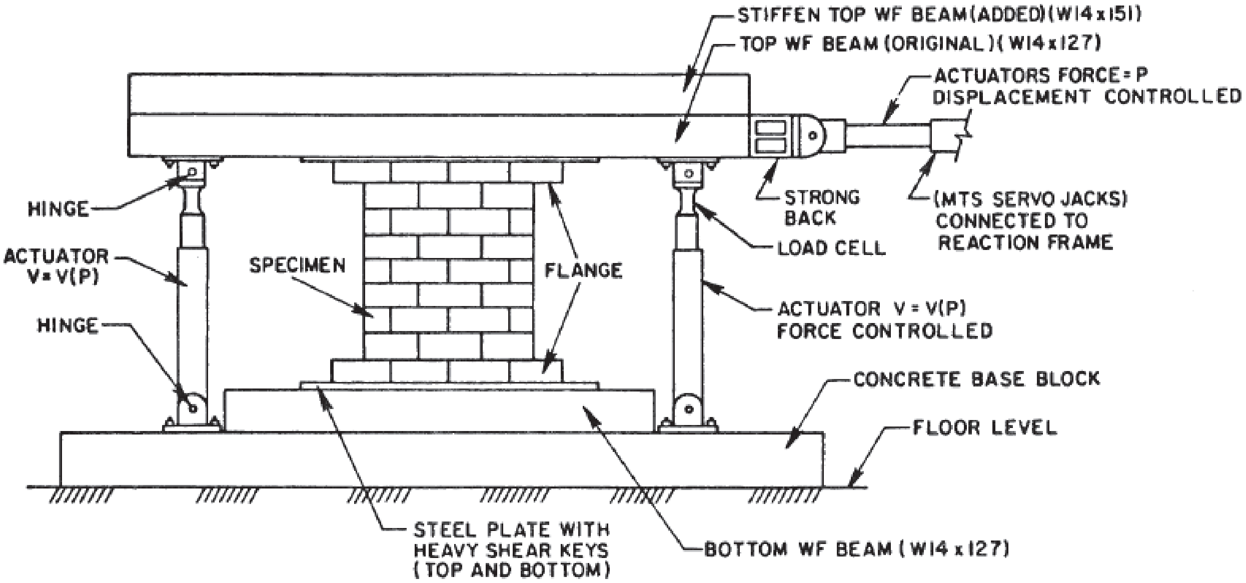

Figure 2.17: Schematic illustration of test setup for masonry wall (Sveinsson et al., 1985)

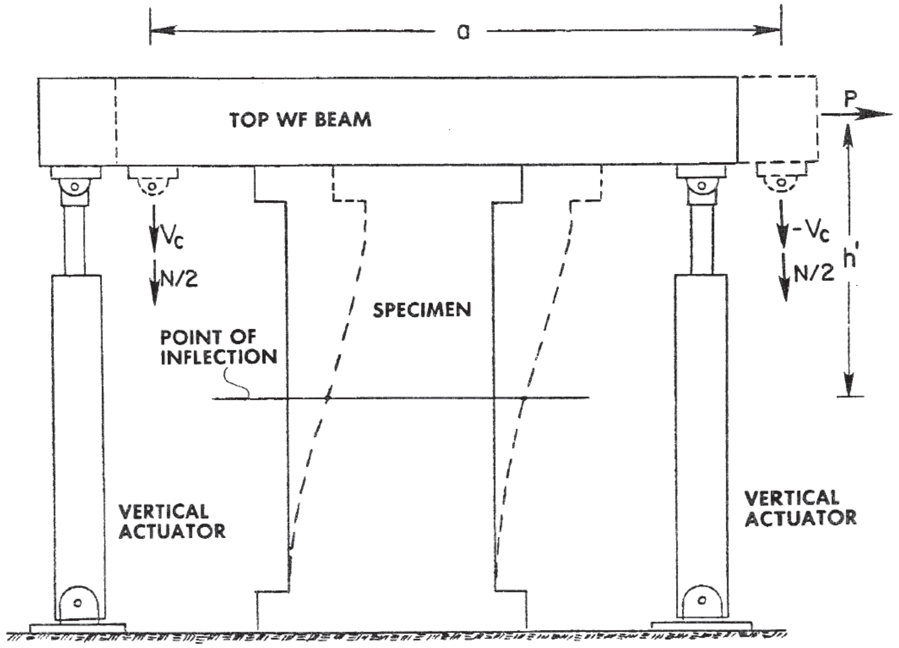

Figure 2.18: Mode of shape of tested walls (Sveinsson et al., 1985)

2.3.1.2.2 Vertical bed join (beam type)

Matsumura (1986) carried out in-plane shear tests on more than 80 masonry wall panels. Two kinds of loading method were used in his research. In one of his loading methods, 25 masonry walls were laid horizontally and subjected to vertical shear loads as shown in Figure 2.19. As can be seen in this test setup, all the walls had a top and bottom RC beam with the same cross-sectional dimensions of the tested masonry wall. Furthermore, both ends of the walls were restrained to vertical movement but they were free to rotate. The masonry walls were subjected to shear loads monotonically in one direction, or one cycle round to get plus and minus maximum shear resistances. This type of test setup is not commonly used because it does not represent the realistic boundary condition of the masonry shear walls. Instead, it could be more representative for RM deep beam.

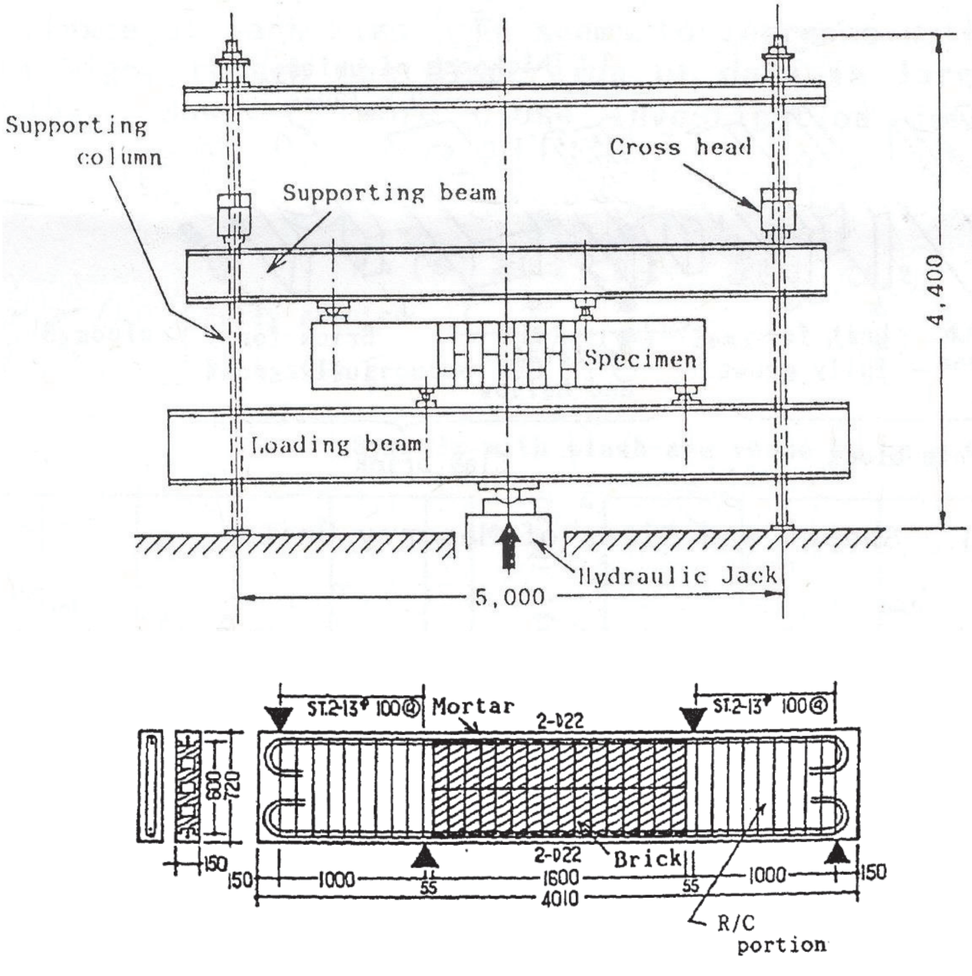

Figure 2.19: In-plane masonry beam shear test (Matsumura, 1988)

2.3.2 MULTI-STORY MASONRY WALLS

Previous experimental work has been conducted on multi-story masonry walls. Due to the limitation in the height and the actuators capacities, most of this work was carried out on scaled walls. Shedid et al. (2010) and Banting and El-Dakhakhani (2012) tested up to three stories fully grouted RM shear walls. Half-scale concrete masonry units were used to construct the tested walls. After pouring the RC base footing, the construction procedure for each story was divided into three stages including: building the tested wall up to the story height, grouting the wall, followed by the construction of the RC slab portion representing the story floor.

The same test-setup was used in both studies as presented in Figure 2.20. After placing the tested wall in the testing frame, the base RC footing was fixed to a strong structural floor through a RC reusable footing to provide a fixed end condition during testing. Two manually operated force-controlled hydraulic actuators were used to apply the axial compression load at the top of the tested specimen. Each actuator was attached to a pair of high-strength threaded rods as shown in Figure 2.21. The two rods were anchored at the bottom to the reusable RC footing through a steel beam on each side, while they were connected to a cross steel beam on the top. To ensure equal force in the two rods, the cross beam pivoted on a roller oriented along the length of the wall and the load was monitored using a load cell at the top of one of the rods.

Lateral displacement was applied at the top of the wall in order to create a zero moment condition at the wall top. The horizontal actuator was attached to a steel-loading beam that was mortared to the top RC slab. To ensure a sufficient connection between the top loading beam and the tested wall and to have a good distribution of the lateral loads along the whole length of the shear wall, the vertical reinforcement of the masonry specimens in addition to vertical steel dowels in the cells that did not contain vertical bars were welded to the loading beam. Two steel box beams were connected to the RC slabs at each level and were pinned to a steel reaction frame on the other side to simulate the high out-of-plane stiffness of the rigid diaphragm floors, as shown in Figure 2.21.

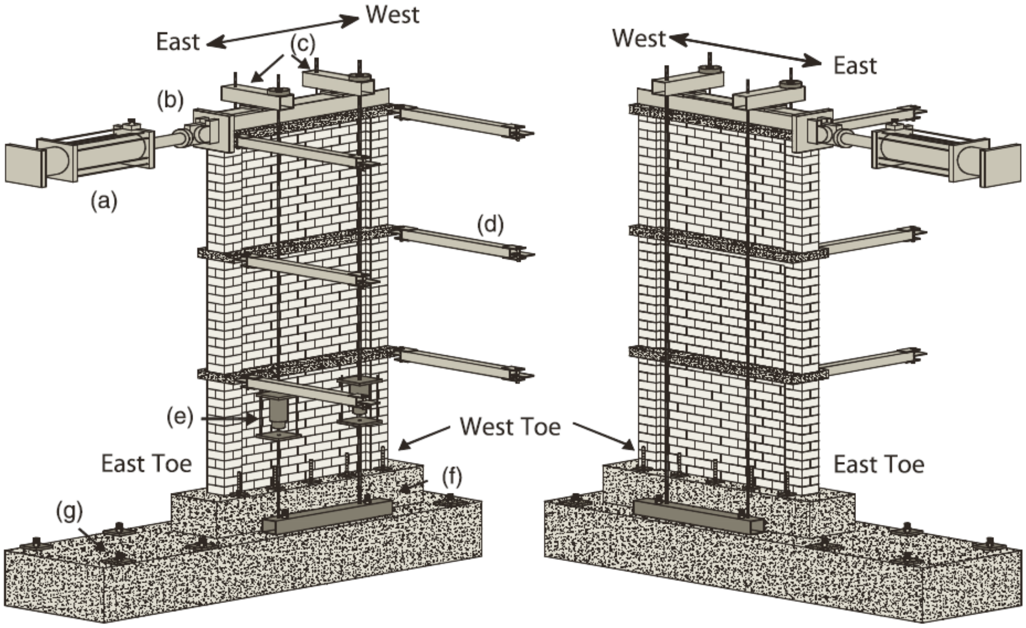

Figure 2.20: Test setup (Banting and El-Dakhakhni, 2012):

(a) lateral loading hydraulic actuator; (b) loading beam; (c) transverse axial load beams with load cells; (d) out-of plane supports (connected to a separate frame not shown); (e) test specimen; (f) test specimen footing; (g) reusable base

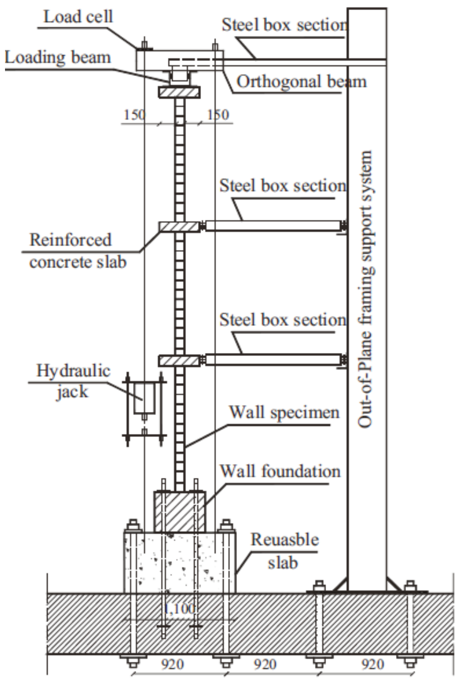

Figure 2.21: Out-of-plane view of test setup (Shedid et al., 2010)

2.4 In-plane Shear Strength Equations

A selection of the available equations for predicting the in-plane shear strength, V_n, of reinforced masonry shear walls is presented and briefly discussed in this section. To make it easier to follow and compare, some of the equations presented below were modified to have the same notations and consistent units, SI units.

2.4.1 Matsumura (1988)

Matsumura (1987, 1988) investigated the shear behaviour of fifty-seven concrete masonry and twenty-three brick masonry walls. Out of the fifty-seven concrete masonry walls, fifteen walls were fully grouted and dominated by shear failure. Based on regression analysis of his test results as well as test results reported by Kaminosono et al. (1985), Matsumura (1988) developed a formula to predict the shear strength as follows:

$$V_n = \left[K_u K_p \left(\frac{0.76}{\left(h_w / d\right) + 0.7} + 0.012 \right) \sqrt{f'_m} + 0.2\sigma_n + 0.18\gamma\delta\sqrt{\rho_h f_{yh} f'_m} \right] (0.875\, b_w\, d) \qquad \text{Eq. 2.3}$$

where:

K_u = factor to account for grout pattern and type of masonry unit,

= 1.0 for fully grouted masonry

= 0.8 for partially grouted brick masonry

= 0.64 for partially grouted concrete masonry

K_p = factor to account for the contribution of the vertical reinforcement ratio in one side,

$$= 1.16\ \rho_{ve}^{0.3}\ ,\ \rho_{ve} = \frac{A_{ve}}{b_w\, d} \times 100$$

A_{ve} = cross sectional area of vertical reinforcing bar(s) in one side, mm^2

b_w = overall wall thickness, web width, (mm)

D = effective depth of the wall for flexural calculation, the distance from the extreme compression fiber to centroid of flexural tension reinforcement which is placed at one side of the wall to resist against flexural moment, mm

σ_n = axial compressive stress per gross area, MPa

h_w = height of wall, mm

γ = factor concerning the action of confine grout

= 1.0 for hoop type reinforcement closing grout within it

= 0.8 for single reinforcing bar with semi-circular hooks at the ends (the 180° standard hook)

= 0.6 for the same reinforcement in partially grouted concrete masonry

δ = factor concerning loading method

= 1.0 for loading which yields inflection point at the mid-height of wall

= 0.6 for loading of cantilever type (single curvature)

This equation includes three contributors to the shear resistance: masonry, axial compressive stress, and horizontal reinforcement. As shown in Eq. 2.3, the masonry shear resistance term includes the effect of the wall height to the effective flexural depth ratio, h_w/d, instead of the shear span to depth ratio, M/Vd_v. Furthermore, only the edge bars in one side were considered contributing to the dowel action. In addition, it can be noticed that the proposed equation for the contribution of the horizontal reinforcement does not seem to have any logical mechanisms. In this equation the effective depth for shear calculations, d_v, was assumed to equal $0.875d$.

In addition to the provided equation for the shear strength, Matsumura (1988) proposed an equation to predict the shear crack load as follows:

$$V_c = \left[K_c \, \frac{1.0}{(h_w / d) + 2} \sqrt{f'_m} + 0.3 \, \alpha \, \sigma_n \right] (0.875 \, b_w \, d) \qquad \text{Eq. 2.4}$$

where:

V_c = shear load corresponding to the first diagonal shear crack

K_c = K_u

α = 1.0 for fully grouted masonry
0.6 for partially grouted masonry

As shown in this equation, Matsumura (1988) considered higher contribution from the axial compressive stress, v_p, toward the shear resistance before cracking, v_c, compared to the shear strength, v_n, for the fully grouted masonry. This contribution is proposed to be $0.3\sigma_n$ for v_c and $0.2\sigma_n$ for v_n, with more than 30% degradation in v_p after cracking. Furthermore, Eq. 2.4 dese not include any contribution of the steel reinforcement before cracking. Comparisons of the test results to the values calculated by Eq. 2.3 and Eq. 2.4 in a relation to h/d are shown in Figure

2.22. Matsumura (1988) reported that about 70% of $Vu_{(test)}/Vu_{(calc.)}$ range within 1±0.2. However, this percentage was decreased to about 60% for $Vc_{(test)}/Vc_{(calc.)}$ as shown in Figure 2.22b.

However, for fully grouted concrete masonry walls, which is the scope of work in this research program, these percentage are about 60 and 55% for $Vu_{(test)}/Vu_{(calc.)}$ and $Vc_{(test)}/Vc_{(calc.)}$, respectively. Also, it can be noticed that the proposed equation for V_n, (Eq. 2.3), is conservative for fully grouted concrete masonry where more than 90% of $Vu_{(calc.)}$ is higher than $Vu_{(test)}$.

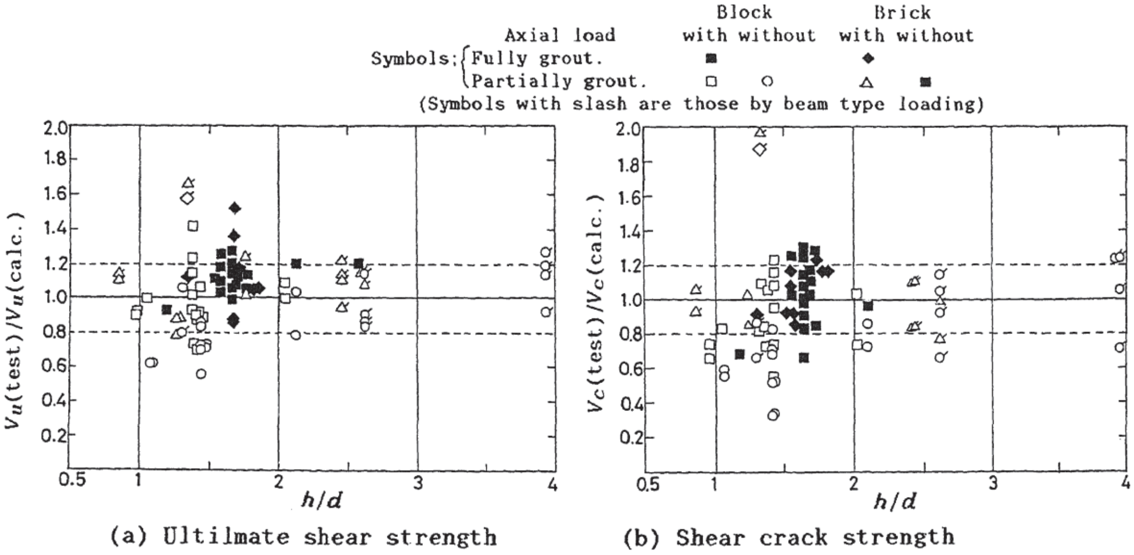

(a) Ultilmate shear strength

(b) Shear crack strength

Figure 2.22: Comparison of test results with calculated values in relation to the height to depth ratio, *h/d* (Matsumura, 1988)

2.4.2 SHING ET AL. (1990)

Shing et al. (1990) tested twenty-two masonry walls to investigate their inelastic flexural and shear behaviour. Using their test results, they developed the following shear strength equation:

$$V_n = \left[0.0217\left(\rho_v\, f_{yv} + \sigma_n\right) + 0.166\right] A_n \sqrt{f'_m} + \left(\frac{l_w - 2d'}{s_h} - 1\right) A_h\, f_{yh} \qquad \text{Eq. 2.5}$$

where:

ρ_v = total vertical reinforcement ratio = $(A_v)_{\text{total}} / A_n$

A_n = net area of masonry section bounded by wall thickness and length of section
in direction of shear force considered, mm^2
$= b_w \, l_w$

d' = distance between wall edge and nearest vertical reinforcing steel bar, mm

s_h = vertical spacing between horizontal reinforcement layers, mm

A_h = area of horizontal reinforcement in one layer (mm^2)

f_{yv}, f_{yh} = yield strength of vertical and horizontal reinforcement, respectively, MPa

Unlike Matsumura's (1988) equation Eq. 2.3, Shing et al. (1990) did not consider a separate component for the axial compressive stress, σ_n, instead, it is included in the masonry contribution. Furthermore, the full amount of the vertical reinforcement is considered in Eq. 2.5. However, the proposed masonry term does not include the effect of the shear span to depth ratio, M/Vd_v, or even the wall aspect ratio, h_w/l_w. The form of the horizontal reinforcement component seems to be derived from a more logical mechanism than the one proposed by Matsumura (1988) in Eq. 2.3. Shing et al. (1990) assumed that following the major diagonal shear crack between the wall corners, the top and bottom horizontal reinforcement layers will not have a sufficient embedment length to develop their yield capacity. Consequently, the horizontal reinforcement term, V_s, proposed in Eq. 2.5 ignores the contribution of the top and bottom layers of the horizontal reinforcement. In addition, it is important to mention that Eq. 2.5 considers the full horizontal length of the wall, l_w, instead of the effective shear depth, d_v, in the calculation of the net area.

2.4.3 ANDERSON AND PRIESTLEY (1992)

Anderson and Priestley (1992) analyzed experimental test results provided by Sveinssion et al. (1985), Matsumura (1987), and Shing et al. (1990) to develop a best fit predictive equation for the in-plane shear strength of a RM shear wall. The proposed equation is significantly more simplified than Eq. 2.3 and Eq. 2.5 because it considers V_n as the sum of three separate independent contributions of V_m, V_p, and V_s. Where V_m, V_p, and V_s, are the shear resistances provided by the masonry, axial compressive stress, and horizontal reinforcement respectively, and were calculated as follows:

$$V_n = \quad C\,k\,\sqrt{f'_m}\;A_n + 0.25\,P + 0.5\,A_v\,f_y\,\frac{d}{s} \qquad \text{Eq. 2.6}$$

where:

C = factor to account for the type of masonry unit used in construction,
= 0.24 for concrete block masonry
= 0.12 for clay brick masonry
K = ductility coefficient factor,
$= 1 - \dfrac{\mu_\Delta - 2}{2}$, $0.0 \leq k \leq 1$, and μ_Δ is the displacement ductility ratio
A_n = net horizontal cross-sectional area of the wall, mm^2
$= b_w\, l_w$
D = distance from extreme compression fiber to centroid of extreme tension bar, mm
A_v = area of horizontal reinforcement in one layer (mm^2)

Unlike the previous equations, the masonry shear resistance term in Eq. 2.6 does not include the contribution made by the dowel action of the vertical reinforcement. Furthermore, Anderson and Priestley (1992) proposed a factor k to account for the degradation in the shear resistance provided by the masonry, V_m, for the inelastic response when the displacement ductility is greater than 2. This factor decreases linearly from 1.0 to 0.0 as the displacement ductility ratio, μ_Δ, increases from 2.0 to 4.0. However, Eq. 2.6 does not consider any influence of the shear span to depth ratio, M/Vd_v, or the wall aspect ratio, h_w/l_w, on V_m.

Anderson and Priestley (1992) explained that as all the walls in the data sets for calibrating Eq. 2.6 had a height to width ratio, h_w/l_w, greater than 1.0 where for most of them, h_w/l_w ranged between 1.0 and 1.6. The walls tested by Shing et al. (1990) had single curvature bending with h_w/l_w equal to 1.0, while some of the other tests, Sveinssion et al. (1985) and Matsumura (1987), had double curvature bending with equal top and bottom moments. Since the proposed Eq. 2.6 did not appear to fit one set of data better than the other, it could indicate that the in-plane shear behaviour of RM shear walls with h_w/l_w greater than unity is not effected by the wall aspect ratio.

Similar to the equation proposed by Matsumura (1988), Eq. 2.6 considers a constant percentage of the axial force that contributes to the shear strength. This percentage was increased from 20% in Eq. 2.3, to 25% in Eq. 2.6. Anderson and Priestley (1992) proposed that only 50% of the yield capacity of the horizontal reinforcement would contribute toward the shear strength, V_n. This contribution is less than the similar expected value for the in-plane shear strength of RC shear walls. At the early stage of loading a RC shear wall, the concrete will carry all the shear stress while the lateral reinforcement will be essentially unstressed. After the initiation of the diagonal cracks, tensile strains will be developed in the reinforcement. Thus, as the cracks widen the tension in the lateral reinforcement, V_s, increases, while the shear resistance by concrete, V_c, decreases. Later, at high deformation the shear strength, V_n, is reached when the increasing of V_s is less than the degradation in V_c.

Anderson and Priestley (1992) clarified that the suggested low contribution of V_s, which is the best-fit value with the experimental results, could be because the masonry is constructed of fine aggregate compared to concrete. Thus, masonry shear walls lose their shear capacity at smaller crack openings. Consequently, the lateral reinforcement does not reach its yield capacity. Another explanation added by Anderson and Priestley (1992) is that some of the tested RM walls from the data sets for validating Eq. 2.6 had 90° bends or straight lateral steel reinforcing bars. Thus, the anchorage of the horizontal reinforcement was not as sufficient as that of the stirrups in RC walls that have a 180° hook around the vertical reinforcement. However, by reviewing the fully grouted tested walls in the data sets for calibrating Eq. 2.6, as in Section 2.2, most of the tested walls had a 180° hook except some walls tested by Sveinssion et al. (1985) that were constructed with lateral steel reinforcing bars with 90° bends.

2.4.4 NATIONAL EARTHQUAKE HAZARDS REDUCTION PROGRAM (NEHRP, 1997)

The Federal Emergency Management Agency (FEMA) and the National Earthquake Hazards Reduction Program (NEHRP) carried out extensive research with the aim of understanding the performance of structural buildings in regions with high seismic activity as a means to minimize building damage. Similar to the equation proposed by Anderson and Priestley (1992), Eq. 2.6, NEHRP (1997) adopted a shear strength equation for masonry as follows:

$$V_n = \quad 0.083\left[4.0 - 1.75\left(\frac{M}{Vd_v}\right)\right] A_n \sqrt{f'_m} + 0.25\,P + 0.5\,A_v\,f_{yh}\,\frac{d_v}{s_h} \qquad \text{Eq. 2.7}$$

where:

$$V_{n(\max)} = 0.5\,A_n\sqrt{f'_m} \qquad \text{for} \quad \frac{M}{V\,d_v} \le 0.25$$

$$V_{n(\max)} = 0.33\, A_n \sqrt{f'_m} \quad \text{for} \quad \frac{M}{V\, d_v} \geq 1.0$$

with linear interpolation for $1.0 \geq \frac{M}{V\, d_v} \geq 0.25$ and $\frac{M}{V\, d_v}$ need not be taken greater than 1.0 in Eq. 2.7.

M, V = the moment and shear at the section under consideration, respectively.

d_v = length of member in direction of shear, mm

= l_w for walls under in-plane loads

A_n = net horizontal cross-sectional area of the wall, mm^2

= $b_w\, l_w$

Compared to Eq. 2.6, the shear resistance provided by the masonry, V_m, in Eq. 2.7, was modified to include a new parameter as the shear span to depth ratio, M/Vd_v. On the other hand, NEHRP (1997) did not consider the degradation in the shear resistance of V_m when the RM wall experiences inelastic response at high displacement ductility, μ_Δ, as proposed in Eq. 2.6. The ratio M/V is equal to the effective wall height, h_e, at which the resultant shear force V acts and causes the overturning moment, M; hence, it is equal to the shear span to depth ratio, h_e/d_v (Anderson and Brzev, 2009). However, the effective depth for shear calculations, d_v, in Eq. 2.7 was assumed to equal the full length of the wall, l_w, in the direction of the in-plane shear loads. Furthermore, the net horizontal cross-sectional area of the wall, $b_w\ l_w$, was used for the shear force contribution by masonry, V_m.

Comparing Eq. 2.6 and Eq. 2.7, it can be noticed that the axial compressive stress contribution, V_p, in both equations is equal to 25% of the applied axial load. In addition, the horizontal reinforcement contribution, V_s, is similar in both of them with a slight difference in the effective depth calculation. Furthermore, both equations ignored the contribution of the vertical reinforcement, due to its dowel action, toward V_n. For non-squat shear walls, where h_w/l_w is greater than 1.0, NEHRP (1997) limited the in-plane shear load capacity to $0.33\,A_n\sqrt{f'_m}$.

2.4.5 UNIFORM BUILDING CODE (UBC, 1997)

The Uniform Building Code UBC (1997) used Eq. 2.8 to calculate the in-plane shear strength of RM shear walls. The nominal shear strength, V_n, was proposed as the sum of the shear resistance provided by the masonry, V_m, combined with the horizontal reinforcement contribution, V_s. Unlike the previous equations, the UBC (1997) equation does not include the contribution of the axial compressive stress. For walls with a shear span to depth ratio, M/Vd_v, higher than the unit, the masonry contribution in Eq. 2.8 is about 47% less than V_m in Eq. 2.7. Moreover, this equation considers the full yield capacity of the horizontal reinforcement compared to 50% of f_y as proposed by NEHRP (1997) and Anderson and Priestley (1992). Similar to most of the existing equations for predicting V_n, M/Vd_v in Eq. 2.8 was limited to values between 0.25 and 1.0. The in-plane shear strength for RM shear is calculated by the UBC (1997) as follows:

$$V_n = 0.083\left[2.8 - 1.6\left(\frac{M}{Vd}\right)\right]A_n\sqrt{f'_m} + A_{sh}\,f_{yh} \le 0.33\,A_n\sqrt{f'_m} \qquad \text{Eq. 2.8}$$

where:

M, V = the moment and shear at the section under consideration, respectively

D = distance from compression face of flexural member to centroid of longitudinal tensile reinforcement, mm, for walls it could be considered as the distance from extreme compression fiber to centroid of extreme tension bar

A_n = net area of masonry section bounded by wall thickness and length of section in direction of shear force considered, mm^2

$= b_w \, l_w$

A_{sh} = total area of distributed shear reinforcement, mm^2

For RM shear walls dominated by flexural/shear or flexural failure, where the nominal shear strength exceeds the shear corresponding to development of its nominal flexural strength, UBC (1997) ignores the in-plane shear resistance provided by masonry inside the plastic hinge region. The plastic hinge region is defined by the base of the shear wall and a plane at a height l_w above the base of the shear walls.

2.4.6 AUSTRALIAN STANDARD AS3700-2001

A simplified equation for in-plane shear strength was provided by the Australian masonry standard (AS3700-2001) as follows:

$$V_n = f_{vr} \; A_n + 0.8 \, f_{yh} \; A_s \qquad \text{Eq. 2.9}$$

where:

f_{vr} = $(1.5 - 0.5 \, h_w / l_w)$, MPa

A_n = the design cross-section area of the wall, the overall width by the wall length

$= b_w \, l_w$, mm^2

A_s = the cross-sectional area of reinforcement, mm^2, as follows:

(i) If $h_w/l_w \leq 1.0$

A_s = the total cross-sectional area of horizontal reinforcement, or total cross-sectional area of vertical reinforcement, whichever is less

(ii) If $h_w/l_w > 1.0$

$A_s = A_{sh} \, l_w/h_w$

where

A_{sh} = total cross-sectional area of anchored horizontal reinforcement

Unlike most of the equations for predicting V_n, Eq. 2.9 does not seem to be derived from any logical mechanisms. The influence of many parameters was ignored in this equation such as: masonry compressive strength, f'_m, axial compressive strength, σ_n, the shear span to depth ratio, M/Vd_v, and displacement ductility, μ_Δ. The above formula (Eq. 2.9) is accompanied with some essential requirement for the reinforcement as follows:

(a) The reinforcement shall be located symmetrically in the cross-section.

(b) The spacing between the vertical reinforcement should be less than $0.75h_w$ and 2000 mm.

(c) The spacing between the horizontal reinforcement $\leq 0.75l_w$ and 3000 mm.

(d) The vertical and horizontal reinforcement ratios shall be not less than 0.13 and 0.07%, respectively. If the reinforcement does not meet these requirements then the wall shall be designed as unreinforced masonry wall.

2.4.7 CANADIAN STANDARDS ASSOCIATION CSA (S304.1-04/ S304-14)

The Canadian Standards Association CSA 2004 provides an equation to calculate the in-plane shear strength of reinforced masonry shear walls as follows:

$$V_n = (v_m b_w d_v + 0.25P_d)\,\gamma_g + 0.6\,A_v\,f_y\,\frac{d_v}{s} \qquad \text{Eq. 2.10}$$

where:

$$(V_n)_{\max} = 0.4\sqrt{f'_m}\,b_w\,d_v$$

v_m = shear strength attributed to the masonry in running bond pattern,

$$0.16\left(2-\frac{M}{V\ d_v}\right)\sqrt{f'_m}$$

$\dfrac{M}{V\ d_v}$ = shear span to depth ratio, shall be taken as not less than 0.25 nor more than 1.0, where, M and V are the moment and shear at the section under consideration, respectively

b_w = overall wall thickness, web width, mm

d_v = effective depth for shear calculations, mm

$d_v \geq 0.8 l_w$ for walls with flexural reinforcement distributed along the length

P_d = axial compressive load on the section under consideration, based on 0.9 times dead load, P_{DL}, including any axial load arising from bending in coupling beams, N

$P_d = 0.9\,P_{DL}$ for solid walls

$P_d = 0.9\,P_{DL} \pm N$ for perforated/coupled walls, walls with door or/and window opening (see Figure 2.23)

γ_g = factor to account for partially grouted walls that are constructed of hollow or semi-solid units

= 1.0 for fully grouted masonry, solid concrete block masonry, or solid brick masonry

$= \dfrac{A_e}{A_g}$ for partially grouted walls, but $\gamma_g \leq 0.5$ (see Figure 2.24)

A_e = effective cross-sectional area of the wall, mm^2

Ag = gross cross-sectional area of the wall, mm^2

A_v = area of horizontal wall reinforcement, mm^2

S = vertical spacing of horizontal reinforcement, mm

CSA S304.1-04 uses a shear strength equation similar to that provided by NEHRP (1997) with some minor modifications. The shear span to depth ratio, M/Vd_v, is multiplied by 2.0 instead of 1.75 as in Eq. 2.7. In addition, the contribution of the horizontal reinforcement was increased from 50 to 60% of the yield strength. Moreover, it can be noticed that M/Vd_v was limited to values between 0.25 and 1.0. Consequently, shear strength attributed to the masonry, v_m, ranged between $0.16\sqrt{f'_m}$ and $0.28\sqrt{f'_m}$.

Although Eq. 2.10 does not consider any degradation in the shear strength at high inelastic lateral deformation as proposed by Anderson and Priestley (1992), the CSA S304.1-04 reduces the shear resistance contribution by the masonry and axial compression load by one-half for moderately ductile RM shear walls with a ductility factor R_d of 2. This reduction factor was further modified in the current standard CSA S304-14 to be 0.75 and 0.5 for R_d of 2 and 3, respectively. However, no reduction factor is proposed for conventional shear walls with R_d equal to 1.5. Similar to Eq. 2.6, Eq. 2.7, and Eq. 2.8, the contribution of the vertical reinforcement toward the shear strength was neglected in Eq. 2.10. It is important to mention that unlike most of the previous equations that consider the net cross-sectional area of the masonry, A_n, as (b_w l_w), the formula provided by the CSA S304-14, Eq. 2.10, considers it as (b_w d_v), where d_v equal $0.8l_w$.

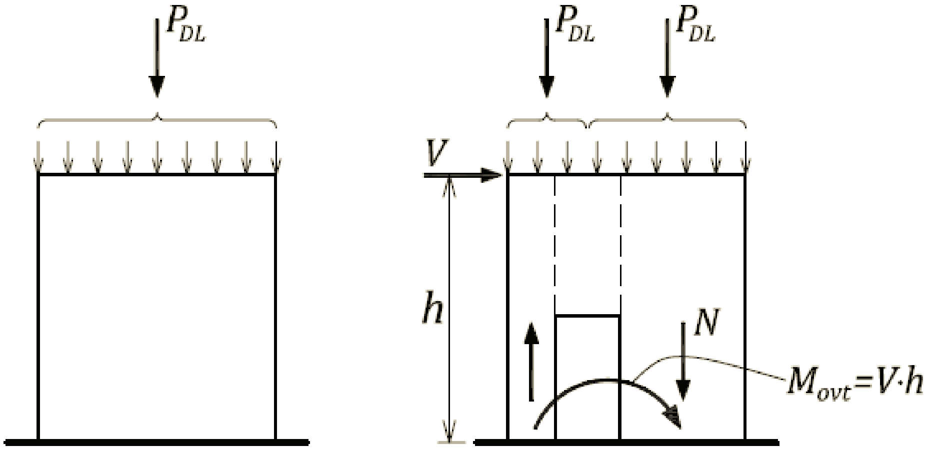

(a) (b)

Figure 2.23: Axial load in masonry walls: (a) solid; (b) perforated (Anderson and Brzev, 2009)

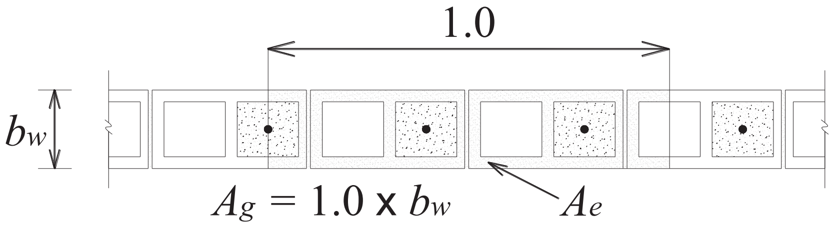

Figure 2.24: Wall cross-sectional area

2.4.8 NEW ZEALAND STANDARD 4230:2004

Based on research conducted by Voon and Ingham (2001 and 2003), the New Zealand Standard Design of Reinforced Concrete Masonry Structures NZS 4230:2004 contains a formula (Eq. 2.11) for calculating the nominal shear strength of RM shear walls, V_n. The total shear stress, v_n, is a sum of contributions of masonry, v_m, axial stress, v_p, and horizontal reinforcement, v_s. These three components are defined by Eq. 2.12, Eq. 2.13, and Eq. 2.14, respectively.

$$V_n = (v_m + v_p + v_s)\, b_w\, d \qquad \text{Eq. 2.11}$$

$$v_m = (C_1 + C_2)\, v_{bm} \qquad \text{Eq. 2.12}$$

$$v_p = 0.9 \frac{N^*}{b_w\, d} \tan\alpha \qquad \text{Eq. 2.13}$$

$$v_s = C_3 \frac{A_v\, f_y}{b_w\, S} \qquad \text{Eq. 2.14}$$

where:

v_n = the total required shear stress (v_m+ v_p+ v_s) shall not exceed the maximum type-dependent total shear stress, v_g, given in Table 2.2

b_w = effective web width, mm, (see Figure 2.25)

D = for walls, d shall be taken as $0.8l_w$, mm, (see Figure 2.25)

C_1 = shear strength coefficient to account for the dowel action of the vertical reinforcement

$=33\,\rho_v \frac{f_{yv}}{300}$, and $\rho_v > 0.07\%$

where ρ_v and f_{yv} are the vertical reinforcement ratio and the yield strength of the vertical reinforcement, respectively

$$\rho_v = \frac{\text{total cross-sectional area of the vertical reinforcement}}{b_w\, d}$$

C_2 = shear strength coefficient to account for the shear span ratio, M/Vl_w,

$=1.5$ for $M/Vl_w < 0.25$

$=0.42[4.0-1.75\,(M/Vl_w)]$ for $0.25 \leq M/Vl_w \leq 1.0$

$=1.0$ for $M/Vl_w > 1.0$

v_{bm} = basic shear stress provided by masonry, MPa, as defined in Table 2.2

v_p = Shear stress provided by axial compression load, MPa, shall not be taken greater than $0.1\,f_m^`$

N^* = axial compression load, N, shall not be taken greater than $0.1\,f_m^`\,A_g$

where A_g is the total cross-sectional area bounded by the wall's external perimeter faces. For rectangular RM wall, $A_g = b_w\, l_w$

α = For a cantilever wall, α is the angle formed between the wall axis and the strut from the point of load application to the centre of the flexural compression zone. For a wall in double bending, α is the angle between the wall axis and the line joining the centres of flexural compression at the top and bottom of the wall (as shown in Figure 2.26)

C_3 = 0.8 for walls

The nominal shear strength, V_n, in Eq. 2.11 is calculated as the total shear stress multiply by the net cross-sectional shear area of the masonry member bounded by $b_w\, d$ as shown in Figure 2.25. Table 2.2 provides the maximum limits for the design compressive strength of masonry, $f_m^`$, and the total shear stress, v_g, to avoid critical shear related failures. Three different observation types, C, B, and A, were defined according to the required level of structure ductility. The concept of maximum allowed shear stress, v_g, which is included in Table 2.2 for observation types A and B masonry is adopted from the Building Code Requirements for Masonry Structures *ACI 530/ASCE 5/TMS 402* (2002).

The masonry shear resistance term, v_m, in Eq. 2.12 includes the summation of two coefficients, C_1 and C_2, which is multiplied by the basic type-dependent shear strength of masonry, v_{bm}. These two factors aim to consider the influence of the vertical reinforcement and the shear span to depth ratio, respectively. Although this equation does not include the effect of the achieved displacement ductility, Table 2.2 presents the degradation in v_{bm} in potential plastic hinges of limited ductile and ductile masonry structures. The New Zealand Standard NZS 4230:2004 specified the values for the structural ductility factor, μ, for the limited ductile and ductile structures as 2 and 20 ($1-T_1$), respectively, where T_1 was defined as the fundamental period of the building with limits of $4 < 20\ (1-T_1) < 6$. The degradation in v_{bm} was assumed to be negligible prior to a ductility ratio of 1.25, followed by a gradual decrease until v_{bm} equal 0.0 at a ductility ratio of 4.

Unlike most of the existing equations for predicting the in-plane shear strength of RM shear walls, the contribution of the axial compression stress in Eq. 2.13 is considered as a dependent component upon the angle α which is resulting from a diagonal compression strut as shown in Figure 2.26. Priestley et al. (1994) discussed the theory behind this assumption. For a cantilever wall, α is the angle formed between the wall axis and the strut from the point of load application to the centre of the flexural compression zone. For a wall in double bending, α is the angle between the wall axis and the line joining the centres of flexural compression at the top and bottom of the wall. The 0.9 term in Eq. 2.13 is proposed to provide a degree of conservatism to the contribution of the axial compression load. It can be noticed that as the axial load increases, the depth of the flexural compression zone, a, increases. Consequently, the rate of axial compressive stress contribution, v_p, will decrease. Limitation is provided to N^* to prevent possible brittle shear failure. Furthermore, v_p is limited to up limit to excess dependence on v_p in a relatively squat masonry wall with an aspect ratio, h_w/l_w, less than 1.0.

Table 2.2: Type Dependent Nominal Strengths, MPa, (NZS 4230:2004)

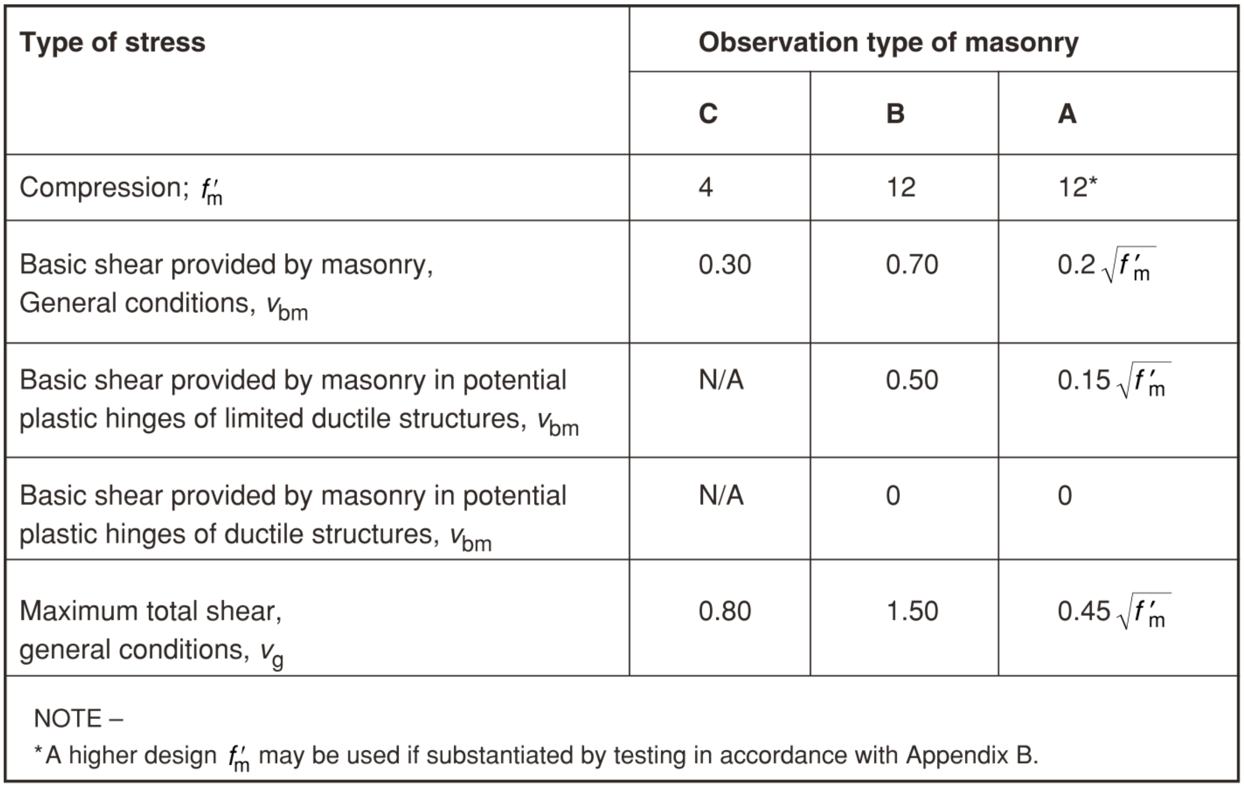

Type of stress	**Observation type of masonry**		
	C	**B**	**A**
Compression; f'_m	4	12	12*
Basic shear provided by masonry, General conditions, v_{bm}	0.30	0.70	$0.2\sqrt{f'_m}$
Basic shear provided by masonry in potential plastic hinges of limited ductile structures, v_{bm}	N/A	0.50	$0.15\sqrt{f'_m}$
Basic shear provided by masonry in potential plastic hinges of ductile structures, v_{bm}	N/A	0	0
Maximum total shear, general conditions, v_g	0.80	1.50	$0.45\sqrt{f'_m}$

NOTE –
*A higher design f'_m may be used if substantiated by testing in accordance with Appendix B.

where

Type C: no construction observation by design engineering or nominated representative

Type B: inspection required to establish that work is carried out generally as specified

Type A: in addition to inspection required by Type B, Type A observation of masonry shall require construction supervision at all critical stages

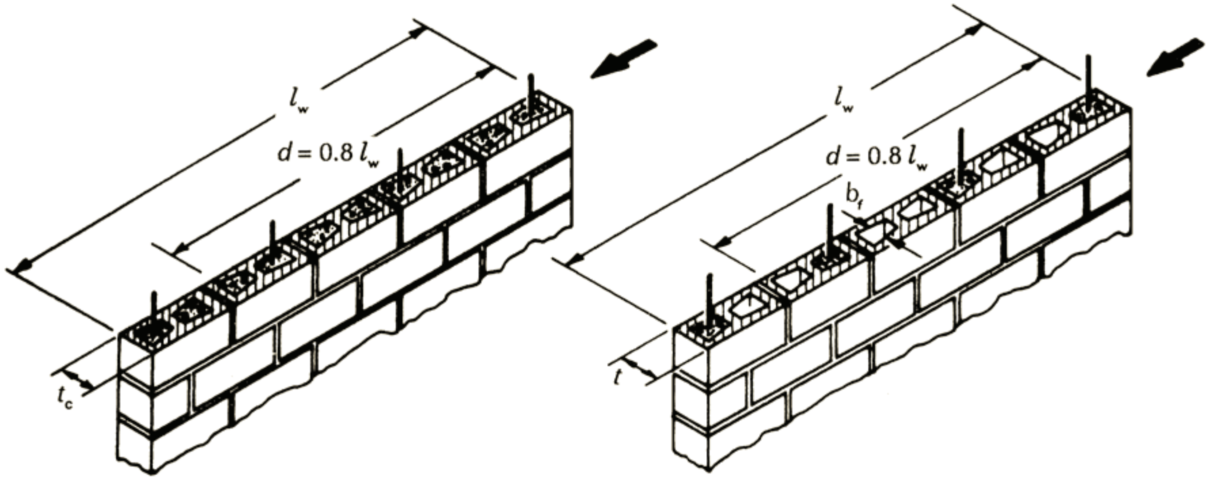

(a) In-plane shear, fully grouted wall
$b_w = t_c$

(b) In-plane shear, partially grouted wall
$d = 0.8\,l_w$, $b_w = t - b_f$

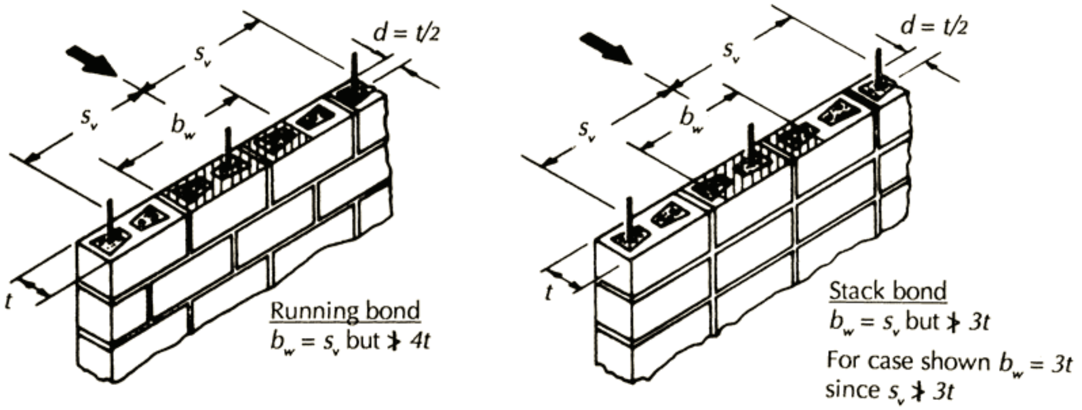

(c) Face load shear, fully grouted wall

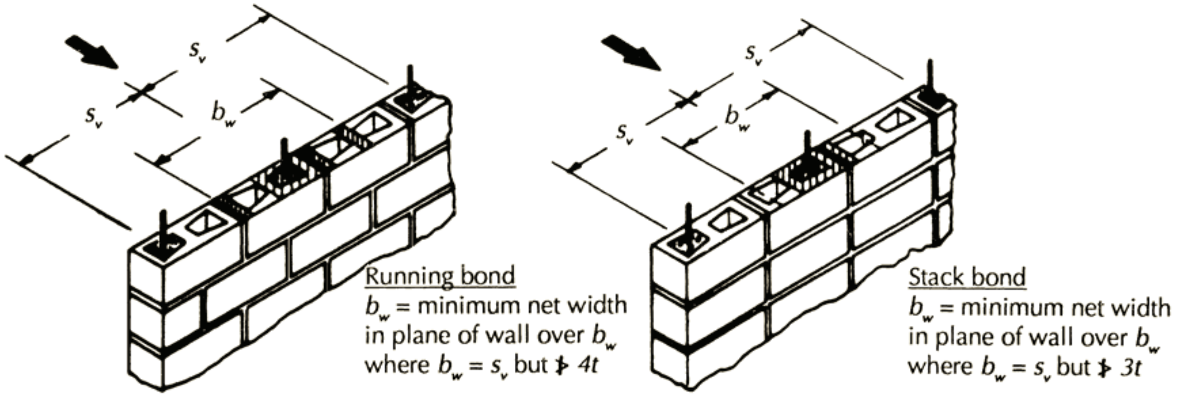

(d) Face load shear, partially grouted wall

Figure 2.25: Effective areas for shear (NZS 4230:2004)

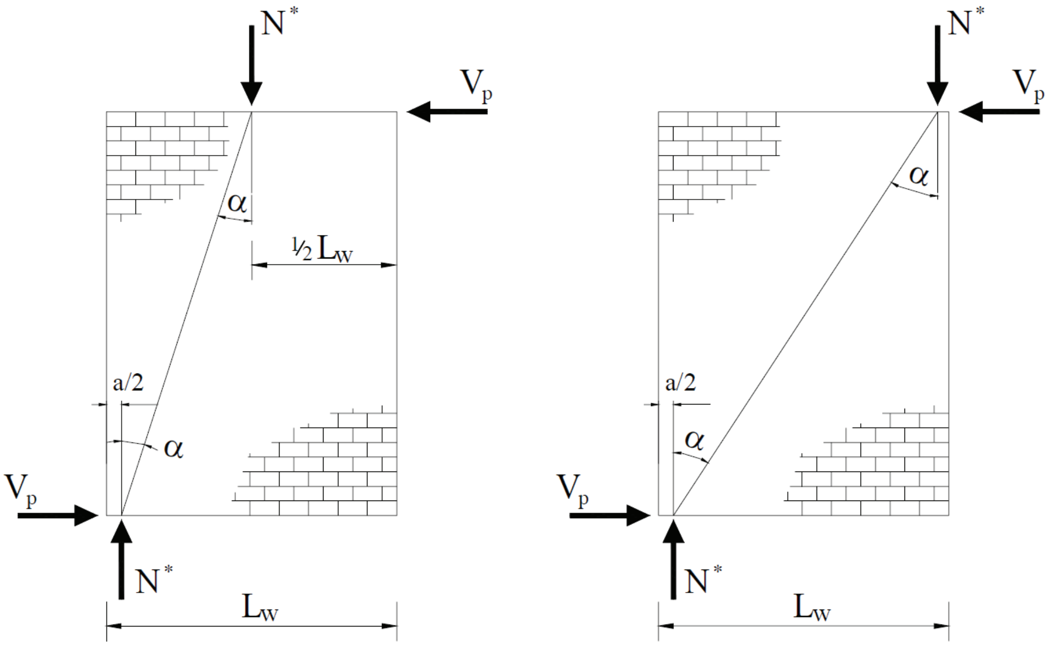

(a) Single Bending

(b) Double Bending

Figure 2.26: Contribution of axial load to wall shear strength (NZS 4230:2004)

The current New Zealand Standard NZS 4230:2004 assumes that 80% of the horizontal reinforcement's yield strength will contribute toward the shear strength, V_n, as shown in Eq. 2.14. Based on the previous discussion, Eq. 2.11 can be re-written for the observation types B and A, which is the common case for masonry structural walls, as follows:

$$V_n = \left[(0.022\rho_v f_{yv} + 0.084 \left(4 - 1.75 \frac{M}{V l_w} \right) \right] (1 - \frac{\mu - 1.25}{2.75}) \sqrt{f'_m} (b_w d) + (0.9 \tan \alpha) N^* + 0.8 A_v f_y \frac{d}{s} \qquad \text{Eq. 2.15}$$

where $1.25 \le \mu \le 4.0$

It is important to mention that the basic shear provided by masonry, v_{bm}, for observation types B and A in Table 2.2 was evaluated according to Eq. 2.15 for a RM shear wall with $M/Vl_w \ge 1.0$ using vertical reinforcement with yield strength, f_{yv}, and a minimum ratio, ρ_v, of 300 MPa and 0.07%, respectively. This produces $v_{bm} = 0.194\sqrt{f'_m}$, for $\mu \le 1.25$, which was then rounded up to give $0.2\sqrt{f'_m}$.

2.4.9 VOON AND INGHAM (2007)

Voon and Ingham (2007) proposed minor modifications to the equation adopted in the NZS 4230:2004 (Eq. 2.15) as follows:

$$V_n = \left[(0.022\rho_v f_{yv} + 0.084 \left(4 - 1.75 \frac{M}{V\, l_w} \right) \right] (1 - \frac{\mu - 1.25}{2.75}) \sqrt{f'_m} (b_w d) + (0.9 \tan \alpha) N^* + A_v f_y \frac{d_{eff}}{s} \qquad \text{Eq. 2.16}$$

As shown in Eq. 2.16, a reduced effective depth of the wall section, d_{eff}, was introduced to the horizontal reinforcement contribution instead of, d, in Eq. 2.15. This reduced effective depth, d_{eff}, takes into account the cover to the vertical reinforcement, the depth of masonry compression zone, and the development length of the horizontal reinforcing bars.

where:

d_{eff} = reduced effective depth of wall section, mm, for the horizontal reinforcement contribution, V_s

= $l_w - (d^{`} + c) - l_{dh}$

l_w = length of masonry wall, mm

$d^{`}$ = distance between wall edge and nearest vertical reinforcing steel bar, mm

C = depth of masonry compression zone, mm

l_{dh} = development length of the horizontal reinforcement, mm, that has 90° hook

= $20d_b$ for $f_y = 300$ MPa

= $35d_b$ for $f_y = 500$ MPa

The depth of the neutral axis, c, was subtracted from the horizontal reinforcing bar, in the calculation of d_{eff}, because of the reinforcement within the compression zone is ineffective to be used as anchorage. Moreover, Voon and Ingham (2007) proposed that 100% of the horizontal reinforcement yield capacity would contribute toward the shear strength, V_n. The shear strength, V_n, in Eq. 2.16 was limited by an upper limit value of $0.33\sqrt{f'_m}\,A_n$ similar to the same value imposed by the NEHRP (1997), and more conservative than the upper limit provided in the NZS 4230:2004 (Eq. 2.11).

2.4.10 MASONRY STANDARDS JOINT COMMITTEE (MSJC) (2013)

Similar to the equation provided by the NEHRP (1997), the MSJC proposed an equation to predict the shear strength of reinforced masonry walls as follows:

$$V_n = 0.083\left[4.0 - 1.75\left(\frac{M}{V\,d_v}\right)\right] A_{nv}\sqrt{f'_m} + 0.25\,P + 0.5\,A_v\,f_y\,\frac{d_v}{s} \qquad \text{Eq. 2.17}$$

where:

$(V_n)_{\max}$ = $0.5\,A_n\sqrt{f'_m}$ for $\frac{M}{V\,d_v} \le 0.25$

$0.33\,A_n\sqrt{f'_m}$ for $\frac{M}{V\,d_v} \ge 1.0$

with linear interpolation for $1.0 \ge \frac{M}{V\,d_v} \ge 0.25$ and $\frac{M}{V\,d_v}$ need not be taken greater than 1.0 in Eq. 2.17

$\frac{M}{V\,d_v}$ = shear span to depth ratio, shall be taken as not less than 0.25 nor more than 1. where, M and V are the moment and shear at the section under consideration, respectively

A_{nv} = net shear area, (mm^2)

$= b_w\,d_v$

d_v = actual depth of a member in direction of shear considered, mm, for rectangular RM walls it could be considered as l_w

The proposed equation by MSJC (2013) is derived from research conducted by Davis (2008). This equation has been compared with results from fifty-six tests of masonry walls dominated by in-plane shear failure. The test data included fully grouted concrete masonry and clay masonry. The walls were selected from research carried out by Shing et al. (1990), Matsumura (1987), Sveinsson et al. (1985), and Voon and Ingham (2006). As reported in his research, the average ratio of the experimental results to the calculated strength using Eq. 2.17 was 1.17 with a coefficient of variation of 0.15. Three others coefficients were evaluated for the contribution of the horizontal reinforcement (0.6, 0.8, and 1.0) instead of 0.5, but Davis (2008) claimed that the best fit to the experimental data was obtained using the 0.5 factor. Although Davis (2008) proposed a ductility coefficient factor, α, to consider the degradation in the shear resistance contribution by masonry in the plastic hinge regions, MSJC (2013) did not approve this degradation in Eq. 2.17. The definition of α and the approach for accounting for strength degradation is the same as that used by Anderson and Priestley (1992). It can be noticed that Eq. 2.17 is the same equation provided by NEHRP (1997), Eq. 2.7, without significant modifications.

2.5 DISCUSSION AND SUMMARY

Many experimental studies have been conducted to investigate the in-plane shear performance of RM shear walls under cyclic lateral loading (e.g. Kaminosono et al., 1985; Matsumura, 1987; Shing et al., 1990; Sveinsson et al., 1985; Voon and Ingham, 2006). Using the best-fit analysis for these test results, in-plane shear strength equations have been developed by different researchers and standards. A selection of these equations were discussed in this chapter and given in a summary form in Table 2.3. To make them easier to follow and compare, some of these equations were re-written and modified to have the same notations and consistent units, SI units. In addition, all the equations are for fully grouted, single bending, rectangular, concrete block RM shear walls.

Table 2.3: Summary of In-Plane Shear Strength Equations

Reference	**In-plane masonry shear strength, V_n[1]**	**Eq.**
Matsumura (1988)	$\left[\left(\frac{0.76}{(h_w/d)+0.7}+0.012\right)0.27\sqrt{f_m^{\prime}}+0.2\sigma_n+0.108\gamma\sqrt{\rho_h f_{yh} f_m^{\prime}}\right](0.875\,t\,d)$	**[2.3]**
Shing et al. (1990)	$(0.0217\sigma_n+0.24)\sqrt{f_m^{`}}\,b_w l_w+\left(\frac{l_w-2d^{\prime}}{s}-1\right)A_{sh}\,f_{yh}$	**[2.5]**
Anderson and Priestley (1992)	$\left(1-\frac{\mu_{\Delta}-2}{2}\right)0.24\sqrt{f_m^{`}}\,b_w l_w+0.25\,P+0.5\,A_{sh}\,f_{yh}\,\frac{d}{s}$	**[2.6]**
NEHRP (1997)	$0.187\sqrt{f_m^{\prime}}\,b_w l_w+0.25P+0.5\,A_{sh}\,f_{yh}\,\frac{l_w}{s}$	**[2.7]**
UBC (1997)	$0.1\sqrt{f_m^{\prime}}\,b_w l_w+\;A_{sh}\,f_{yh}$	**[2.8]**
AS3700-2001	$\left(1.5-0.5\frac{h_w}{l_w}\right)b_w l_w+0.8\,A_s^{*}\,f_{yh}$	**[2.9]**
CSA S304-14[2]	$0.13\,k\sqrt{f_m^{\prime}}\,b_w l_w+0.25\,k\,P^{*}+0.48\,A_{sh}\,f_{yh}\,\frac{l_w}{s}$	**[2.10]**
NZS 4230:2004	$(1-\frac{\mu-1.25}{2.75})\,0.22\sqrt{f_m^{\prime}}\,b_w l_w+(0.9\tan\alpha)\,P+0.64A_{sh}\,f_{yh}\,\frac{l_w}{s}$	**[2.15]**
Voon and Ingham(2007)	$(1-\frac{\mu-1.25}{2.75})\,0.22\sqrt{f_m^{\prime}}\,b_w l_w+(0.9\tan\alpha)P+A_{sh}\,f_{yh}\,\frac{d_{eff}}{s}$	**[2.16]**
MSJC (2013)	$0.187\sqrt{f_m^{\prime}}\,b_w l_w+0.25P+0.5\,A_{sh}\,f_{yh}\,\frac{l_w}{s}$	**[2.17]**

[1] all the equations for concrete block, fully grouted, single bending, rectangular, $M/Vd_v > 1.0$,

$\rho_{sv} = 0.78\%$ (20M in each cell), f_{yv} =430MPa

[2] k = 1.0, 0.75, 0.5 for R_d of 1.5, 2.0, 3.0, respectively.

From Table 2.3, the main parameters that influence the in-plane shear strength can be summarized as: the compressive strength of the masonry f'_m, the shear span to depth ratio, M/Vd_v, the displacement ductility, μ_Δ, the vertical reinforcement ratio, ρ_v, the axial compressive stress, σ_n, the horizontal reinforcement ratio, ρ_h, and the wall cross-section dimensions, b_w and l_w, in addition to the yield strength of the vertical and horizontal reinforcement.

Due to the complexity of the interactions between these parameters, no effective mechanistic model has been proposed for the accurate prediction of the nominal shear strength of RM walls. To simplify the task of calculating the nominal shear strength of RM shear walls, V_n, Anderson and Priestley (1992) proposed the first effective equation (Eq. 2.6) that considered V_n as the sum of three independent terms as shown in Eq. 2.18: masonry, V_m, axial compression load, V_p, and horizontal reinforcement, V_s. They also proposed a factor k to consider the degradation of the shear resistance provided by the masonry, V_m, when the wall reaches its inelastic performance level.

$$V_n = V_m + V_P + V_S \qquad \text{Eq. 2.18}$$

NEHRP (1997) modified Eq. 2.6 to consider the effect of the shear span to depth ratio, M/Vd_v, on the masonry term and proposed Eq. 2.7. The shear resistance degradation in V_m was replaced by a limitation in the total nominal shear strength, V_n, with respect to M/Vd_v as shown in Eq. 2.7. This equation (Eq. 2.7) is widely used in North American codes including CSA (S304-14) and MSJC (2013), with slight modifications as presented in Eq. 2.10 and Eq. 2.17. The NZS equation and the one modified by Voon and Ingham (2007), Eq. 2.15 and Eq. 2.16, respectively, modified the masonry term in Eq. 2.7 to take into account the effects of the dowel action and the displacement ductility. Furthermore, the axial compressive stress contribution, V_p, was considered as a dependent component upon the angle, α, resulting from a diagonal compression strut (see Figure 2.26).

In summary, that main two parameters for accurate prediction of the nominal in-plane shear strength of RM shear walls; the shear strength degradation model, as discussed earlier in Chapter 1, and the contribution of the horizontal reinforcement. It was demonstrated that all of the proposed equations were developed based on the results of experimental work conducted over the past 30 years. There are two main concerns about these experimental results. The first one is that most of the tested walls did not achieve their initial shear strength, V_i. Consequently, the reported failure loads represented the lateral force corresponding to the interaction between the flexural performance and the shear strength envelope at the strength degradation zone. The second concern relates to the horizontal reinforcement contribution, which was not measured experimentally. Most of the previous researchers calculated the lateral reinforcement resistance based on the difference between the maximum lateral loads achieved for different horizontal reinforcement ratios, neglecting the influence of the redistribution in the resistance shares of the horizontal reinforcement and the masonry. This discussion shows the need for this research to be conducted to consider these concerns and to develop a more accurate equation for predicting the in-plane shear strength of RM shear walls.

CHAPTER 3

EXPERIMENTAL WORK

3.1 INTRODUCTION

Similar to reinforced concrete (RC) buildings, reinforced masonry (RM) shear walls are a popular lateral load resisting system for RM structures. There are several failure modes for RM shear walls. One of the possible failure mechanisms is diagonal shear failure. The shear behaviour of RM shear walls at the plastic hinge zone is more complicated than the flexural behaviour due to the interaction between the nonlinear responses of their constituent materials, namely: concrete masonry blocks, mortar, grout, and steel reinforcement. Although some experimental data have been reported in the literature, more experimental work is needed to provide a better understanding of the inelastic behaviour of RM shear walls. Accordingly, experimental work is conducted to evaluate the in-plane shear behaviour of RM shear walls and presented in this chapter. The first part of the chapter describes the studied parameters along with the test matrix and the details of the studied walls. The properties of the materials used in the construction of the walls are discussed in the second part, followed by the test setup and instrumentation. A short overview of the testing procedure, including the loading protocol, is presented at the end of the chapter.

The experimental work for this study involved the testing of nine full-scale fully grouted rectangular RM shear walls to evaluate the effect of the studied parameters on the shear behaviour of the walls. All the tested walls and their auxiliary specimens were constructed in the structures laboratory at Concordia University by certified masons following all the requirements of the Canadian Standards CSA S304.1 (2004) and CSA A179 (2004). The main variables considered were:

- Horizontal reinforcement ratio, ρ_h
- Level of the axial compressive stress, σ_n
- Shear span to depth ratio, M/Vd_v
- Horizontal reinforcement anchorage end detail
- Vertical spacing of horizontal reinforcement, S_v
- Horizontal spacing of vertical reinforcement, S_h

3.2 TEST LAYOUT

To achieve the research objectives, nine full-scale fully grouted rectangular RM shear walls were tested under in-plane axial compressive stress, top moment, and cyclic lateral excitations. All the walls were designed and detailed such that they failed in shear before reaching their flexural capacity. The experimental work was conducted in two phases. In the first phase, five RM shear walls were constructed and tested to investigate the effect of the first three parameters: the horizontal reinforcement ratio, ρ_h, the level of axial compressive stress, σ_n, and the shear span to depth ratio, M/Vd_v, on the in-plane shear behaviour. The test results of these five walls along with other available experimental data from previous researchers were used to evaluate the contribution of the masonry, V_m, axial load, V_p, and the horizontal reinforcement, V_s, to the shear capacity, V_n, equation in the current Canadian Standards, CSA S304-14 “Design of Masonry Structures”. This led to a proposed more accurate equation to predict the in-plane shear strength, V_n, with respect to the displacement ductility of the RM shear wall.

In the second phase, four walls were tested to study the effect of the reinforcement detailing, including the horizontal reinforcement anchorage end detail and the spacing between the horizontal and vertical reinforcement, on the overall shear performance. Based on the results of these four walls, reinforcement detailing requirements are proposed for the plastic hinge zone to enhance the inelastic behaviour of RM shear walls in terms of shear capacity, lateral displacement ductility, and energy dissipation. Figure 3.1 shows the layout of a typical tested wall.

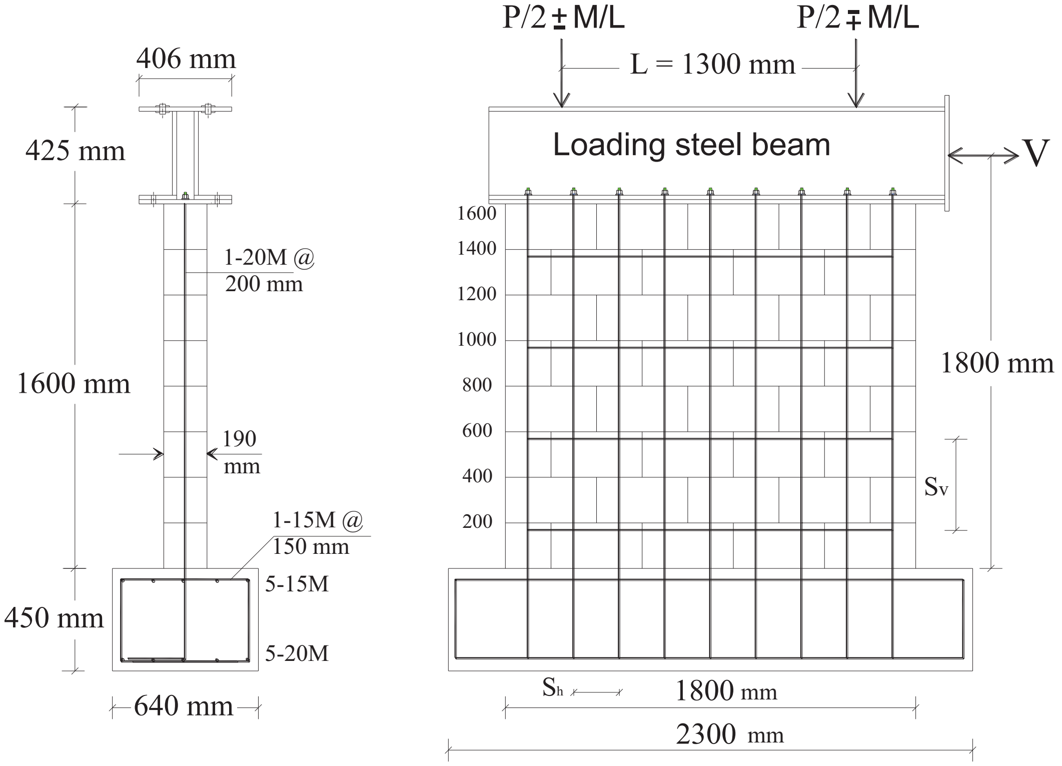

Figure 3.1: Dimensions of a typical tested RM shear wall

All the walls had the same dimensions, 1.8 m x 1.6 m x 0.19 m, and each one was constructed on a reinforced concrete (RC) foundation with dimensions of 2.3 m x 0.64 m x 0.45 m (see Figure 3.1). The walls were subjected to cyclic lateral excitations at a height of 1.80 m from the top of the RC foundation in order to keep the shear span to depth ratio, M/Vd_v, higher than 1.0. All the loads were transferred to the tested walls through a stiff built-up steel loading beam. The vertical reinforcement of the RM walls was anchored to the bottom flange of the loading beam as can be seen in Figure 3.1. Table 3.1 presents the test matrix of the studied walls including the reinforcement details and the studied parameters.

Table 3.1: Test Matrix of Nine RM Shear Walls

Wall ID	Reinforcement		Studied Parameter					
	Vertical	Horizontal	ρ_h %	σ_n MPa	M/Vd$_v$	Horizontal Reinf. end detail	S$_v$ mm	S$_h$ mm
W-Ref	20M@200	10M@400	0.13	1.0	1.2	180° hook	400	200
W-ρ_h0	20M@200	–––	0.0	1.0	1.2	–––	–––	200
W-σ_n0	20M@200	10M@400	0.13	0.0	1.2	180° hook	400	200
W-σ_n1.5	20M@200	10M@400	0.13	1.5	1.2	180° hook	400	200
W-M/Vd_v1.8	20M@200	10M@400	0.13	1.0	1.8	180° hook	400	200
W-90°	20M@200	10M@400	0.13	1.0	1.2	90° hook	400	200
W-Str	20M@200	10M@400	0.13	1.0	1.2	Straight	400	200
W-S$_v$800	20M@200	15M@800	0.13	1.0	1.2	180° hook	800	200
W-S$_h$800	30M@800	15M@800	0.13	1.0	1.2	180° hook	800	800

All the walls were vertically reinforced with 20M bar in each cell with a vertical reinforcement ratio, ρ_v, of 0.79%, except wall W-S$_h$800 that had a 30M bar in the first, middle, and last cells with ρ_v equal to 0.61%. The first wall, W-Ref, was designed to be a reference wall for the remaining tested walls. Wall W-Ref had uniformly distributed horizontal reinforcing bars, 10M@400 mm, which were attached using a standard 180^o hook around the outermost vertical bars. A constant axial compressive stress of 1.0 MPa was applied to the studied wall, W-Ref, before applying the in-plane cyclic lateral displacements and it remained constant throughout the whole test. Wall W-ρ_h0 was constructed without horizontal reinforcement. Comparing the behaviour of walls W-Ref and W-ρ_h0 enabled evaluation of the horizontal reinforcement contribution, V_s, towards the nominal shear strength, V_n, and its influence on the displacement ductility of the wall. The effect of the horizontal reinforcement on the redistribution of the shear resistances provided by the masonry, V_m, and the axial compressive stress, V_p, is discussed later in Chapter 4.

As mentioned in Chapter 2, the axial compressive stress has a contribution, V_p, to the in-plane nominal shear resistance of masonry shear walls, V_n. Most of the existing masonry shear strength predictive equations consider a constant percentage of the total axial compressive stress that contributes to V_n. In order to evaluate the effect of the compressive axial stress on the overall in-plane shear behaviour of masonry shear walls, walls W-σ_n0 and W-σ_n1.5 were duplicates of wall W-Ref, but with externally applied axial compressive stresses of 0.0 and 1.5 MPa, respectively, instead of 1.0 MPa for wall W-Ref.

One of the important parameters that affects the inelastic behaviour and ductility of RM shear walls is the shear span to depth ratio, M/Vd_v. Wall W-M/Vd_v1.8 was subjected to a top moment of 0.9V kN.m, where V is the lateral load from the horizontal actuator, which makes the overall shear span to depth ratio, M/Vd_v, equal to 1.875 as compared to a value of 1.25 for wall W-Ref. Out of the eight horizontally reinforced walls, the anchorage end detail of the horizontal reinforcement for walls W-90° and W-Str were 90^o hook and straight bar, respectively, as shown in Figure 3.2. The impact of the horizontal reinforcement anchorage end detail on the seismic response of RM shear walls was assessed based on the test results of walls W-Ref, W-90°, and W-Str.

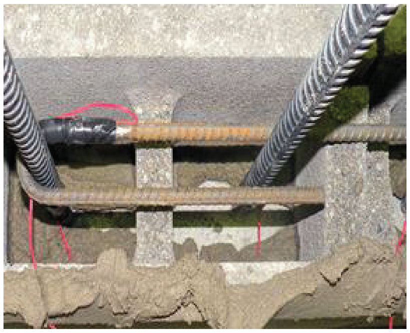

(a) 180° hook

(b) 90° hook (c) Straight bar

Figure 3.2: Horizontal reinforcement end details of tested RM shear walls: (a) W-Ref; (b) W-90°; (c) W-Str

Unlike wall W-Ref, wall W-S_v800 was constructed with horizontal reinforcement of 15M@ 800 mm, in order to study the effect of vertical spacing between horizontal bars. Wall W-S_h800 is a duplicate of wall W-S_v800, except that the vertical reinforcement was concentrated in the first, middle, and end cells. Each cell has a 30M bar with a total vertical reinforcement ratio, ρ_v, of 0.61% compared to ρ_v of 0.79% for the rest of the tested walls. However, this slight difference in ρ_v can be neglected since most of the existing equations for the nominal in-plane shear strength, V_n, including the design equations given in the Canadian standard CSA S304-14 and the Masonry Standards Joint Committee MSJC-2013, do not consider the contribution of the vertical reinforcement. In addition to the effect of the studied parameters on the in-plane nominal shear strength, V_n, their impact on the seismic performance and the crack propagation is discussed in the next chapter. Figures 3.3 shows details of the tested RM shear walls.

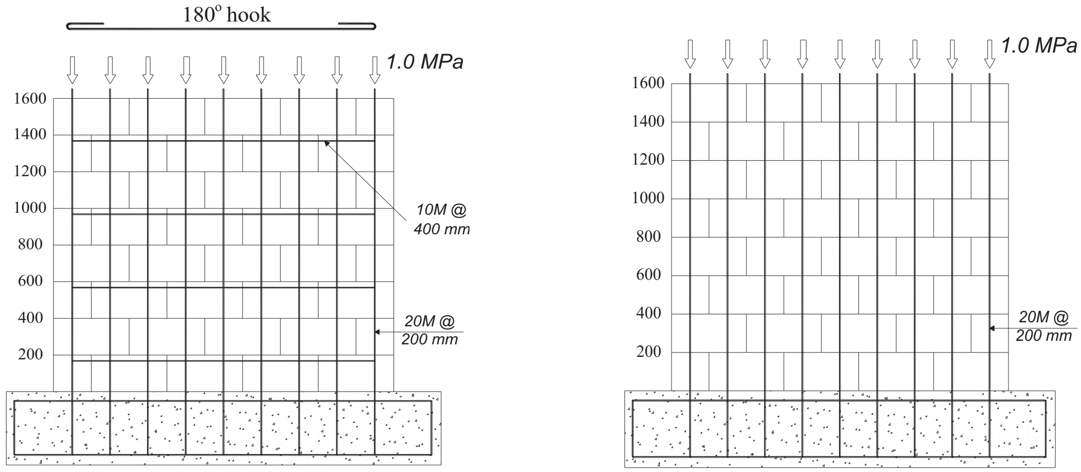

W-Ref W-ρ_h0

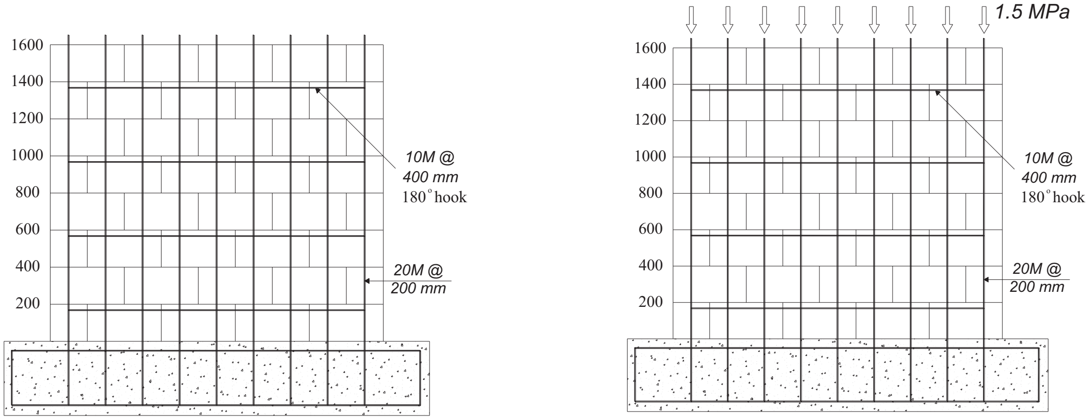

W-σ_n0 W-σ_n1.5

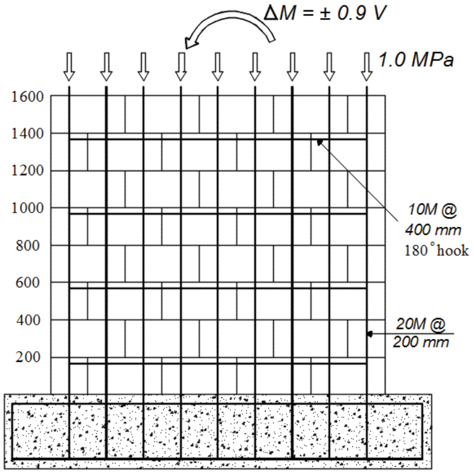

W-M/Vd_v1.5

Figure 3.3: Details of the tested RM shear walls

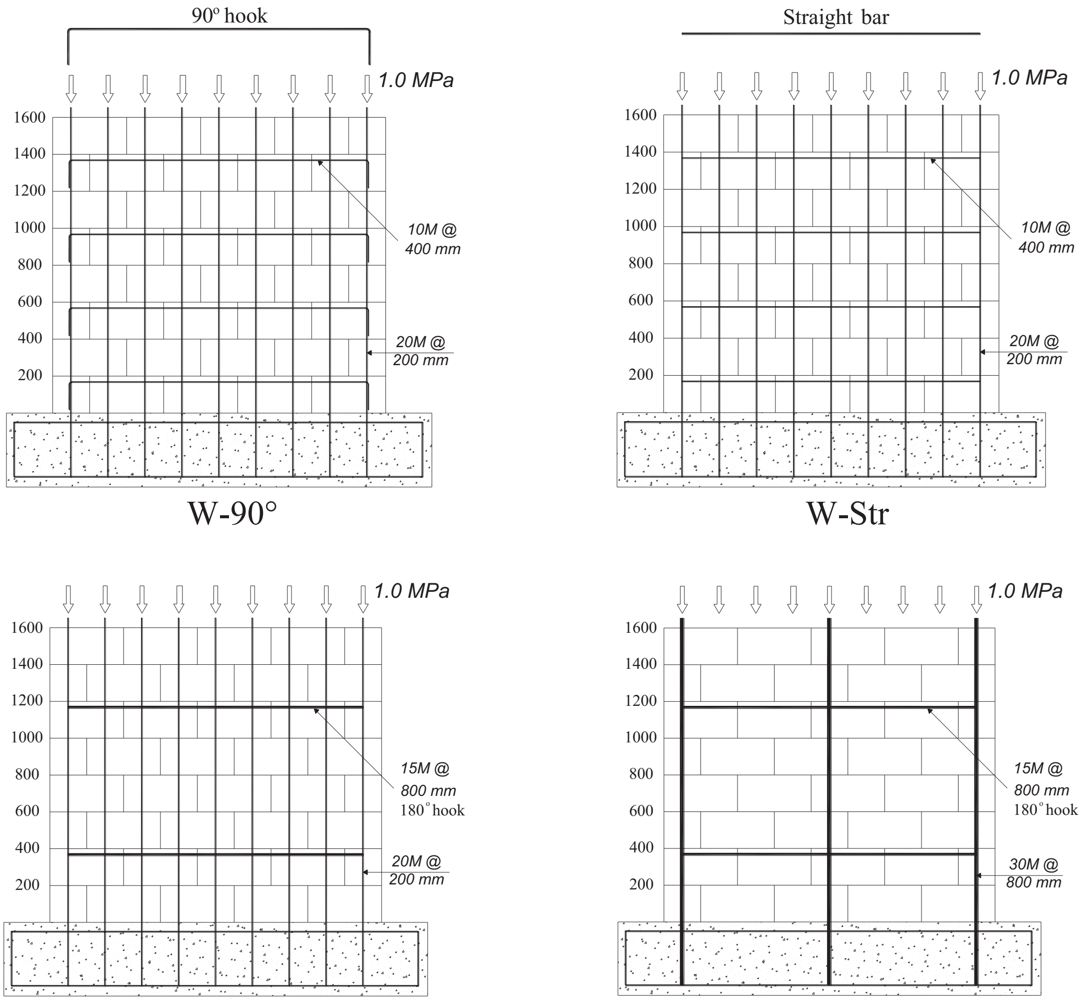

W-90° W-Str

W-S_v800 W-S_h800

Figure 3.3(continued): Details of the tested RM shear walls

3.3 CONSTRUCTION MATERIALS AND AUXILIARY LABORATORY TESTS

3.3.1 CONSTRUCTION OF THE RM SHEAR WALLS' FOUNDATION

To provide a fixed end condition at the base of the tested walls, each tested wall was constructed on a reinforced concrete (RC) foundation that was designed to be stiff and not to deform significantly during testing of the walls. The vertical reinforcement of each tested wall was bent into its RC foundation with an embedded sufficient length to transfer the base moment of the wall to the RC foundation. In order to connect the tested wall to the top loading steel beam (see section 3.4 Test Setup), the vertical reinforcement was threaded 100 mm from the top as shown in Figure 3.4.

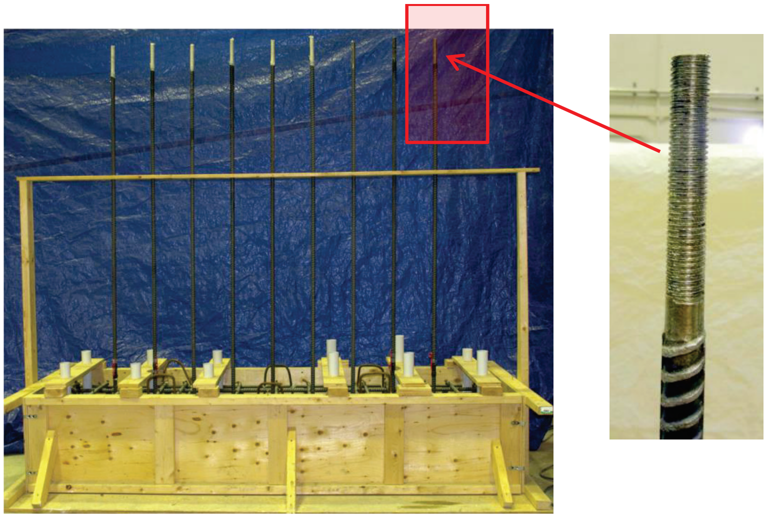

Figure 3.4: Threaded part of the vertical reinforcement of the studied RM shear walls

Each of The RC foundation was 2.3 m long x 0.64 m wide x 0.45 m high and was reinforced longitudinally with 5-15M and 5-20M at the top and bottom, respectively. In addition to the longitudinal reinforcement, horizontal reinforcement of 15M@150 mm c/c was provided in the top and bottom of the RC foundation. A temporary timber frame was used to hold the vertical reinforcement of the tested walls in place during pouring of the concrete into the foundation formwork, see Figure 3.5a. Twelve vertical openings were created in the foundation using plastic tubes with a 50 mm outer diameter. These openings were created to accommodate high tensile strength threaded rods that were used to fix the RC foundation to a strong floor during testing. A ready mix concrete of f_c' equal to 30 MPa was used for the RC foundation as shown in Figure 3.5.

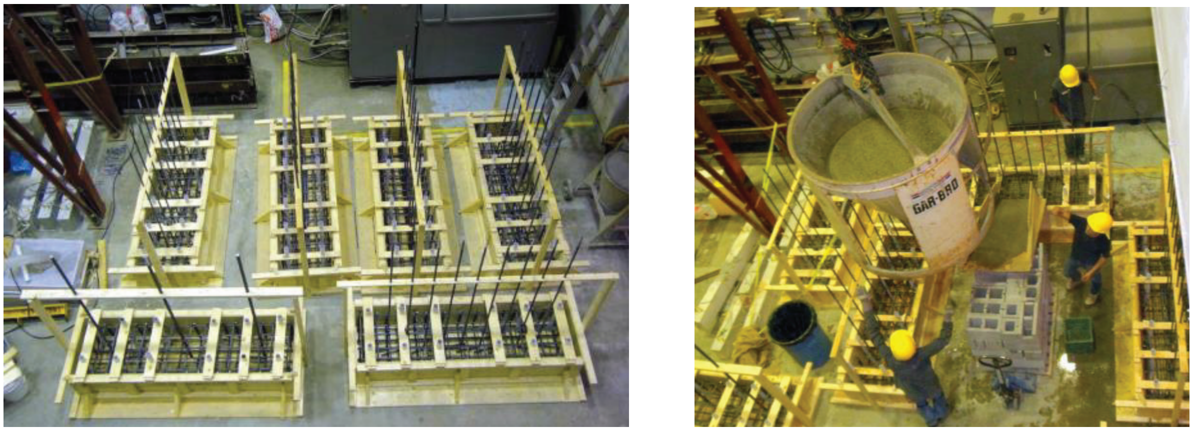

(a) (b)

Figure 3.5: Tested walls' foundation: (a) RC foundation formwork; (b) pouring ready mix concrete

The compressive strength of the concrete in the foundation was measured experimentally using six standard 100 mm diameter x 200 mm high cylinders. The average compressive strength for the cylinders after 7 days was 30.5 MPa (c.o.v. = 5.1%) and it was 39.5 MPa (c.o.v. = 6.6%) at the beginning of testing. In addition to the compressive strength test, splitting tensile strength tests were conducted on three concrete cylinders resulting in an average splitting tensile strength of 4.2 MPa (c.o.v. = 4.4%).

3.3.2 CONCRETE MASONRY UNITS (CMUS)

Lightweight knock-out concrete masonry units (CMUs) were used to construct all the tested walls and the required auxiliary specimens. The knock-out units are concrete masonry units that have knock-out webs that can be removed to accommodate the horizontal reinforcement as can be seen in Figure 3.6.

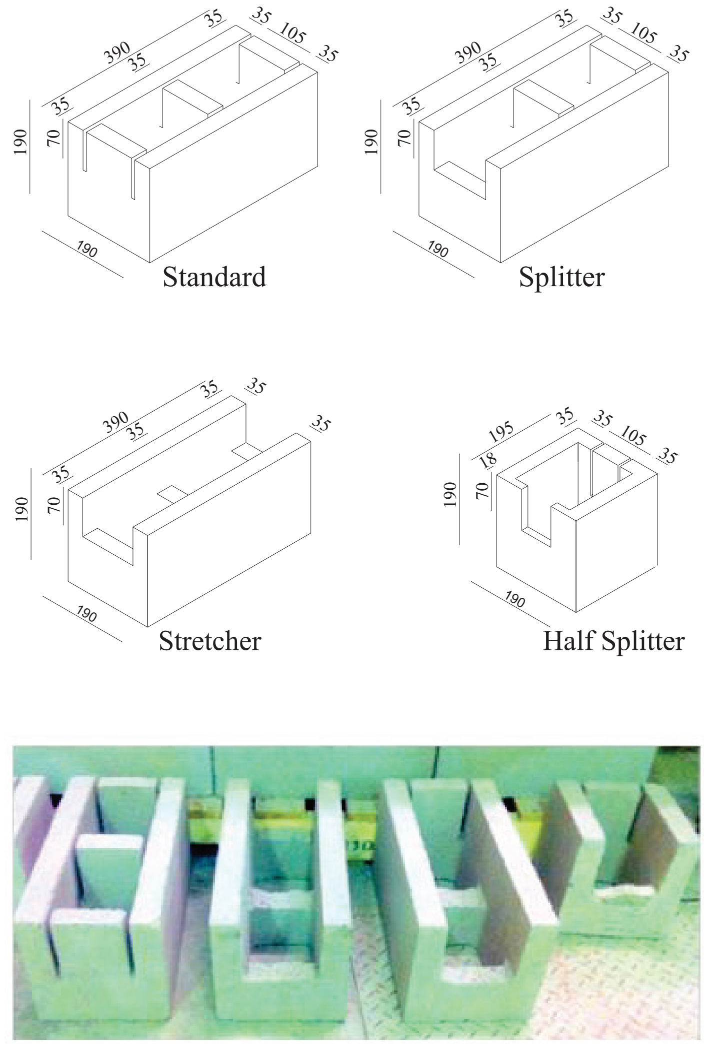

Standard

Splitter

Stretcher

Half Splitter

Figure 3.6: Full-scale CMUs with knock-out webs

The CMUs have standard dimensions of 390 mm x 190 mm x 190 mm with a net cross-sectional area of 383 cm^2. The average weight of the lightweight knock-out CMU is 12.9 kg (c.o.v. = 3.1%), which is almost 72% of a standard CMU' normal weight. The minimum nominal compressive strength of the blocks was reported by the supplier's specifications as 15.0 MPa. This type of blocks can be classified as H/15/C/O following the standard classification in the Canadian Standards CSA A165.1-14. The H/15/C/O refers to a hollow unit with a minimum specified compressive strength of 15.0 MPa, a density between 1700-1800 kg/m^3, maximum water absorption of 225 kg/m^3, and no limit on moisture content at time and point of shipment.

The knock-out was selected in order to provide grout continuity in both the vertical and the horizontal directions compared to the standard two-cell hollow blocks that provide grout continuity in the vertical direction only. This continuity of the grout will prevent any planes of weakness between the concrete masonry units. Furthermore, it will enhance the behaviour of the fully grouted RM structural walls in the horizontal direction; consequently, its capability to resist lateral loads will increase. Moreover, using lightweight concrete blocks in masonry building improves the mason's productivity. Five blocks were tested to measure the compressive strength of lightweight knock-out CMUs. Figure 3.7 shows the compression test setup in addition to the different modes of failure.

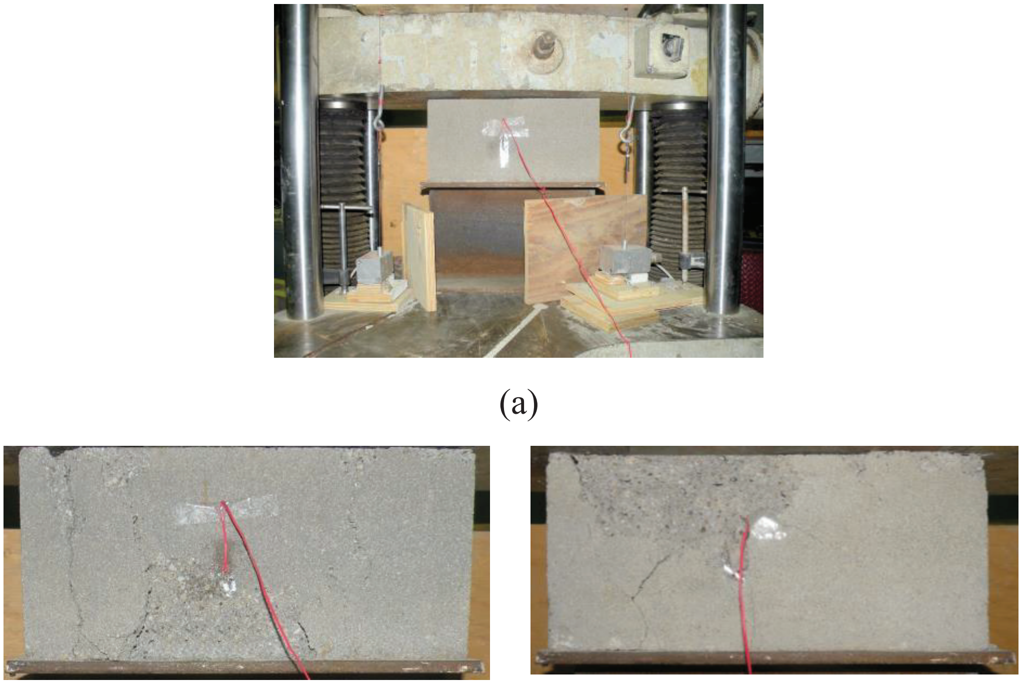

(a)

(b)

(c)

Figure 3.7: Compression test on lightweight knock-out CMUs: (a) test setup; (b) vertical cracks followed by crushing; (c) diagonal cracks followed by crushing

The Canadian Standards CSA A165.1-14 provides the following equation to calculate the compressive strength based on the average net cross-sectional area.

$$f'_{bl} = f_{av}(1 - 1.64v) \quad = \quad f_{av} - 1.64s \qquad \text{Eq. 3.1}$$

where;

f'_{bl} = specified compressive strength, MPa

f_{av} = average compressive strength of the test results, MPa

v = coefficient of variation = s / f_{av}

s = standard deviation = $\sqrt{\frac{\sum(\mathrm{x} - \mathrm{x_m})^2}{\mathrm{n} - 1}}$, MPa

- x = an individual test result, MPa
- $\mathrm{x_m}$ = f_{av} , average of individual test results, MPa
- n = number of masonry units tested = 5

Based on the test results and Eq. 3.1, the compressive strength of the lightweight knock-out CMUs, f'_{bl}, normal to the bed joint was measured as 16.7 MPa (c.o.v. = 4.8%).

3.3.3 MORTAR

The concrete masonry units were joined together using 10 mm type S mortar joints and were laid in a running bond as can be seen in Figure 3.8. Mortar type S is recommended for structural elements that are subjected to high lateral loads, such as the tested shear walls in this research. After several trials, a mixture of one volumetric unit of masonry cement, 2.75 units of sand and 0.7 units of water was chosen following the specific requirements in the Canadian Standards CSA A179-04. The workability of the mortar has a major effect on the construction process of masonry structures as it directly affects the mason's work by facilitating or impeding the construction quality. The definition of workability is slightly subjective as it relies on the mason's evaluation of the mortar. Consequently, the mortar workability was evaluated in terms of fresh mortar flow using the flow table test described in the standard test method ASTM 1437-13.

Figure 3.8: Running bond pattern

Through the standard flow test, fresh mortar was used to fill a standard frustum conical shape with a diameter of 100 mm on a flow table. The mortar sample was then dropped 25 times within 15 seconds. As the mortar was dropped, it spread out on the flow table as shown in Figure 3.9. The initial and the final diameters of the mortar sample were used to calculate the flow using the following equation:

$$\text{flow} = \frac{D_f - D_i}{D_i} \times 100 \qquad \text{Eq. 3.2}$$

Where D_i and D_f are the initial and the final diameters of the mortar sample, respectively. The average flow was measured as 112.16% (c.o.v. = 3.8%). Twenty-four randomly selected mortar cubes were constructed to measure their compressive strength. The mortar was moulded into 50 mm cubes using moulds meeting the requirements of the standard ASTM 1437-13 as shown in Figure 3.10a. Half of the mortar cubes were tested after 7 days and the rest were tested at the beginning of testing the RM shear walls. The compressive strength after 7 days and at the beginning of testing the walls was 8.5 MPa (c.o.v. =8.8%) and 13.7 MPa (c.o.v. = 7.8%), respectively. Figure 3.10 shows the test setup and the different modes of failure.

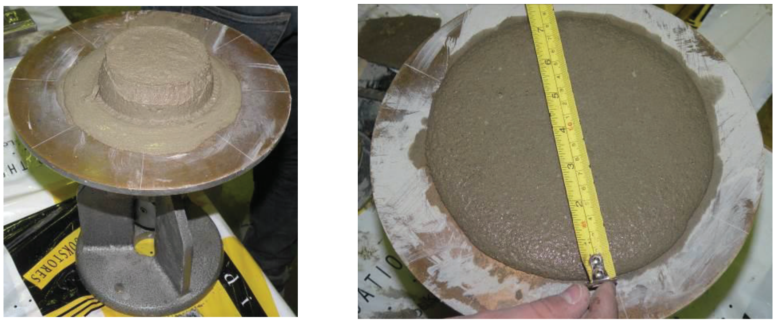
(a) (b)

Figure 3.9: Flow table test: (a) prior to dropping on the table; (b) after 25 drops

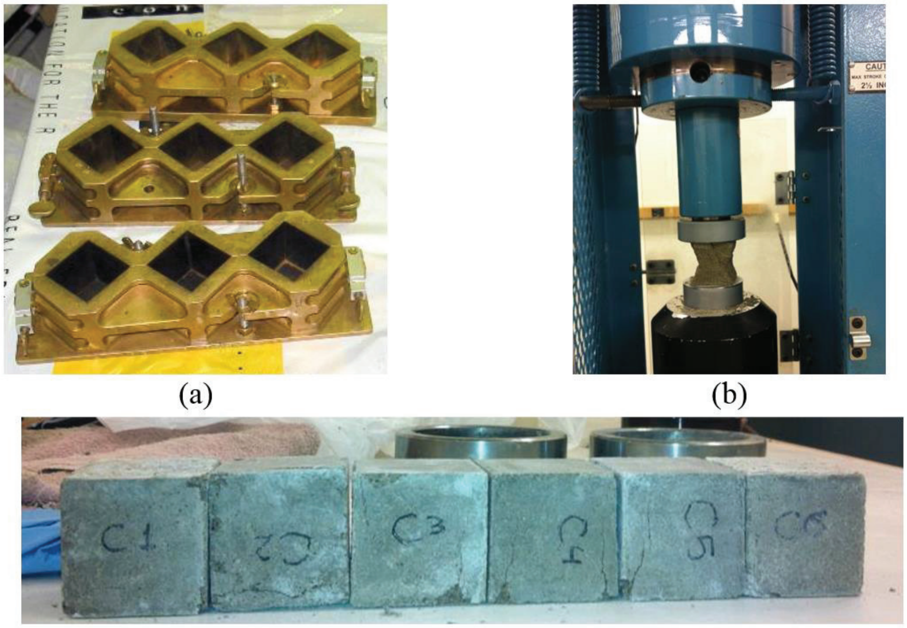

(a) (b)

(c)

Figure 3.10: Mortar compressive strength test: (a) mortar cubes moulds; (b) compression test setup; (c) modes of failure

3.3.4 GROUT

All the tested RM shear walls were fully grouted as shown in Figure 3.11. The grout used in this experimental work, categorized as “coarse grout”, was mixed in the laboratory in accordance with CSA A179-04. The grout mixture had one volumetric unit of Portland cement, 2.4 units of fine aggregate (sand), two units of coarse aggregates with a maximum size of 7 mm (¼″), and 0.9 units of water. A grout with a high workability was necessary to ensure filling all the cells of the tested walls. The slump test of the fluid grout was done every day during the construction of the walls and was measured as a 270 mm average slump (see Figure 3.12).

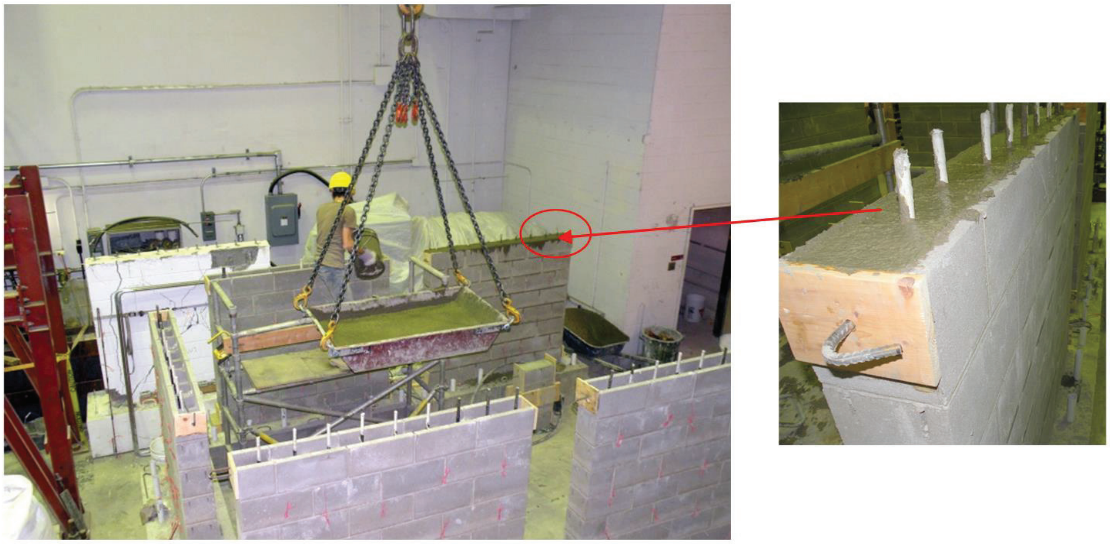

Figure 3.11: Grouting the tested RM shear walls

Figure 3.12: Slump test for grout

The compressive strength of the grout has a considerable effect on the behaviour of fully grouted masonry structural elements. Twenty cylinders of coarse grout 100 mm in diameter by 200 mm long were constructed randomly during the construction of the walls in order to evaluate their compressive strength. The average compressive strength at the age of 7 days and at the beginning of walls testing was 21.6 MPa (c.o.v. = 8.4%) and 29.4 MPa (c.o.v. = 7.3%), respectively. Figure 3.13 shows the compressive strength test for the grout cylinder.

(a) (b)

Figure 3.13: Compressive strength test for grout: (a) prior to failure; (b) after failure

3.3.5 STEEL REINFORCEMENT

All the studied walls were reinforced either in the vertical direction or in both vertical and horizontal directions. Standard steel reinforcing bars in the Canadian market, 10M and 15M, were used for the horizontal bars, while 20M and 30M bars represented the vertical reinforcement. In addition, the RC foundations were reinforced with 15M and 20M steel reinforcing bars. Samples were taken from each diameter and were tested to determine their tensile stress-strain characteristics in accordance with the test methods and definitions in ASTM A615M-13 and A370-14. Figure 3.14 shows the tensile test setup for the different steel reinforcement bars using a Tinius-Olsen testing machine, as well as the failure modes of the tested bars. To monitor the tensile deformation of the tested samples during the tensile loading until failure, two strain gauges were installed on each tested sample. In addition, a Linear Variable Differential Transformer (LVDT) extensometer was attached to the tested samples, as shown in Figure 3.14(a). Figure 3.15 shows the average stress-strain curves for the different used steel reinforcing bars. As presented in this figure, the yield point or yield plateau can be well defined for both the vertical and horizontal reinforcement. The average yield strength of the bars, f_y, was measured as 430 MPa (c.o.v. =3.2%) with an average modulus of elasticity, E_s, equal to 196 GPa (c.o.v. =1.85%).

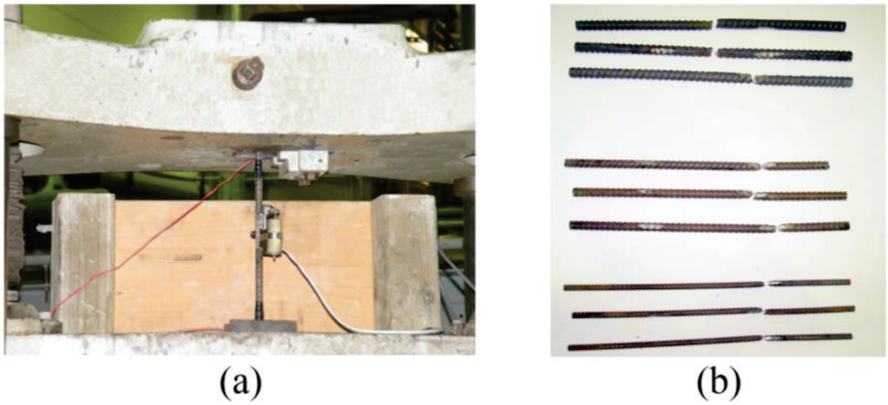
(a)
(b)

Figure 3.14: Tension test for steel reinforcement bars: (a) test setup; (b) modes of failure

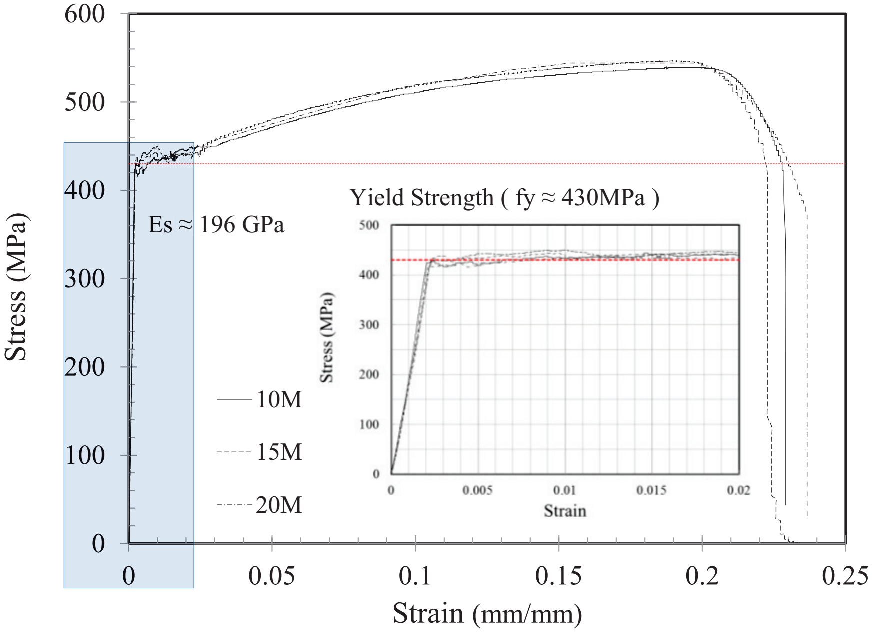

Figure 3.15: Average stress-strain curves for different steel reinforcement diameters

3.3.6 MASONRY

After evaluating the behaviour of masonry constituent materials separately, i.e. the knock-out CMUs, the mortar and the grout, experimental auxiliary tests were carried out to characterize the behaviour of fully grouted masonry prisms. Uniaxial compression tests normal to the bed joint in addition to in-plane beam tests were conducted to evaluate the compressive, indirect tensile, and shear performance of the masonry prisms.

3.3.6.1 Uniaxial compression tests

Fully grouted masonry prisms are expected to have a similar behaviour to concrete in that they will have a strong compressive capacity as compared to their weak tensile resistance. The compressive strength of masonry prism, f'_m, has a significant effect on the performance of masonry structural elements. Although the Canadian standard CSA S304.1 (2004) provides empirical values for the design masonry compressive strength, f'_m, using the mortar type and the masonry unit strength, still the values from the uniaxial compression test are more representative for the compressive strength of the tested walls as compared to these proposed values. The Canadian standard CSA S304.1 (2004) specifies the minimum prism size of fully grouted hollow blocks to be at least one masonry unit in width and three courses in height with a height-to-thickness ratio, *h/t*, greater than or equal to two.

Throughout the uniaxial compression tests, 16 fully grouted unreinforced masonry (URM) prisms were constructed and tested to measure the compressive strength, f'_m, the modulus of elasticity in compression normal to the bed joint, E_m, and the axial strain at maximum strength, ε_o. The effect of the bond pattern and the height-to-thickness ratio, *h/t*, on the previous measured properties was also evaluated. The 16 prisms were divided into four groups as presented in Table 3.2 and Figure 3.16. In each group, at least three replicates of URM prism were tested to consider variations in the masonry materials' properties.

Table 3.2: Compression Prisms Configurations

Group ID*	Number of prisms	*h* mm	*t* mm	*h*/*t*	Bond Pattern
G1-P4R	5	800	200	4	running bond
G2-P3S	3	600	200	3	stack bond
G3-P4S	5	800	200	4	stack bond
G4-P8S	3	1600	200	8	stack bond

* P = Prism
3, 4, 8 = height-to-thickness ratio
R, S = Bond pattern; running bond or stack.

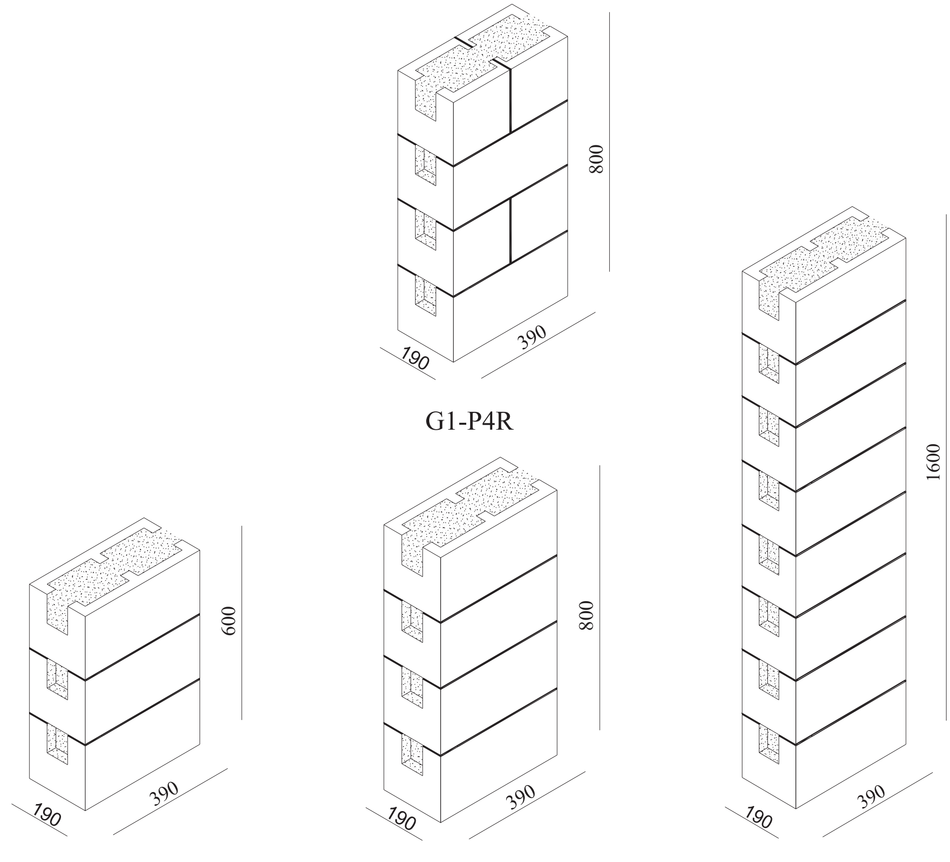

G1-P4R

G2-P3S G3-P4S G4-P8S

Figure 3.16: Dimensions of the compression unreinforced masonry prisms

In the first Group, G1-P4R, five URM prisms were constructed using the typical configuration of compression test for masonry prisms following the Canadian standard CSA S304.1 (2004) requirements. The masonry compressive strength, f'_m, the modulus of elasticity, E_m, and the axial strain at maximum strength, ε_o, were measured and calculated in accordance with the test results of this group. Each prism in group G1-P4R was four concrete masonry units high by one unit long (800 mm high x 390 mm long x 190 mm thick) and was constructed with alternating courses of whole units and two half units, using ½-½ running, as shown in Figure 3.16. The half units were cut from the whole CMUs using a wet masonry saw and the cut ends of the half units were facing outwards.

There are many parameters that could affect the compressive strength of a masonry prism, f'_m. In addition to the tested prisms in group G1-P4R, a total of 11 prisms were tested and divided into 3 groups: G2-P3S, G3-P4S, and G4-P8S (see Table 3.2). The test results of these prisms aimed to investigate the effect of the bond pattern and height-to-thickness ratio, *h/t*, on the compression behaviour of the masonry prisms. All 11 prisms were constructed in a stack bond pattern. Three different height-to-thickness ratios, *h/t*, were considered in this study: 3, 4, and 8 for groups G2-P3S, G3-P4S, and G4-P8S, respectively. The tested prisms in group G4-P8S had a height-to-thickness ratio equal to 8 that represents the full height of a vertical strip of the studied RM shear wall in this experimental program. Comparing the test results of groups G1-P4R and G3-P4S shows the effect of the bond pattern on the compression behaviour of the masonry prism for the same height-to-thickness ratios equal to 4.

All 16 URM prisms were built and grouted at the same time of constructing the tested walls using the same construction materials that were used to build the studied RM shear walls. Before grouting, the cores were cleaned out to be free of any mortar droppings and vertical wooden boards were attached to both sides of the prisms to allow the cells to be filled with grout as shown in Figure 3.17. Two 10M bars were pre-embedded horizontally inside the prisms before grouting to be used for measuring the axial deformation during testing. During the grouting process, the grout was compacted in layers by rodding to ensure complete filling of all cells and was finished to a height of 25 mm above the top surface of the prisms. They were then cured for the first 7 days sealed under polyethylene, similar to the studied walls. Similar to all the auxiliary tests, the masonry prisms were tested at the beginning of testing the walls at an age of more than 28 days.

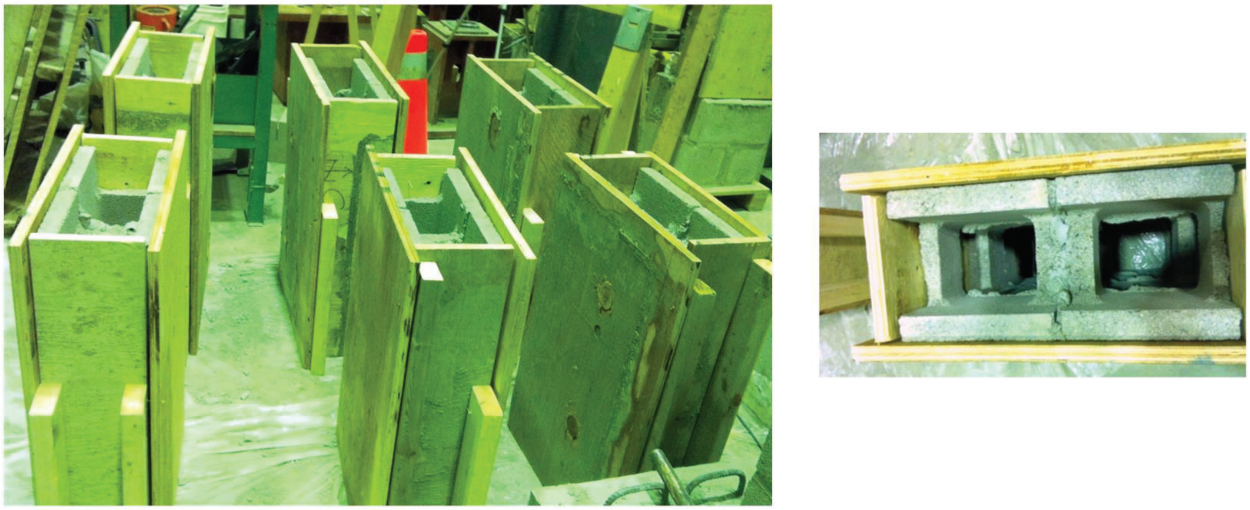

Figure 3.17: Construction of the compression prisms

Figure 3.18 shows the typical uniaxial compressive test setup for the fully grouted masonry prisms. The test setup consists of: a reaction steel frame that transfers the load to a strong floor system; a 3000 kN hydraulic cylinder for the application of the axial compression force on the test units; a stiff rectangular loading steel plate for uniform distribution of the axial load; and a stiff steel beam footing supporting the tested prisms. The loading cylinder was connected to a hydraulic pump to control the loading rate. Before testing, all the prisms were capped at their top and bottom with strong mortar with a thickness of 10 mm. All the specimens were loaded up to one-half of the expected maximum load with a small loading rate of 40 kN/min. The loading rate was then adjusted such that the remaining load was applied at a uniform rate to reach the expected failure load in not less than 1 min nor more than 2 min. This loading rate was selected in accordance with the Canadian Standards CSA S304.1 (2004) requirements. The load was measured and recorded from the load cell that was attached to the cylinder. The vertical displacement of the prisms was measured using two cable-extension transducers (potentiometers) attached at the two sides of the tested prisms using the embedded thrown 10M bars. In addition to the vertical displacement, the horizontal deformation was also measured during testing.

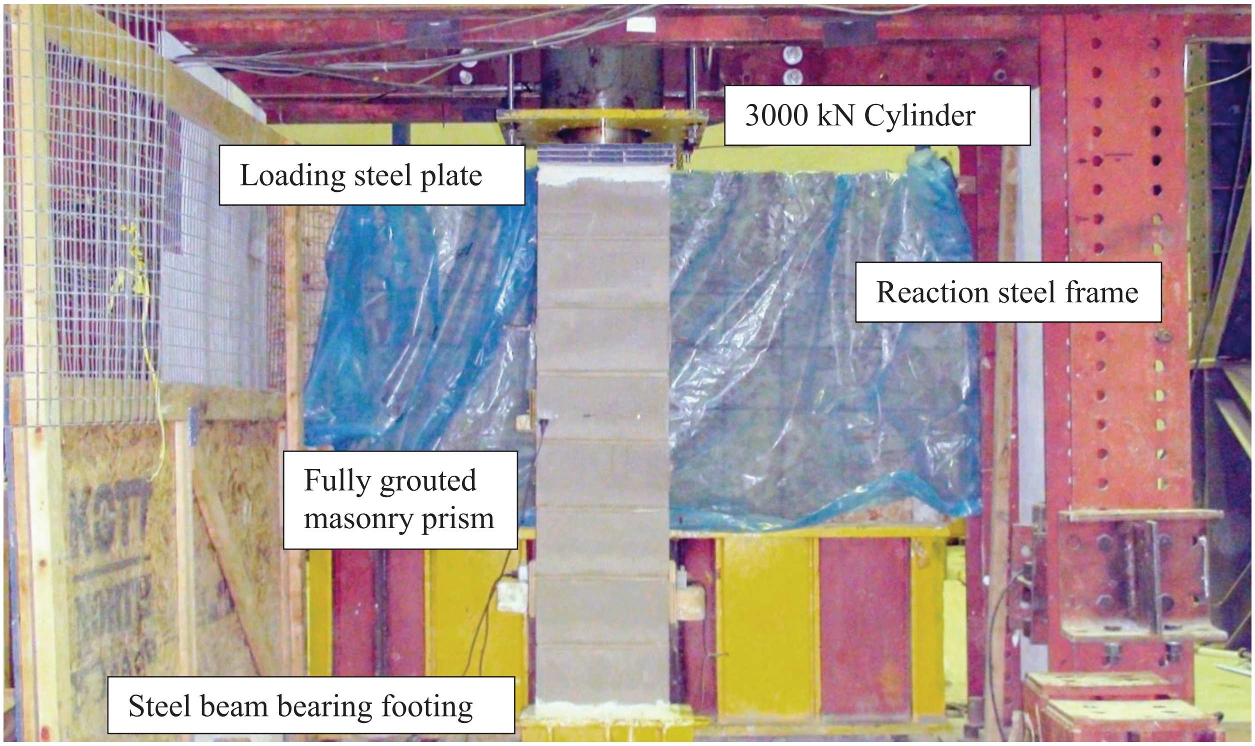

Figure 3.18: Typical uniaxial compression test setup for masonry prisms

The masonry compressive strength, f'_m, of each individual specimen was calculated as the maximum load divided by the effective cross-sectional area, A_e. The modulus of elasticity in compression normal to the bed joint, E_m, was measured over a stress range extending from 0.05

to 0.33 of the measured average prism compressive strength. Table 3.3 shows the prism compressive strength, f'_m, axial strain at maximum strength, ε_o, and modulus of elasticity, E_m, of all tested prisms. It is important to mention that one of the prisms in group G3-P4S was cracked when it was moved for testing. Therefore, the results of this prism were eliminated from Table 3.3.

Table 3.3: Test Results of Compression Prisms

Group ID	f'_m (MPa)	Avg. f'_m c.o.v. (%)	ε_o^* (mm/mm)	Avg. ε_o c.o.v. (%)	E_m / f'_m **	Avg. E_m / f'_m c.o.v. (%)
G1-P4R (typical standard test)	11.9	13.1 (7.6)	0.0028	0.0025 (11.4)	491	529 (17.4)
	12.6		0.0021		681	
	14.2		0.0023		550	
	14.0		0.0025		453	
	12.7		0.0027		473	
G2-P3S	13.4	13.4 (8.1)	0.0028	0.0025 (12.5)	650	606 (13.4)
	14.7		0.0022		512	
	12.7		0.0025		655	
G3-P4S	13.2	12.8 (7.4)	0.0022	0.0026 (12.0)	711	625 (12.8)
	11.7		0.0027		654	
	12.6		0.0029		614	
	13.9		0.0028		521	
G4-P8S	10.9	9.8 (10.7)	0.0026	0.0029 (9.9)	616	598 (4.9)
	8.9		0.0032		564	
	9.5		0.0029		613	

*Strain at maximum stress, f'_m.

** E_m, was measured over a stress range extending from 0.05 to 0.33 of f'_m.

3.3.6.1.1 Test results of G1-P4R: running bond prisms

Five URM prisms with a height-to-thickness ratio, *h/t*, equal to 4 were constructed in ½-½ running bond pattern using the same construction materials that were used to build the studied walls. The axial deformations were measured during testing using two displacement transducers (potentiometers) over a gauge length of 600 mm on both sides of the tested prism and recorded as well as the applied load continuously up to the failure point. Figure 3.19 shows the failure modes of the tested prisms. The average masonry compressive strength, f'_m, and the corresponding axial strain, ε_o, were measured as 13.1 MPa (c.o.v. = 7.6%) and 0.0025 (c.o.v. = 11.4%), respectively. Furthermore, the average modulus of elasticity, E_m, was calculated as 6.9 GPa (c.o.v. = 17.4%). Comparing the average experimental value of the modulus of elasticity, 6.9 GPa, which is equal to $529f'_m$, with the empirical value proposed by the Canadian standard for design of masonry structures CSA S304-14, $850f'_m$, shows that the Canadian standard overestimates the modulus of elasticity, E_m, of masonry. The stress-strain relationships for the tested prisms in group G1-P4R under the uniaxial compression test normal to the bed joint are presented in Figure 3.20.

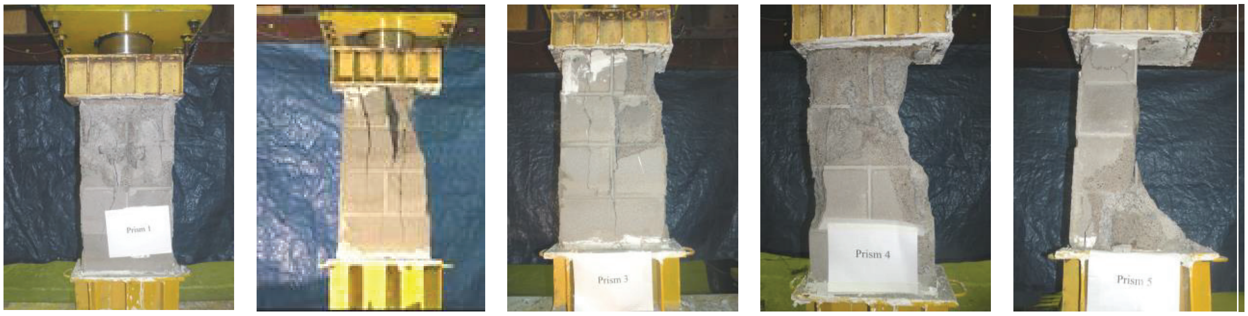

P4R-1 P4R-2 P4R-3 P4R-4 P4R-5

Figure 3.19: Failure modes for URM prisms in group G1-P4R

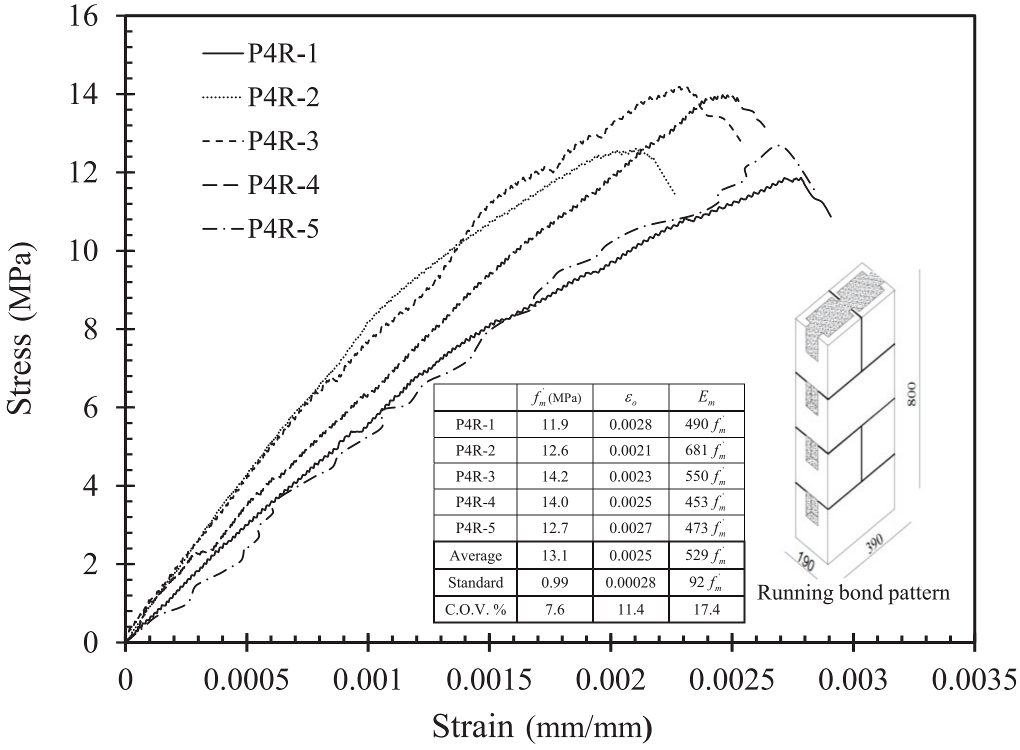

	$f_m^`$ (MPa)	ε_o	E_m
P4R-1	11.9	0.0028	490 $f_m^`$
P4R-2	12.6	0.0021	681 $f_m^`$
P4R-3	14.2	0.0023	550 $f_m^`$
P4R-4	14.0	0.0025	453 $f_m^`$
P4R-5	12.7	0.0027	473 $f_m^`$
Average	13.1	0.0025	529 $f_m^`$
Standard	0.99	0.00028	92 $f_m^`$
C.O.V. %	7.6	11.4	17.4

Figure 3.20: Compressive stress-strain relationship for typical standard URM prisms

3.3.6.1.2 Effect of bond pattern on the compressive strength of masonry prisms

To investigate the effect of bond pattern on the compression behaviour of masonry prisms, five prisms were constructed in group G3-P4S in the same manner as the prisms in group G1-P4R were built, except that a stack bond pattern was utilized in Group G3-P4S instead of the running bond pattern of group G1-P4R. One of the prisms in G3-P4S was cracked during moving the prisms. Therefore, the results of this prism were ignored. Figure 3.21 shows the damage at the end of the test for the prisms in group G3-P4S. As shown in Table 3.3, the average compressive strength, f'_m, the corresponding axial strain, ε_o, and the modulus of elasticity, E_m, were measured as 12.8 MPa (c.o.v. = 7.4%), 0.0026 (c.o.v. = 12.0%), and 8.0 GPa (c.o.v. = 12.8%), respectively. The stress-strain relationships for the tested prisms in group G3-P4S with stack bond are shown in Figure 3.22. Figure 3.23 shows a comparison between the average compressive stress-strain relationship of masonry prisms with stack and running bond pattern construction.

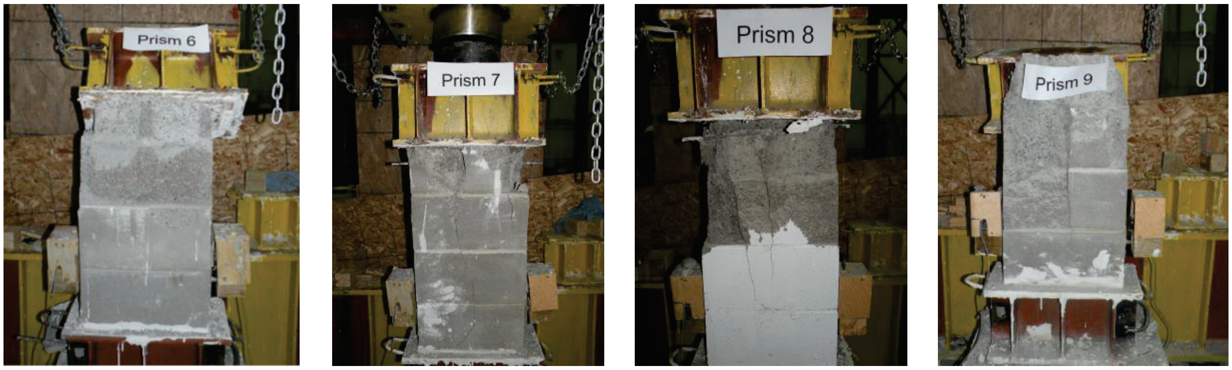
P4S-1 P4S-2 P4S-3 P4S-4

Figure 3.21: Failure modes for URM prisms in group G3-P4S

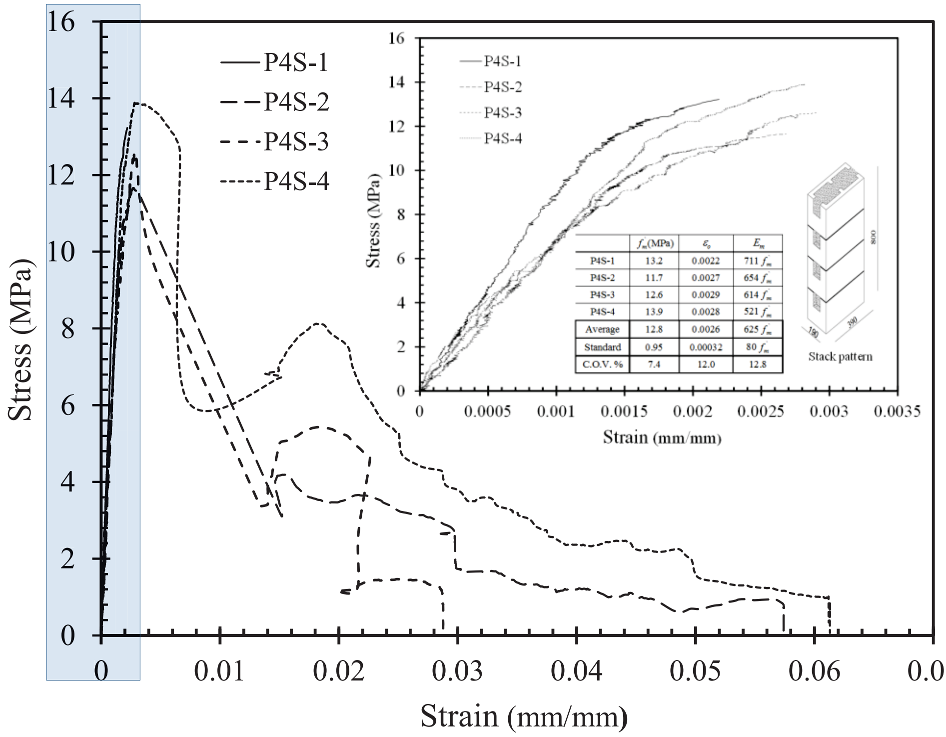

	f'_m(MPa)	ε_o	E_m
P4S-1	13.2	0.0022	711 f'_m
P4S-2	11.7	0.0027	654 f'_m
P4S-3	12.6	0.0029	614 f'_m
P4S-4	13.9	0.0028	521 f'_m
Average	12.8	0.0026	625 f'_m
Standard	0.95	0.00032	80 f'_m
C.O.V. %	7.4	12.0	12.8

Figure 3.22: Compressive stress-strain relationship for tested prisms in group G3-P4S

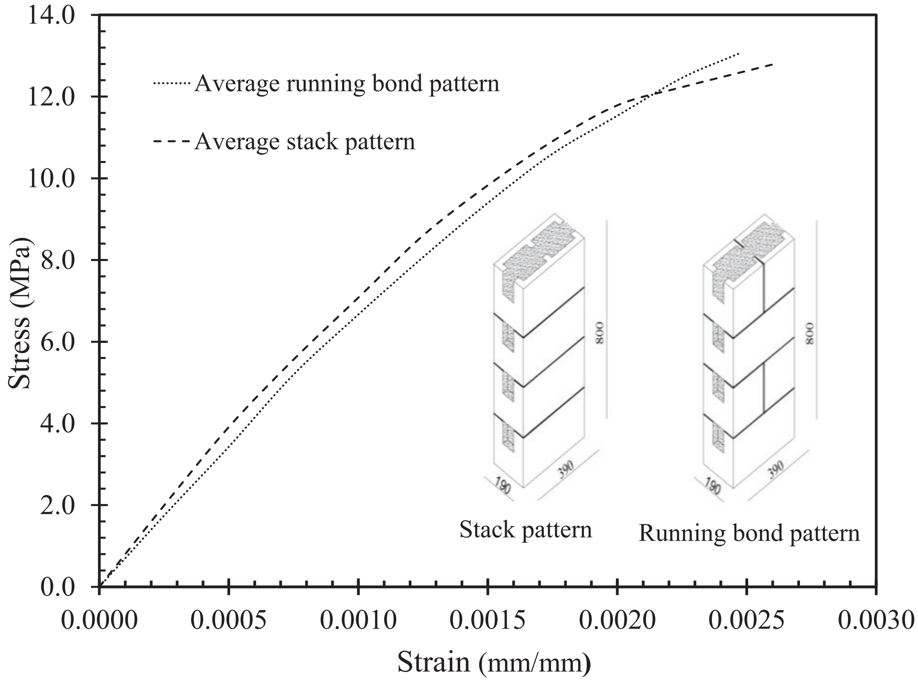

Figure 3.23: Average compressive stress-strain relationship of masonry prisms for different bond patterns

Based on the test results in Table 3.3 and as shown in Figure 3.23, the compressive behaviour of the two patterns is very close where the differences in the average compressive strength, f'_m, and the corresponding axial strain, ε_o, and the modulus of elasticity, E_m, were less than 15%. Shedid (2009) arrived at similar results by testing masonry prisms with different bond patterns. These results conclude that the bond pattern has no significant effect on the compressive strength of the masonry prism, f'_m. However, the bond pattern still has an effect on the overall behaviour of masonry walls.

3.3.6.1.3 Effect of height-to-thickness ratio (*h/t*)

In addition to the tested prisms in group G3-P4S with a height-to-thickness ratio, *h/t*, equal to 4, two others height-to-thickness ratios of 3 and 8 were considered in order to evaluate the effect of *h/t* on the compressive strength of masonry prism, f'_m. The tested prisms in group G4-P8S with a height-to-thickness ratio equal to 8 represent the full height of a vertical strip of the studied RM shear wall in this experimental program. Figure 3.24 shows the typical failure mode of the prisms in G4-P8S. The average compressive stress-strain relationship of masonry prisms with different *h/t* ratios can be seen in Figure 3.25. As can be observed from this figure, increasing the height-to-thickness ratio, *h/t,* results in a lower compressive strength of grouted prisms. As shown in Table 3.3, the values f'_m and E_m decreased from 13.4 MPa and 8.1 GPa, respectively, for *h/t* equal to 3 (group G2-P3S), to 9.8 MPa and 5.9 GPa for *h/t* equal to 8 (group G4-P4S), respectively. The Canadian standard CSA S304-14 considers this degradation in the masonry strength numerically by means of a correction factor related to the height-to-thickness ratio, *h/t*.

Figure 3.24: Typical failure mode for URM prisms in group G4-P8S with *h/t* equal to 8

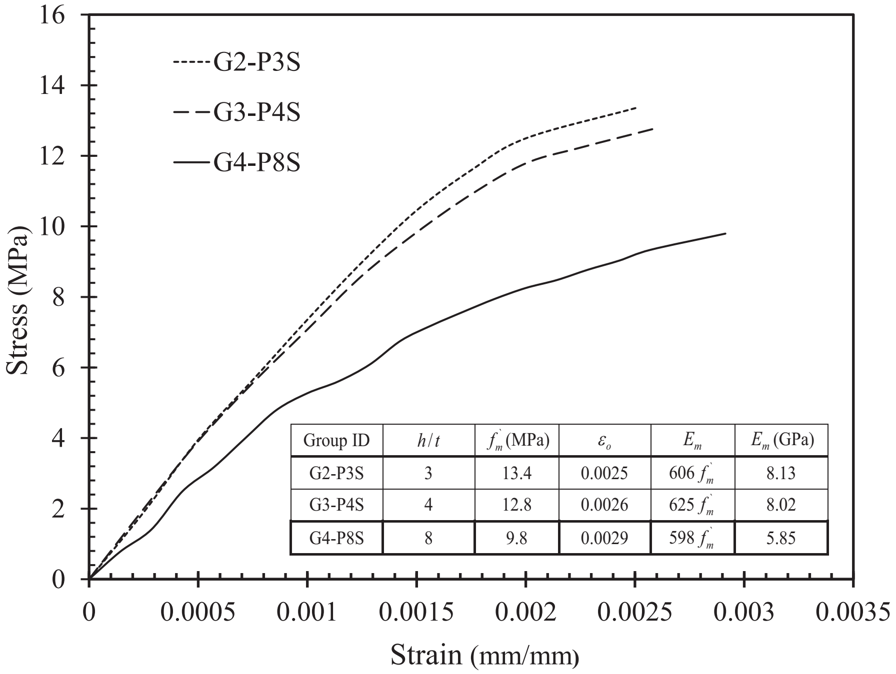

Group ID	h/t	$f_m^`$ (MPa)	ε_o	E_m	E_m (GPa)
G2-P3S	3	13.4	0.0025	$606\ f_m^`$	8.13
G3-P4S	4	12.8	0.0026	$625\ f_m^`$	8.02
G4-P8S	8	9.8	0.0029	$598\ f_m^`$	5.85

Figure 3.25: Average compressive stress-strain relationship of masonry prisms for different height-to-thickness ratios

The Canadian standard CSA S304.1-04 provides a correction factor for masonry compressive strength, f'_m, of 0.8, 0.9, and 0.95 for tested prisms with height-to-thickness ratio, *h/t*, equal to 2, 3, and 4, respectively. These values were further modified in the current version CSA S304-14 to be 0.85, 0.9, and 0.95 for the same *h/t* ratios, where linear interpolation may be used. Both versions CSA S304.1-04 and CSA S304-14 specified a limit on the height-to-thickness ratio, *h/t*, to a value of five, where at this ratio it is assumed that the end effects due to machine platens becomes small and that the failure pattern becomes similar to that of full story height walls. However, the CSA S304-14 mentioned that at higher *h/t* ratios the compressive strength might be decreased due to slenderness and that the designer can take this reduction into account. Figure 3.26 shows the given correction factors by the Canadian standards CSA S304.1-04 and CSA S304-14 versus the experimental results. The experimental values were calculated based on the assumption that the effect of the height-to-thickness ratio is limited to a value of eight using the following equation:

$$Correction\ factor = \frac{(f'_m)_{at\ h/t=8}}{(f'_m)_{at\ h/t\ lesst\ than 8}} \qquad \text{Eq. 3.3}$$

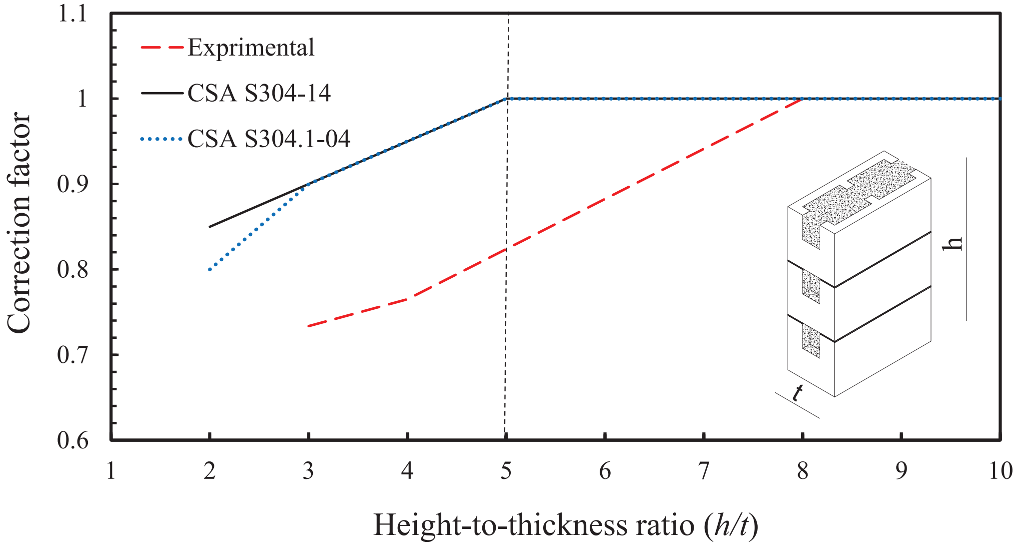

Figure 3.26: Masonry compressive strength correction factor for different masonry prisms height-to-thickness ratios, *h/t*

As can be seen in Figure 3.26, the correction factors obtained from these experimental results are less than the adopted values in the Canadian standards, which indicates that the correction factors in both the CSA S304.1-04 and CSA S304-14 overestimate the compressive strength of masonry at high values of *h/t* ratios. Liu (2012) arrived at similar conclusion by testing masonry prisms with different height-to-thickness ratios

3.3.6.1.4 Uniaxial compression test for grouted concrete masonry units

In addition to the compression tests for masonry prisms, five knock-out concrete masonry units were grouted and tested separately under axial compressive stress till failure. As can be observed from Figure 3.27, the typical failure mode of one grouted block was dominated by vertical cracking in the outside shells of the concrete block followed by a separation between the two cells. However, the two cores of grout did not experience any visible cracks or crushing. Comparing this failure mechanism with the failure mode of the prisms with *h/t* ratio equal to 4 (see Figure 3.19) indicates that testing one grouted block does not represent the real compressive behaviour of a masonry structural element under axial compression loads. This confirms the CSA S304-14 requirement for the minimum prism height of three courses. The average compressive strength, f'_m, the corresponding axial strain, ε_o, and the modulus of elasticity, E_m, were measured as 11.2 MPa (c.o.v. = 6.6%), 0.002 (c.o.v. = 11.0%), and 6.5 GPa (c.o.v. = 4.3%), respectively.

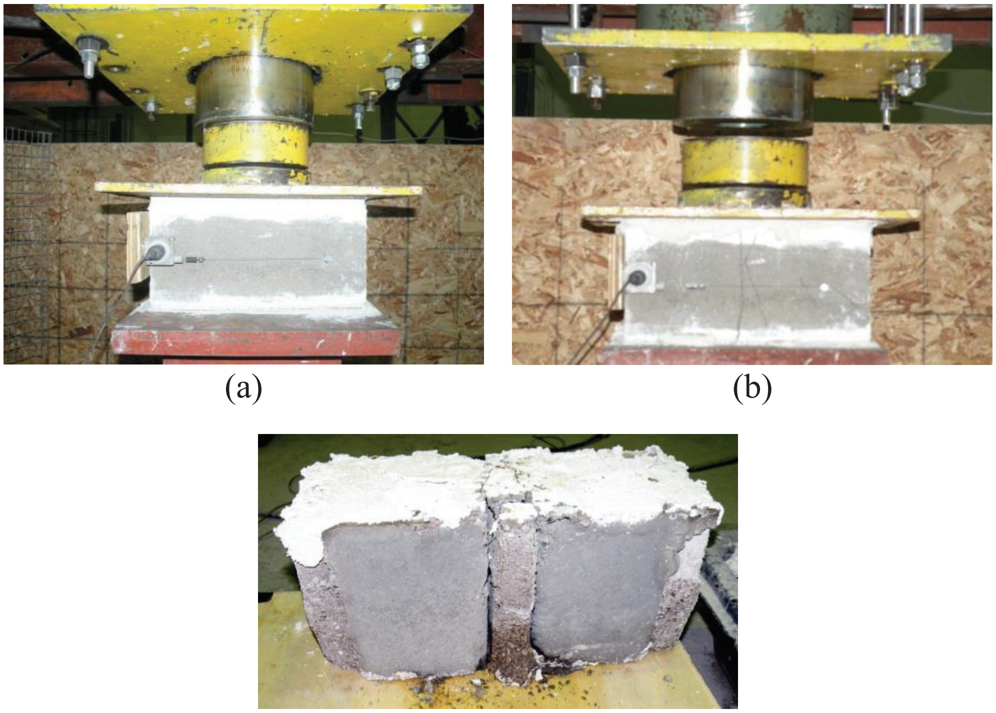
(a)

(b)

(c)

Figure 3.27: Uniaxial compression test for grouted concrete masonry unit: (a) prior to failure; (b) initiation of cracks; (c) after failure

3.3.7 IN-PLANE BEAM TESTS

In addition to the uniaxial compression tests, in-plane beam tests were carried out according to ASTM E518-10. Nine fully grouted masonry prisms were constructed using three different configurations as shown in Table 3.4. Three replicates of each beam configuration were tested in order to account for the variations in the properties of the masonry materials, namely: concrete block, mortar, and grout. All the tested prisms had the same dimensions of one unit in length with seven courses in height and were built with a stack bond pattern as shown in Figure 3.28. The beams BF200 and BF400 were designed to be dominated by flexural failure while the expected mode of failure for beam BS200-20M is shear failure. The flexural prisms were constructed without reinforcement in order to evaluate the flexural tensile strength of masonry, f_t (also called the modulus of rupture), and the maximum masonry tensile strain. On the other hand, the prisms BS200-20M were constructed with a vertical reinforcement of 2-20M, one in each cell, in order to increase their flexural capacity, hence forcing the prisms to fail in shear.

All the prisms were built and grouted at the same time as construction of the full-scale walls using the same construction materials. Later, the beam specimens were subjected to a four point loading test with a span-to-depth ratio of 3.0, higher than the minimum limit of 2.5 as described in ASTM E518-10. Figure 3.28 presents the typical in-plane masonry beam test setup. As shown in this figure, three cable-extension transducers (potentiometers) were used to measure the vertical displacements and were attached to the centre of the three middle courses, respectively. The load was applied at a constant rate such that the total load was applied in not less than 1.0 nor more than 3.0 min.

Table 3.4: Configurations of In-Plane Masonry Beam Prisms

Beam ID*	Number of tested beams	L_1 mm	A_s	Expected mode of failure
BF200	3	200	----	Flexural
BF400	3	400	---	Flexural
BS200-20M	3	200	2-20M	Shear

* B = Beam
F,S = Failure mode; flexural or shear
200, 400 = shear span value

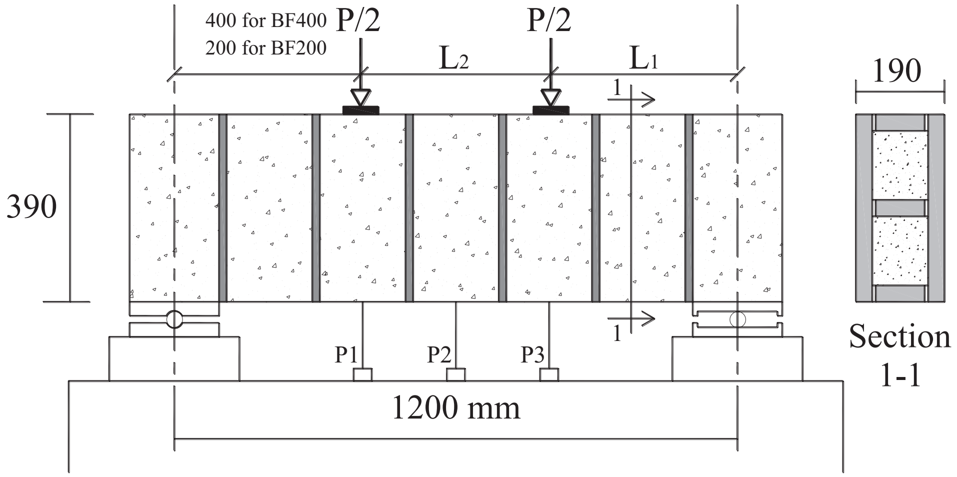

Figure 3.28: Test setup for in-plane masonry beam prisms

The maximum flexural tensile stress, f_t, was calculated using Eq. 3.4, according to ASTM E518-10. The weight of the tested masonry beams was ignored in the calculations since it is negligible compared to the applied load.

$$f_t = \frac{3\, P_{max}\, L_2}{b\, h^2} \qquad \text{Eq. 3.4}$$

where:

f_t = maximum flexural tensile stress, MPa

P_{max} = maximum applied load indicated by the testing machine, N

L_1 = shear span, mm = $(1200 - L_2)/2$

b = beam width, mm = 190 mm

h = beam height, mm = 390 mm

The curvature in the pure flexural zone was measured using the vertical displacement readings from the potentiometers P1, P2, and P3 as shown in Figure 3.28. Figure 3.29 and (Eqs. 3.5 to 3.9) present the steps suggested by Haach (2009) for calculating the masonry flexural mechanical properties.

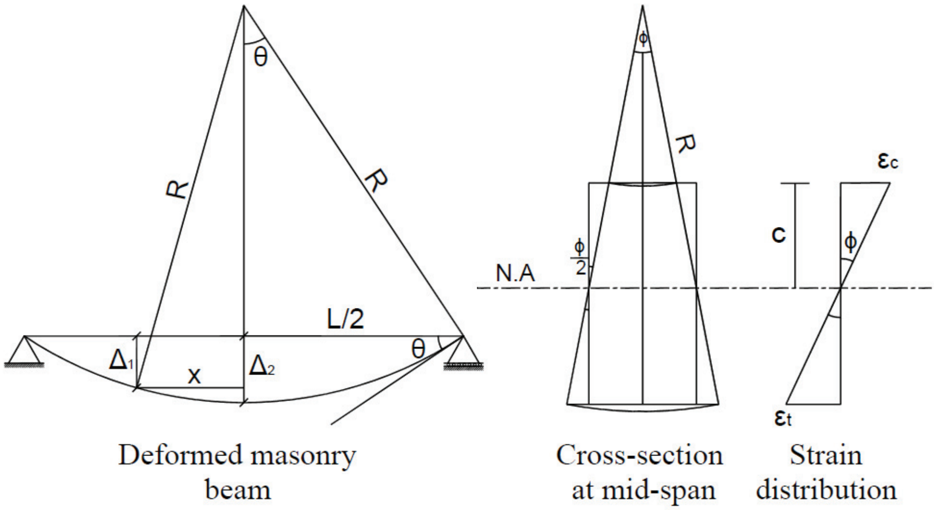

Figure 3.29: Deformed masonry beam prism under in-plane loading

$$f = \frac{3\,P\,L_2}{b\,h^2} \qquad \text{Eq. 3.5}$$

$$R = \frac{x^2 + (\Delta_2 - \Delta_1)^2}{2\,(\Delta_2 - \Delta_1)} \qquad \text{Eq. 3.6}$$

$$\phi = \frac{1}{R} \qquad \text{Eq. 3.7}$$

$$\varepsilon = \phi c = \frac{\phi h}{2} \qquad \text{Eq. 3.8}$$

$$E_{m,f} = \frac{f}{\varepsilon} \qquad \text{Eq. 3.9}$$

where:

Δ_l = average of displacement readings of P1 and P3, mm

ϕ = curvature in the pure bending zone, 1/mm

ε = strain at the extreme tensile fibers

3.3.7.1 In-plane beam flexural test

Table 3.5 and Figure 3.31 show the flexural test results for the in-plane masonry beam prisms BF200 and BF400. The prisms with a shear span of 200 mm, BF200, reached an average maximum load and deflection at mid-span of 83.8 kN (c.o.v. = 9.7%) and 1.27 mm (c.o.v. = 12.32%), respectively, compared to 44.8 kN (c.o.v. = 7.9%) and 0.65 mm (c.o.v. = 4.74%) for the prisms with a shear span of 400, BF400. The average flexural tensile strength, f_t , for the six beams was measured as 1.80 MPa (c.o.v. = 9.5%) with a corresponding average maximum tensile strain of 0.00046 (c.o.v. = 13.3%).

Comparing the experimental value of the average flexural tensile strength, 1.80 MPa, with the value proposed by the Canadian standard for design of masonry structures, CSA S304-14, for grouted hollow block, 0.65 MPa, shows that the Canadian standard underestimates the flexural tensile capacity of masonry. In fact, the experimental results seems to be closer to the value suggested by the Canadian standard for design of concrete structures, CSA A23.3-14, with some modifications to accommodate fully grouted masonry concrete blocks as follows:

$$f_t = 0.6\lambda_{ge}\sqrt{f'_g} \qquad \text{Eq. 3.10}$$

where;

f_t = flexural tensile strength of masonry, MPa

λ_{ge} = factor to account for the effective cross-sectional area of grout,

$$= A_{grout}/A_{gross}$$

f'_g = compressive strength of grout, MPa

In Eq. 3.10, the compressive strength of concrete, f'_c, is replaced by the compressive strength of grout, f'_g. In addition, a new factor is introduced, λ_{ge}, to account for the effective cross-sectional area of grout. This equation could be explained by observing the failure modes of the tested beam prisms as shown in Figure 3.31. As can be seen in this figure, the grout is the main contributor to the tensile strength of grouted masonry, while the contribution of the masonry block and mortar can be neglected.

Table 3.5: Flexural Test Results of Masonry Beam Subjected to In-Plane loading

Beam ID	P_{max} kN	Δ_{max} mm	θ_{max} rad	ϕ_{max} 1/mm ($\times10^{-6}$)	f_t MPa	ε_t ----
BF200-1	94.6	1.16	0.0015	2.5	1.96	0.00048
BF200-2	81.2	1.44	0.0014	2.3	1.69	0.00044
BF200-3	75.7	1.19	0.0011	1.8	1.57	0.00035
BF400-1	41.0	0.69	0.0016	2.7	1.70	0.00052
BF400-2	48.0	0.63	0.0014	2.3	1.99	0.00044
BF400-3	45.4	0.64	0.0015	2.5	1.89	0.00049
Average			0.0014	2.3	1.80	0.00046
Standard			0.00019	0.31	0.17	6.1×10^{-5}
C.O.V. %			13.3	13.3	9.5	13.3

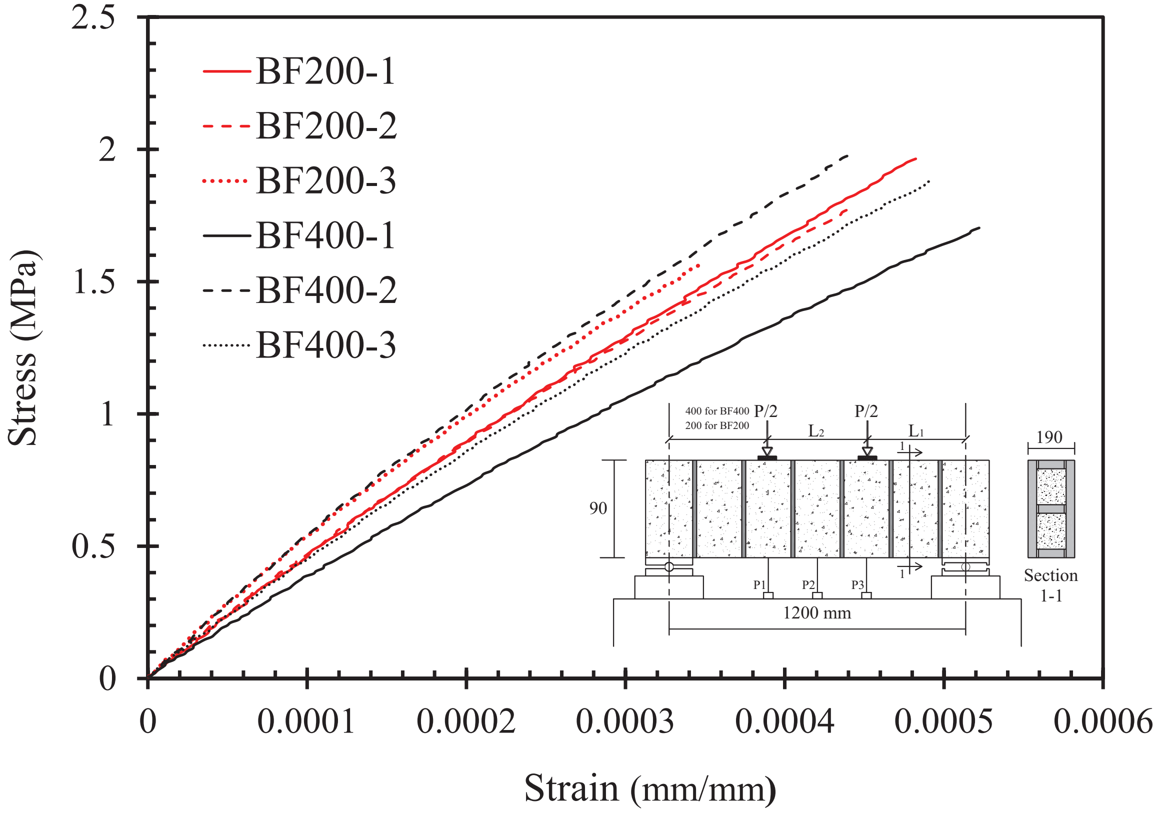

Figure 3.30: Stress-strain relationships at mid-span section of masonry beam prisms under in-plane flexural test

Applying the measured compressive strength of the grout, 29.4 MPa, as presented in section 3.3.4, and λ_{ge} of 0.46 in Eq. 3.10 will provide an expected flexural tensile strength, f_t , of 1.5 MPa. This proposed equation is still more conservative than the experimental results because of neglecting the contribution of the masonry concrete block and mortar, as well as the confinement action of the concrete block to the grout. Further experimental work is needed to consider more variations such that the proposed equation (Eq. 3.10) can be verified.

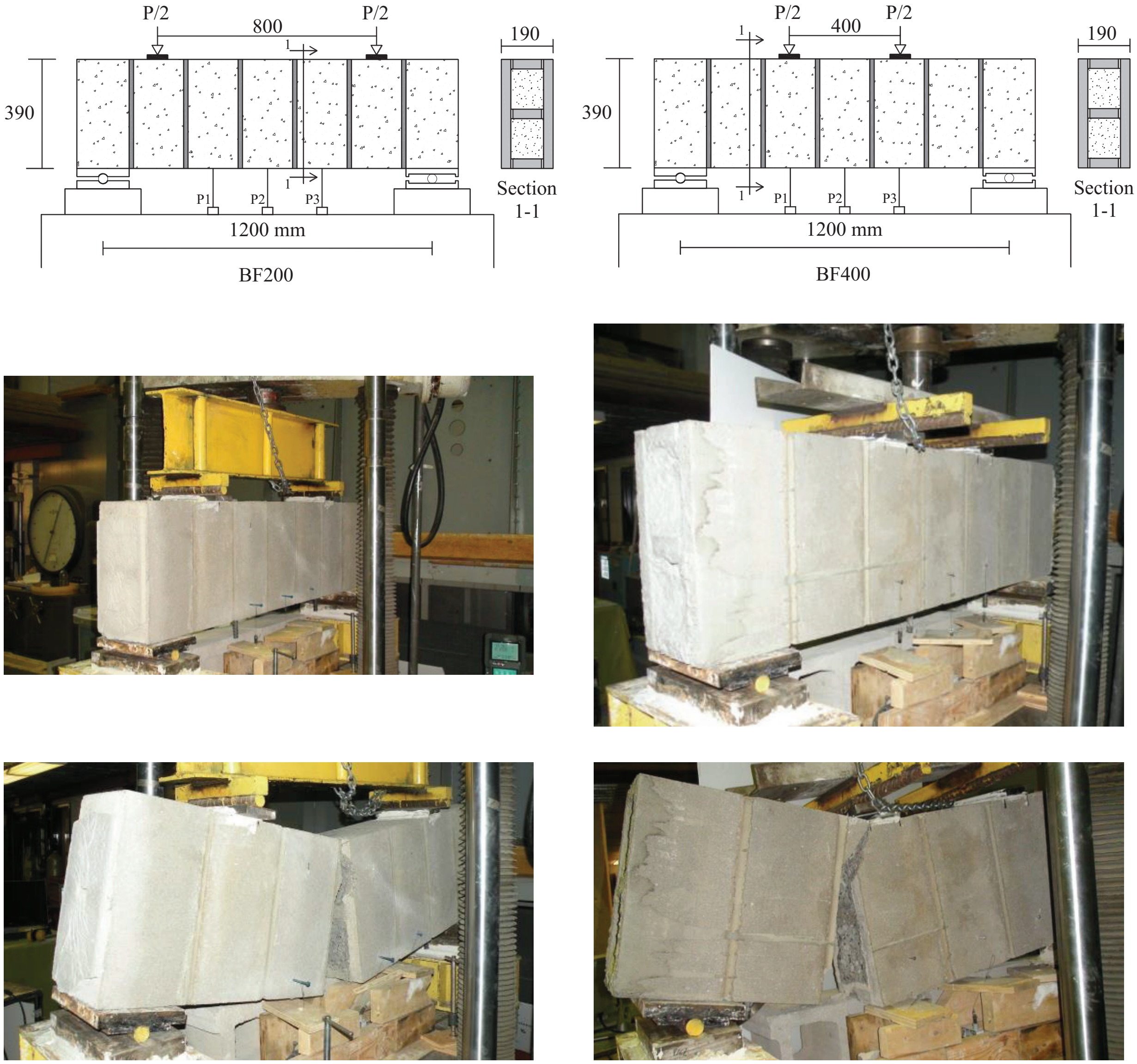

(a) (b)

Figure 3.31: In-plane beam flexural test: (a) BF-200 mm shear span; (b) BF-400 mm shear span

3.3.7.2 In-plane beam shear test

Three reinforced masonry prisms were constructed with a vertical reinforcement of 2-20M, one in each cell, to increase their flexural capacity. The beams BS200-20M were tested with a shear span of 200 mm in order to have a diagonal shear failure. Figure 3.32 shows the configuration of the tested beams in addition to the typical mode of failure. Adding the 2-20M vertical reinforcement increased the average maximum load from 83.8 kN (c.o.v. = 9.7%) for beams BF200, to 331 kN (c.o.v. = 11.7%) for beams BS200. The average deflection at the mid-span corresponding to the maximum load was measured as 5.56 mm (c.o.v = 7.2%). Figure 3.33 shows the load-deflection relationships at the mid-span section for the three tested beams.

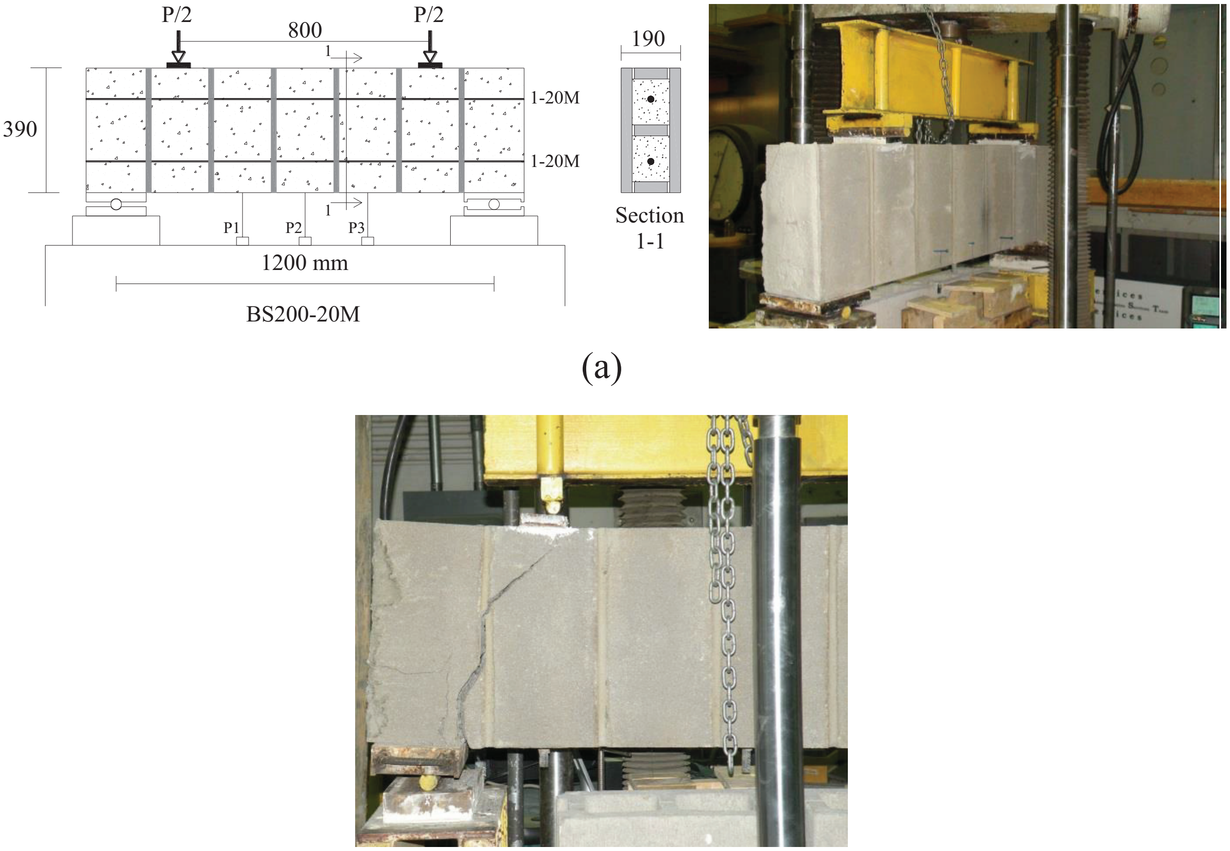

(a)

(b)

Figure 3.32: In-plane beam shear test: (a) test setup; (b) typical mode of failure

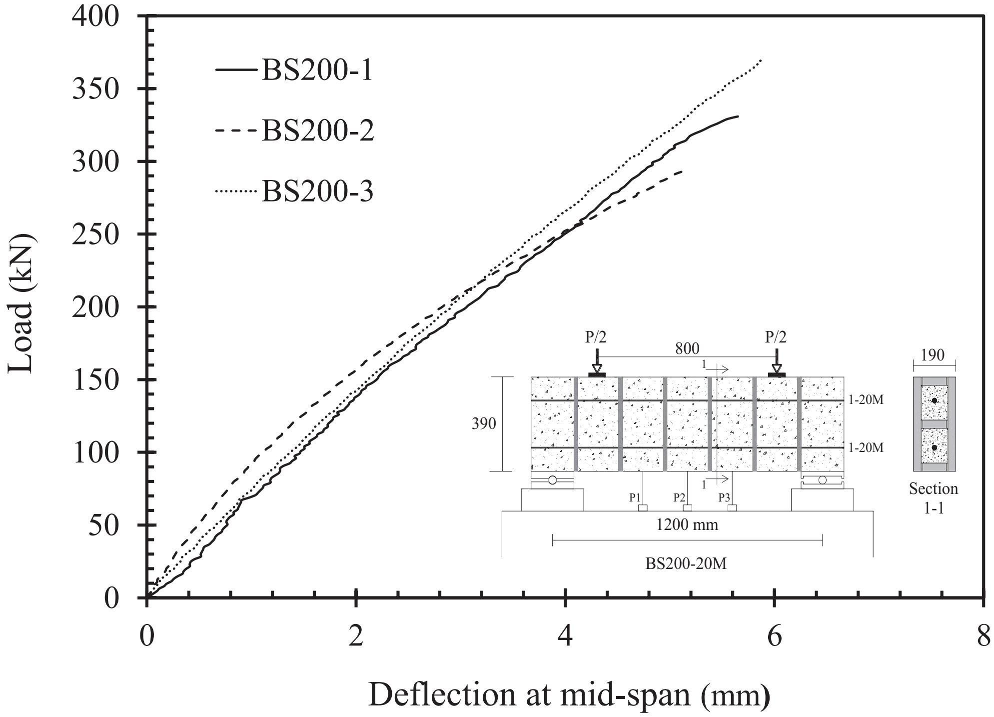

Figure 3.33: Load-deflection relationship at mid-span section of masonry beam prisms under in-plane shear test

3.3.8 SUMMARY OF MATERIAL PROPERTIES

Characterizing the mechanical properties of the masonry constituent materials and assemblies is essential for understanding the behaviour of reinforced masonry shear walls under in-plane loading, and for proper analyses of the experimental and numerical results. Section 3.3 has provided a detailed characterization of the mechanical behaviour of reinforced masonry shear wall components, namely: knock-out concrete block, mortar, grout, and steel reinforcement in addition to masonry prisms. Table 3.6 summarizes the mechanical properties of the materials used to construct the tested RM shear walls. All the properties were determined from standardized testing methods that are given in the same table. Based on the auxiliary laboratory test results in this section, a new equation was proposed for the masonry flexural tensile strength, f_t , of grouted masonry structural element. This equation is similar to the suggested one by the Canadian standard for design of concrete structures, CSA A23.3-14, with some modification to consider the contribution of the grouted area. Further experimental work is needed for verification of this proposed equation.

Table 3.6: Summary of Material Mechanical Properties

Material	Characteristic	Strength (C.O.V.)	Reference
Type S mortar	Cube compressive strength, f'_{mo}	7d- 8.5 MPa (8.8%) 28d- 13.7 MPa (7.8%)	CSA A179-04
	Flow Table Test	112.16% (3.8%)	ASTM C1437-13
Knock out concrete block	Weight	12.9 kg (3.1%)	-----
	Block compressive strength, f'_b	16.7 MPa (4.8%)	CSA A165.1-14
Footing Concrete	Cylinder compressive strength ,	7d- 30.5 MPa (5.1%) 28d- 39.5 MPa (6.6%)	ASTM C39M-12
	Splitting tensile strength, f_r	28d- 4.2 MPa (4.4%)	ASTM C496M - 11
Coarse grout	Cylinder compressive strength, f'_g	7d- 21.6 MPa (8.4%) 28d- 29.4 MPa (7.3%)	ASTM C476-10 CSA A179-04
Steel reinforcement	Yield strength, f_y	430 MPa (3.2%)	ASTM A615M-13 A370-14
	Modulus of Elasticity, E_s	196 GPa (1.85%)	
	Ultimate strength	536 MPa (2.7%)	
4-course running bond prism	Prism Compressive strength , f'_m	13.1 MPa (7.6%)	ASTM C1314-12 CSA S304-14
	Axial strain at maximum strength, ε_o	0.0025 (11.4%)	
	Modulus of elasticity, E_m	6.9 GPa (17.4%)	
7-course stack bond beam	Prism tensile strength , f_t	1.8 MPa (9.5%)	ASTM E518-10 CSA S304-14
	Tensile strain at maximum strength, ε_t	0.00046 (13.3%)	

3.4 TEST SETUP

All the studied walls were tested under in-plane loads. Three MTS hydraulic actuators with a maximum capacity of 1000 kN and a maximum displacement stroke of ± 200 mm each were used to apply the loads as shown in Figure 3.34. Two actuators were installed vertically and were used to apply the axial compression force and the top moment (when applicable) that act on the top of the wall. The cyclic in-plane horizontal displacements were applied using the horizontal actuator. The RC base foundation of the wall specimens was connected to a strong floor using a

RC footing with a depth of 600 mm to provide a fixed constraint condition at the base of the tested walls. All the loads were transferred to the tested walls through a stiff built-up steel loading beam. The vertical reinforcement of the studied walls was anchored to the bottom flange of the loading beam as shown in Figure 3.35. The three actuators were synchronized to apply the shear force, axial load and top moment that represent the acting loads on the plastic hinge panel of the whole RM shear wall. Two out-of-plane steel back-to-back angles connected the loading steel beam (through slotted holes) to a strong-resistance concrete wall to prevent any out-of-plane displacement (see Figure 3.36).

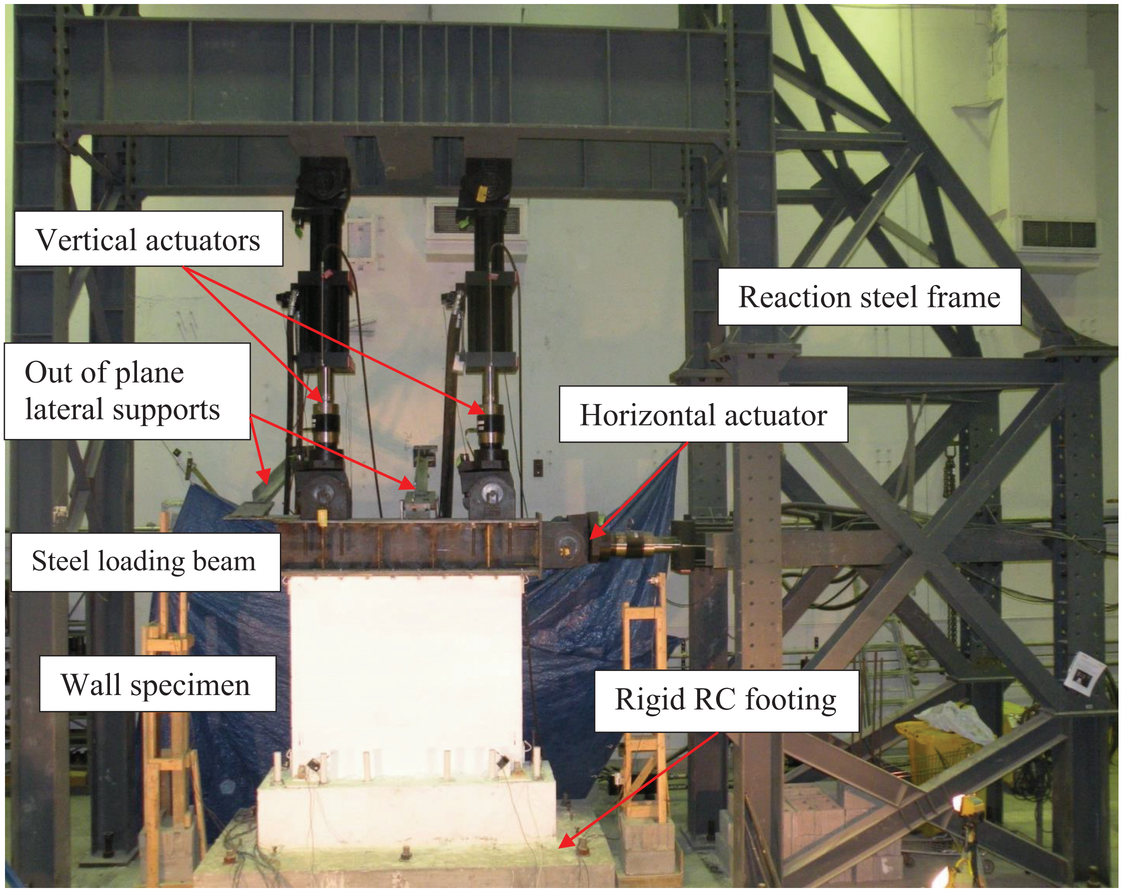

Figure 3.34: Test setup for RM shear wall

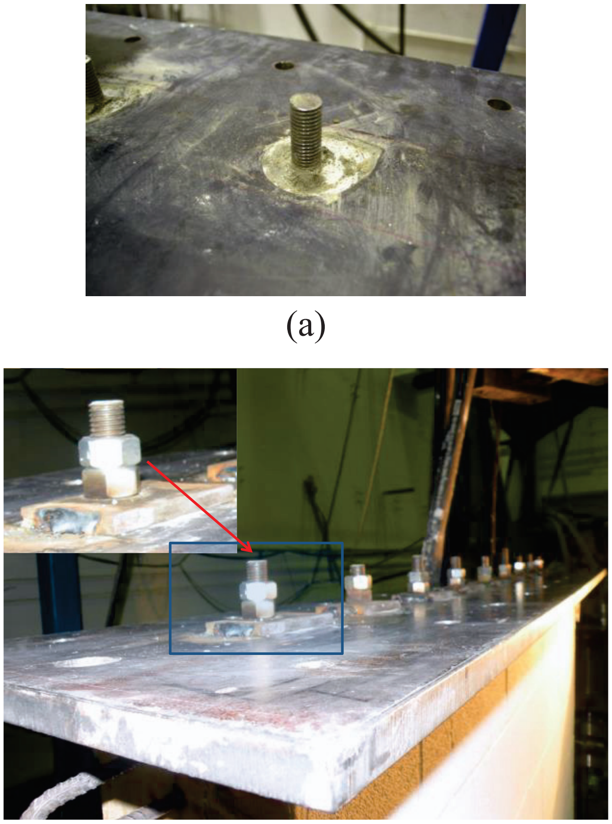
(a)

(b)

Figure 3.35: Connection between the tested RM shear walls and bottom flange of the loading steel beam: (a) hole filled with strong mortar; (b) anchorage

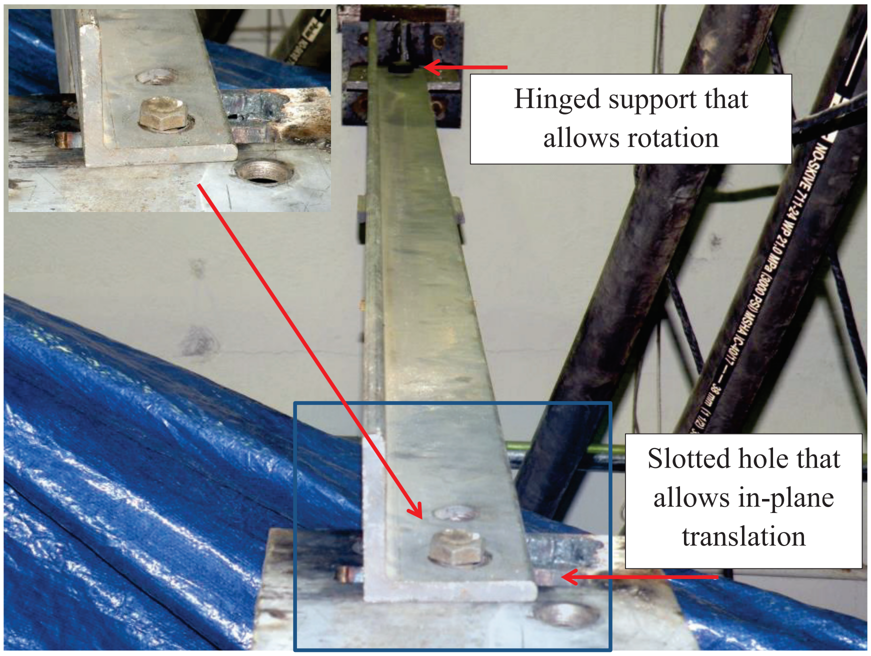

Figure 3.36: Out-of-plane lateral support

3.5 INSTRUMENTATION AND TESTING PROTOCOL

Two different types of instruments were used to monitor the deformations of the tested walls. Nine potentiometers were attached externally to each of the tested RM shear walls to measure the horizontal, vertical, and diagonal displacements as shown in Figure 3.37. The target displacement was measured as the difference between the average reading of P2 and P9 and the movement in the base foundation, P8, if any. The shear sliding displacement was calculated as the difference in the readings between P3 and P8. Potentiometers P4 and P7 were attached to the tested wall to measure the flexural tensile and compressive deformations, while P5 and P6 were used to measure the overall diagonal shear deformations. P1 was attached to the top loading steel beam to monitor any sliding between the loading beam and the tested wall.

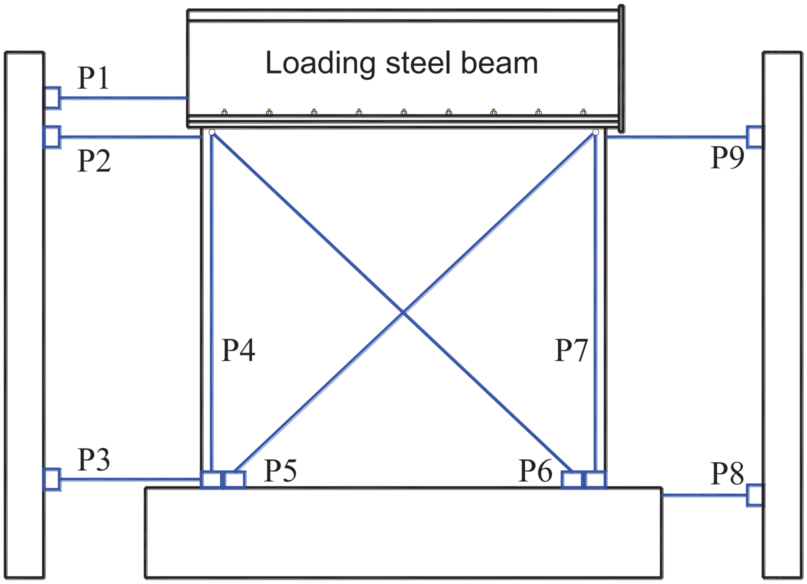

Figure 3.37: Location of displacement potentiometers

In addition to the potentiometers, 5 mm strain gauges were attached to the steel reinforcement bars to record the local strains during loading of the walls as shown in Figure 3.38. Four strain gauges were installed at the wall-footing interface of the two outermost vertical reinforcement bars on each side, to define the yield load. To measure the axial strain distribution in the horizontal reinforcement, five-5 mm strain gauges were installed and equally distributed along the total length of each bar. Using the experimentally measured stress-strain relationship and the cross-section area for the steel reinforcing bars, the average tension force in each bar was calculated to measure the horizontal reinforcement contribution, V_s, to the in-plane shear strength, V_n, as will be discussed in Section 4.3.1.1

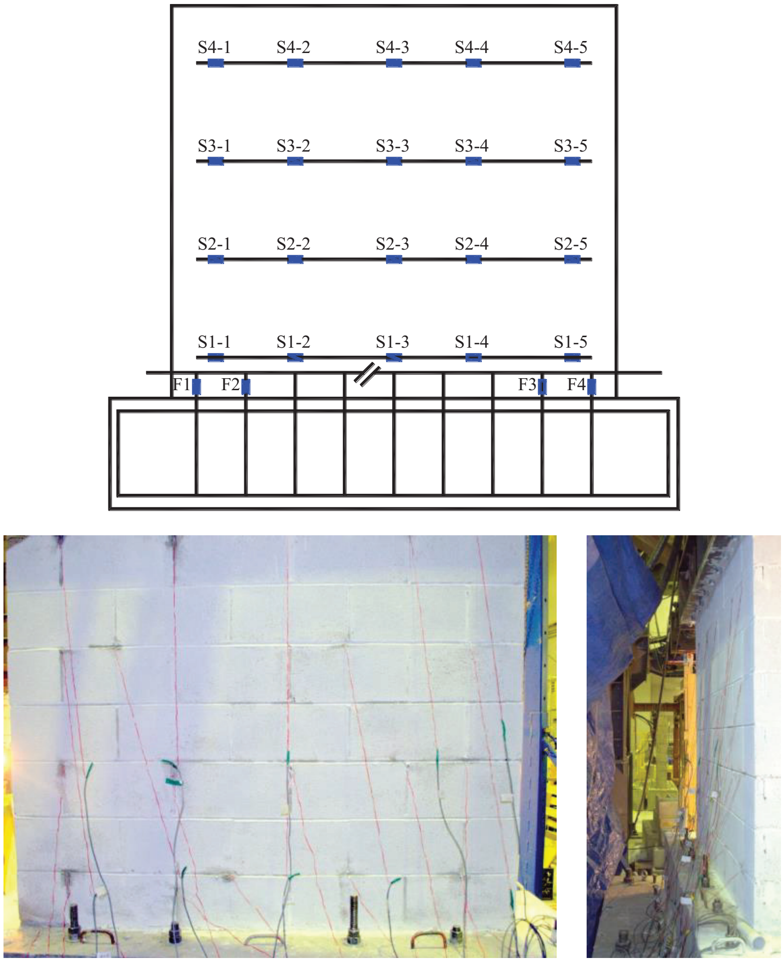

Figure 3.38: Location of strain gauges

The loads were applied in two phases. In the first phase, the total vertical compression load was applied using load-control protocol. The readings of the potentiometers P4 and P7 and the strain gauges attached to the vertical reinforcement were used to calculate the masonry modulus of elasticity, E_m. It was then compared to the value measured from the axial/flexure tests of the masonry prisms/beams, respectively. Next, the test protocol was switched to displacement-control. In this second phase, in-plane lateral displacements were introduced at the mid-height of the loading steel beam, according to the loading histories proposed by FEMA 461 (2007) (see Figure 3.39). In each stage of lateral loading, two displacement cycles were completed for each target displacement increment. The yield load was determined when the strain gauge located at the wall-footing interface reached the yield strain level. Failure was defined as the point on the loading curve where the lateral resistance dropped to 80% of the maximum lateral load recorded, in whichever direction this first occurred. Consequently, the displacement capacity $\Delta_{0.8Que}$ and the displacement ductility $\mu_{\Delta 0.8Que}$ were measured at the failure point.

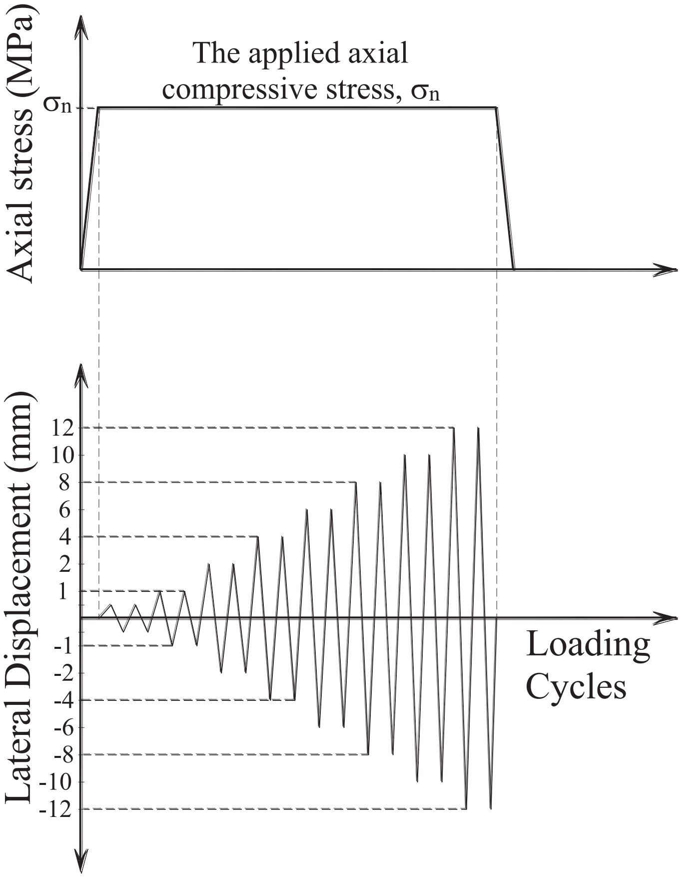

Figure 3.39: Loading procedure

CHAPTER 4

EXPERIMENTAL RESULTS

4.1 INTRODUCTION

Throughout the experimental work, nine single-story reinforced masonry (RM) shear walls were tested to investigate their in-plane shear behaviour. The effects of several parameters were considered in the test matrix, namely: horizontal reinforcement ratio, ρ_h, level of the axial compressive stress, σ_n, shear span to depth ratio, M/Vd_v, horizontal reinforcement anchorage end detail, vertical spacing of horizontal reinforcement, S_v, and horizontal spacing of vertical reinforcement, S_h. This chapter provides a detailed discussion of the test results and observations made during the experimental testing of the nine RM shear walls. The following section provides a summary of the measured lateral strength and displacements in addition to the lateral force-displacement hysteresis and failure modes for all walls.

As an example, a detailed analysis of the results of the reference wall W-Ref, including aspects related to force-based, displacement-based, and performance-based design approaches, is given in Section 4.3. This is followed by a separate discussion on the influence of each parameter on these three different design approaches. The last section provides more discussion and proposes equations for the in-plane lateral stiffness degradation, equivalent viscous damping, and effective stiffness for seismic calculations. Most of the current design standards for masonry structures classify RM shear walls according to their ductility in terms of a ductility-related seismic force modification factor, R_d. The test results showed that the wall effective elastic stiffness has a direct impact on the relation between the experimental displacement ductility, $\mu_{\Delta e}$, and R_d.

4.2 GENERAL TEST RESULTS RELATED TO LATERAL FORCE-DISPLACEMENT RESPONSE

This section presents general test results, including the generated hysteretic loops for each wall, in addition to a summary of the recorded strength and displacements properties. The experimental measurements for strength, displacements, and ductility are defined as follows:

Δ_{ye} = lateral yield displacement, it was taken as the average between the top lateral displacements that are corresponding to the first yield in the vertical reinforcement in each direction;

Q_{ye} = lateral yield force, was defined at the lateral yield displacement, Δ_{ye}, on the backbone curve;

Q_{ue} = peak lateral force;

Δ_{Que} = lateral displacement at the peak lateral force, Q_{ue};

$\Delta_{0.8Que}$ = lateral displacement defined at a drop in wall capacity to 80% of Q_{ue};

$\mu_{\Delta Que}$ = lateral displacements ductility at peak force;

$\mu_{\Delta 0.8Que}$ = lateral displacements ductility at a drop in wall capacity to 80% of Q_{ue}; and

$\mu_{\Delta e1\%}$ = lateral displacements ductility corresponding to the top drift of 1.0%

The test results indicated that all tested walls exhibited shear dominated response with diagonal cracks as shown in Figure 4.1. Figure 4.2 presents the hysteretic force-displacement response for each wall against the top drift. The variation in the lateral force-displacement envelopes for all walls due to the influence of the studied parameters is given in Figure 4.3. Table 4.1 and Table 4.2 summarize the force-based results for tested walls in push and pull directions, respectively, including the crack, yield, and ultimate capacities in addition to the top drift of 1%. As shown in these tables and Figure 4.3, all tested walls had a similar behaviour in both push and pull directions with a general symmetric resistance. Thus, only the results in the push direction were considered for the evaluation of the studied parameters.

W-Ref W-ρ_h0

W-σ_n0 W-σ_n1.5

Figure 4.1: Crack pattern of tested walls at failure in push direction

W-M/Vd_v1.8

W-90°

W-Str

W-S_v800

W-S_h800

Figure 4.1(continued): Crack pattern of tested walls at failure in push direction

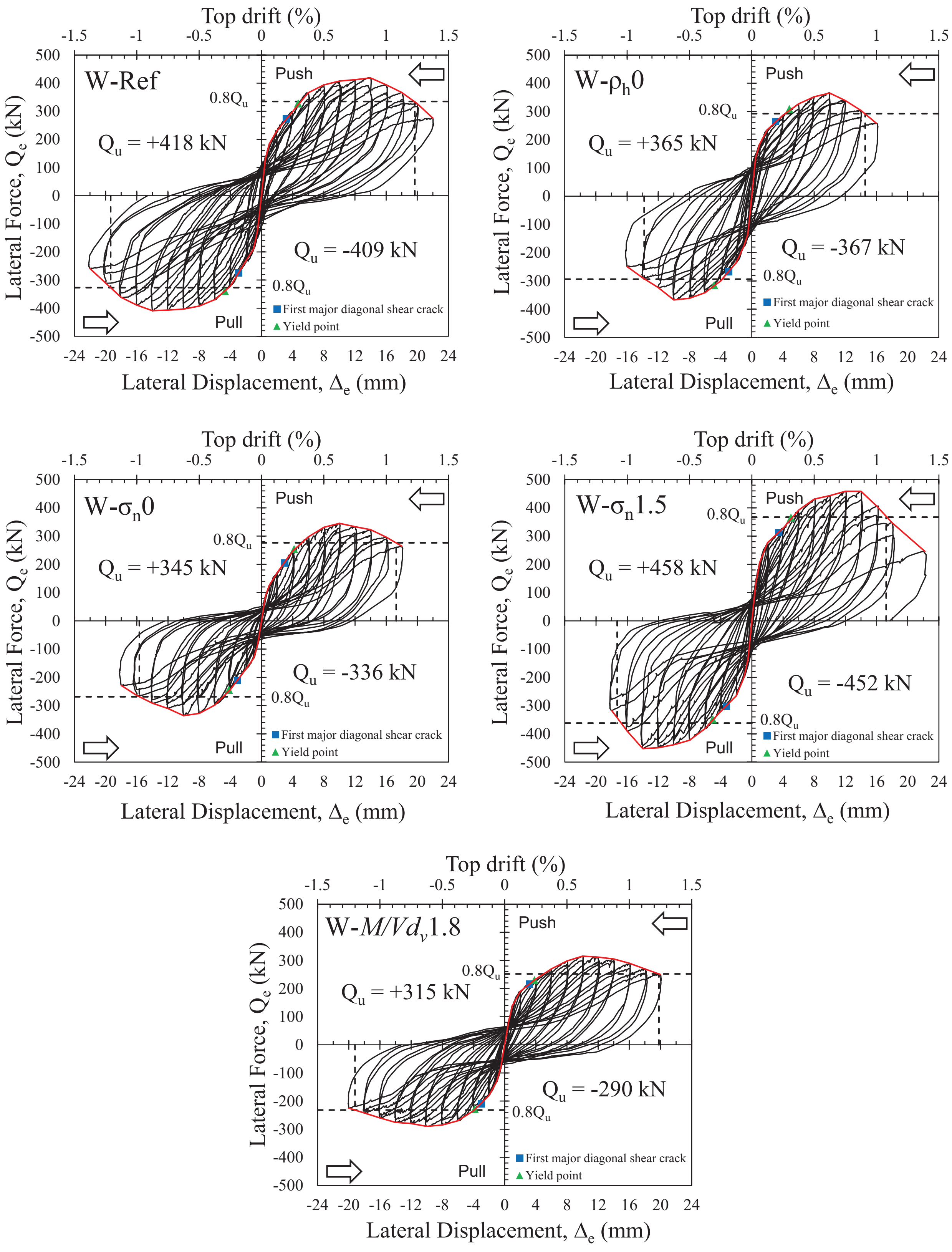

Figure 4.2: Hysteretic force-displacement response of tested walls

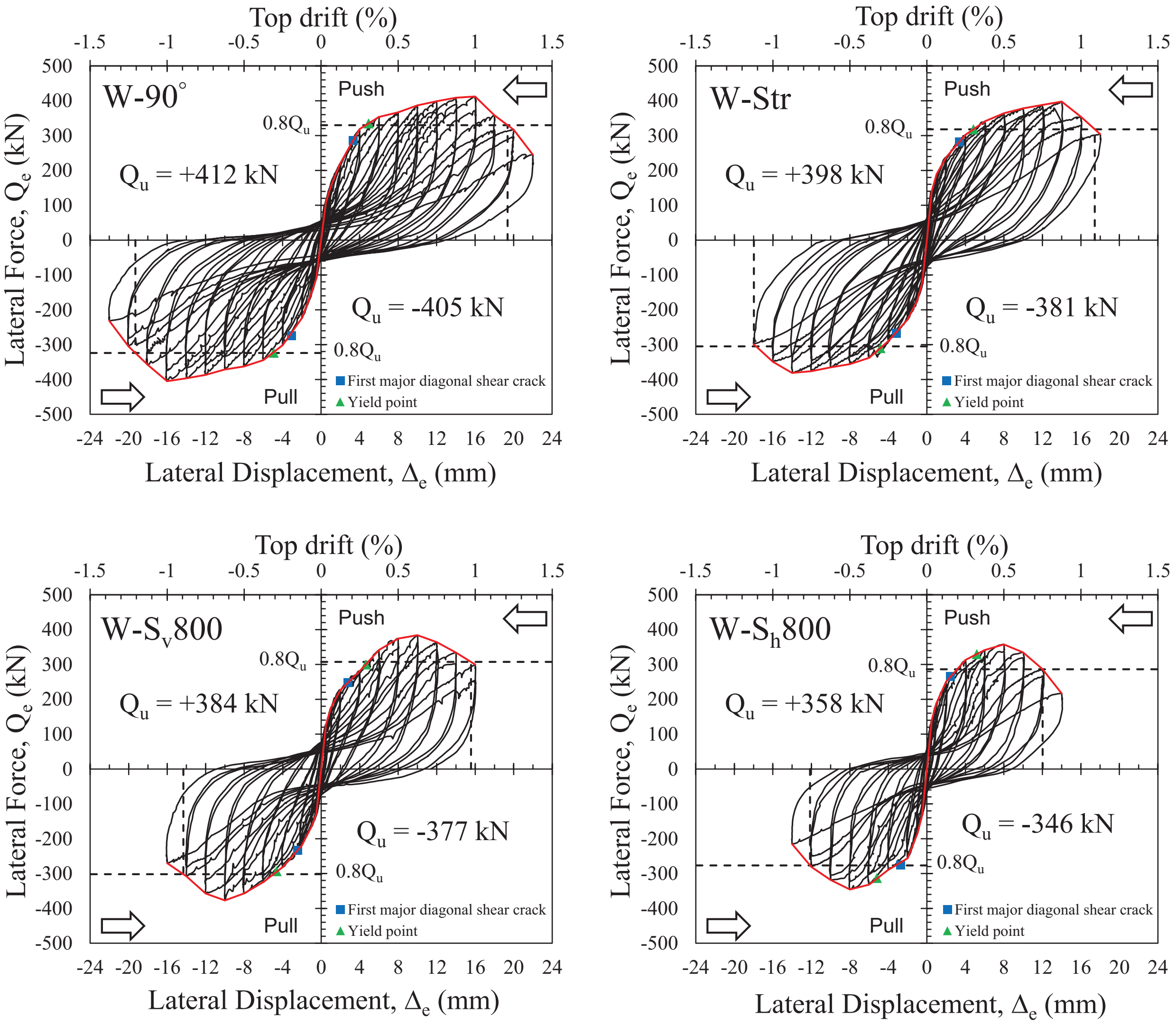

Figure 4.2(continued): Hysteretic force-displacement response of tested walls

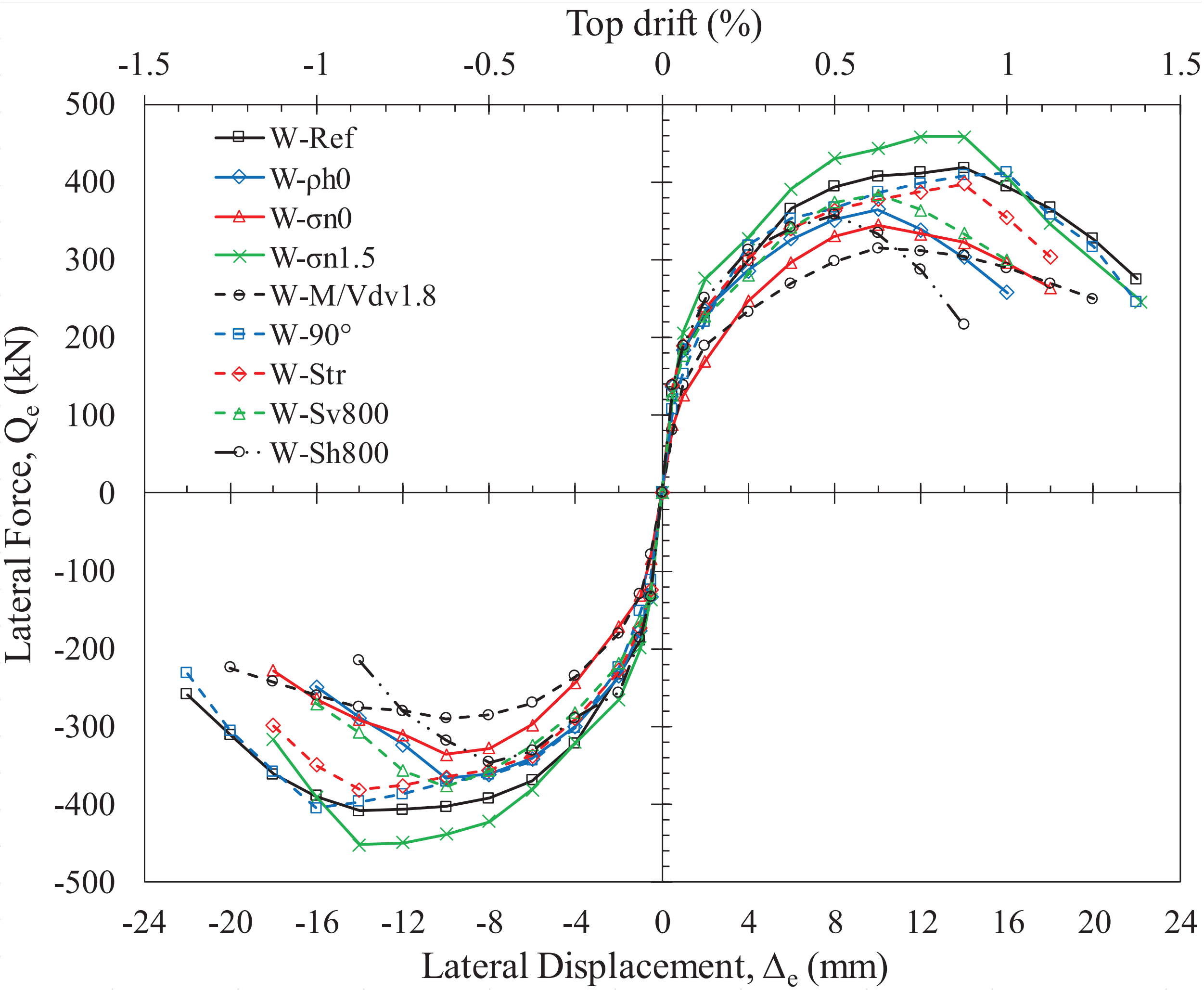

Figure 4.3: Lateral force-displacement envelopes for all walls

Table 4.1: Summary of Experimental Force and Displacement Capacities of all Walls in Push Direction

Wall ID	Test Results (push direction)									
	Yield		Peak		Failure	Displacement ductility			First crack[1]	
	Q_{ye}	Δ_{ye}	Q_{ue}	Δ_{Que}	$\Delta_{0.8Que}$	$\mu_{\Delta Que}$	$\mu_{\Delta 0.8Que}$	$\mu_{\Delta e1\%}$	Δ_{FCe}	Q_{FCe}
	(kN)	(mm)	(kN)	(mm)	(mm)	—	—	—	(mm)	(kN)
W-Ref	328	4.7	418	14.0	19.7	3.0	4.2	3.4	3.2	272
W-ρ_h0	309	4.8	365	10.0	14.6	2.1	3.0	3.3	3.1	265
W-σ_n0	254	4.2	345	10.0	17.3	2.4	4.1	3.8	3.0	209
W-σ_n1.5	365	5.0	458	14.0	17.2	2.8	3.4	3.2	3.4	312
W-M/Vd_v1.8	230	3.8	315	10.0	19.8	2.6	5.2	4.2	3.2	216
W-90°	335	4.9	412	16.0	19.4	3.2	3.9	3.2	3.3	287
W-Str	318	4.8	398	14.0	17.4	2.9	3.6	3.3	3.4	281
W-S_v800	300	4.6	384	10.0	15.6	2.2	3.4	3.5	2.8	248
W-S_h800	330	5.2	358	8.0	12.0	1.5	2.3	N/A	2.6	265

[1] First major diagonal crack

Table 4.2: Summary of Experimental Force and Displacement Capacities of all Walls in Pull Direction

Wall ID	Test Results (pull direction)									
	Yield		Peak		Failure	Displacement ductility			First crack[1]	
	Q_{ye}	Δ_{ye}	Q_{ue}	Δ_{Que}	$\Delta_{0.8Que}$	$\mu_{\Delta Que}$	$\mu_{\Delta 0.8Que}$	$\mu_{\Delta e1\%}$	Δ_{FCe}	Q_{FCe}
	(kN)	(mm)	(kN)	(mm)	(mm)	—	—	—	(mm)	(kN)
W-Ref	-339	-4.7	-409	-14.0	-19.4	3.0	4.1	3.4	-2.9	-274
W-ρ_h0	-315	-4.8	-367	-10.0	-13.8	2.1	2.9	3.3	-3.0	-269
W-σ_n0	-244	-4.2	-336	-10.0	-15.7	2.4	3.7	3.8	-3.1	-212
W-σ_n1.5	-349	-5.0	-452	-14.0	-17.3	2.8	3.4	3.2	-3.3	-306
W-M/Vd_v1.8	-225	-3.7	-290	-10.0	-19.2	2.7	5.3	4.4	-3.0	-210
W-90°	-323	-4.9	-405	-16.0	-19.3	3.3	4.0	3.3	-3.1	-275
W-Str	-310	-4.8	-381	-14.0	-18.0	2.9	3.8	3.4	-3.0	-268
W-S_v800	-294	-4.6	-377	-10.0	-14.3	2.2	3.1	3.5	-2.4	-234
W-S_h800	-313	-5.2	-346	-8.0	-12.1	1.5	2.3	N/A	-2.7	-275

[1] First major diagonal crack

4.3 ANALYSIS OF TEST RESULTS FOR WALL W-REF

4.3.1 OVERVIEW OF FORCE-BASED SEISMIC DESIGN APPROACH

Force-Based Design (FBD) is one of the current approaches for seismic design, which is widely used in many modern seismic codes including the National Building Code of Canada (NBCC 2010). In this approach, the behaviour of structures is simulated by a single-degree-of-freedom (SDOF) system. As such, the design seismic base shear is obtained from the estimated equivalent fundamental mode period and the mass of structure participating in the first mode. The design force from this approach is mostly limited by certain level of deformations in terms of ductility or inter-story drifts.

Early structures were designed for seismic forces based on their elastic behaviour. This assumption was very conservative for RC and RM buildings due to their limited tensile capacity, and therefore the cross-sections of structural elements needed to be relatively large; this significantly increased the total cost of building. At the first World Conference on Earthquake Engineering, Housner (1956) and Tabinashi (1956) suggested that the design of structures for reduced seismic loads could be acceptable by allowing certain levels of inelastic deformation to dissipate energy. Riddell (2008) pointed out that during the large seismic events of Long Beach (1933) and El Centro (1940), under-designed structures that exceeded their theoretical capacity did not collapse but survived with large inelastic deformations. The total energy imposed on a similarly designed elastic system could therefore be dissipated by an inelastic response, which is the principle underpinning the equal energy assumption. Based on this assumption, the equivalent elastic-perfectly plastic system is expected to deflect more than the elastic one such that equal energy for these parallel systems is achieved as shown in Figure 4.4a. On the other hand, Veletsos and Newmark (1960) concluded that an approach that equates the maximum displacement of the elastic system and the equivalent inelastic one is the most reasonable for relatively small magnitudes of damping as presented in Figure 4.4b. However, for structural systems that experience a long period of vibration with frequencies up to 2 Hz., the equal displacement approach is more accurate (El-Dakhakhni, 2014); instead, in the frequency range from 2 to 8 Hz, the equal energy approach applies.

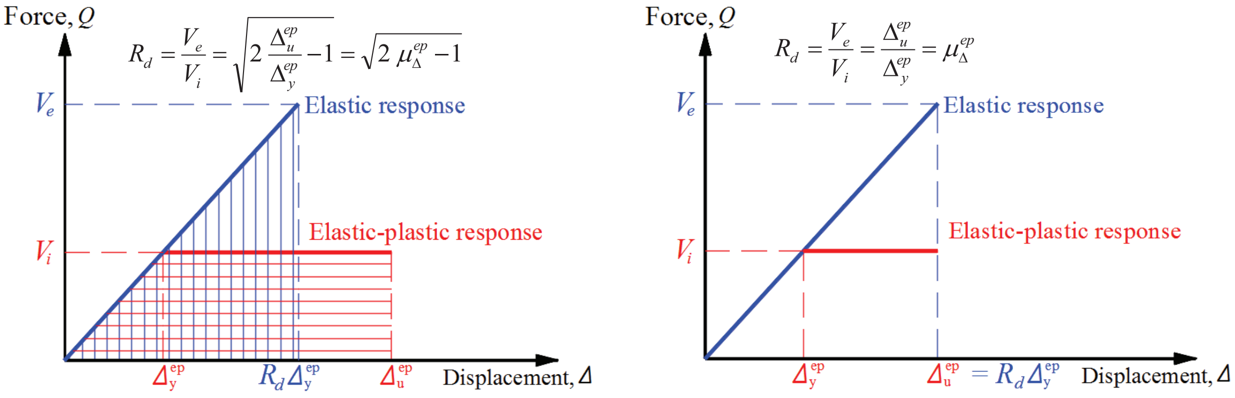

(a) Equal energy

(b) Equal displacement

Figure 4.4: Equal energy and equal displacement approaches for R_d calculation

For the calculation of the reduced force demands imposed on an inelastic system, V_i, relative to an equivalent elastic load, V_e, a Ductility-related seismic force Modification Factor D.M.F, referred to as R_d in NBCC (2010), was proposed using one of the following equations:

$$R_d = \frac{V_e}{V_i} = \sqrt{2\frac{\Delta_u^{ep}}{\Delta_y^{ep}} - 1} = \sqrt{2\,\mu_\Delta^{ep} - 1} \qquad \text{Eq. 4.1}$$

$$R_d = \frac{V_e}{V_i} = \frac{\Delta_u^{ep}}{\Delta_y^{ep}} = \mu_\Delta^{ep} \qquad \text{Eq. 4.2}$$

Where Δ_y^{ep} and Δ_u^{ep} are the yield and ultimate lateral displacement of the equivalent elastic-perfectly plastic curve, while, μ_Δ^{ep} is the equivalent displacement ductility. As shown in figure

4.4, using the equal energy approach results in unequal ultimate displacements; whereas, the energy dissipated by the elastic system is higher than the one in the inelastic system when using the equal displacement approach. Since most of the RM structures have a long period of vibration, the Canadian seismic design codes follow the equal displacement principle for calculating R_d (Eq. 4.2).

There are several ways to define the equivalent elastic-plastic force-displacement relationship with an equal displacement and energy of a real seismic force resistance system (SFRS), such as RM shear walls. As shown in Figure 4.5, the equivalent elastic-perfectly plastic response can be characterized by three parameters, namely: the effective elastic stiffness, K_e^{ep}, the ultimate displacement, Δ_u^{ep}, and the yield displacement, Δ_y^{ep}. The effective elastic stiffness, K_e^{ep}, is commonly calculated based on the yield secant stiffness, which is determined as a ratio between the experimental yield load, Q_{ye}, and its corresponding displacement, Δ_{ye}. However, K_e^{ep} could be defined also as the secant gross un-cracked stiffness, K_{ge}, up to $0.5Q_{ue}$ or until the first major diagonal crack is observed (Banting, 2013). The ultimate displacement, Δ_u^{ep}, refers mostly to the failure point or the demand level of deformation using the equal displacement approach. Generally, the maximum displacement of the plastic plateau is limited to the experimental displacement corresponding to: the peak lateral force, Δ_{Que}, a drift limit of 1.0%, $\Delta_{1\%}$, or, a drop in wall capacity to 80% of Q_u, $\Delta_{0.8Que}$. The last parameter for the characterization of the equivalent elastic-plastic curve is the yield displacement, Δ_y^{ep}, or the intersection between the elastic and plastic behaviour. This point can be determined on the elastic line using the same energy approach by equating the area under the real force-displacement relationship and the equivalent elastic-plastic response until Δ_u^{ep}. Figure 4.5 shows an example of the equivalent energy elastic-perfectly plastic response, using the secant yield stiffness and the ultimate displacement corresponding to a drop in wall capacity to 80% of Q_u.

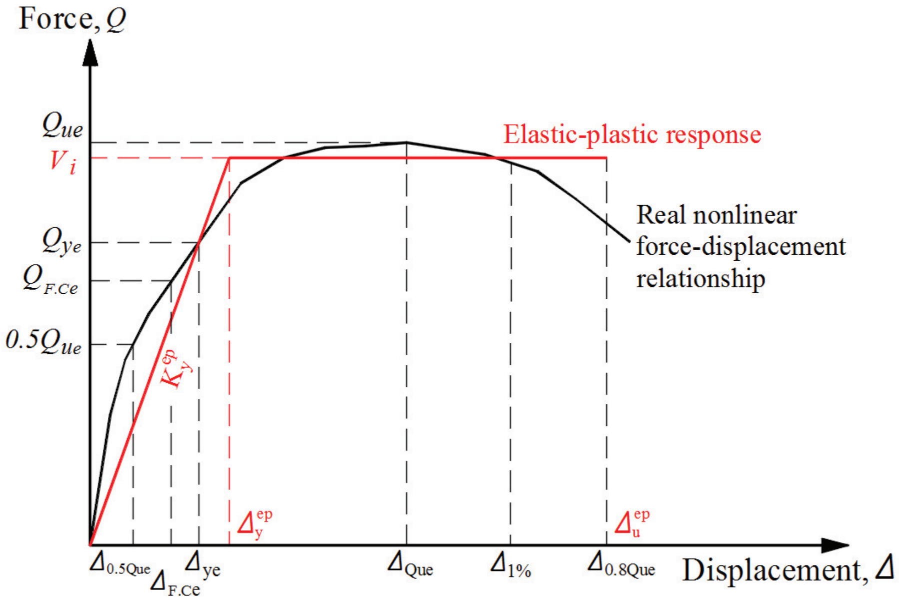

Figure 4.5: Different approaches for equivalent elastic-perfectly plastic response of a nonlinear force-displacement relationship

In addition to the ductility-related force modification factor, R_d, another factor was given in NBCC (2010) as R_o, overstrength-related force modification factor, such that the design base shear for the building is calculated by dividing the elastic base shear force by the product of R_d R_o. This R_o factor is proposed based on the fact that the real capacity of a structural element is higher than the calculated value. Mitchell et al. (2003) suggested that R_o is made up of five components as given in the following formulation:

$$R_o = R_{size} R_\phi R_{yield} R_{sh} R_{mesh} \qquad \text{Eq. 4.3}$$

Where R_{size} accounts for the restricted choices of masonry unit; R_ϕ accounts for the difference between nominal and factor resistance and is equal to $1/\phi$, where ϕ is the material resistance factor; R_{yield} is the ratio of actual yield strength to minimum specified yield capacity; R_{sh} is the overstrength due to strain hardening developing in the material at the expected level of deformation of the structure; and R_{mech} accounts for the additional resistance from mobilizing the full capacity of the structure such that a collapse mechanism is formed. After some rounding of these factors, R_o was proposed as 1.5 for RM shear walls.

In the United States seismic design codes (i.e. American Society of Civil Engineering, ASCE 7-10), the value of the R_d R_o is replaced by an overall force reduction factor, R, which accounts for both the ductility and overstrength, whereas, another factor Ω_o is used to separate the overstrength factor as shown in Figure 4.6. More discussion about the seismic performance factors R and Ω_0 can be found in FEMA P695 (2009).

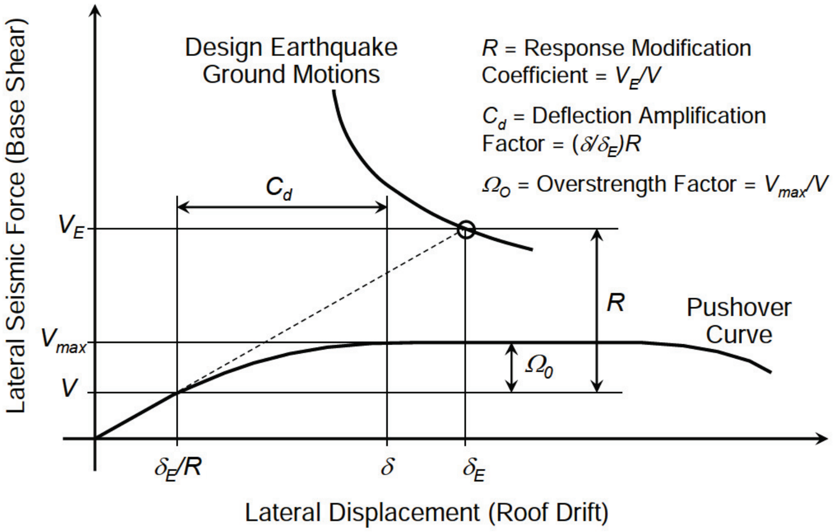

Figure 4.6: Illustration of seismic performance factors R and Ω_0 (FEMA P695, 2009)

Throughout the analysis of the test results of wall W-Ref using the FBD approach, the horizontal reinforcement resistance contribution, V_s, in addition to the resistance share of the masonry and axial compressive stress, V_{m+p}, are evaluated separately. Moreover, the ductility-related seismic force modification factor, R_d, is calculated using different approaches and these values are compared to the experimentally measured lateral displacement ductilities. A discussion about these values is provided in the following sections.

4.3.1.1 Horizontal reinforcement resistance (V_s)

To calculate the in-plane shear resistance provided by the horizontal reinforcement, V_s, the axial strain distribution along the horizontal reinforcing bars was measured using five-5 mm strain gauges that were installed and equally distributed along the total length of each horizontal bar (see Figure 4.7). The strain gauges had a capacity of 15000 microstrain, $\mu\varepsilon$, which is less than the measured strain hardening (see Figure 3.15). Hence, the axial tensile stress in each bar was limited to its yield capacity, f_y. Using the experimentally measured stress-strain relationship of reinforcement, Figure 4.8 shows the stress distribution of the horizontal reinforcing bars at different levels of lateral excitations. Consequently, the average tension stress, f_s, in each bar was calculated while considering the crack pattern as follows: for bar 1 (average of f1-1, f1-2, and f1-3); for bar 2 (average of f2-2, f2-3, and f2-4); for bar 3 (average of f3-2, f3-3, and f3-4); and for bar 4 (average of f4-2, f4-3, and f4-4). The tension forces in the horizontal reinforcing bars were then summed to calculate V_s. By subtracting the measured V_s from the measured in-plane lateral force, Q_e, the masonry and axial compressive stress resistance, V_{m+p}, was calculated.

Figure 4.9 presents the contribution of the horizontal reinforcement, V_s, to the in-plane shear capacity of wall W-Ref at different levels of experimental displacement ductility, $\mu_{\Delta e}$. As shown in this figure, the horizontal reinforcement reached its yield capacity at high displacement ductility and lateral top drift of 3.0 and 0.88%, respectively; by contrast, at low deformations levels this contribution was minor. Also, it can be noticed that the rate of increasing V_s became higher after the initiation of diagonal cracks, which means that as the cracks increased and became wider as the horizontal reinforcement provided more resistance, V_s.

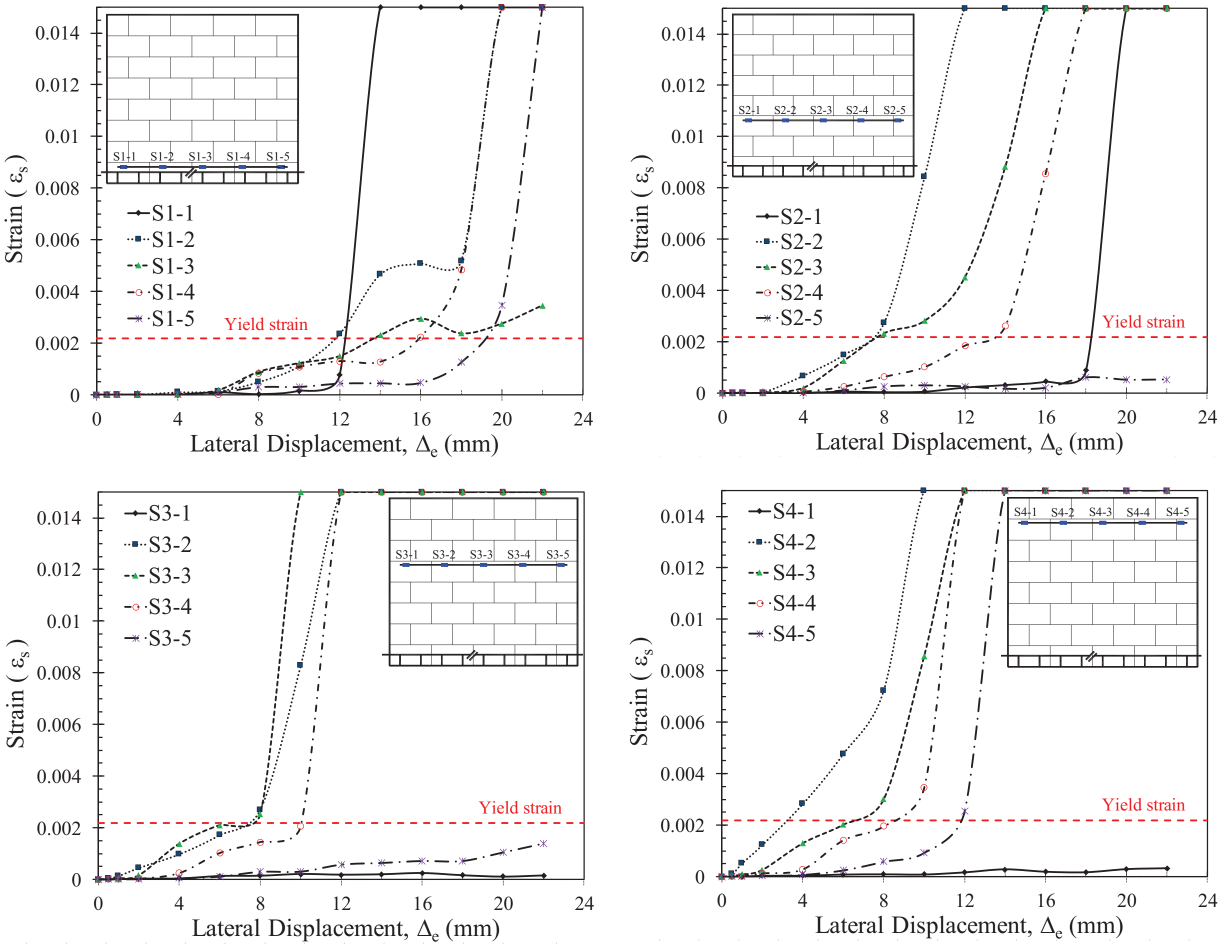

Figure 4.7: Lateral strain-displacement envelopes of horizontal reinforcing bars for wall W-Ref

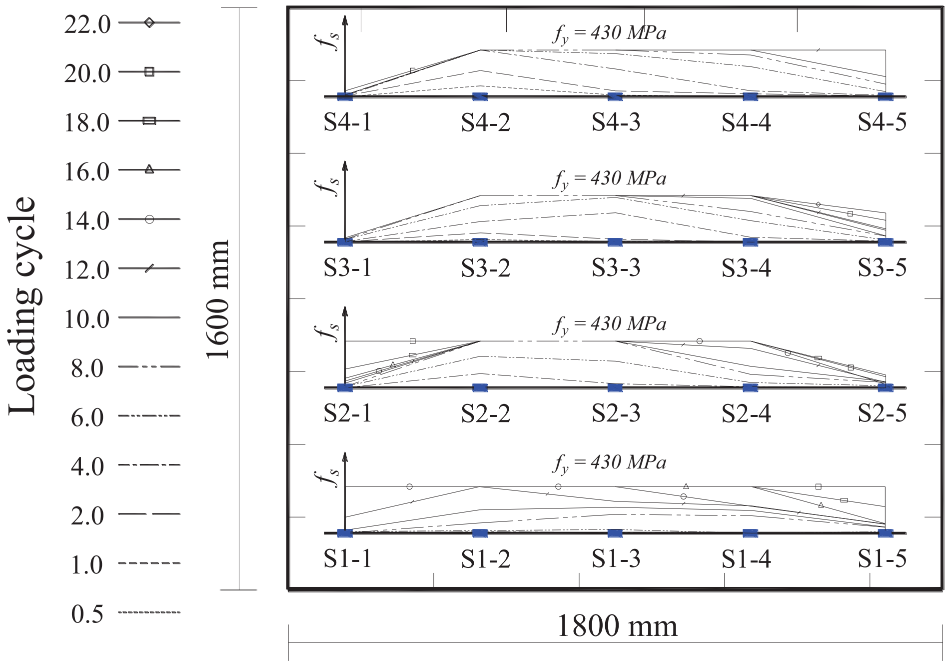

Figure 4.8: Stress distribution of horizontal reinforcing bars for wall W-Ref

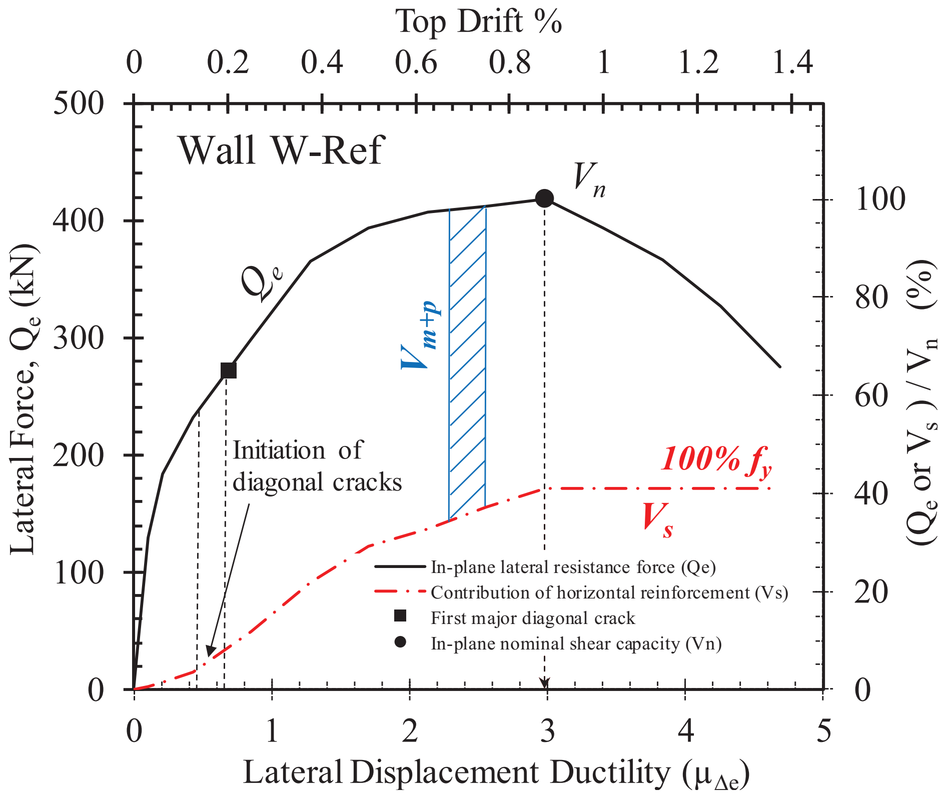

Figure 4.9: Horizontal reinforcement resistance, V_s, for wall W-Ref

4.3.1.2 Masonry and axial compressive stress resistance (V_{m+p})

The resistance shares of the masonry and axial compressive stress, V_{m+p}, in addition to the horizontal reinforcement, V_s, are given in Figure 4.10. At low deformation levels, the in-plane lateral resistance of wall W-Ref is mainly provided by the masonry and axial compression force, V_{m+p}, meanwhile, V_s was negligible. By increasing the level of deformations, the masonry reached its tensile strength capacity; hence, minor diagonal cracks occurred. These cracks decreased the rate of V_{m+p} contribution; instead, it resulted in higher resistance provided by the horizontal reinforcement, $V_{s.}$ As the cracks increased and became wider as the contribution rate of V_{m+p} decreased until the masonry reached its capacity, $(V_{m+p})_{\max}$, followed by a degradation in the provided resistance by the masonry and axial compressive stress. As long as the increasing in V_s is higher than the reduction in V_{m+p} as the tested wall gained more resistance.

Wall W-Ref reached its nominal in-plane shear capacity, V_n, when the horizontal reinforcement achieved its yield strength, then, degradation in the wall resistance occurred with the same rate of the reduction in V_{m+p}. From Figure 4.10, it can be noticed that the resistance shares provided by the masonry and axial compressive stress, V_{m+p}, and the horizontal reinforcement, V_s, did not reach their capacities at the same level of top drift. The resistance provided by the masonry and axial compressive stress, V_{m+p}, achieved its maximum contribution of $0.66V_n$ at a displacement ductility, μ_Δ, equal to 1.27 while V_s was $0.22V_n$. However, the horizontal reinforcement resistance, V_s, reached its yield capacity at μ_Δ of 3.0 with a contribution of $0.41V_n$. It was observed that the corresponding V_{m+p} at μ_Δ of 3.0 reduced gradually to $0.59V_n$. After the tested wall reached its capacity, V_n, the degradation in V_{m+p} became more rapid.

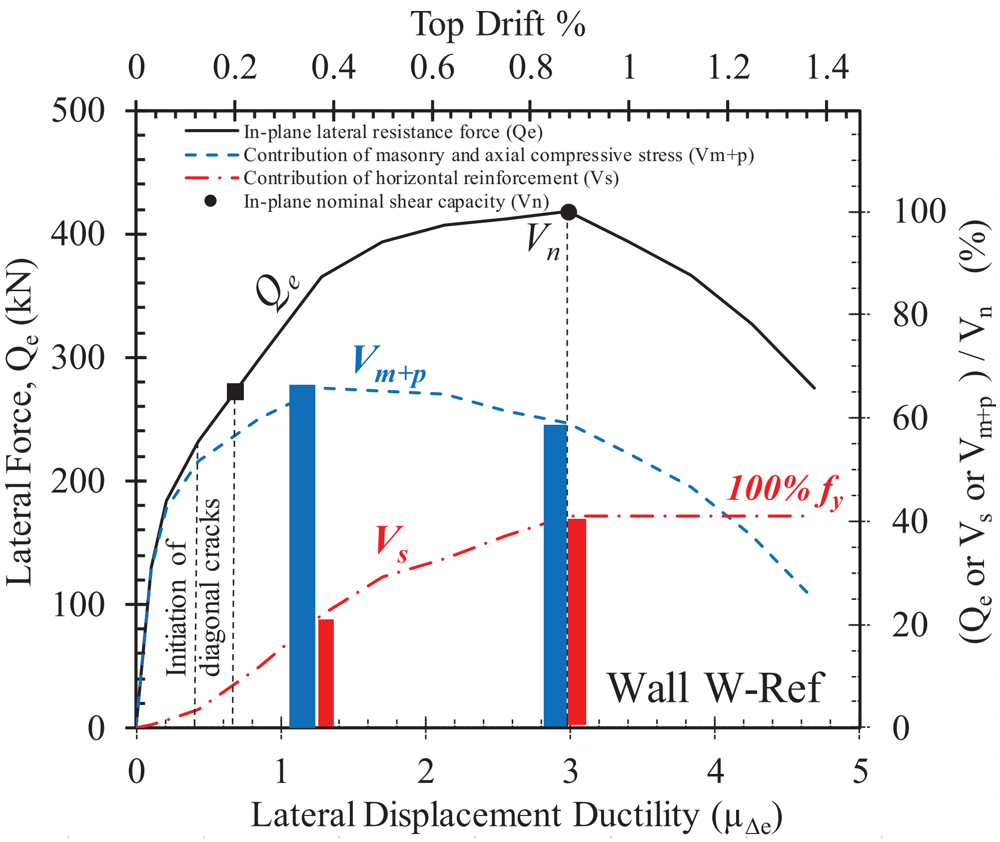

Figure 4.10: In-plane shear resistance provided by masonry and axial compressive stress, V_{m+p}, and horizontal reinforcement, V_s, for wall W-Ref

4.3.1.3 Idealized elastic-perfectly plastic response

To define the equivalent energy elastic-plastic response of wall W-Ref, three values of the effective elastic stiffness were considered as follow: K_y^{ep}, based on the secant yield stiffness; $K_{0.5}^{ep}$, based on the secant gross un-cracked stiffness up to $0.5Q_{ue}$; and K_{FC}^{ep}, based on the secant gross un-cracked stiffness until the first major diagonal crack is observed. Moreover, the ultimate displacement, Δ_u^{ep}, was taken at: the peak lateral force, Δ_{Que}; a drift limit of 1.0%, $\Delta_{1\%}$, and corresponding to a drop in wall capacity to 80% of Q_{ue}, $\Delta_{0.8Que}$. The yield displacement, Δ_y^{ep}, was calculated using equal energy approach by equating the area under the experimental force-displacement envelope and the equivalent elastic-plastic response until Δ_u^{ep}.

Figure 4.11 presents the nine equivalent energy elastic-perfectly plastic responses versus the experimental force-displacement envelope for wall W-Ref. Moreover, Table 4.3 summarizes the displacement ductility, μ_{Δ}^{ep}, and the inelastic lateral force, V_i, for each of the equivalent elastic-plastic responses and their ratios to $\mu_{\Delta e}$ and Q_{ue}, respectively. As disused earlier, the ductility-related seismic force modification factor, R_d, in NBCC (2010) was proposed equal to μ_{Δ}^{ep} based on the equal displacement approach between the equivalent elastic system and the elastic-perfectly plastic response (see Figure 4.4a).

As shown in Table 4.3, the value of R_d is sensitive to the followed approach for determining the equivalent elastic-plastic response. The ductility reduction factor, R_d, varies from 2.1 to 7.1 with a range of 0.76 to 1.72 of the corresponding $\mu_{\Delta e}$. The smallest value was found when using the secant yield stiffness, K_y^{ep}, and the ultimate displacement corresponding to the peak lateral force, Δ_{Que}. Alternatively, when the effective elastic stiffness was defined based on the gross un-cracked stiffness at $0.5Q_{ue}$, $K_{0.5}^{ep}$, and the failure point was taken at a drop in the wall force capacity to 80% of Q_{ue}, R_d reached 7.1. The inelastic lateral force, V_i, ranged between 0.9 to 1.04 Q_{ue}. The results of this analysis show that although the equivalent response has both equal displacement and energy with the real nonlinear behaviour, still it does not guarantee a safe design ($V_i \geq Q_{ue}$) if R_d is taken as μ_{Δ}^{ep}.

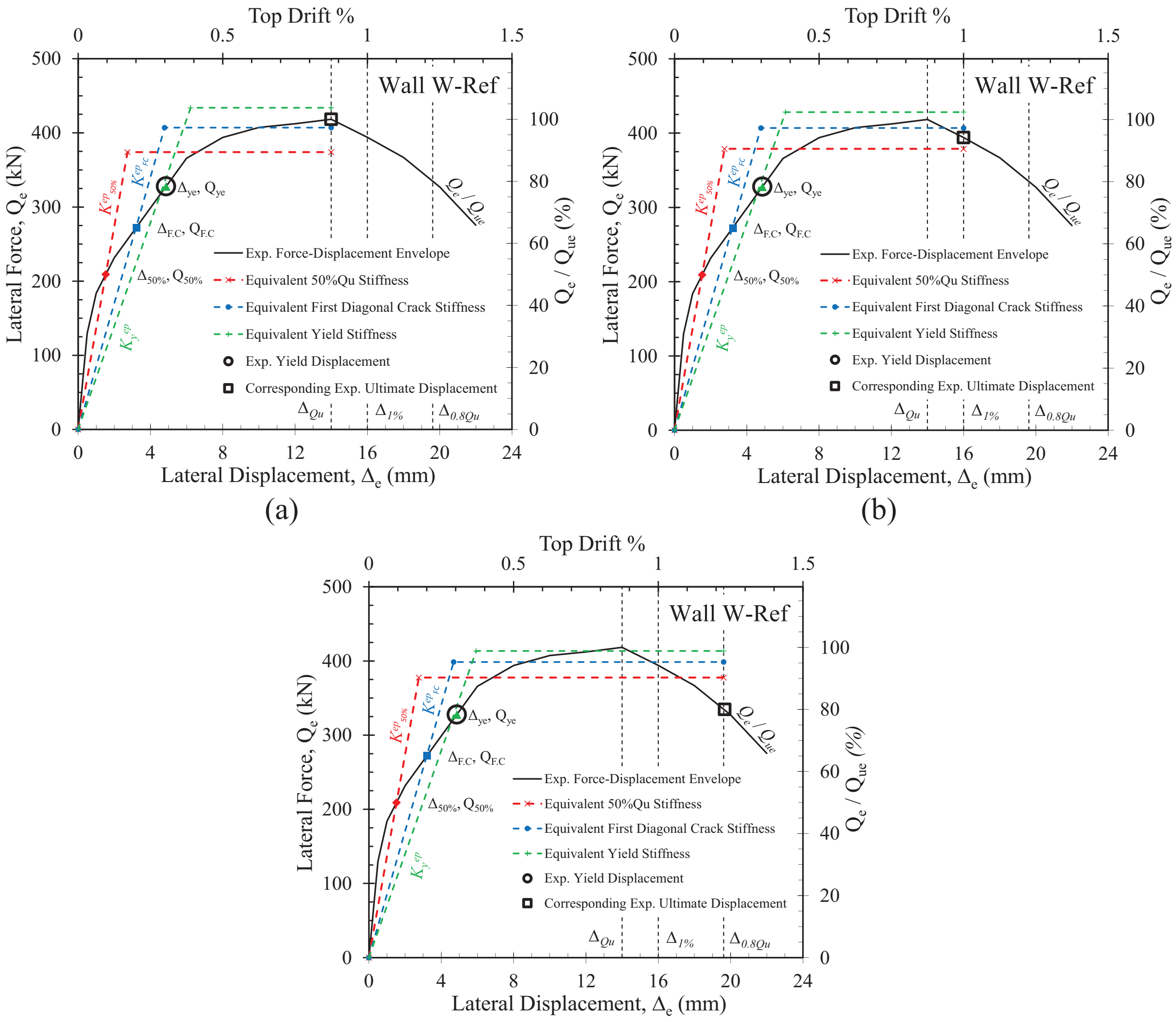

(a)

(b)

(c)

Figure 4.11: Experimental lateral force-displacement envelope vs. equivalent elastic-perfectly plastic response using equal energy approach at ultimate displacement corresponding to: (a) Δ_{Que}; (b) $\Delta_{1\%}$; (c) $\Delta_{0.8Que}$

Table 4.3: Ductility-Related Seismic Force Modification Factor, R_d, for Wall W-Ref Based on Equivalent Elastic-Perfectly Plastic Response

	Ultimate displacement, Δ_u^{ep}, mm												$\frac{\mu_\Delta^{ep} V_i}{\mu_{\Delta e} Q_{ue}}$ = $\frac{R_{d,\max}}{\mu_{\Delta e}}$
	At peak lateral force, Δ_{Que}, 14.0				At a drift limit of 1.0%, $\Delta_{1\%}$, 16.0				At a drop to 0.8 Q_u, $\Delta_{0.8Que}$, 19.7				
	$\mu_{\Delta e} = 3.0$				$\mu_{\Delta e} = 3.4$				$\mu_{\Delta e} = 4.2$				
	μ_Δ^{ep}	V_i	$\mu_\Delta^{ep}/\mu_{\Delta e}$	V_i/Q_{ue}	μ_Δ^{ep}	V_i	$\mu_\Delta^{ep}/\mu_{\Delta e}$	V_i/Q_{ue}	μ_Δ^{ep}	V_i	$\mu_\Delta^{ep}/\mu_{\Delta e}$	V_i/Q_{ue}	
	–	kN	–	–	–	kN	–	–	–	kN	–	–	
$^1K_{0.5}^{ep}$	5.1	374	1.72	0.89	5.8	379	1.70	0.91	7.1	378	1.70	0.90	1.54
$^2K_{F.C}^{ep}$	2.9	407	0.98	0.97	3.3	407	0.98	0.97	4.2	399	1.00	0.95	0.96
$^3K_y^{ep}$	2.3	434	0.76	1.04	2.6	428	0.77	1.02	3.3	414	0.79	0.99	0.78

$^1K_{0.5}^{ep}$ based on the gross un-cracked secant stiffness, K_{ge}, up to $0.5Q_{ue}$

$^2K_{F.C}^{ep}$ based on the gross un-cracked secant stiffness, K_{ge}, until the first major diagonal crack is observed

$^3K_y^{ep}$ based on the yield secant stiffness

Since both of the real behaviour and the equivalent energy elastic-plastic response has equal ultimate displacement, each effective elastic stiffness, K_e, has a constant value for the component of $(\mu_\Delta^{ep} V_i)/(\mu_{\Delta e} Q_{ue})$ regardless of the value of the ultimate displacement, Δ_u, as given in Table 4.3. This value could be defined as the maximum value of R_d, as a ratio of $\mu_{\Delta e}$, that satisfies safe design ($V_i \geq Q_{ue}$) when using a certain value of K_e. For example, if K_e is taken as $K_{0.5}^{ep}$ for wall W-Ref, R_d could be taken up to 1.54 $\mu_{\Delta e}$. Alternatively, for less effective elastic stiffness value, K_y^{ep}, the maximum value of R_d is 0.78 $\mu_{\Delta e}$ such that a safe design is achieved.

The effective elastic stiffness that produces $(\mu_\Delta^{ep} V_i)/(\mu_{\Delta e} Q_{ue})$ equal to 1.0, results in $V_i = Q_{ue}$ when R_d is taken as $\mu_{\Delta e}$. This effective elastic stiffness could be termed as the idealized effective elastic stiffness, K_{id}^{ep}, with equal displacement. This idealized stiffness could be calculated as the ratio of the peak lateral load, Q_{ue}, to the yield displacement as given in Figure 4.12 below. Hence, to keep $V_i \geq Q_{ue}$ while using R_d equal to $\mu_{\Delta e}$, the effective elastic stiffness should be taken higher than K_{id}^{ep}. Unlike the equivalent response, this idealized elastic-perfectly plastic response does not provide equal energy.

Figure 4.13 and Figure 4.14 present an example for the relation between the experimentally measured force-displacement envelope and the equivalent elastic performance when using the secant yield stiffness, K_y^{ep}, and the idealized effective elastic stiffness, K_{id}^{ep}, respectively.

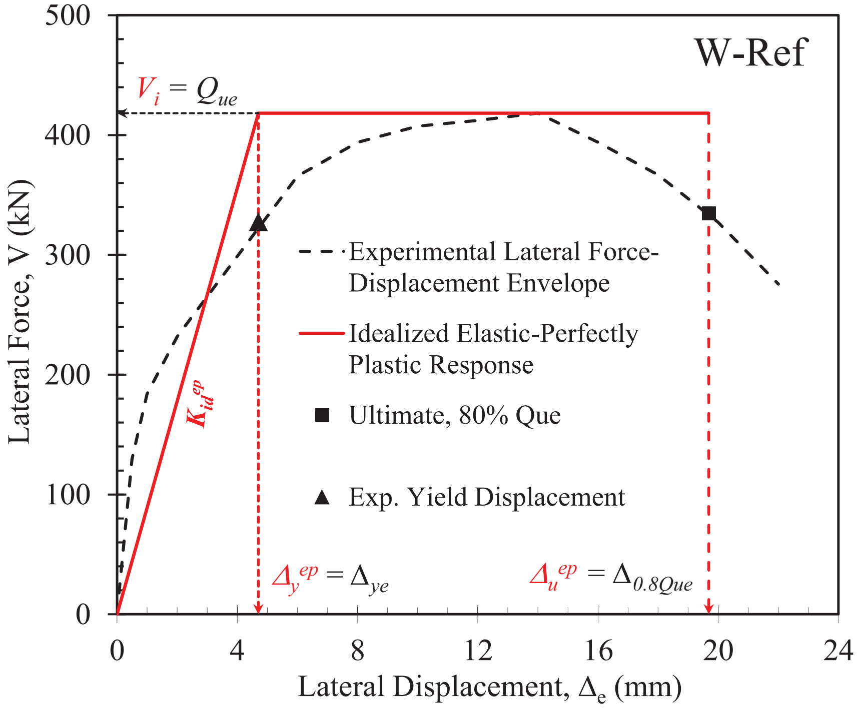

Figure 4.12: Idealized elastic-perfectly plastic response of wall W-Ref

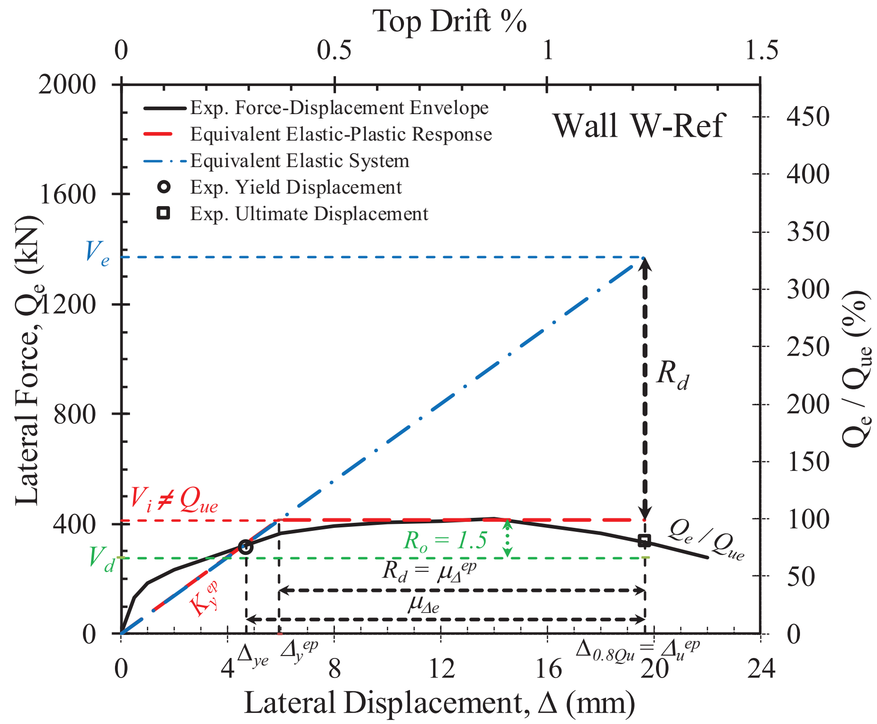

Figure 4.13: Experimental force-displacement envelope vs. equivalent energy elastic-perfectly plastic response vs. equivalent elastic performance

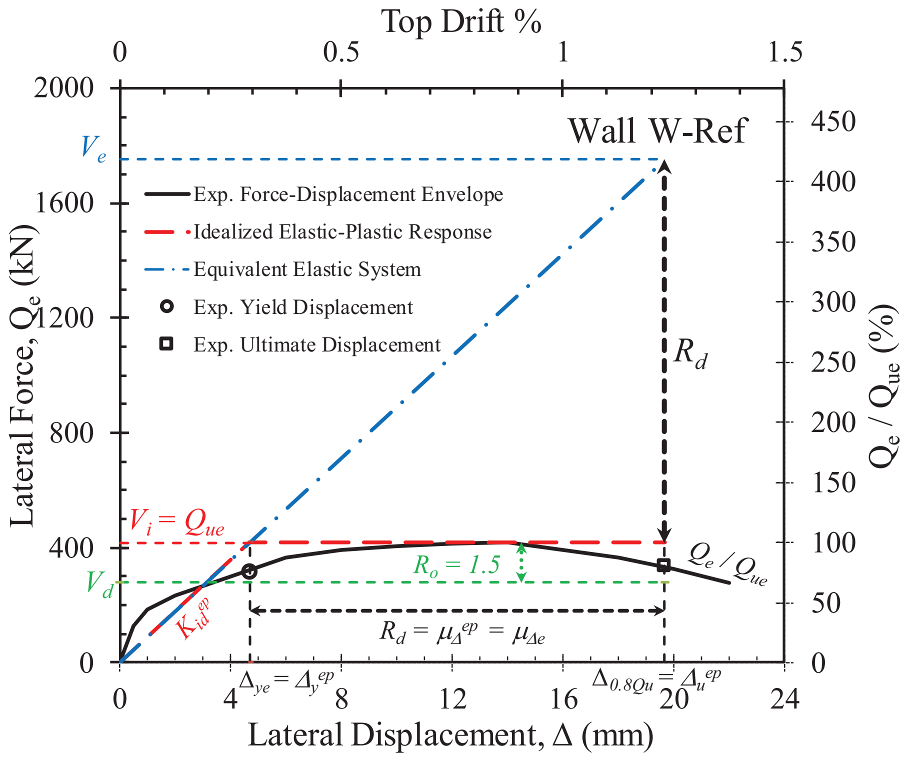

Figure 4.14: Experimental force-displacement envelope vs. idealized elastic-perfectly plastic response vs. equivalent elastic performance

4.3.2 OVERVIEW OF DISPLACEMENT-BASED SEISMIC DESIGN APPROACH

The Displacement-Based seismic Design (DBD) approach was first introduced by Priestley (1993) and was followed by considerable attention from researchers. The fundamentals of the DBD procedure are formulated in Figure 4.15. Similar to the force-based seismic design approach, the analysis and design of the DBD approach represents the behaviour of a building or structural element by an equivalent single-degree-of-freedom (SDOF) system with an effective height, h_e, and mass, m_e, (see Figure 4.15a). Unlike the FBD that intends to keep the inter-story drifts to less than a certain limit when the structure is subjected to the design seismic force, the DBD aims to achieve a target level of building performance under a specified level of seismic intensity in terms of demand top drift or lateral displacement, Δ_d. Moreover, the DBD characterizes the equivalent SDOF system by a linear behaviour using a secant stiffness at Δ_d, while the FBD defines it in terms of yield and ultimate displacement capacity as shown in Figure 4.15b. For the demand level of ductility, the equivalent viscous damping ratio, ξ, can be determined based on the type of structure. Thus, with Δ_d and ξ, the effective period, T_e, can be found (Figure 4.15d). Based on the effective mass and period, the effective stiffness of the equivalent SDOF system, K_e, at Δ_d can be found by inverting the normal equation for the period of a SDOF oscillator as follows:

$$K_e = \frac{4\,\pi^2\, m_e}{T_e^2} \qquad \text{Eq. 4.4}$$

Furthermore, the design lateral force can be calculated using Eq. 4.5. More discussion about the DBD approach can be found in Priestley et al. (2007) and El-Dakhakhni (2014).

$$F = V_{base} = K_e\, \Delta_d \qquad \text{Eq. 4.5}$$

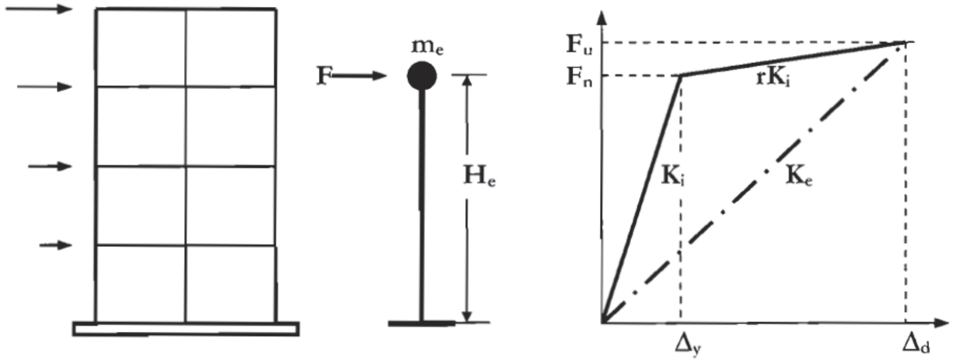

(a) SDOF Simulation

(b) Effective Stiffness K_e

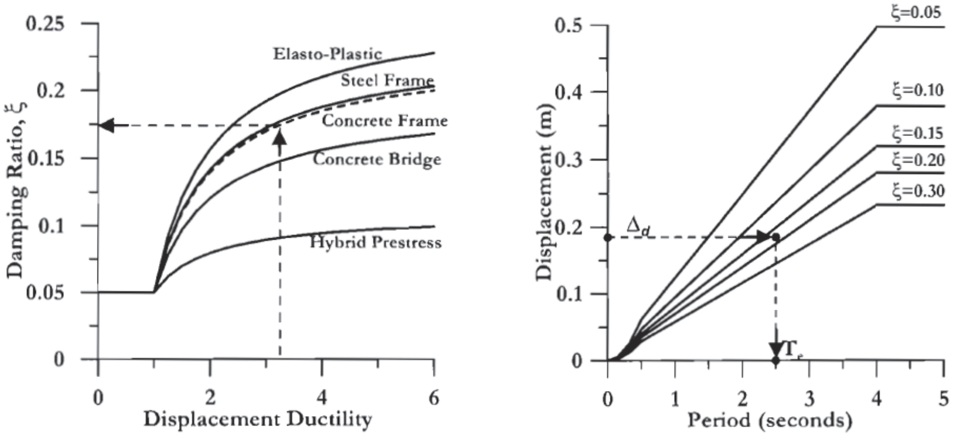

(c) Equivalent damping vs. ductility

(d) Design Displacement Spectra

Figure 4.15: Fundamentals of direct displacement-based seismic design approach (Priestley et al., 2007)

Stiffness degradation, energy dissipation, and equivalent viscous damping are important aspects that need to be considered when evaluating the seismic performance of RM shear walls, as well as when modeling their cyclic response. In this analysis, these three parameters are calculated for each tested wall and taken into account when evaluating the effect of studied parameters.

4.3.2.1 Stiffness degradation

Lateral stiffness is one of the main aspects to estimate the fundamental natural period, T_a, of a RC or RM structure; in addition, the acting lateral force on structures will be distributed among the shear walls based on their stiffness. Using the elastic or the equivalent cracked stiffness is a conservative choice, especially at high levels of ductility accompanied by yielding of reinforcement. Thus, it is important to predict an accurate effective stiffness of inelastic structures at the desired level of top drift. Priestley et al. (2007) suggested an effective secant stiffness at any loading cycle, $K_{s,i}$, which is defined as the ratio between the lateral force resistance, Q_i, and the corresponding top lateral displacement, Δ_i. Figure 4.16 exemplifies the calculation of the secant stiffness for wall W-Ref. As shown in this figure, unlike the elastic theory, there is a significant reduction in the secant stiffness by increasing the level of imposed top displacement relative to the initial gross stiffness, K_g, which was calculated at the first cycle of ± 0.5 mm. This stiffness degradation could be a good index for the level of damage in RM shear walls. The secant stiffness degradation can be calculated as follows:

$$\textit{Stiffness Degradation}\,(\%) \quad = \quad \frac{K_{s,i}}{K_g} \times 100 \qquad \text{Eq. 4.6}$$

where $K_{s,i}$ and K_g are the secant stiffness at any loading cycle and the initial gross stiffness, respectively. Figure 4.17 shows the secant stiffness and the stiffness degradation of wall W-Ref against the lateral displacement ductility and top drift. The right vertical axis, (%), represents the percentage of the experimental lateral resistance, Q_e, to the peak force, Q_{ue}, as well as the stiffness degradation ratio, $K_{s,i}/K_g$. As presented in this figure, Wall W-Ref has an initial experimental gross lateral stiffness equal to 259 kN/mm. Increasing the level of top drift resulted in more damage in the wall; thus, more degradation in the secant stiffness. At the ultimate lateral force, Q_{ue}, the secant stiffness was calculated as 30 kN/mm, which is almost 11.5% of the initial gross stiffness, K_g. The secant stiffness reached to 35%, 27%, and 9.5% of K_g at the first major diagonal crack, first yield, and at 1% top drift, respectively, while it was 7.0% at failure, when the wall capacity was dropped to $0.8Q_{ue}$.

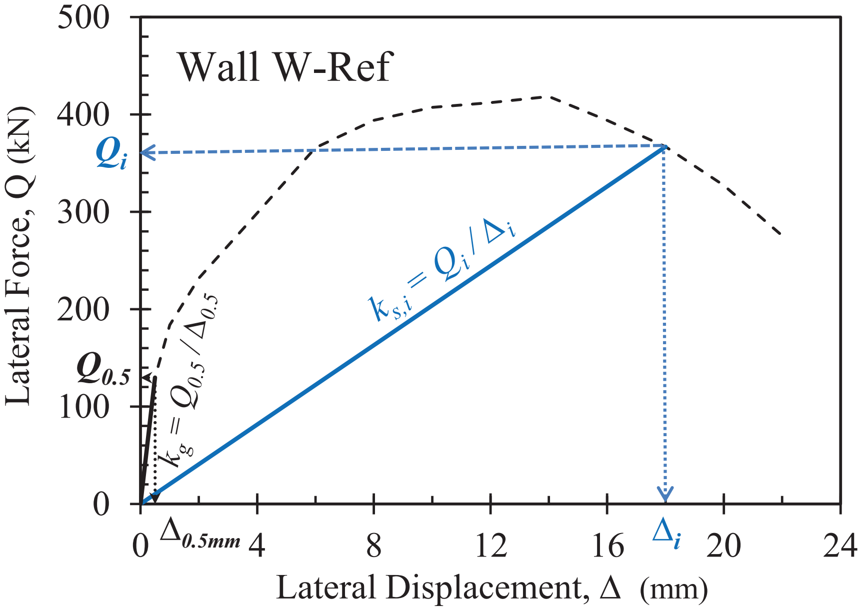

Figure 4.16: Secant stiffness, K_s, from the lateral force-displacement envelope

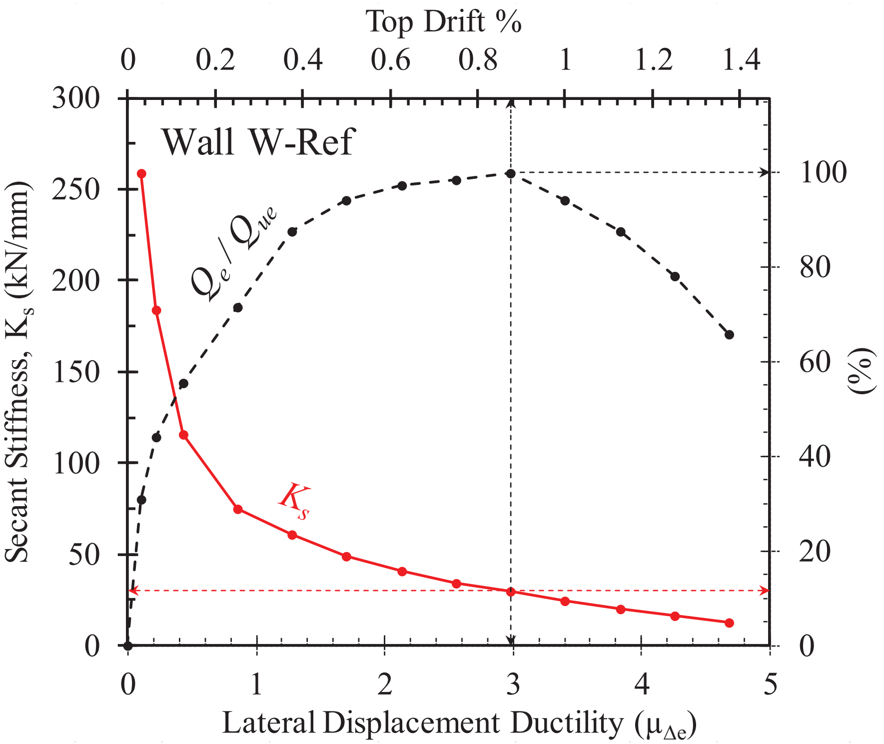

Figure 4.17: Stiffness degradation of wall W-Ref

4.3.2.2 Energy dissipation (E_d)

The capacity of shear walls to dissipate energy is another important aspect in seismic design and in analysis of their cyclic response. Figure 4.18 shows an example of the calculation of the dissipated and strain energy at a drift limit of 1% for wall W-Ref. The energy dissipation, E_d, is defined as the area enclosed within the inelastic hysteretic force-displacement response, the horizontally hatched region, as proposed by Hose and Seible (1999). However, the elastic stored strain energy, E_s, is calculated as the area under the equivalent linear elastic response, i.e. the vertically hatched area.

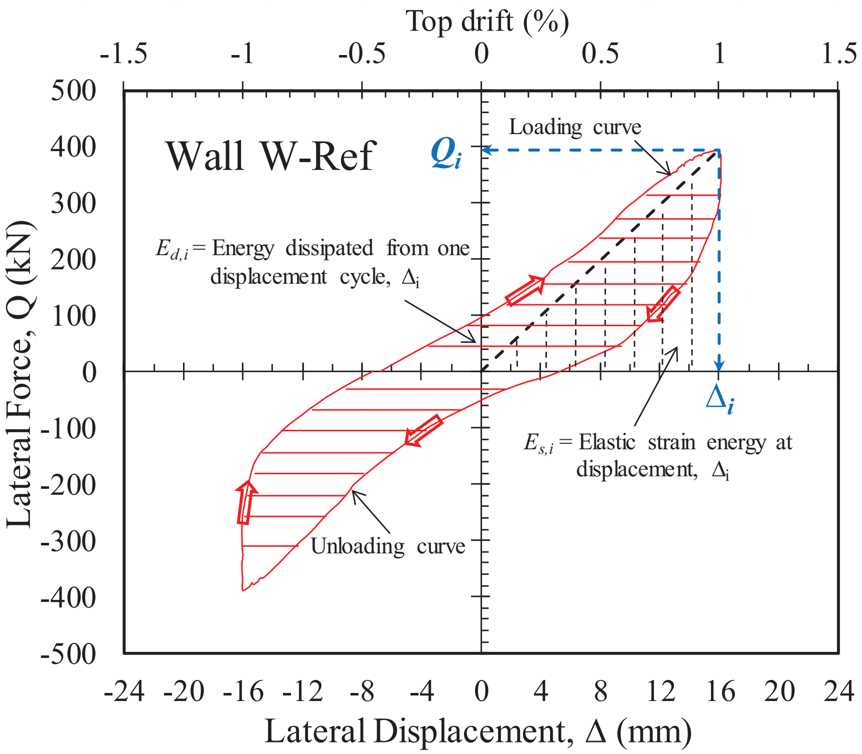

Figure 4.18: Calculation of energy dissipation

4.3.2.3 Equivalent viscous damping ratio (ζ_{eq})

The energy dissipation within different structural systems at the inelastic behaviour can be quantified through hysteric damping. Chopra (2000) described the hysteric damping by an equivalent viscous damping ratio, ζ_{eq}, using an equal area approach by equating the energy dissipated by a viscous damper with the energy dissipated from non-linear behaviour using the following equation:

$$\zeta_{eq} = \frac{1}{4\pi}\frac{E_d}{E_s} \qquad \text{Eq. 4.7}$$

where E_d and E_s are the energy dissipation and the stored strain energy from the hysteric response of one displacement cycle under quasi-static loading, respectively, as shown in Figure 4.18. Damping is generally specified for the whole structure rather than for an individual element. However, most RM structures are typically constructed with RM shear walls that are connected together by rigid diaphragms. Consequently, the trend of damping for a structural element such as shear walls, with respect to the top drift or the displacement ductility, can provide an indication for the overall response of RM structures. Figure 4.19 presents the energy dissipation, E_d, the stored strain energy, E_s, and the equivalent viscous damping ratio, ζ_{eq}, of wall W-Ref at different levels of top drift and displacement ductility.

The left vertical axis shows the values of the experimentally measured energy while the secondary vertical axis, (%), represents the percentage of the experimental lateral resistance, Q_e, to the ultimate force, Q_{ue}, and the equivalent viscous damping ratio, ζ_{eq}. The figure shows that the energy dissipated by the tested RM wall increased at higher levels of deformation. The energy dissipated from one displacement cycle at displacement ductility equal to 4.0, is almost 4.2 times the energy dissipated at the cycle of first yield. However, the equivalent viscous damping ratio, ζ_{eq}, ranged between 9% and 17% with an average of 14% (c.o.v. = 15%).

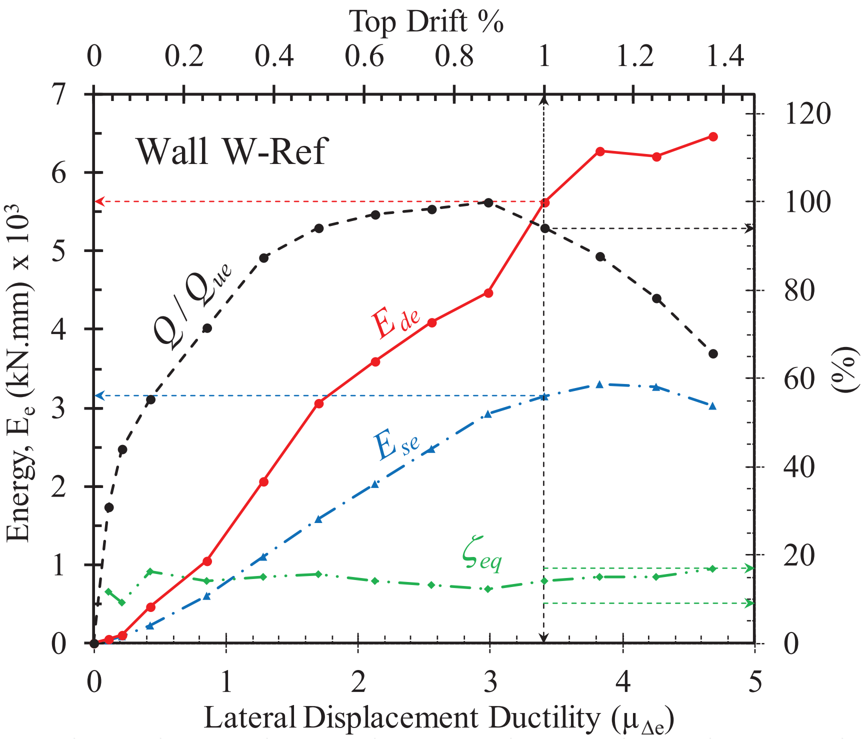

Figure 4.19: Energy dissipation, stored strain energy, and equivalent viscous damping ratio of wall W-Ref

4.3.3 OBSERVATION RELATED TO PERFORMANCE-BASED DESIGN

Figure 4.20 shows the crack pattern of wall W-Ref at different levels of top drift. Minor shear cracks were observed at the cycle of ±2.00 mm. However, the first sign of diagonal cracking damage occurred at lateral top displacement of +3.2 mm during the cycle of +4.0 mm (see Figure 4.20a). This first damage consisted of six diagonal cracks in the top left diagonal part of the tested wall with varied angels. It can be noticed that the angle of the cracks is steeper, the closer they are to the compression zone. Moreover, similar cracks were observed in the pull direction. By increasing the imposed lateral top displacement, the cracks extended, increased, and gradually spread over the wall diagonals.

Through the cycle of ±6.00 mm, initial horizontal cracks appeared in the bed joint of the extreme cells from both sides in the first and second course from the base. Cracks continued to form in this manner until the tested wall reached its peak lateral load as shown in Figure 4.20b. During the post-peak behaviour, the cracks were significantly wider and the face shell started to spall in addition to crushing in the east toe. Figure 4.21 presents the final crack pattern after the 1st cycle of imposed top lateral displacement, Δ, equal to +22.0 mm.

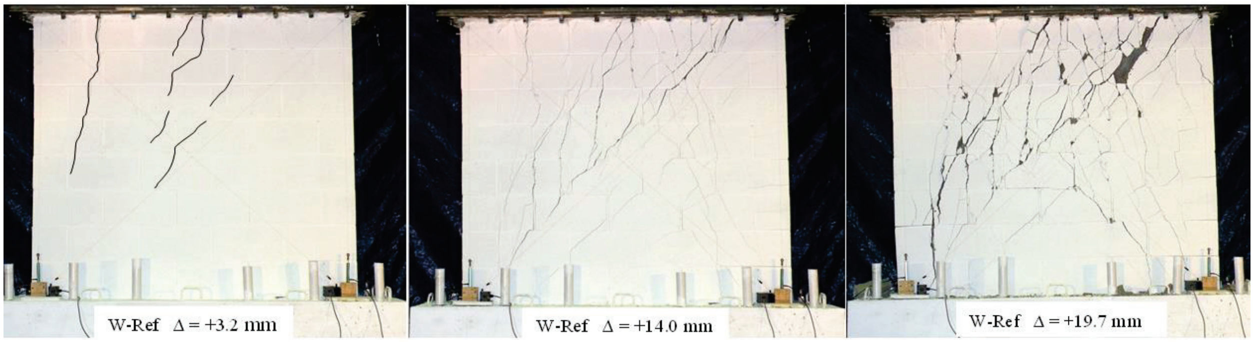

(a) (b) (c)

Figure 4.20: Crack pattern of wall W-Ref at: (a) first major diagonal crack; (b) lateral peak load Q_{ue}; (c) when the lateral load resistance dropped to 80% of Q_{ue}

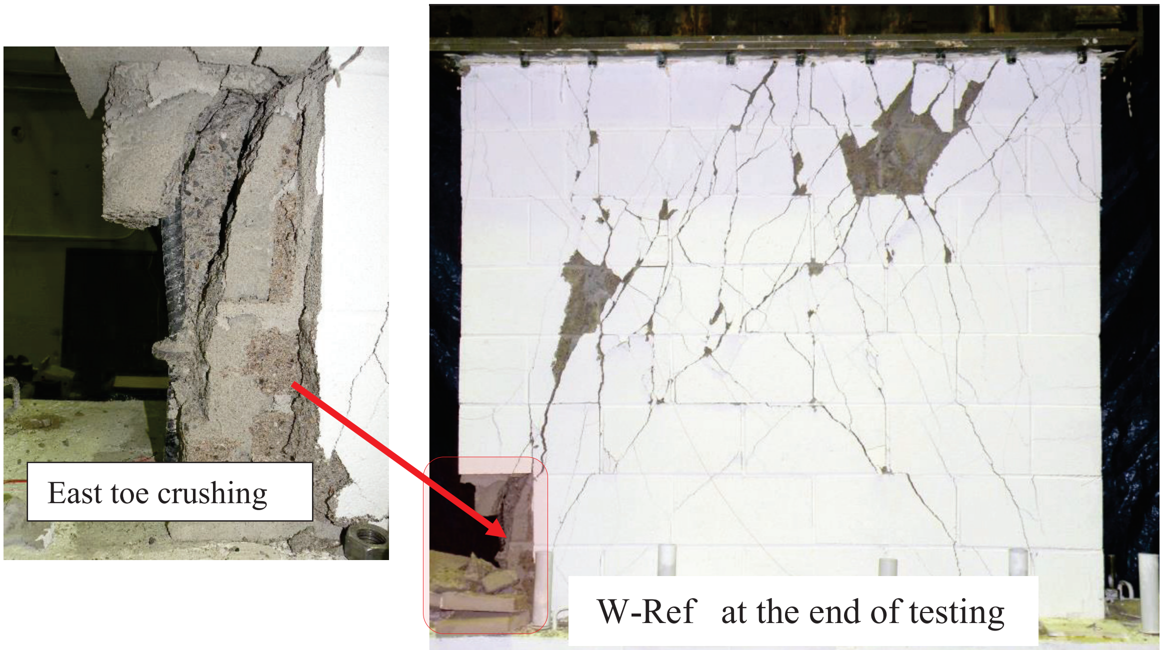

Figure 4.21: Final crack pattern of tested wall W-Ref

4.4 EFFECT OF STUDIED PARAMETERS ON IN-PLANE SHEAR BEHAVIOUR OF RM SHEAR WALLS

4.4.1 EFFECT OF HORIZONTAL REINFORCEMENT RATIO (ρ_h)

To evaluate the effect of the horizontal reinforcement on the in-plane shear performance of RM shear walls, two RM walls, W-Ref and W-ρ_h0, were tested with and without horizontal reinforcement, respectively. Wall W-Ref was horizontally reinforced with 10M@400 mm with a ratio ρ_h of 0.13%.

4.4.1.1 Force-based design

Figure 4.22 shows the effect of horizontal reinforcement in enhancing the in-plane shear behaviour of RM walls in terms of shear strength and displacement ductility. Providing horizontal reinforcement with a ratio of 0.13% increased the shear capacity from 365 to 418 kN. In addition, the tested wall W-Ref was able to achieve a higher displacement ductility, $\mu_{\Delta 0.8Que}$, of 4.2 compared to 3.0 for wall W-ρ_h0. However, it is clear from the test results that the horizontal reinforcement does not have a significant effect on the pre-crack behaviour and it has a minor effect on the yield capacity since it increased from 309 kN for wall W-ρ_h0 to 328 kN for wall W-Ref with just a 6% increase. This minor effect could be attributed to the confinement action of the horizontal reinforcement.

The experimentally measured resistance shares provided by masonry and axial compressive stress, W-Ref-V_{m+p}, and horizontal reinforcement, W-Ref-V_s, of wall W-Ref against the lateral resistance of wall W-ρ_h0, which is provided only by masonry and axial compressive stress and can be written as W-ρ_h0-V_{m+p}, are given in Figure 4.22. As shown in this figure, when wall W-

ρ_h0 was constructed without horizontal reinforcement, W-ρ_h0-V_{m+p} reached to 365 kN at displacement ductility of 2.1 followed by a rapid degradation in the strength to 292 kN, $0.8Q_{ue}$, at μ_Δ equal to 3.0. Instead, the inclusion of horizontal reinforcement in wall W-Ref resulted in re-distribution of the resistance provided by W-Ref-V_{m+p}. The masonry and axial compressive stress achieved their ultimate lateral resistance of 275 kN at μ_Δ equal to 1.28. Although this contribution is 25% less than W-ρ_h0-V_{m+p}, the figure shows that the behaviour of the masonry material became more ductile to retain similar dissipated energy by the material.

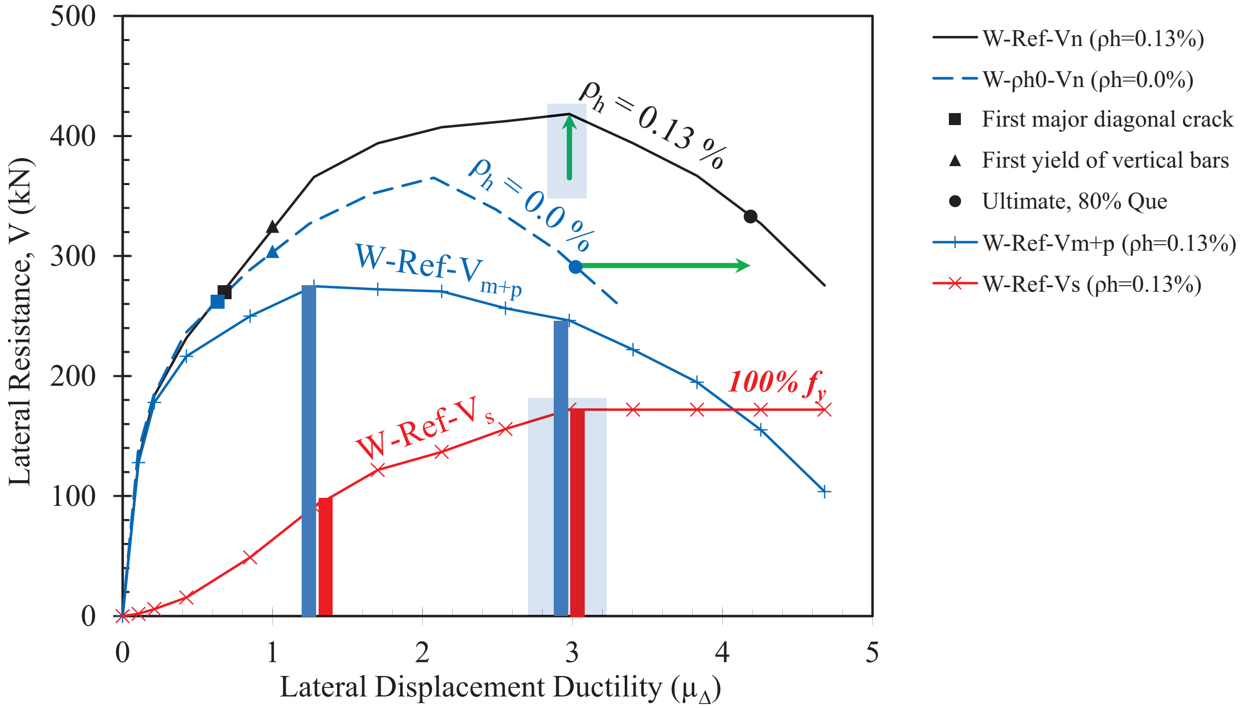

	Q_{ye}	Δ_{ye}	Q_{ue}	Δ_{Que}	$\Delta_{0.8Que}$	$\mu_{\Delta Que}$	$\mu_{\Delta 0.8Que}$	$\mu_{\Delta e1\%}$	Δ_{FCe}	Q_{FCe}
	(kN)	(mm)	(kN)	(mm)	(mm)	—	—	—	(mm)	(kN)
W-Ref	328	4.7	418	14.0	19.7	3.0	4.2	3.4	3.2	272
W-ρ_h0	309	4.8	365	10.0	14.6	2.1	3.0	3.3	3.1	265

Figure 4.22: Effect of horizontal reinforcement on in-plane shear strength of RM shear walls

As discussed in Chapter 2, most of the existing design equations for in-plane shear strength of RM shear walls, V_n, only consider a percentage of the horizontal reinforcement yield capacity contributing to V_n. The reason for this is that previous researchers did not measure the resistance provided by the horizontal reinforcement, V_s, experimentally but rather quantified V_s based on the difference between the achieved maximum lateral loads for tested RM walls with different horizontal reinforcement ratios. This quantification approach overlooks the effect of the re-distribution in the shear resistance shares between the reinforcement and the masonry, especially at high levels of displacement ductility. The presented test results here support this explanation since the measured resistance provided by the horizontal reinforcement reached 100% of its yield capacity. However, if the peak lateral load, Q_{ue}, of walls W-Ref and W-ρ_h0 was compared, it would falsely appear that the resistance provided by the horizontal reinforcement is 53 kN, which is only 30% of its yield capacity.

The equivalent energy elastic-plastic response of wall W-ρ_h0 using the nine alternative methods is given in Figure 4.23. The value of μ_{Δ}^{ep} ranged between 1.5 and 9.4 and the corresponding V_i varied between 1.18 Q_{ue} and 0.86 Q_{ue}. Using the effective elastic stiffness as $K_{0.5}^{ep}$ or K_{FC}^{ep} are conservative choices that would result in a factor of safety equal to 2.45 or 1.15 when R_d is taken as $\mu_{\Delta e}$, respectively. On the other hand, if the secant yield stiffness, K_{y}^{ep}, is considered, the ductility-related seismic force modification factor, R_d, can not be taken more than 0.85$\mu_{\Delta e}$. Figure 4.24 presents the idealized elastic-plastic response for both walls. The idealized effective elastic stiffness, K_{id}^{ep}, is increased from 76 kN/mm for wall W-ρ_h0 to 89 kN/mm for wall W-Ref. These values represents 28% and 34% of the initial gross stiffness, K_g, for each wall, respectively. Consequently, the stiffness of the equivalent SDOF system for wall W-ρ_h0 should be taken higher than 0.28 of its gross stiffness. However, when wall W-Ref achieved higher levels of inelastic deformation, this limit increased to 0.34.

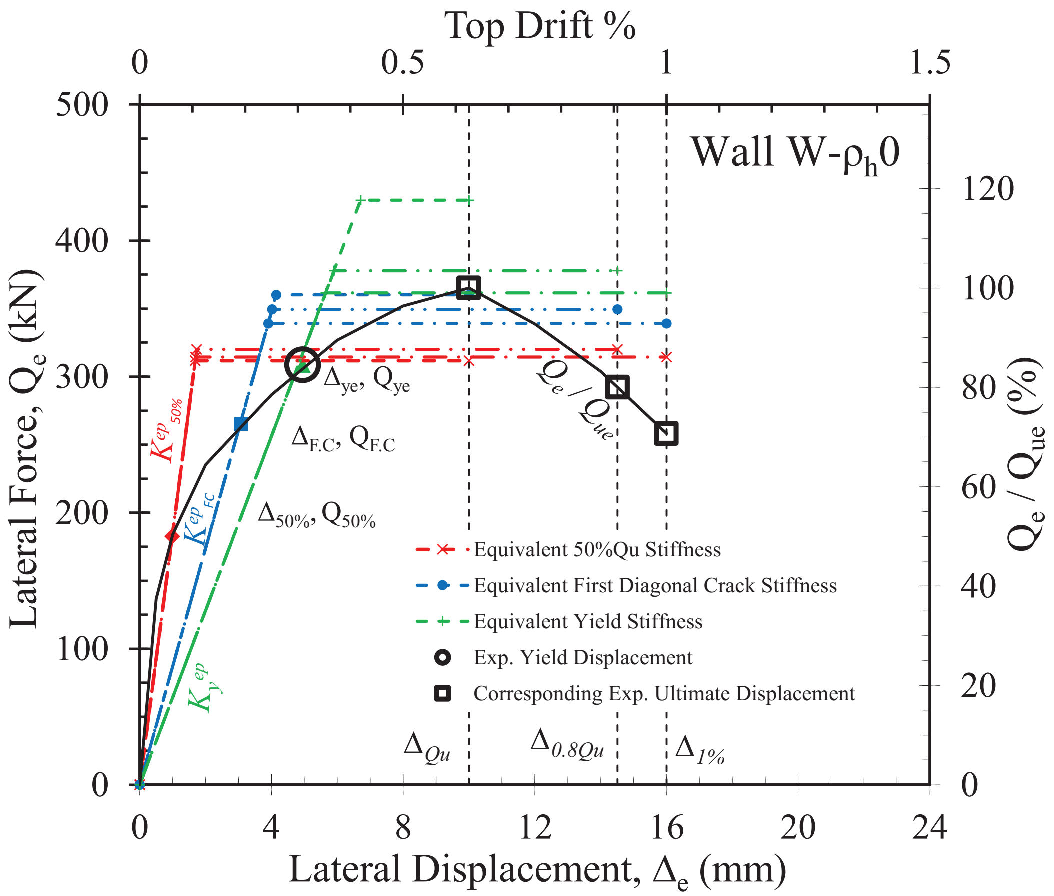

	Ultimate displacement, Δ_u^{ep} , mm												$\frac{\mu_\Delta^{ep} V_i}{\mu_{\Delta e} Q_{ue}}$ = $\frac{R_{d,\max}}{\mu_{\Delta e}}$
	At peak lateral force, Δ_{Que}, 10.0				At a drift limit of 1.0%, $\Delta_{1\%}$, 16.0				At a drop to 0.8 Qu, $\Delta_{0.8Que}$, 14.6				
	$\mu_{\Delta e} = 2.1$				$\mu_{\Delta e} = 3.3$				$\mu_{\Delta e} = 3.0$				
	μ_Δ^{ep}	V_i	$\mu_\Delta^{ep} / \mu_{\Delta e}$	V_i / Q_{ue}	μ_Δ^{ep}	V_i	$\mu_\Delta^{ep} / \mu_{\Delta e}$	V_i / Q_{ue}	μ_Δ^{ep}	V_i	$\mu_\Delta^{ep} / \mu_{\Delta e}$	V_i / Q_{ue}	
	–	kN	–	–	–	kN	–	–	–	kN	–	–	
$^1K_{0.5}^{ep}$	5.9	312	2.86	0.85	9.4	314	2.84	0.86	8.4	320	2.79	0.88	2.45
$^2K_{F.C}^{ep}$	2.4	360	1.16	0.99	4.1	339	1.24	0.93	3.6	349	1.20	0.96	1.15
$^3K_y^{ep}$	1.5	430	0.72	1.18	2.8	361	0.85	0.99	2.5	378	0.82	1.03	0.85

Figure 4.23: Equivalent energy elastic-perfectly plastic responses for walls W-ρh0

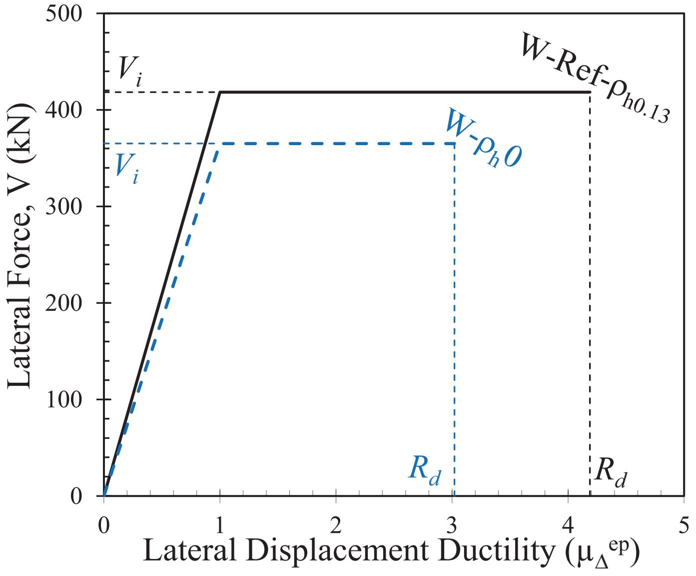

Figure 4.24: Effect of horizontal reinforcement on idealized elastic-plastic response

4.4.1.2 Displacement-based design

The effect of the horizontal reinforcement on the in-plane lateral stiffness and stiffness degradation is given in Figure 4.25. Figure 4.25a presents the relation between the top drift and secant stiffness, left axis, against the lateral experimental resistance force, right axis, of walls W-Ref and W-ρ$_h$0. Both walls had a similar initial gross stiffness, K_g, with an average of 266 kN/mm.

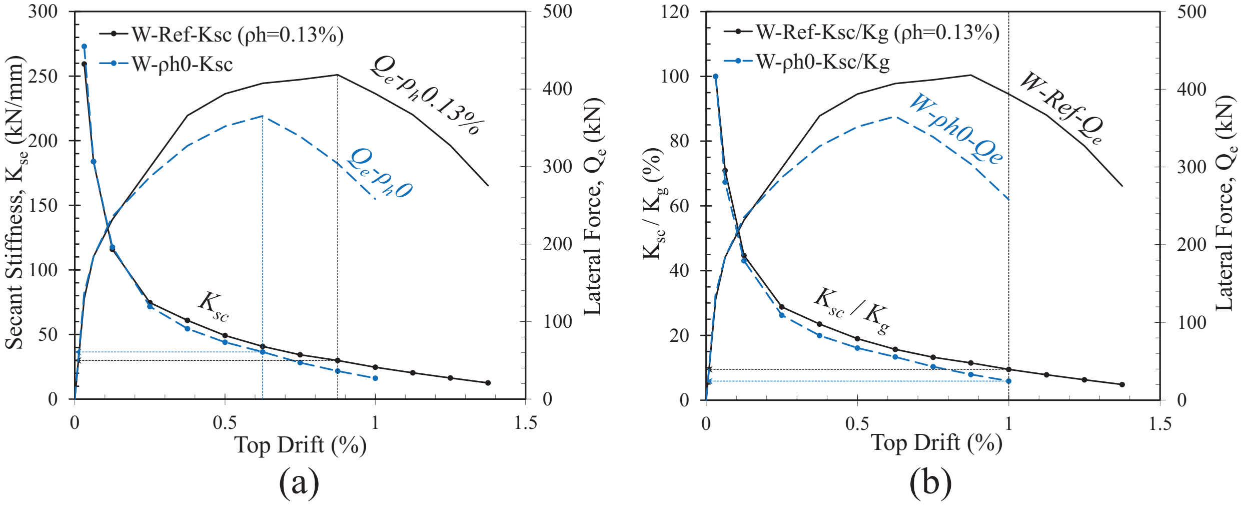

(a) (b)

Figure 4.25: Effect of horizontal reinforcement on stiffness degradation: (a) K_{sc}; (b) K_{sc}/K_g

The horizontal reinforcement did not have a significant effect on K_{sc} at low levels of deformation up to the first sign of crack damage. The two walls had about 65% reduction in their initial stiffness at the first diagonal crack. However, providing steel reinforcement enhanced the stiffness degradation in the post-crack behaviour. At a drift limit of 1%, the secant stiffness of Wall W-Ref was 25.0 kN/mm, which is 10% of K_g compared to 16.0 kN/mm for wall W-ρ_h0 with 94% reduction in its initial stiffness at the same top drift (see Figure 4.25b).

Another aspect that needs to be considered when designing RM shear walls using the DBD approach is the energy dissipation. Figure 4.26 presents the total dissipated energy by both walls against the top drift. As shown in this figure, the two tested walls dissipated similar total energy at a drift value of 1.0%. However, at this drift limit, wall W-ρ_h0 had about 30% degradation in its shear capacity while wall W-Ref had only 6% degradation. On the other hand, wall W-Ref dissipated total energy with about 63% higher than wall W-ρ_h0 when both walls reached their failure point, $0.8Q_{ue}$, as shown in Figure 4.26. For wall W-ρ_h0 that was constructed without horizontal reinforcement, the equivalent viscous damping ratio, ζ_{eq}, ranged between 13% and 23% with an average of 17% (c.o.v. = 17.8%). Providing lateral reinforcement in wall W-Ref, resulted in an average of 14.0% (c.o.v. = 15.0%).

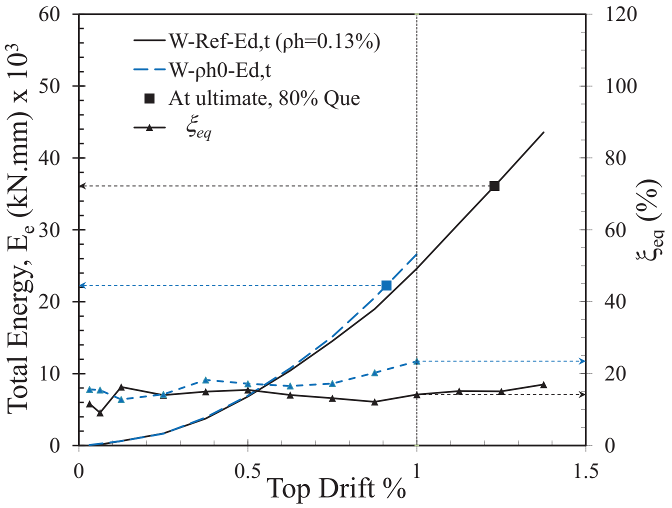

Figure 4.26: Effect of horizontal reinforcement on energy dissipation

4.4.1.3 Performance-based design

Figure 4.27 shows the crack pattern for the two tested walls at different levels of deformation. The first sign of cracking for both walls W-ρh0 and W-Ref occurred at a similar top drift of 0.2%. This observation confirms that the horizontal reinforcement does not have a significant effect on pre-crack behaviour. However, by increasing the imposed top lateral displacement, the main diagonal crack of wall W-ρh0 became wider. Distributing the horizontal reinforcement along the height of wall W-Ref replaced the major diagonal cracks with sets of minor cracks. These minor cracks were formed and gradually spread over the wall diagonals, as the initial diagonal cracks did not widen significantly. Moreover, the presence of the horizontal reinforcement delayed the corresponding top drift to the maximum load, Q_{ue}, to 0.88% for wall W-Ref instead of 0.63% for wall W-ρh0 (see Figure 4.27b). At a similar top drift of 0.91%, wall W-ρ_h0 had a drop in its shear capacity to $0.8Q_{ue}$ with severe damage, whereas wall W-Ref reached the failure displacement, $\Delta_{0.8Q_{ue}}$, at a top drift of 1.23% with major damage. Finally, the failure mode of wall W-ρ_h0 can be classified as a brittle shear failure with two major diagonal cracks, while the behaviour of wall W-Ref is characterized by more ductile performance (see Figure 4.27c).

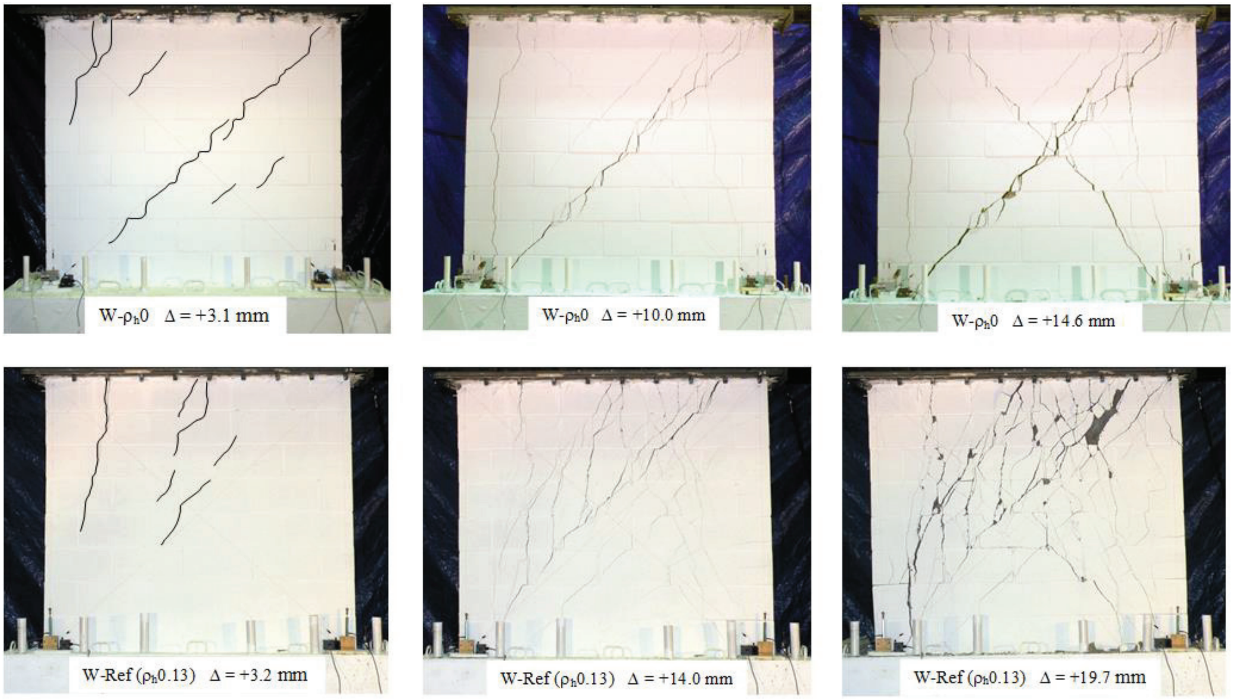

(a) (b) (c)

Figure 4.27: Effect of horizontal reinforcement on crack pattern at: (a) first major diagonal cracks; (b) lateral peak load Q_{ue}; (c) when the lateral load dropped to 80% of Q_{ue}

4.4.2 EFFECT OF AXIAL COMPRESSIVE STRESS (σ_n)

In addition to wall W-Ref, which is tested under σ_n of 1.0 MPa, two walls W-σ_n0 and W-σ_n1.5 were tested under 0.0 and 1.5 MPa, respectively. The influence of axial compressive stress, σ_n, on in-plane shear resistance, stiffness degradation, energy dissipation, and crack pattern is presented and discussed in the following sections.

4.4.2.1 Force-based design

The relation between the in-plane lateral force resistance against the displacement ductility of the three tested walls, W-σ_n0, W-Ref, and W-σ_n1.5, is illustrated in Figure 4.28. Increasing the axial compressive stress from 0.0 to 1.0 and 1.5 MPa resulted in a higher ultimate lateral force, Q_{ue}, from 345 to 418 and 458 kN, respectively. Similar influence on diagonal crack load can be noticed. The measured average yield displacement and the corresponding lateral load for wall W-σ_n0 were 4.2 mm and 254 kN, respectively. These values increased to 4.7 mm and 328 kN for wall W-σ_n1.0 and 5.0 mm and 365 kN for wall W-σ_n1.5. However, this increase in the shear strength was followed by a reduction in the displacement ductility capacity, $\mu_{\Delta e}$. At a top drift of 1.0%, $\mu_{\Delta e1\%}$ decreased from 3.8 to 3.4 and 3.2 for walls W-σ_n0, W-σ_n1.0, and W-σ_n1.5, respectively. Moreover, the achieved ductility at failure, $\mu_{\Delta 0.8Que}$, was measured as 3.4 for wall W-σ_n1.5 compared to 4.1 for wall W-σ_n0.

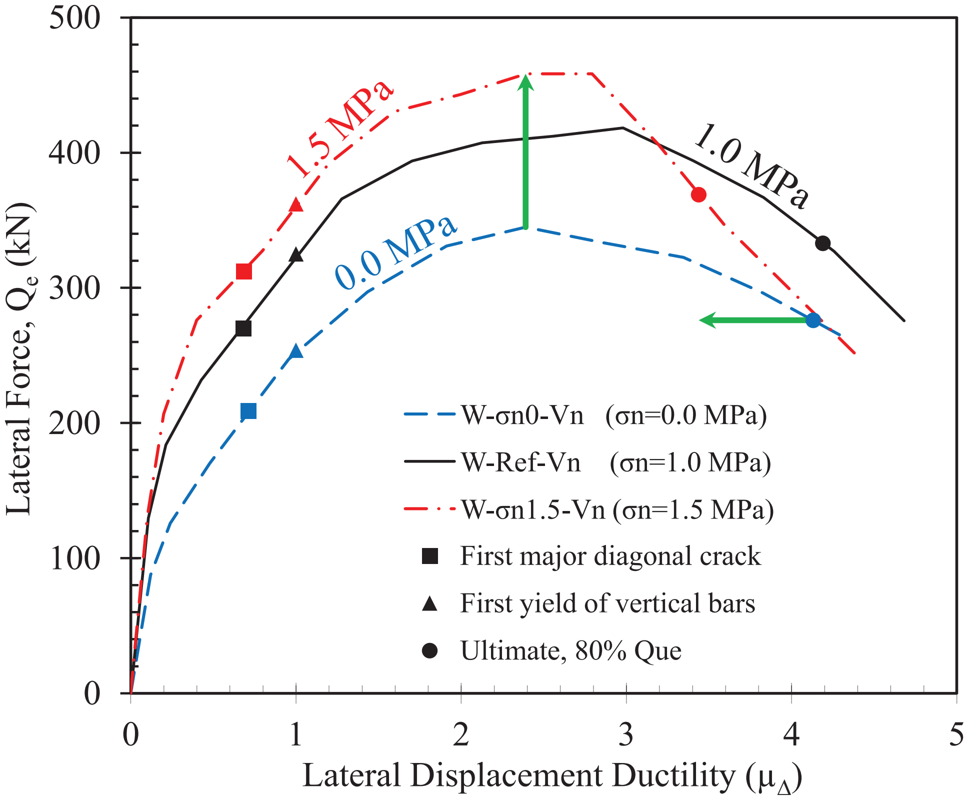

	Q_{ye}	Δ_{ye}	Q_{ue}	Δ_{Que}	$\Delta_{0.8Que}$	$\mu_{\Delta Que}$	$\mu_{\Delta 0.8Que}$	$\mu_{\Delta e1\%}$	Δ_{FCe}	Q_{FCe}
	(kN)	(mm)	(kN)	(mm)	(mm)	—	—	—	(mm)	(kN)
W-σ_n0	254	4.2	345	10.0	17.3	2.4	4.1	3.8	3.0	209
W-Ref	328	4.7	418	14.0	19.7	3.0	4.2	3.4	3.2	272
W-σ_n1.5	365	5.0	458	14.0	17.2	2.8	3.4	3.2	3.4	312

Figure 4.28: Effect of axial compressive stress on in-plane shear strength of RM shear walls

The shear resistance provided by the horizontal reinforcement, V_s, was calculated using the measured strain data along the total length of each horizontal steel reinforcing bar and the sum is presented in Figure 4.29a. Consequently, the combined contribution of the masonry and axial stress, $V_{(m+p)}$, was calculated by subtracting the horizontal reinforcement resistance, V_s, from the measured lateral load. As shown in Figure 4.29b, the maximum combined contributions of the masonry and axial stress, $V_{(m+p)max}$, increased from 182 kN for wall W-σ_n0 to 275 and 336 kN for walls W-Ref and W-σ_n1.5, respectively. Since wall W-σ_n0 was tested without axial compressive stress, the improvement in $V_{(m+p)max}$ for walls W-Ref and W-σ_n1.5 can be assumed as V_p, the resistance provided by the axial compressive stress only. Hence, V_p was calculated as 0.27P and 0.3P when σ_n was 1.0 and 1.5 MPa, respectively, where P is the equivalent compression axial load of σ_n. Nevertheless, comparing the ultimate lateral force resistances, Q_{ue}, of the three walls shows that V_p is only contributing 0.21P and 0.23P for walls W-σ_n1.0 and W-σ_n1.5, respectively. These different values of V_p could be explained by delaying in the resistance provided by the horizontal reinforcement, V_s, as the axial compression load increased (see Figure 4.29a). In addition, V_p reached its maximum contribution at early levels of displacement ductility, followed by a reduction in its resistance share as $\mu_{\Delta e}$ increased until the tested walls reached their capacity, V_n.

Earlier researchers such as Sveinssion et al. (1985), Matsumura (1988), Shing et al. (1990), and Voon and Ingham (2006), evaluated the in-plane shear resistance provided by the axial compressive stress, σ_n, based on differences in the achieved ultimate lateral force, Q_{ue}, by testing RM walls under varying levels of σ_n. The test results presented here show that using this approach is underestimating V_p, since increasing σ_n results in a higher $V_{(m+p)max}$ that is accompanied by a reduction in the corresponding V_s, as shown in Figure 4.30.

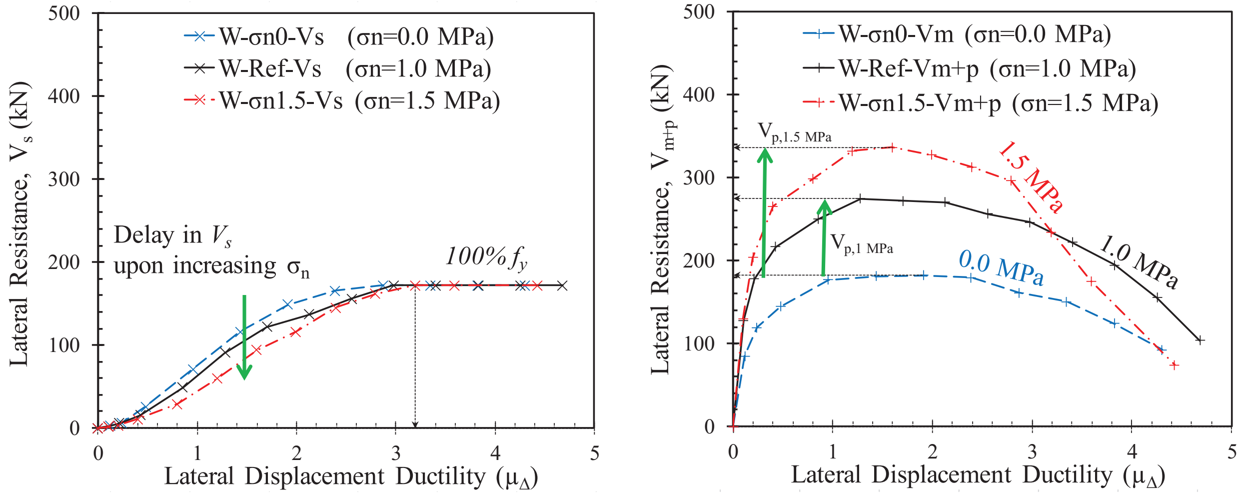

(a) (b)

Figure 4.29: Effect of axial compressive stress on shear resistance shares provided by: (a) horizontal reinforcement, V_s; (b) masonry and axial compressive stress, V_{m+p}

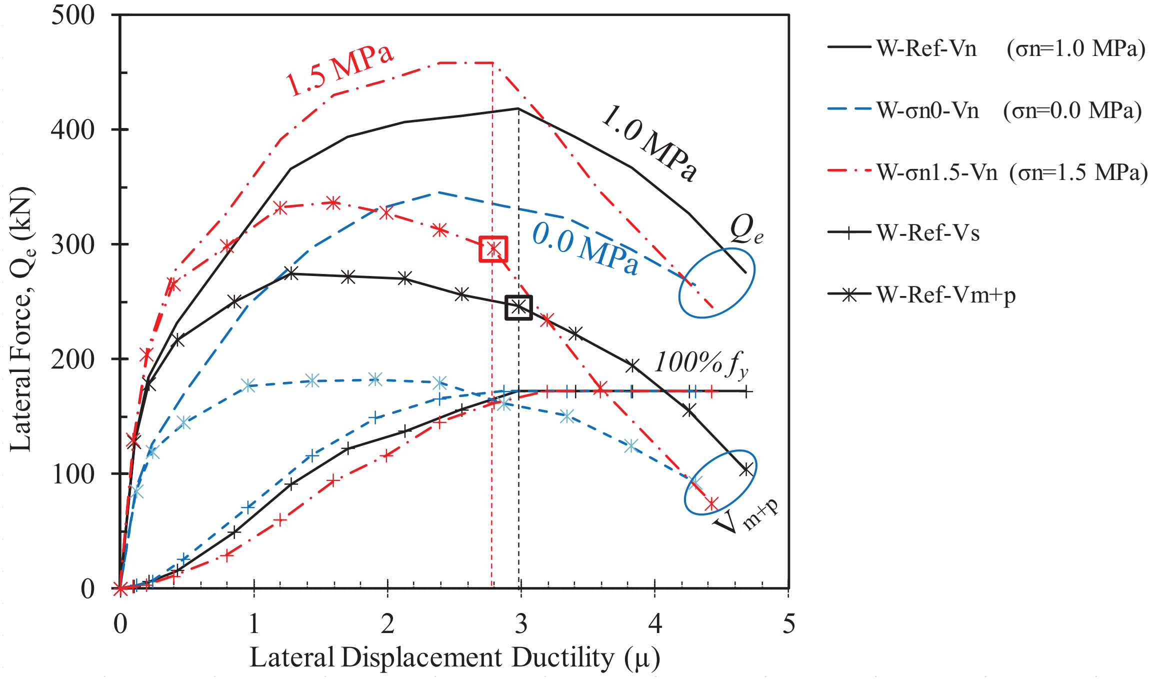

Figure 4.30: Evaluation of V_p at different levels of σ_n

For seismic design purposes, the equivalent energy elastic-perfectly plastic responses for walls W-σ_n0 and W-σ_n1.5 are defined and illustrated in Figure 4.31 and Figure 4.32, respectively. The variation in μ_{Δ}^{ep} was narrow for Wall W-σ_n0, from 1.7 to 4.6, compared to wall W-σ_n1.5 that has a wider range of 2.1 to 7.4. This could be due to the small differences between 50% Q_{ue}, first major shear cracks, and yield points on the experimental lateral force-displacement envelop of Wall W-σ_n0 (see Figure 4.31). Increasing the axial compressive stress, σ_n, from 0.0 to 1.5 MPa resulted in a more elastic behaviour accompanied by a wide difference between $K_{0.5}^{ep}$, K_{FC}^{ep}, and K_{y}^{ep}.

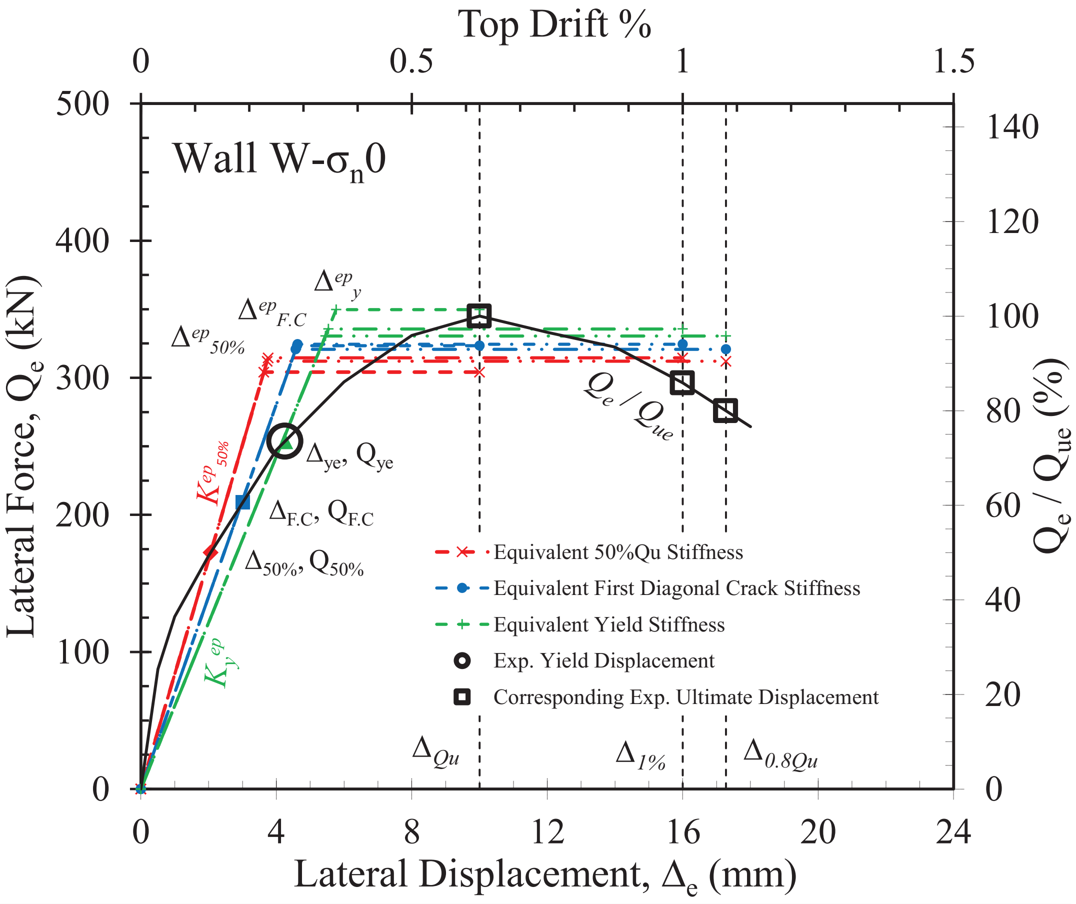

	Ultimate displacement, Δ_u^{ep}, mm												$\frac{\mu_{\Delta}^{ep} V_i}{\mu_{\Delta e} Q_{ue}} = \frac{R_{d,\max}}{\mu_{\Delta e}}$
	At peak lateral force, Δ_{Que}, 10.0				At a drift limit of 1.0%, $\Delta_{1\%}$, 16.0				At a drop to 0.8 Q_u, $\Delta_{0.8Que}$, 17.3				
	$\mu_{\Delta e} = 2.4$				$\mu_{\Delta e} = 3.8$				$\mu_{\Delta e} = 4.1$				
	μ_{Δ}^{ep}	V_i	$\mu_{\Delta}^{ep}/\mu_{\Delta e}$	V_i/Q_{ue}	μ_{Δ}^{ep}	V_i	$\mu_{\Delta}^{ep}/\mu_{\Delta e}$	V_i/Q_{ue}	μ_{Δ}^{ep}	V_i	$\mu_{\Delta}^{ep}/\mu_{\Delta e}$	V_i/Q_{ue}	
	–	kN	–	–	–	kN	–	–	–	kN	–	–	
$^1K_{0.5}^{ep}$	2.8	304	1.15	0.88	4.3	314	1.11	0.91	4.6	312	1.12	0.90	1.02
$^2K_{F.C}^{ep}$	2.2	323	0.91	0.94	3.5	324	0.90	0.94	3.8	321	0.91	0.93	0.85
$^3K_{y}^{ep}$	1.7	350	0.73	1.01	2.9	336	0.76	0.97	3.2	330	0.77	0.96	0.74

Figure 4.31: Equivalent energy elastic-perfectly plastic responses for walls W-σ_n0

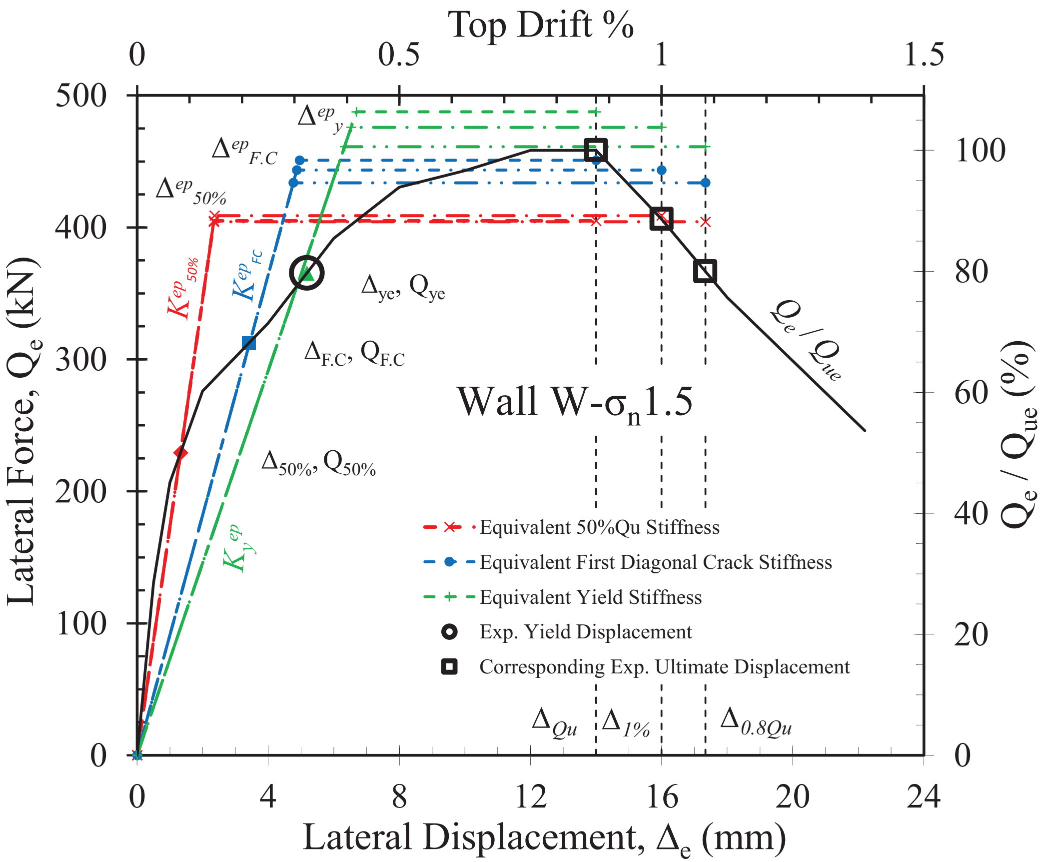

	Ultimate displacement, Δ_u^{ep}, mm												$\frac{\mu_\Delta^{ep} V_i}{\mu_{\Delta e} Q_{ue}} = \frac{R_{d,\max}}{\mu_{\Delta e}}$
	At peak lateral force, Δ_{Que}, 14.0				At a drift limit of 1.0%, $\Delta_{1\%}$, 16.0				At a drop to 0.8 Q_u, $\Delta_{0.8Que}$, 17.2				
	$\mu_{\Delta e} = 2.8$				$\mu_{\Delta e} = 3.2$				$\mu_{\Delta e} = 3.4$				
	μ_Δ^{ep}	V_i	$\mu_\Delta^{ep} / \mu_{\Delta e}$	V_i / Q_{ue}	μ_Δ^{ep}	V_i	$\mu_\Delta^{ep} / \mu_{\Delta e}$	V_i / Q_{ue}	μ_Δ^{ep}	V_i	$\mu_\Delta^{ep} / \mu_{\Delta e}$	V_i / Q_{ue}	
	–	kN	–	–	–	kN	–	–	–	kN	–	–	
[1] $K_{0.5}^{ep}$	6.0	405	2.14	0.88	6.8	409	2.12	0.89	7.4	404	2.15	0.88	1.89
[2] $K_{F.C}^{ep}$	2.8	451	1.01	0.98	3.3	443	1.03	0.97	3.6	434	1.05	0.95	1.00
[3] K_y^{ep}	2.1	488	0.75	1.06	2.5	476	0.77	1.04	2.7	461	0.79	1.01	0.80

Figure 4.32: Equivalent energy elastic-perfectly plastic responses for wall W-σn1.5

Using the effective elastic stiffness as K_{FC}^{ep} or K_y^{ep} for wall W-σn0 does not provide a safe design if R_d is taken equal to $\mu_{\Delta e}$. However, calculating V_i for wall W-σn0 based on $K_{0.5}^{ep}$ and R_d equal to $\mu_{\Delta e}$ results in a factor of safety of 1.02. On the other hand, taking the effective elastic stiffness for wall W-σn1.5 as K_{FC}^{ep} offers the most economic safe design but $K_{0.5}^{ep}$ and K_y^{ep} lead to overdesign and an unsafe inelastic seismic design force, V_i, for the case of R_d equal to $\mu_{\Delta e}$. The idealized elastic-plastic responses, with equal displacements, for walls W-σ_n0, W-Ref, and W-σ_n1.5 are given in Figure 4.33.

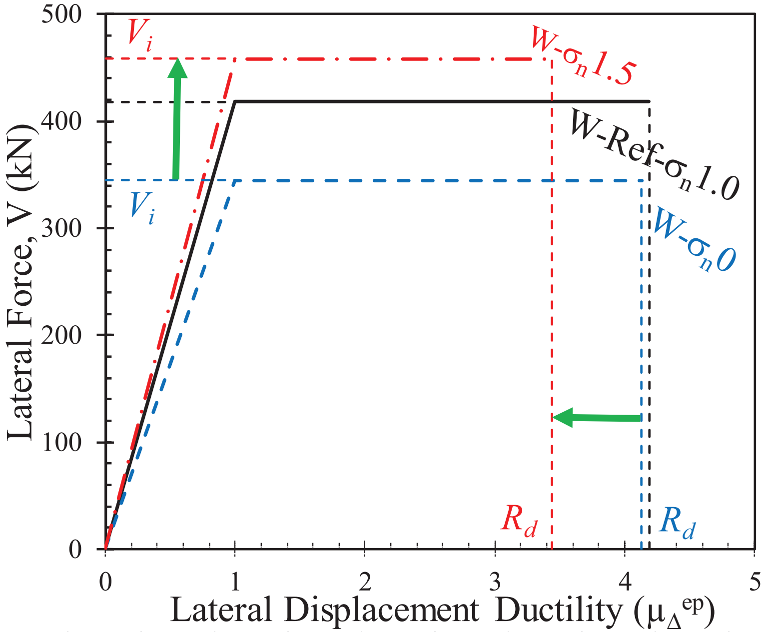

Figure 4.33: Effect of axial compressive stress on idealized elastic-plastic response

4.4.2.2 Displacement-based design

Figure 4.34 shows the effect of the axial compressive stress on the stiffness degradation. The values of the secant stiffness at different levels of top drift for the three tested walls are presented in Figure 4.34a, while Figure 4.34b shows the top drift against stiffness degradation. At an early stage of loading, the axial compressive stress had a considerable effect on the secant stiffness since at a top drift of 0.125%, $K_{s,2mm,}$ was equal to 85, 116, and 138 kN/mm for walls W-σ_n0, W-Ref, and W-σ_n1.5, respectively. However, at a drift limit of 1%, the three walls had about 90% degradation in their initial gross stiffness. During the post-peak behaviour, wall W-σ_n1.5 had a rapid degradation in its secant stiffness related to the stiffness at the peak load, K_{sc}/K_{Que}, compared to walls W-σ_n0 and W-Ref as shown in Figure 4.34-c. Nevertheless, a similar effect was not observed by comparing the post-peak stiffness degradation between wall W-σ_n0 and W-Ref.

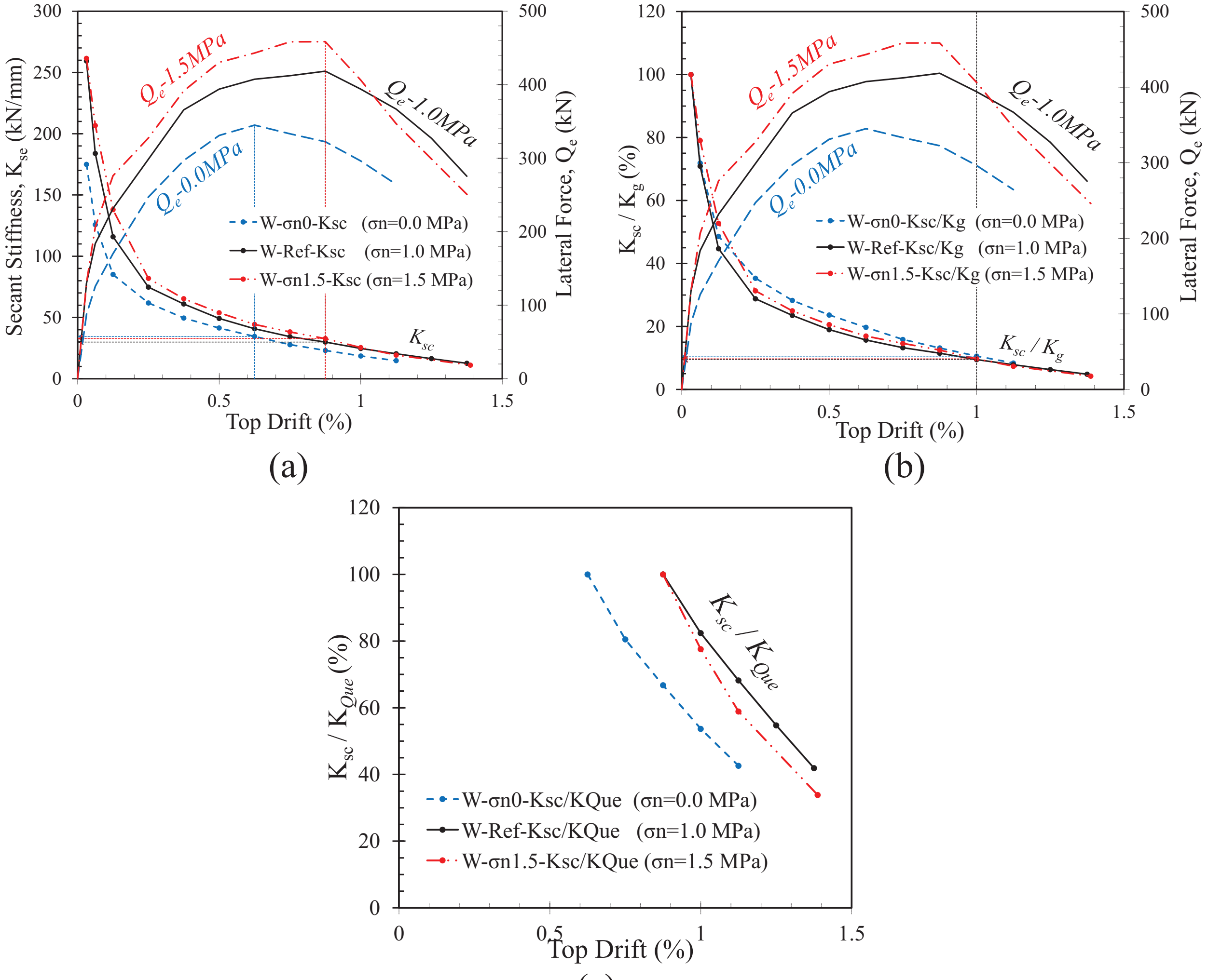

(a)

(b)

(c)

Figure 4.34: Effect of axial compressive stress on stiffness degradation: (a) K_{sc}; (b) K_{sc}/K_g; (c) K_{sc}/K_{Que}

The effect of axial compressive stress on the total energy dissipation and the equivalent viscous damping ratio, ζ_{eq}, is illustrated in Figure 4.35. At a drift limit of 1.0%, increasing the axial compressive stress from 0.0 to 1.0 and 1.5 MPa resulted in higher total dissipated energy by 22% and 36%, respectively. On the other hand, the axial compressive stress does not seem to have a considerable effect on ζ_{eq}. Ignoring the first stage of loading, the equivalent viscous damping ratio, ζ_{eq}, ranged between 12% and 18% for the three tested walls.

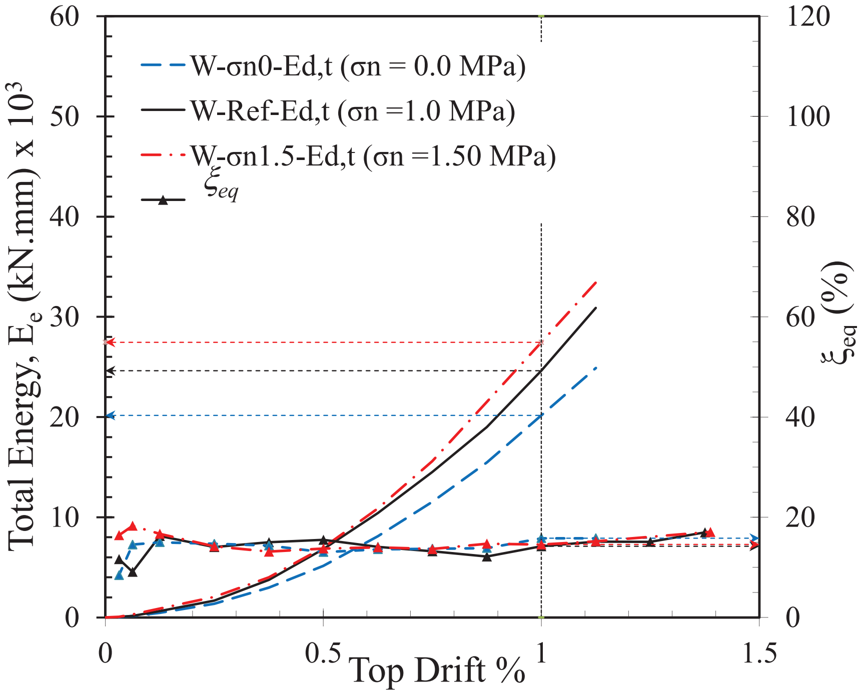

Figure 4.35: Effect of axial compressive stress on Energy dissipation

4.4.2.3 Performance-based design

Figure 4.36 shows the cracking patterns for the three tested walls at different stages: first major diagonal cracks, lateral peak load, Q_u, and when the lateral load dropped to 80% of Q_u. In general, the three walls exhibited a mixed shear-flexural behaviour with a high contribution from the shear deformation towards the overall performance. Figure 4.36a shows the first sign of cracking for the tested walls. The crack pattern in wall W-σ_n0 shows the ability of the test setup to equally distribute the applied lateral load along the length of the tested wall. Furthermore, increasing the axial compressive stress, σ_n, resulted in a higher angle between the diagonal shear cracks and the bed joint plane, θ, followed by less intensity of the initiated cracks. These remarks support the previous conclusion that increasing σ_n enhanced the initial stiffness of tested walls.

At a top drift of 0.63%, wall W-σ_n0 achieved its ultimate lateral load resistance with major damage; however, wall W-σ_n1.5 reached its capacity at higher top drift of 0.88% with less damage (see Figure 4.36b). For the post-peak behaviour, wall W-σ_n1.5 shows more stability with less damage compared to walls W-Ref and W-σ_n0. This could be attributed to the enhancement of the aggregate interlocking at high levels of compressive stress. Nevertheless, the absence of σ_n in wall W-σ_n0 increased the sliding deformation at the top course at late loading stages close to the failure displacement as shown in Figure 4.36c.

From the performance of three tested walls it could be concluded that although the plastic hinge is mostly expected at the base where the maximum loads are, shear failure could occur at the top of a RM shear wall in a multi-story building with a high sliding deformation, since the gravity loads are less than at the base. However, this type of failure is more common in partially grouted masonry walls without sufficient vertical reinforcement, i.e. dowel action.

The effect of axial compressive stress on the crack pattern can be explained by the principal stresses using Mohr's circle. Figure 4.37 presents the principal stresses acting on a masonry panel where a two-dimensional state of stress develops in the wall: axial compressive stress, σ_n, and shear stress. The principal stresses due to uniform shear stress and before applying σ_n are given in Figure 4.37b as σ_t, σ_c, and v with an angle of θ. When the principal tensile stress, σ_t, exceeds the tensile strength of masonry, the initiation of diagonal shear cracks takes place in masonry walls. However, the presence of the axial compressive stress, σ_n, increases the principal compressive stresses to be σ_n'; meanwhile, it reduces the principal tensile stresses to σ_t' due to the compressive field created by σ_n as shown in Figure 4.37c. Hence, to reach the same tensile strength, σ_t, a higher value of shear stress, v', is required (see Figure 4.37d). Moreover, it is clear from the same figure that increasing σ_n results in a higher angle of the principal stresses, θ'.

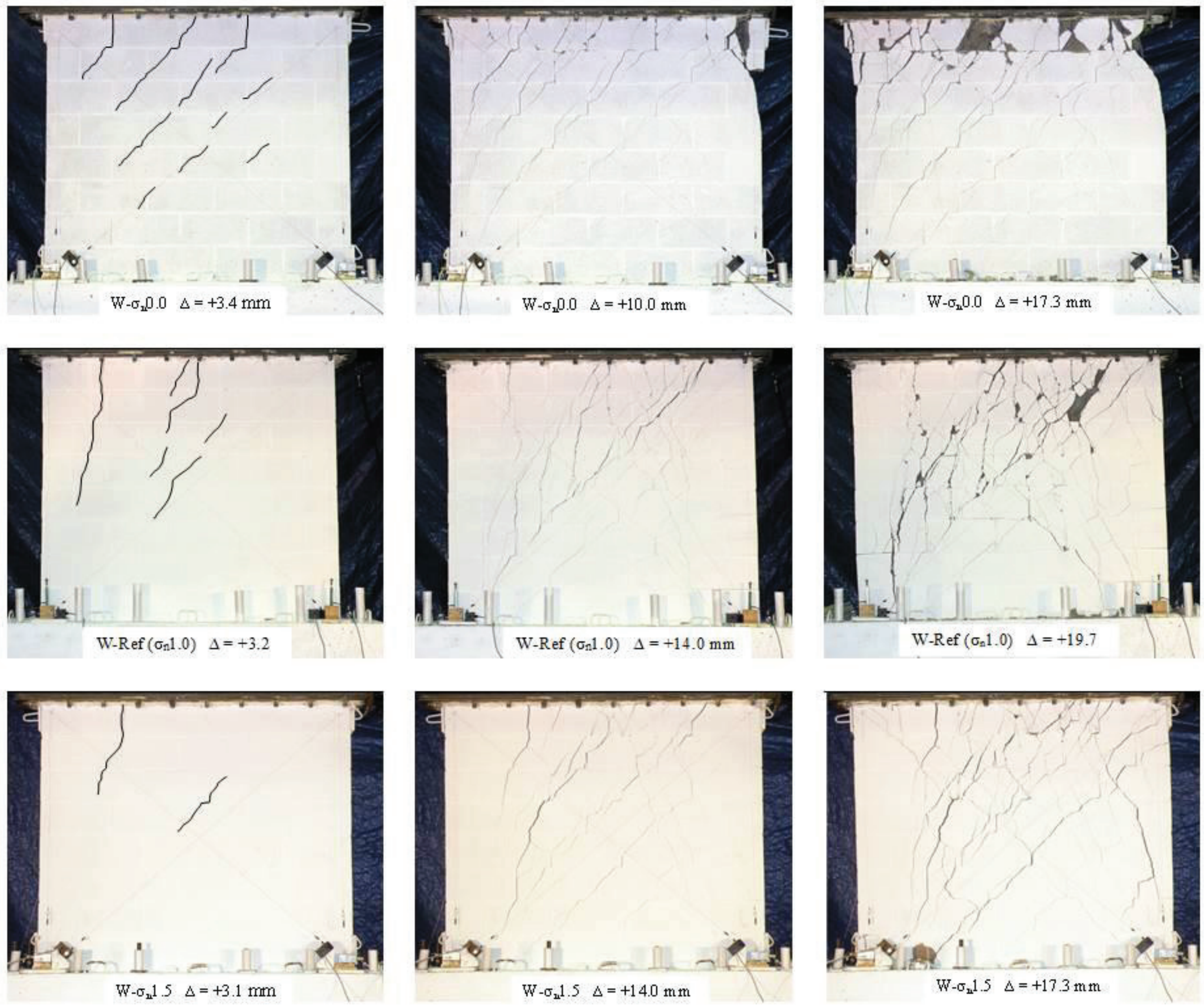

(a) (b) (c)

Figure 4.36: Effect of axial compressive stress on crack pattern at: (a) first major diagonal cracks; (b) lateral peak load Q_{ue}; (c) when the lateral load dropped to 80% of Q_{ue}

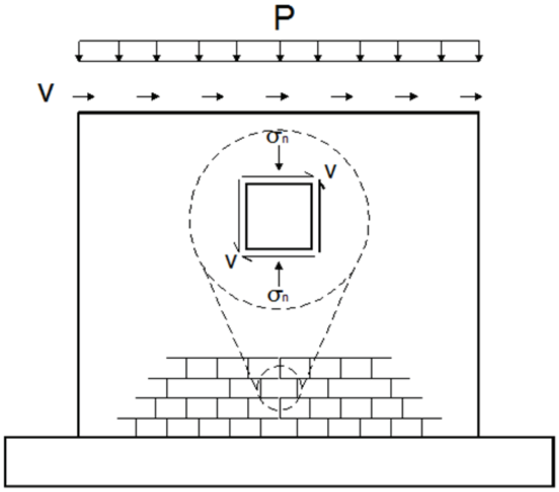

(a) State of stress

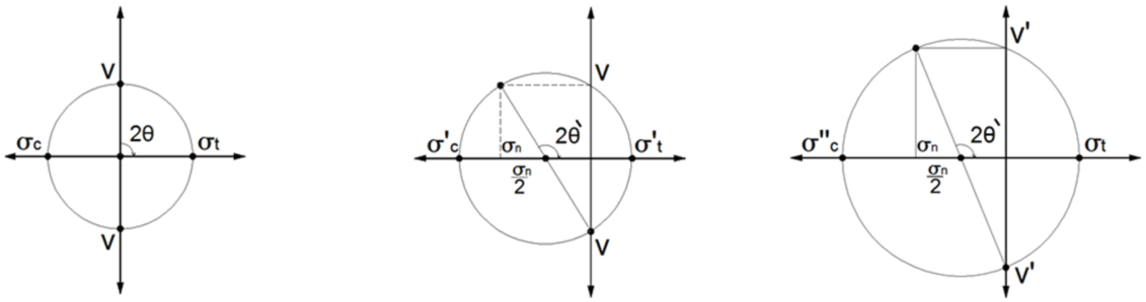

(b) (c) (d)

Figure 4.37: Principal stresses acting on the masonry wall under different levels of axial compressive stress, σ_n

4.4.3 EFFECT OF SHEAR SPAN TO DEPTH RATIO (*M/Vd*$_v$)

One of the important parameters that influence the inelastic behaviour of RM shear walls is the shear span to depth ratio, M/Vd_v. Most of the existing design codes for masonry structures, including the North American codes, limit the effect of M/Vd_v to an upper limit of 1.0. Wall W-M/Vd_v1.8 was subjected to a top moment of 0.9V kN.m, where V is the lateral load from the horizontal actuator. Instead, Wall W-Ref was tested without a top moment. As proposed by the Canadian Standards Association CSA S304-14, the effective shear depth, d_v, was taken as 0.8 l_w. Thus, the value of M/Vd_v for walls W-Ref and W-M/Vd_v1.8 are 1.25 and 1.875, respectively. Since both walls had the same dimensions and reinforcement, comparison between their behaviours is provided in the next section that evaluates the effect of M/Vd_v on the in-plane shear performance of RM shear walls.

4.4.3.1 Force based-design

The test results presented in Figure 4.38 show a reduction in the achieved ultimate force, Q_{ue}, by 25% due to increasing M/Vd_v from 1.25 to 1.875. This loss in the shear resistance is accompanied by enhancement in the displacement ductility, $\mu_{\Delta 0.8Qu}$, from 4.2 to 5.2. Moreover, the crack strength of wall W-M/Vd_v1.8 was 30% less than wall W-Ref. As can be seen in Figure 4.38, Wall W-M/Vd_v1.8 achieved its yield capacity at a lateral load, Q_{ye}, of 230 kN compared to 328 kN when the same wall was tested without a top moment.

Figure 4.39 illustrates the effect of M/Vd_v on shear resistance shares provided by horizontal reinforcement, V_s, and masonry and axial compressive stress, V_{m+p}. The shear span to depth ratio does not have a significant effect on V_s since the horizontal reinforcement in both walls reached its yield capacity at the same μ_Δ of 3.0. At an early stage of ductility, the shear resistance provided by V_s in wall W-M/Vd_v1.8 was higher than W-Ref because wall W-M/Vd_v1.8 reached its inelastic deformations earlier. On the other hand, the aforementioned reduction in Q_{ue} due to increasing M/Vd_v from 1.25 to 1.875, could be due to the losses in $(V_{m+p})_{\max}$ as shown in Figure 4.39b. In wall W-Ref, the masonry and axial compressive stress contributed with an ultimate resistance of 275 kN at μ_Δ of 1.27 followed by rapid strength degradation. This behaviour became more ductile in wall W-M/Vd_v1.8 with less capacity, $(V_{m+p})_{\max}$, equal to 155 kN.

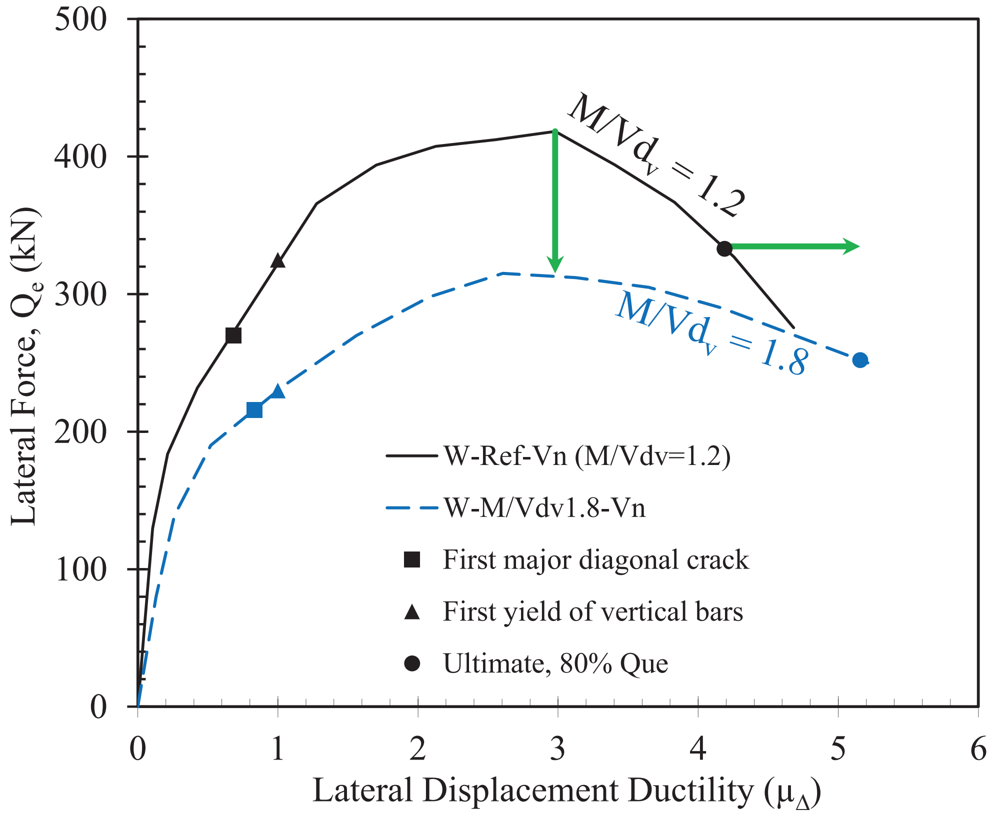

	Q_{ye}	Δ_{ye}	Q_{ue}	Δ_{Que}	$\Delta_{0.8Que}$	$\mu_{\Delta Que}$	$\mu_{\Delta 0.8Que}$	$\mu_{\Delta e1\%}$	Δ_{FCe}	Q_{FCe}
	(kN)	(mm)	(kN)	(mm)	(mm)	—	—	—	(mm)	(kN)
W-Ref	328	4.7	418	14.0	19.7	3.0	4.2	3.4	3.2	272
W-*M/Vd*$_v$1.8	230	3.8	315	10.0	19.8	2.6	5.2	4.2	3.2	216

Figure 4.38: Effect of shear span to depth ratio, *M/Vd$_v$*, on in-plane shear strength of RM shear walls

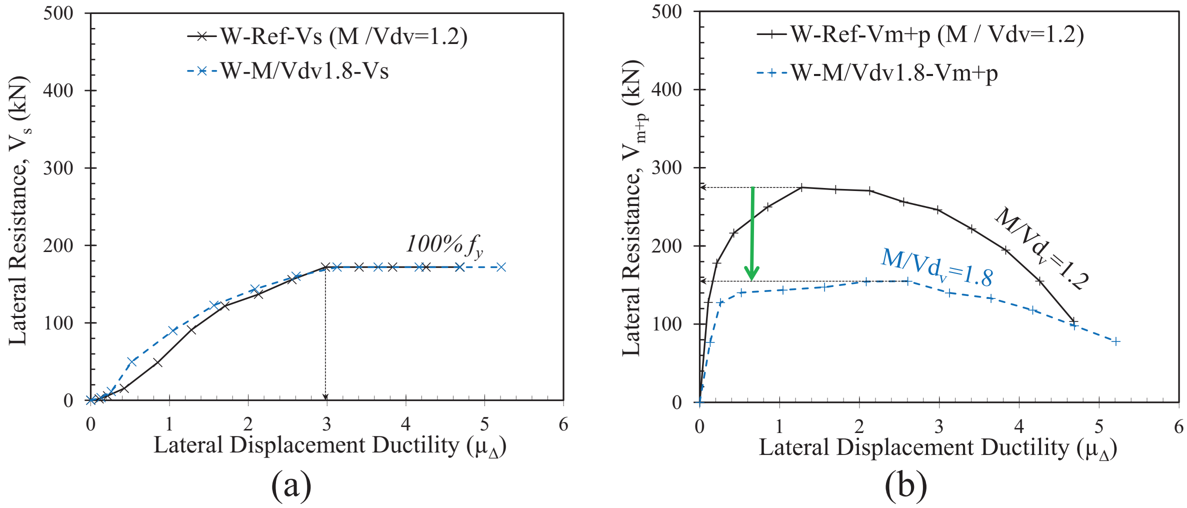

(a) (b)

Figure 4.39: Effect of shear span to depth ratio, *M/Vd$_v$*, on shear resistance shares provided by: (a) horizontal reinforcement, *V_s*; (b) masonry and axial compressive stress, *V_{m+p}*

The test results of walls W-Ref and W-M/Vd_v1.8 show that limiting the effect of shear span to depth ratio to an upper value of 1.0, as provided in most of the masonry design codes, is overestimating the in-plane shear strength of RM shear walls, V_n, at high values of M/Vd_v, which might lead to an unsafe design. This experimentally measured reduction in the shear capacity could be explained by considering the interaction between the flexural and shear performances, as shown in Figure 4.40. Both walls had same dimensions and reinforcement such that they have the same shear strength envelope and moment capacity. Increasing M/Vd_v results in a reduction in the lateral force that corresponds to the flexural capacity of the wall. Consequently, this lower lateral force intersects with the shear strength envelope at a lower capacity along with higher displacement ductility.

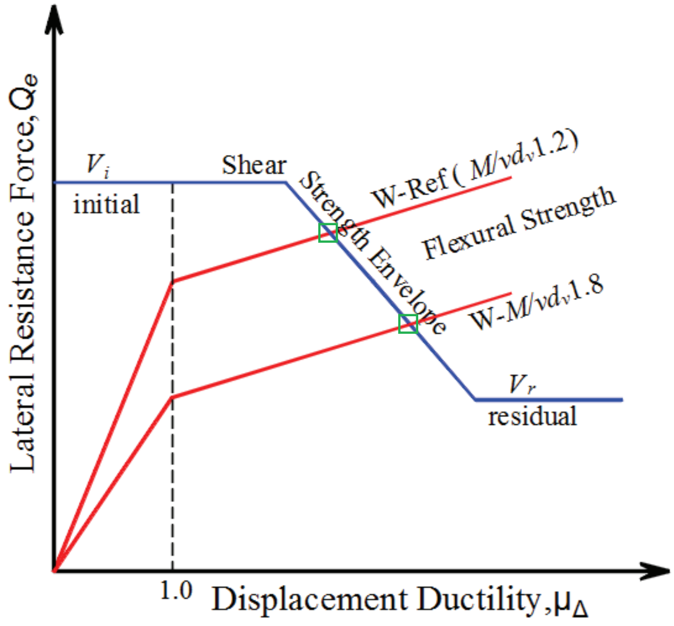

Figure 4.40: Interaction between flexural and shear performance of walls: W-Ref and W-M/Vd_v1.8

Due to the ductile behaviour of wall W-M/Vd_v1.8, the value of μ_{Δ}^{ep} is sensitive to the method followed in characterizing the equivalent energy elastic-plastic response as shown in Figure 4.41. The displacement ductility of the elastic-plastic response, μ_{Δ}^{ep}, varied between 1.9 and 8.1;

whereas, the corresponding V_i has a narrow range of $0.84Q_{ue}$ to $1.02Q_{ue}$. For a safe seismic design using the FBD approach, the value of R_d cannot be taken more than $0.73\mu_{\Delta e}$ if the secant yield stiffness, K_y^{ep}, is considered. On the other hand, using a more conservative effective stiffness, such as K_{50}^{ep}, allows use of R_d up to 1.41 $\mu_{\Delta e}$.

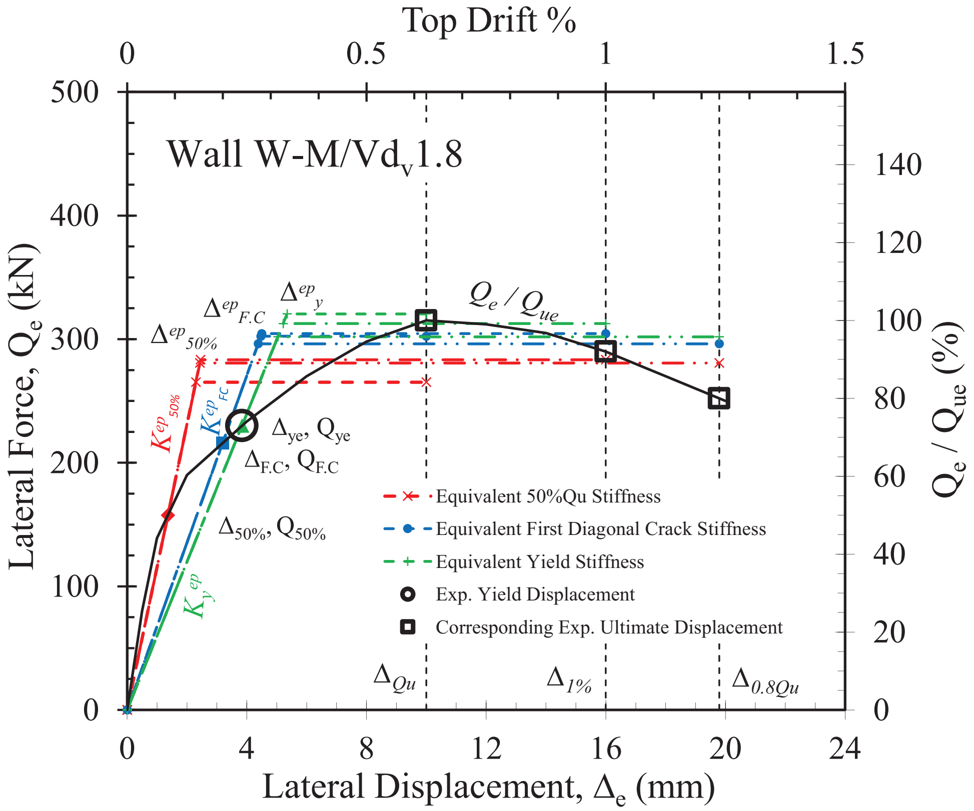

	Ultimate displacement, Δ_u^{ep}, mm												$\frac{\mu_\Delta^{ep} V_i}{\mu_{\Delta e} Q_{ue}} = \frac{R_{d,\max}}{\mu_{\Delta e}}$
	At peak lateral force, Δ_{Que}, 10.0				At a drift limit of 1.0%, $\Delta_{1\%}$, 16.0				At a drop to 0.8 Q_u, $\Delta_{0.8Que}$, 19.8				
	$\mu_{\Delta e} = 2.6$				$\mu_{\Delta e} = 4.2$				$\mu_{\Delta e} = 5.2$				
	μ_Δ^{ep}	V_i	$\mu_\Delta^{ep}/\mu_{\Delta e}$	V_i/Q_{ue}	μ_Δ^{ep}	V_i	$\mu_\Delta^{ep}/\mu_{\Delta e}$	V_i/Q_{ue}	μ_Δ^{ep}	V_i	$\mu_\Delta^{ep}/\mu_{\Delta e}$	V_i/Q_{ue}	
	–	kN	–	–	–	kN	–	–	–	kN	–	–	
$^1K_{0.5}^{ep}$	4.4	265	1.67	0.84	6.5	283	1.56	0.90	8.1	281	1.58	0.89	1.41
$^2K_{F.C}^{ep}$	2.2	302	0.86	0.96	3.6	304	0.85	0.97	4.5	296	0.88	0.94	0.82
$^3K_y^{ep}$	1.9	320	0.72	1.02	3.1	313	0.74	0.99	3.9	302	0.76	0.96	0.73

Figure 4.41: Equivalent energy elastic-perfectly plastic responses for wall W-*M/Vd*$_v$1.8

The idealized effective elastic stiffness, K_{id}^{ep}, for wall W-*M/Vd*$_v$1.8 was calculated as 82 kN/mm which is almost 50% of its initial gross stiffness, K_g. However, K_{id}^{ep} is equal to $0.35K_g$ for wall W-Ref. Hence, for higher shear span to depth ratio, *M/Vd*$_v$, more conservative stiffness for the equivalent elastic system, K_e, needs to be considered such that safe seismic design is achieved. The effect of shear span to depth ratio, M/Vd_v, on idealized elastic-plastic response is presented in Figure 4.42.

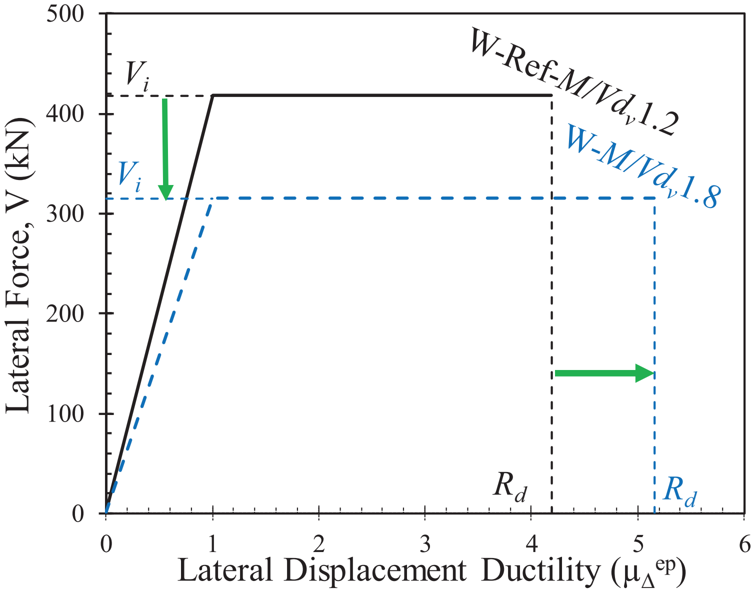

Figure 4.42: Effect of shear span to depth ratio, M/Vd_v, on idealized elastic-plastic response

4.4.3.2 Displacement-based design

Increasing the shear span to depth ratio, M/Vd_v, reduces the initial gross stiffness, K_g. Wall W-M/Vd_v1.8 had K_g equal to 160 kN/mm compared to 259 kN/mm for wall W-Ref that has M/Vd_v of 1.25. However, the difference in the secant stiffness at the same level of top drift became smaller as the tested walls reached higher levels of deformation (see Figure 4.43a). Both walls reached their peak lateral load at the same secant stiffness of 30 kN/mm. However, wall W-Ref achieved its maximum resistance at a higher top drift of 0.875% compared to 0.625% for wall M/Vd_v1.8. On the other hand, increasing M/Vd_v enhanced the stiffness degradation as shown in Figure 4.43b. Wall W-M/Vd_v1.8 had about 50% reduction in its initial stiffness at a top drift of 0.18%, while wall W-Ref had the same stiffness degradation at earlier levels of deformation with a top drift of 0.11%. At a drift limit of 1%, the values of K_{sc} were 9.5% and 11.3% of the corresponding K_g when M/Vd_v was equal to 1.25 and 1.875, respectively. Moreover, Wall W-M/Vd_v1.8 had a gradually degradation in its secant stiffness related to the secant stiffness at the peak load, K_{sc}/K_{Que}, compared to wall W-Ref as shown in Figure 4.43c.

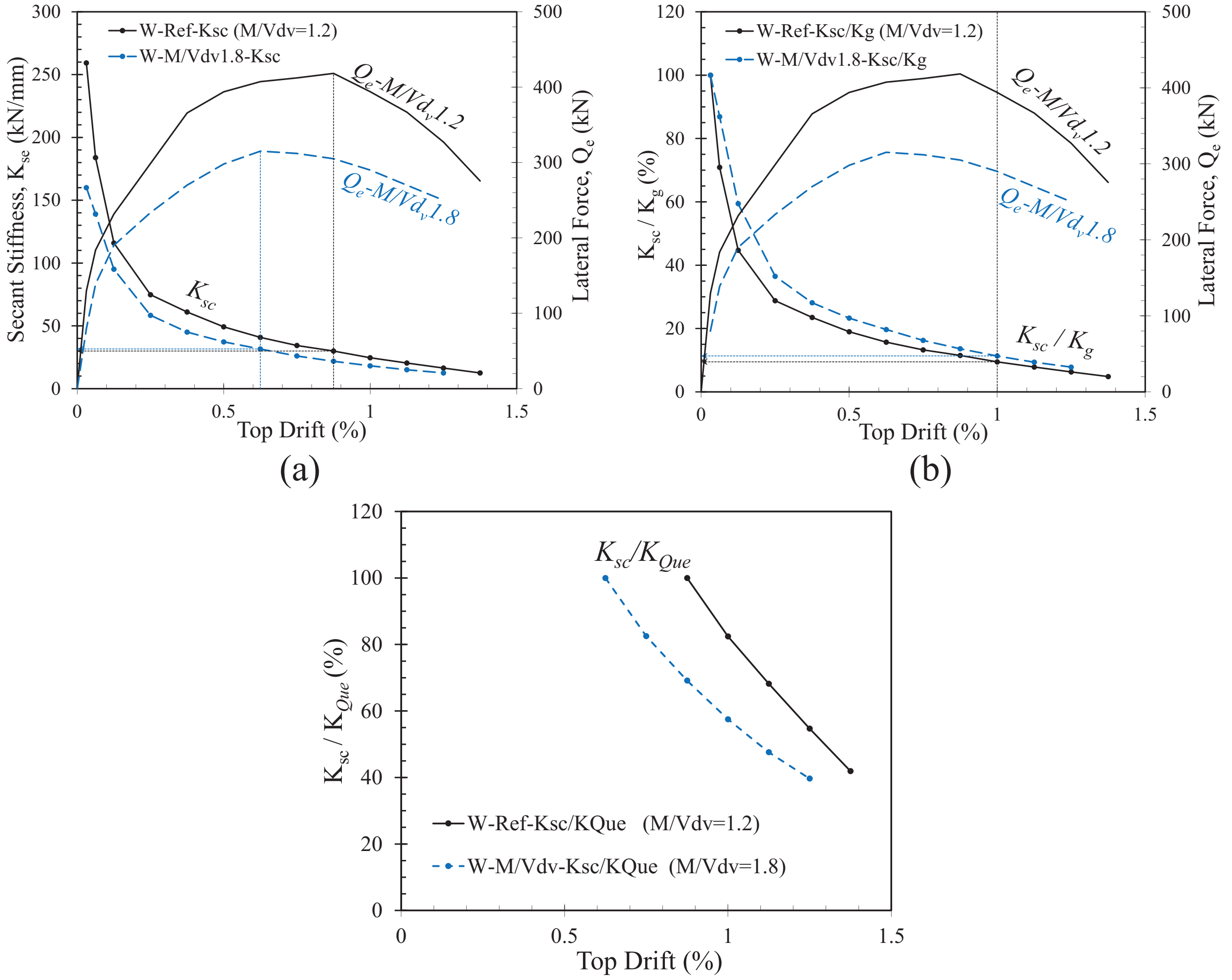

(a) (b)

(c)

Figure 4.43: Effect of shear span to depth ratio, M/Vd_v, on stiffness degradation: (a) K_{sc}; (b) K_{sc}/K_g; (c) K_{sc}/K_{Que}

The impact of the M/Vd_v on the total dissipated energy and the equivalent viscous damping ratio, ζ_{eq}, is given in Figure 4.44. Although Wall W-M/Vd_v1.8 had a more ductile performance than wall W-Ref, still wall W-Ref was able to dissipate more energy. At a top drift of 1%, wall

W-Ref with M/Vd_v of 1.25 dissipated 30% higher energy than wall W-M/Vd_v1.8. This percentage decreased to 26% when both walls had a drop in their in-plane lateral force capacity to 80% of Q_{ue}. The shear span to depth ratio did not show a significant influence on ζ_{eq}. After a top drift of 0.25% and until failure, both walls had an average equivalent viscous damping ratio, ζ_{eq}, of 14.4% (c.o.v. = 9.1%).

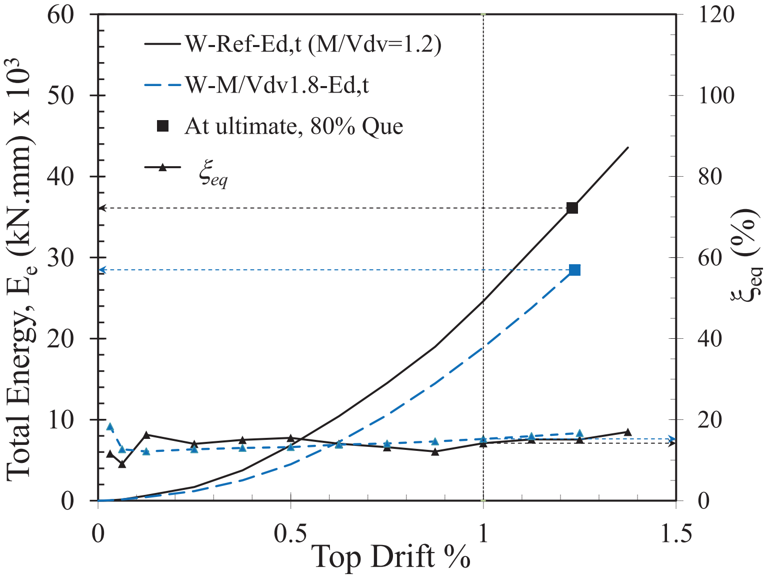

Figure 4.44: Effect of shear span to depth ratio, M/Vd_v, on energy dissipation

4.4.3.3 Performance-based design

Wall W-Ref with M/Vd_v equal to 1.25 and wall W-M/Vd_v1.8 had similar crack propagation as shown in Figure 4.45. Both walls were characterized by moderately ductile failure. Initial diagonal crack damage was observed at a top drift of 0.2% for both walls. As the imposed in-plane top lateral displacement increased, more cracks were formed and gradually spread over the wall diagonals. Wall W-M/Vd_v1.8 reached its lateral load capacity at early levels of deformation when subjected to top displacement of +10.0 mm; instead, Wall W-Ref was able to gain more resistance until Δ_e equal to +14.0 mm. Yet, wall W-M/Vd_v1.8 required more number of loading cycles to lose 20% of its shear strength, Q_{ue}, compared to Wall W-Ref. The two tested walls reached their failure point at almost the same Δ_e with an average top drift of 1.23%. However, increasing M/Vd_v from 1.25 to 1.875 resulted in higher levels of axial compressive stress on the end zones. Hence, buckling failure was observed in W-M/Vd_v1.8 as shown in Figure 4.45c. Nevertheless, this failure occurred in the wall cover outside the confined core as presented in Figure 4.46. Moreover, the right side view of the final crack pattern for wall W-M/Vd_v1.8 does not show any inside crushing in the grout, which could explain the enhancement in the stiffness degradation during the post-peak behaviour.

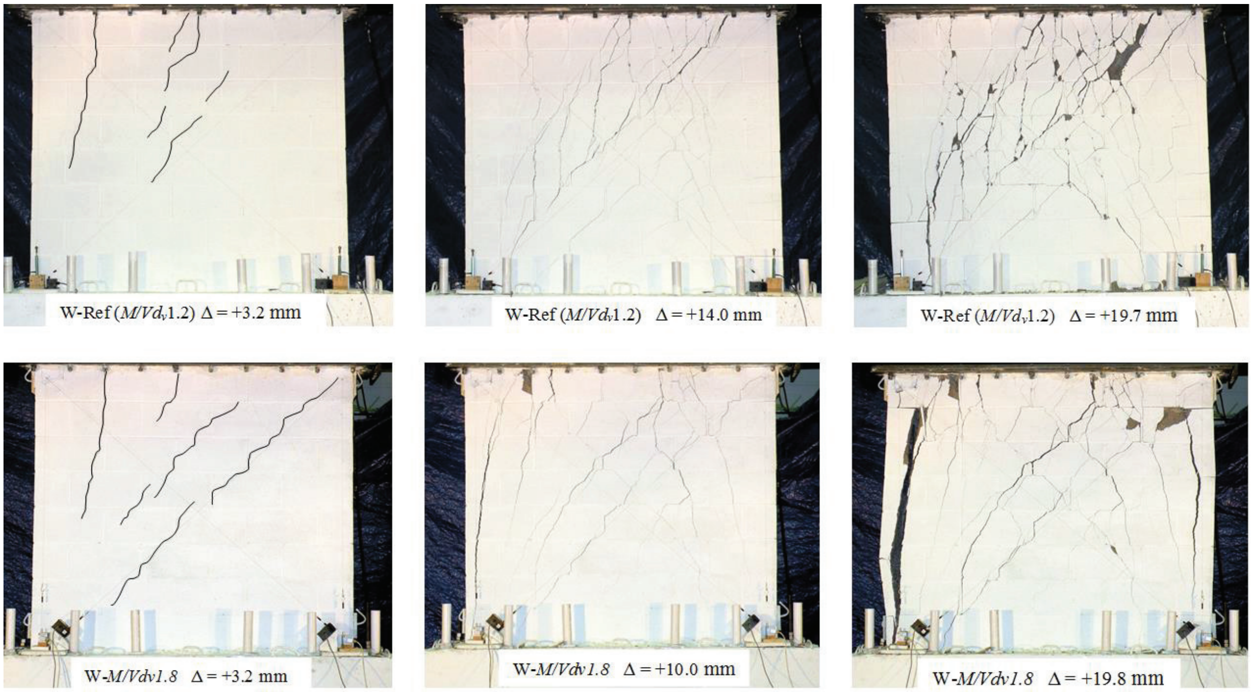

(a) (b) (c)

Figure 4.45: Effect of shear span to depth ratio, M/Vd_v, on crack pattern at: (a) first major diagonal cracks; (b) lateral peak load Q_{ue}; (c) when the lateral load dropped to 80% of Q_{ue}

W-*M/Vdv1.8* at the end of testing

Right side view

Figure 4.46: Final crack pattern of tested wall W-M/Vd_v1.8

4.4.4 EFFECT OF HORIZONTAL REINFORCEMENT ANCHORAGE END DETAIL

The Canadian Standards Association CSA S304 for design of masonry structures classifies RM shear walls according to their ductility. The previous version CSA S304.1-04 classified it as follows: conventional construction shear walls (R_d = 1.5); limited ductility shear walls (R_d = 1.5); and moderately ductile shear walls (R_d = 2.0). However, modifications have been made to this classification in the current version, CSA S304-14, such that the limited ductility shear wall was removed and a new class introduced for ductile shear walls (R_d = 3.0). The plastic hinge region was defined for moderately ductile and ductile RM shear walls, with R_d equal to 2.0 and 3.0, respectively. In this region, additional seismic reinforcement detailing is required where inelastic flexural curvature occurs.

The height of the plastic hinge region, h_p, above the critical section of the wall is limited to the greater of $l_w/2$ or $h_w/6$ but not greater than $1.5l_w$, where l_w is taken as the length of the longest RM shear wall in the building. On the other hand, for R_d = 3.0 the lower limit is taken as $(0.5l_w+0.1h_w)$ but not less than $0.8l_w$. According to the seismic reinforcement requirements for moderately ductile RM shear walls in CSA S304-14, the anchorage of the horizontal reinforcing bars in the plastic hinge region shall have 90°, or more, standard hook at the ends of the conventional and moderately ductile walls, whereas a 180° standard hook is required for the ductile shear walls. However, in the previous CSA S304.1-04, only a 180° standard hook was mandatory for ductile wall classes, including the limited ductile. For the conventional construction RM shear walls with R_d equal to 1.5 and outside the plastic hinge region for other R_d values, a 90° standard hook is required. However, some international codes (e.g. New Zealand, NZS 4230:2004) accept the 90° anchorage hook for ductile RM shear walls.

As discussed in Chapter 2, only a few studies have considered the effect of the lateral reinforcement anchorage end detail on its contribution to the in-plane shear strength of RM walls, one of which is the experimental work conducted by Sveinsson et al. (1985). Throughout the experimental work in Chapter 3, three different types of horizontal reinforcement anchorage details were evaluated. Wall W-Ref was constructed with 180° standard hook horizontal reinforcing bars, while walls W-90° and W-str had 90º hook and straight bars, respectively. The impact of the horizontal reinforcement anchorage end detail on the in-plane seismic performance of RM shear walls is presented in this section.

4.4.4.1 Force-based design

Since the horizontal reinforcement did not show a significant effect on the pre-crack behaviour with minor impact on the yield capacity, its anchorage end detail is not expected to have a considerable influence on the in-plane shear performance of RM shear wall prior to the yield load. Figure 4.47 shows that the 180° hook is the most effective anchorage end detail in terms of lateral force capacity and ductility. However, wall W-90° reached a similar shear capacity as wall W-Ref with a 7.0% less displacement ductility, μ_Δ. On the other hand, constructing wall W-Str with straight horizontal reinforcing bars resulted in a reduction in both shear capacity and displacement ductility. Wall W-Str reached an ultimate lateral load, Q_{ue}, of 398 kN compared to 418 kN for wall W-Ref, followed by a rapid degradation in its in-plane lateral force resistance. At a 20% reduction in Q_{ue}, the straight horizontal reinforcement had the least ductile behaviour with $\mu_{\Delta 0.8Que}$ equal to 3.6; whereas, walls W-Ref and W-90° achieved $\mu_{\Delta 0.8Que}$ of 4.2 and 3.9, respectively.

The three tested walls W-Ref, W-90°, and W-Str were horizontally reinforced with four bars that were uniformly distributed along the height. The first bar was placed at the first row followed by 400 mm vertical spacing between bars. The readings of the lateral bars strain gauges show that the first bar from the base footing for wall W-Str did not have a sufficient development length, l_d, to reach its yield strength. Therefore, the in-plane shear resistance provided by its horizontal reinforcement, V_s, just reached 84% of its yield capacity. On the other hand, providing 180° and 90° hook anchorage for walls W-Ref and W-90°, respectively, were more effective. Hence, all of their horizontal bars achieved their yield strength as shown in Figure 4.48a. This could explain the reduction in the reached ultimate lateral force, Q_{ue}, for wall W-Str.

Figure 4.48b presents the masonry and axial compressive stress contribution, V_{m+p}, at different levels of displacement ductility for the three tested walls. The slight variation in these relations show that the horizontal reinforcement anchorage detail has a negligible effect on V_{m+p} up to the peak lateral force resistance, Q_{ue}; however, it has a considerable influence on the resistance degradation of V_{m+p}. Wall W-Ref had a gradual reduction in V_{m+p} compared to walls W-90° and W-Str. This enhancement could be attributed to the sufficient confinement of the 180° hook anchorage compared to the other end details as shown in Figure 4.49.

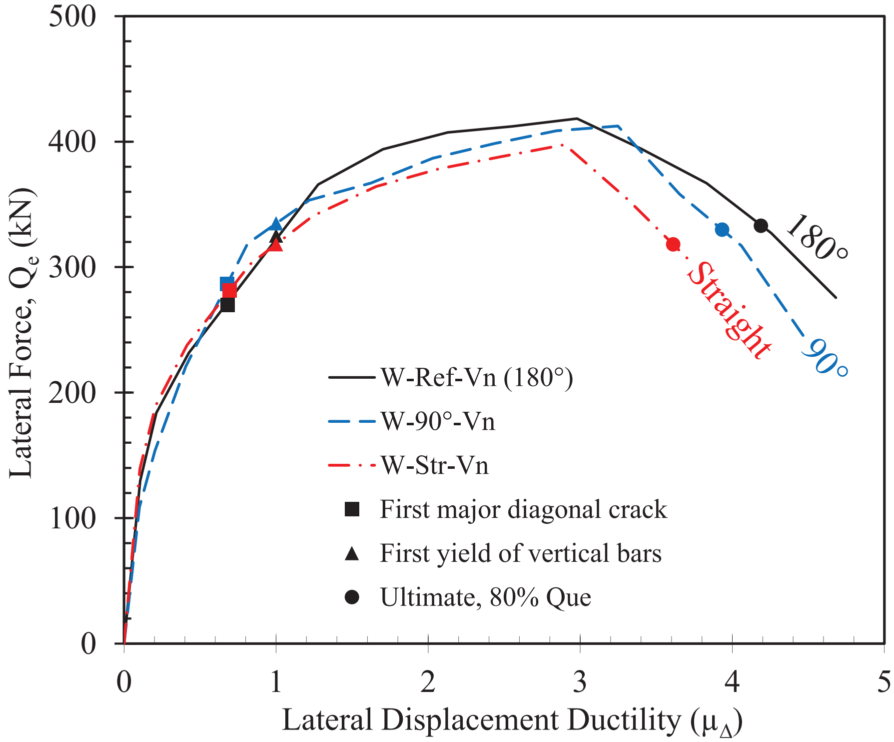

	Q_{ye}	Δ_{ye}	Q_{ue}	Δ_{Que}	$\Delta_{0.8Que}$	$\mu_{\Delta Que}$	$\mu_{\Delta 0.8Que}$	$\mu_{\Delta e1\%}$	Δ_{FCe}	Q_{FCe}
	(kN)	(mm)	(kN)	(mm)	(mm)	—	—	—	(mm)	(kN)
W-Ref-180°	328	4.7	418	14.0	19.7	3.0	4.2	3.4	3.2	272
W-90°	335	4.9	412	16.0	19.4	3.2	3.9	3.2	3.3	287
W-Str	318	4.8	398	14.0	17.4	2.9	3.6	3.3	3.4	281

Figure 4.47: Effect of horizontal reinforcement anchorage end detail on in-plane shear strength of RM shear walls

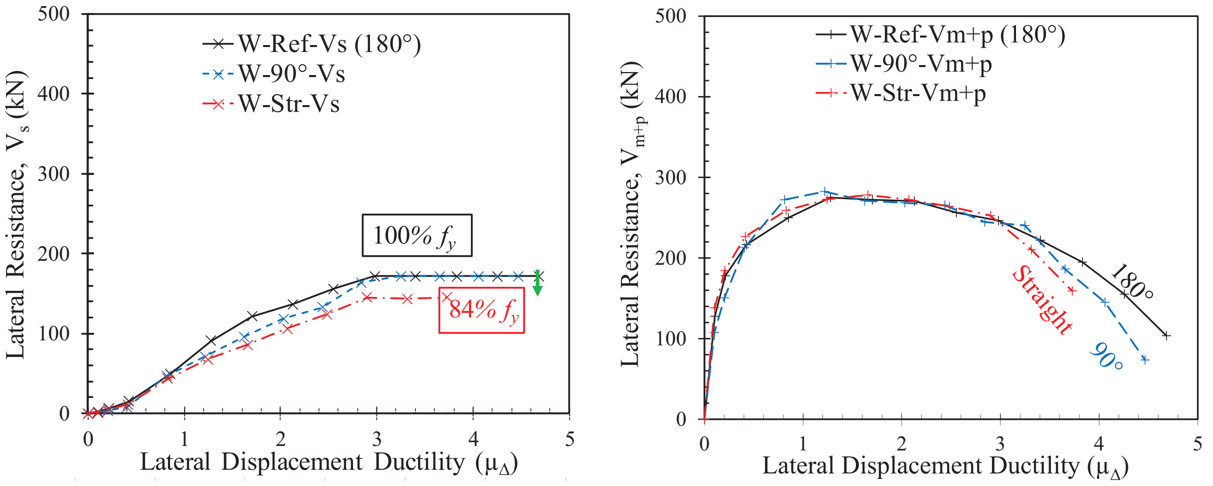

(a) (b)

Figure 4.48: Effect of horizontal reinforcement anchorage end detail on shear resistance shares provided by: (a) horizontal reinforcement, V_s; (b) masonry and axial compressive stress, V_{m+p}


(a) (b)

Figure 4.49: In-plane lateral confinement of vertical reinforcement using: (a) 180° hook; (b) 90° hook anchorage end detail

It can be concluded from the test results of walls W-Ref, W-90°, and W-Str, and from the previous discussion that the horizontal reinforcement anchorage end detail in RM shear walls has two main functions. The first one is to provide a sufficient development length such that the horizontal bars can reach their yield strength, while the second is to improve the confinement of the extreme vertical bars and the grout in the end zones under compressive stress. These two functions are responsible for the enhancement of the in-plane lateral strength and displacement ductility, respectively. Since the 90° and 180° hooks were able to provide the needed development length, the lateral resistance provided by the horizontal reinforcement in both walls reached its yield capacity. Even though both walls reached similar in-plane shear resistance, the 90° hook was not as sufficient for confinement as the 180° hook. Consequently, wall W-Ref achieved higher displacement ductility. These conclusions could explain the seismic reinforcement requirements provided in CSA S304-14, where a 180° hook is necessary inside the plastic hinge region of ductile shear walls due to the expected high level of plastic deformations.

Instead, inside the plastic hinge region for low ductile (moderately ductile) RM shear walls or anywhere outside this region where the main aspect for design is related to force capacity, a 90° hook is acceptable.

Although the 180° and 90° hook is more efficient than the straight bar, using them may cause congestion at the end zone for narrow blocks. Moreover, the reduction in Q_{ue} when using straight horizontal bars is still minor; it was less than 5% between walls W-Ref and W-Str. Therefore, to facilitate the construction process, it is suggested that straight horizontal bars could be permitted in regions where high ductility is not required; for example, in higher floors outside the critical region with high demands of the conventional construction shear walls. The height of the critical region could be taken as h_p, similar to the plastic hinge region. Furthermore, it could be argued to use straight horizontal reinforcement outside the plastic hinge region of moderately ductile RM shear walls where R_d equals 2.0.

Figure 4.50 and Figure 4.51 show the equivalent energy elastic-perfectly plastic responses for walls W-90° and W-Str, respectively. The maximum value for the ratio $R_d/\mu_{\Delta e}$ that could be taken for a safe design ($V_i \geq Q_{ue}$) was calculated as 1.38, 1.02, and 0.81 for wall W-90°, and 2.02, 1.02, and 0.8 for wall W-Str when using $K_{0.5}^{ep}$, K_{FC}^{ep}, or K_{y}^{ep} as the effective stiffness for the equivalent elastic response, respectively. However, the horizontal reinforcement anchorage end detail did not have a considerable effect on the idealized effective elastic stiffness, K_{id}^{ep}, as can be seen in Figure 4.52. The values of K_{id}^{ep} for the three tested walls, W-Ref, W-90°, and W-Str, were calculated as 89, 84, and 82 kN/mm, respectively, with insignificant differences.

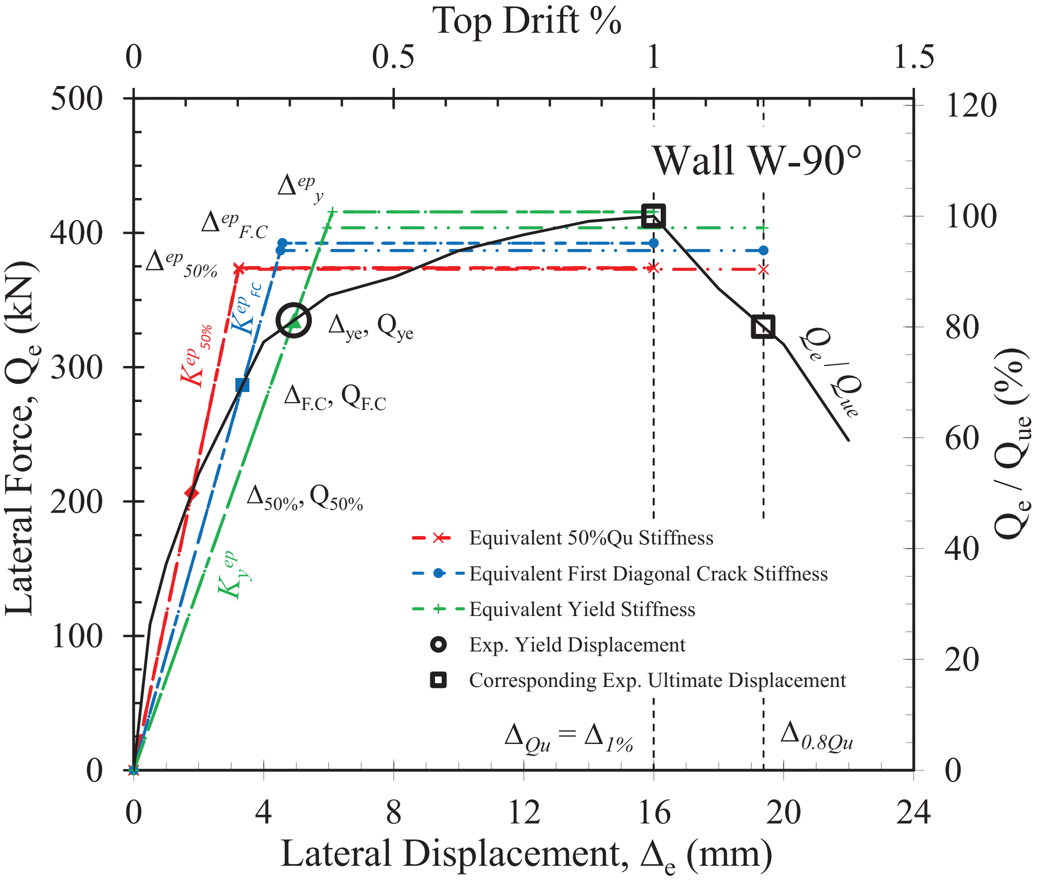

	Ultimate displacement, Δ_u^{ep}, mm												$\frac{\mu_\Delta^{ep} V_i}{\mu_{\Delta e} Q_{ue}} = \frac{R_{d,\max}}{\mu_{\Delta e}}$
	At peak lateral force, Δ_{Que}, 16.0				At a drift limit of 1.0%, $\Delta_{1\%}$, 16.0				At a drop to 0.8 Qu, $\Delta_{0.8Que}$, 19.4				
	$\mu_{\Delta e} = 3.2$				$\mu_{\Delta e} = 3.2$				$\mu_{\Delta e} = 3.9$				
	μ_Δ^{ep}	V_i	$\mu_\Delta^{ep}/\mu_{\Delta e}$	V_i/Q_{ue}	μ_Δ^{ep}	V_i	$\mu_\Delta^{ep}/\mu_{\Delta e}$	V_i/Q_{ue}	μ_Δ^{ep}	V_i	$\mu_\Delta^{ep}/\mu_{\Delta e}$	V_i/Q_{ue}	
	–	kN	–	–	–	kN	–	–	–	kN	–	–	
$^1K_{0.5}^{ep}$	4.9	374	1.52	0.91	4.9	374	1.52	0.91	6.0	373	1.53	0.90	1.38
$^2K_{F.C}^{ep}$	3.5	392	1.08	0.95	3.5	392	1.08	0.95	4.3	387	1.09	0.94	1.02
$^3K_y^{ep}$	2.6	416	0.81	1.01	2.6	416	0.81	1.01	3.3	404	0.83	0.98	0.81

Figure 4.50: Equivalent energy elastic-perfectly plastic responses for wall W-90°

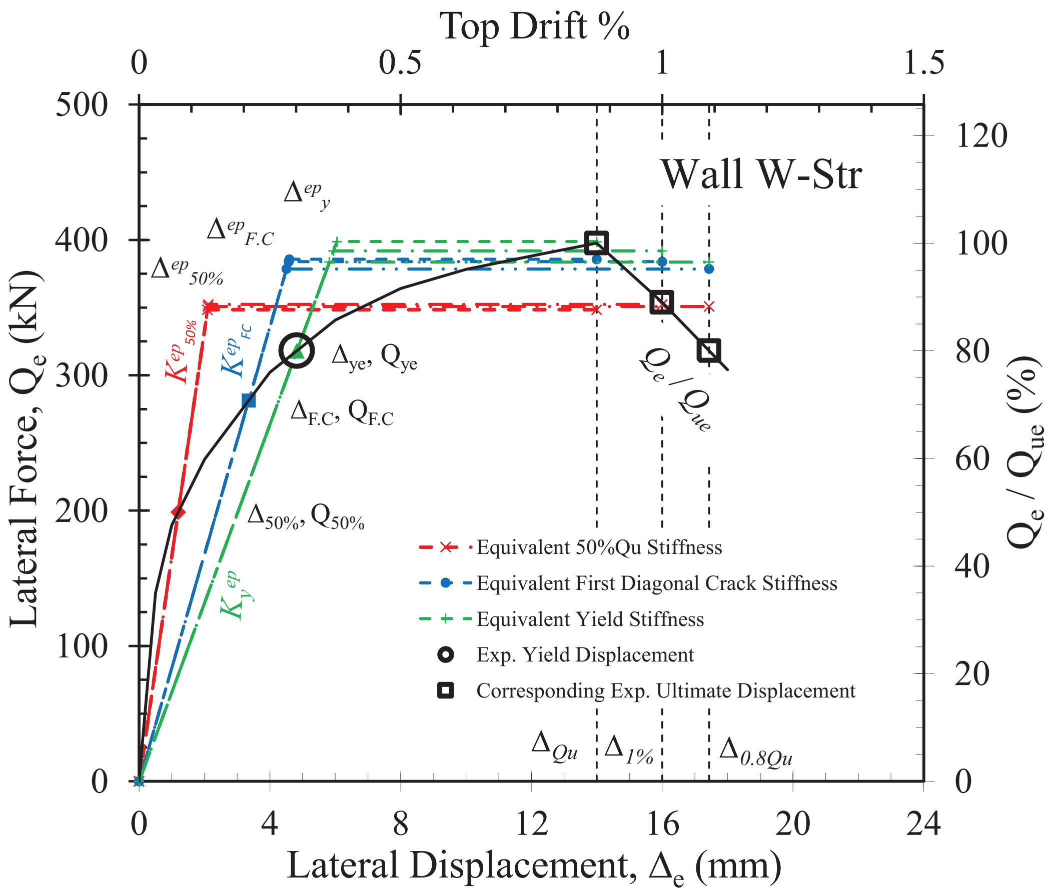

	Ultimate displacement, Δ_u^{ep} , mm												$\frac{\mu_\Delta^{ep} V_i}{\mu_{\Delta e} Q_{ue}}$ = $\frac{R_{d,\max}}{\mu_{\Delta e}}$
	At peak lateral force, Δ_{Que}, 14.0				At a drift limit of 1.0%, $\Delta_{1\%}$, 16.0				At a drop to 0.8 Qu, $\Delta_{0.8Que}$, 17.4				
	$\mu_{\Delta e}$ = 2.9				$\mu_{\Delta e}$ = 3.3				$\mu_{\Delta e}$ = 3.6				
	μ_Δ^{ep}	V_i	μ_Δ^{ep} / $\mu_{\Delta e}$	V_i / Q_{ue}	μ_Δ^{ep}	V_i	μ_Δ^{ep} / $\mu_{\Delta e}$	V_i / Q_{ue}	μ_Δ^{ep}	V_i	μ_Δ^{ep} / $\mu_{\Delta e}$	V_i / Q_{ue}	
	–	kN	–	–	–	kN	–	–	–	kN	–	–	
$^1K_{0.5}^{ep}$	6.7	348	2.31	0.88	7.6	352	2.28	0.89	8.3	351	2.29	0.88	2.02
$^2K_{F.C}^{ep}$	3.0	386	1.05	0.97	3.5	384	1.06	0.97	3.9	379	1.07	0.95	1.02
$^3K_y^{ep}$	2.3	399	0.80	1.00	2.7	392	0.81	0.99	3.0	384	0.83	0.96	0.80

Figure 4.51: Equivalent energy elastic-perfectly plastic responses for wall W-Str

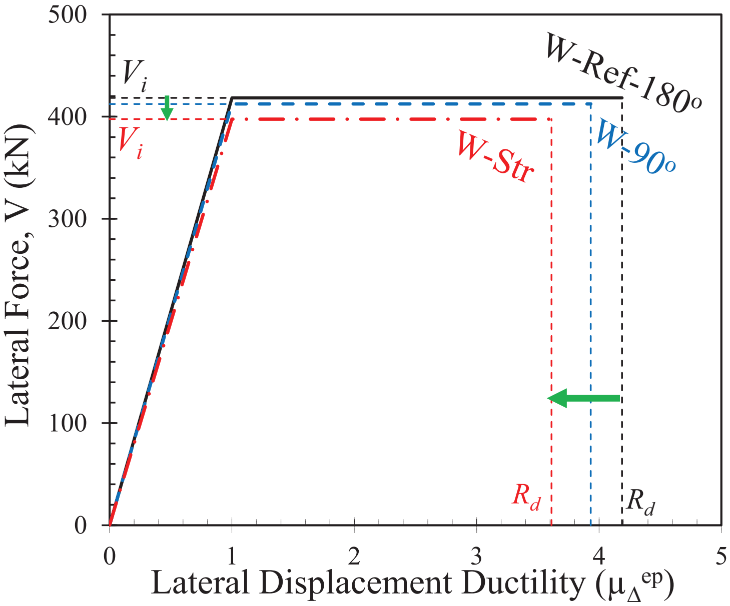

Figure 4.52: Effect of horizontal reinforcement anchorage end detail on idealized elastic-plastic response

4.4.4.2 Displacement-based design

The measured secant stiffness, K_{sc}, in addition to the stiffness degradation, K_{sc}/K_g, for the three tested walls, W-Ref (180°), W-90°, and W-Str at, different levels of top drift are given in Figure 4.53a and b, respectively. As shown in these figures, the anchorage end detail of the horizontal reinforcement does not have a significant effect on the stiffness degradation up to the peak load. Both walls W-Ref and W-Str reached their ultimate resistance at a drift limit of 0.875% with a degradation in their initial gross stiffness, K_g, equal to 88.5% and 89.8%, respectively. On the other hand, wall W-90° lost 88% of its K_g at a top drift of 1.0%. During the post-peak behaviour, wall W-Ref that was constructed with a 180° hook had more gradually stiffness degradation compared to the other two end details due to its efficient confinement. However, walls W-90° and W-Str had rapid reduction in their secant stiffness with almost the same slope as shown in Figure 4.53c.

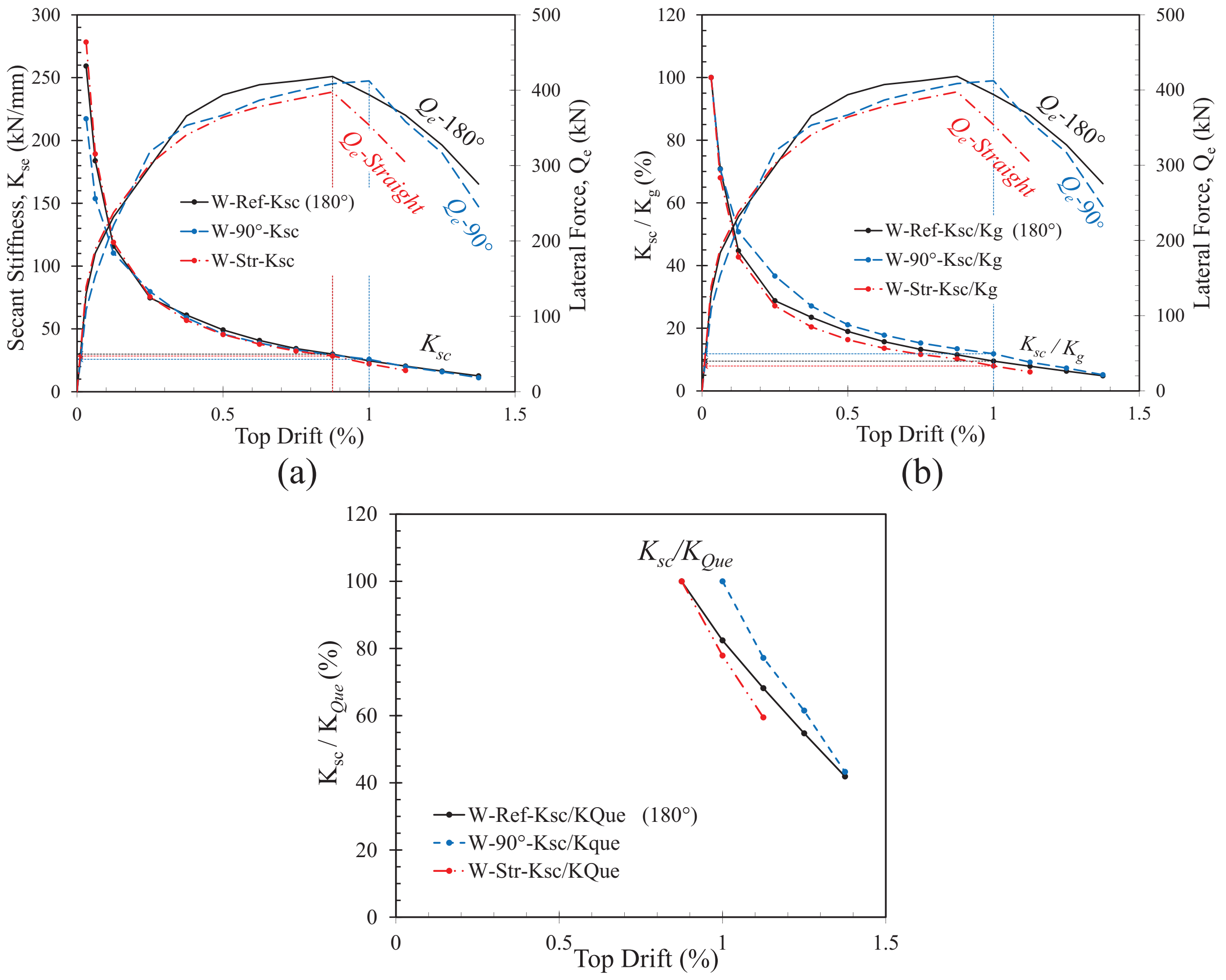

(a)

(b)

(c)

Figure 4.53: Effect of horizontal reinforcement anchorage end detail on stiffness degradation: (a) K_{sc}; (b) K_{sc}/K_g; (c) K_{sc}/K_{Que}

Overall, the three evaluated end details, 180° hook, 90° hook, and straight bar, had no considerable impact on the total dissipated energy up to a drift limit of 1.0%. However, due to the rapid degradation in the secant stiffness for walls W-90° and W-Str after they reached their Q_{ue}, wall W-Ref was able to dissipate 32% and 18% more energy than walls W-90° and W-Str when they reached their failure points, which was defined at a drop in wall capacity to 80% of Q_{ue}. Figure 4.54 presents the effect of the horizontal reinforcement anchorage end detail on the energy dissipation and equivalent viscous damping ratio, ζ_{eq}.

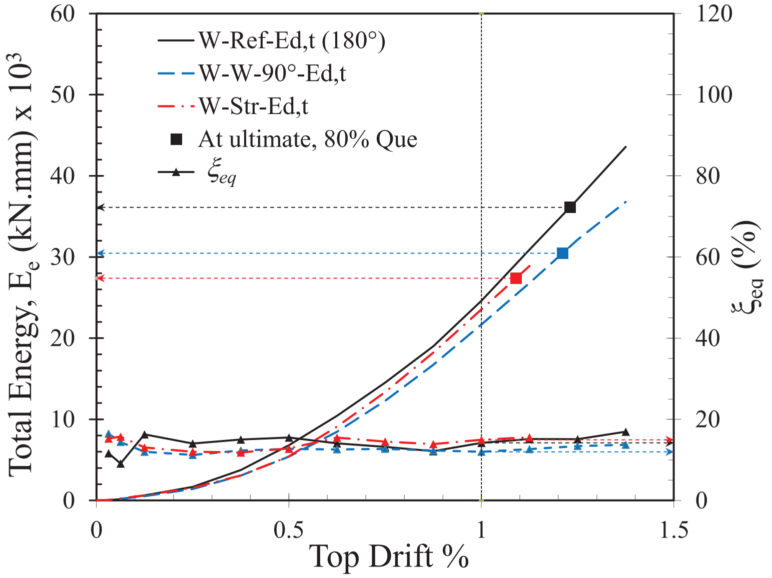

Figure 4.54: Effect of horizontal reinforcement anchorage end detail on energy dissipation

4.4.4.3 Performance-based design

The effect of horizontal reinforcement anchorage end detail on the crack pattern of the three tested walls at first major diagonal cracks, lateral peak load Q_{ue}, and when the lateral load dropped to 80% of Q_{ue}, is depicted in Figure 4.55. In general, the walls constructed with 180° and 90° hooks had similar crack propagation, whereas wall W-Str was characterized by more brittle behaviour. The initial diagonal crack damage appeared during the +4.0 mm loading cycle for the three walls with a slight difference in the top drift. Walls W-Ref and W-Str reached their ultimate resistance at Δ_e equal to +14.0 mm followed by a degradation in the lateral resistance. On the other hand, Wall W-90° was able to achieve another displacement increment before reaching its in-plane shear capacity with almost a constant resistance between Δ_e of +14.0 and +16.0 mm. At the peak load, Q_{ue}, wall W-Str had two major diagonal cracks that started from the middle length of the top to the bottom corners. These main cracks were accompanied by a small number of minor cracks. However, anchoring the lateral reinforcement at the end of walls W-Ref and W-90°, replaced these major diagonal cracks in wall W-Str, with sets of minor cracks along the diagonal axes. Increasing the imposed top lateral displacement resulted in the major diagonal cracks of wall W-Str became wider and they went through the thickness of the wall. On the other hand, the cracks in walls W-Ref and W-90° did not widen significantly; instead, face shell spalling was observed at drift limit of 1.1% (see Figure 4.55c). As a conclusion, not providing a sufficient development length for the horizontal bars at the ends of the tested wall resulted in a sort of brittle shear failure. It can be noticed that wall W-Str had a performance with a mixed crack propagation of walls W-ρh0 and W-Ref as shown in Figure 4.27.

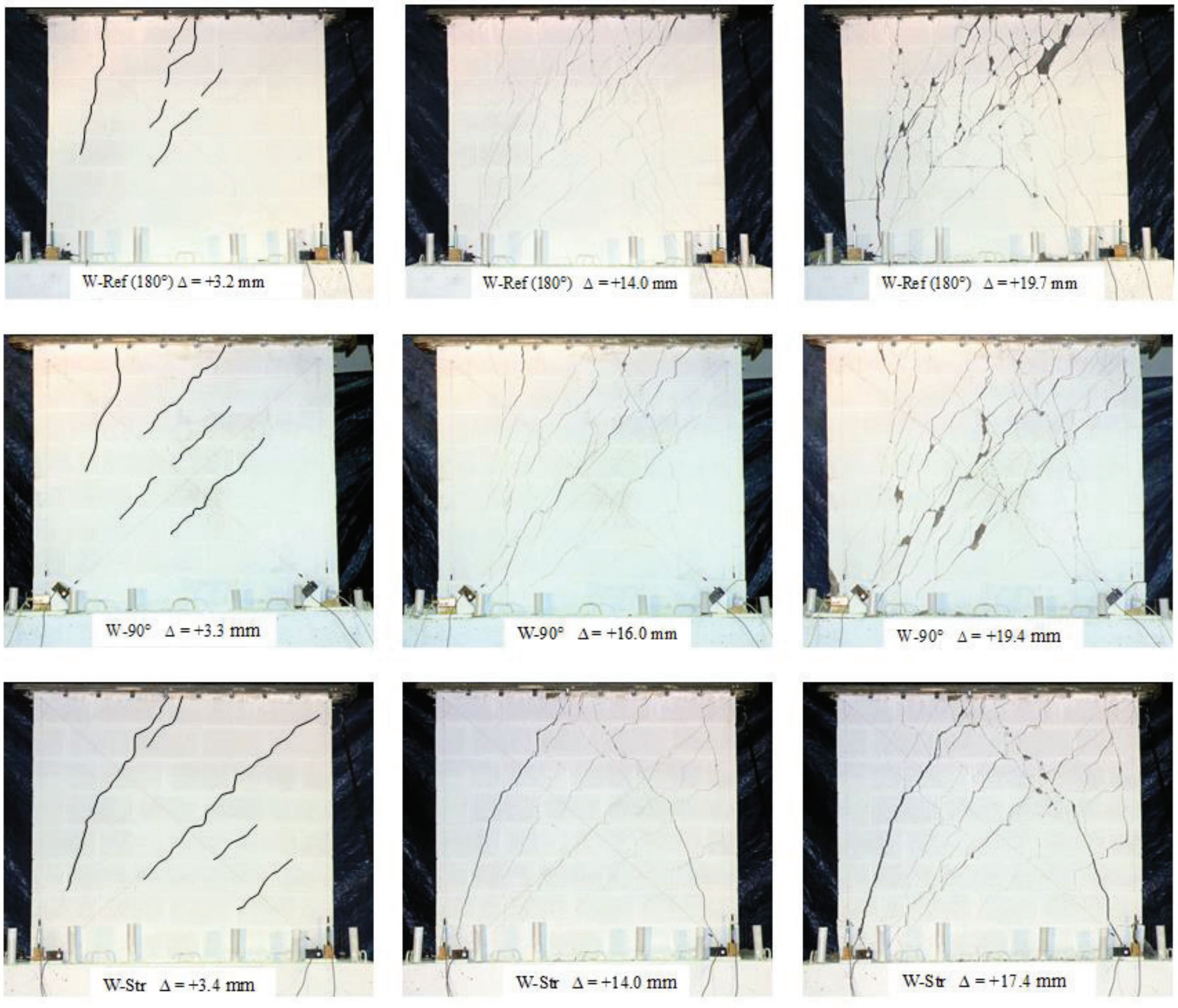

(a) (b) (c)

Figure 4.55: Effect of horizontal reinforcement anchorage end detail on crack pattern at: (a) first major diagonal cracks; (b) lateral peak load Q_{ue}; (c) when the lateral load dropped to 80% of Q_{ue}

4.4.5 EFFECT OF THE SPACING BETWEEN THE HORIZONTAL AND VERTICAL REINFORCEMENT (S_v AND S_h)

All the design equations for in-plane shear strength, V_n, that are presented in Table 2.3 neglect the effect of the spacing between the vertical and horizontal reinforcement; instead, they just consider the reinforcement ratios. However, to account for this effect, the masonry design codes provide some limitations for the maximum spacing of the vertical and horizontal reinforcement. The current version of the Canadian standard for design of masonry structures, CSA S304-14, defines the bond beam as a course or courses of a masonry wall grouted and reinforced in the horizontal direction with reinforcing bars. The bond beam may serve as a horizontal wall tie, as a bearing surface for structural element member, or as a beam. The joint reinforcement commonly refers to the embedded horizontal reinforcement in the mortar joints as shown in Figure 4.56. The reinforcement shear resistance, V_s, in RM shear walls is mainly provided by the horizontal steel bars in the bond beam and/or the joint reinforcement. However, the joint reinforcement is more common for partially grouted RM shear wall, which is beyond the scope of this research.

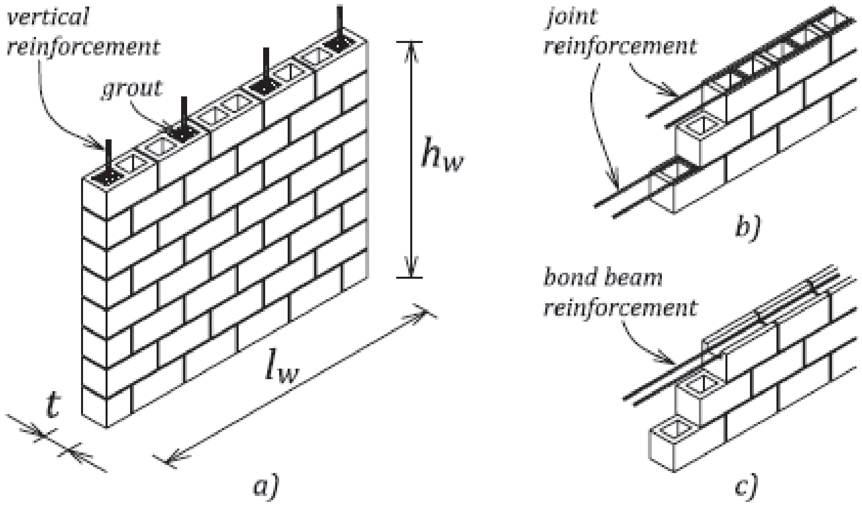

Figure 4.56: Typical reinforced concrete masonry block wall: a) vertical reinforcement; b) joint; c) bond beam reinforcement (Anderson and Brzev, 2009)

In general, the Canadian standard CSA S304-14 limits the maximum spacing between the horizontal reinforcement, S_v, for seismic design to 1200 mm where only bond beams are used; 400 mm where only joint reinforcement is provided; or 2400 mm for bond beams and 400 mm for joint reinforcement where both are used. However, S_v shall not exceed $0.5l_w$ for bond beams. In addition, the maximum spacing of vertical reinforcement S_h, shall be the lesser of 12(t+10) mm or 2400 mm for seismic hazard index, $I_EF_aS_a(0.2)$, less than 0.75; or half of these values if $I_EF_aS_a(0.2) \geq 0.75$. For better seismic performance, S_v is limited to 600 mm instead of 1200 mm inside the plastic hinge region of ductile shear walls ($R_d = 3.0$). Moreover, for moderately ductile and ductile RM shear walls, $S_{h,max}$ shall be taken as 6(t+10) mm, 1200 mm, or $0.25l_w$, whichever is less, whatever the value of the seismic hazard index. However, $S_{h,max}$ need not be less than 600 or 400 mm where the spacing required for strength is greater than 600 or 400 mm for R_d equals 2.0 or 3.0, respectively. These minimum limits are provided to ensure flexural failure mode.

To investigate the effect of S_v on the in-plane shear behaviour, wall W-S_v800 was constructed with horizontal reinforcement of 15M@800 mm instead of 10M@400 mm for wall W-Ref, where both walls had the same horizontal reinforcement ratio, ρ_h, of 0.13%. In Addition, walls W-Ref and W-S_v800 had vertical reinforcement of 20M bar in each cell with a vertical reinforcement ratio, ρ_v, of 0.79%. Wall W-S_h800 is a duplicate of wall W-S_v800 except that the vertical reinforcement was concentrated in the first, middle, and end cells. Each cell had a 30M bar with a total vertical reinforcement ratio, ρ_v, of 0.61% compared to ρ_v of 0.79% for the rest of the tested walls. However, this slight difference in ρ_v can be neglected since most of the existing equations for the nominal in-plane shear strength, V_n, including the design equations given in the Canadian standard CSA S304-14 and the Masonry Standards Joint Committee MSJC-2013 do not consider any contribution from the vertical reinforcement.

4.4.5.1 Force-based design

Although Walls W-Ref, W-S_v800, and W-S_h800 have the same theoretical in-plane shear strength, V_n, according to most of masonry design codes, such as CSA S304-14 and MSJC-2013, the experimental results show a significant reduction in V_n and $\mu_{\Delta e}$ by increasing the spacing of the vertical and horizontal bars. Figure 4.57 presents the effect of the spacing of reinforcement on the in-plane shear strength of the tested walls. Using horizontal reinforcement of 15M@800 mm instead of 10M@400 mm, with the same ρ_h of 0.13%, resulted in a reduction in Q_{ue} from 418 to 384 kN. Moreover, wall W-S_v800 achieved a displacement ductility, $\mu_{\Delta 0.8Que}$, of 3.4 compared to 4.2 for wall W-Ref. On the other hand, concentrating the vertical reinforcement in the first, middle, and last cells, as in wall W-S_h800, instead of distributing it in each cell with smaller areas, as in wall W-S_v800, led to a more brittle behaviour accompanied with less strength. Wall W-S_h800 had Q_{ue} and $\mu_{\Delta 0.8Que}$ equal to 358 kN and 2.3, respectively. These values are about 93% and 68% of the corresponding measured values for wall W-S_v800 and 85% and 55% for wall W-Ref, respectively. However, wall W-S_h800 achieved a yield strength of 330 kN, which is almost 10% higher than W-S_v800, at a top drift equal to 0.32%. Khattab and Drysdale (1993) arrived at similar results by testing unreinforced and reinforced masonry panels (1.2 m x 1.2 m) under uniform stresses applied in two orthogonal directions. Based on their test results, they concluded that increasing the horizontal reinforcement ratio can be beneficial to both shear strength and ductility of RM panels compared to unreinforced panels when distributing the reinforcement.

Wall W-S_v800 reached in-plane lateral resistance of 265 kN at a displacement of $0.62\Delta_y$ before the major diagonal cracks occurred compared to 248 kN and $0.6\Delta_y$ for wall W-S_h800 and

272 kN and $0.68\Delta_y$ for wall W-Ref, respectively. These values provide additional evidence that the horizontal reinforcement does not have a significant influence on the pre-crack behaviour compared to its effect on the post-crack performance as discussed earlier.

For better understanding of the behaviour of the three tested walls, the resistances shares provided by horizontal reinforcement, V_s, and masonry and axial compressive stress, V_{m+p}, were evaluated separately and are given in Figure 4.58. Increasing the spacing of reinforcement resulted in a reduction in the horizontal reinforcement contribution, which was responsible for the losses in Q_{ue}. Constructing Wall W-Ref with uniformly distributed vertical and horizontal reinforcement with small spacing allowed the lateral reinforcement to achieve its yield capacity. On the other hand, $V_{s,max}$ only reached $0.81f_y$ when the spacing between the bond beams in wall W-S_v800 was increased to 800 mm. Moreover, the results of wall W-S_h800 show that the spacing of vertical reinforcement has indirect impact on the contribution of V_s. Although both walls W-S_v800 and W-S_h800 had the same distribution of the horizontal reinforcement, 15M@800 mm, V_s was not able to contribute more than 69% of its yield resistance in wall W-S_h800 compared to 81% of f_y in wall W-S_v800 as shown in Figure 4.58-. This reduction in V_s is due to the redistribution of the vertical reinforcement, since the 20M@200 mm vertical reinforcement in wall W-S_v800 was replaced by 30M vertical bars with spacing of 800 mm in wall W-S_h800.

By subtracting the provided horizontal reinforcement resistance, V_s, from the measured lateral force, the combined contribution of the masonry and axial compressive stress, $V_{(m+p)}$, was calculated for each wall and is presented in Figure 4.58b. As shown in this figure, the three walls almost reached the same $V_{(m+p)max}$ at close displacement ductility values. However, the overall loss in the displacement ductility, $\mu_{\Delta 0.8Que}$, from 4.2 to 3.4 and 2.3 for walls W-Ref, W-S_v800, and W-S$_h$800, respectively, could be attributed to the rapid degradation in $V_{(m+p)}$ in walls W-S$_h$800 and W-S$_v$800 compared to more gradually reduction in wall W-Ref.

Finally, from the results of the tested walls and the previous discussion it can be concluded that the amount and distribution of reinforcement has a significant effect on the in-plane shear capacity, with a major impact on the achieved displacement ductility. Hence, the current values for the maximum spacing of reinforcement in the Canadian standard CSA S304-14 need to be modified by specifying more conservative limits.

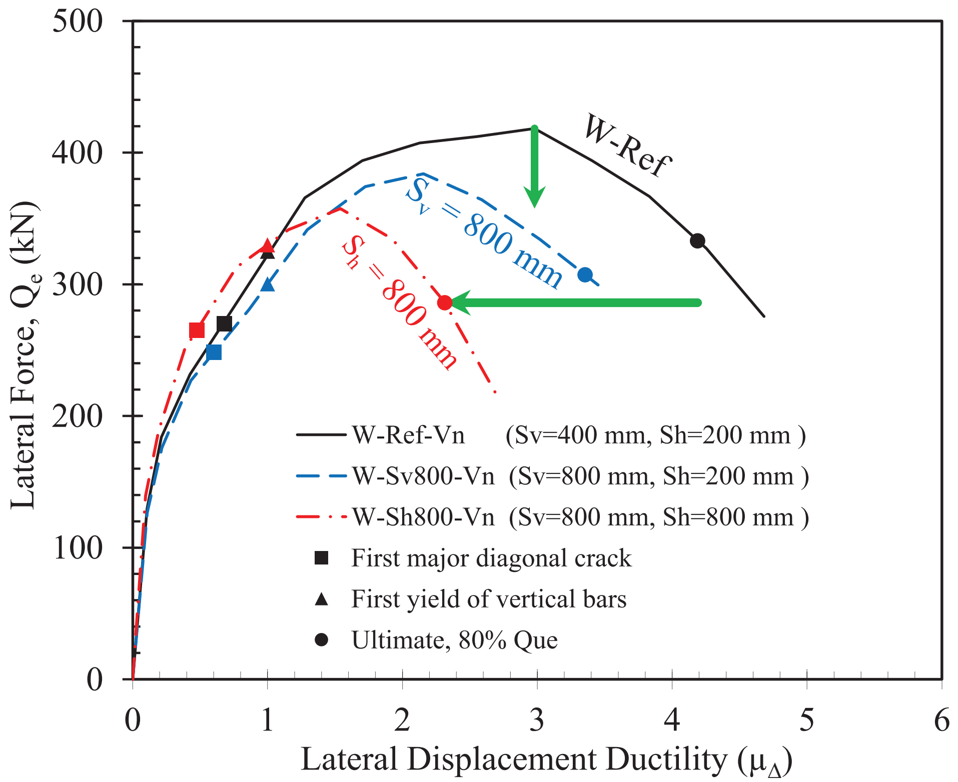

	Q_{ye}	Δ_{ye}	Q_{ue}	Δ_{Que}	$\Delta_{0.8Que}$	$\mu_{\Delta Que}$	$\mu_{\Delta 0.8Que}$	$\mu_{\Delta e1\%}$	Δ_{FCe}	Q_{FCe}
	(kN)	(mm)	(kN)	(mm)	(mm)	—	—	—	(mm)	(kN)
[1]W-Ref	328	4.7	418	14.0	19.7	3.0	4.2	3.4	3.2	272
[2] W-S$_v$800	300	4.6	384	10.0	15.6	2.2	3.4	3.5	2.8	248
[3] W-S$_h$800	330	5.2	358	8.0	12.0	1.5	2.3	N/A	2.6	265

[1] W-Ref (S$_v$ = 400 mm, S$_h$ = 200 mm)
[2] W-S$_v$800 (S$_v$ = 800 mm, S$_h$ = 200 mm)
[3] W-S$_h$800 (S$_v$ = 800 mm, S$_h$ = 800 mm)

Figure 4.57: Effect of the spacing of reinforcement on in-plane shear strength of RM shear walls

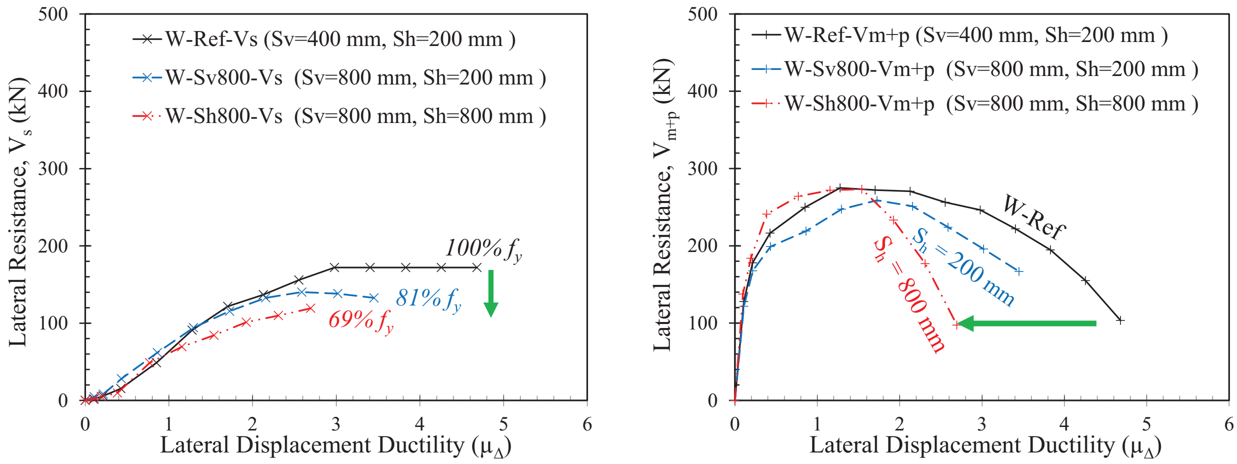

(a) (b)

Figure 4.58: Effect of spacing of reinforcement on shear resistance shares provided by: (a) horizontal reinforcement, V_s; (b) masonry and axial compressive stress, V_{m+p}

In lieu of modeling the nonlinear behaviour of RM shear walls using a SDOF system, the equivalent energy elastic-perfectly plastic responses for walls W-S_v800 and W-S_h800 were defined and are presented in Figure 4.59 and Figure 4.60, respectively. Moreover, Figure 4.61 shows the effect of the spacing of reinforcement on the idealized effective elastic stiffness, K_{id}^{ep}, for the tested walls. Using the effective elastic stiffness as $K_{0.5}^{ep}$ or K_{FC}^{ep} for wall W-S_v800 resulted in a factor of safety of 1.76 and 1.07 if R_d is taken as equal to $\mu_{\Delta e}$. However, if K_y^{ep} was considered in modeling, a conservative value of R_d should be considered since it cannot be taken more than 0.78 $\mu_{\Delta e}$. Since wall W-S_h800 had a 20% reduction in its peak load before reaching a 1.0% top drift, the equivalent energy elastic-perfectly plastic responses when Δ_u^{ep} equals to $\Delta_{1\%}$ was not applicable. In addition, there is no elastic-perfectly plastic response that can provide equal energy with the real nonlinear force-displacement behaviour if Δ_u^{ep} is taken as Δ_{Que}. That is because of the slight difference between Q_{ye} and Q_{ue} as shown in Figure 4.60.

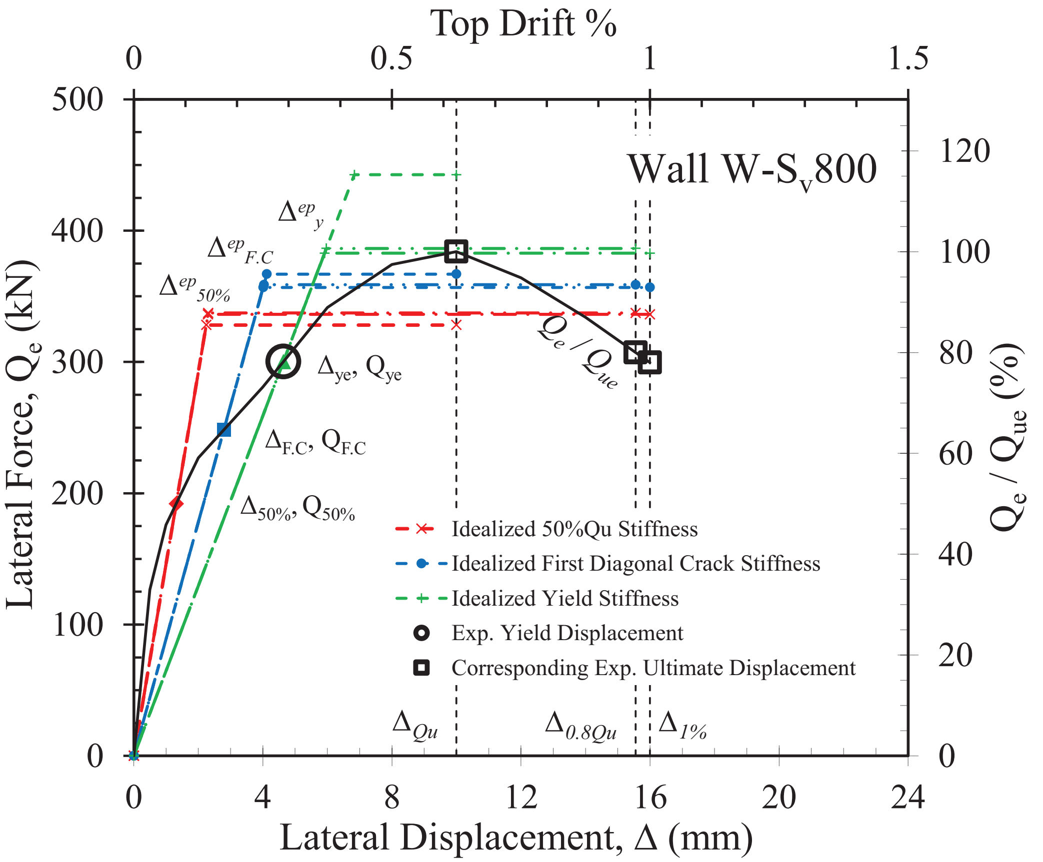

	Ultimate displacement, Δ_u^{ep}, mm											
	At peak lateral force, Δ_{Que}, 10.0				At a drift limit of 1.0%, $\Delta_{1\%}$, 16.0				At a drop to 0.8 Q_u, $\Delta_{0.8Que}$, 15.6			
	$\mu_{\Delta e} = 2.2$				$\mu_{\Delta e} = 3.5$				$\mu_{\Delta e} = 3.4$			
	R_d	V_i	$R_d / \mu_{\Delta e}$	V_i / Q_{ue}	R_d	V_i	$R_d / \mu_{\Delta e}$	V_i / Q_{ue}	R_d	V_i	$R_d / \mu_{\Delta e}$	V_i / Q_{ue}
	–	kN	–	–	–	kN	–	–	–	kN	–	–
$K^{ep}_{0.5}$	4.5	328	2.07	0.85	7.0	336	2.02	0.88	6.7	337	2.01	0.88
$K^{ep}_{F.C}$	2.4	367	1.12	0.96	4.0	357	1.16	0.93	3.9	359	1.15	0.93
K^{ep}_{y}	1.5	443	0.68	1.15	2.7	383	0.78	1.00	2.6	386	0.78	1.01

Figure 4.59: Equivalent energy elastic-perfectly plastic responses for wall W-S$_v$800

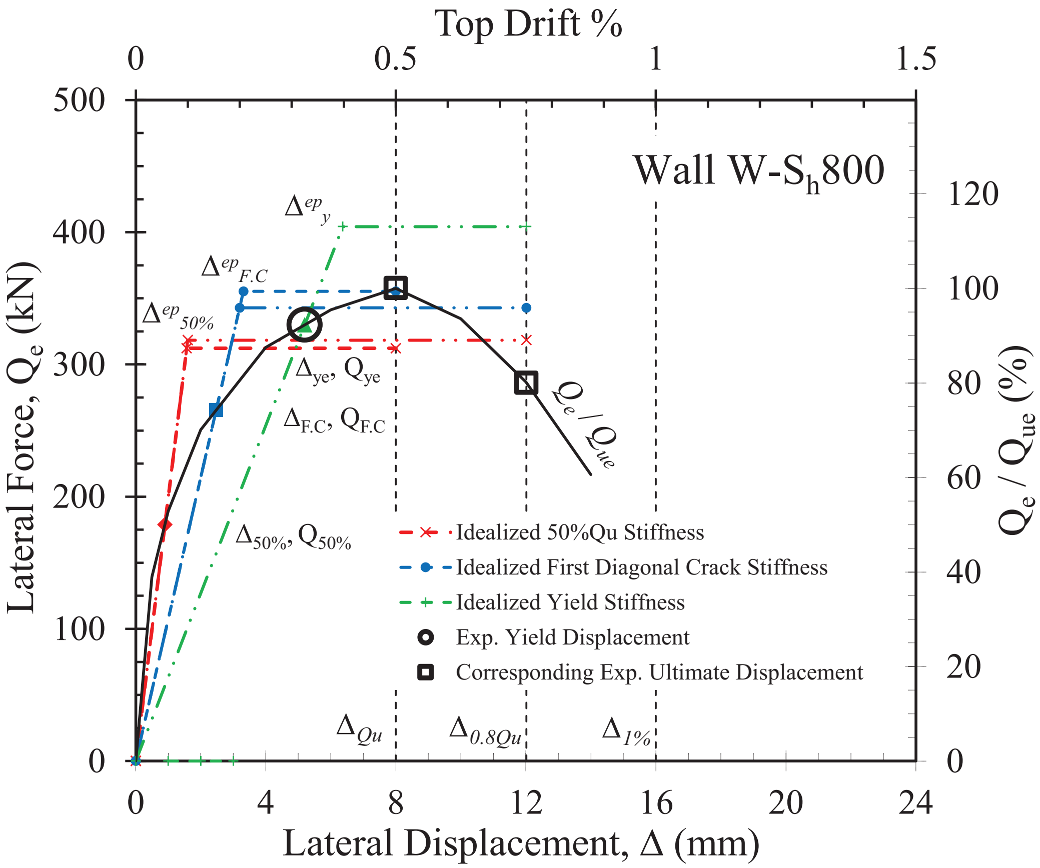

	Ultimate displacement, Δ_u^{ep}, mm											
	At peak lateral force, Δ_{Que}, 8.0				At a drift limit of 1.0%, $\Delta_{1\%}$, N/A				At a drop to 0.8 Q$_u$, $\Delta_{0.8Que}$, 12.0			
	$\mu_{\Delta e}$ = 1.5				$\mu_{\Delta e}$ = N/A				$\mu_{\Delta e}$ = 2.3			
	R_d	V_i	$R_d / \mu_{\Delta e}$	V_i / Q$_{ue}$	R_d	V_i	$R_d / \mu_{\Delta e}$	V_i / Q$_{ue}$	R_d	V_i	$R_d / \mu_{\Delta e}$	V_i / Q$_{ue}$
	–	kN	–	–	–	kN	–	–	–	kN	–	–
$K_{0.5}^{ep}$	5.1	312	3.32	0.87	N/A	N/A	N/A	N/A	7.5	318	3.25	0.89
$K_{F.C}^{ep}$	2.4	355	1.57	0.99	N/A	N/A	N/A	N/A	3.8	343	1.63	0.96
K_y^{ep}	N/A	N/A	N/A	N/A	N/A	N/A	N/A	N/A	1.9	404	0.82	1.13

Figure 4.60: Equivalent energy elastic-perfectly plastic responses for wall W-S$_h$800

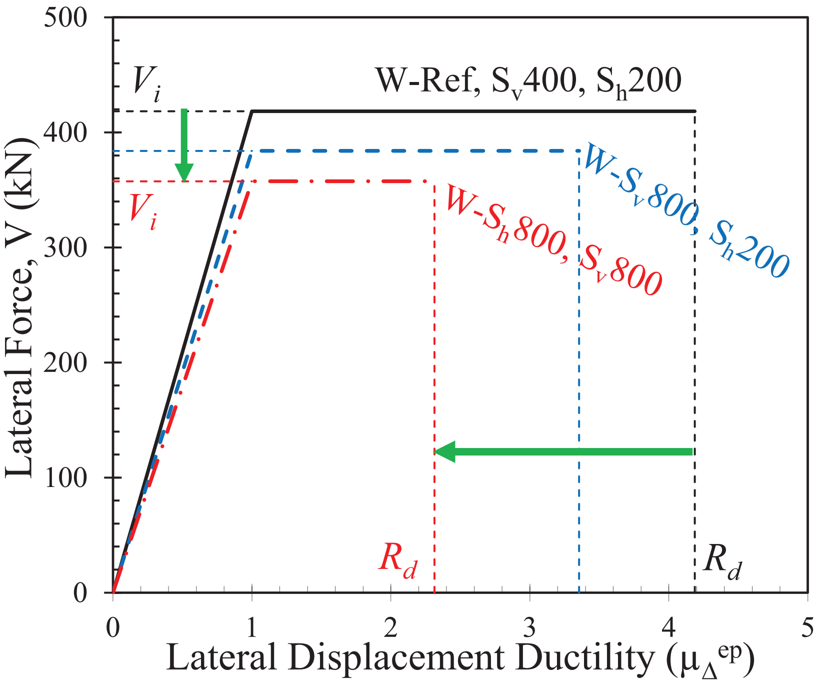

Figure 4.61: Effect of the spacing of reinforcement on idealized elastic-plastic response

4.4.5.2 Displacement-based design

Figure 4.62 presents the secant stiffness, K_{sc}, and the stiffness degradation, K_{sc}/K_g, of walls W-Ref, W-S_v800, and W-S_h800 at different levels of deformations. The three walls had almost the same initial gross stiffness, K_g, with similar force-displacement response up to a top drift of 0.25%; thereafter, wall W-S_h800 had a significant degradation in its secant stiffness compared to wall W-Ref. At a drift limit of 1.0%, wall W-Ref had a secant stiffness of $0.095K_g$. Increasing the spacing between the horizontal reinforcement from 200 to 800 mm resulted in more reduction. At the same top drift, K_{sc} of wall W-S_v800 was measured as $0.074K_g$, which means a 25% loss in the corresponding lateral force resistance, Q_e. When the spacing of vertical reinforcement was also increased, wall W-S_h800 was not even able to achieve a drift limit of 1.0%. However, it had stiffness degradation, K_{sc}/K_g equal to 0.1, at top drift of 0.7% compared to wall W-Ref that reached same degradation at top drift equal to 1%.

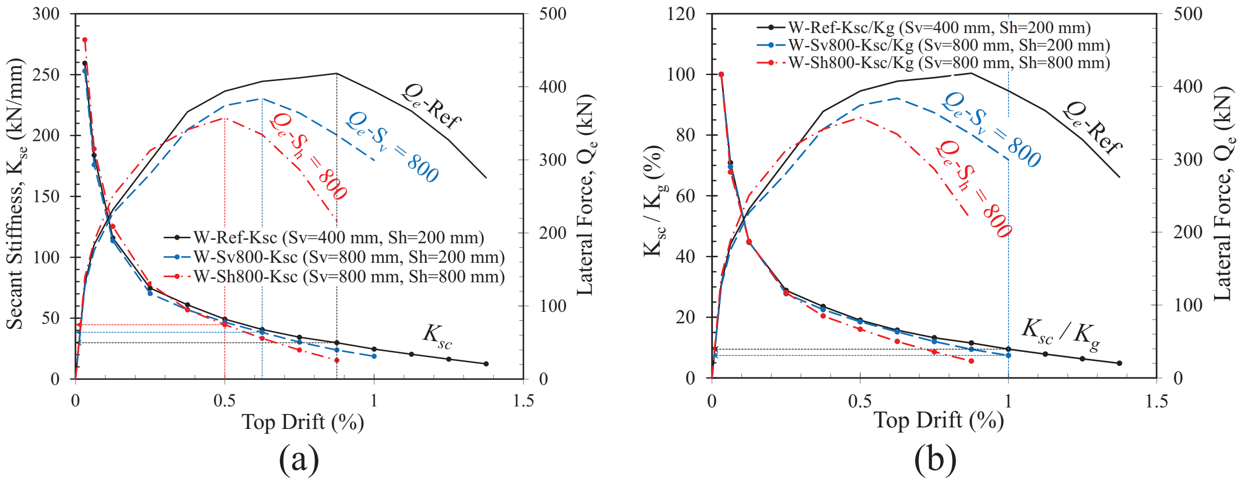

Figure 4.62: Effect of the spacing of reinforcement on stiffness degradation: (a) K_{sc}; (b) K_{sc}/K_g

The spacing of reinforcement shows a major impact on the total energy dissipated by tested RM shear walls under in-plane cyclic lateral excitations. At 0.75% top drift, the three walls had the same total dissipated energy. Nevertheless, wall W-S_h800 was suffering extensive damage while wall W-Ref had a set of minor cracks. Distributing the vertical reinforcement in each cell relatively enhanced the behaviour of wall W-S_v800 compared to wall W-S_h800 and resulted in higher energy dissipation. However, Figure 4.63 shows that wall W-Ref was able to dissipate energy 2.7 and 1.7 times the energy dissipated by walls W-S_h800 and W-S_v800, respectively, when reaching the same drop in the lateral capacity, $0.8Q_{ue}$. This enhancement in the efficiency of dissipating energy was as a direct result of distributing the horizontal and vertical reinforcement with small spacing.

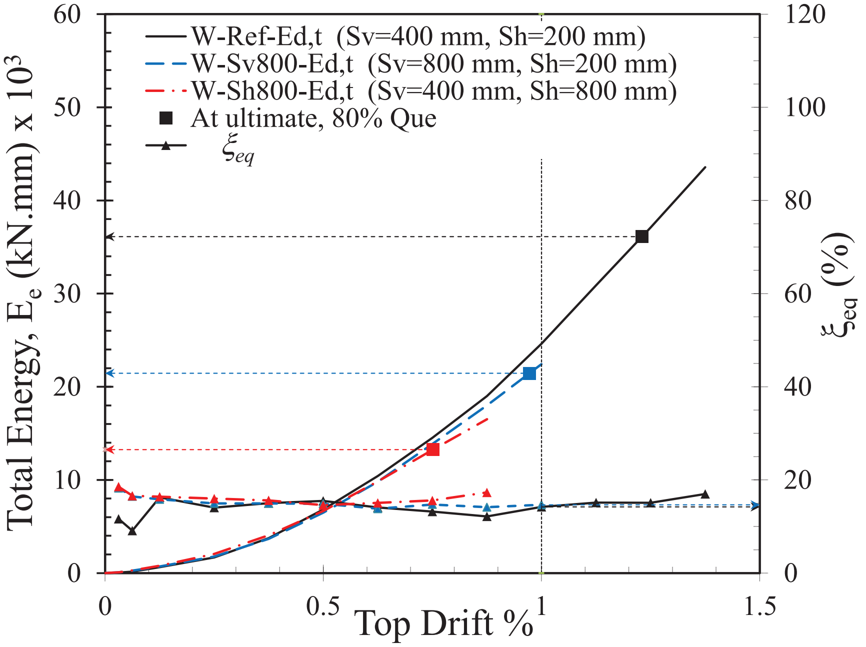

Figure 4.63: Effect of the spacing of reinforcement on energy dissipation

4.4.5.3 Performance-based design

Masonry walls have directional properties that vary according to the orientation of the mortar joints relative to the applied principal stresses. The presence of grout and reinforcement enhance this behaviour by creating continuity in the stress flow. Although all tested walls were constructed using knock-out concrete masonry units to provide some sort of grout continuity in the horizontal direction, the distribution of horizontal and vertical reinforcement still had a major impact on stress flow. This can be seen from the shear crack penetration as depicted in the photographs in Figure 4.64. Concentrating the horizontal reinforcement at the top and bottom of wall W-S_v800, or concentrating the lateral and vertical reinforcement in wall W-S_h800, leads to a localized failure mechanism at the boundaries of the tested walls. Unlike wall W-Ref that reached a top lateral displacement, Δ_e, of 19.7 mm without a significant crushing or spalling of the face shell, wall W-S_v800 had completely separated parts at an earlier imposed Δ_e equals to

+15.6. Moreover, wall W-S$_h$800 lost more than 40% of its in-plane shear capacity at target displacement Δ_e = +14.0 mm with instability of the loading system, which led to termination of the test. However, the final crack pattern of wall W-S$_v$800 in Figure 4.64 shows the discontinuity in the stress flow since no significant damage occurred in the main core of grout compared to the severe damage at the wall ends.

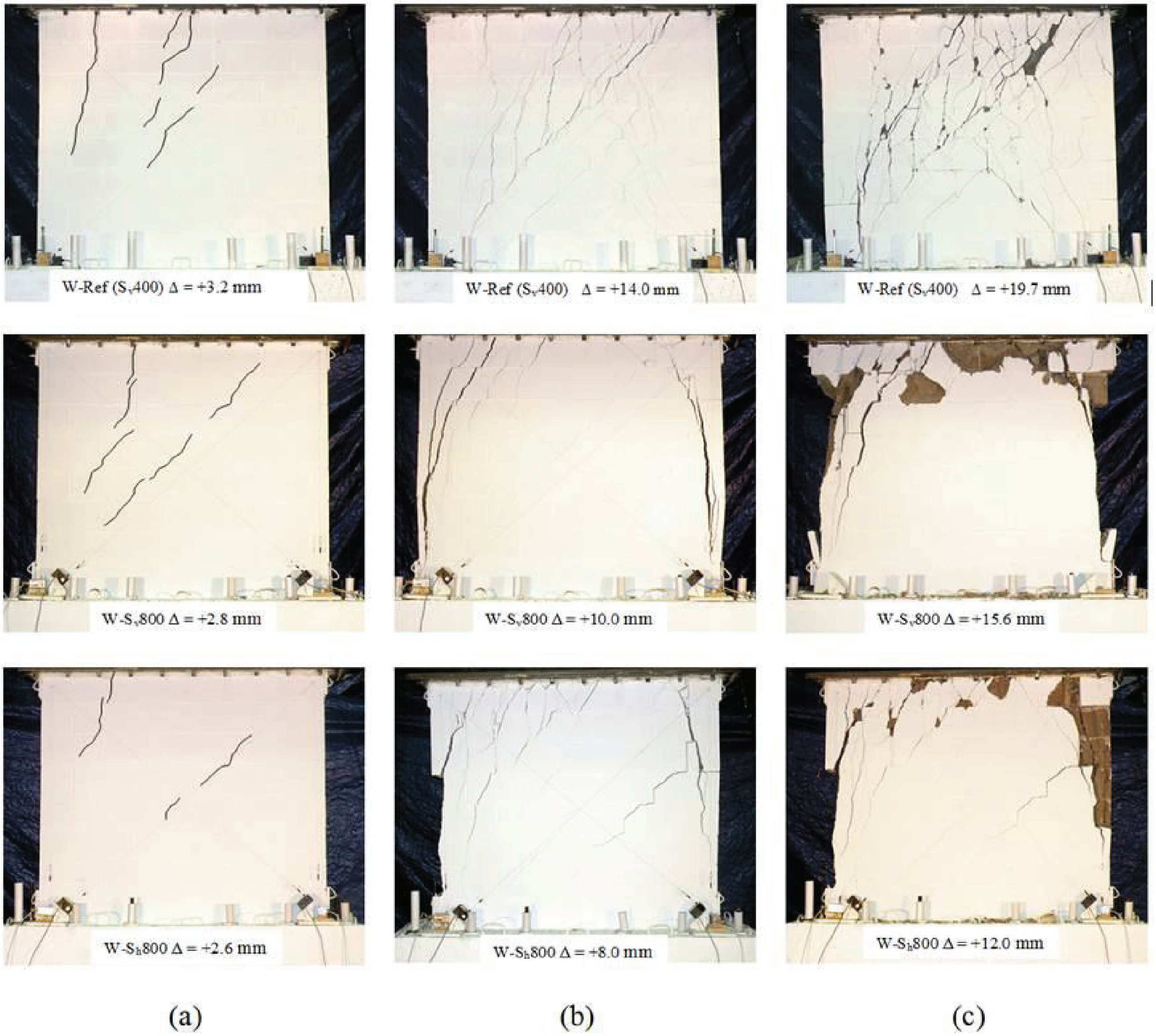

Figure 4.64: Effect of the spacing of reinforcement on crack pattern at: (a) first major diagonal cracks; (b) lateral peak load Q_{ue}; (c) when the lateral load dropped to 80% of Q_{ue}

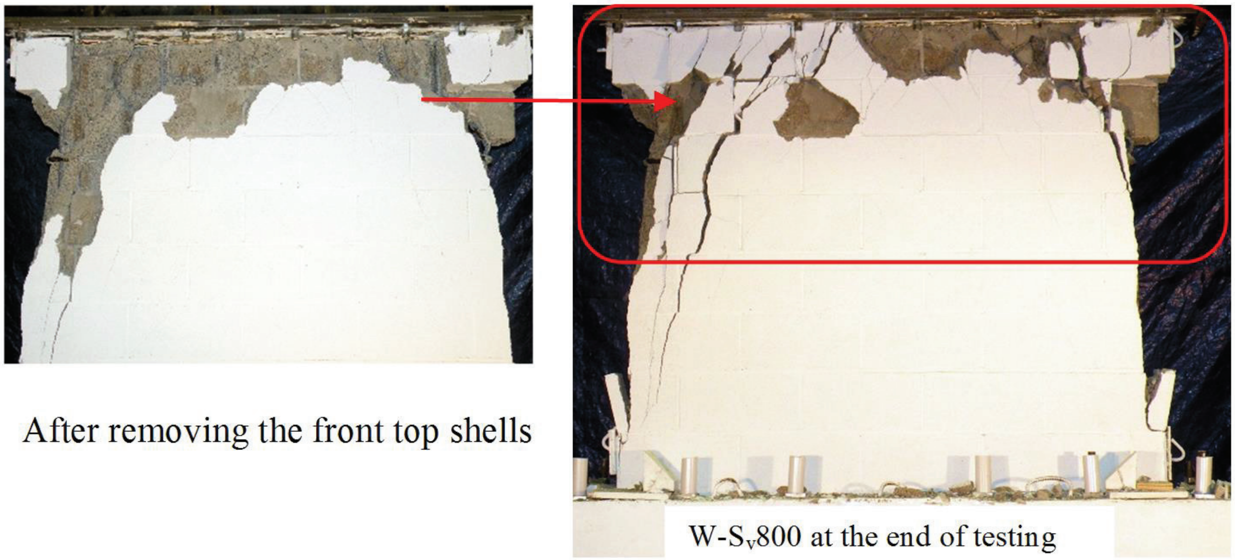

After removing the front top shells

W-S_v800 at the end of testing

Figure 4.65: Final crack pattern of tested wall W-S_v800

Unlike the seismic reinforcement requirements provided in CSA S304-14, the Standards Association of New Zealand NZS 4230:2004 for design of reinforced concrete masonry structures provide more conservative limits for the spacing of reinforcement. According to NZS 4230:2004, the spacing between the vertical reinforcement inside the plastic hinge region should not be taken more than 400 mm with a minimum of 4 vertical bars. In addition, it should be uniformly distributed along the length of the wall. Moreover, the horizontal reinforcement shall be uniformly distributed throughout the height of the wall with a maximum spacing of 400 mm in case of a RM building with not greater than 3 stories or 12 m height. This maximum limit becomes 200 mm in walls greater than 3 stories or 12 m in height.

Based on the test results of walls W-S_v800 and W-S_h800 compared to wall W-Ref, in addition to the previous discussion, the author of this research strongly suggests that the requirements for maximum spacing of reinforcement in NZS 4230:2004 to be adopted in the upcoming version of Canadian Standard CSA S304 for design of masonry structures, to replace the current values.

4.5 DISCUSSION OF TEST RESULTS FOR ALL TESTED WALLS

4.5.1 STIFFNESS DEGRADATION

The experimentally measured secant stiffness, $K_{sc,e}$, for all tested walls against the top drift and the experimentally displacement ductility are given in Figure 4.66. The experimental initial gross stiffness, K_g, which was calculated at the first cycle of ± 0.5 mm, ranged between 279 and 160 kN/mm. Both walls W-σ_{n0} and W-$MV/d_v1.8$ had the smallest K_g of 175 and 160 kN/mm, respectively, yet it can be noticed that this variation in the initial secant stiffness became minor as the imposed top displacement increased.

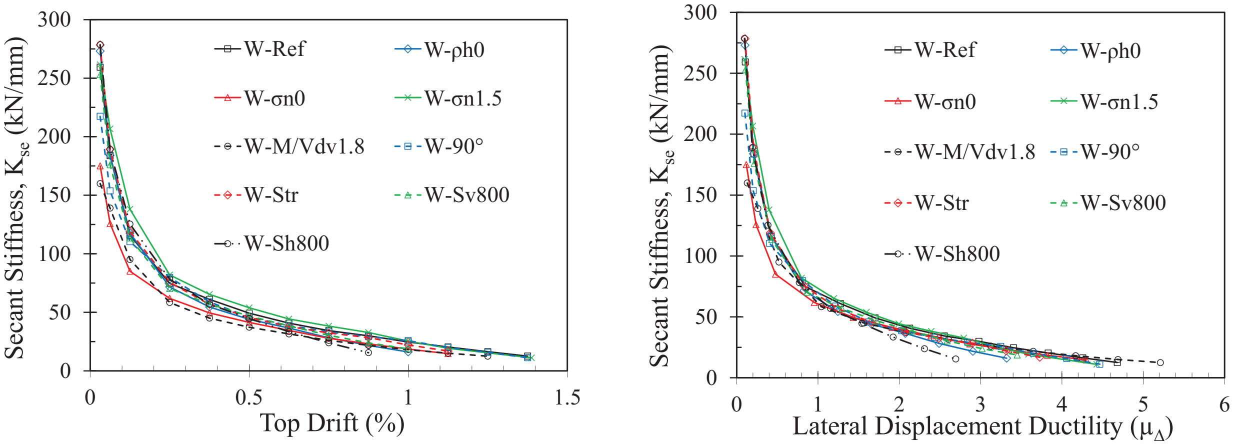

(a) (b)

Figure 4.66: Secant stiffness of all tested walls versus: (a) top drift; (b) displacement ductility

Figure 4.67 presents the values of the secant stiffness degradation, K_{sc}/K_g, for each wall based on the experimental force-displacement envelope. From the test results, it is clear that there is a rapid reduction in K_{sc} at the first stage of loading followed by a relatively gradually degradation in the stiffness as the level of deformation increased. As shown in Figure 4.67a, at a top drift limit of 1.0%, the secant stiffness of the tested walls ranged between 6.0% and 12.0 % of their initial stiffness. However, at the experimental yield displacement, the tested walls recorded more than 50% reduction in their initial stiffness (see Figure 4.67b).

Based on the test results, empirical equations for the stiffness degradation of RM shear walls relative to their top drift limit or displacement ductility are proposed as follows:

$$\frac{K_{sc}}{K_g}(\%) \quad = \quad \frac{7.5}{(Top\,drift\,\%)^{0.75}} \leq 100 \qquad \text{Eq. 4.8}$$

$$\frac{K_{sc}}{K_g}(\%) \quad = \quad \frac{18.5}{(\mu_\Delta)^{0.85}} \leq 100 \qquad \text{Eq. 4.9}$$

The two equations are plotted against the measured values in Figure 4.66 and Figure 4.67, respectively. As shown in these figures, the proposed equations provide somewhat conservative but adequate values. More than 98% of the recorded stiffness degradation is higher than the values obtained from Eq. 4.8 and Eq. 4.9. Using Eq. 4.8 results in a reduction in the initial secant stiffness, K_g, by 88%, 92.5%, and 95.5% at a drift limit of 0.5, 1.0, and 2.0%, respectively. Moreover, at a displacement ductility of 1.0, 2.0, 3.0, and 4.0, K_{sc}/K_g is equal to 18.5%, 10.0%, 7.0%, and 5.5%, respectively, when using Eq. 4.9.

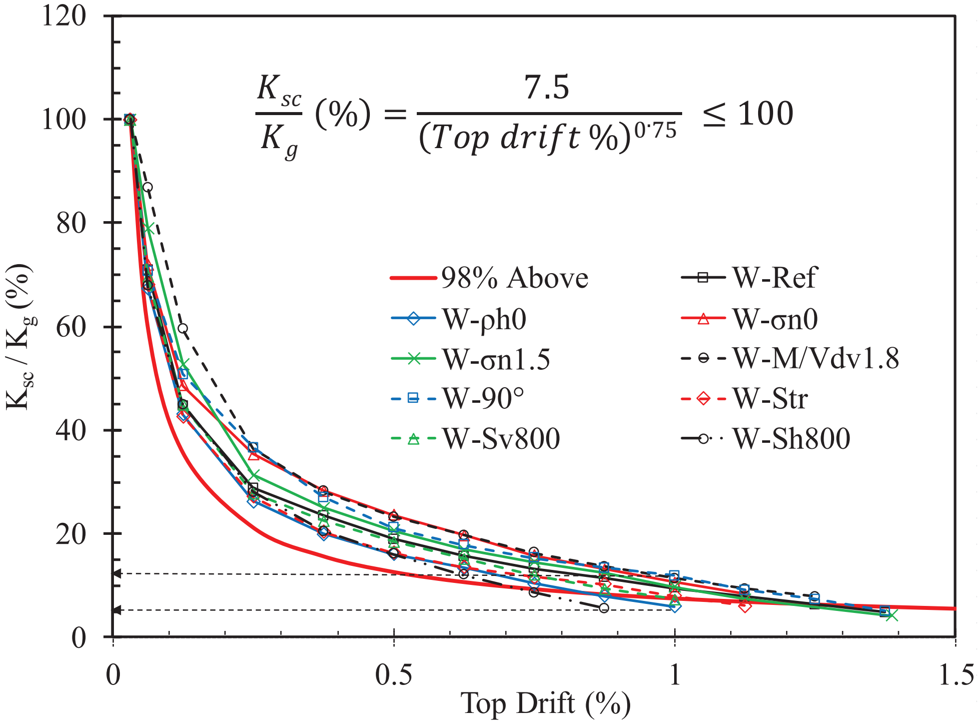

(a)

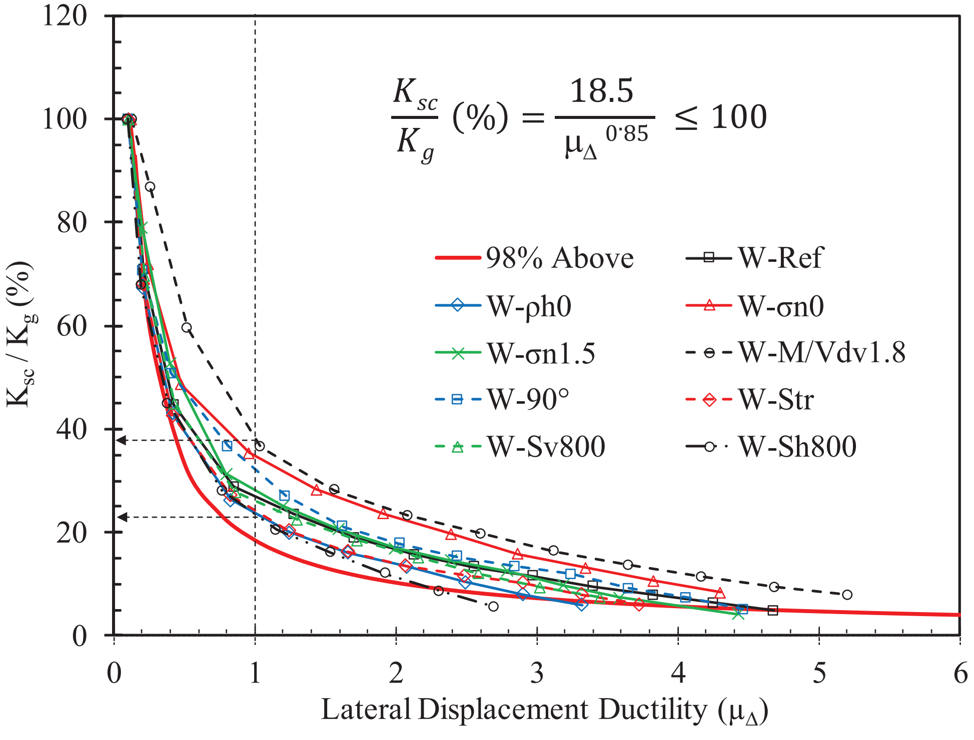

(b)

Figure 4.67: Secant stiffness degradation of all tested walls versus: (a) top drift; (b) displacement ductility

4.5.2 EQUIVALENT VISCOUS DAMPING

The equivalent viscous damping ratio, ζ_{eq}, was defined experimentally using the equal area approach by equating the energy dissipated by a viscous damper with the energy dissipated from the force-displacement response using Eq. 4.7. The calculated values of ζ_{eq} for each wall are plotted in Figure 4.68a against the top drift and Figure 4.68b at different levels of displacement ductility. The values of ζ_{eq} ranged between 8.4% and 23.4% with higher values at larger nonlinear deformations. Based on the common assumption of 5% elastic damping, ξ_{el}, Priestley et al. (2007) suggested the following equation for the damping-ductility relationships:

$$\xi_{eq} = 0.05 + C_3 \left(\frac{\mu_\Delta - 1}{\mu_\Delta \, \pi} \right) \qquad \text{Eq. 4.10}$$

where the coefficient C_3 varies between 0.1 and 0.7 and can be taken as 0.444 for masonry wall buildings. Based on the best-fit analysis for the tested walls in this research work, Eq. 4.11 and Eq. 4.12 were proposed for ζ_{eq} function in the top drift and displacement ductility, respectively. The elastic damping, ξ_{el} was assumed as 8% in these equations. The calculated values of ζ_{eq} using Eq. 4.10 and Eq. 4.12 are plotted against the experimental values and given in Figure 4.68.

$$\xi_{eg}\,(\%) = 8 + (4.0)\sqrt{Top\ drift\ (\%)} \qquad \text{Eq. 4.11}$$

$$\xi_{eg}\,(\%) = 8 + (2.0)\sqrt{\mu_\Delta} \qquad \text{Eq. 4.12}$$

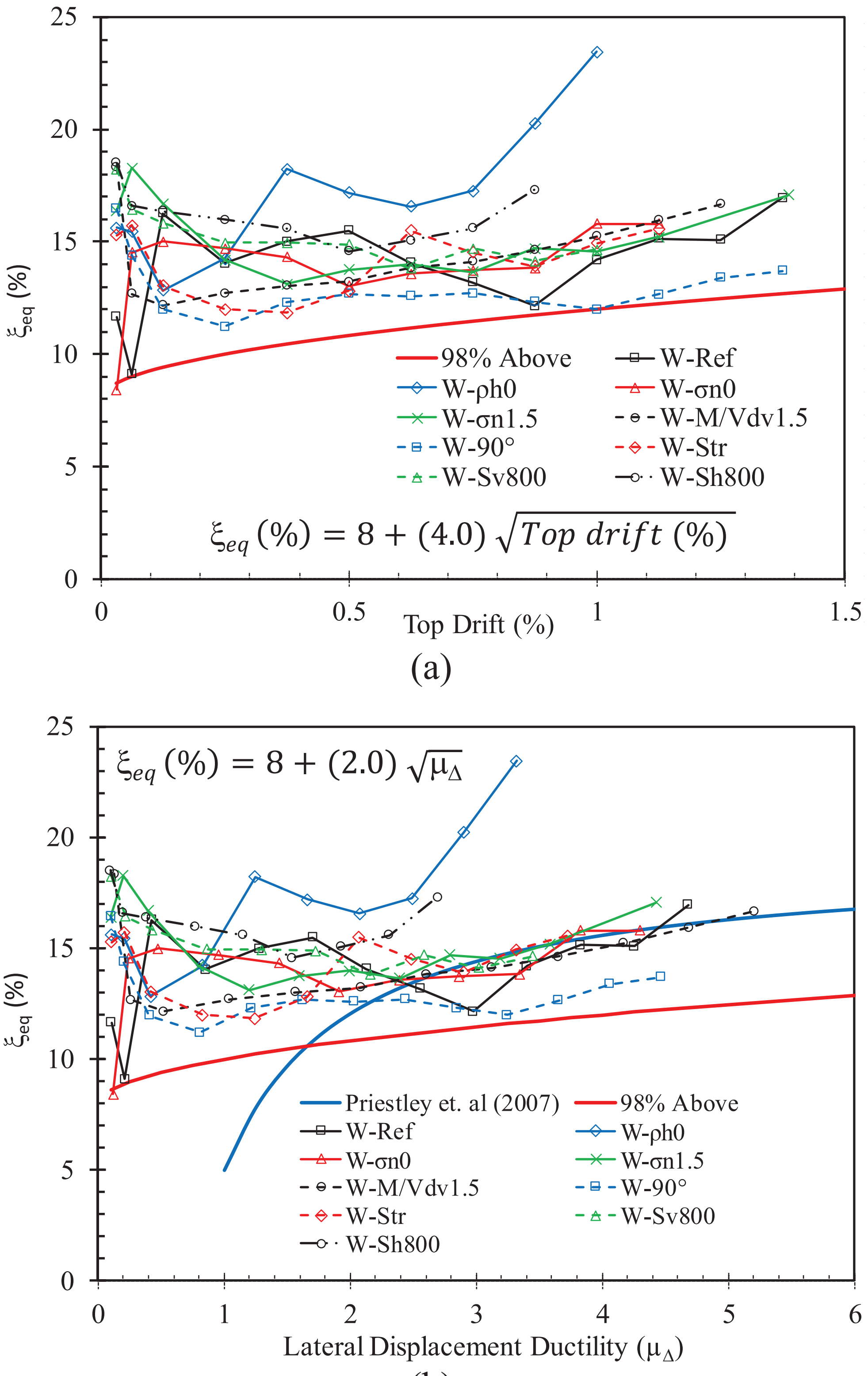

(a)

(b)

Figure 4.68: Equivalent viscous damping of all tested walls versus: (a) top drift; (b) displacement ductility

4.5.3 DUCTILITY-RELATED FORCE MODIFICATION FACTOR (*R_d*)

To account for the nonlinear behaviour of RM structures, the design seismic forces and deformations may be calculated based on reduced section properties. The current version of the Canadian code CSA S304-14 for design of masonry structures permits the use of effective section properties as follows:

$$I_e = I_g\,(0.3 + \frac{P_s}{A_g\,f'_m}) \quad \text{where } I_{cr} \geq I_e \leq I_g \qquad \text{Eq. 4.13}$$

$$A_e = A_g\,(0.3 + \frac{P_s}{A_g\,f'_m}) \quad \text{where } A_{cr} \geq A_e \leq A_g \qquad \text{Eq. 4.14}$$

where P_s is the factored axial dead and live loads determined at the base of the wall for the seismic load combinations. This reduction in the section properties is similar to what was proposed in the previous version, CSA A23.3-04, for seismic design of reinforced concrete shear walls but less conservative Eq. 4.15.

$$\alpha_w = 0.6 + \frac{P_s}{f'_c\,A_g} \leq 1.0 \qquad \text{Eq. 4.15}$$

where α_w is the section property reduction factor used for wall effective stiffness properties. Hence, the effective axial cross-section area, A_e, and the effective moment of inertia, I_e, to be used in seismic analysis can be calculated as $\alpha_w\,A_g$ and $\alpha_w\,I_g$, respectively. Both Eq. 4.13 and Eq. 4.15 define the effective stiffness properties as function in the axial force without considering the ductility-related force modification factor, R_d. However, Eq. 4.15 was further modified in the current version of CSA A23.3-14 for design of concrete structures to account for R_d as follows:

$$\alpha_w = 1.0 - 0.35\left(\frac{R_d\,R_o}{\gamma_w} - 1.0\right) \geq 0.5 \; and \leq 1.0 \qquad \text{Eq. 4.16}$$

where γ_w is wall overstrength factor equal to the ratio of the load corresponding to nominal moment resistance of the wall system to the factored load on the wall system, but need not be taken as less than 1.3, and may be taken equal to R_o. This equation limits the effective stiffness of the equivalent elastic system, K_e, between 0.5 and 1.0 of the initial cross stiffness, K_g, as shown in Figure 4.69. Taking γ_w as R_o, results in K_e equal to $0.825K_g$ and $0.65K_g$ for conventional construction and moderately ductile RC shear walls, respectively. Moreover, for ductile shear walls with R_d higher than 2.4, up to 50% reduction in the stiffness can be considered. This reduction factor in Eq. 4.16 assumes that as the RC shear walls become more ductile, with higher R_d, smaller value of K_e could be taken up to $0.5K_g$. However, this inverse relationship between α_w and R_d does not agree with the experimental results in this research, which is discussed in the following paragraphs.

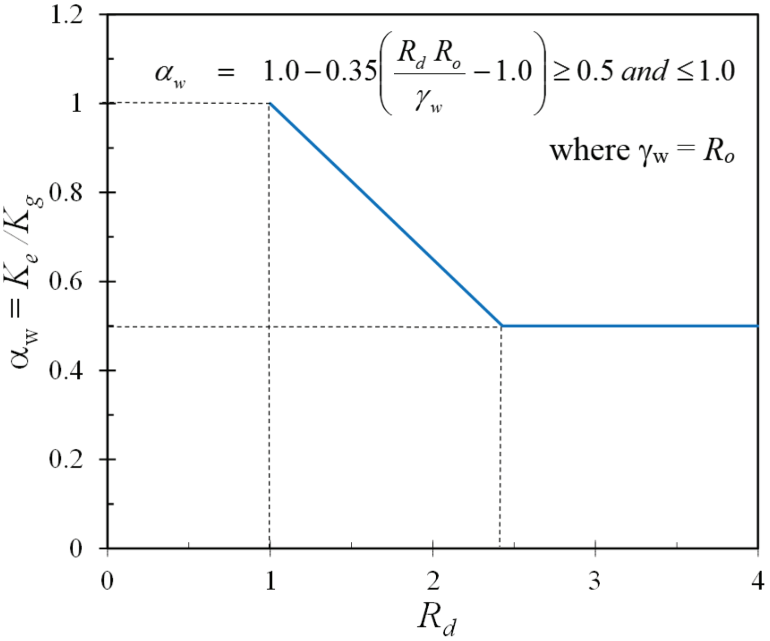

Figure 4.69: Section property reduction factor, α_w, for seismic design (CSA A23.3-14)

In order to define the equivalent energy elastic-plastic response of the tested walls, three values of the effective elastic stiffness were considered as follows: $K_{0.5}^{ep}$, based on the secant gross un-cracked stiffness up to $0.5Q_{ue}$; K_{FC}^{ep}, based on the secant gross un-cracked stiffness until the first major diagonal crack is observed; and K_{y}^{ep}, based on the secant yield stiffness. In addition, the idealized effective elastic stiffness, K_{id}^{ep}, was calculated for each wall. Using K_{id}^{ep} results in $V_i = Q_{ue}$ when R_d is taken as $\mu_{\Delta e}$. This idealized stiffness is calculated as the ratio of the peak lateral load, Q_{ue}, to the yield displacement, Δ_{ye}. Moreover, the initial gross stiffness, K_g, was measured experimentally as the secant stiffness at the first cycle of ± 0.5 mm. Table 4.4 presents a summary of these different stiffness values for each wall and their degradation compared to K_g; it also shows the corresponding maximum value of R_d that could be taken such that a safe design is achieved $V_i \geq Q_{ue}$.

Table 4.4: Summary of Effective Elastic Stiffness of Tested Walls

		Equivalent energy elastic-perfectly plastic response									Idealized response		
		$K_{0.5}^{ep}$			$K_{F.C}^{ep}$			K_{y}^{ep}			K_{id}^{ep}		
	K_g	$K_{0.5}^{ep}$	$\frac{K_{0.5}^{ep}}{K_g}$	$\frac{R_{d,\max}}{\mu_{\Delta e}}$	$K_{F.C}^{ep}$	$\frac{K_{F.C}^{ep}}{K_g}$	$\frac{R_{d,\max}}{\mu_{\Delta e}}$	K_{y}^{ep}	$\frac{K_{y}^{ep}}{K_g}$	$\frac{R_{d,\max}}{\mu_{\Delta e}}$	K_{id}^{ep}	$\frac{K_{id}^{ep}}{K_g}$	$Rd = \mu_{\Delta 0.8Que}$
	kN/mm	kN/mm	—	—	kN/mm	—	—	kN/mm	—	—	kN/mm	—	—
W-Ref	259	137	0.53	1.54	85	0.33	0.96	70	0.27	0.78	89	0.34	4.2
W-ρ_h0	273	185	0.68	2.45	87	0.32	1.15	64	0.23	0.85	76	0.28	3.0
W-σ_n0	175	84	0.48	1.02	70	0.40	0.85	61	0.35	0.74	82	0.47	4.1
W-σ_n1.5	261	173	0.66	1.89	91	0.35	1.00	73	0.28	0.80	91	0.35	3.4
W-M/Vd_v1.8	160	116	0.72	1.41	68	0.42	0.82	60	0.37	0.73	82	0.51	5.2
W-90°	217	116	0.53	1.38	86	0.39	1.02	68	0.31	0.81	84	0.39	3.9
W-Str	278	166	0.60	2.02	84	0.30	1.02	66	0.24	0.80	82	0.30	3.6
W-S_v800	253	146	0.58	1.76	89	0.35	1.07	65	0.26	0.78	83	0.33	3.4
W-S_h800	279	199	0.72	2.90	107	0.38	1.56	63	0.23	0.92	69	0.25	2.3

According to the test results in Table 4.4, the secant gross un-cracked stiffness up to $0.5Q_{ue}$, $K_{0.5}^{ep}$, ranged between (0.48 to 0.72)K_g; however, K_{FC}^{ep} and K_{y}^{ep} varied between (0.3 to 0.42)K_g and (0.23 to 0.37)K_g, respectively. Using one of these effective stiffness, results in a different relationship between R_d and $\mu_{\Delta e}$. To model a RM shear wall with an elastic response using $K_{0.5}^{ep}$, R_d need not to be taken more than $\mu_{\Delta e}$. Nevertheless, at a lower effective stiffness, a more conservative value for R_d has to be considered. The ductility-related force modification factor, R_d, is limited to 0.82 $\mu_{\Delta e}$ and 0.73 $\mu_{\Delta e}$ when K_{FC}^{ep} and K_y^{ep} are taken in the elastic analysis, respectively. To keep R_d equal to $\mu_{\Delta e}$, the idealized effective elastic stiffness with equal displacement, K_{id}^{ep}, was defined such that using effective stiffness higher than K_{id}^{ep} results in a safe seismic design. The experimentally measured stiffness reduction factor, K_{id}^{ep}/K_g, versus R_d equal to $\mu_{\Delta 0.8Que}$ is plotted in Figure 4.70. Based on these results, a best-fit equation for the section property reduction factor, α_w, is defined as follows:

$$\alpha_w \quad = \quad \left[0.3+\left(R_d-3.0\right)0.16\right] \geq 0.3 \, and \leq 0.52 \qquad \text{Eq. 4.17}$$

Except for wall W-σ_n1.5, all walls were tested under a constant axial compressive stress, σ_n, of 1.0 MPa, hence they all have the same α_w according to Eq. 4.13. Furthermore, with the assumption that γ_w is equal to R_o, α_w was calculated for each wall using Eq. 4.16 and the values presented in Figure 4.70. As shown in this figure, Eq. 4.13 in the current version of the Canadian standard for design of masonry structures CSA S304-14 does not seem to be based on realistic assumptions since it is independent of R_d. Moreover, this equation is overestimating the effect of the effective elastic stiffness, K_e, at high displacement ductility, which leads to unsafe design. Although Eq. 4.16 takes into account the effect of R_d, still this equation has an inverse trend with the experimental values such that a high factor of safety is considered for conventional shear walls; instead, it provides critical values of K_e for ductile RC shear walls. However, since R_d is limited to 3.5 and 3.0 in design codes CSA A23.3-14 and CSA S304-14, respectively, both equations are still valid and safe.

In lieu of a more accurate, conservative but adequate, equivalent static seismic design force using the FBD approach, Eq. 4.18 is proposed for the section property reduction factor, α_w. This equation provides a similar level of safety at different values of R_d compared to the other equations as shown in Figure 4.70.

$$\alpha_w = 0.4 + 0.1\left(\frac{R_d\, R_o}{\gamma_w} - 2\right) \geq 0.4 \; and \leq 0.7 \qquad \text{Eq. 4.18}$$

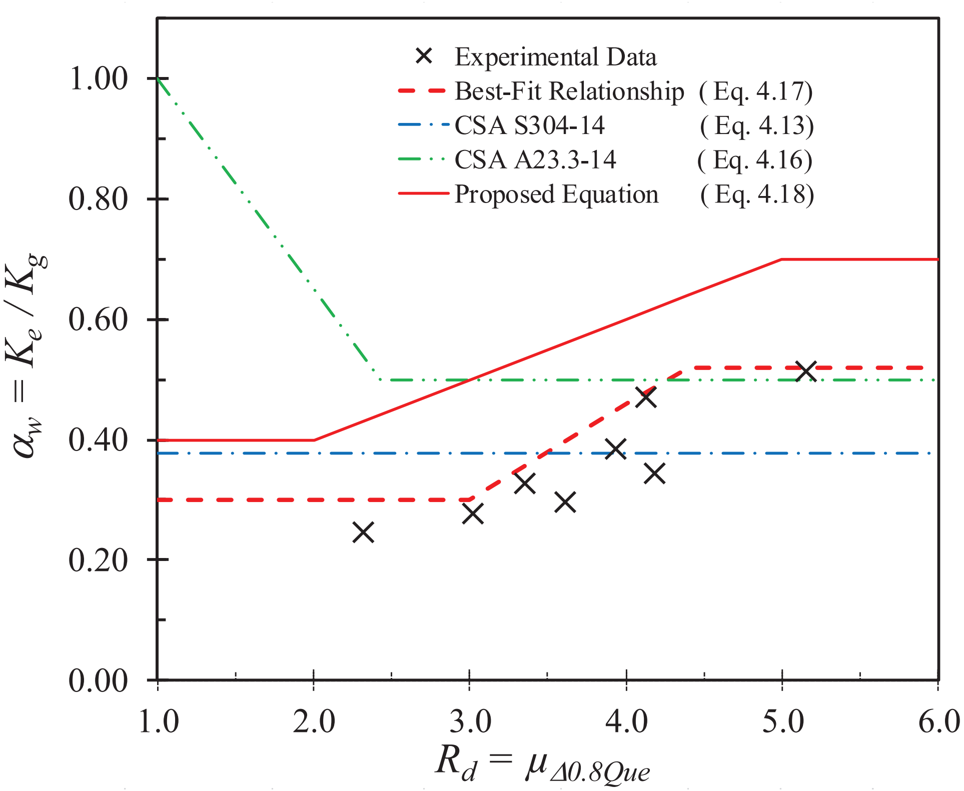

Figure 4.70: Section property reduction factor, α_w, versus the ductility-related force modification factor, R_d

To evaluate the efficiency of the proposed formula for α_w (Eq. 4.18) against the provided equations in the Canadian codes for design of RM and RC shear walls, a simplified analysis is conducted and the results are summarized in Table 4.5. The theoretical initial gross stiffness for tested walls was calculated based on the flexural and shear deformations using the following equation:

$$K_{g,th} = 1/\left(\frac{h_w^3}{3E_m I_g} + k\frac{h_w}{G_m A_g}\right) \qquad \text{Eq. 4.19}$$

where:

E_m = modulus of elasticity of masonry, shall be taken as 850 f'_m (According to CSA S304-14), and f'_m was measured as 13.1 MPa

G_m = 0.4 E_m (Drysdale and Hamid, 2008)

k = Shear shape factor (1.2 for all walls)

The effective stiffness of the equivalent elastic system, K_e, was then defined based on $K_{g,th}$ using the three different Eqs. 4.13, 4.16, and 4.18. Assuming that the elastic system is achieving the same ultimate displacement of the tested walls, the equivalent elastic force, V_e, was determined as $K_e \times \Delta_e$. Thus, V_i was calculated as V_e / R_d according to Eq. 4.2 using the equal displacement approach. The ratio of V_i to Q_{ue} was evaluated based on R_d being equal to the experimental displacement ductility, $\mu_{\Delta e}$, without limitation and with an upper limit of 3.0 as defined in the National Building Code of Canada (NBCC 2010) for the ductile RM shear walls. Two values of the ultimate displacement were considered in this analysis: $\Delta_{e1\%}$ at 1.0% top drift and $\Delta_{0.8Que}$ at a drop in wall capacity to 80% of Q_{ue} with their corresponding displacement ductility. Table 4.5 presents the results when Δ_e is taken as $\Delta_{0.8Que}$. Moreover, the effect of the section property reduction factor, α_w, on the equivalent inelastic seismic design force, V_i, when R_d is equal to $\mu_{\Delta 0.8Que}$ and $\mu_{\Delta 1\%}$ is given in Figure 4.71.

The results presented in Table 4.5 and Figure 4.71 support the efficiency of Eq. 4.18. However, the equation for α_w in the current version of the Canadian code CSA S304-14 for design of masonry structures provides the minimum ratios of V_i/Q_{ue} compared to the other equations. This ratio ranged from 0.7 to 1.9 when no limit for R_d is considered; instead, if R_d is limited to 3.0, V_i varied from (1.2 to 2.4) Q_{ue}. Although Eq. 4.16 provides more conservative values for α_w, which is limited between 0.5 and 1.0, compared to the proposed equation (Eq. 4.18) that limits α_w from 0.4 to 0.7, using Eq. 4.18 still results in higher ratios for V_i/Q_{ue}. This ratio varied from 1.3 to 2.9 and 2.3 to 4.0 when using the proposed equation Eq. 4.18; instead, when taking Eq. 4.16, CSA A23.3-14, V_i/Q_{ue} was found from 1.0 to 3.0 and 1.6 to 3.2 without limiting and with limiting R_d to 3.0, respectively. Based on this analysis, the current equation (Eq. 4.13) need be modified further in the upcoming version of CSA S304; thus, a new class for special ductile RM shear walls with R_d equal to 4.0 could be introduced.

Table 4.5: Summary of Equivalent Inelastic Seismic Design Forces using Different Equations for the Section Property Reduction Factor, α_w.

		Unit	W-Ref	W-ρ_h0	W-σ_n0	W-σ_n1.5	W-M/Vd_v1.8	W-90°	W-Str	W-S_v800	W-S_h800
Experimental Data	$P_s / f'_m A_g$	—	0.076	0.076	0.076	0.115	0.076	0.076	0.076	0.076	0.076
	Q_{ue}	kN	418	365	345	458	315	412	398	384	358
	$\Delta_{0.8Que}$	mm	19.7	14.6	17.3	17.2	19.8	19.4	17.4	15.6	12.0
	$\mu_{\Delta 0.8Que}$	—	4.2	3.0	4.1	3.4	5.2	3.9	3.6	3.4	2.3
	$K_{g,th}$ (Eq. 4.19)	kN/mm	386	386	386	386	157	386	386	386	386
CSA S304-14	α_w	—	0.38	0.38	0.38	0.41	0.38	0.38	0.38	0.38	0.38
	$K_e = K_{g,th} \times \alpha_w$	kN/mm	145	145	145	160	59	145	145	145	145
	$V_e = K_e \times \Delta_e$	kN	2861	2117	2513	2759	1169	2817	2535	2262	1748
	$^1 V_i / Q_{ue}$	—	1.63	1.92	1.76	1.75	0.72	1.74	1.77	1.76	2.11
	$^2 V_i / Q_{ue}$	—	2.28	1.93	2.43	2.01	1.24	2.28	2.13	1.96	2.11
CSA A23.3-14	α_w	—	0.50	0.50	0.50	0.50	0.50	0.50	0.50	0.50	0.54
	$K_e = K_{g,th} \times \alpha_w$	kN/mm	193	193	193	193	78	193	193	193	209
	$V_e = K_e \times \Delta_e$	kN	3802	2813	3339	3328	1553	3743	3369	3005	2509
	$^1 V_i / Q_{ue}$	—	2.17	2.55	2.34	2.11	0.96	2.31	2.35	2.33	3.03
	$^2 V_i / Q_{ue}$	—	3.03	2.57	3.23	2.42	1.64	3.03	2.82	2.61	3.03
Proposed Equation	α_w	—	0.62	0.50	0.61	0.54	0.70	0.59	0.56	0.54	0.43
	$K_e = K_{g,th} \times \alpha_w$	kN/mm	239	194	237	210	110	229	217	207	167
	$V_e = K_e \times \Delta_e$	kN	4705	2824	4093	3619	2174	4441	3780	3219	2003
	$^1 V_i / Q_{ue}$	—	2.69	2.56	2.87	2.30	1.34	2.74	2.63	2.50	2.42
	$^2 V_i / Q_{ue}$	—	3.75	2.58	3.95	2.63	2.30	3.59	3.17	2.79	2.42

[1] based on $R_d = \mu_{\Delta 0.8Qu}$

[2] based on $R_d = \mu_{\Delta 0.8Que}$ and limited to 3.0 for ductile RM shear wall

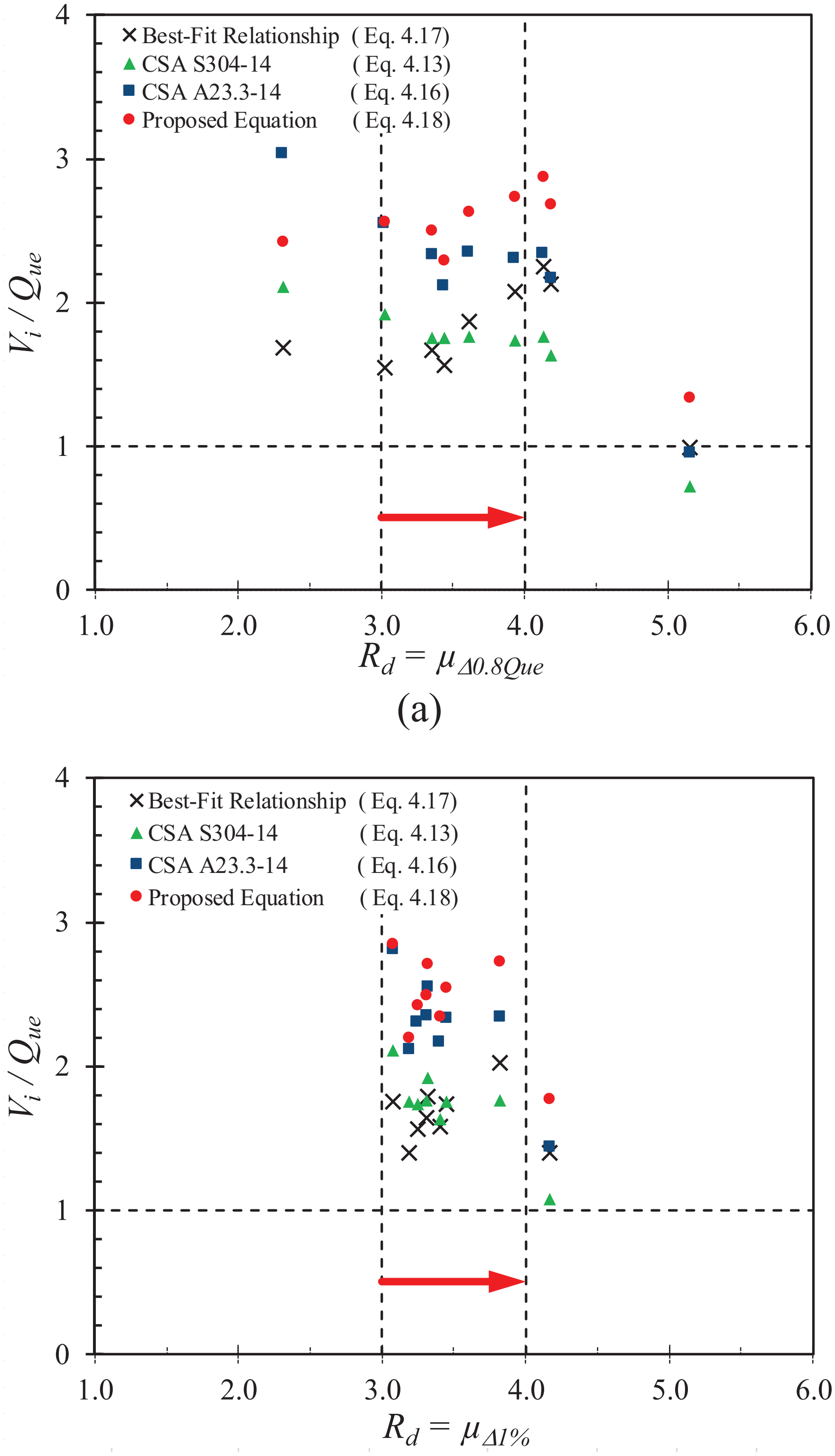

Figure 4.71: Effect of the section property reduction factor, α_w, on equivalent inelastic seismic design force when R_d equal to: (a) $\mu_{\Delta 0.8Que}$; (b) $\mu_{\Delta 1\%}$

CHAPTER 5

NUMERICAL SIMULATION

5.1 INTRODUCTION

Masonry walls have directional properties that vary according to the orientation of the mortar joints relative to the applied principal stresses (Facconi et al., 2013). The presence of grout and reinforcement enhance this behaviour by creating continuity in the stress flow, making the behaviour of fully grouted reinforced masonry (RM) walls similar to that of reinforced concrete (RC) walls (Colotti, 2001). In recent years, numerical models based on finite element (FE) method have been developed to simulate the structural behaviour of masonry. FE analysis is a cost effective tool to predict the performance of structural elements.

There are different approaches for modeling masonry walls, such as the discrete and smeared approaches. In the discrete approach, the properties of each of the constituent materials, namely: masonry units, mortar, grout, and steel reinforcing bars are modeled separately. The smeared approach instead considers the blended properties of the masonry materials. The smeared approach is widely used to model RC structural elements to study their nonlinear behaviour (Shing et al., 1992). Similarly, this approach is suitable to model fully grouted concrete masonry units, as the influence of mortar joints can be neglected (Ewing et al., 1988; and Shing et al., 1992). More discussion about the difference between the two approaches can be found in Galvez et al. (2002). Some of the available numerical models are based on the Modified Compression Field Theory (MCFT) developed by Vecchio and Collins (1986). This theory differs from the original compression field theory that takes into consideration the tensile stresses in the concrete between cracks (Vecchio and Collins, 1986).

5.1.1 MODIFIED COMPRESSION FIELD THEORY (MCFT)

The MCFT can be defined as "An analytical model for predicting the load-deformation response of two-dimensional reinforced concrete elements subjected to in-plane normal and shear stresses" (Güner, 2008). In this theory, the equilibrium and compatibility conditions within the shell element are considered in terms of average stresses and strains. The MCFT was developed by testing many RC panels using a special panel element test setup at the University of Toronto. The shell elements were subjected to various combinations of uniform axial stresses in both directions, f_x and f_y, and a uniform shear stress, v_{xy}. Figure 5.1 shows the deformed shape of a membrane element under in-plane stresses. The deformed shape is assumed to have straight and parallel edges and can be defined by ε_x and ε_y as axial strains and γ_{xy} as the shear strain (Vecchio and Collins, 1986). The MCFT models a cracked concrete element as an orthotropic material using a smeared rotating crack approach. Wong et al. (2013) summarized the MCFT assumptions as follows:

- uniformly distributed reinforcement;
- uniformly distributed and rotating cracks;
- uniformly applied shear and normal stresses;
- unique stress state for each strain state, without consideration of strain history;
- strains and stresses are averaged over a distance including several cracks;
- orientations of principal strain, θ_ε, and orientations of principal stress, θ_f, are the same;
- perfect bond between reinforcement and concrete;

- independent constitutive relationships for concrete and reinforcement;
- negligible shear stresses in reinforcement.

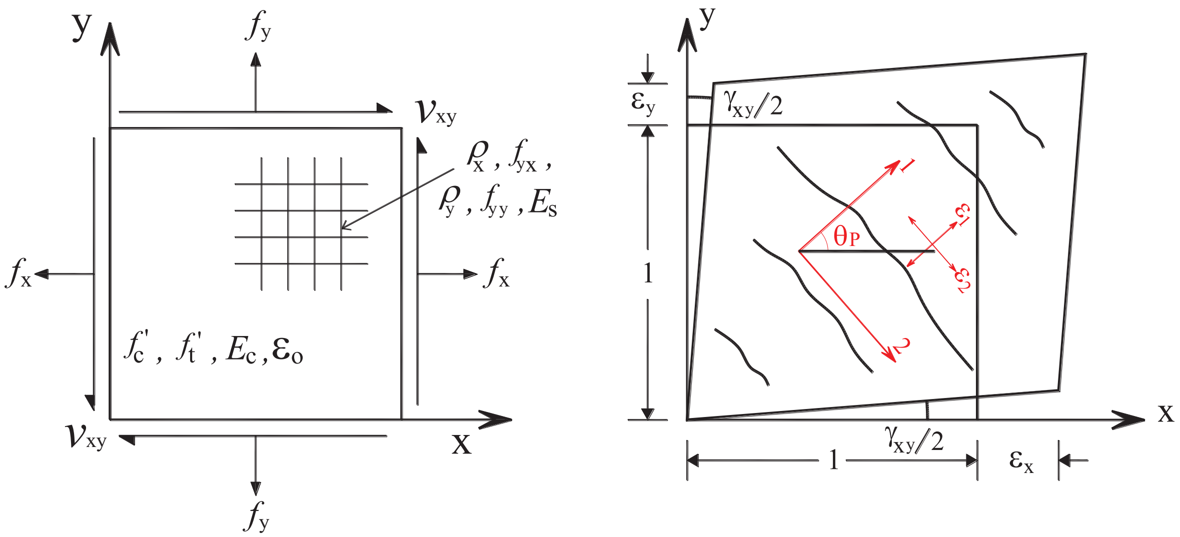

Figure 5.1: Membrane element subjected to in-plane stresses: (a) stresses; (b) deformations

Three sets of relationships are included in this theory: compatibility relationships for concrete and reinforcement average strains; equilibrium relationships involving average stresses in the concrete and reinforcement; and constitutive relationships for cracked concrete and reinforcement. Based on the perfect bond assumption in this theory, the average strains in concrete were assumed to be equal to the strains in the reinforcement in the x and y directions, denoted by ε_x and ε_y, respectively, (see Figure 5.1b). The resulting state of strains can be calculated using Mohr's circle as presented in Figure 5.2.

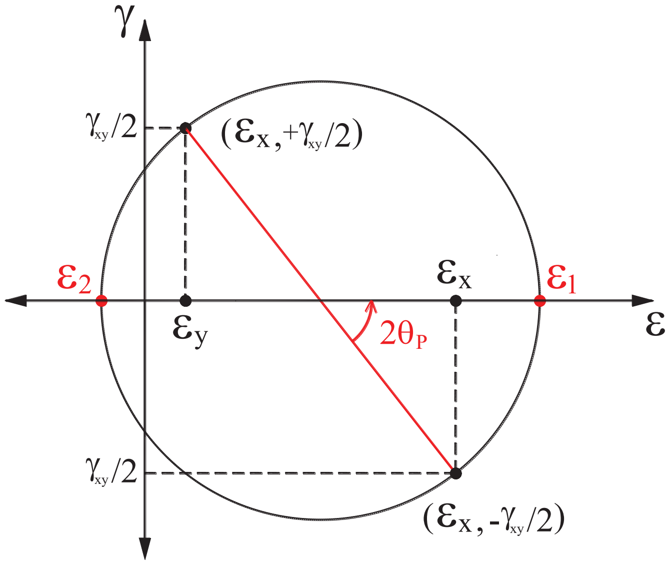

Figure 5.2: State of strain in a membrane element

The average principal tensile strain, ε_1, and the average principal compressive strain, ε_2, in addition to the angle between the principal tensile strains/stresses with respect to the x-axis, θ_p, can be expressed by the following equations:

$$\varepsilon_1 = 0.5\left[(\varepsilon_x+\varepsilon_y)+((\varepsilon_x-\varepsilon_y)^2+\gamma_{xy}{}^2)^{0.5}\right] \qquad \text{Eq. 5.1}$$

$$\varepsilon_2 = 0.5\left[(\varepsilon_x+\varepsilon_y)-((\varepsilon_x-\varepsilon_y)^2+\gamma_{xy}{}^2)^{0.5}\right] \qquad \text{Eq. 5.2}$$

$$\theta_p = \theta_{p\varepsilon} = \theta_{pf} = 0.5\tan^{-1}\left(\frac{\gamma_{xy}}{\varepsilon_x-\varepsilon_y}\right) \qquad \text{Eq. 5.3}$$

where positive shear would cause a clockwise rotation of the membrane element about the element centre. θ_ε and θ_f are the orientations of the average principal tensile strains and stresses with respect to the x-axis, respectively. Figure 5.3 presents the free body diagram of a reinforced concrete element subjected to in-plane stresses. Assuming the in-plane stresses are uniformly distributed over each side area of the membrane element with a constant value, equilibrium relationships can be derived based on the average stresses in the concrete and in the reinforcement.

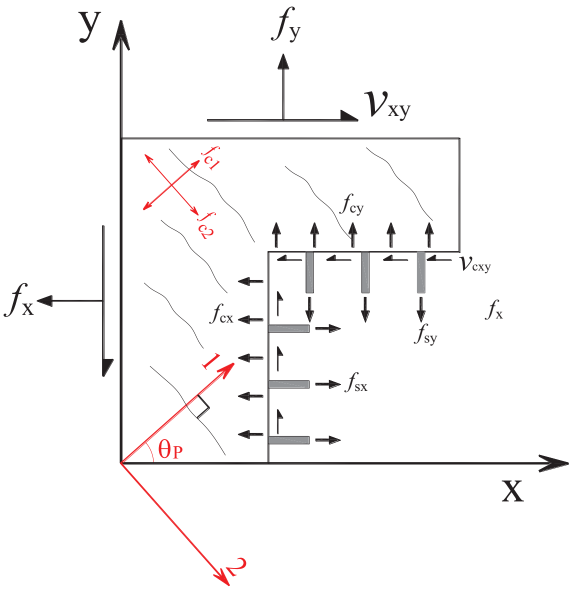

Figure 5.3: Free body diagram of reinforced concrete membrane element

Applying an equilibrium of forces in the x and y directions will result in a balance between the applied in-plane stresses, f_x and f_y, and the internal average stresses in the concrete, f_{cx} and f_{cy}, and in the reinforcement, f_{sx} and f_{sy}, respectively. By neglecting the dowel action of reinforcement, the applied shear stresses, v_{xy} , are entirely carried by the average shear stresses in concrete, v_{cxy} . Using Mohr's circle of stress, the average concrete stresses can be related to the average principal tensile stress in concrete, f_{c1}. These equilibrium relationships for the average stresses are summarized as follows:

$$f_x = \left(f_{c1} - \cot(90-\theta_p) \times \upsilon_{cxy}\right) + \rho_{sx} f_{sx} \qquad \text{Eq. 5.4}$$

$$f_y = \left(f_{c1} - \tan(90-\theta_p) \times \upsilon_{cxy}\right) + \rho_{sy} f_{sy} \qquad \text{Eq. 5.5}$$

where ρ_{sx} and ρ_{sy} are the reinforcement ratios in the x and y directions, respectively. To relate the strains in the compatibility relationships with the stresses in the equilibrium, Vecchio and Collins (1986) tested thirty panels with dimensions of 890 x 890 x 70 mm under in-plane stresses. Based on the test results, constitutive models for cracked concrete in compression and tension were developed. More discussion about the Modified Compression Field Theory (MCFT) can be found in Vecchio and Collins (1986).

5.1.2 DISTURBED STRESS FIELD MODEL (DSFM)

Tensile failure in matrix-aggregate composite can be called a crack and modeled as a geometrical discontinuity. One of the current approaches for crack modeling is the smeared crack approach, where the crack is assumed to be distributed over the area of the element. In nonlinear finite-element analysis of reinforced concrete, there are two main approaches for modeling cracked concrete: fixed crack models and rotating crack models. In fixed crack models, it is assumed that the crack directions remain fixed in the direction of the first crack. In some models, new discrete cracks may form at alternate inclinations. Alternatively, in rotating crack models, a gradual reorientation is assumed to occur in the principal stress and in the principal strain directions with respect to any change in the crack direction. Rots and Blaauwendraad (1989) provide more details about crack models.

When the crack shear slip is significant, the assumption "the orientations of principal strain, θ_ε, and the orientations of principal stress, θ_f, are the same" will not be accurate. In this case, the rotation of the principal stress tends to lag behind the rotation of the principal strain field. In such elements, the MCFT overestimates the shear stiffness and strength. The Disturbed Stress Field Model (DSFM), (Vecchio, 2000), and the MCFT have the same conceptual model. The DSFM, however, includes the crack shear slip deformation in the formulation of compatibility relations. Figure 5.4 shows the deformation due to crack shear slip.

Considering the compatibility conditions in a reinforced concrete element with a discontinuous slip crack surface, the DSFM expresses the total strains ε_x, ε_y, and γ_{xy}, as the sum of strains due to smeared cracks, ε_{cx}, ε_{cy}, and γ_{cxy}, and the strains due to shear slip, ε_x^s, ε_y^s, and γ_{xy}^s. The compatibility, equilibrium, and constitutive relationships were defined using Mohr's circle, and then the crack slip, δ_s, the crack width, w, and the crack slip shear strain, γ_{xy}^s, were determined.

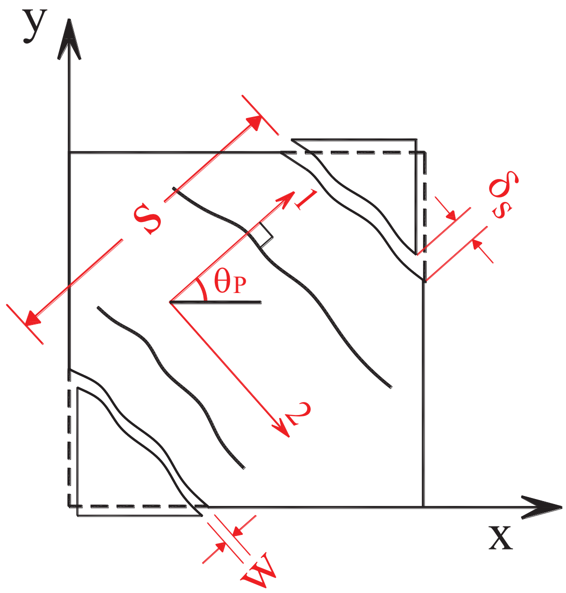

Figure 5.4: Deformation due to crack shear slip

5.2 FINITE ELEMENT MODELING

The program VecTor2 (Wong et al. 2013) was used in this study to numerically simulate the in-plane shear behaviour of reinforced masonry shear walls. This software was developed at the University of Toronto. The developers defined the software as a nonlinear finite element analysis (NLFEA) program for modeling two-dimensional reinforced concrete membrane structures. VecTor2 adopts a smeared, rotating-crack formulation for reinforced concrete based on the Modified Compression Field Theory (MCFT) and the Disturbed Stress Field Model (DSFM). The walls studied in this numerical simulation were subjected to in-plane axial compression and cyclic lateral loads (as shown in Figure 5.5). Figure 5.6 provides a flow chart that summarizes the algorithm of the nonlinear finite element analysis program, VecTor2. As shown in this flow chart, this software uses displacement-based finite element methods for structural analysis. This method results in a system of equations relating the unknown nodal displacements to the known external applied forces, using the structural elements stiffness matrix. Although VecTor2 was developed to model reinforced concrete membrane elements, the presence of grout and reinforcement enhance the directional behaviour of masonry by creating continuity in the stress flow and thereby making the behaviour of fully grouted RM walls similar to that of RC walls.

The behaviour of RM shear walls panels was simulated using the smeared approach. The masonry materials, including concrete block, mortar, and grout were modeled as one material with homogeneous properties. The word "masonry" in this numerical simulation will refer to the homogeneous material. Furthermore, the vertical and horizontal reinforcement cross-section areas were smeared along the membrane element area in the vertical and horizontal directions, respectively.

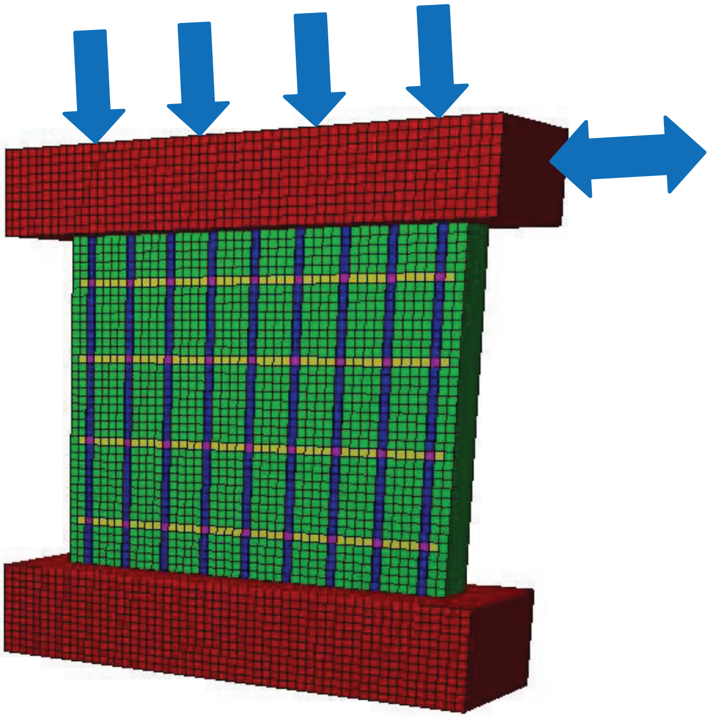

Figure 5.5: Finite element modeling for RM walls

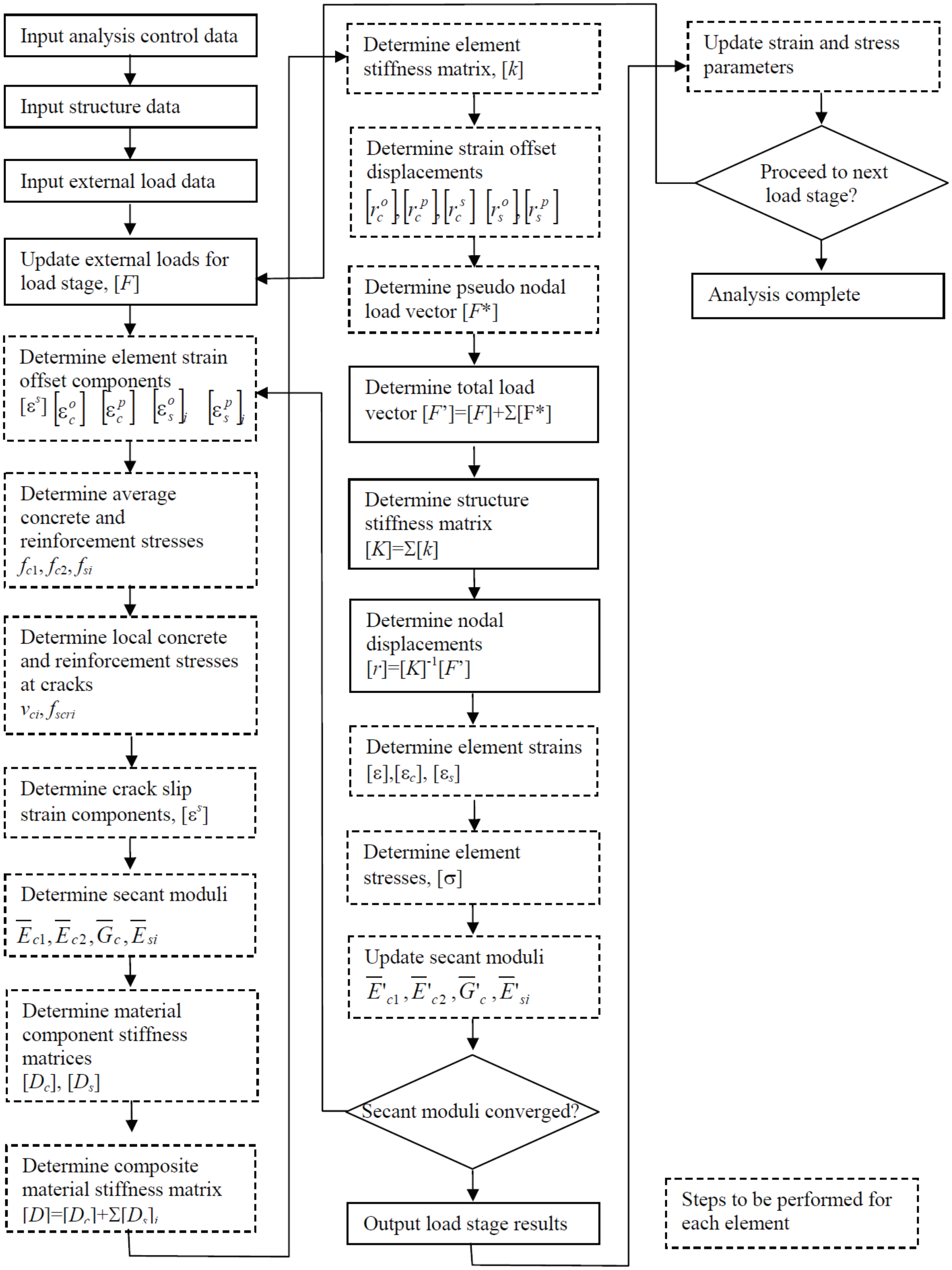

Figure 5.6: Vector2 nonlinear finite element analysis algorithm

(VecTor2&formworks user's manual, Wong et al. 2013)

5.2.1 ELEMENT TYPE

VecTor2 has three element categories in its element library, distinguished by the type of materials. The first category is for modeling concrete elements and it consists of triangular, rectangular, and quadrilateral elements. Discrete reinforcing bars can be modeled using the linear truss bar element in the second element category. The last category is for modeling bond-slip using non-dimensional links and contact elements. Since all the reinforcement in the studied walls were modeled using the smeared approach with an assumption of full bonding between the masonry and the reinforcement, only the elements in the first category are considered in this section. Figure 5.7 presents the three different element types in the first category for modeling concrete elements with or without smeared reinforcement.

All the elements are plane elements with a uniform thickness, t. Each node can translate in x and y directions with a total of 6 or 8 degrees of freedom for elements with 3 or 4 nodes, respectively. The displacement of any point in the element is expressed as a linear combination of the x and y coordinates. The element strains ε_x, ε_y, and γ_{xy} are related to the nodal displacements. For the quadrilateral element, the solver divides it into two constant strain triangles sharing the shortest diagonal, as shown in Figure 5.7c. The program then analyzes the two triangles separately for the nodal displacements. For accuracy, the software developers limited the use of the constant strain triangle and quadrilateral elements to accommodate edges that are not parallel to the x or y axes and to make transitions in element size. The plane stress rectangle element was selected to model the studied walls. The element is defined by four nodes in counterclockwise sequence (see Figure 5.7b).

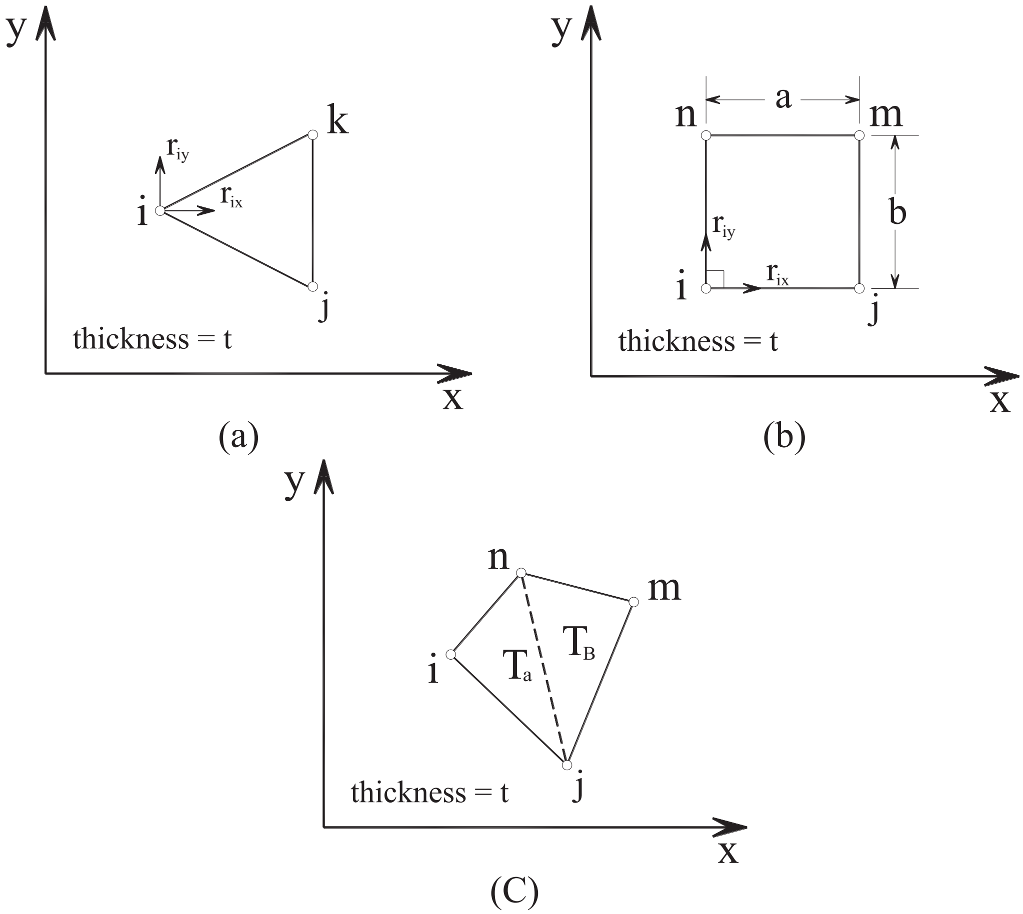

Figure 5.7: Masonry element types: (a) triangular, (b) rectangular, and (c) quadrilateral elements

Figure 5.8 shows the meshing of the finite element modeling for a RM wall. As shown in this figure, five different plane stress rectangle elements were defined and used in this modeling. The first one has a high compressive masonry strength with a high percentage of reinforcement in both the x and y directions, and was assigned for the top loading beam and the base foundation to make sure that they will be rigid during the loading of the studied walls. The other four elements were assigned to the studied walls. Out of the four elements, one element was defined without reinforcement, and the other three elements were defined with smeared reinforcement in the x or y or x and y directions (see Figure 5.8).

The arrangement of these wall elements was selected based on the spacing between the horizontal and vertical reinforcement. In this smeared approach, the bond between the steel reinforcement and the masonry was assumed to be fully bonded, as the de-bonding failure mode was not one of the studied failure modes. To simulate the boundary conditions during the laboratory test, all the joints at the base of the foundation were restrained in the x and y translation, while all the other joints were assigned to be free.

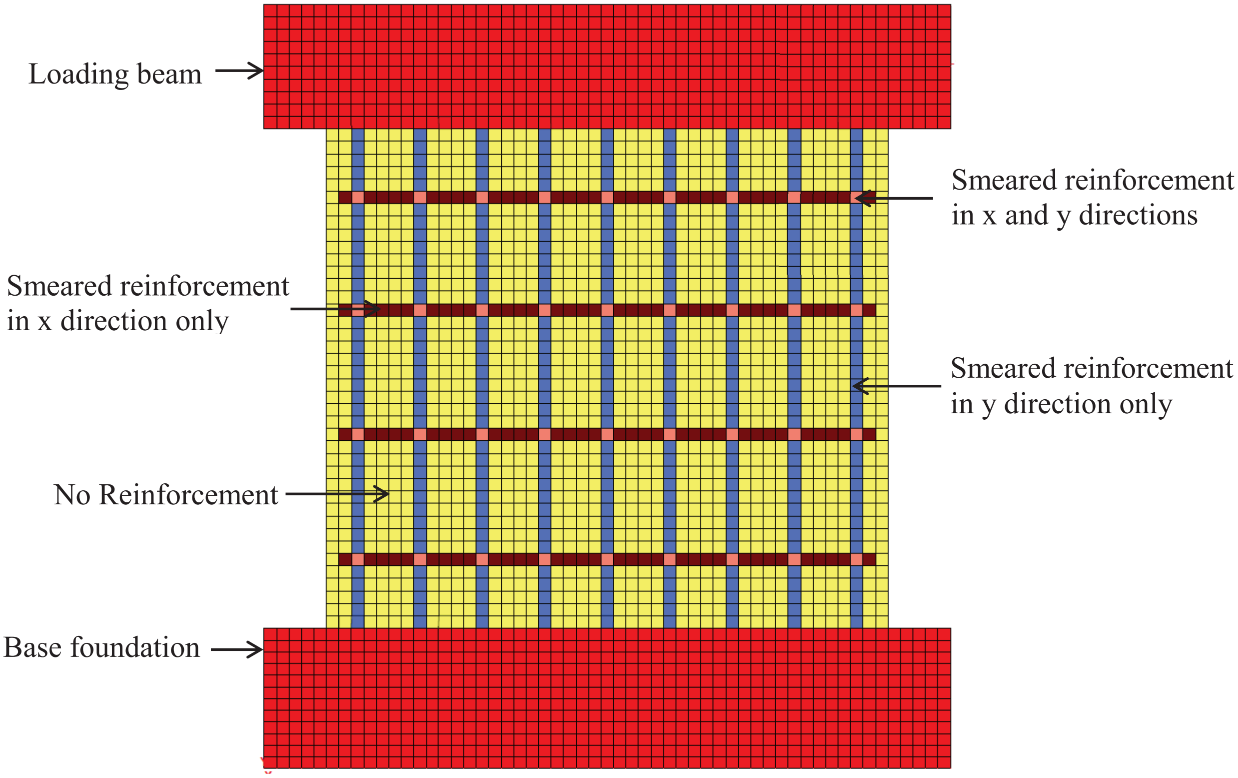

Figure 5.8: Finite element meshing for the studied RM walls

One of the parameters that has a major influence on the accuracy of the FE numerical simulation of concrete or masonry structural elements that involve cracking is the mesh sensitivity. In order to select the optimized mesh size that provides an acceptable level of precision for the output with respect to the CPU time, a sensitivity analysis was performed. The tested wall, W-Ref, was modeled using four different mesh sizes as shown in Figure 5.9. The numerical outputs were then compared to the test results to evaluate the influence of the mesh densities. The mesh sizes were selected based on the actual concrete block’s dimensions. In the first mesh densities, the wall geometry was meshed with 55 elements and 74 nodes. The other mesh densities' CPU time consumption were measured relative to this mesh size. Plane element size equal to 200 mm x 200 mm that represent the actual dimension of the concrete block cell was selected for the second mesh`s densities, Mesh 2. The last two mesh sizes were taken such that the masonry block cell is divided into 3 and 5 elements, respectively.

Figure 5.10 presents the lateral load-displacement backbone curves resulted from the different mesh densities for wall W-Ref, including the test results. As shown in this figure, modeling wall W-Ref using a fine mesh, Mesh 4, provides a better level of accuracy compared to that of the other mesh densities. Increasing the element size from Mesh 4 to Mesh 1 increases both the lateral strength and the ductility of the modeled wall by a significant percentage. Those increases are related to the reinforcement modeling approach. In this numerical simulation, the reinforcing bars were modeled using a smeared approach such that the vertical and horizontal reinforcement cross-section areas were smeared along the membrane element area in the vertical and horizontal directions, respectively. Using a large mesh size in the first mesh densities was a result of modeling the RM wall using only one type of element with smeared reinforcement in both the x and y directions (see Figure 5.9). In this manner, the steel reinforcing bars are simulated as a thin sheet with an area equal to the in-plane area of the wall. Conversely, using a small mesh size of 40 mm x 40 mm provides a more accurate simulation of the distributions of the reinforcing bars as shown in Figure 5.9, and thus low level of error. As can be seen in Figure 5.11, using a finer mesh size in Mesh 4 compared to Mesh 1 decreases the error in predicting the peak lateral load for wall W-Ref from 13% to less than 2%. Based on the results of this sensitivity analysis, a plane element size of 40 mm x 40 mm was selected to model the RM shear walls in this numerical simulation.

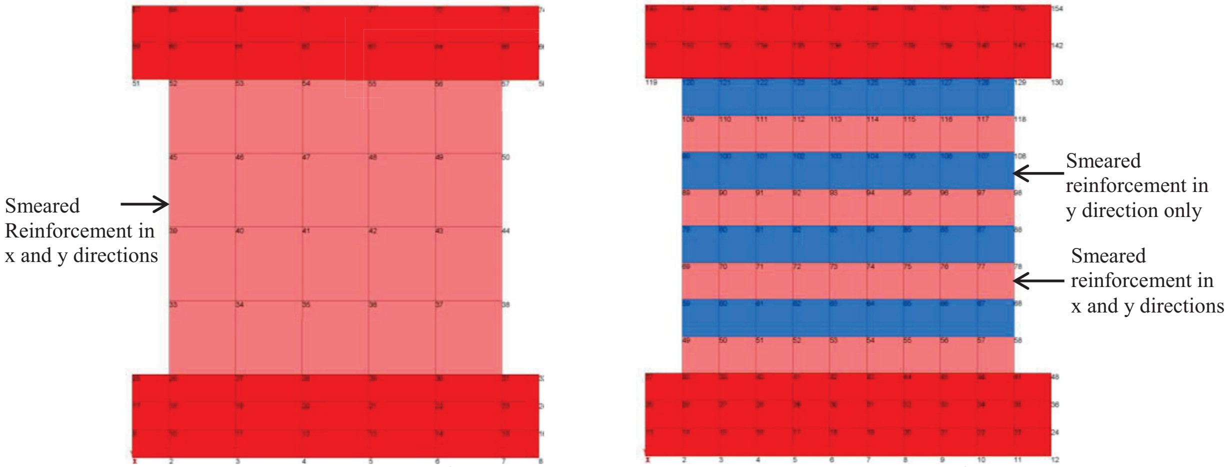

Mesh 1 (360 X 400) mm^2
74 Nodes
55 Elements

Mesh 2 (200 x 200) mm^2
154 Nodes
127 Elements

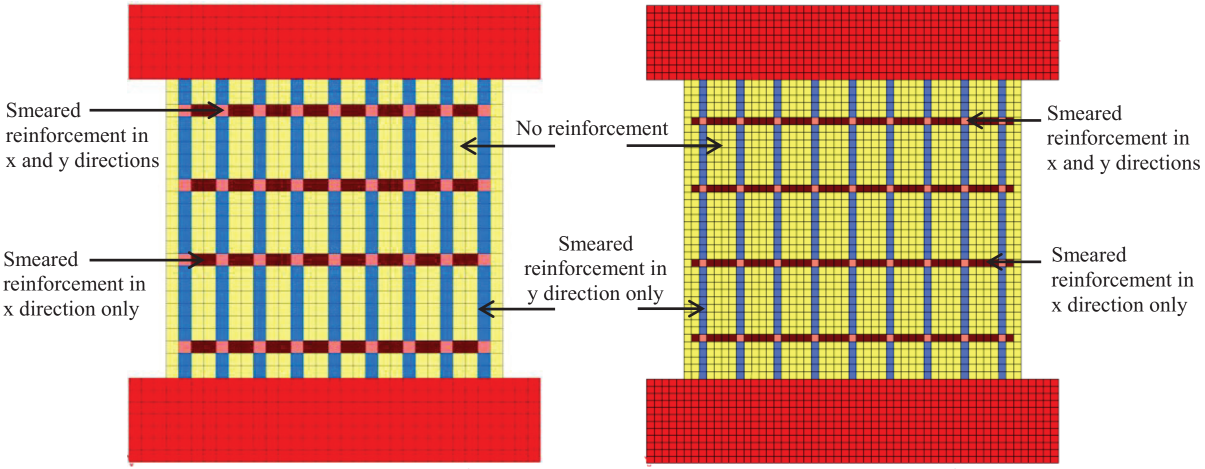

Mesh 3 (66.67 X 66.67) mm^2
1154 Nodes
1077 Elements

Mesh 4 (40 X 40) mm^2
3138 Nodes
3010 Elements

Figure 5.9: Different mesh densities evaluated in the mesh sensitivity analysis

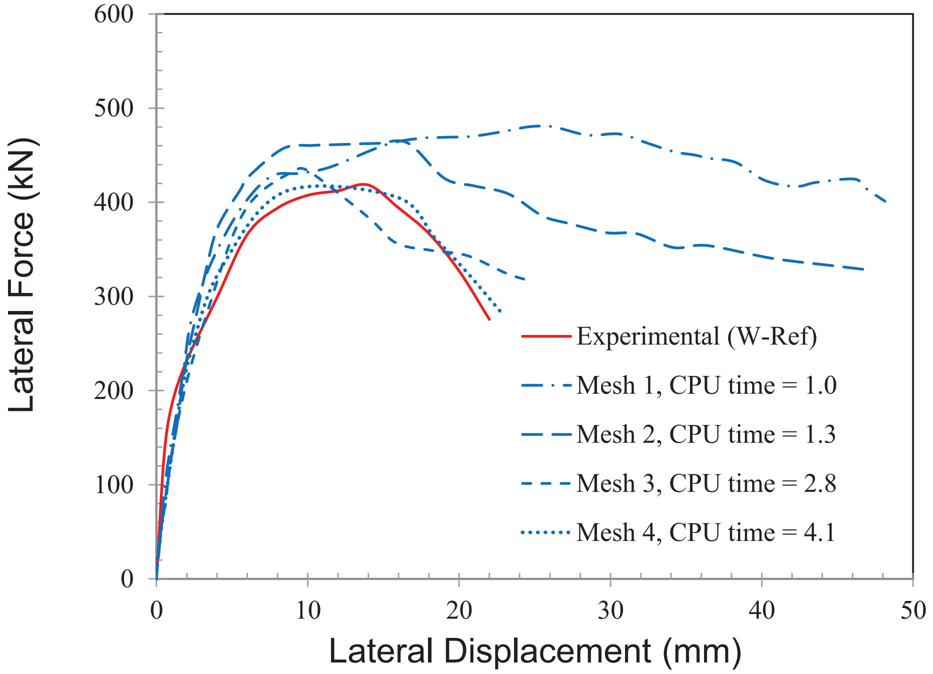

Figure 5.10: Lateral load-displacement backbone curves resulted from different mesh densities for the tested wall, W-Ref

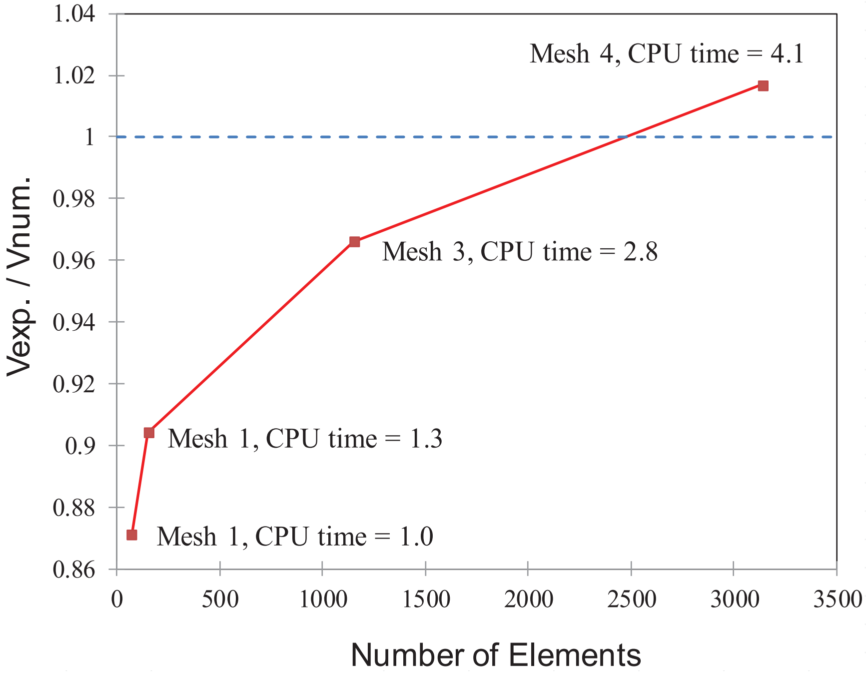

Figure 5.11: Effect of mesh size on the predicted lateral load capacity for wall W-Ref

5.2.2 MATERIAL MODELS

VecTor2 provides many material models for concrete and reinforcement. At each load step, the stresses and strains in each element are calculated; the structure's stiffness is then determined based on pre-defined models. Many of these models include multiple options that may produce a divergence in the results. Some of these models were selected based on the measured mechanical properties of the masonry and reinforcement materials in Section 3.3. Other models were chosen after multiple trials, having reached a good agreement between the numerical and experimental cyclic lateral load-displacement response of wall W-Ref. Next, the same models were used to simulate the behaviour of the other tested walls to verify the numerical results. This section provides a brief discussion of the models selected for the different materials.

5.2.2.1 Models for masonry material

As mentioned earlier, the behaviour of fully grouted and well-reinforced masonry walls is similar to the behaviour of RC walls under in-plane stresses (Pauley and Priestley 1992). Thus, all the models available for concrete material in VecTor2's library are considered viable selections for representing the masonry. Different models must be considered when modeling masonry material, such as:

- The compressive stress-strain relationship in both the pre-peak and post-peak behaviour, including the confinement effect and compression softening;
- The tensile stress-strain relationship, including the models for tension softening and tension splitting; and
- The hysteretic response, the crack width, and the crack slip check.

5.2.2.1.1 Compressive behaviour of masonry

One of the most important models that influence the response of numerically simulated RM shear walls is the stress-strain relationship of masonry under uniaxial compressive stress. The compressive stress-strain curve for masonry can be divided into two parts; pre-peak and post-peak response. All the pre-peak models in VecTor2 compute the peak compressive stress, f_p, and the corresponding strain, ε_p, by adjusting the unconfined input data for the compressive strength of masonry prism, f'_m, and its corresponding strain, ε_o, by the strength enhancement due to confinement.

The VecTor2 software provides five models that can be used to define the ascending branch. The first model is the linear response, realized by assuming a perfect elastic-plastic compression curve. Despite the fact that the concrete block and mortar, exhibit a linear elastic behaviour in compression, the presence of grout changes this behaviour so that it is nonlinear at a low level of compressive stresses. This behaviour change is a result of the softening in the stiffness due to the internal micro-cracks that form at the interface between the cement paste and the aggregates in the grout mixture. The Hognestad parabola (1951) is another model provided by the program. This simple compression response assumes a symmetric parabola curve about ε_p in which the stress equals to zero at zero and $2\varepsilon_p$ strains. In addition to these two models, three others: Popovics (1973), Popovics (high strength), and Hoshikuma et al. (1997) can be used to define the pre-peak response of masonry material.

Using the experimental results of the tested masonry prisms, Figure 5.12 shows the average compression pre-peak response of the masonry prisms versus the different models provided by VecTor2. As shown in this figure, the Hoshikuma et al. (1997) and Popovics (1973) models offer an accurate prediction for the pre-peak behaviour. The compressive stress-strain ascending branch in this study was defined by Hoshikuma et al.`s model using the following equation:

$$f_{mi} = E_m \, \varepsilon_{mi} \left(1 - \frac{1}{n} \left(\frac{\varepsilon_{mi}}{\varepsilon_{pi}} \right)^{n-1} \right) \quad for \quad \varepsilon_{mp} < \varepsilon_{mi} < 0 \qquad \text{Eq. 5.6}$$

$$n = \frac{E_m}{E_m - E_{sec}} \quad , \quad E_{sec} = \frac{f_{mp}}{\varepsilon_{mp}}$$

where f_{mi} and ε_{mi} are the compressive stress and strain at any point, respectively, f_{mp} and ε_{mp} are the peak compressive stress and its corresponding strain from the experimental results, respectively, and E_m and E_{sec} are the initial and secant tangents, respectively. Facconi et al. (2013) recommended this equation to model masonry walls because it considers the initial modulus of elasticity independently of the compressive strength and strain at peak. The masonry prism with h/t equal to 8, representing a full-scale vertical strip of the tested walls, were used for the input data; f_{mp}, ε_{mp}, E_m and E_{sec}, to define the pre-peak model. After the principal compressive stress reaches the masonry peak compressive strength, f_{mp}, degradation in the masonry resistance occurs by increasing the level of compressive strains along the descending branch. The post-peak stiffness dictates the ductility of a structural element subjected to displacement excitations such as the response of shear walls in seismic events. Consequently, the selection of the compression post-peak model has a significant effect on the predicted load-deformation response, and as a result, on the level of displacement ductility.

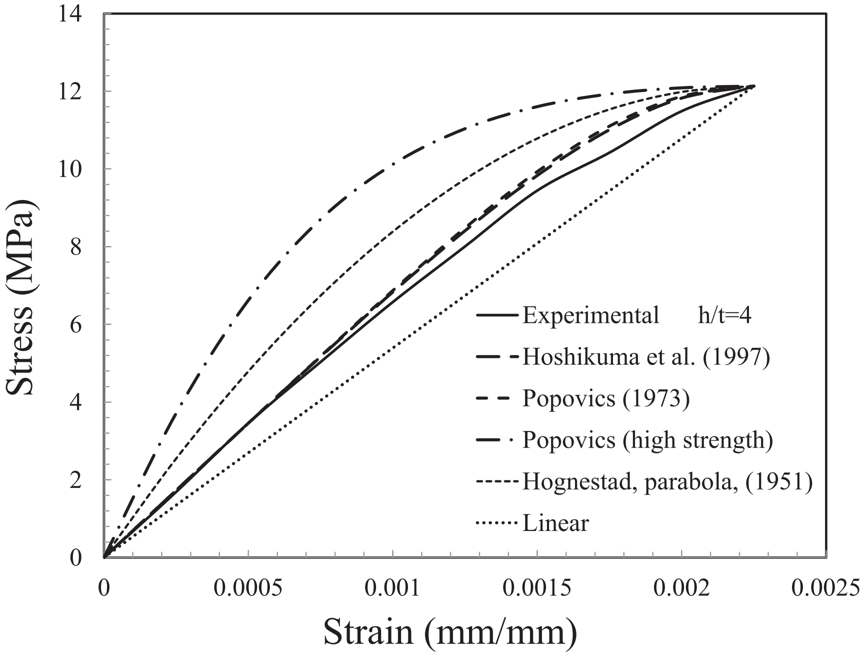

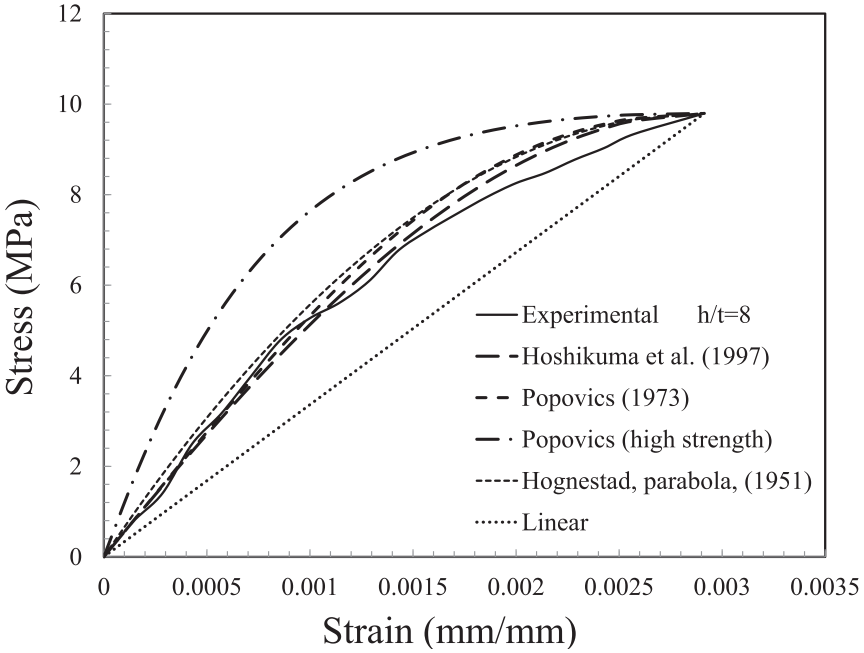

Figure 5.12: Experimental vs compression pre-peak models in VecTor2 for masonry prisms with: (a) *h/t* =4; (b) *h/t* =8

Similar to the pre-peak response, VecTor2 provides different models to predict the compression post-peak behaviour of masonry, such as: the Modified Park-Kent (1982), Popovics/Mander (1988), Hoshikuma et al. (1997) and Seenz/Spacone (2002) models. All of these models have a residual branch with a constant value equal to $0.2f_{mp}$. On the other hand, each of these models has a different equation for the descending branch. The post-peak model proposed by Hoshikuma et al (1997) was selected to model the descending branch of the masonry compressive stress-strain relationship, as recommended by Facconi et al. (2013) (see Figure 5.13). More details about the equations that define this model can be found in Wong et al. (2013).

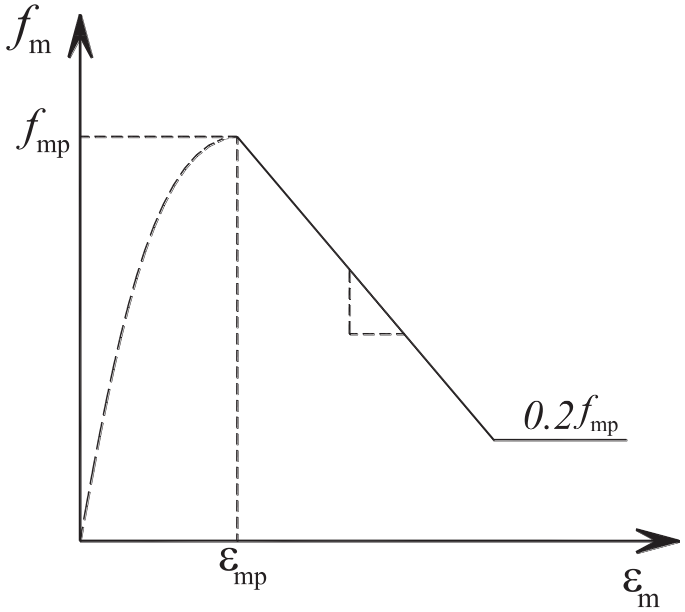

Figure 5.13: Hoshikuma et al. (1997) model used to represent the post-peak compression behaviour of masonry

After the initiation of cracks in RM walls, the peak compressive strength and the initial stiffness will reduce. This phenomenon is known as compression softening. The compression softening models provided by the program calculate this reduction by multiplying the peak compressive stress, f_{mp}, and its corresponding strain, ε_{mp}, by a softening parameter, β_d.

The compression softening parameter, β_d, was determined by statistical analysis of the stress-strain states from tested panels (Vecchio and Collins, 1992). This softening parameter ranges between zero and one. The software provides three options for compression softening. In the first option, no compression softening is considered such that the compression response is assumed independent of the coexisting tensile strains. Otherwise, only strength softening or strength and strain softening are considered in the second and third options, respectively, (see Figure 5.14). In this numerical study, only softening in the compression strength was considered.

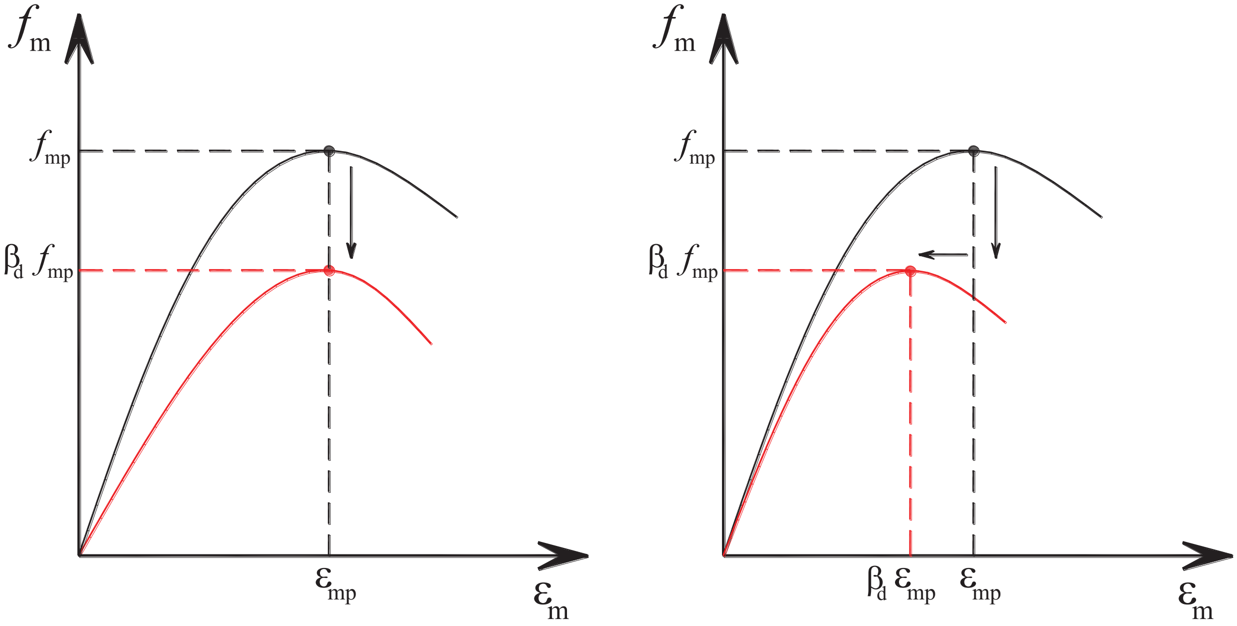

Figure 5.14 Compression softening models: (a) strength only; (b) strength and strain

5.2.2.1.2 Tensile behaviour of masonry

Similar to concrete and most of the cementitious materials, masonry exhibits a brittle behaviour under tensile stress. The pre-peak tensile response of masonry can be defined in a linear-elastic relation as follows:

$$f_{mt} = E_m \varepsilon_{mt} \quad for \quad 0 < \varepsilon_{mt} < \varepsilon_{mcr}$$ Eq. 5.7

$$\varepsilon_{mcr} = \frac{f_{mcr}}{E_m}$$ Eq. 5.8

where f_{mt} and ε_{mt} are the principal tensile stress and strain at any point, respectively, f_{mcr} and ε_{mcr} are the tensile strength and its corresponding strain, respectively, and E_m, is the elasticity modulus of masonry. The input value for the masonry tensile strength was 1.8 MPa (see Table 3.6). When the principal tensile stress exceeds the tensile strength of masonry, the initiation of cracks takes place in masonry walls, followed by a sudden drop in the masonry tensile stresses to zero at the cracks` free surfaces. The presence of reinforcement enhances the tensile post-peak response of RM walls due to the bond action that allows tensile stresses to flow between the cracks. Increasing the level of deformations leads to wider cracks and as a result, the bond action reduces near the cracks` surfaces. Furthermore, the masonry tensile strength reduces gradually to zero. Meanwhile, the tensile stress is redistributed to the reinforcement. Thus, the amount of reinforcement and the bond mechanism have a critical influence on the degradation slope. This behaviour is known as tension stiffening. Neglecting the phenomenon of the tension stiffening will lead to a sudden reduction in the tensile resistance, carried to zero by the masonry upon cracking. There are many proposed models for tension stiffening, such as: the Modified Bentz model which is derived from the work done by Bentz (2000), Vecchio (1992), Collins-Mitchell (1987), and Tension chord (Kaufmann and Marti, 1998) models. After several trials, the Modified Bentz model was selected, as it provides a more accurate degradation branch in the lateral load-displacement response of wall W-Ref.

As a consequence of the cyclic loading, there is degradation in the stress-strain response relationships of masonry under loading, unloading, and reloading. As such, the hysteretic response of masonry has an impact on the strength and ductility of masonry shear wall models. The hysteretic response models define the relation between the stress-strain curve under monotonic and cyclic loading. Palermo and Vecchio (2002) proposed a model for the hysteretic response that includes the damage in the reloading curve (see Figure 5.15). As shown in this figure, when unloading the masonry element to a zero load there is a plastic offset of strains, ε^p. Increasing the level of deformations will increase the value of this offset. Furthermore, when reloading the masonry element a reduction in the stiffness accrues, leading to losses in the strength at the same strain. In addition to these models, many mechanisms were considered for modeling the behaviour of the masonry material, including: tension softening, shear slip along crack surfaces, cracking stress calculation, and crack width check.

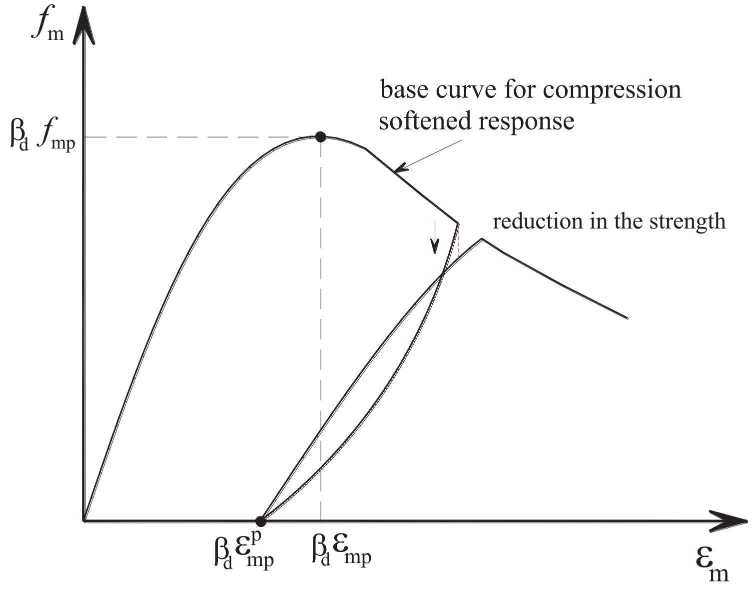

Figure 5.15: Palermo model of masonry hysteretic response in compression (Palermo and Vecchio, 2002)

5.2.2.2 Models for steel reinforcing bars

All the walls tested in the experimental program were reinforced either in the vertical direction or in both the vertical and horizontal directions. The standard steel reinforcing bars in the Canadian market, 10M and 15M, were used for the horizontal bars, while the vertical bars were either 20M or 30M. Samples were taken from each type of reinforcing bar and subjected to tensile testing to determine their stress-strain characteristics in accordance with test methods and definitions in the ASTM A615 Standard (ASTM 2013). The steel reinforcing bars show a ductile behaviour as presented in Figure 5.16. Based on the test results, the stress-strain behaviour of steel reinforcement material can be defined in a trilinear relationship that includes an initial linear-elastic response followed by a yield plateau and then a linear strain-hardening phase until failure. The VecTor2 program calculates the reinforcement stress, f_s, in tension and compression as follows:

$$f_s = \begin{cases} E_s \varepsilon_s & \text{for} \quad |\varepsilon_s| \le \varepsilon_y \ \varepsilon_s \\ f_y & \text{for} \quad \varepsilon_y \le |\varepsilon_s| \le \varepsilon_{sh} \\ f_y + E_{sh}\,(\varepsilon_s - \varepsilon_{sh}) & \text{for} \quad \varepsilon_{sh} \le |\varepsilon_s| \le \varepsilon_u \\ 0 & \text{for} \quad \varepsilon_u \le |\varepsilon_s| \end{cases} \qquad \text{Eq. 5.9}$$

$$\varepsilon_u = \varepsilon_{sh} + \frac{\left(f_u - f_y\right)}{E_{sh}} \qquad \text{Eq. 5.10}$$

where ε_s, ε_y, ε_{sh}, and ε_u are the steel reinforcement strain, yield strain, strain at the onset of strain hardening, and the ultimate strain, respectively. E_s and E_{sh} are the elastic modulus and the strain hardening modulus, respectively, and f_y and f_u are the yield and ultimate strength, respectively. Figure 5.16 presents the modeled stress-strain response of steel reinforcement versus the experimental relationship. This model represents the behaviour of the steel reinforcement under monotonic loading. For RM shear walls subjected to lateral cyclic loading, the hysteretic response of the steel reinforcement has an influence on the level of displacement ductility. The hysteretic response Seckin model (1981) with a Bauschinger effect was selected for the steel reinforcement (see Figure 5.17).

The contribution of the vertical reinforcement towards the lateral shear resistance, i.e. the dowel action, was modeled using Tassios' model (1987). This contribution is computed as a function of the shear slip, δ_s, at the crack, as shown earlier in Figure 5.4. The reinforcement cross-sectional area was smeared along the membrane element area. It is important to mention that reinforcement buckling was ignored in this model.

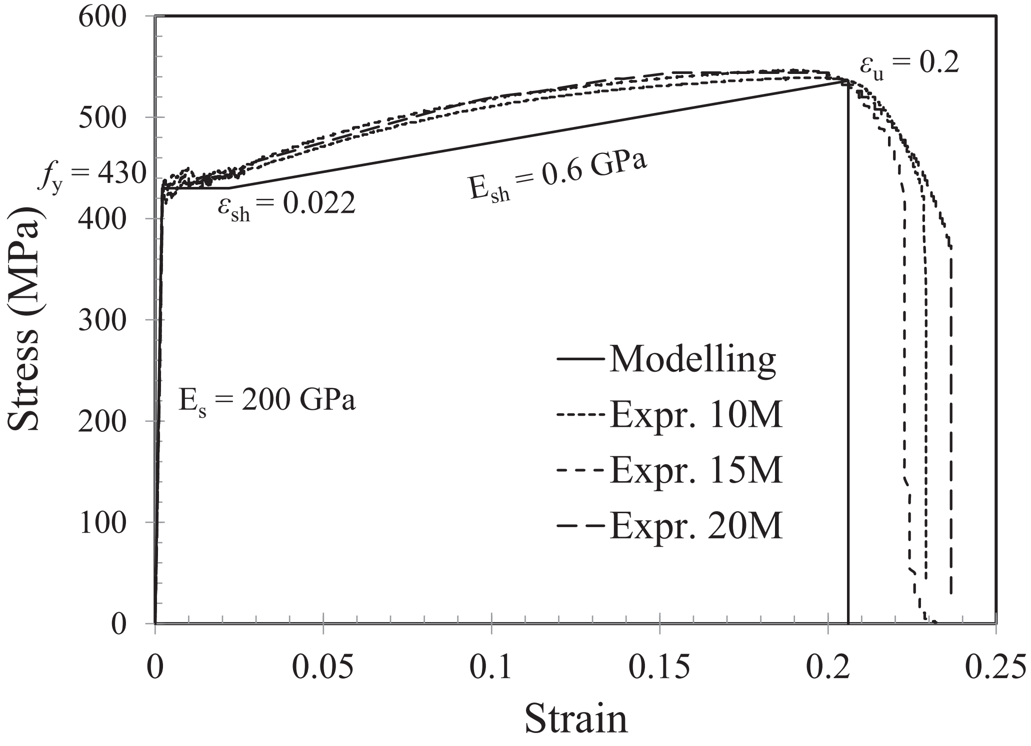

Figure 5.16: Ductile steel reinforcement stress-strain response: Modeling vs. Experimental

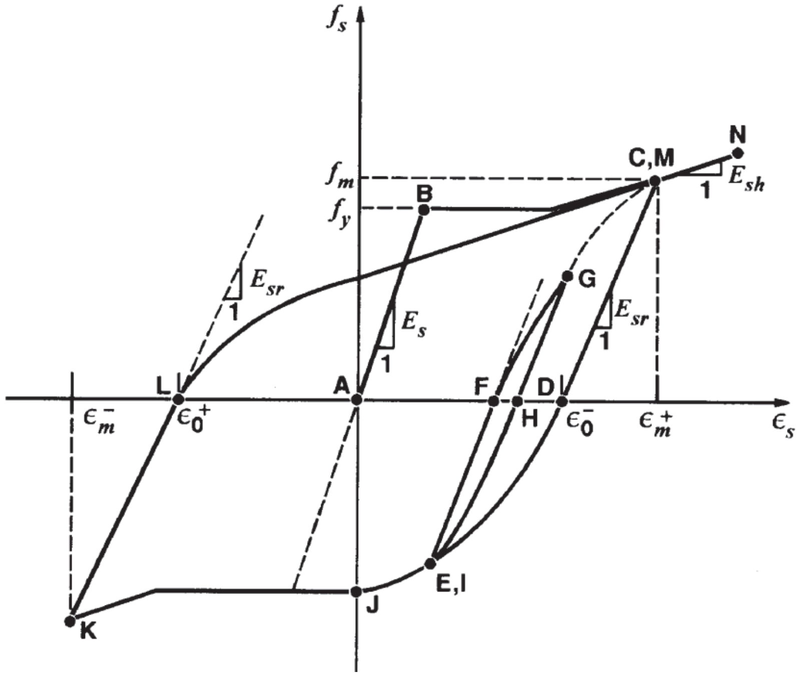

Figure 5.17: Seckin model (1981) of reinforcement hysteretic response (Vecchio, 1999)

Table 5.1 summarizes the different models that were selected for the behaviour of the masonry and steel reinforcement materials. The analysis models, including the strain history, strain rate effects, and the geometric nonlinearity are shown in the same table. Wong et al. (2013) present more details and discussions about these models.

Table 5.1: Models for Numerical Simulation

Homogeneous masonry material	Model
Compression pre-peak	Hoshikuma et al. (1997)
Compression post-peak	Hoshikuma et al. (1997)
Compression softening	Vecchio 1992-B (e1/e0-Form)
Tension softening	Nonlinear (Hordijk)
Tension stiffening	Modified Bentz 2003
Confinement strength	Kupfer / Richart (1969)
Dilatation	Variable-Kupfer et al. (1969)
Cracking criterion	Mohr-Coulomb (Stress)
Crack stress calculation	Advanced (Lee 2009)
Crack width check	Crack limit (Agg/2.5)
Hysteresis response	Nonlinear with plastic offsets Palermo and Vecchio (2002)
Crack slip calculation	Vecchio-Lai (Cyclic)

Reinforcement bar material	Model
Stress-strain	Ductile (trilinear relationship)
Dowel action	Tassios (1987)
Hysteresis response	Seckin with bauschinger (1981)

Analysis parameters	Model
Strain history	Previous loading considered
Strain rate effects	CEB (full)
Geometric nonlinearity	Considered

5.2.3 LOADING PROTOCOL

The loads were applied in two sequential phases, axial and lateral. In the first phase, a load-control protocol was used to apply the total vertical compression load that was uniformly distributed and applied on the top joints of the loading beam. In the second phase, in-plane cyclic static displacements were applied at the middle height joint of the right side of the loading beam, according to the loading histories proposed by FEMA 461 (2007). In each stage of lateral loading, two displacement cycles were completed for each target displacement, with an incremental gain of 2mm for each stage. These load protocols were selected to represent the same load protocols that were followed for the experimentally tested walls that will be used to verify this FE models. The yield load was determined when the strain at the wall-footing interface of the outermost vertical reinforcing bars reached the yield strain level. Furthermore, the failure was defined as the point on the envelope lateral load - deformation relationship where the lateral resistance dropped to 80% of the maximum lateral load recorded, in whichever direction this occurs first. Consequently, the displacement capacity $\Delta_{80\%Qu}$ and the displacement ductility $\mu_{\Delta 80\%Qu}$ were measured at the same point of failure. In order to obtain a realistic post-peak non-linear behaviour for shear walls, it is important to determine the suitable displacement increment rate. Many parameters influence the selection of the displacement increment rate, such as the element dimensions and the maximum expected displacement (Güner, 2008). Based on several trials, the most suitable and practical applied displacement increment rate was found to be from 0.2 to 0.4 mm, according to the wall aspect ratio. Figure 5.18 presents snapshots of VecTor2 output.

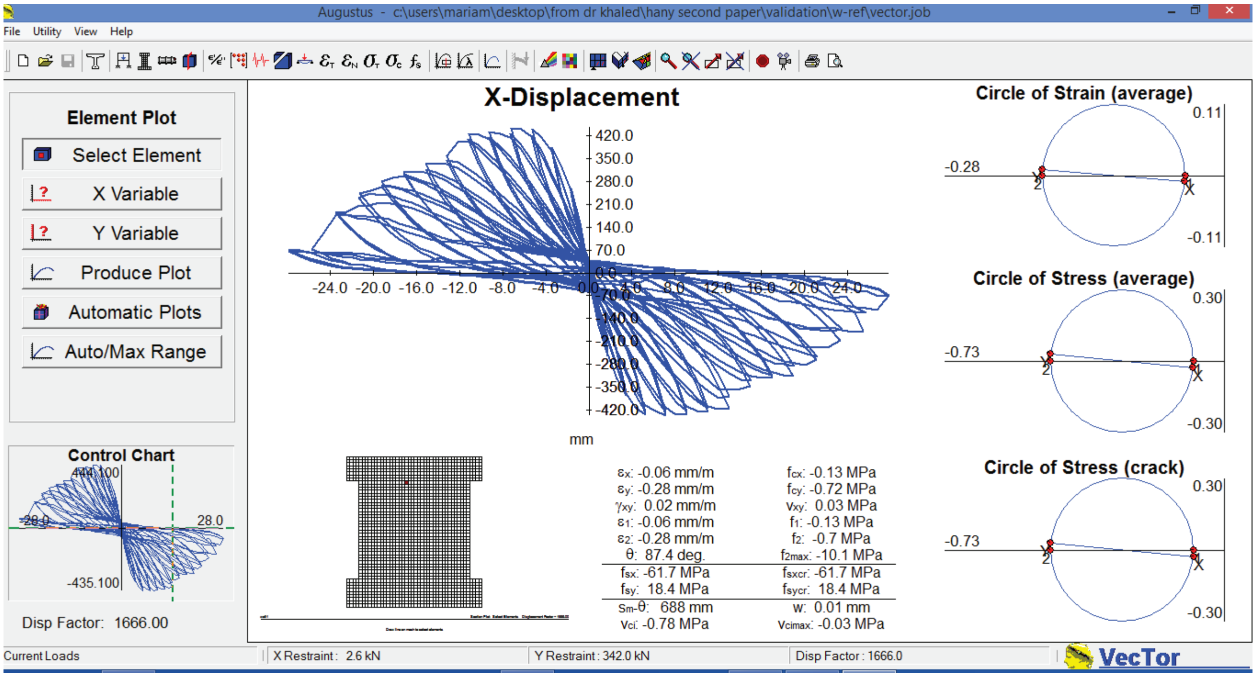

Disp Factor: 1666.00

ε_x: -0.06 mm/m
ε_y: -0.28 mm/m
γ_{xy}: 0.02 mm/m
ε_1: -0.06 mm/m
ε_2: -0.28 mm/m
θ: 87.4 deg.
f_{sx}: -61.7 MPa
f_{sy}: 18.4 MPa
$s_{m\text{-}\theta}$: 688 mm
v_{ci}: -0.78 MPa

f_{cx}: -0.13 MPa
f_{cy}: -0.72 MPa
v_{xy}: 0.03 MPa
f_1: -0.13 MPa
f_2: -0.7 MPa
f_{2max}: -10.1 MPa
f_{sxcr}: -61.7 MPa
f_{sycr}: 18.4 MPa
w: 0.01 mm
v_{cimax}: -0.03 MPa

Current Loads
X Restraint: 2.6 kN
Y Restraint: 342.0 kN
Disp Factor: 1666.0

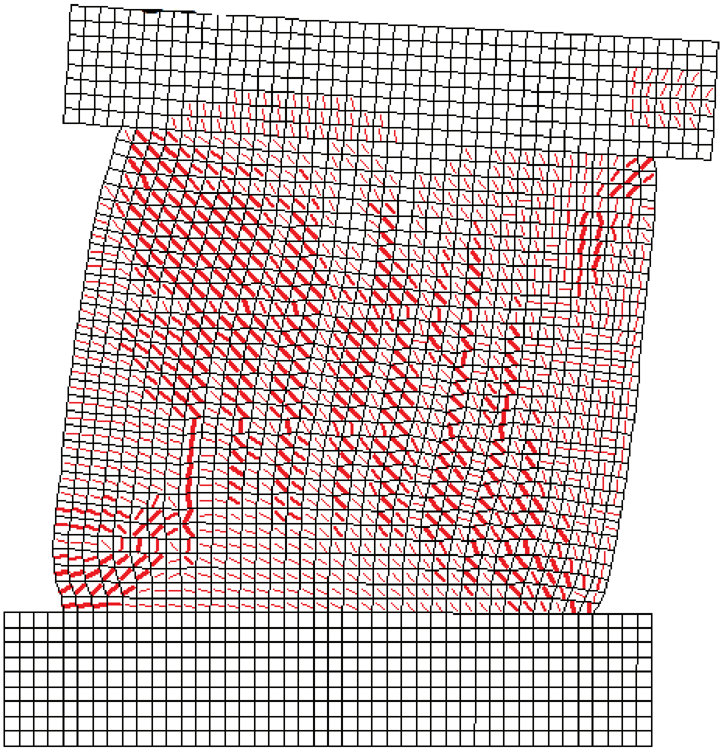

Figure 5.18: Snapshots of VecTor2 output

5.3 VERIFICATION OF THE FE MODELING

The results of the tested walls in the experimental work were used to verify the FE modeling. Out of the nine walls, two walls were tested to investigate the influence of the horizontal reinforcement anchorage end detail on the in-plane shear behaviour, including the reinforcement contribution, V_s. Since one of the assumptions in this numerical modeling is that there is a full bond between the masonry and the reinforcement, the results of these two walls, W-90° and W-Str, were eliminated from the modeling verification.

All the tested walls had the same dimensions, 1.8 m x 1.6 m x 0.19 m, and were constructed on reinforced concrete (RC) foundations with dimensions of 2.3 m long x 0.64 m wide x 0.45 m high. The walls were subjected to a cyclic lateral displacement at a height of 1.80 m from the top of the RC foundation in order to keep the shear span to depth ratio, M/Vd_v, higher than 1.0. The loads were transferred to the tested walls through a stiff built-up steel loading beam. The first wall, W-Ref, was designed to be a reference wall for the remaining tested walls. Wall W-Ref had a horizontal reinforcement of 10M@400 mm, uniformly distributed along the height of the wall and hooked using the standard 180° bend around the outermost wall vertical reinforcing bars. Wall W-Ref was vertically reinforced with a 20M bar in each cell. A constant axial compressive stress of 1.0 MPa was applied to the studied wall before applying the in-plane cyclic lateral displacements, and that stress remained until the failure occurred.

Wall W-ρ_h0 is a duplicate of wall W-Ref, but without horizontal reinforcement. Walls W-σ_n0 and W-σ_n1.5 are also duplicates of wall W-Ref, but with externally applied axial compressive stresses of 0.0 and 1.5 MPa, respectively. Wall W-M/Vd_v1.5 was subjected to a top moment of 0.9V kN.m to represent a shear span to depth ratio, M/Vd_v, equal to 1.5, compared to a value of 1.0 for wall W-Ref, where V is the lateral load from the horizontal actuator.

Unlike wall W-Ref, wall W-S_v800 was constructed with horizontal reinforcement of 15M@ 800 mm, in order to study the influence of the vertical spacing between horizontal bars. Wall W-S_h800 is a duplicate of wall W-S_v800 except that the vertical reinforcement was concentrated in the first, middle, and end cells. Each cell has a 30M bar with a vertical reinforcement ratio,ρ_v , of 0.61% compared to ρ_v of 0.79% for the rest of the tested walls.

The selected models for the masonry and steel reinforcement material as well as the analysis parameters were calibrated using the test results of the reference wall, W-Ref. The numerical cyclic load-displacement responses of the seven walls were then verified with the experimental hysteresis loops, using the same models. Wall W-M/Vd_v1.5 was modeled with a height of 2.7 m to have a shear-span to depth ratio of 1.5 compared to the reference wall, W-Ref, in the tested walls. The cyclic static displacements were applied at the middle height joint of the right side of the loading beam, whereas the lateral displacement was measured at a height of 1.8 m, as shown in Figure 5.19. Figure 5.20 shows the experimental versus the numerical cyclic lateral load-displacement response for the seven tested RM walls. Furthermore, Figure 5.21 presents a comparison between the maximum lateral forces from the numerical simulation predictions and the measured values from the experimental work.

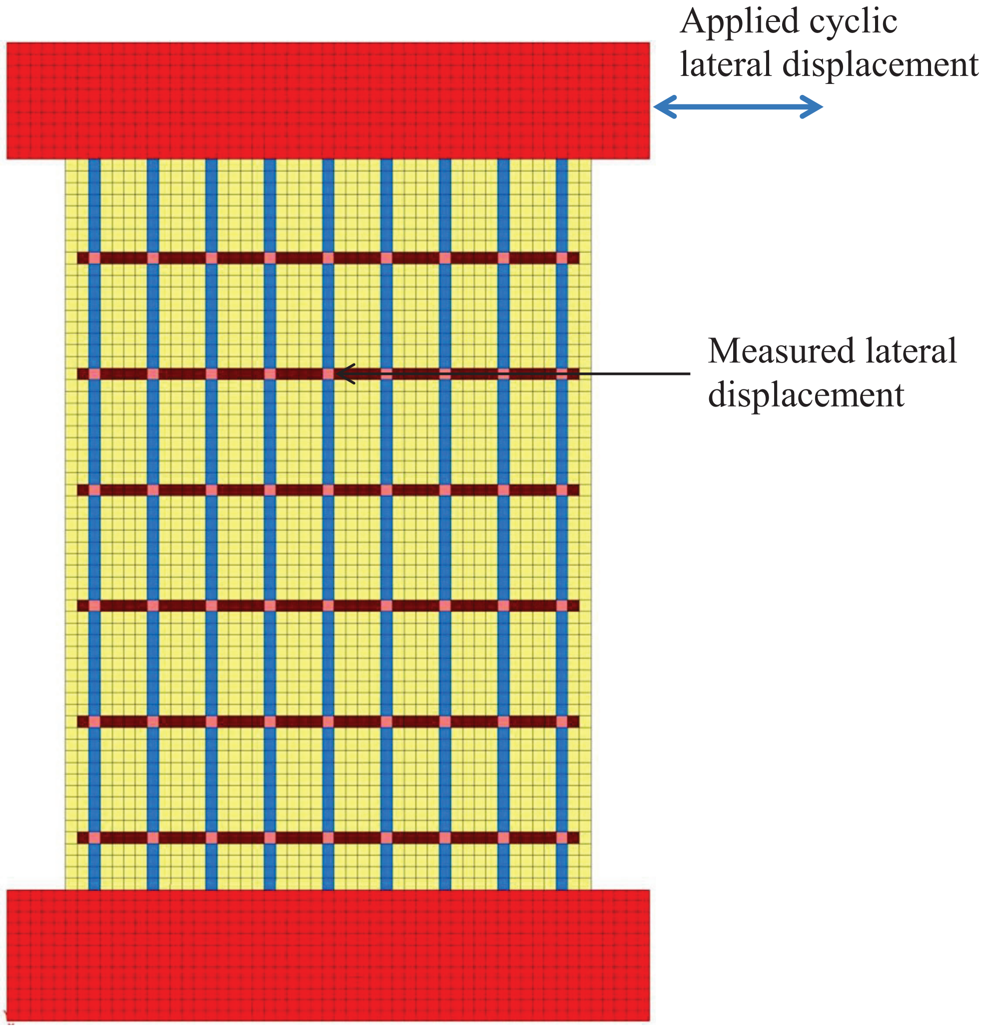

Figure 5.19: Finite element model for wall W-M/Vd_v1.5

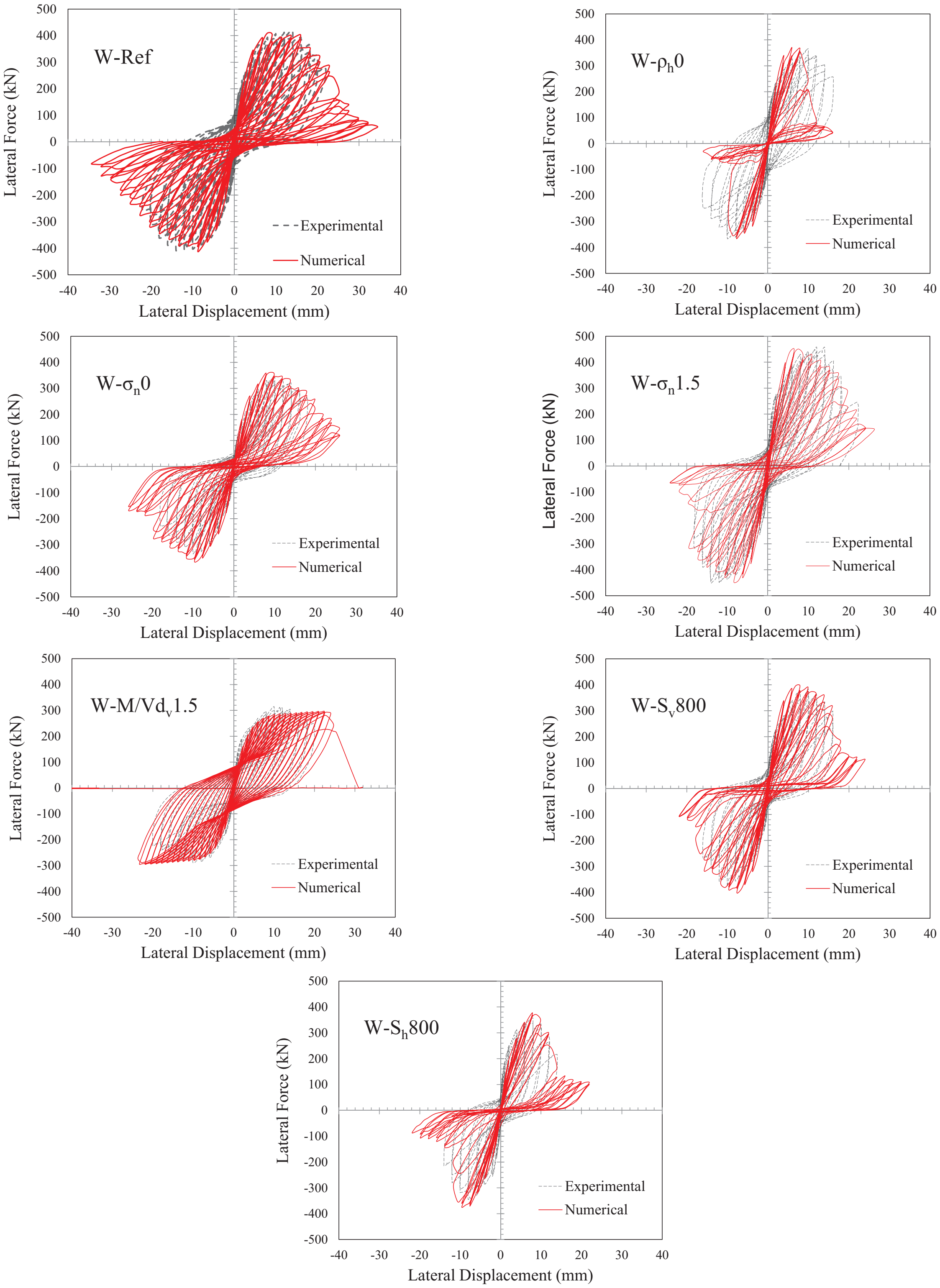

Figure 5.20: Experimental vs. numerical cyclic lateral load-displacement response of tested RM shear walls

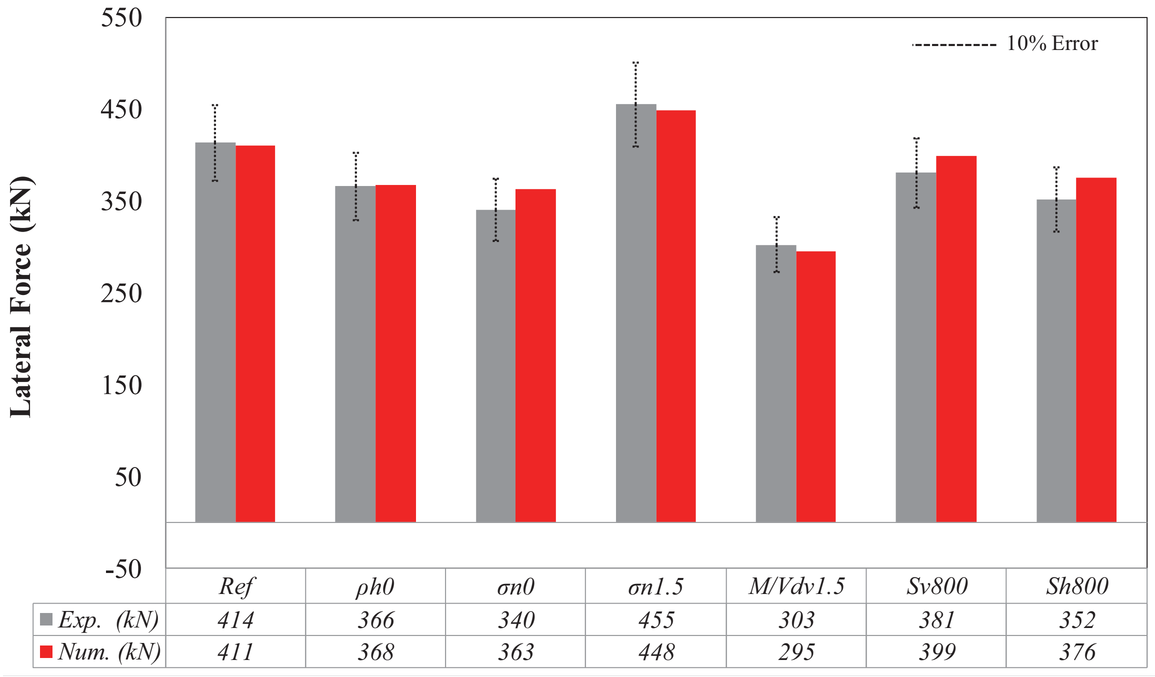

Figure 5.21: Experimental vs. numerical maximum lateral force for the studied RM walls

There are two main observations that can be made from these figures. The first one is that the developed numerical models provide an acceptable level of accuracy to predict the maximum lateral force, as the percentage of error is within ±10% for all the tested walls (as depicted in Figure 5.21). In addition, the models have a good match with the experimental hysteresis loops for the walls with uniform distributed reinforcement in both directions. On the other hand, for the walls with no horizontal reinforcement, such as wall W-ρ_h0, or with large spacing between the vertical bars, like W-S_h800, the numerical models were not able to predict an accurate post-peak response.

The explanation for this behaviour refers to both the Modified Compression Field Theory (MCFT) and the Disturbed Stress Field Model (DSFM), developed based on the test results of membrane-reinforced concrete elements. Moreover, all the models provided in the VecTor2 program are for concrete materials and not for masonry. The assumption to simulate the behaviour of masonry as a homogenous material and thereby using the concrete models was based on having a sufficient amount of well-distributed reinforcement in both directions to transfer the applied stresses. If this condition is not satisfied, the provided post-peak models for concrete materials are not accurate at presenting the post-peak masonry response.

5.4 PARAMETRIC STUDY

After validating the FE modeling using the experimental results, a parametric study was conducted to investigate the in-plane shear behaviour of RM shear walls. A total of eight walls were considered in this study. All the studied walls were reinforced with a constant horizontal and vertical reinforcement ratio of 0.13% and 0.79%, respectively. The length of all the walls was 1.8 m, while the height varied based on the wall aspect ratio. Standard concrete block with dimensions of 400 mm x 200 mm x 190 mm was assumed to be used to construct the studied walls. The influences of three parameters were evaluated in this study, namely: the horizontal reinforcement distribution, the level of the axial compressive stress, and the wall aspect ratio. Two values for each parameter were considered: horizontal reinforcement spacing of 200 mm and 800 mm c/c; axial compressive stress of 0.0 and 1.0 MPa; and wall aspect ratios of 1 and 2. The dimensions, reinforcement details, and the applied axial compressive stress for the eight walls are given in Table 5.2. Moreover, Table 5.3 presents a summary of the numerical results for studied walls. The effect of each parameter on the in-plane shear behaviour of RM shear walls is discussed separately in the next section.

Table 5.2: Matrix of the Studied Walls in the Parametric Study

Wall ID	Length (L) mm	Height (H) mm	Aspect ratio (H/L)	Reinforcement		Axial Stress (MPa)	Axial Load (kN)
				Horizontal	Vertical		
Wall 1	1800	1800	1	D8@200	20M@200	0	0
Wall 2	1800	1800	1	15M@800	20M@200	0	0
Wall 3	1800	1800	1	D8@200	20M@200	1	342
Wall 4	1800	1800	1	15M@800	20M@200	1	342
Wall 5	1800	3600	2	D8@200	20M@200	0	0
Wall 6	1800	3600	2	15M@800	20M@200	0	0
Wall 7	1800	3600	2	D8@200	20M@200	1	342
Wall 8	1800	3600	2	15M@800	20M@200	1	342

Table 5.3: Results of the Studied Walls in the Parametric Study

Wall ID	Q_y kN	Q_u kN	Δ_y mm	Δ_{Qu} mm	$\Delta_{80\%Qu}$ mm	$\mu_{\Delta 80\%Qu}$ ------
Wall 1	314	357	6.8	14.2	23.8	3.5
Wall 2	305	363	6.6	13.7	21.5	3.3
Wall 3	371	420	6.0	8.9	17.3	2.9
Wall 4	365	399	6.1	9.1	15.4	2.52
Wall 5	147	195	13.1	25.6	64.0	4.9
Wall 6	148	193	13.5	30.0	63.0	4.7
Wall 7	223	245	16.1	24.0	46.0	2.9
Wall 8	226	241	16.2	22.0	50.0	3.1

where:

Q_y = the lateral yield load that is corresponding to the first yield in the vertical reinforcement;

Q_u = the peak lateral load;

Δ_y = the lateral displacement at the yield lateral load, Q_y;

Δ_{Qu} = the lateral displacement at the peak lateral load, Q_u;

$\Delta_{80\%Qu}$ = the lateral displacement defined at a drop in wall capacity to 80% of Q_u;

$\mu_{\Delta Qu}$ = the lateral displacements ductility at peak load; and

$\mu_{\Delta 80\%Qu}$ = the lateral displacements ductility at a drop in wall capacity to 80% of Q_u.

5.4.1 EFFECT OF HORIZONTAL REINFORCEMENT DISTRIBUTION ON MASONRY SHEAR STRENGTH

As can be seen in Figure 5.22, distributing the horizontal reinforcement along the height of a wall (i.e. using smaller diameter horizontal reinforcement that are closely spaced) has a minor effect on the shear strength for RM shear walls (for the same horizontal reinforcement ratio). A reduction of 5% in V_n was recorded when replacing the D8 @ 200 mm horizontal reinforcing bars in wall 3 with 15M @ 800 mm in wall 4. However, this slight difference disappears at low axial compressive stress or high wall aspect ratio. Instead, it can be clearly observed that providing horizontal reinforcement with close spacing enhances the post-peak behaviour; hence, the displacement ductility. This enhancement could be attributed to the close spacing between the horizontal reinforcement that enables the distribution of the shear stresses throughout the wall after the initiation of the diagonal shear cracks. Otherwise, the overall effect of the horizontal reinforcement becomes negligible at high values of wall aspect ratio since the shear wall will be more characterized by flexural deformations.

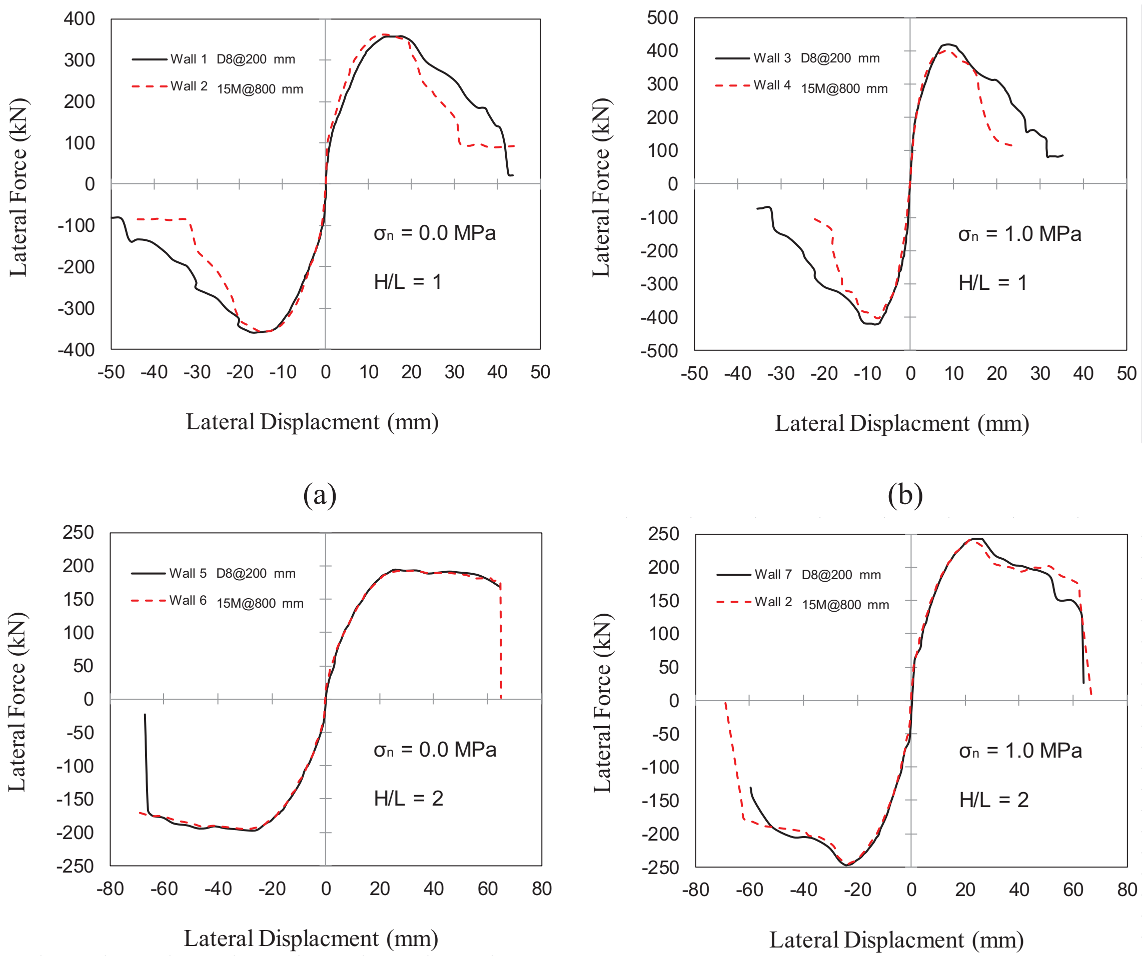

(a) (b)

(c) (d)

Figure 5.22: Effect of horizontal reinforcement distribution on RM shear behaviour

5.4.2 EFFECT OF AXIAL COMPRESSIVE STRESS ON MASONRY SHEAR STRENGTH

The comparison between the different walls in Figure 5.23 shows that the axial compressive stress has a favorable influence on the shear strength, while it has an unfavorable effect on the lateral load degradation. Similar to the horizontal reinforcement distribution, increasing the wall aspect ratio decreases the effect of the axial compressive stress on the displacement ductility.

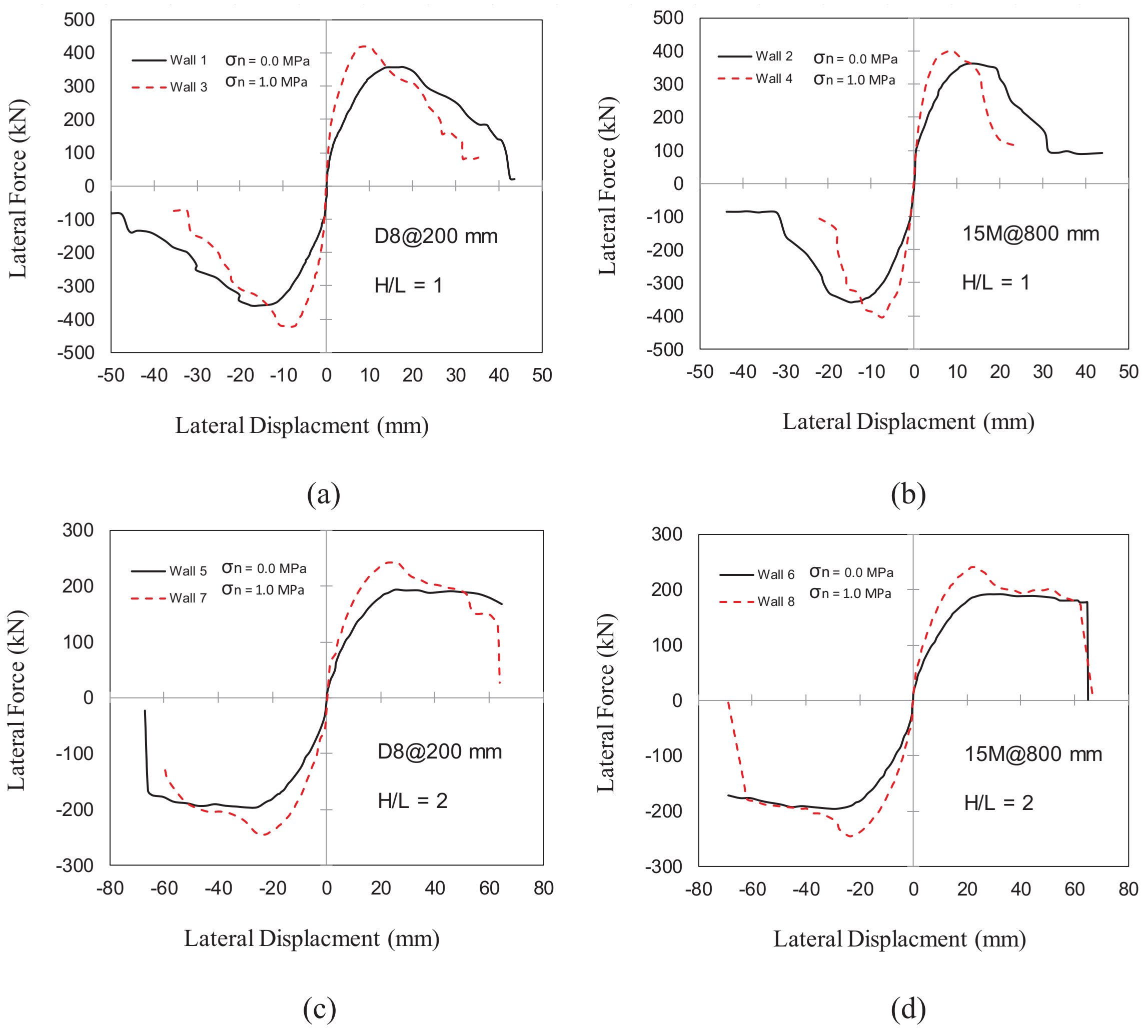

(a) (b)

(c) (d)

Figure 5.23: Effect of axial compressive stress on RM shear behaviour

5.4.3 EFFECT OF WALL ASPECT RATIO (H/L) ON MASONRY SHEAR STRENGTH

Increasing the wall aspect ratio, H/L, from 1.0 to 2.0 has a significant influence on the displacement ductility. This mainly refers to the fact that increasing the H/L ratio triggers the flexural failure mechanism before reaching the shear capacity of the wall (as shown in Figure 5.24).

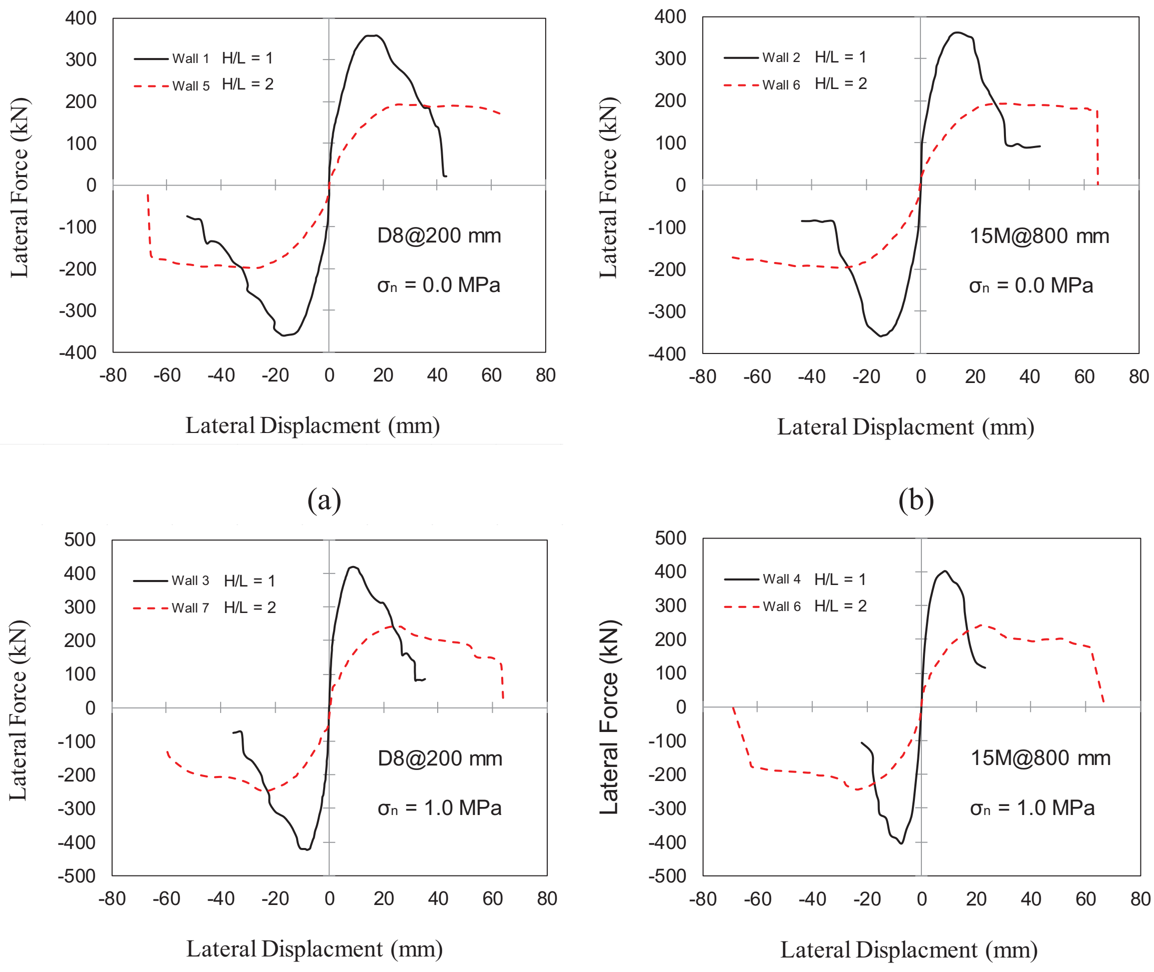

(a) (b) (c) (d)

Figure 5.24: Effect of wall aspect ratio on RM shear behaviour

5.5 DISCUSSION AND SUMMARY

In recent years, numerical models based on the finite element method (FEM) have been developed to simulate the nonlinear behaviour of masonry walls. Nonlinear finite element (FE) models were developed here to represent the behaviour of reinforced masonry (RM) shear walls. VecTor2, software that adopts a smeared, rotating-crack formulation for reinforced concrete based on the Modified Compression Field Theory (MCFT) and the Disturbed Stress Field Model (DSFM) was used in this study. Although all the proposed material models in this program are for concrete, these models show a good ability to predict the behaviour of fully grouted RM walls under the condition of having a sufficient amount of closely spaced reinforcement in both vertical and horizontal directions.

Moreover, a mesh sensitivity analysis was performed to evaluate the influence of mesh size on the precision of the output results. Throughout this analysis, the tested wall W-Ref was modeled using four different mesh densities. From analysis of the results, it is concluded that mesh size has a major impact on the accuracy of the numerical simulation, especially when using the smeared approach to model the reinforcing bars. Using a finer mesh size reduced the error in predicting the lateral load capacity for wall W-Ref from 13% to less than 2%. Further, a verification of the numerical modeling was accomplished using the test results of seven single-story fully grouted RM shear walls. The verification of the FE models shows a good agreement between the numerical and the experimental results.

A parametric study was conducted to evaluate the influence of horizontal reinforcement distribution, the level of axial compressive stress, and the wall aspect ratio on the in-plane shear behaviour of RM shear walls. The results of this numerical study showed that the horizontal reinforcement distribution has a minor effect on the shear strength. It does, however, enhance the displacement ductility. Increasing the level of axial compressive stress also increases the shear strength. Furthermore, the wall aspect ratio has a significant influence on the overall shear behaviour. It is important to mention that the results and conclusions of this numerical simulation are limited to fully grouted walls with uniformly distributed reinforcement in both the x and y directions. Further work is required to consider different failure mechanisms, as well as to investigate the influence of different materials models.

CHAPTER 6

PROPOSED EQUATION FOR IN-PLANE SHEAR STRENGTH OF RM SHEAR WALLS

6.1 INTRODUCTION

Many experimental studies have been conducted to investigate the in-plane shear performance of RM shear walls under cyclic in-plane lateral loading. Using the best-fit analysis for these test results, in-plane shear strength equations were developed by different researchers and standards. A selection of these equations was briefly discussed in Section 2.4 and is summarized in Table 6.1. To make it easier to follow and compare the equations, some of these equations were re-written and modified to have the same notations and consistent SI units. The main parameters that control the in-plane shear strength of RM shear walls can be summarized from the table as: the compressive strength of the masonry f'_m, the shear span to depth ratio, M/Vd_v, the displacement ductility, μ_Δ, the vertical reinforcement ratio, ρ_v, the axial compressive stress, σ_n, the horizontal reinforcement ratio, ρ_h, and the wall cross-section dimensions, b_w and l_w, in addition to the yield strength of the vertical and horizontal reinforcement.

To simplify the task of calculating the nominal shear strength of RM shear walls, V_n, Anderson and Priestley (1992) proposed the first effective equation that considered V_n as the sum of three independent terms: masonry, V_m, axial compression load, V_p, and horizontal reinforcement, V_s. They also proposed a factor k to consider the degradation of the shear resistance provided by the masonry, V_m, when the wall reaches its inelastic performance level.

Table 6.1: In-Plane Shear Strength Equations for RM Shear Walls

Reference	In-plane Masonry Shear Strength, V_n	Eq.
Matsumura (1988)	$\left[K_u K_p \left(\frac{0.76}{(h_w/d)+0.7}+0.012\right)\sqrt{f'_m}+0.2\sigma_n+0.18\gamma\,\delta\sqrt{\rho_h\,f_{yh}\,f'_m}\right](0.875\,b_w\,d)$	**(2.3)**
Shing et al. (1990)	$\left[0.0217\left(\rho_v\,f_{yv}+\sigma_n\right)+0.166\right]A_n\sqrt{f_m^{\backprime}}+\left(\frac{l_w-2d'}{s_h}-1\right)A_h\,f_{yh}$	**(2.5)**
Anderson and Priestley (1992)	$C\,k\sqrt{f_m^{\backprime}}\;A_n+0.25\,P+0.5\,A_{sh}\,f_{yh}\,\frac{d}{s_h}$	**(2.6)**
NEHRP (1997)	$0.083\left[4.0-1.75\left(\frac{M}{Vd_v}\right)\right]A_n\sqrt{f'_m}+0.25\,P+0.5\,A_v\,f_{yh}\,\frac{l_w}{s_h}$	**(2.7)**
UBC (1997)	$0.083\left[2.8-1.6\left(\frac{M}{V\,d}\right)\right]A_n\sqrt{f'_m}+\;A_{sh}\,f_{yh}$	**(2.8)**
AS3700-2001	$\left(1.5-0.5\,\frac{h_w}{l_w}\right)A_n+0.8\,A_s^{*}\,f_{yh}$	**(2.9)**
CSA S304-14	$\left(0.16(2-\frac{M}{V\,d_v})\sqrt{f_m^{\backprime}}\;b_w d_v+0.25P_d\right)\gamma_g\,k+0.6\,A_{sh}\,f_{yh}\,\frac{d_v}{s_h}$	**(2.10)**
NZS 4230:2004	$\left[0.022\,\rho_v\,f_{yv}+0.084\left(4.0-1.75\,\frac{M}{Vd_v}\right)\right](1-\frac{\mu-1.25}{2.75})\sqrt{f'_m}\,b_w\,d+(0.9\tan\alpha)P+0.64A_{sh}\,f_{yh}\,\frac{l_w}{s_h}$	**(2.15)**
Voon and Ingham(2007)	$\left[0.022\,\rho_v\,f_{yv}+0.084\left(4.0-1.75\,\frac{M}{Vd_v}\right)\right](1-\frac{\mu-1.25}{2.75})\sqrt{f'_m}\,b_w\,d+(0.9\tan\alpha)P+A_{sh}\,f_{yh}\,\frac{d_{eff}}{s_h}$	**(2.16)**
MSJC (2013)	$0.083\left[4.0-1.75\left(\frac{M}{Vd_v}\right)\right]A_n\sqrt{f'_m}+0.25\,P+0.5\,A_v\,f_{yh}\,\frac{l_w}{s_h}$	**(2.17)**

NEHRP (1997) modified Eq. 2.6 to consider the effect of the shear span to depth ratio, *M/Vd*$_v$, on the masonry term and proposed Eq. 2.7. However, Eq. 2.7 does not take into account the degradation in the shear resistance provided by masonry, V_m, at higher levels of ductility. The equation proposed by NEHRP (1997) is widely used in North American codes, including CSA (S304-14) and MSJC (2013), with slight modifications as presented in Eq. 2.10 and Eq. 2.17. The NZS equation and the one modified by Voon and Ingham (2007), Eq. 2.15 and Eq. 2.16

respectively, modified the masonry term in Eq. 2.7 to take into account the effects of the dowel action and the displacement ductility. Furthermore, the axial compression load contribution, V_p, was modified to consider the angle, α, resulting from a diagonal compression strut.

Most of the previous researchers quantified the in-plane shear resistance provided by the masonry, V_m, axial compression load, V_p, and horizontal reinforcement, V_s, based on the difference between the achieved maximum lateral loads for tested RM walls with different values of the studied parameters. The experimental results in Chapter 4 show that this quantification approach overlooks the effect of the re-distribution in the shear resistance shares between V_m, V_p, and V_s, especially at high levels of displacement ductility. Moreover, Most of the equations presented in Table 6.1 do not consider the interaction between the flexural performance and the shear strength envelope at the strength degradation zone. According to these findings, an equation that aims for more accurately predicting the in-plane shear strength of RM shear walls was developed and verified with the experimental results from this study and other researchers. Furthermore, statistical analysis was performed to evaluate the accuracy of the proposed equation against the given equations.

6.2 PROPOSED EQUATION FOR IN-PLANE SHEAR STRENGTH OF RM SHEAR WALLS

Using the results of the tested shear walls and based on the effects of the studied parameters in Chapter 4, an equation for predicting the in-plane shear strength, V_n, of RM shear walls is proposed as follows:

$$V_{\mathrm{n}} = \left[(V_m + V_p)\,\gamma_g\, k_1 + V_s\, k_2\right] k_\phi \qquad \text{Eq. 6.1}$$

where:

$(V_n)_{\max}$ = $0.4\sqrt{f'_m}\, b_w\, d_v$, kN, as adopted in CSA S304-14

V_m = shear resistance provided by masonry, kN

$$\left[0.02\,\rho_v\, f_{yv} + 0.14\left(2.5-\frac{h_e}{d_v}\right)\right]\sqrt{f'_m}\, b_w\, d_v$$

ρ_v = total vertical reinforcement ratio = $(A_{st})_{\text{total}} / b_w\, d$

A_{st} = total cross-sectional area of vertical reinforcement, mm^2

b_w = overall web width, which does not include flanges or projections formed by intersecting walls when calculating factored shear resistance of walls, mm

d = distance from extreme compression fiber to centroid of tension reinforcement, mm, for uniform distributed vertical reinforcement, it could be taken as the distance from extreme compression fiber to centroid of extreme tension bar

f_{yv} = yield strength of vertical reinforcement, MPa

h_e = effective height, shall be taken as M/V, mm, where, M and V are the moment and shear at the section under consideration, respectively

d_v = effective depth for shear calculations, mm

$d_v \geq 0.8 l_w$ for walls with flexural reinforcement distributed along the length

l_w = wall length, mm

$\dfrac{h_e}{d_v}$ = shear span to depth ratio, shall be taken as not less than 1.0 nor more than 2.0

f'_m = compressive strength of masonry normal to the bed joint at 28 d, MPa

V_p = shear resistance provided by the axial compression load, kN

$= (\tan\alpha\ P_d)$

α = angle formed between the wall axis and the strut from the point of load application to the centre of the flexural compression zone for a cantilever wall. For a wall in double bending (pier), α is the angle between the wall axis and the line joining the centres of flexural compression at the top and bottom of the wall (as defined in NZS 4230:2004)

For simplifying , $\tan\alpha = 0.4\dfrac{l_w}{h_e}$ (see Figure 6.2)

P_d = axial compression load on the section under consideration, based on 0.9 times dead load, P_{DL}, including any axial load arising from bending in coupling beams, N, (as defined in CSA S304-14) and shall not be taken greater than ($0.1\, f'_m A_g$)

$$P_d = 0.9\, P_{DL} \text{ for solid walls}$$

$$P_d = 0.9\, P_{DL} \pm N$$ for perforated/coupled walls, walls with door or/and window opening (see Figure 2.23 in Chapter 2)

γ_g = factor to account for partially grouted walls that are constructed of hollow or semi-solid units and is taken according to CSA S304-14 (see Figure 2.24 in Chapter 2)

= 1.0 for fully grouted masonry, solid concrete block masonry, or solid brick masonry

= $\dfrac{A_e}{A_g}$ for partially grouted walls, but $\gamma_g \leq 0.5$)

A_e = effective cross-sectional area of the wall, mm^2

A_g = gross cross-sectional area of the wall, mm^2

k_1 = ductility related modification factor for in-plane shear resistance provided by masonry and axial compression load, V_{m+p}, (see Figure 6.4)

$$= 1 - \frac{\mu_\Delta - 1.5}{4.5} \quad , \quad 0.0 \leq k_1 \leq 1,$$ and μ_Δ is the displacement ductility

V_s = shear strength attributed to horizontal reinforcement, kN

$$= 0.4 \frac{A_{sv}}{S_v} d_{eff}\ f_{yh}$$

A_{sv} = cross-sectional area of horizontal reinforcement, mm^2

S_v = vertical spacing of horizontal reinforcement, mm

d_{eff} = reduced effective depth of wall section for the calculation of the in-plane shear resistance provided by horizontal reinforcement, V_s, mm. Shall be taken as 0.8 times the smaller between l_w and h_e (see Figure 6.3)

f_{yh} = yield strength of horizontal reinforcement, MPa

k_2 = ductility related modification factor for in-plane shear resistance provided by the horizontal reinforcement, V_s, (see Figure 6.4)

$= 1 + \dfrac{\mu_\Delta - 1.5}{1.65}, 1.0 \le k_2 \le 2.5$, and μ_Δ is the displacement ductility

k_ϕ = factor concerning loading method

= 1.0 for loading of cantilever type (single curvature)

= 0.80 for loading resulting in inflection point at the mid-height of walls (double curvature)

6.2.1 IN-PLANE SHEAR RESISTANCE PROVIDED BY MASONRY (V_m)

Matsumura (1988) and most of the given equations in Table 6.1 proposed that the in-plane shear resistance provided by masonry, V_m, has a proportional relation with $\sqrt{f'_m}$. Although the vertical reinforcement ratio, ρ_v, was not one of the studied parameters in the current experimental work, the effect of the vertical reinforcement distribution on the behaviour of wall W-S$_h$800 showed that it has a significant influence on the stress flow; hence, the achieved peak lateral load. In addition, increasing ρ_v results in a higher flexural strength. Therefore, the shear strength envelope intersects with the lateral force that corresponds to the flexural capacity of the wall at higher V_n as shown in Figure 6.1. Consequently, the proposed masonry term, V_m, in Eq. 6.1 takes this effect into account. The shear resistance provided by the vertical reinforcement in Eq. 6.1 is proposed as provided by Shing et al. (1990). The same contribution of ρ_v is also adopted in the design equation of V_n in the New Zealand Standard Design of Reinforced Concrete Masonry Structures NZS 4230:2004 (Eq. 2.15). However, since 1992 when Anderson and Priestley ignored the impact of the vertical reinforcement on the in-plane shear strength, V_n, of RM shear walls in their proposed equation, most of design equations given in North American codes, such as CSA S304-2014 and MSJC-2013, does not consider ρ_v in predicting V_n.

The shear span to depth ratio, h_e/d_v, is another parameter that has a considerable effect on V_m. Unlike the vertical reinforcement, increasing h_e/d_v results in a lower shear strength as can be seen in Figure 6.1. The proposed term for the effect of h_e/d_v in Eq. 6.1, which is equal to $0.14\,(2.5 - h_e / d_v)$, closely matches that used in the NEHRP (1997) expression (Eq. 2.7) which can be written as $0.145\,(2.3 - h_e / d_v)$. However, the test results of walls W-Ref and W-*M/Vdv*1.8 show that limiting the effect of shear span to depth ratio to an upper value of 1.0, as provided in most of the masonry design codes, is overestimating the in-plane shear strength of RM shear walls, V_n, at a high values of h_e/d_v, which might lead to an unsafe design. Consequently, the upper limit of h_e/d_v was extended to a value of 2.0 instead of 1.0. This value, 2.0, is proposed based on the assumption that at values of h_e/d_v higher than 2.0 the RM shear walls are dominated more by flexural behaviour, then the corresponding lateral force of the flexural capacity would be close to the residual shear strength, V_r. Nevertheless, h_e/d_v should not be taken less than 1.0 since this equation is not adopted for squat shear walls.

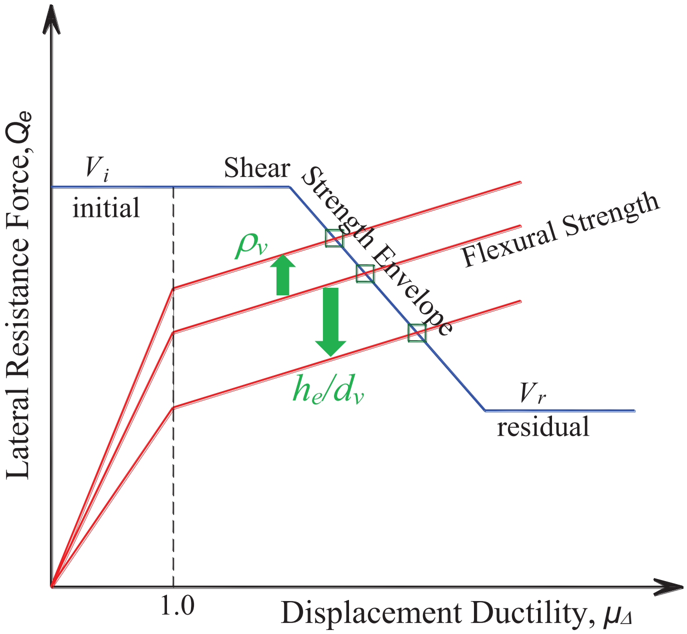

Figure 6.1: Effect of vertical reinforcement ratio, ρ_v, and shear span to depth ratio, h_e/d_v on the in-plane shear resistance provided by masonry, V_m

6.2.2 IN-PLANE SHEAR RESISTANCE PROVIDED BY AXIAL COMPRESSION LOAD (V_P)

Similar to the equation proposed by Matsumura (1988), Anderson and Priestley (1992) consider a constant percentage of the axial compression load, P, that contributes to the shear strength; this percentage was increased from 20% in Eq. 2.3, to 25% in Eq. 2.6. This 25% contribution was later adopted by NEHRP (1997), CSA S304-2014, and MSJC-2013. However, Priestley et al. (1994) concluded that the axial compression load enhances the shear capacity of RC columns by the arch action forming an inclined strut. Hence, the shear strength was assumed to increase by the horizontal component of the diagonal compression strut. The same approach was incorporated in the shear design equation for RM shear walls in NZS 4230:2004. As shown in Figure 6.2, for a cantilever RM wall, a compression strut is formed between the points of the applied axial load, P_d, and the resultant compression force of the flexural compression zone. Consequently, the horizontal component, V_p, can be calculated as ($P_d \tan \alpha$).

For simplicity, the depth of the compression zone, c, can be assumed as $0.2l_w$ and the resultant force is acting at the middle of the compression zone with a distance of $0.1l_w$ from the extreme compression fiber. This assumption results in tan α equal to $0.4l_w/h_e$ when the axial compression load is applied at the centre of the wall. On the other hand, for RM piers that are subjected to double bending, the effective height h_e will be reduced (i.e. $h_e = h_w/2$) resulting in the same equation for tan α. However, at high values of axial compression loads, the depth of the compression zone, c, will increase so that the assumption of c being equal to $0.2l_w$ becomes an overestimation of tan α. Consequently, the value of P_d in the proposed equation is defined as 0.9 times dead load, P_{DL}, including any axial load arising from bending in the coupling beams, N, (as shown by Figure 2.23 in Chapter 2), and it is limited to ($0.1\, f'_m A_g$) in order to provide a reasonable degree of conservatism.

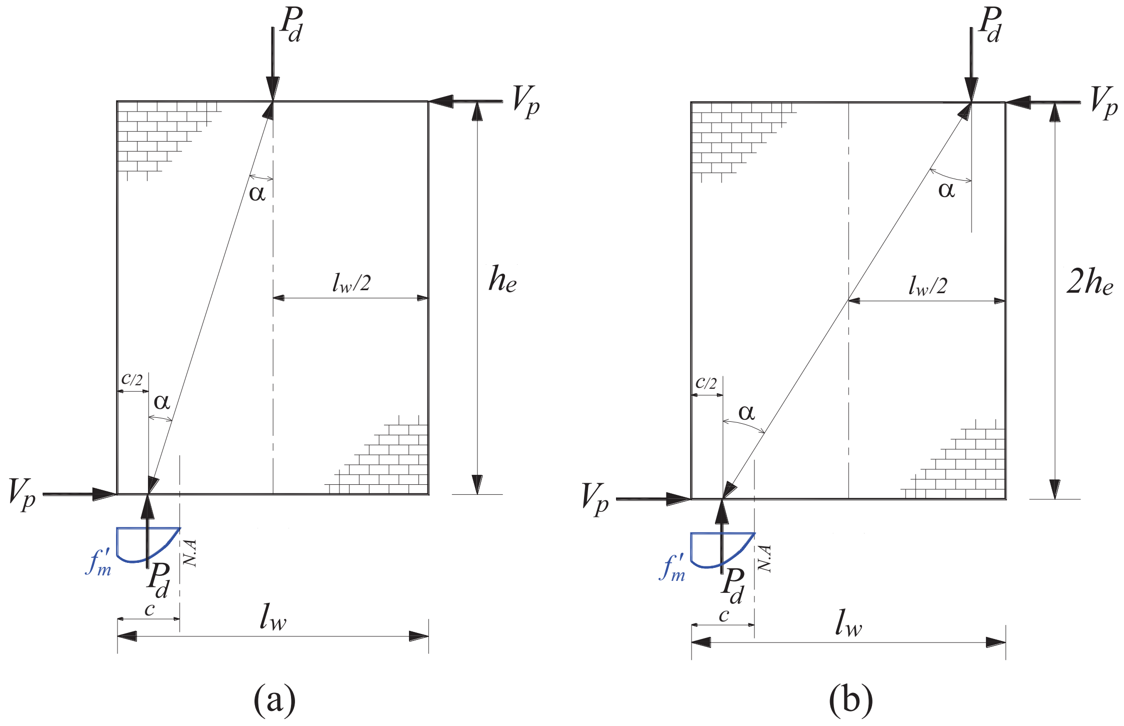

Figure 6.2: In-plane shear resistance provided by axial compression load for: (a) RM shear walls with single curvature; (b) RM piers with double curvature

6.2.3 IN-PLANE SHEAR RESISTANCE PROVIDED BY HORIZONTAL REINFORCEMENT (V_S)

The results of the tested walls in Chapter 4 show that the horizontal reinforcement could reach its yield capacity at high levels of deformation; and on the contrary, at low displacement ductility this contribution is minor. Based on this observation, the horizontal reinforcement was assumed to have contributed with a conservative value of 40% of its yield capacity, that increases at higher levels of the displacement ductility, μ_Δ, using modification factor k_2. The number of the horizontal reinforcing bars that contribute to V_s shall be calculated based on reduced effective depth of wall section, d_{eff}, which is taken as 0.8 times the smaller between l_w and h_e as shown in

Figure 6.3. However, for RM cantilever shear walls with an aspect ratio, h_w/l_w, more than one, d_{eff} is equal to d_v.

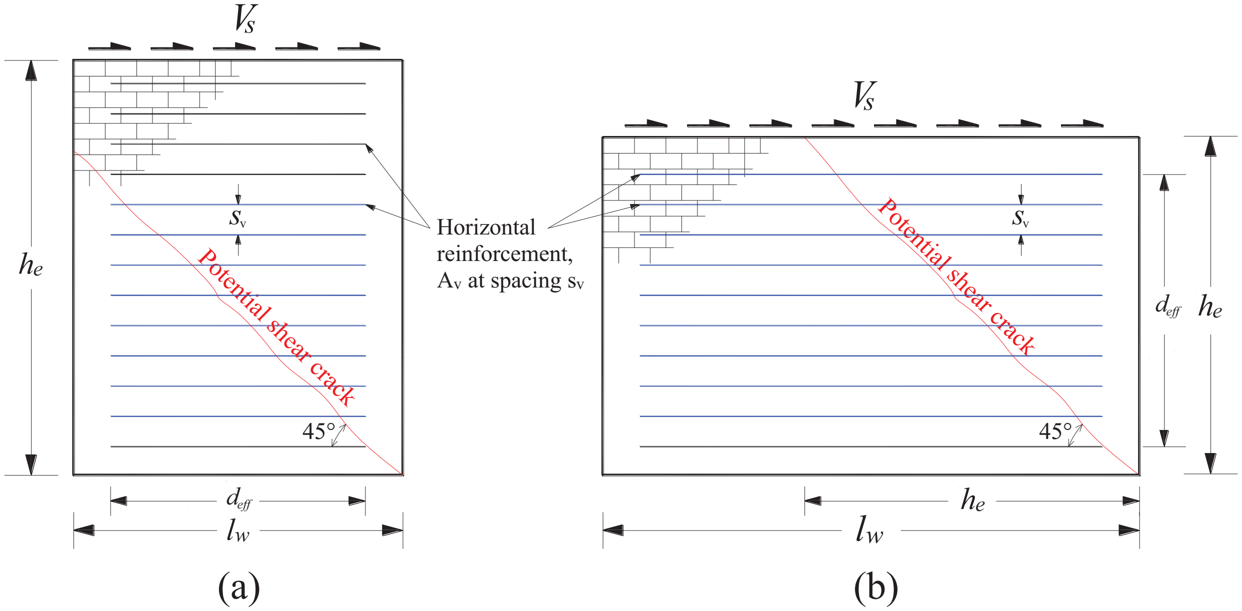

Figure 6.3: In-plane shear resistance provided by horizontal reinforcement for RM shear walls: (a) $h_e > l_w$; (b) $h_e < l_w$

6.2.4 MODIFICATION FACTORS

Four modification factors are proposed in Eq. 6.1 to take into account the effect of grouting, higher demands of displacement ductility, and loading method. Since the main objective of this study is to evaluate the inelastic behaviour of fully grouted RM shear walls only (partially grouted walls were beyond the scope of this research and therefore not one of the studied parameters), the factor γ_g to account for partially grouted walls is proposed according to CSA S304-14 (see Section 2.4.7 in Chapter 2). The results of the nine RM tested walls showed that after the initiation of diagonal cracks and yielding of the vertical reinforcement, there is a significant reduction in the in-plane shear resistance provided by the masonry and axial compression load, V_{m+p}, accompanied with an increase in V_s. To take account of this behaviour, ductility related modification factors, k_1 and k_2, are proposed as shown in Figure 6.4.

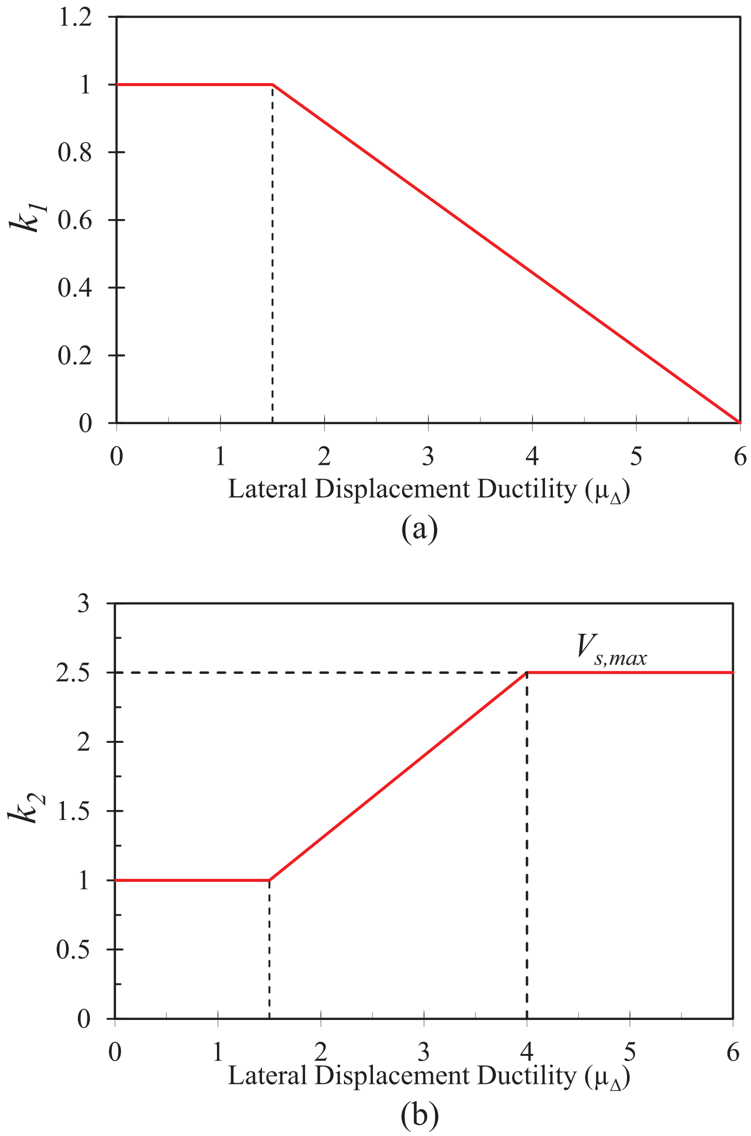

Figure 6.4: Ductility related modification factors for the in-plane shear resistance provided by: (a) masonry and axial compression load, V_{m+p}; (b) horizontal reinforcement, V_s

The experimental results of the tested walls with closely spaced reinforcement in both directions, vertical and horizontal, showed that the in-plane shear resistance provided by V_{m+p} was able to maintain more than 50% of its capacity at high levels of inelastic deformation, μ_Δ = 4.0. Consequently, k_1 is proposed assuming a linear degradation in V_{m+p} from μ_Δ = 1.5 to zero contribution at μ_Δ = 6.0. On the other hand, to benefit from the increasing in the in-plane shear resistance provided by horizontal reinforcement, V_s, at high levels of displacement ductility, k_2

could be used. This factor is assumed to increase linear from 1.0 at μ_Δ = 1.5 to 2.5 (when the horizontal reinforcement reaches its yield capacity) at μ_Δ = 4.0. However, the increase in V_s in the proposed factor k_2 is limited to fully grouted RM shear walls with closely spaced reinforcement in both directions, vertical and horizontal. Finally, the sum of the three contributions, V_m, V_p, and V_s, is multiplied by K_ϕ, which is equal to 1.0 for cantilever walls with single curvature or 0.8 for piers with double curvature.

6.3 EXPERIMENTAL DATA SOURCES

To verify the accuracy of the proposed equation for predicting the in-plane shear strength of RM shear walls, a brief survey of previous experimental work on fully grouted RM walls dominated by shear failure was conducted, which resulted in a total of 64 reliable RM walls and piers, in addition to the nine tested RM walls in this study. The test results were collected from the following six sources:

1. Twenty one piers were tested by Sveinsson et al. (1985) at the University of California at Berkeley;
2. Eighteen piers were tested by Matsumura (1985) at Japan's Building Research Institute, Ministry of Construction;
3. Eight piers were tested by Okamoto et al. (1987) at Japan's Building Research Institute, Ministry of Construction;
4. Ten cantilever walls were tested by Shing et al. (1990) at the University of Colorado;
5. Seven cantilever walls were tested by Voon and Ingham (2006) at the University of Auckland;
6. Nine cantilever walls were tested in this study at Concordia University.

Table 6.2: Summary of Experimental Database

Data Source		Total studied walls	Cantilever walls (single curvature)		Piers (double curvature)	
			Concrete block	Clay brick	Concrete block	Clay brick
1	Sveinsson et al., (1985)	21			10	11
2	Matsumura (1985)	18			14	4
3	Okamoto et al. (1987)	8			5	3
4	Shing et al. (1990)	10	8	2		
5	Voon and Ingham (2003)	7	7			
6	Current study	9	9			
Total		73	24	2	29	18
			26		47	

During significant earthquakes in the twentieth century, many masonry structures suffered severe damage due to their limited inelastic deformation capacity. Consequently, a coordinated research program between the U.S. and Japan was conducted at the beginning of the 1980s to investigate the seismic performance of reinforced masonry structures. One of the main program objectives was to develop design criteria for reinforced masonry buildings and their structural components, including RM shear walls. The coordinated program included comprehensive experimental studies by several researchers, including Sveinsson et al. (1985), Matsumura (1985), Okamoto et al. (1987), and Shing et al. (1990). After this extensive research, there was a gap in the experimental data until Voon and Ingham (2006) carried out an experimental study in New Zealand that investigated the in-plane shear strength of RM shear walls. However, there is still a lack of experimental data for fully grouted RM shear walls dominated by shear failure. The following remarks are related to the collected experimental data in addition to the nine tested RM walls in this study:

a) The experimental tests conducted in this analysis were limited to full-scale fully grouted RM shear walls; work conducted on scaled walls are not considered in this study.
b) All collected walls were dominated by diagonal shear failure except five concrete block walls tested by Sveinsson et al. (1985) that had sliding/diagonal shear failure.
c) All the walls tested by Sveinsson et al. (1985); Matsumura (1985); and Okamoto et al. (1987) were subjected to in-plane lateral forces at their middle height and were fixed against rotation along both top and bottom edges (i.e. under double curvature). This test setup was used to simulate the behaviour of RM piers; hence, the effective height, h_e, is equal to $h_w/2$. On the other hand, Shing et al. (1990) and Voon and Ingham (2006) carried out their tests on cantilever RM shear walls (i.e. under single curvature) similar to the way it was conducted in this current study.
d) Sveinsson et al. (1985) defined the displacement ductility as a ratio of the maximum relative lateral displacement experienced by the tested wall before failure to the crack displacement, without considering the first yield point of vertical reinforcement, which results in overestimating the displacement ductility, μ_Δ. In addition, the failure point was not clearly defined since all walls were loaded until the first demand lateral displacement after the strength degradation was initiated. Although the experimental lateral force-displacement envelope for each of the tested walls by Sveinsson et al. (1985) was reported in their test results, only the crack point was defined on each envelope. Hence, for more reasonable values of μ_Δ for the verification purpose of the studied equations, the equivalent elastic-perfectly plastic response using the idealized equal energy effective

stiffness was generated for each wall using the given experimental lateral force-displacement envelopes. Thus, the experimental displacement ductility, $\mu_{\Delta e}$, in Table 6.3 is taken as equal to the idealized ductility, $\mu^{ep}_{\Delta id}$. All the generated equivalent elastic-perfectly plastic responses of the walls tested by Sveinsson et al. (1985) are given in Appendix A.

e) The reinforcement yield strength, f_y, was not given for some of the tested walls by Matsumura (1985) but was reported to have ranged between 320-450 MPa. Therefore, an average value of the yield strength, f_y, was taken for these walls as 385 MPa.

f) The results of the four fully grouted brick masonry walls tested by Matsumura (1985) did not show a significant effect of the horizontal reinforcement on their shear capacity. The author attributed this to the existence of many grouting faults because of inadequate grouting during construction of the walls. However, these four walls were retested and the results reported by Matsumura (1988), which were used in this analysis.

g) Only the achieved peak lateral loads were reported for most of the walls tested by Matsumura (1985) and Kaminosono et al. (1988), without providing any information about their lateral force-displacement responses. Hence, for these walls and any other walls in the experimental data where their displacement ductility was not reported, it was assumed that they were able to reach μ_{Δ} equal to 2.5.

h) Finally, it is important to mention that the proposed equation by Matsumura (1988) is based on data sources 2 and 3, whereas the proposed equation by Shing et al. (1990) only considered their results, data source 4. However, Anderson and Priestley (1992) used the test results from data sources 1, 2, and 4 to propose the best-fit equation for V_n, which was further modified in NEHRP (1997). On the other hand, the adopted design equations for

V_n in NZS 4230:2004 and MSJC (2013) were verified using data sources, 1, 2, and 4, in addition to data source 5 that came from walls tested by Voon and Ingham (2006). It should be noted that the main data for these sources 1, 2, 4 and 5 are coming from testing RM piers. However, only few studies have considered data source 3, such as Fattal and Todd (1991) and Banting (2013).

Variations in the main variables of the 73 studied specimens are presented in Figure 6.5 with the values tabulated in Table 6.3. In addition, more details about the properties of the tested walls are given in Appendix A. The studied walls were constructed with a wide range of f'_m that varied between 13.1 and 31.4 MPa. To evaluate the in-plane shear resistance provided by axial compression load, V_p, the studied walls were subjected to different levels of σ_n that varied between 0.0 and 5.9 MPa. These values of σ_n represented up to 26% of the corresponding f'_m as shown in Figure 6.5(c). However, all walls were tested under axial compressive stress less than 3.0 MPa, except the two walls tested by Okamoto et al. (1987) that were subjected to 3.9 and 5.9 MPa respectively.

All the studied walls were vertically reinforced with different ratios. The majority of the RM piers tested by Sveinsson et al. (1985) had light reinforcement with ρ_v less than 0.5%, while, Matsumura (1985) tested heavy verticaly reinforcement walls with ρ_v up to 1.3%. On the other hand, to evaluate the contribution of the horizontal reinforcement, V_s, to the in-plane shear strength, V_n, some of the walls were constructed without horizontal reinforcement but instead the others were horizontally reinforced with ρ_h up to 0.68%. As can be seen from Figure 6.5(h), there are few walls that were tested to investigate the effect of the shear span to depth ratio, h_e/d_v; however, among all the walls this ratio ranged from 0.56 to 2.5. Figure 6.5(j) shows that a considerable number of the tested cantilever walls were able to reach high levels of inelastic deformation with displacement ductility, μ_Δ, more than 3.0.

The following are some observations that can be made. The experimental testing carried out by Voon and Ingham (2006) was intended to investigate the shear capacity of concrete masonry walls when subjected to low levels of axial compressive stress, from 0.0 to 0.5 MPa, and horizontally reinforced with low ratios, $\rho_h \leq 0.062\%$. However, the experimental studies conducted by other researchers in the U.S. and Japan, in addition to this current study, involved higher ratios. In addition, the collected walls had a wide variation in the main parameters, which have a significant effect on the in-plane shear strength, V_n, of RM shear walls, such as: f'_m; σ_n, $\rho_v f_{yv}$, $\rho_h f_{yh}$, h_e/d_v, and μ_Δ. From the above, it could be said that a proposed equation for predicting V_n that simulates the contributions of this large range of parameter variations with good accuracy proves to effectively represent the shear strength of RM shear walls.

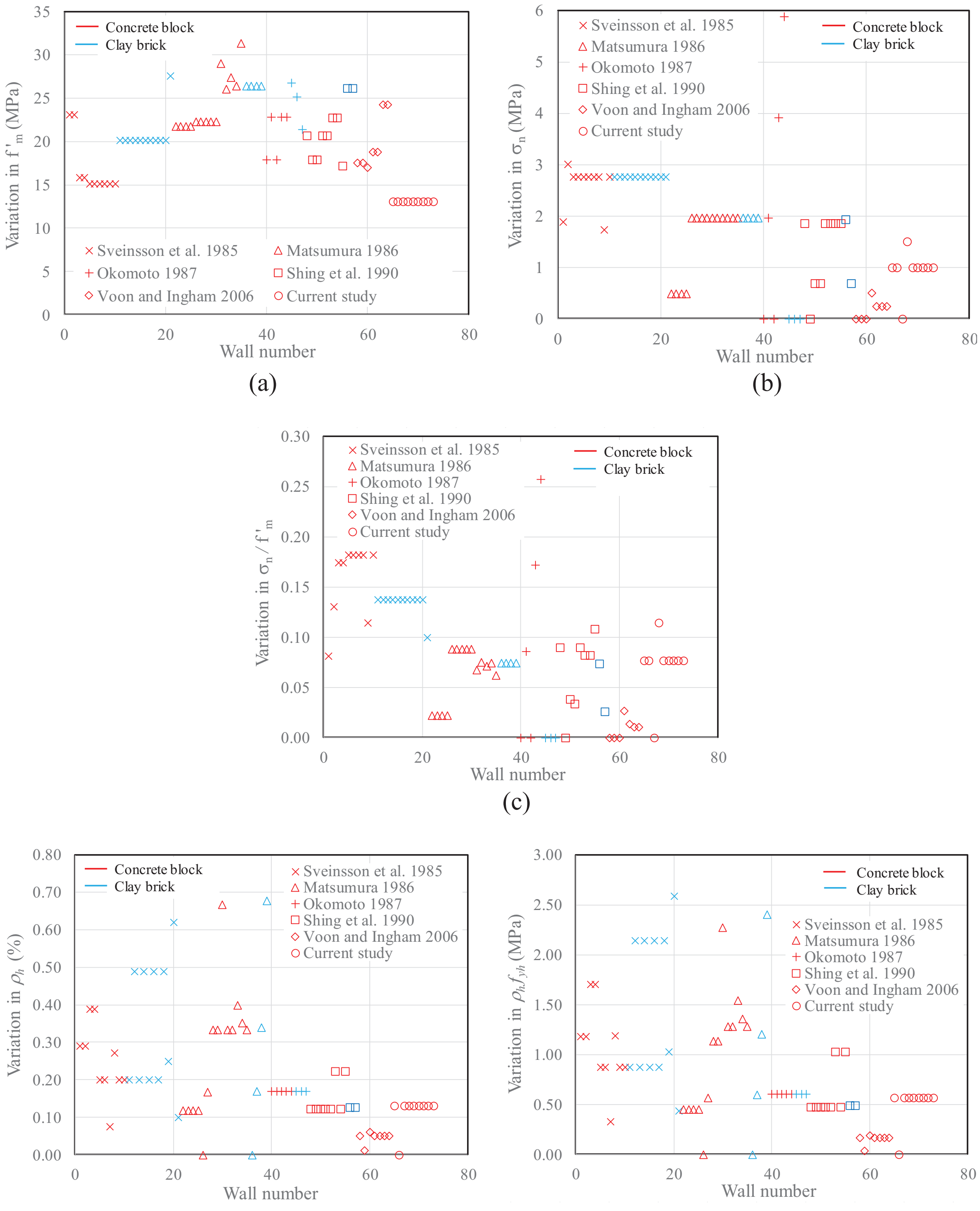

(a) (b) (c) (d) (e)

Figure 6.5: Variation in main variables for the studied specimens

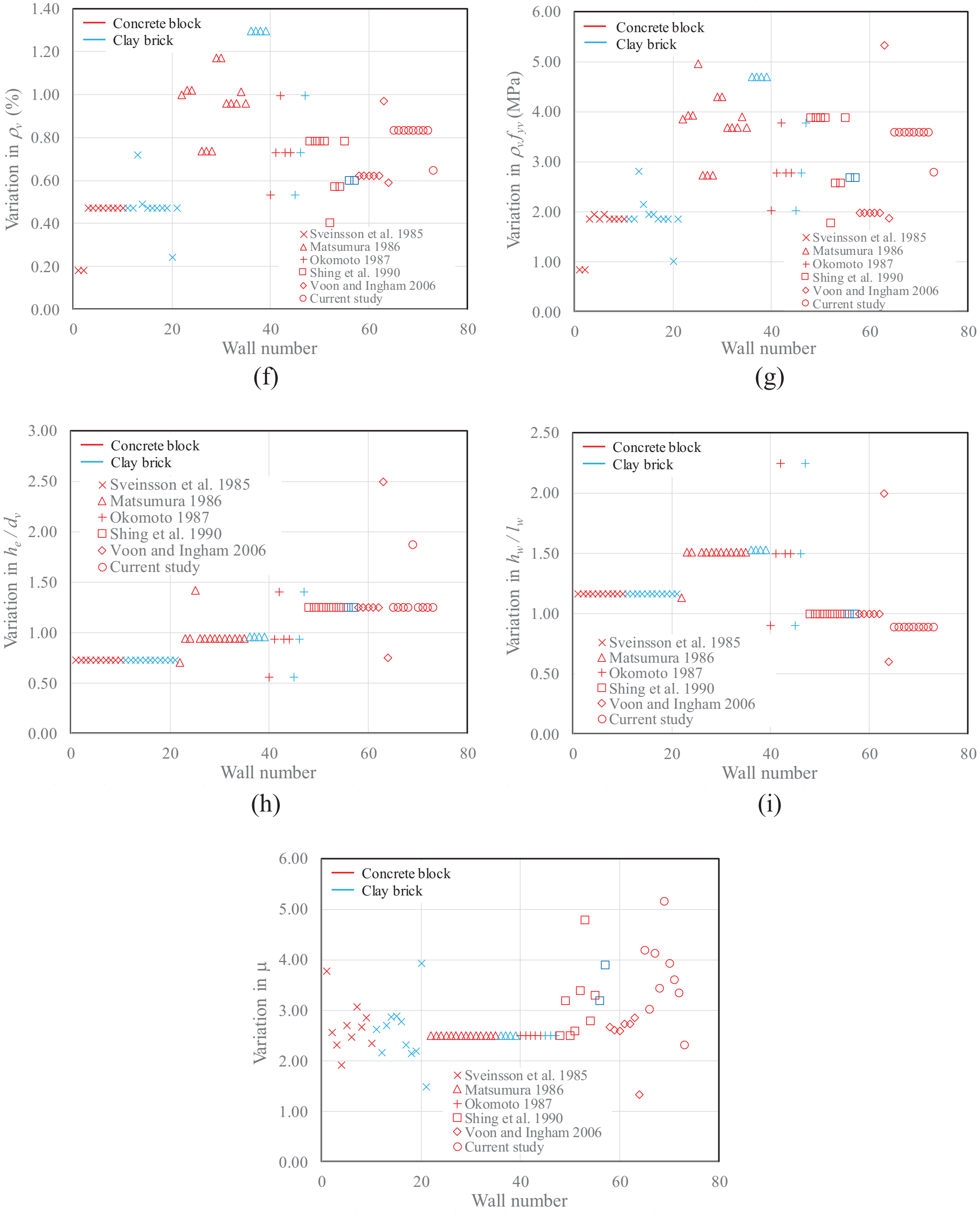

(f) (g)

(h) (i)

(j)

Figure 6.5(continued): Variation in main variables for the studied specimens

Table 6.3: Main Variables of the Studied Specimens

Source	Specimen no.	Specimen label	Mode of failure*	f'_m	σ_n	$\frac{\sigma_n}{f'_m}$	ρ_h	$\rho_h f_{yh}$	ρ_v	$\rho_v f_{yv}$	$\frac{h_w}{l'_w}$	$\frac{h_e}{d_v}$ **	μ_Δ
				MPa	MPa	—	%	MPa	%	MPa	—	—	—
Sveinsson et al., (1985)	1	HCBL-11-13	S	23.2	1.9	0.08	0.29	1.18	0.18	0.84	1.17	0.73	3.8
	2	HCBL-11-15	S	23.2	3.0	0.13	0.29	1.18	0.18	0.84	1.17	0.73	2.6
	3	HCBL-11-17	S	15.8	2.8	0.17	0.39	1.71	0.47	1.85	1.17	0.73	2.3
	4	HCBL-11-18	S	15.8	2.8	0.17	0.39	1.71	0.47	1.94	1.17	0.73	1.9
	5	HCBL-11-20	S	15.1	2.8	0.18	0.20	0.88	0.47	1.85	1.17	0.73	2.7
	6	HCBL-11-21	S	15.1	2.8	0.18	0.20	0.88	0.47	1.94	1.17	0.73	2.5
	7	HCBL-11-23	S	15.1	2.8	0.18	0.08	0.33	0.47	1.85	1.17	0.73	3.1
	8	HCBL-11-24	S	15.1	2.8	0.18	0.27	1.19	0.47	1.85	1.17	0.73	2.7
	9	HCBL-11-25	S	15.1	1.7	0.11	0.20	0.88	0.47	1.85	1.17	0.73	2.9
	10	HCBL-11-26	S	15.1	2.8	0.18	0.20	0.88	0.47	1.85	1.17	0.73	2.3
	11	HCBR-11-19	S	20.1	2.8	0.14	0.20	0.88	0.47	1.85	1.17	0.73	2.6
	12	HCBR-11-20	S/S	20.1	2.8	0.14	0.49	2.15	0.47	1.85	1.17	0.73	2.2
	13	HCBR-11-21	S	20.1	2.8	0.14	0.20	0.88	0.72	2.81	1.17	0.73	2.7
	14	HCBR-11-22	S/S	20.1	2.8	0.14	0.49	2.15	0.49	2.14	1.17	0.73	2.9
	15	HCBR-11-23	S	20.1	2.8	0.14	0.20	0.88	0.47	1.94	1.17	0.73	2.9
	16	HCBR-11-24	S/S	20.1	2.8	0.14	0.49	2.15	0.47	1.94	1.17	0.73	2.8
	17	HCBR-11-25	S	20.1	2.8	0.14	0.20	0.88	0.47	1.85	1.17	0.73	2.3
	18	HCBR-11-26	S/S	20.1	2.8	0.14	0.49	2.15	0.47	1.85	1.17	0.73	2.2
	19	HCBR-11-27	S	20.1	2.8	0.14	0.25	1.03	0.47	1.85	1.17	0.73	2.2
	20	HCBR-11-28	S/S	20.1	2.8	0.14	0.62	2.59	0.24	1.00	1.17	0.73	3.9
	21	HCBR-11-30	S	27.6	2.8	0.10	0.10	0.44	0.47	1.85	1.17	0.73	1.5
Matsumura (1986)	22	KW4-1	S	21.8	0.5	0.02	0.12	0.45	1.00	3.85	1.13	0.71	2.5
	23	KW3-1	S	21.8	0.5	0.02	0.12	0.45	1.02	3.93	1.51	0.95	2.5
	24	KW3S-1	S	21.8	0.5	0.02	0.12	0.45	1.02	3.93	1.51	0.95	2.5
	25	KW2-1	S	21.8	0.5	0.02	0.12	0.45	1.29	4.97	2.28	1.42	2.5
	26	WS2	S	22.3	2.0	0.09	0.00	0.00	0.74	2.73	1.51	0.95	2.5
	27	WS4	S	22.3	2.0	0.09	0.17	0.57	0.74	2.73	1.51	0.95	2.5
	28	WS5	S	22.3	2.0	0.09	0.33	1.14	0.74	2.73	1.51	0.95	2.5
	29	WS9	S	22.3	2.0	0.09	0.33	1.14	1.17	4.30	1.51	0.95	2.5
	30	WS10	S	22.3	2.0	0.09	0.67	2.27	1.17	4.30	1.51	0.95	2.5
	31	WS9-2	S	29.0	2.0	0.07	0.33	1.29	0.96	3.69	1.51	0.95	2.5
	32	WSB21	S	26.1	2.0	0.08	0.33	1.29	0.96	3.69	1.51	0.95	2.5
	33	WSB22	S	27.4	2.0	0.07	0.40	1.54	0.96	3.69	1.51	0.95	2.5
	34	WSB3	S	26.4	2.0	0.07	0.35	1.36	1.01	3.90	1.51	0.95	2.5
	35	WSB4	S	31.4	2.0	0.06	0.33	1.29	0.96	3.69	1.51	0.95	2.5
	36	WSR2-2	S	26.4	2.0	0.07	0.00	0.00	1.30	4.70	1.53	0.96	3.8
	37	WSR4-2	S	26.4	2.0	0.07	0.17	0.60	1.30	4.70	1.53	0.96	2.6
	38	WSR5-2	S	26.4	2.0	0.07	0.34	1.20	1.30	4.70	1.53	0.96	2.3
	39	WSR6-2	S	26.4	2.0	0.07	0.68	2.41	1.30	4.70	1.53	0.96	1.9

Specimens with gray shading were constructed with clay brick

* S for diagonal shear failure and S/S for diagonal/sliding shear failure

** Shear span to depth ratio, where h_e is effective height, was taken as *M/V*, and d_v is effective depth for shear calculations, was taken as *0.8lw*

Table 6.3(continued): Main Variables of the Studied Specimens

Source	Specimen no.	Specimen label	Mode of failure *	f'_m	σ_n	$\frac{\sigma_n}{f'_m}$	ρ_h	$\rho_h f_{yh}$	ρ_v	$\rho_v f_{yv}$	$\frac{h_w}{l'_w}$	$\frac{h_e}{d'_v}$ **	μ_Δ
				MPa	MPa	——	%	MPa	%	MPa	——	——	——
Okomoto (1987)	40	WS1	S	17.9	0.0	0.00	0.17	0.60	0.53	2.03	0.90	0.56	2.5
	41	WS4	S	22.8	2.0	0.09	0.17	0.60	0.73	2.78	1.50	0.94	2.5
	42	WS7	S	17.9	0.0	0.00	0.17	0.60	1.00	3.78	2.25	1.41	2.5
	43	WSN1	S	22.8	3.9	0.17	0.17	0.60	0.73	2.78	1.50	0.94	2.5
	44	WSN2	S	22.8	5.9	0.26	0.17	0.60	0.73	2.78	1.50	0.94	2.5
	45	WSR1	S	26.8	0.0	0.00	0.17	0.60	0.53	2.03	0.90	0.56	2.5
	46	WSR4	S	25.2	0.0	0.00	0.17	0.60	0.73	2.78	1.50	0.94	2.5
	47	WSR7	S	21.4	0.0	0.00	0.17	0.60	1.00	3.78	2.25	1.41	2.5
Shing et al. (1990)	48	S-3	S	20.7	1.9	0.09	0.12	0.47	0.78	3.89	1.00	1.25	2.5
	49	S-4	S	17.9	0.0	0.00	0.12	0.47	0.78	3.89	1.00	1.25	3.2
	50	S-5	S	17.9	0.7	0.04	0.12	0.47	0.78	3.89	1.00	1.25	2.5
	51	S-7	S	20.7	0.7	0.03	0.12	0.47	0.78	3.89	1.00	1.25	2.6
	52	S-9	S	20.7	1.9	0.09	0.12	0.47	0.40	1.79	1.00	1.25	3.4
	53	S-13	S	22.8	1.9	0.08	0.22	1.03	0.57	2.58	1.00	1.25	4.8
	54	S-14	S	22.8	1.9	0.08	0.12	0.47	0.57	2.58	1.00	1.25	2.8
	55	S-16	S	17.2	1.9	0.11	0.22	1.03	0.78	3.89	1.00	1.25	3.3
	56	S-21	S	26.2	1.9	0.07	0.13	0.49	0.60	2.69	1.00	1.25	3.2
	57	S-22	S	26.2	0.7	0.03	0.13	0.49	0.60	2.69	1.00	1.25	3.9
Voon and Ingham (2006)	58	A1	S	17.6	0.0	0.00	0.05	0.16	0.62	1.98	1.00	1.25	2.7
	59	A2	S	17.6	0.0	0.00	0.01	0.04	0.62	1.98	1.00	1.25	2.6
	60	A4	S	17.0	0.0	0.00	0.06	0.19	0.62	1.98	1.00	1.25	2.6
	61	A7	S	18.8	0.5	0.03	0.05	0.16	0.62	1.98	1.00	1.25	2.7
	62	A8	S	18.8	0.3	0.01	0.05	0.16	0.62	1.98	1.00	1.25	2.7
	63	A9	S	24.3	0.3	0.01	0.05	0.16	0.97	5.34	2.00	2.50	2.9
	64	A10	S	24.3	0.3	0.01	0.05	0.16	0.59	1.88	0.60	0.75	1.3
Current study	65	W-Ref	S	13.1	1.0	0.08	0.13	0.57	0.84	3.59	0.89	1.25	4.2
	66	W-ρ_h0	S	13.1	1.0	0.08	0.00	0.00	0.84	3.59	0.89	1.25	3.0
	67	W-σ_n0	S	13.1	0.0	0.00	0.13	0.57	0.84	3.59	0.89	1.25	4.1
	68	W-σ_n1.5	S	13.1	1.5	0.11	0.13	0.57	0.84	3.59	0.89	1.25	3.4
	69	W-M/Vd_v1.8	S	13.1	1.0	0.08	0.13	0.57	0.84	3.59	0.89	1.88	5.2
	70	W-90°	S	13.1	1.0	0.08	0.13	0.57	0.84	3.59	0.89	1.25	3.9
	71	W-Str	S	13.1	1.0	0.08	0.13	0.57	0.84	3.59	0.89	1.25	3.6
	72	W-S_v800	S	13.1	1.0	0.08	0.13	0.57	0.84	3.59	0.89	1.25	3.4
	73	W-S_h800	S	13.1	1.0	0.08	0.13	0.57	0.65	2.80	0.89	1.25	2.3

Specimens with gray shading were constructed with clay brick

* S for diagonal shear failure and S/S for diagonal/sliding shear failure

** Shear span to depth ratio, where h_e is effective height, was taken as *M/V*, and d_v is effective depth for shear calculations, was taken as *0.8lw*

6.4 VERIFICATION OF IN-PLANE SHEAR STRENGTH EQUATIONS

The predicted in-plane shear resistances provided by masonry, V_m, axial compression load, V_p, horizontal reinforcement, V_s, in addition to, the nominal shear strength, V_n, for each wall were calculated using the ten equations given in Table 6.1 along with the proposed equation (Eq. 6.1). The results are presented in Tables A.2, A.3, A.4, and A.5 of Appendix A, along with Table A.6 that provides a comparison between the accuracy of the eleven equations in terms of $V_{experimental}/V_{predicted}$.

For a more accurate evaluation of the efficiency of the studied equations including the proposed equation for predicting V_n, a statistical analysis was performed and comparisons made between the average, standard deviation, coefficient of variation, smallest value, and largest value. Furthermore, the 95th and 99th percentile values were calculated assuming normally distributed data; hence, the 95th percentile is 1.645 standard deviations from the average, while, the 99th percentile is 2.33 standard deviations from the average.

During the statistical analysis, the experimental data was divided into three data sets based on the detailed results concerning the behaviour of tested walls and how far the testing approach simulated the actual behaviour of RM shear walls. The three data sets were defined as follows:

1. Data set one (7 cantilever walls): this data set includes the first seven RM shear walls tested in this current study. Walls W-S_v800 and W-S_h800 were not included in this data set since they were tested with large spacings of the horizontal and vertical reinforcement to evaluate the effect of distributing the reinforcement along the height and length of RM walls.

2. Data set two (24 cantilever walls): the experimental data in data set one was extended to include the tested walls by Shing et al. (1990) and Voon and Ingham (2006), since these walls were tested under single curvature which is more representative of the real behaviour of RM shear walls. Moreover, their test results together with the data given in Chapter 4 provide more results, including the yield point of vertical reinforcement and the hysteretic force-displacement response of tested walls. Conversely, most of the reported results from the experimental studies conducted on masonry piers by Sveinsson et al. (1985), Matsumura (1985), and Kaminosono et al. (1988), provide little information on the force-displacement responses of their tested piers.
3. Data set three (68 cantilever walls and piers): although the total number of tested walls is 73, only 68 walls were considered in this data set. Comparing the predicted shear strength, $V_{predicted}$, using different equations with the reported experimental peak lateral load, $V_{experimental}$, from the five tested masonry walls by Kaminosono et al. (1988), WS1, WS7, WSR1, WSR4, and WSR7, shows that these piers were able to achieve high levels of unpredicted shear strength. None of the equations was able to predict a close value to the reported $V_{experimental}$ for these walls. As shown in Table 6.3, these walls were tested under axial compression stress equal to 0.0 MPa. Hence, if they were subjected to an axial compression load during testing, this could cause high values of $V_{experimental}$. However, most of the given equations in Table 6.1, including Shing et al. (1990), Anderson and Priestley (1992), NEHRP (1997), NZS 4230:2004, MSJC (2013), and CSA S304-14, did not consider all tested walls by Kaminosono et al. (1988) in their data source. On the other hand, only Matsumura (1988) who considered them in his proposed equation. Consequently, only walls WS4, WSN1,

and WSN2 were taken from Kaminosono et al. (1988) in this statistical analysis, which resulted in a total of 68 cantilever walls and piers.

Table 6.4 presents the results of the statistical comparisons between the eleven equations for predicting V_n using the three data sets. In the statistical comparisons, the values of the 95th and 99th percentile were considered. These values are well known when evaluating the safety of design equations. The 95th percentile value of the ($V_{experimental}/V_{predicted}$) ratios means that 95% of the tested walls will achieve in-plane shear strength, $V_{experimental}$, higher than this value multiplied by the predicted strength, $V_{predicted}$; similarly, the 99th percentile refers to 99% of the walls. For example, the 95th and 99th percentile values when using the proposed equation for data set one are equal to 1.1 and 1.02 respectively, hence, it can be expected that 95% of the tested shear strength will exceed 1.1 times the strength calculated using Eq. 6.1, while, 99% of the tested walls will reach $V_{experimental}$ higher than $1.02V_{predicted}$.

For a safe prediction, the minimum value of ($V_{experimental}/V_{predicted}$) ratios needs to be more than one. However, most of the design codes provide a strength reduction factor, ϕ, which is taken less than one for safe design. This means that the design value for shear strength, V_{design}, is equal to $\phi V_{predicted}$. Consequently, the minimum ($V_{experimental}/V_{predicted}$) ratio can go up to ϕ relying on this safe limit. The following researchers compared the 95th percentile with the strength-reduction factor, ϕ: Voon (2007) for the equation adopted in the New Zealand Standard Design of Reinforced Concrete Masonry Structures NZS 4230:2004 (Eq. 2.5), and Davis (2008) for the equation given in US Masonry Standards Joint Committee MSJC-2013 (Eq. 2.7). This means that there is a 5% probability that $V_{experimental}$ is less than V_{design}. On the other hand, some researchers more conservatively defined the safe value of ϕ as equal to or less than the 99th percentile value, such as Sherwood and Sarhat (2010), when evaluating the effective shear design equations for reinforced masonry beams.

Table 6.4: Statistical Comparisons between Shear Equations for Different Data Sets

Data Set		$V_{experimental} / V_{predicted}$									
		Matsumura (1988)	Shing et al. (1990)	Anderson & Priestley (1992)	NEHRP (1997) MSJC (2013)	UBC (1997)	AS3700-2001	CSA S304-14	NZS 4230:2004	Voon & Ingham (2007)	Proposed Equation
	Eq.	(2.3)	(2.5)	(2.6)	(2.7)	(2.8)	(2.9)	(2.10)	(2.15)	(2.16)	(6.1)
Data Set 1 Current study (7 walls)	Average	0.99	0.89	2.10	0.98	1.54	0.81	2.04	1.58	1.52	1.32
	STDV	0.11	0.14	0.78	0.13	0.65	0.14	0.51	0.54	0.42	0.13
	C.O.V. (%)	11.3	16.1	37.2	13.1	42.3	16.9	25.1	34.0	27.6	9.8
	Minimum	0.76	0.67	1.50	0.73	1.02	0.61	1.44	1.15	1.07	1.14
	Maximum	1.10	1.13	3.72	1.16	2.97	1.01	3.11	2.75	2.36	1.50
	95th Percentile	0.81	0.66	0.81	0.77	0.47	0.58	1.20	0.70	0.83	1.10
	99th Percentile	0.73	0.56	0.28	0.68	0.02	0.49	0.85	0.33	0.55	1.02
Data Set 2 (24 walls)	Average	0.99	0.97	1.69	1.05	1.54	0.97	2.14	1.55	1.46	1.35
	STDV	0.15	0.16	0.74	0.14	0.38	0.21	0.36	0.44	0.37	0.14
	C.O.V. (%)	14.6	16.2	43.8	13.5	24.7	21.3	16.7	28.4	25.5	10.2
	Minimum	0.73	0.55	1.00	0.73	1.00	0.61	1.44	1.01	0.97	1.13
	Maximum	1.26	1.19	3.73	1.32	2.97	1.30	3.11	2.75	2.49	1.71
	95th Percentile	0.75	0.71	0.47	0.82	0.91	0.63	1.55	0.83	0.85	1.12
	99th Percentile	0.65	0.60	N/A	0.72	0.65	0.49	1.31	0.52	0.59	1.03
Data Set 3 (68 walls)	Average	1.05	1.12	1.41	1.02	1.36	1.24	1.91	1.17	1.18	1.38
	STDV	0.16	0.26	0.55	0.14	0.49	0.43	0.41	0.42	0.34	0.20
	C.O.V. (%)	15.3	23.3	38.8	13.6	36.5	34.5	21.5	35.5	28.6	14.6
	Minimum	0.55	0.55	0.14	0.67	0.60	0.61	0.96	0.48	0.60	0.90
	Maximum	1.42	1.87	3.73	1.32	3.48	2.91	3.11	2.75	2.49	1.85
	95th Percentile	0.79	0.69	0.51	0.79	0.54	0.54	1.24	0.49	0.62	1.05
	99th Percentile	0.68	0.51	0.14	0.69	0.20	0.24	0.96	0.20	0.39	0.91

The strength reduction factor, ϕ, for in-plane shear design of RM shear walls ranges between 0.75 and 0.8 for different masonry design codes. In most of the US design codes, such as UBC (1997), NEHRP (1997), and MSJC (2013) it is defined as 0.8, whereas a more conservative value of 0.75 is adopted in AS3700-2001 and NZS 4230:2004. Unlike the aforementioned codes, the Canadian Standards Association CSA S304-2014 does not consider a strength reduction factor, instead using a resistance factor for the material. The resistance factors for masonry, ϕ_m, and steel, ϕ_s, are 0.6 and 0.85 respectively. Since the in-plane shear strength equation adopted in CSA S304-14 contains three terms of V_m, V_p, V_s, where (V_m+V_p) is multiplied by ϕ_m and V_s is multiplied by ϕ_s, the average strength reduction factor, ϕ, for statistical compression purposes was calculated for all walls according to the following equation and it gives a value of 0.69 (c.o.v = 5.3%).

$$\phi = \left[\phi_m (V_m + V_p) + \phi_s (V_s)\right] / V_n \qquad \text{Eq. 6.2}$$

The proposed equation was calibrated using data set one to have a sufficient level of conservative prediction that results in a 99th percentile value of $(V_{experimental}/V_{predicted})$ ratios higher than 1.0 instead of ϕ, and then it was verified with other data sets. This conservative limit was set intentionally because most seismic design codes, including the National Building Code of Canada (NBCC 2010), calculate the design seismic base shear for a building by dividing the elastic base shear force, V_e, by the product of R_d R_o. This R_o factor is proposed based on the fact that the real capacity of a structural element is higher than the calculated value. Mitchell et al. (2003) suggested that R_o is made up of five components (see Eq. 4.3), Chapter 4), one of these components is R_ϕ that accounts for the difference between nominal and factor resistance and is equal to $1/\phi$, where ϕ is the material resistance factor. Consequently, reconsidering this factor, ϕ, in the probability of failure is effectively duplicating this safety limit, which could lead to unsafe seismic design.

Based on the analyzed results using data set one, both equations proposed by Matsumura (1988) and adopted in MSJC (2013) have the closest average ratio to 1.0; however, both of the 99th and 95th percentile values using MSJC (2013) are smaller than the strength reduction factor, ϕ, of 0.8 suggested by MSJC (2013). Likewise, using codes UBC (1997), NEHRP (1997), AS3700-2001, and NZS 4230:2004 result in 95th percentile values less than the adopted values for ϕ. On the other hand, the proposed equation (Eq. 6.1) and the given equation in CSA S304-14 were the only two equations that have 99th percentile values higher than one. However, using the equation given in the Canadian design code results in very conservative values to cover the large variation of ($V_{experimental}/V_{predicted}$) ratios with a range between 1.44 to 3.11 (c.o.v. = 25.1%); instead, the proposed equation has the narrowest variation among all equations with c.o.v. = 9.8%. Similar observations can be made when using data set two and three (see Table 6.4). Figure 6.6 shows the calculated ratios of ($V_{experimental}/V_{predicted}$) for all walls, along with the average, 95th percentile, and 99th percentile values for data set three using each equation separately. Although the five tested walls by Kaminosono et al. (1988) were not considered in the statistical analysis, their high ($V_{experimental}/V_{predicted}$) ratios are shaded and shown in this figure.

Generally, the tested walls in the experimental data can be classified based on the type of masonry units as concrete block and clay brick, or, based on the loading approach as cantilever walls with one curvature or piers with double curvature. To add more confidence in the ability of the proposed equation to provide the same level of accuracy for all kinds of RM shear walls, the statistical analysis was performed using the results of the studied walls constructed by concrete block and clay brick separately, the results of which are presented in Table 6.5. Likewise, the studied walls were divided into cantilever walls and piers, with the results of the statistical compression given in Table 6.6. As shown in these tables, the proposed equation is the only equation that provides the same level of safety among all of the equations for different types of walls with 95% of the experimental results higher than the predicted values, and a 99% of tested shear strength higher than 0.87 of $V_{predicted}$. On the other hand, each of the other equations has at least one or more of the 95th percentile values less than the strength reduction factor. Even using the adopted equation in CSA S304-14, which generally has high 99th percentile values, for predicting the in-plane shear strength of clay brick walls, results in a 99th percentile value of 0.42 smaller than its strength reduction factor.

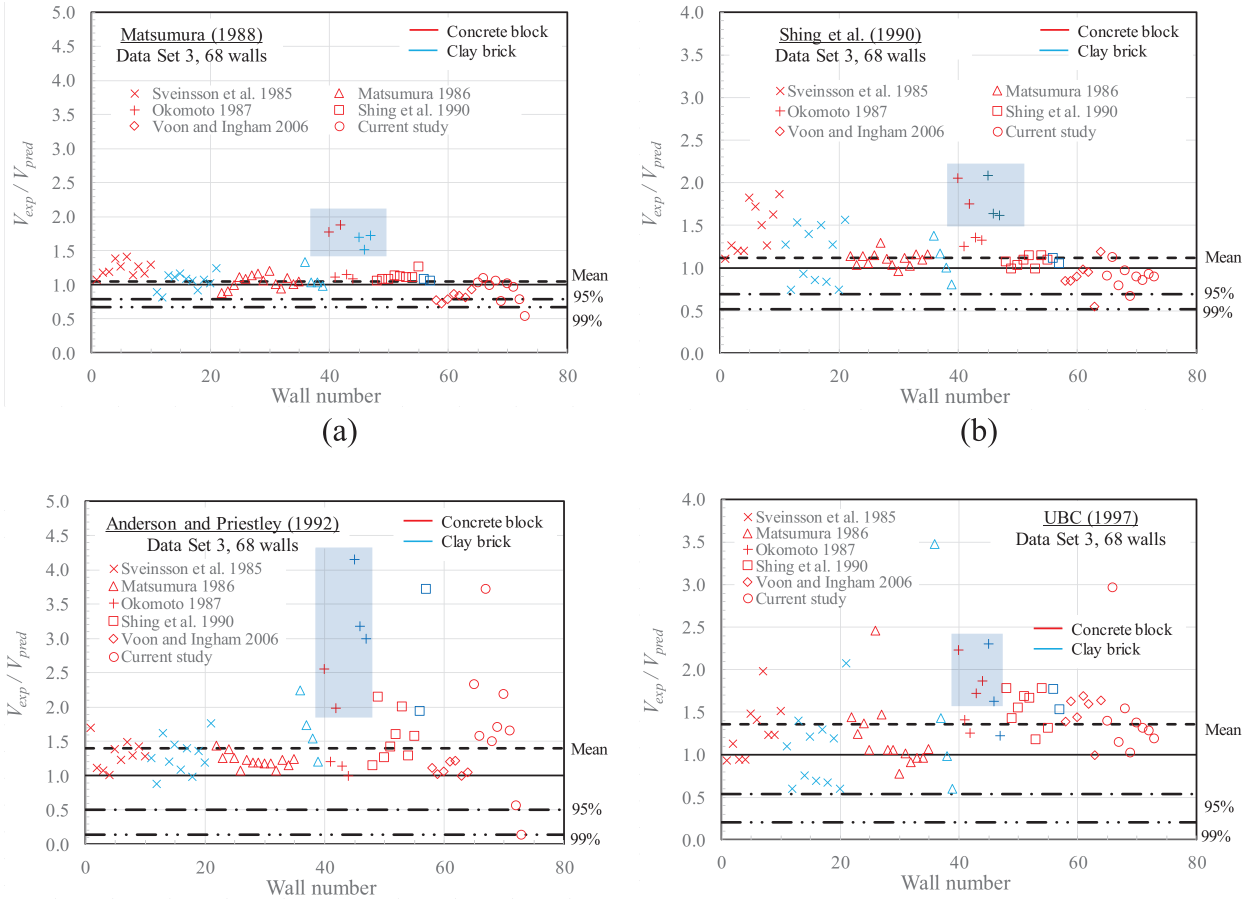

(a) (b)

(c) (d)

Figure 6.6: Experimental results versus the predicted in-plane shear strength using eleven different equations

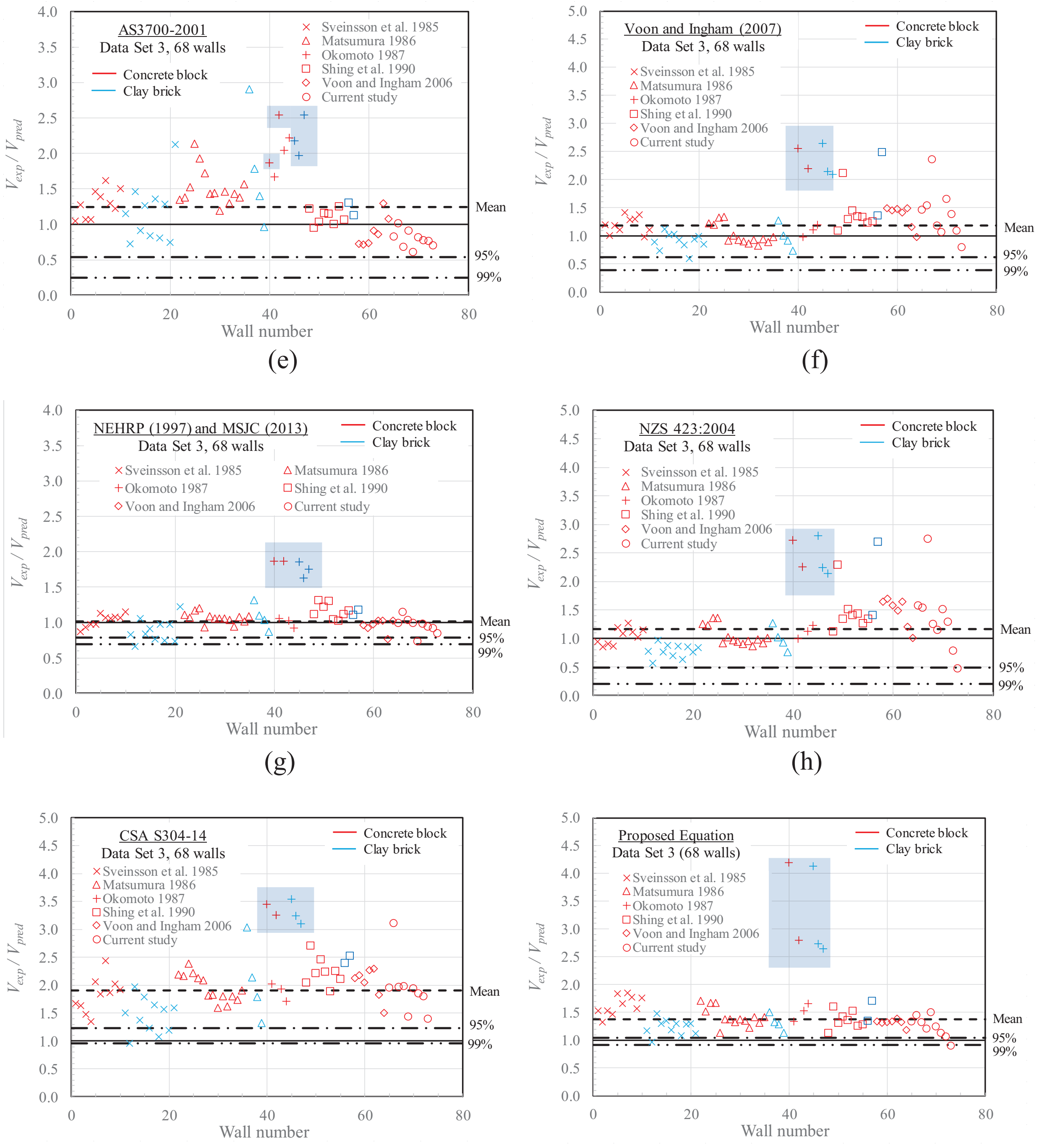

(e) (f)

(g) (h)

(i) (j)

Figure 6.6(continued): Experimental results versus the predicted in-plane shear strength using eleven different equations

Table 6.5: Statistical Comparisons between Shear Equations for Different Types of Loading Approaches - Cantilever Walls and Piers

Data Set		$V_{experimental} / V_{predicted}$									
		Matsumura (1988)	Shing et al. (1990)	Anderson & Priestley (1992)	NEHRP (1997) MSJC (2013)	UBC (1997)	AS3700-2001	CSA S304-14	NZS 4230:2004	Voon & Ingham (2007)	Proposed Equation
	Eq.	(2.3)	(2.5)	(2.6)	(2.7)	(2.8)	(2.9)	(2.10)	(2.15)	(2.16)	(6.1)
Cantilever Walls Current study (26 walls)	Average	0.97	0.97	1.59	1.04	1.51	0.95	2.10	1.48	1.42	1.32
	STDV	0.17	0.15	0.80	0.14	0.37	0.21	0.38	0.49	0.39	0.17
	C.O.V. (%)	17.5	15.7	50.4	13.8	24.7	21.9	18.0	33.3	27.2	12.6
	Minimum	0.55	0.55	0.14	0.73	1.00	0.61	1.40	0.48	0.80	0.90
	Maximum	1.26	1.19	3.73	1.32	2.97	1.30	3.11	2.75	2.49	1.71
	95th Percentile	0.69	0.72	0.27	0.80	0.90	0.61	1.48	0.67	0.79	1.05
	99th Percentile	0.57	0.61	N/A	0.70	0.64	0.47	1.22	0.33	0.52	0.93
Piers (42 walls)	Average	1.10	1.22	1.29	1.01	1.26	1.43	1.80	0.98	1.03	1.42
	STDV	0.13	0.27	0.25	0.14	0.54	0.43	0.39	0.19	0.19	0.21
	C.O.V. (%)	12.0	22.2	19.4	13.5	42.8	30.3	21.7	19.4	18.3	15.2
	Minimum	0.82	0.74	0.88	0.67	0.60	0.73	0.96	0.57	0.60	0.96
	Maximum	1.42	1.87	2.24	1.31	3.48	2.91	3.03	1.36	1.42	1.85
	95th Percentile	0.89	0.77	0.88	0.78	0.37	0.72	1.15	0.67	0.72	1.06
	99th Percentile	0.79	0.59	0.71	0.69	0.00	0.42	0.89	0.54	0.59	0.91

Table 6.6: Statistical Comparisons between Shear Equations for different Types of Masonry Units - Concrete Block and Clay Brick

Data Set		$V_{experimental} / V_{predicted}$									
		Matsumura (1988)	Shing et al. (1990)	Anderson & Priestley (1992)	NEHRP (1997) MSJC (2013)	UBC (1997)	AS3700-2001	CSA S304-14	NZS 4230:2004	Voon & Ingham (2007)	Proposed Equation
	Eq.	(2.3)	(2.5)	(2.6)	(2.7)	(2.8)	(2.9)	(2.10)	(2.15)	(2.16)	(6.1)
Concrete block Current study (51 walls)	Average	1.05	1.12	1.35	1.04	1.39	1.22	1.98	1.23	1.23	1.41
	STDV	0.17	0.26	0.50	0.11	0.40	0.38	0.33	0.37	0.30	0.20
	C.O.V. (%)	16.4	22.9	36.8	11.0	28.7	31.3	16.7	30.3	24.3	14.2
	Minimum	0.55	0.55	0.14	0.73	0.77	0.61	1.35	0.48	0.80	0.90
	Maximum	1.42	1.87	3.72	1.32	2.97	2.22	3.11	2.75	2.36	1.85
	95th Percentile	0.77	0.70	0.53	0.85	0.73	0.59	1.44	0.62	0.74	1.08
	99th Percentile	0.65	0.52	0.19	0.77	0.46	0.33	1.21	0.36	0.53	0.94
Clay brick (17 walls)	Average	1.06	1.13	1.56	0.96	1.26	1.30	1.71	0.98	1.04	1.28
	STDV	0.12	0.28	0.66	0.19	0.72	0.56	0.56	0.49	0.42	0.18
	C.O.V. (%)	11.7	25.2	42.2	19.5	57.1	42.6	32.4	49.8	40.1	13.8
	Minimum	0.82	0.74	0.88	0.67	0.60	0.73	0.96	0.57	0.60	0.96
	Maximum	1.34	1.57	3.73	1.31	3.48	2.91	3.03	2.70	2.49	1.71
	95th Percentile	0.86	0.66	0.48	0.65	0.08	0.39	0.80	0.18	0.36	0.99
	99th Percentile	0.77	0.47	0.03	0.52	N/A	0.01	0.42	N/A	0.07	0.87

6.5 MODIFICATION IN THE PROPOSED EQUATION FOR CODIFICATION

Similar to other codes, the Canadian Standards Association CSA S304 for design of masonry structures classifies RM shear walls according to their ductility. However, the ductility of RM shear walls is commonly defined based on the Ductility-related seismic force Modification Factor, referred to as R_d in NBCC (2010), not based on the displacement ductility, μ_Δ. The previous version of the Canadian code, CSA S304.1-04, classified RM shear walls as follows: conventional construction shear walls (R_d = 1.5); limited ductility shear walls (R_d = 1.5); and moderately ductile shear walls (R_d = 2.0). However, modifications have been made to this classification in the current version, CSA S304-14, such that the limited ductility shear wall was removed and a new class introduced for ductile shear walls (R_d = 3.0). Unlike the equation proposed by Anderson and Priestley (1992), the in-plane shear strength equation adopted in CSA S304-14 (see Eq. 2.10 in Table 6.1) does not include the effect of the displacement ductility, μ_Δ; instead, it reduces the shear resistance provided by the masonry and axial compression load, V_{m+p}, by a factor based on the value of R_d. This reduction factor is equal to 0.75 and 0.5 for R_d of 2 and 3, respectively.

Practically, displacement ductility, μ_Δ, is not easy to define and is not well known by engineers and designers; however, it is more commonly used for experimental work and research purpose. On the other hand, R_d is the most representative factor for ductility of RM shear walls in design codes. Consequently, to simplify the proposed equation (Eq. 6.1) for design purposes, such that it can be easily handled by designers, the ductility related modification factors, k_1 and k_2, are modified to be functions of R_d as shown in Table 6.7.

Table 6.7: Ductility Related Modification Factors for the Proposed Equation

R_d	Proposed Equation (Eq. 6.1)		CSA S304-14 (Eq. 2.10)	
	k_1 for (V_{m+P})	k_2 for (V_s)	k_1 for (V_{m+P})	k_2 for (V_s)
1.5	1	1	1	1
2	0.75	1.5	0.75	1
3	0.5	2.0	0.5	1
4	0.25	2.5	N/A	N/A

A summary of the statistical comparison between the accuracy of the proposed equation for predicting in-plane shear strength of RM shear walls using data set 3, 68 walls, against the studied equations and the modified one in terms of V_{exp}/V_{pred}, is given in Figure 6.7 along with the average, 95th and 99th percentile values, and the strength reduction factor, ϕ. Although all the equations have an average higher than one, only the adopted equation in CSA S304-14 and the proposed equations have 99th percentile values higher than the strength reduction factor, ϕ. Moreover, the modified equation has a 99th percentile value higher than one. However, the Canadian equation predicted very conservative values with an approximate average of 50% of the real capacity in order to overcome the large variation of ($V_{experimental}/V_{predicted}$) ratios that range from 0.96 to 3.11 with a c.o.v. = 21.5%. On the other hand, the proposed equation provides an acceptable level of conservatism with much better variation that is tightly distributed around the average. The minimum and maximum values of ($V_{experimental}/V_{predicted}$) are 0.9 and 1.85 respectively, with a c.o.v. = 14.6%. Although, the modified equation has a wider variation than the proposed one, which is a function of the displacement ductility, it is nevertheless the only equation that has a minimum ($V_{experimental}/V_{predicted}$) ratio higher than one, with a c.o.v. = 16.1%.

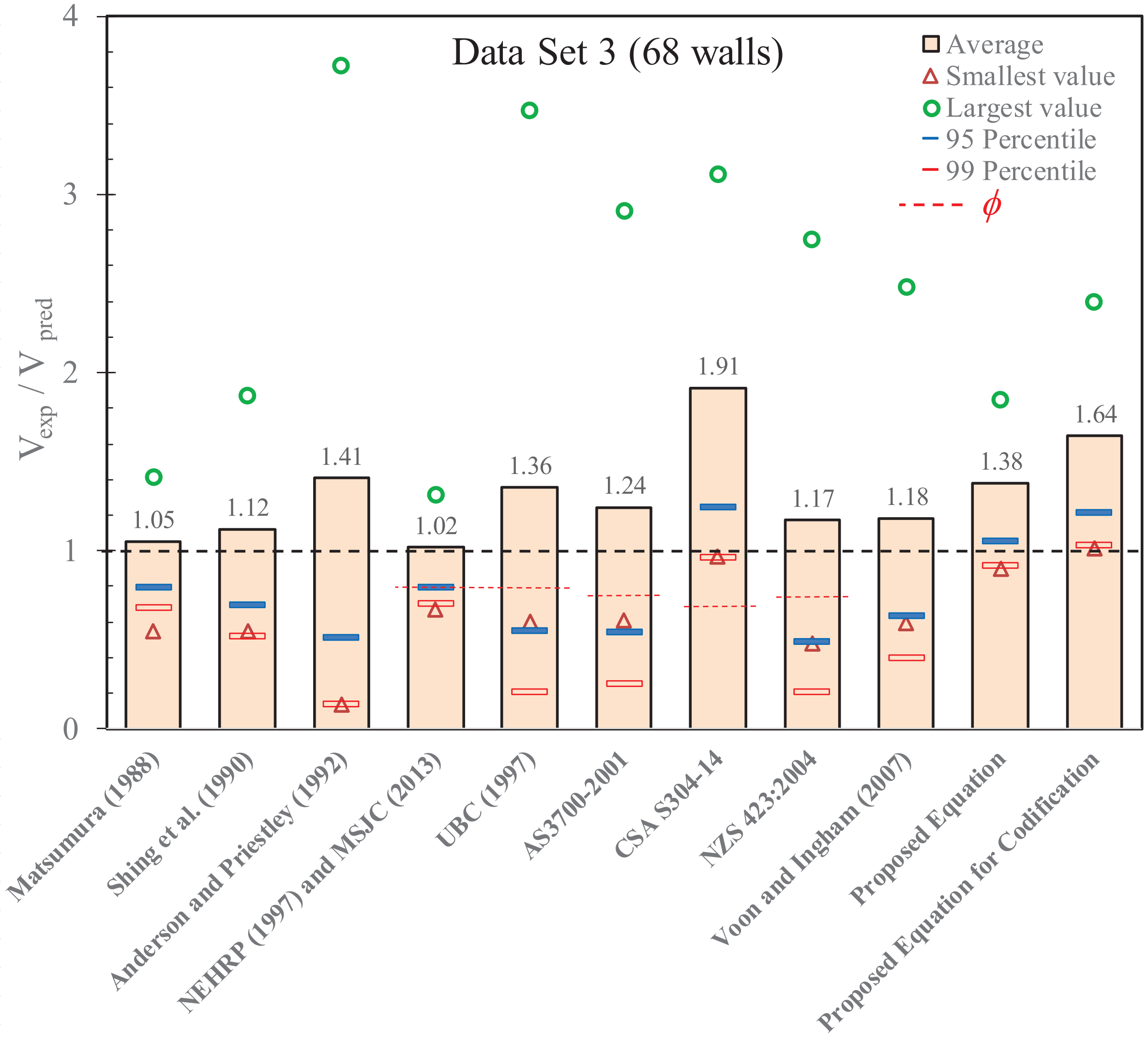

Figure 6.7: Statistical comparisons between the accuracy of shear equations for predicting in-plane shear strength, in terms of V_{exp}/V_{pred}

CHAPTER 7

SUMMARY AND CONCLUSIONS

7.1 INTRODUCTION

Reinforced masonry (RM) shear walls are the key structural elements that are widely used to resist lateral loads in masonry buildings due to their capability to provide lateral strength, stiffness, and energy dissipation. The flexural behaviour of RM shear walls is well defined and follows the simple flexural theory of reinforced concrete structures based on plane-section assumption. On the other hand, the shear behaviour of RM shear walls in the plastic hinge region is more complex due to the interaction between the nonlinear responses of their constituent materials, namely: concrete masonry blocks, mortar, grout, and steel reinforcement. The main objective of this research was to evaluate the inelastic behaviour of fully grouted RM shear walls that are dominated by shear failure. To achieve the research objective, the study involved experimental, numerical, and analytical research. Section 7.2 presents a summary of the study and the motivation for each goal, while conclusions are drawn and summarized in Section 7.3 based on the study's results and findings. In the last section, recommendations are provided for future related research with the aim of improving the inelastic performance of RM buildings.

7.2 SUMMARY OF THE STUDY

During significant earthquakes in the twentieth century, many masonry structures suffered severe damage due to their limited inelastic deformation capacity. Consequently, at the beginning of the 1980s a coordinated research program between the U.S. and Japan conducted a series of comprehensive experiments to investigate the seismic performance of reinforced masonry structures. Most of the tested walls were subjected to in-plane lateral forces at their middle height, and were fixed against rotation along both top and bottom edges (i.e. under double curvature) to simulate the behaviour of masonry piers. After this extensive research, there was a gap in the experimental data until Voon and Ingham (2006) carried out an experimental study in New Zealand that investigated the in-plane shear strength of RM shear walls. However, there is still a lack of experimental data for fully grouted RM shear walls dominated by shear failure, which shows the need for more experimental tests to be carried out on RM walls with single curvature (cantilever wall) that provide a more realist simulation of shear walls.

The experimental work in this study involved the testing of nine full-scale fully grouted rectangular RM shear walls that were subjected to in-plane axial compressive stress, top moment, and cyclic lateral excitations to evaluate the effect of the following parameters on their in-plane shear behaviour:

- Horizontal reinforcement ratio, ρ_h
- Level of the axial compressive stress, σ_n
- Shear span to depth ratio, M/Vd_v
- Horizontal reinforcement anchorage end detail
- Vertical spacing of horizontal reinforcement, S_v
- Horizontal spacing of vertical reinforcement, S_h

In addition to the tested walls, a total of 16 fully grouted unreinforced masonry (URM) prisms were tested under a uniaxial compression load normal to the bed joint, to study the effect of the bond pattern and the height-to-thickness ratio, h/t, on the measured compressive strength of masonry, f'_m. Furthermore, in-plane beam tests were carried out to evaluate the indirect tensile, and shear performance of masonry prisms.

The effort, time, and cost spent in the experimental work show the need to develop a cost effective tool to predict the performance of structural elements with larger variation in the studied parameters. Nonlinear finite element FE models were developed in this research to simulate the behaviour of RM shear walls under cyclic in-plane lateral loading. After the verification of the FE models using the results of the tested walls in the experimental work, a parametric study was performed to consider more variations in some of the studied parameters in the experimental work.

A survey of widely used equations for predicting the in-plane shear strength of RM shear walls, V_n, was conducted, with the result that most of the equations were developed based on the results of experimental work conducted over the past 30 years. There are two main concerns about these experimental results. The first one is that most of the tested walls did not achieve their initial shear strength, V_i. Consequently, the reported failure lateral loads represented the lateral force corresponding to the interaction between the flexural performance and the shear strength envelope at the strength degradation zone. The second concern relates to the horizontal reinforcement contribution, which was not measured experimentally. Most of the previous researchers evaluated the in-plane shear resistance provided by horizontal reinforcement based on the difference between the maximum lateral loads achieved for different horizontal reinforcement ratios, neglecting the influence of the redistribution in the resistance shares of the horizontal reinforcement and the masonry. Consequently, an equation for predicting the in-plane shear strength of RM shear walls that provides greater accuracy was developed as a result of this study and is proposed in this thesis.

7.3 CONCLUSIONS

The research presented in this thesis was carried out in three phases: experimental, numerical, and analytical. The following conclusions for *fully grouted reinforced* masonry shear walls are drawn from the research reported in the preceding chapters.

7.3.1 CONCLUSIONS BASED ON EXPERIMENTAL RESULTS

Based on the auxiliary laboratory test results on masonry prisms, it can be concluded that:

1. The height-to-thickness ratio, *h/t*, of tested prisms under a uniaxial compression load has a considerable effect on the measured masonry compressive strength, f'_m. On the other hand, the bond pattern of masonry prisms does not significantly influence the measured f'_m.
2. The Canadian standard CSA S304-14 underestimates the masonry flexural tensile strength, f_t, of the grouted masonry structural element. In fact, the results of tested in-plane beam prisms seems to be closer to the value suggested by the Canadian standard for design of concrete structures, CSA A23.3-14, with some modifications to consider the effect of the grouted area.

The effects of several parameters were considered in the experimental work. The results of the nine tested fully grouted RM shear walls in this study support the following conclusions:

1. Providing horizontal reinforcement to masonry shear walls enhances their in-plane shear behaviour in terms of shear strength and displacement ductility. However, the horizontal reinforcement does not have a significant influence on the pre-crack behaviour and it has a minor effect on the yield capacity. On the other hand, the

experimentally measured in-plane shear resistance provided by the horizontal reinforcement, V_s, reached to 100% of its yield capacity at high displacement ductility, $\mu_\Delta = 3$, when the tested walls were constructed with closely spaced reinforcement in both vertical and horizontal directions.

2. Increasing the axial compressive stress, σ_n, resulted in a higher shear strength accompanied with more brittle failure. Likewise, it enhances the initial stiffness but it is followed by rapid stiffness degradation. From the performance of tested walls under different levels of σ_n, it can be concluded that although the plastic hinge is mostly expected at the base where the maximum loads are, shear failure could occur at the top of a RM shear wall in a multi-story building with a high sliding deformation, since the gravity loads are less than at the base. However, this type of failure is more common in partially grouted masonry walls without sufficient vertical reinforcement, i.e. limited dowel action.
3. The test results of walls W-Ref and W-M/Vd_v1.8 with shear span to depth ratio, M/Vd_v equal to 1.25 and 1.875, respectively, show a significant reduction in the shear strength when M/Vd_v is increased. However, W-M/Vd_v1.8 was able to achieve higher levels of displacement ductility. This reduction in the shear capacity could be explained by considering the interaction between the flexural and shear performances. Both walls had same dimensions and reinforcement such that they have the same shear strength envelope and moment capacity. Increasing M/Vd_v results in a reduction in the lateral force that corresponds to the flexural capacity of the wall. Consequently, this lower lateral force intersects with the shear strength envelope at a lower capacity along with higher displacement ductility.

4. Three different types of horizontal reinforcement anchorage details were evaluated in this experimental work: 180° standard hook, 90^o hook, and straight bars. Based on the test results, the 180° standard hook was the most efficient in terms of strength and ductility comparted to the 90^o hook that had similar strength with less ductility. On the other hand, the tested walls with straight horizontal bars achieved the smallest values for strength and displacement ductility among the three anchorage details. However, using the 180° standard hook or 90^o hook may cause congestion at the end zone for narrow blocks. Moreover, the reduction in Q_{ue} when using straight horizontal bars is still minor; it was less than 5% between walls W-Ref (180° standard hook) and W-Str. Therefore, to facilitate the construction process, it is suggested that straight horizontal bars could be permitted in regions where high ductility is not required; for example, in higher floors outside the critical region with high demands of the conventional construction shear walls. The height of the critical region could be taken as h_p, similar to the plastic hinge region. Furthermore, it could be argued to use straight horizontal reinforcement outside the plastic hinge region of moderately ductile RM shear walls where R_d equals 2.0.
5. The spacing of the reinforcement has a considerable effect on the stress flow, and thereby on the behaviour of RM shear walls. Tested walls that were constructed with closely spaced reinforcement were able to reach higher strength and ductility compared to similar walls with large spacing when using the same reinforcement ratio. Hence, the current values for the maximum spacing of reinforcement in the Canadian standard CSA S304-14 need to be modified by specifying more conservative limits.

6. All walls had a rapid reduction in their stiffness at early stages of loading. At the experimental yield displacement, the tested walls recorded more than 50% degradation in their initial stiffness. Moreover, at a top drift limit of 1.0%, the secant stiffness of the tested walls ranged between 6.0% and 12.0% of their initial stiffness.

   The equivalent viscous damping ratio, ζ_{eq}, was defined experimentally using the equal area approach by equating the energy dissipated by a viscous damper with the energy dissipated from the force-displacement response. The values of ζ_{eq} ranged between 8.4% and 23.4% with higher values at larger nonlinear deformations.

   Based on the test results, empirical equations for the stiffness degradation of RM shear walls along with the equivalent viscous damping ratio, ζ_{eq}, relative to their top drift limit or displacement ductility, are proposed and presented in this study.

7. To account for the nonlinear behaviour of RM structures, the design seismic forces may be calculated based on section property reduction factor, α_w. This factor has a direct impact on the relation between the experimental ductility, μ_Δ, and the ductility-related force modification factor, R_d. Unlike the current version of CSA A23.3-14 for design of concrete structures, the equation adopted in the CSA S304-14 for α_w does not include the effect of R_d. An equation for α_w is proposed and verified using the results of the tested walls, which was shown to be more efficient than the current equations in both codes, in terms of safety and economy.

7.3.2 CONCLUSIONS BASED ON NUMERICAL SIMULATION

Nonlinear finite element (FE) models were developed to represent the behaviour of reinforced masonry (RM) shear walls. Based on the numerical simulation, the following conclusions were drawn:

1. The material models used for modeling concrete structural elements show a good ability to predict the behaviour of fully grouted RM walls under the condition of having a sufficient amount of closely spaced reinforcement in both vertical and horizontal directions.
2. A mesh sensitivity analysis was performed to evaluate the influence of mesh size on the precision of the output results. From the results, it is concluded that mesh size has a major impact on the accuracy of the numerical simulation, especially when using the smeared approach to model the reinforcing bars. Using a finer mesh size reduced the error in predicting the lateral load capacity for wall W-Ref from 13% to less than 2%.
3. The verification of the FE models using the results of the tested RM shear walls shows a good agreement between the numerical and the experimental results.
4. A parametric study was conducted to consider more variations in the effect of the horizontal reinforcement distribution, the level of axial compressive stress, and the wall aspect ratio on the in-plane shear behaviour of RM shear walls. The results of this numerical study agreed with the experimental conclusions.

7.3.3 CONCLUSIONS BASED ON ANALYTICAL STUDY

Most of the previous researchers quantified the in-plane shear resistance provided by the masonry, V_m, axial compression load, V_p, and horizontal reinforcement, V_s, based on the difference between the achieved maximum lateral loads for tested RM walls with different values of the studied parameters. The experimental results in this research show that this quantification approach overlooks the effect of the re-distribution in the shear resistance shares between V_m, V_p, and V_s, especially at high levels of displacement ductility. Moreover, most of the existing equations for in-plane shear strength of RM shear walls do not consider the interaction between the flexural performance and the shear strength envelope at the strength degradation zone. According to these findings, Eq. 6.1 was developed to better predict the in-plane shear strength of RM shear walls and considered the effect of the following observations:

- The vertical reinforcement has a considerable effect on the stress flow, and consequently on the achieved peak lateral load. In addition, increasing ρ_v results in a higher flexural strength. Therefore, the shear strength envelope intersects with the lateral force that corresponds to the flexural capacity of the wall at higher V_n with less ductility.
- The test results of walls W-Ref and W-M/Vd_v1.8 show that limiting the effect of shear span to depth ratio, M/Vd_v, to an upper value of 1.0, as provided in most of the masonry design codes, is overestimating the in-plane shear strength of RM shear walls, V_n, at high values of M/Vd_v, which might lead to an unsafe design. Consequently, the upper limit of h_e/d_v was extended to a value of 2.0 instead of 1.0. This value, 2.0, is proposed based on the assumption that at values of M/Vd_v higher than 2.0 the RM shear walls are dominated more by flexural behaviour, then the corresponding lateral force of the flexural capacity would be close to the residual shear strength, V_r. This assumption is supported by the

results of the nonlinear FE models in the parametric study. Nevertheless, h_e/d_v should not be taken less than 1.0 since this equation was not verified for squat shear walls.

- Unlike most of design equations given in North American codes that consider a constant percentage of the axial compression load contributing to the in-plane shear strength of RM shear walls, the proposed equation takes into account the effect of the angle, α, resulting from a diagonal compression strut from the point of load application to the centre of the flexural compression zone.
- Four modification factors are proposed in Eq. 6.1 to consider the effect of grouting, higher demands of displacement ductility, and loading method. The results of the nine RM tested walls showed that after the initiation of diagonal cracks and yielding of the vertical reinforcement, there is a significant reduction in the in-plane shear resistance provided by the masonry and axial compression load, V_{m+p}, while there is an increase in V_s. Ductility related modification factors, k_1 and k_2, for V_{m+p} and V_s , respectively, are proposed to take account of this behaviour. These factors are given in terms of the displacement ductility, such that k_1 is proposed assuming a linear degradation in V_{m+p} from $\mu_\Delta = 1.5$ up to zero contribution at $\mu_\Delta = 6.0$. On the other hand, the in-plane resistance provided by the horizontal reinforcement, V_s, increases linear from $\mu_\Delta = 1.5$ to its yield capacity at $\mu_\Delta = 4.0$. However, for codification and to simplify the proposed equation (Eq. 6.1) for design purposes, such that it can be easily handled by designers, the ductility related modification factors, k_1 and k_2, are modified to be functions of R_d. The values of k_1 and k_2 are proposed as 1.0, 0.75, 0.5, 0.25 and 1.0, 1.5, 2.0, 2.5 for R_d equal to 1.5, 2, 3, 4, respectively.

The proposed equation was verified with results of 64 *fully grouted* RM wall tests from five sources in the literature, in addition to the nine tested RM walls in this study. Then, statistical analysis was performed to evaluate the accuracy of the proposed equation against ten widely used equations, including the design equations given in the Canadian Standards Association CSA S304-2014, the US Masonry Standards Joint Committee MSJC-2013, and the Standards Association of New Zealand NZS 4230:2004. During the statistical analysis the values of the 95th and 99th percentile were calculated and compared with the strength reduction factor, ϕ, for in-plane shear design of RM shear walls. Moreover, the experimental data were divided into different data sets to add more confidence in the ability of the proposed equation to provide the same level of accuracy for all kinds of RM shear walls (i.e. concrete block, clay brick, single curvature, double curvature). The results of the statistical analysis support the following:

1. The proposed equation is the only equation that provides the same level of safety among all of the equations for different types of walls with 95% of the experimental results higher than the predicted values, and a 99% of tested shear strength higher than 0.87 of $V_{predicted}$. On the other hand, each of the other equations has at least one or more of the 95th percentile values (based on the data set) less than the strength reduction factor.
2. In general, for the data set that includes all walls, all the equations have an average higher than one, however, only the adopted equation in CSA S304-14 and the proposed equation have 99th percentile values higher than the strength reduction factor, ϕ. On the other hand, the Canadian equation predicted very conservative values with an approximate average of 50% of the real capacity in order to overcome the large variation of ($V_{experimental}/V_{predicted}$) ratios that range from 0.96 to 3.11 with a c.o.v. = 21.5%. Alternatively, the proposed equation provides an acceptable level of conservatism with much better variation that is tightly distributed around the average.

The minimum and maximum values of ($V_{experimental}/V_{predicted}$) are 0.9 and 1.85 respectively, with a c.o.v. = 14.6%. Although the equation proposed for codification (using R_d instead of μ_Δ) has a wider variation than the Eq. 6.1, it is nevertheless the only equation that has a minimum ($V_{experimental}/V_{predicted}$) ratio higher than one, with a c.o.v. = 16.1%.

7.4 FUTURE RESEARCH

The main objective of this study was to investigate the in-plane shear behaviour of RM shear walls. The conclusions drawn from this research are limited to the studied parameters. However, there are still some parameters that this study did not cover and which need to be investigated. Consequently, the following recommendations are made for future research:

1. The test results show that the correction factor for compressive strength of masonry, f'_m, which is adopted in the CSA S304-14 overestimates the compressive strength of masonry. However, this conclusion is limited to small numbers of tested prisms with three values of the height-to-thickness ratio, *h/t*. Hence, comprehensive experimental work is needed to cover a wide variation of the effect of *h/t*, on f'_m. Also, it was observed that the Canadian standard CSA S304-14 underestimates the masonry flexural tensile strength, f_t, of the grouted masonry structural element. Moreover, an equation was proposed for f_t similar to the one given by the Canadian standard for design of concrete structures, CSA A23.3-14, with some modifications to consider the effect of the grouted area. This equation needs to be verified by testing a large number of prisms.

2. The results of the tested walls are limited to rectangular cross-section single story RM shear walls. Consequently, further experimental work is needed to consider different complex geometries for walls with boundary elements. In addition, it is also recommended to perform tests on full-scale multi-story RM shear walls, which is more representative of real structures.
3. All the tested walls were subjected to in-plane cyclic static lateral excitations. Therefore, the response of RM shear walls subjected to bi-directional loading needs to be investigated experimentally. Moreover, it is recommended to perform shake table testing on RM shear walls to take into account the dynamic effects of seismic forces that only act for a short duration.
4. The survey conducted of previous experimental studies shows that the effect of some parameters on the in-plane shear behaviour of RM shear walls, such as the shear span to depth ratio, M/Vd_v, and the spacing and ratio of vertical reinforcement, need to be considered with wide variations.
5. In practice, RM shear walls do not act individually. Consequently, it is important to link the behaviour of RM shear walls with the performance of a complete structural system. Hence, it is recommended to perform experimental tests and numerical simulation to investigate seismic performance of RM buildings.
6. All the reinforcement in the numerical simulation was modeled using the smeared approach with an assumption of full bonding between the masonry and the reinforcement. Hence, the de-bonding failure mechanism was not considered and consequently the effect of the anchorage end detail of the horizontal reinforcement. It is therefore recommended to develop more nonlinear FE models using the discrete

approach for reinforcement; comparisons with the results of this study could help researchers to perform an accurate numerical simulation of RM shear walls.

References

Anderson, D. L., and Brzev, S. (2009). “Seismic design guide for masonry buildings.” Canadian Concrete Masonry Producers Association, Toronto, Canada, 317p (www.ccmpa.ca).

Anderson, D. L., and Priestley, M. J. N. (1992). “In plane shear strength of masonry walls.” Proceedings of the 6th Canadian Masonry Symposium, Saskatoon, Canada, pp. 223-234.

AS (Australian Standard). (2007). “Masonry structures.” AS 3700-2001, Sydney, Australia.

ASTM (American Society for Testing and Material). (2010). “Minimum design loads for buildings and other structures.” ASCE 7-10, American Society of Civil Engineers, Reston, Virginia, USA.

ASTM (American Society for Testing and Material). (2010). “Standard test methods for flexural bond strength of masonry.” E518-10, ASTM International, West Conshohocken, Pa., USA.

ASTM (American Society for Testing and Material). (2010). “Standard specification for grout for masonry.” C476-10, ASTM International, West Conshohocken, Pa., USA.

ASTM (American Society for Testing and Material). (2012). “Standard test method for compressive strength of cylindrical concrete specimens.” C39/C39M-12, ASTM International, West Conshohocken, Pa., USA.

ASTM (American Society for Testing and Material). (2012). “Standard test method for splitting tensile strength cylindrical concrete specimens.” C496/C496M-11, ASTM International, West Conshohocken, Pa., USA.

ASTM (American Society for Testing and Material). (2012). “Standard test method for compressive strength of masonry prisms.” C1314-12, ASTM International, West Conshohocken, Pa., USA.

ASTM (American Society for Testing and Material). (2013). “Standard test method for flow of hydraulic cement mortar.” C1437-13, ASTM International, West Conshohocken, Pa., USA.

ASTM (American Society for Testing and Material). (2013). “Standard specification for deformed and plain carbon-steel bars for concrete reinforcement.” A615/A615M-13, ASTM International, West Conshohocken, Pa., USA.

ASTM (American Society for Testing and Material). (2014). “Standard test methods and definitions for mechanical testing of steel products.” A370-14, ASTM International, West Conshohocken, Pa., USA.

ATC (Applied Technology Council). (1981). “Seismic design guidelines for highway bridges.” ATC-6, Berkeley, USA.

ATC (Applied Technology Council). (1998). “Evaluation of earthquake damaged concrete and masonry wall buildings.” Federal Emergency Management Agency FEMA-307, Washington, USA.

Banting, B. R. (2013). "Seismic performance quantification of concrete block masonry structural walls with confined boundary elements and development of the normal strain-adjusted shear strength expression (NSSSE)." Ph.D. thesis, McMaster University, Hamilton, Canada.

Banting, B. R., and El-Dakhakhni, W. W. (2012). "Force- and displacement-based seismic performance parameters for reinforced masonry structural walls with boundary elements." Journal of Structural Engineering (ASCE), Vol. 138, No. 12, pp. 1477-1491.

Bentz, E. C. (2000). "Sectional analysis of reinforced concrete structures." Ph.D. thesis, University of Toronto, Toronto, Canada.

Chen, J., Hidalgo, P. A., Mayes, R. L., Clough, R. W., and McNiven, H. D. (1978). "Cyclic loading tests of masonry single piers, Volume 2-height to width ratio of 1." Report No. UCB/EERC-78/28, Earthquake Engineering Research Centre, University of California, Berkeley, USA.

Chopra, A. K. (2007). "Dynamics of structures: Theory and applications to earthquake engineering." Third Edition, Pearson Prentice Hall, Upper Saddle River, New Jersey, USA.

Collins, M. P., and Mitchell, D. (1997). "Prestressed concrete structures." Response Publications, Canada, 766 pp.

Colotti, V. (2001). “Modeling of flexural and shear response in reinforced masonry walls under seismic loading.” The Masonry Society (TMS) Journal, Vol. 19, No. 1, pp. 37-48.

CSA (Canadian Standards Association). (2004). “Design of concrete structures.” CSA A23.3-04, CSA, Mississauga, Canada.

CSA (Canadian Standards Association). (2004). “Design of masonry structures.” CSA S304.1-04, CSA, Mississauga, Canada.

CSA (Canadian Standards Association). (2004). “Mortar and grout for unit masonry.” CSA A179-04, CSA, Mississauga, Canada.

CSA (Canadian Standards Association). (2014). “Concrete block masonry units.” CSA A165.1-14, CSA, Mississauga, Canada.

CSA (Canadian Standards Association). (2014). “Design of concrete structures.” CSA A23.3-14, CSA, Mississauga, Canada.

CSA (Canadian Standards Association). (2014). “Design of masonry structures.” CSA S304-14, CSA, Mississauga, Canada.

Davis, C. L. (2008). “Evaluation of design provisions for in-plane shear in masonry walls.” M.Sc. thesis, Washington State University, USA.

Dickie, J. E., and Lissel, S. L. (2011). “In-plane shear test method for reinforced concrete masonry and comparison of test results.” Proceedings of 9th Australasian Masonry Conference, Queenstown, New Zealand.

El-Dakhakhni, W. (2014). “Resilient reinforced concrete block shear wall systems for the next-generation of seismic codes.” Proceedings of 9th International Masonry Conference, Guimarães, Portugal.

ElMapruk, H. J. (2010). “Shear strength of partially grouted squat masonry shear walls.” M.Sc. thesis, Washington State University, USA.

Ewing, R. D., El-Mustapha, A. M., and Kariotis, J.C. (1988). “A finite element computer program for the nonlinear static analysis of reinforced masonry walls.” Proceedings of 8th International Brick and Block Masonry Conference, Dublin, Ireland, Vol. 3, pp 1119-1130.

Facconi, L. G., Plizzari, F., and Vecchio, F. (2013). “Disturbed stress field model for unreinforced masonry.” Journal of Structural Engineering (ASCE), Vol. 140, No. 4.

Fattal, S. G., and Todd, D. R. (1991). “Ultimate strength of masonry shear walls: Prediction vs test results.” NISTIR 4633, Building and Fire Research Laboratory, Gaithersburg, Md.

FEMA (Federal Emergency Management Agency). (2007). “Interim testing protocols for determining the seismic performance characteristics of structural and nonstructural components.” FEMA Report No. 461, Washington, USA.

FEMA (Federal Emergency Management Agency). (2009). “Quantification of building seismic performance factors.” FEMA P695, Washington, USA.

Fujisawa, M., Kawashima, T., and Yamaguchi, Y. (1986). “Seismic capacity of reinforced masonry walls: effect of shear span ratio.” Proceedings of 4th Canadian Masonry Symposium, Fredericton, Canada.

Galvez, J. C., Cervenka, J., Cendon, D. A., and Saouma, V. (2002). “A discrete crack approach to normal/shear cracking of concrete.” Cement and Concrete Research, Vol. 32, No. 10, pp. 1567-1585.

Güner, S. (2008). “Performance assessment of shear-critical reinforced concrete plane frames.” Ph.D. thesis, University of Toronto, Toronto, Canada.

Haach, V. (2009). “Development of a design method for reinforced masonry subjected to in-plane loading based on experimental and numerical analysis.” Ph.D. thesis, University of Minho, Guimarães, Portugal.

Haach, V., Vasconcelos, G., and Lourenço, P. (2010). “Experimental analysis of reinforced concrete block masonry walls subjected to in-plane cyclic loading.” Journal of Structural Engineering (ASCE), Vol. 136, No. 4, pp. 452-462.

Hidalgo, P. A., Mayes, R. L., McNiven, H. D., and Clough, R. W. (1978). “Cyclic loading tests of masonry single piers.” Volume 1, Report No. UCB/EERC-78/27, Earthquake Engineering Research Centre, University of California, Berkeley, USA.

Hidalgo, P. A., Mayes, R. L., McNiven, H. D., and Clough, R. W. (1979). “Cyclic loading tests of masonry single piers.” Volume 3, Report No. UCB/EERC-79/12, Earthquake Engineering Research Centre, University of California, Berkeley, USA.

Hognestad, E. (1951). “A study on combined bending and axial load in reinforced concrete members.” Bulletin series No. 399, University of Illinois, Engineering Experiment Station, IL, USA, 128 pp.

Hose, Y. D., and Seible, F. (1999). “Performance evaluation database for concrete bridge components and systems under simulated seismic loads.” Pacific Earthquake Engineering Research Center (PEER), Report No. 1999/11, College of Engineering, University of California, Berkley, USA.

Hoshikuma, J., Kawashima, K., Nagaya, K., and Taylor, A.W. (1997). “Stress-strain model for confined reinforced concrete in bridge piers”. Journal of Structural Engineering (ASCE), Vol. 123, No. 5, pp. 624-633.

Housner, G. W. (1956). “Limit design of structures to resist earthquakes.” Proceedings of the 1st World Conference on Earthquake Engineering, Earthquake Engineering Research Institute, Berkeley, USA, pp. 5-1 – 5-13.

Ingham, J. M., Davidson, B. J., Brammer, D. R., and Voon, K. C. (2001). “Testing and codification of partially grout-filled nominally-reinforced concrete masonry subjected to in-plane cyclic loads.” The Masonry Society (TMS) Journal, Vol. 19, No. 1, pp. 83-96.

Kaminosono, T., Teshigowara, M., Hiraishi, H., Fujisawa, M., and Nakaoka, A. (1988). “Experimental study on seismic performance of reinforced masonry walls.” Proceedings of the 9th World Conference on Earthquake Engineering, Tokyo-Kyoto, Japan, pp. 109-114.

Kaufmann, W., and Marti, P. (1998). "Structural concrete: cracked membrane model." Journal of Structural Engineering (ASCE), Vol. 124, No. 12, pp. 1467-1475.

Khattab, M.M., and Drysdale, R.G. (1993). "The effect of reinforcement on the shear response of grouted concrete masonry." The Masonry Society (TMS) Journal, Vol. 12, No.1, 38-44.

Kwon, M., and Spacone, E. (2002). "Three-dimensional finite element analyses of reinforced concrete columns." Computers and Structures. Vol. 80, No. 2, pp.199-212.

Liu, J. (2012). "The effect of height-to-thickness ratio on the compressive strength of concrete masonry." M.Sc. thesis, University of Windsor, Windsor, Canada.

Mander, J. B., Priestley, M. J. N., and Park. R. (1988). "Theoretical stress-strain model for confined concrete." Journal of Structural Engineering (ASCE), Vol. 114, No. 8, pp. 1804-1826.

Matsumura, A. (1985). "Effect of shear reinforcement in concrete masonry walls." First Joint Technical Coordinating Committee on Masonry Research-U.S.-Japan Coordinated Earthquake Research Program, Tokyo, Japan.

Matsumura, A. (1986). "Shear strength of reinforced hollow unit masonry walls." Second Meeting of the U.S.-Japan Joint Technical Coordinating Committee on Masonry Research, Keystone, USA.

Matsumura, A. (1988). “Effectiveness of shear reinforcement in fully grouted hollow clay masonry walls.” Fourth Meeting of the U.S.-Japan Joint Technical Coordinating Committee on Masonry Research, San Diego, USA, pp. 1-10.

Matsumura, A. (1988). “Shear strength of reinforced masonry walls.” Proceedings of the 9th World Conference on Earthquake Engineering, Vol. 7, Tokyo, Japan, pp. 121-126.

Minaie, E., Mota, M., Moon, F. L., and Hamid, A. A. (2010). “In-plane behavior of partially grouted reinforced concrete masonry shear walls.” Journal of Structural Engineering (ASCE), Vol. 136, No. 9, pp. 1089-1097.

Mitchell, D., Tremblay, R., Karacabeyli, E., Paultre, P., Saatcioglu, M., and Anderson, D. L. (2003). “Seismic force modification factors for the proposed 2005 edition of the National Building Code of Canada.” Canadian Journal of Civil Engineering, Vol. 30, No. 2, pp. 308–327.

Mosallam, A., and Banerjee, S. (2011). “Enhancement in in-plane shear capacity of unreinforced masonry (URM) walls strengthened with fiber reinforced polymer composites.” Composites: Part B, Vol. 42, No. 6, pp. 1657-1670.

MSJC (Masonry Standards Joint Committee). (2002). “Building code requirements for masonry structures.” TMS 402/ ACI 530/ASCE 5, The Masonry Society, American Concrete Institute, and American Society of Civil Engineers, Boulder, CO, Farmington Hills, MI, and Reston, VA, USA.

MSJC (Masonry Standards Joint Committee). (2013), “Building code requirements for masonry structures.” TMS 402/ ACI 530/ASCE 5, The Masonry Society, American

Concrete Institute, and American Society of Civil Engineers, Boulder, CO, Farmington Hills, MI, and Reston, VA, USA.

NBCC (National Building Code of Canada). (2010), National Research Council of Canada, Ottawa, Canada.

NEHRP (National Earthquake Hazards Reduction Program). (1997). “Recommended provisions for seismic regulations for new buildings and other structures, Part-1 provisions.” Building Seismic Safety Council, Washington, USA.

Nolph, S., and ElGawady, M. (2012). “Static cyclic response of partially grouted masonry shear walls.” Journal of Structural Engineering (ASCE), Vol. 138, No. 7, pp. 864-879.

Oan, A. (2013). "Diagonal shear of partially grouted concrete masonry panels." Ph.D. thesis, University of Calgary, Canada.

Oan, A. F., and Shrive, N. (2012). “Effect of construction method on shear resistance of concrete masonry walls.” Proceedings of 15th International Brick and Block Masonry Conference, Florianópolis, Brazil.

Okamoto, S., Yamazaki, Y., Kaminosono, T., Teshigawara, M., and Hirashi, H. (1987). “Seismic capacity of reinforced masonry walls and beams.” Proceedings of the 18th Joint Meeting of the U.S.-Japan Cooperative Program in Natural Resource Panel on Wind and Seismic Effects, NBSIR 87-3540, National Institute of Standards and Technology, Gaithersburg, pp. 307-319.

Palermo, D., and Vecchio, F. J. (2002). “Behaviour and analysis of reinforced concrete walls subjected to reversed cyclic loading.” Publication No. 2002-01, Department of Civil Engineering, University of Toronto, 351 pp.

Pauley, T., and Priestley, M. J. N. (1992). “Seismic design of reinforced concrete and masonry buildings.” Wiley, New York, 744 pp.

Popovics, S. (1973). “A numerical approach to the complete stress-strain curve of concrete.” Cement and Concrete Research, Vol. 3, No. 5, pp. 583-599.

Priestley, M. J. N., Verma, R., and Xiao, Y. (1994). “Seismic shear strength of reinforced concrete columns.” Journal of Structural Engineering (ASCE), Vol. 120, No. 8, pp. 2310-2329.

Priestley, N. (2003). “Myths and fallacies in earthquake engineering-conflicts between design and reality.” Bulletin of the New Zealand National Society for Earthquake Engineering (NZNSEE), Vol. 26, No. 3, pp. 329-341.

Priestley, N., Calvi, G., and Kowalsky, M. (2007). “Displacement-based seismic design of structures.” IUSS Press, Pavia, Italy.

Riddell, R. (2008). “Inelastic response spectrum: Early history.” Earthquake Engineering and Structural Dynamics, Vol. 37, No. 8, pp. 1175-1183.

Rots, J. G., and Blaauwendraad, J. (1989). “Crack models for concrete: discrete or smeared? fixed, multi-directional or rotating?.” Heron Journal, Vol. 34, No. 1.

SANZ (Standards Association of New Zealand). (2004). “Design of reinforced concrete masonry structures.” NZS 4230:2004, Wellington, New Zealand.

Sarhat, S. R., and Sherwood, E. G. (2010). “Effective shear design of reinforced masonry beams.” The Masonry Society (TMS) Journal, Vol. 28, No. 2, pp. 27-39.

Scott, B. D., Park, R., and Priestley, M. J. N. (1982). “Stress-strain behavior of concrete confined by overlapping hoops at low and high strain rates.” American Concrete Institute (ACI) Journal, Vol. 79, No. 1, pp. 13-27.

Seckin, M. (1981). “Hysteretic behaviour of cast-in-place exterior beam-column-slab subassemblies.” Ph.D. thesis, University of Toronto, Toronto, Canada.

Shedid, M. T. (2009). “Ductility of concrete block shear wall structures.” Ph.D. thesis, McMaster University, Hamilton, Canada.

Shedid, M. T., El-Dakhakhni, W. W., and Drysdale, R. G. (2010). “Alternative strategies to enhance the seismic performance of reinforced concrete-block shear wall systems.” Journal of Structural Engineering (ASCE), Vol. 136, No. 6, pp. 676-689.

Shing P. B., Lotfi, H. R., Lofti, A., Barzegarmehrabi, A., and Bunner, J. (1992). “Finite element analysis of shear resistance of masonry wall panels with and without confining frames.” Proceedings of 10th World Conference on Earthquake Engineering, Colorado, USA. pp 2581-2586.

Shing, P. B., Brunner, J. D., and Lotfi, H. R. (1993). "Evaluation of shear strength of reinforced masonry walls." The Masonry Society (TMS) Journal, Vol. 12, No. 1, pp. 65-77.

Shing, P. B., Klamerua, E., Spaeh, H., and Noland, J. L. (1988). "Seismic performance of reinforced masonry shear walls." Proceedings of the 9th World Conference on Earthquake Engineering, Vol. 7, Tokyo, Japan, pp. 103-108.

Shing, P. B., Noland, J. L., Klamerus, E., and Schuller, M. (1989). "Inelastic behaviour of concrete masonry shear walls." Journal of Structural Engineering (ASCE), Vol. 15, pp. 2204-2225.

Shing, P. B., Noland, J. L., Spaech, H., Klamerus, E., and Schuller, M. (1991). "Response of single-story reinforced masonry shear walls to in-plane lateral loads." TCCMAR Report No. 3.1(a)-2.

Shing, P. B., Schuller, M., and Hoskere, V. S. (1990). "In-plane resistance of reinforced masonry shear walls." Journal of Structural Engineering (ASCE), Vol. 116, No. 3, pp. 619-640.

Shing, P. B., Schuller, M., and Hoskere, V. S. (1990). "Strength and ductility of reinforced masonry shear walls." Proceedings of the 5th North America Masonry Conference, University of Illinois, Urbana-Champaign, pp. 309-320.

Sveinsson, B. I., Mayes, R. L., and McNiven, H. D. (1985). "Cyclic loading of masonry single piers – Volume 4: Additional tests with height to width ratio of 1." Report No.

UCB/EERC-85/15, Earthquake Engineering Research Centre, University of California, Berkeley. USA.

Tabinashi, R. (1956). “Studies on the nonlinear vibrations of structures subjected to destructive earthquakes.” Proceedings of the 1st World Conference on Earthquake Engineering, Earthquake Engineering Research Institute, Berkeley, USA, pp. 6-1 – 6-16.

Tassios, T., and Vintzēleou, E. (1987). “Concrete-to-Concrete Friction.” Journal of Structural Engineering (ASCE), Vol. 113, No. 4, pp. 832-849.

Uniform Building Code. (UBC). (1997). “International conference of building officials.” Volume 2, Whittier, USA.

Vecchio, F. J. (1992). “Finite element modeling of concrete expansion and confinement.” Journal of Structural Engineering (ASCE), Vol. 118, No. 9, pp. 2390-2406.

Vecchio, F. J. (1999). “Towards cyclic load modeling of reinforced concrete.” American Concrete Institute (ACI) Structural Journal, Vol. 96, No. 2, pp. 193-202.

Vecchio, F. J. (2000). “Disturbed stress field model for reinforced concrete: formulation.” Journal of Structural Engineering (ASCE), Vol. 126, No. 9, pp. 1070-1077.

Vecchio, F. J., and Collins, M. P. (1986). “The modified compression-field theory for reinforced concrete elements subject to shear.” American Concrete Institute (ACI) Journal, Vol. 83, No. 2, pp. 219-231.

Veletsos, A. S., and Newmark, N. M. (1960). "Effect of inelastic behaviour on the response of simple systems to earthquake motions." Proceedings of the 2nd World Conference on Earthquake Engineering, Science Council of Japan, Japan, Vol. 2, pp. 895-912.

Vliet, M. R. A. (2004). "Shear tests on masonry panels; literature survey and proposal for experiments." TNO Building and Construction Research, Report No. 2004-CI-R0171.

Voon, K. C. (2007). "In-plane seismic design of concrete masonry structures." Ph.D. thesis, The University of Auckland, Auckland, New Zealand.

Voon, K. C., and Ingham, J. M. (2001). "Towards suitable shear strength provisions for inclusion in the New Zealand masonry design standard." Proceedings of the 6th Australasian Masonry Conference, Adelaide, South Australia, pp. 393-402.

Voon, K. C., and Ingham, J. M. (2003). "Shear strength of concrete masonry walls." School of Engineering Report No. 611, University of Auckland, New Zealand.

Voon, K. C., and Ingham, J. M. (2006). "Experimental in-plane shear strength investigation of reinforced concrete masonry walls." Journal of Structural Engineering (ASCE), Vol. 132, No. 3, pp. 400-408.

Voon, K. C., and Ingham, J. M. (2007). "Design expression for the in-plane shear strength of reinforced concrete masonry." Journal of Structural Engineering (ASCE), Vol. 133, No. 5, pp. 706-713.

Wong, P. S., Vecchio, F. J., and Trommels, H. (2013). "VecTor2 & formworks user's manual." Second Edition, Dept. of Civil Engineering, University of Toronto, Toronto, Canada.

APPENDIX A

PROPERTIES OF AVAILABLE TEST RESULTS

This appendix provides more details related to Chapter 6. To verify the accuracy of the proposed equation for predicting the in-plane shear strength of RM shear walls, a brief survey of previous experimental work on fully grouted RM walls dominated by shear failure was conducted, which resulted in a total of 64 reliable RM walls and piers, in addition to the nine tested RM walls in this study. The test results were collected from the following six sources:

1. Twenty one piers were tested by Sveinsson et al., (1985) at the University of California at Berkeley;
2. Eighteen piers were tested by Matsumura (1985) at Japan's Building Research Institute, Ministry of Construction;
3. Eight piers were tested by Okamoto et al. (1987) at Japan's Building Research Institute, Ministry of Construction;
4. Ten cantilever walls were tested by Shing et al. (1990) at the University of Colorado;
5. Seven cantilever walls were tested by Voon and Ingham (2006) at the University of Auckland;
6. Nine cantilever walls were tested in this study at Concordia University.

Sveinsson et al. (1985) defined the displacement ductility as a ratio of the maximum relative lateral displacement experienced by the tested wall before failure to the crack displacement without considering the first yield point of vertical reinforcement, which results in overestimating the displacement ductility, μ_Δ. In addition, the failure point was not clearly defined since all walls were loaded until the first demand lateral displacement after the strength degradation was initiated. Although the experimental lateral force-displacement envelope for each of the tested walls was reported in their test results, only the crack point was defined in each envelope. Hence, for more reasonable values of μ_Δ for the verification purpose of the studied equations, the equivalent elastic-perfectly plastic response using the idealized equal energy effective stiffness was generated for each wall using the given experimental lateral force-displacement envelope. Thus, the experimental displacement ductility, $\mu_{\Delta e}$, was taken as equal to the idealized one, $\mu_{\Delta id}^{ep}$. All the generated equivalent elastic-perfectly plastic responses of the walls tested by Sveinsson et al. (1985) are presented in Figures A.1 and A.2.

Table A.1 provides all the properties of the 73 RM walls used in this analysis. Out of the 73 walls, 20 walls were constructed using clay brick masonry units, while the others were built with concrete blocks. The shaded rows represent the tested RM clay brick walls. The predicted in-plane shear resistances provided by masonry, V_m, axial compression load, V_p, horizontal reinforcement, V_s, and the nominal shear strength, V_n, for each wall were calculated using the ten equations given in Table 6.1 along with the proposed equation in Chapter 6, and presented separately in Tables A.2, A.3, A.4, and A.5, respectively. A comparison between the accuracy of the eleven equations in terms of $V_{experimental}/V_{predicted}$ is given in Table A.6.

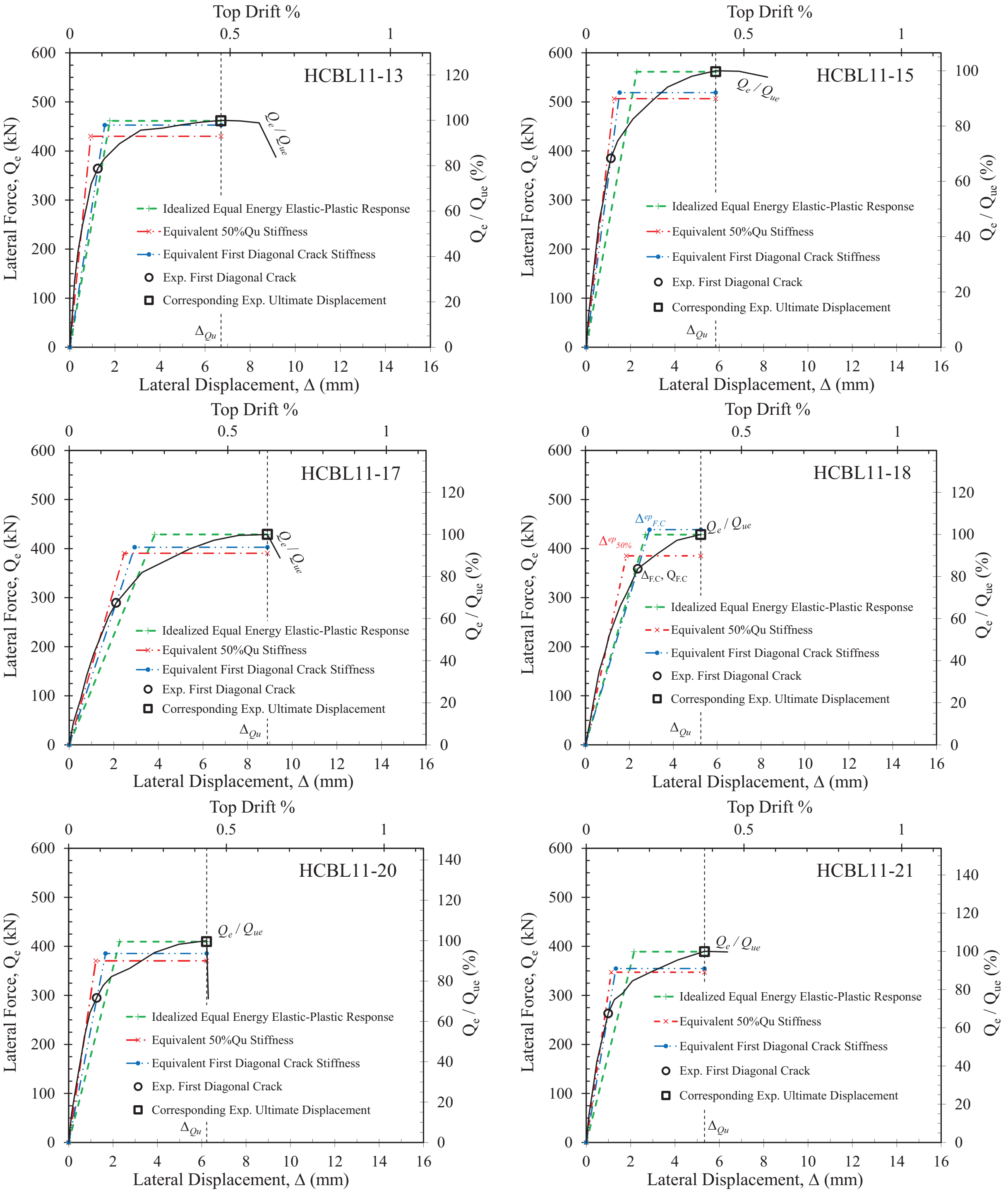

Figure A.1: The equivalent elastic-perfectly plastic responses for the concrete block RM piers tested by Sveinsson et al. (1985) using the idealized equal energy effective stiffness

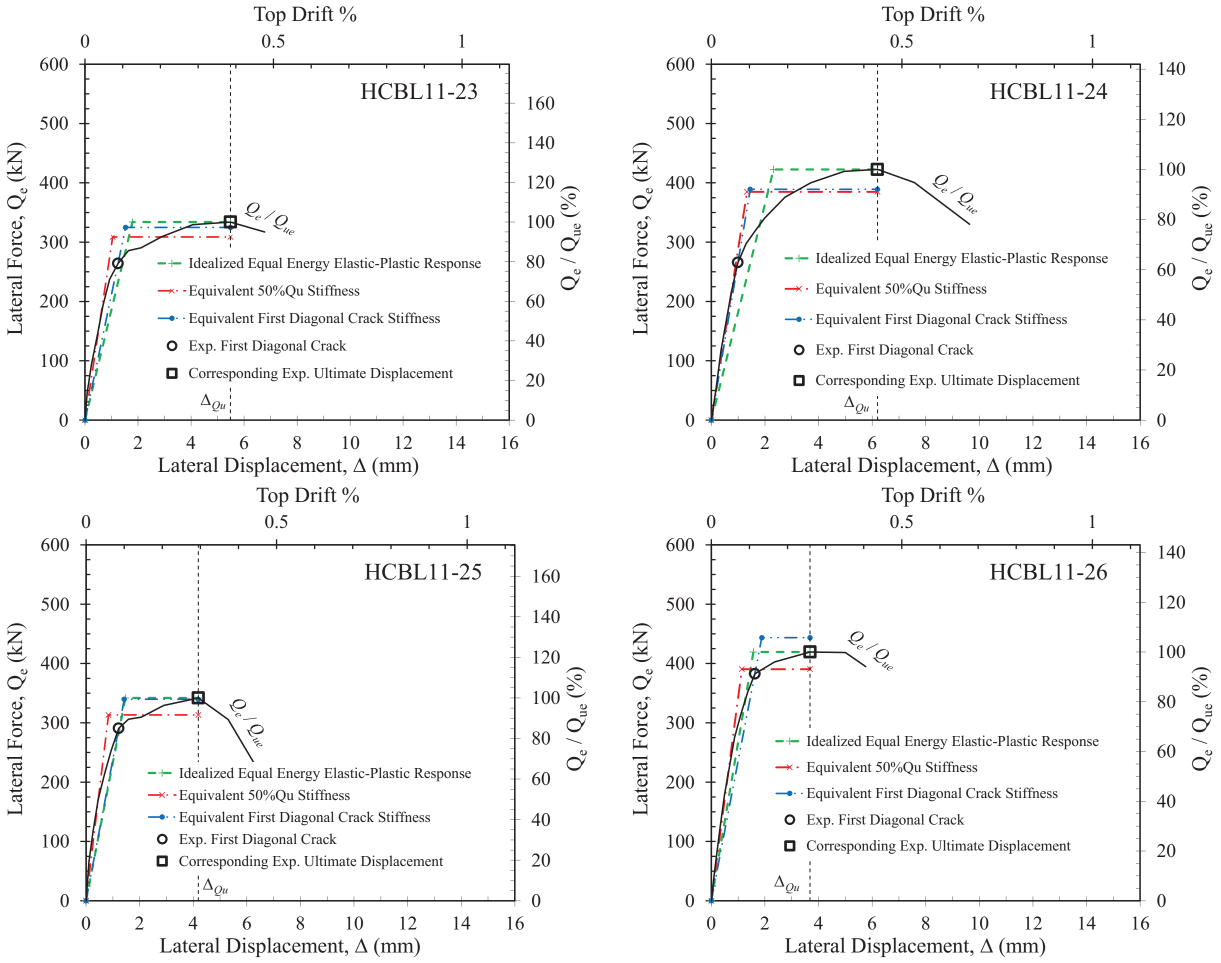

Figure A.1(continued): The equivalent elastic-perfectly plastic responses for the concrete block RM piers tested by Sveinsson et al. (1985) using the idealized equal energy effective stiffness

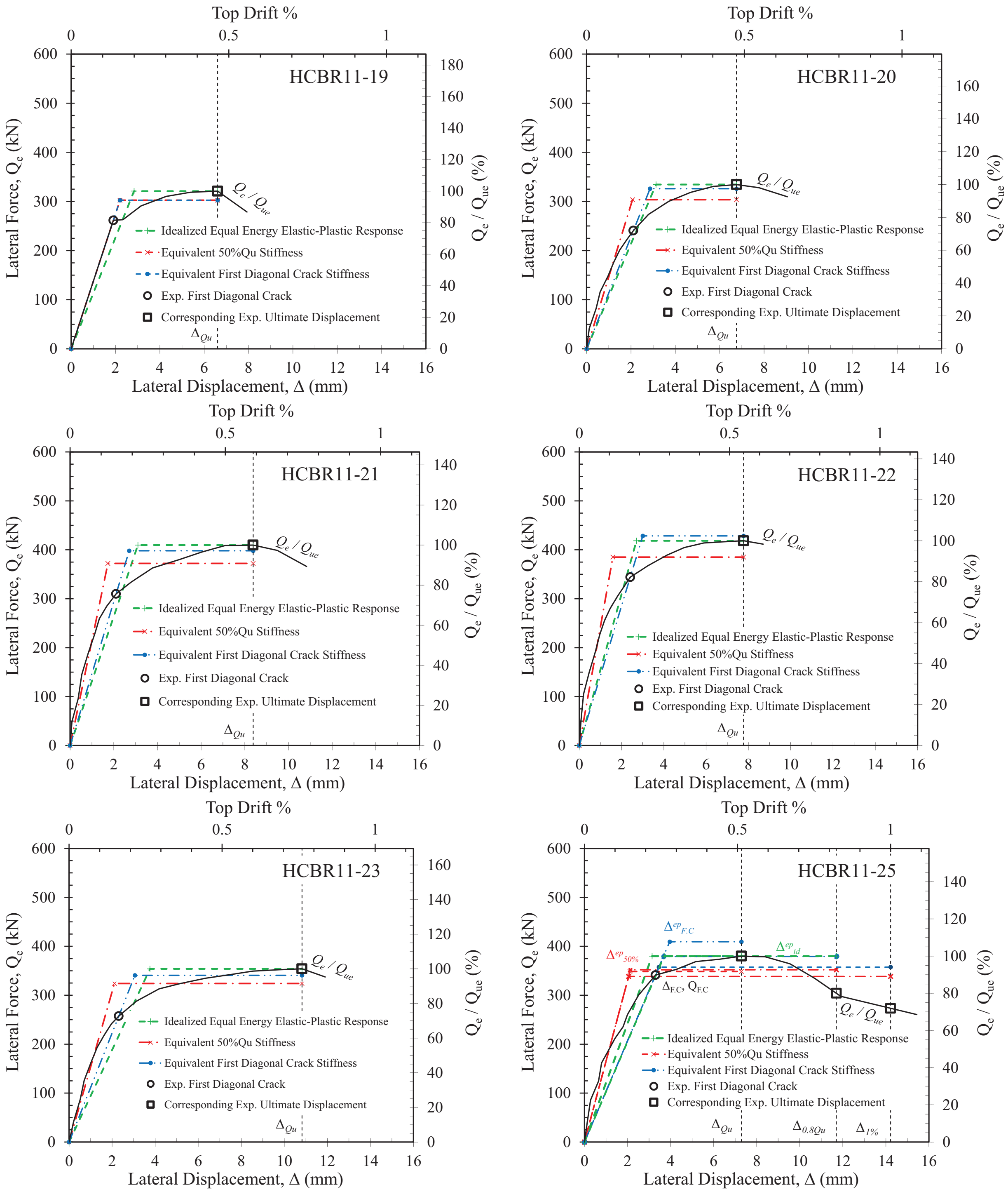

Figure A.2: The equivalent elastic-perfectly plastic responses for the clay brick RM piers tested by Sveinsson et al. (1985) using the idealized equal energy effective stiffness

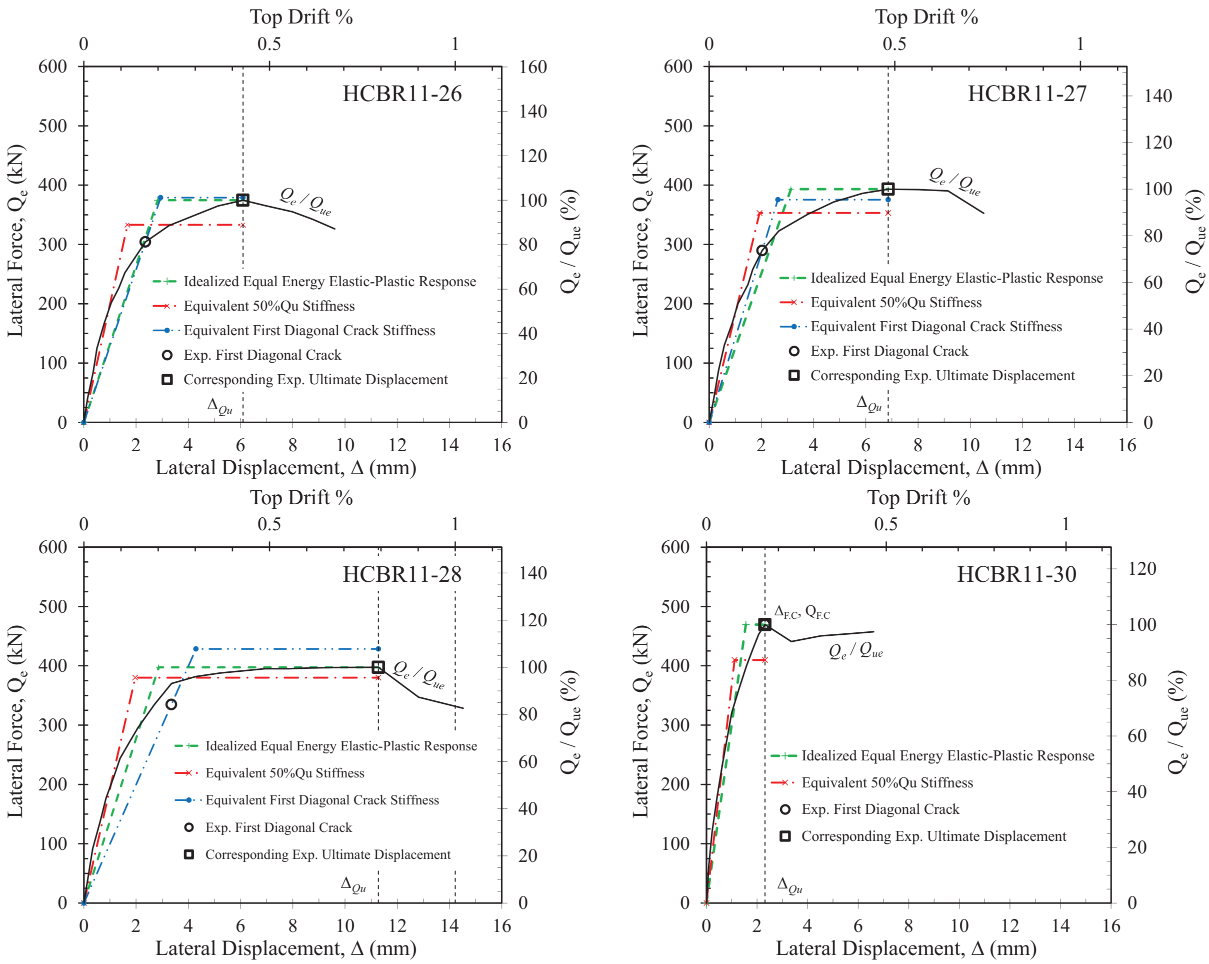

Figure A.2(continued): The equivalent elastic-perfectly plastic responses for the clay brick RM piers tested by Sveinsson et al. (1985) using the idealized equal energy effective stiffness

Table A.1: Properties of Studied RM Walls in the Experimental Database

Source	Specimen no.*	Specimen label	Mode of failure**	Specimen dimensions				Reinforcement								V_{max}
				h_w	lw	b_w	d	ρ_v	f_{yv}	ρ_h	S_h	f_{yh}	f'_m	σ_n	μ_Δ	
				mm	mm	mm	mm	%	MPa	%	mm	MPa	MPa	MPa	___	kN
Sveinsson et al., (1985)	1	HCBL-11-13	S	1422	1219	194	1143	0.18	465	0.29	407	356	23.2	1.88	3.8	461
	2	HCBL-11-15	S	1422	1219	194	1143	0.18	465	0.29	407	356	23.2	3.01	2.6	561
	3	HCBL-11-17	S	1422	1219	143	1143	0.47	391	0.39	438	359	15.8	2.76	2.3	429
	4	HCBL-11-18	S	1422	1219	143	1143	0.47	410	0.39	438	359	15.8	2.76	1.9	428
	5	HCBL-11-20	S	1422	1219	143	1143	0.47	391	0.20	438	700	15.1	2.76	2.7	410
	6	HCBL-11-21	S	1422	1219	143	1143	0.47	410	0.20	438	700	15.1	2.76	2.5	389
	7	HCBL-11-23	S	1422	1219	143	1143	0.47	391	0.08	438	146	15.1	2.76	3.1	334
	8	HCBL-11-24	S	1422	1219	143	1143	0.47	391	0.27	438	146	15.1	2.76	2.7	423
	9	HCBL-11-25	S	1422	1219	143	1143	0.47	391	0.20	438	700	15.1	1.74	2.9	342
	10	HCBL-11-26	S	1422	1219	143	1143	0.47	391	0.20	438	700	15.1	2.76	2.3	419
	11	HCBR-11-19	S	1422	1219	143	1143	0.47	391	0.20	438	700	20.1	2.76	2.6	321
	12	HCBR-11-20	S/S	1422	1219	143	1143	0.47	391	0.49	438	286	20.1	2.76	2.2	334
	13	HCBR-11-21	S	1422	1219	143	1143	0.72	391	0.20	438	700	20.1	2.76	2.7	410
	14	HCBR-11-22	S/S	1422	1219	143	1143	0.49	438	0.49	438	286	20.1	2.76	2.9	418
	15	HCBR-11-23	S	1422	1219	143	1143	0.47	410	0.20	438	700	20.1	2.76	2.9	354
	16	HCBR-11-24	S/S	1422	1219	143	1143	0.47	410	0.49	438	286	20.1	2.76	2.8	384
	17	HCBR-11-25	S	1422	1219	143	1143	0.47	391	0.20	438	700	20.1	2.76	2.3	380
	18	HCBR-11-26	S/S	1422	1219	143	1143	0.47	391	0.49	438	286	20.1	2.76	2.2	374
	19	HCBR-11-27	S	1422	1219	143	1143	0.47	391	0.25	410	361	20.1	2.76	2.2	393
	20	HCBR-11-28	S/S	1422	1219	143	1143	0.24	410	0.62	417	146	20.1	2.76	3.9	397
	21	HCBR-11-30	S	1422	1219	143	1143	0.47	391	0.10	438	146	27.6	2.76	1.5	469
Matsumura (1986)	22	KW4-1	S	1800	1590	150	1500	1.00	385	0.12	385	400	21.8	0.49	2.5	403
	23	KW3-1	S	1800	1190	150	1100	1.02	385	0.12	385	400	21.8	0.49	2.5	263
	24	KW3S-1	S	1800	1190	150	1100	1.02	385	0.12	385	400	21.8	0.49	2.5	290
	25	KW2-1	S	1800	790	150	700	1.29	385	0.12	385	400	21.8	0.49	2.5	174
	26	WS2	S	1800	1190	190	1095	0.74	370	0.00	0	0	22.3	1.96	2.5	324
	27	WS4	S	1800	1190	190	1095	0.74	370	0.17	340	400	22.3	1.96	2.5	447
	28	WS5	S	1800	1190	190	1095	0.74	370	0.33	340	200	22.3	1.96	2.5	502
	29	WS9	S	1800	1190	190	1095	1.17	367	0.33	340	200	22.3	1.96	2.5	505
	30	WS10	S	1800	1190	190	1095	1.17	367	0.67	340	200	22.3	1.96	2.5	637
	31	WS9-2	S	1800	1190	190	1095	0.96	385	0.33	385	400	29.0	1.96	2.5	548
	32	WSB21	S	1800	1190	190	1095	0.96	385	0.33	385	400	26.1	1.96	2.5	486
	33	WSB22	S	1800	1190	190	1095	0.96	385	0.40	385	400	27.4	1.96	2.5	594
	34	WSB3	S	1800	1190	190	1095	1.01	385	0.35	385	400	26.4	1.96	2.5	534
	35	WSB4	S	1800	1190	190	1095	0.96	385	0.33	385	400	31.4	1.96	2.5	587
	36	WSR2-2	S	1700	1110	190	1000	1.30	363	0.00	0	0	26.4	1.96	3.8	450
	37	WSR4-2	S	1700	1110	190	1000	1.30	363	0.17	354	400	26.4	1.96	2.6	448
	38	WSR5-2	S	1700	1110	190	1000	1.30	363	0.34	354	200	26.4	1.96	2.3	485
	39	WSR6-2	S	1700	1110	190	1000	1.30	363	0.68	354	200	26.4	1.96	1.9	519

Specimens with gray shading were constructed with clay brick

* S for diagonal shear failure and S/S for diagonal/sliding shear failure

Table A.1(continued): Properties of Studied RM Walls in the Experimental Database

Source	Specimen no.	Specimen label	Mode of failure *	Specimen dimensions				Reinforcement								V_{max}
				h_w	lw	b_w	d	ρ_v	f_{yv}	ρ_h	S_h	f_{yh}	f'_m	σ_n	μ_Δ	
				mm	mm	mm	mm	%	MPa	%	mm	MPa	MPa	MPa	___	kN
Okomoto (1987)	40	WS1	S	1800	2000	190	1905	0.53	379	0.17	400	355	17.9	0.00	2.5	1018
	41	WS4	S	1800	1200	190	1105	0.73	379	0.17	400	355	22.8	1.96	2.5	449
	42	WS7	S	1800	800	190	705	1.00	379	0.17	400	355	17.9	0.00	2.5	311
	43	WSN1	S	1800	1200	190	1105	0.73	379	0.17	400	355	22.8	3.92	2.5	548
	44	WSN2	S	1800	1200	190	1105	0.73	379	0.17	400	355	22.8	5.88	2.5	596
	45	WSR1	S	1800	2000	190	1905	0.53	379	0.17	400	355	26.8	0.00	2.5	1189
	46	WSR4	S	1800	1200	190	1105	0.73	379	0.17	400	355	25.2	0.00	2.5	529
	47	WSR7	S	1800	800	190	705	1.00	379	0.17	400	355	21.4	0.00	2.5	310
Shing et al. (1990)	48	S-3	S	1830	1830	143	1727	0.78	496	0.12	406	386	20.7	1.86	2.5	456
	49	S-4	S	1830	1830	143	1727	0.78	496	0.12	406	386	17.9	0.00	3.2	354
	50	S-5	S	1830	1830	143	1727	0.78	496	0.12	406	386	17.9	0.69	2.5	385
	51	S-7	S	1830	1830	143	1727	0.78	496	0.12	406	386	20.7	0.69	2.6	431
	52	S-9	S	1830	1830	143	1727	0.40	441	0.12	406	386	20.7	1.86	3.4	427
	53	S-13	S	1830	1830	143	1727	0.57	448	0.22	406	462	22.8	1.86	4.8	500
	54	S-14	S	1830	1830	143	1727	0.57	448	0.12	406	386	22.8	1.86	2.8	467
	55	S-16	S	1830	1830	143	1727	0.78	496	0.22	406	462	17.2	1.86	3.3	536
	56	S-21	S	1830	1830	137	1727	0.60	448	0.13	406	386	26.2	1.93	3.2	469
	57	S-22	S	1830	1830	137	1727	0.60	448	0.13	406	386	26.2	0.69	3.9	407
Voon and Ingham (2006)	58	A1	S	1800	1800	140	1700	0.62	318	0.05	400	325	17.6	0.00	2.7	210
	59	A2	S	1800	1800	140	1700	0.62	318	0.01	1800	325	17.6	0.00	2.6	186
	60	A4	S	1800	1800	140	1700	0.62	318	0.06	800	310	17.0	0.00	2.6	212
	61	A7	S	1800	1800	140	1700	0.62	318	0.05	400	325	18.8	0.50	2.7	262
	62	A8	S	1800	1800	140	1700	0.62	318	0.05	400	325	18.8	0.25	2.7	247
	63	A9	S	3600	1800	140	1700	0.97	550	0.05	400	325	24.3	0.25	2.9	206
	64	A10	S	1800	3000	140	2900	0.59	318	0.05	400	325	24.3	0.25	1.3	585
Current study	65	W-Ref	S	1600	1800	190	1700	0.84	430	0.13	400	430	13.1	1.00	4.2	414
	66	W-ρ_h0	S	1600	1800	190	1700	0.84	430	0.00	0.0	0.0	13.1	1.00	3.0	366
	67	W-σ_n0	S	1600	1800	190	1700	0.84	430	0.13	400	430	13.1	0.00	4.1	340
	68	W-σ_n1.5	S	1600	1800	190	1700	0.84	430	0.13	400	430	13.1	1.50	3.4	455
	69	W-M/Vd_v1.8	S	1600	1800	190	1700	0.84	430	0.13	400	430	13.1	1.00	5.2	303
	70	W-90°	S	1600	1800	190	1700	0.84	430	0.13	400	430	13.1	1.00	3.9	409
	71	W-Str	S	1600	1800	190	1700	0.84	430	0.13	400	430	13.1	1.00	3.6	389
	72	W-S_v800	S	1600	1800	190	1700	0.84	430	0.13	800	430	13.1	1.00	3.4	381
	73	W-S_h800	S	1600	1800	190	1700	0.65	430	0.13	800	430	13.1	1.00	2.3	352

Specimens with gray shading were constructed with clay brick

* S for diagonal shear failure and S/S for diagonal/sliding shear failure

Table A.2: Predicted In-Plane Shear Resistance Provided by Masonry (V_m)

Source	Specimen no.	Specimen label	μ_Δ	V_m (kN)									
				Matsumura (1988)	Shing et al. (1990)	Anderson and Priestley (1992)	NEHRP (1997) MSJC (2013)	UBC (1997)	AS3700-2001	CSA S304-14	NZS 4230:2004	Voon and Ingham (2007)	Proposed Equation
Sveinsson et al., (1985)	1	HCBL-11-13	3.8	212	208	31	281	170	216	92	20	20	102
	2	HCBL-11-15	2.6	212	208	196	281	170	216	112	129	129	157
	3	HCBL-11-17	2.3	173	141	140	171	104	160	76	101	101	112
	4	HCBL-11-18	1.9	124	142	166	171	104	160	89	126	126	125
	5	HCBL-11-20	2.7	169	138	105	168	102	160	63	76	76	98
	6	HCBL-11-21	2.5	121	139	124	168	102	160	70	91	91	106
	7	HCBL-11-23	3.1	169	138	76	168	102	160	55	55	55	87
	8	HCBL-11-24	2.7	169	138	108	168	102	160	64	78	78	99
	9	HCBL-11-25	2.9	169	138	93	168	102	160	59	67	67	94
	10	HCBL-11-26	2.3	169	138	134	168	102	160	73	97	97	109
	11	HCBR-11-19	2.6	194	159	64	193	117	160	75	93	93	116
	12	HCBR-11-20	2.2	194	159	86	193	117	160	90	125	125	132
	13	HCBR-11-21	2.7	194	174	61	193	117	160	73	96	96	122
	14	HCBR-11-22	2.9	160	164	53	193	117	160	68	78	78	110
	15	HCBR-11-23	2.9	140	161	52	193	117	160	67	76	76	108
	16	HCBR-11-24	2.8	140	161	58	193	117	160	71	84	84	112
	17	HCBR-11-25	2.3	194	159	79	193	117	160	85	114	114	126
	18	HCBR-11-26	2.2	194	159	87	193	117	160	90	125	125	132
	19	HCBR-11-27	2.2	194	159	85	193	117	160	89	123	123	131
	20	HCBR-11-28	3.9	160	146	3	193	117	160	64	4	4	66
	21	HCBR-11-30	1.5	228	187	110	226	137	160	149	200	200	181
Matsumura (1986)	22	KW4-1	2.5	346	273	200	278	170	223	115	171	171	199
	23	KW3-1	2.5	210	204	150	185	103	133	70	118	118	150
	24	KW3S-1	2.5	210	204	150	185	103	133	70	118	118	150
	25	KW2-1	2.5	105	145	100	103	55	43	44	75	75	86
	26	WS2	2.5	228	235	192	237	132	168	90	137	137	176
	27	WS4	2.5	228	235	192	237	132	168	90	137	137	176
	28	WS5	2.5	228	235	192	237	132	168	90	137	137	176
	29	WS9	2.5	270	269	192	237	132	168	90	155	155	197
	30	WS10	2.5	270	269	192	237	132	168	90	155	155	197
	31	WS9-2	2.5	308	292	219	270	150	168	103	169	169	215
	32	WSB21	2.5	292	277	208	257	142	168	97	160	160	204
	33	WSB22	2.5	300	284	213	263	146	168	100	164	164	209
	34	WSB3	2.5	299	283	209	258	143	168	98	164	164	208
	35	WSB4	2.5	321	304	228	281	156	168	107	176	176	224
	36	WSR2-2	3.8	271	280	98	239	130	155	90	161	161	205
	37	WSR4-2	2.6	271	280	98	239	130	155	90	161	161	205
	38	WSR5-2	2.3	271	280	98	239	130	155	90	161	161	205
	39	WSR6-2	1.9	271	280	98	239	130	155	90	161	161	205

Specimens with gray shading were constructed with clay brick

Table A.2(continued): Predicted In-Plane Shear Resistance Provided by Masonry (V_m)

Source	Specimen no.	Specimen label	μ_Δ	V_m (kN)									
				Matsumura (1988)	Shing et al. (1990)	Anderson and Priestley (1992)	NEHRP (1997) MSJC (2013)	UBC (1997)	AS3700-2001	CSA S304-14	NZS 4230:2004	Voon and Ingham (2007)	Proposed Equation
Okomoto (1987)	40	WS1	2.5	423	335	290	429	273	399	185	227	227	251
	41	WS4	2.5	233	241	196	243	135	171	93	141	141	180
	42	WS7	2.5	109	153	116	120	64	57	52	79	79	92
	43	WSN1	2.5	233	241	196	243	135	171	93	141	141	180
	44	WSN2	2.5	233	241	196	243	135	171	93	141	141	180
	45	WSR1	2.5	517	409	177	524	334	399	226	277	277	307
	46	WSR4	2.5	245	254	103	255	142	171	97	148	148	189
	47	WSR7	2.5	119	168	63	131	70	57	56	86	86	100
Shing et al. (1990)	48	S-3	2.5	290	292	214	222	119	262	95	151	151	187
	49	S-4	3.2	270	272	106	207	110	262	71	75	75	139
	50	S-5	2.5	270	272	199	207	110	262	89	140	140	174
	51	S-7	2.6	290	292	200	222	119	262	91	141	141	182
	52	S-9	3.4	238	241	86	222	119	262	76	49	49	116
	53	S-13	4.8	277	273	0	233	124	262	80	0	0	60
	54	S-14	2.8	277	273	180	233	124	262	88	111	111	161
	55	S-16	3.3	265	267	91	203	108	262	70	64	64	132
	56	S-21	3.2	289	284	62	240	128	251	82	77	77	146
	57	S-22	3.9	289	284	8	240	128	251	82	10	10	110
Voon and Ingham (2006)	58	A1	2.7	241	218	169	197	105	252	79	101	106	134
	59	A2	2.6	241	218	176	197	105	252	81	103	121	137
	60	A4	2.6	237	215	176	194	103	252	80	103	102	135
	61	A7	2.7	249	226	167	204	109	252	79	98	101	136
	62	A8	2.7	249	226	167	204	109	252	79	98	103	136
	63	A9	2.9	204	342	170	232	124	126	85	131	134	123
	64	A10	1.3	549	425	497	507	311	504	331	466	470	410
Current study	65	W-Ref	4.2	276	297	0	231	123	361	79	0	0	98
	66	W-ρ_h0	3.0	276	297	145	231	123	361	79	100	100	162
	67	W-σ_n0	4.1	276	297	0	231	123	361	79	0	0	102
	68	W-σ_n1.5	3.4	276	297	84	231	123	361	79	57	57	139
	69	W-M/Vd_v1.8	5.2	276	297	0	231	123	361	79	0	0	30
	70	W-90°	3.9	276	297	10	231	123	361	79	7	7	112
	71	W-Str	3.6	276	297	58	231	123	361	79	40	40	130
	72	W-S_v800	3.4	276	297	495	231	123	361	79	66	66	144
	73	W-S_h800	2.3	356	276	2338	231	123	361	106	159	159	187

Specimens with gray shading were constructed with clay brick

Table A.3: Predicted In-Plane Shear Resistance Provided by Axial Compression Load (V_p)

Source	Specimen no.	Specimen label	μ_Δ	V_p (kN)									
				Matsumura (1988)	Shing et al. (1990)	Anderson and Priestley (1992)	NEHRP (1997) MSJC (2013)	UBC (1997)	AS3700-2001	CSA S304-14	NZS 4230:2004	Voon and Ingham (2007)	Proposed Equation
Sveinsson et al., (1985)	1	HCBL-11-13	3.8	73	46	111	111			50	287	287	151
	2	HCBL-11-15	2.6	117	74	178	178			97	353	353	286
	3	HCBL-11-17	2.3	79	41	120	120			73	178	178	155
	4	HCBL-11-18	1.9	79	41	120	120			85	178	178	171
	5	HCBL-11-20	2.7	79	41	120	120			62	170	170	132
	6	HCBL-11-21	2.5	79	41	120	120			68	170	170	142
	7	HCBL-11-23	3.1	79	41	120	120			54	170	170	118
	8	HCBL-11-24	2.7	79	41	120	120			63	170	170	134
	9	HCBL-11-25	2.9	50	26	76	76			37	170	170	126
	10	HCBL-11-26	2.3	79	41	120	120			72	170	170	147
	11	HCBR-11-19	2.6	79	47	120	120			64	226	226	180
	12	HCBR-11-20	2.2	79	47	120	120			77	226	226	205
	13	HCBR-11-21	2.7	79	47	120	120			62	226	226	176
	14	HCBR-11-22	2.9	79	47	120	120			57	226	226	167
	15	HCBR-11-23	2.9	79	47	120	120			57	226	226	167
	16	HCBR-11-24	2.8	79	47	120	120			60	226	226	172
	17	HCBR-11-25	2.3	79	47	120	120			72	226	226	197
	18	HCBR-11-26	2.2	79	47	120	120			77	226	226	205
	19	HCBR-11-27	2.2	79	47	120	120			76	226	226	204
	20	HCBR-11-28	3.9	79	47	120	120			54	226	226	110
	21	HCBR-11-30	1.5	79	55	120	120			108	310	310	329
Matsumura (1986)	22	KW4-1	2.5	19	12	29	29			16	78	78	64
	23	KW3-1	2.5	14	9	22	22			12	43	43	36
	24	KW3S-1	2.5	14	9	22	22			12	43	43	36
	25	KW2-1	2.5	9	6	15	15			8	18	18	16
	26	WS2	2.5	71	45	111	111			62	216	216	182
	27	WS4	2.5	71	45	111	111			62	216	216	182
	28	WS5	2.5	71	45	111	111			62	216	216	182
	29	WS9	2.5	71	45	111	111			62	216	216	182
	30	WS10	2.5	71	45	111	111			62	216	216	182
	31	WS9-2	2.5	71	52	111	111			62	216	216	182
	32	WSB21	2.5	71	49	111	111			62	216	216	182
	33	WSB22	2.5	71	50	111	111			62	216	216	182
	34	WSB3	2.5	71	49	111	111			62	216	216	182
	35	WSB4	2.5	71	54	111	111			62	216	216	182
	36	WSR2-2	3.8	65	46	103	103			58	195	195	168
	37	WSR4-2	2.6	65	46	103	103			58	195	195	168
	38	WSR5-2	2.3	65	46	103	103			58	195	195	168
	39	WSR6-2	1.9	65	46	103	103			58	195	195	168

Specimens with gray shading were constructed with clay brick

Table A.3(continued): Predicted In-Plane Shear Resistance Provided by Axial Compression Load (V_p)

Source	Specimen no.	Specimen label	μ_Δ	V_p (kN)									
				Matsumura (1988)	Shing et al. (1990)	Anderson and Priestley (1992)	NEHRP (1997) MSJC (2013)	UBC (1997)	AS3700-2001	CSA S304-14	NZS 4230:2004	Voon and Ingham (2007)	Proposed Equation
Okomoto (1987)	40	WS1	2.5	0	0	0	0			0	0	0	0
	41	WS4	2.5	72	46	112	112			63	220	220	185
	42	WS7	2.5	0	0	0	0			0	0	0	0
	43	WSN1	2.5	144	93	224	224			126	257	257	216
	44	WSN2	2.5	216	139	335	335			189	257	257	216
	45	WSR1	2.5	0	0	0	0			0	0	0	0
	46	WSR4	2.5	0	0	0	0			0	0	0	0
	47	WSR7	2.5	0	0	0	0			0	0	0	0
Shing et al. (1990)	48	S-3	2.5	80	48	122	122			69	175	175	152
	49	S-4	3.2	0	0	0	0			0	0	0	0
	50	S-5	2.5	30	17	45	45			25	65	65	56
	51	S-7	2.6	30	18	45	45			24	65	65	55
	52	S-9	3.4	80	48	122	122			55	175	175	113
	53	S-13	4.8	80	50	122	122			55	175	175	52
	54	S-14	2.8	80	50	122	122			60	175	175	139
	55	S-16	3.3	80	44	122	122			55	162	162	108
	56	S-21	3.2	80	54	121	121			54	174	174	120
	57	S-22	3.9	29	19	43	43			19	62	62	32
Voon and Ingham (2006)	58	A1	2.7	0	0	0	0			0	0	0	0
	59	A2	2.6	0	0	0	0			0	0	0	0
	60	A4	2.6	0	0	0	0			0	0	0	0
	61	A7	2.7	21	12	32	32			16	50	50	37
	62	A8	2.7	10	6	16	16			8	25	25	18
	63	A9	2.9	10	7	16	16			8	13	13	9
	64	A10	1.3	18	11	26	26			24	71	71	70
Current study	65	W-Ref	4.2	57	27	86	86			38	139	139	55
	66	W-ρ_h0	3.0	57	27	86	86			38	139	139	91
	67	W-σ_n0	4.1	0	0	0	0			0	0	0	0
	68	W-σ_n1.5	3.4	85	40	128	128			58	181	181	102
	69	W-M/Vd_v1.8	5.2	57	27	86	86			38	139	139	17
	70	W-90°	3.9	57	27	86	86			38	139	139	63
	71	W-Str	3.6	57	27	86	86			38	139	139	73
	72	W-S_v800	3.4	57	27	86	86			38	139	139	80
	73	W-S_h800	2.3	57	27	86	86			52	139	139	112

Specimens with gray shading were constructed with clay brick

Table A.4: Predicted In-Plane Shear Resistance Provided by Horizontal Reinforcement (V_s)

Source	Specimen no.	Specimen label	μ_Δ	V_s (kN)									
				Matsumura (1988)	Shing et al. (1990)	Anderson and Priestley (1992)	NEHRP (1997) MSJC (2013)	UBC (1997)	AS3700-2001	CSA S304-14	NZS 4230:2004	Voon and Ingham (2007)	Proposed Equation
Sveinsson et al., (1985)	1	HCBL-11-13	3.8	146	162	131	139	325	223	134	178	78	123
	2	HCBL-11-15	2.6	146	162	131	139	325	223	134	178	78	85
	3	HCBL-11-17	2.3	107	173	139	149	350	240	143	190	84	83
	4	HCBL-11-18	1.9	107	173	139	149	350	240	143	190	84	70
	5	HCBL-11-20	2.7	75	46	71	76	175	120	73	98	43	49
	6	HCBL-11-21	2.5	75	46	71	76	175	120	73	98	43	45
	7	HCBL-11-23	3.1	46	43	27	29	67	46	27	37	32	21
	8	HCBL-11-24	2.7	87	157	97	104	242	166	100	133	58	66
	9	HCBL-11-25	2.9	75	46	71	76	175	120	73	98	112	52
	10	HCBL-11-26	2.3	75	46	71	76	175	120	73	98	112	43
	11	HCBR-11-19	2.6	86	46	71	76	175	120	73	98	43	48
	12	HCBR-11-20	2.2	135	239	175	187	438	300	179	239	105	97
	13	HCBR-11-21	2.7	86	46	71	76	175	120	73	98	43	49
	14	HCBR-11-22	2.9	135	239	175	187	438	300	179	239	105	127
	15	HCBR-11-23	2.9	86	46	71	76	175	120	73	98	43	52
	16	HCBR-11-24	2.8	135	239	175	187	438	300	179	239	105	123
	17	HCBR-11-25	2.3	86	46	71	76	175	120	73	98	112	42
	18	HCBR-11-26	2.2	135	239	175	187	438	300	179	239	276	97
	19	HCBR-11-27	2.2	93	103	84	89	212	145	86	114	67	47
	20	HCBR-11-28	3.9	148	340	211	225	538	369	216	288	168	207
	21	HCBR-11-30	1.5	72	58	36	38	89	61	37	49	42	14
Matsumura (1986)	22	KW4-1	2.5	89	69	51	54	109	77	52	69	81	31
	23	KW3-1	2.5	65	42	37	41	109	58	39	52	59	31
	24	KW3S-1	2.5	65	42	37	41	109	58	39	52	59	31
	25	KW2-1	2.5	42	14	24	27	109	38	26	34	37	28
	26	WS2	2.5	0	0	0	0	0	0	0	0	0	0
	27	WS4	2.5	93	65	59	64	173	91	62	82	93	50
	28	WS5	2.5	132	173	118	128	345	183	123	164	185	99
	29	WS9	2.5	132	173	118	128	345	183	123	164	185	99
	30	WS10	2.5	187	345	236	257	691	365	247	329	370	199
	31	WS9-2	2.5	160	147	134	145	391	207	140	186	209	113
	32	WSB21	2.5	152	147	134	145	391	207	140	186	209	113
	33	WSB22	2.5	170	176	160	174	468	248	167	223	251	135
	34	WSB3	2.5	157	155	141	154	413	219	147	197	221	119
	35	WSB4	2.5	167	147	134	145	391	207	140	186	209	113
	36	WSR2-2	3.8	0	0	0	0	0	0	0	0	0	0
	37	WSR4-2	2.6	95	56	57	63	183	96	61	81	89	50
	38	WSR5-2	2.3	135	158	114	127	366	191	122	162	178	99
	39	WSR6-2	1.9	191	315	229	254	731	382	244	325	356	199

Specimens with gray shading were constructed with clay brick

Table A.4(continued): Predicted In-Plane Shear Resistance Provided by Horizontal Reinforcement (V_s)

Source	Specimen no.	Specimen label	μ_Δ	V_s (kN)									
				Matsumura (1988)	Shing et al. (1990)	Anderson and Priestley (1992)	NEHRP (1997) MSJC (2013)	UBC (1997)	AS3700-2001	CSA S304-14	NZS 4230:2004	Voon and Ingham (2007)	Proposed Equation
Okomoto (1987)	40	WS1	2.5	150	161	109	114	183	147	110	147	172	53
	41	WS4	2.5	98	70	63	69	183	98	66	88	99	53
	42	WS7	2.5	56	24	40	46	183	65	44	59	62	47
	43	WSN1	2.5	98	70	63	69	183	98	66	88	99	53
	44	WSN2	2.5	98	70	63	69	183	98	66	88	99	53
	45	WSR1	2.5	183	161	109	114	183	147	110	147	172	53
	46	WSR4	2.5	103	70	63	69	183	98	66	88	99	53
	47	WSR7	2.5	61	24	40	46	183	65	44	59	62	47
Shing et al. (1990)	48	S-3	2.5	58	82	58	62	137	110	59	79	92	63
	49	S-4	3.2	54	82	58	62	137	110	59	79	92	80
	50	S-5	2.5	54	82	58	62	137	110	59	79	92	63
	51	S-7	2.6	58	82	58	62	137	110	59	79	92	66
	52	S-9	3.4	58	82	58	62	137	110	59	79	92	85
	53	S-13	4.8	90	179	127	134	298	238	129	172	200	215
	54	S-14	2.8	61	82	58	62	137	110	59	79	92	70
	55	S-16	3.3	79	179	127	134	298	238	129	172	200	179
	56	S-21	3.2	64	82	58	62	137	110	59	79	92	80
	57	S-22	3.9	64	82	58	62	137	110	59	79	92	96
Voon and Ingham (2006)	58	A1	2.7	31	28	20	21	46	37	20	26	35	23
	59	A2	2.6	14	0	4	5	9	7	4	6	7	5
	60	A4	2.6	33	22	23	24	43	34	23	31	40	26
	61	A7	2.7	32	28	20	21	46	37	20	26	35	23
	62	A8	2.7	32	28	20	21	46	37	20	26	35	23
	63	A9	2.9	36	28	20	21	83	33	20	26	33	24
	64	A10	1.3	61	55	33	34	46	37	33	44	59	13
Current study	65	W-Ref	4.2	66	129	91	97	172	138	93	124	144	155
	66	W-ρ_h0	3.0	0	0	0	0	0	0	0	0	0	0
	67	W-σ_n0	4.1	66	129	91	97	172	138	93	124	144	155
	68	W-σ_n1.5	3.4	66	129	91	97	172	138	93	124	144	134
	69	W-M/Vd$_v$1.8	5.2	66	129	91	97	172	138	93	124	144	155
	70	W-90°	3.9	66	129	91	97	172	138	93	124	102	152
	71	W-Str	3.6	66	129	91	97	172	138	93	124	102	140
	72	W-S$_v$800	3.4	150	86	91	97	172	138	93	279	144	131
	73	W-S$_h$800	2.3	233	86	91	97	172	138	93	433	144	92

Specimens with gray shading were constructed with clay brick

Table A.5: Predicted In-Plane Shear strength (V_n)

Source	Specimen no.	Specimen label	μ_Δ	V_n (kN)									
				Matsumura (1988)	Shing et al. (1990)	Anderson and Priestley (1992)	NEHRP (1997) MSJC (2013)	UBC (1997)	AS3700-2001	CSA S304-14	NZS 4230:2004	Voon and Ingham (2007)	Proposed Equation
Sveinsson et al., (1985)	1	HCBL-11-13	3.8	431	417	272	531	496	440	276	486	386	301
	2	HCBL-11-15	2.6	474	445	504	598	496	440	344	660	561	423
	3	HCBL-11-17	2.3	358	355	400	440	454	400	291	470	363	280
	4	HCBL-11-18	1.9	310	357	426	440	454	400	317	495	388	293
	5	HCBL-11-20	2.7	322	225	297	364	277	280	198	344	289	224
	6	HCBL-11-21	2.5	275	226	316	364	277	280	211	358	304	234
	7	HCBL-11-23	3.1	293	222	223	316	168	205	137	262	257	181
	8	HCBL-11-24	2.7	335	335	325	391	344	326	227	381	307	239
	9	HCBL-11-25	2.9	293	209	240	319	277	280	169	335	350	217
	10	HCBL-11-26	2.3	322	225	326	364	277	280	218	365	380	239
	11	HCBR-11-19	2.6	360	252	256	390	292	280	213	417	362	275
	12	HCBR-11-20	2.2	408	445	381	500	555	460	346	590	456	347
	13	HCBR-11-21	2.7	360	267	253	390	292	280	209	420	365	278
	14	HCBR-11-22	2.9	374	450	348	500	555	460	304	544	410	323
	15	HCBR-11-23	2.9	305	253	244	390	292	280	198	400	346	261
	16	HCBR-11-24	2.8	354	447	353	500	555	460	310	549	416	326
	17	HCBR-11-25	2.3	360	252	270	390	292	280	231	438	453	292
	18	HCBR-11-26	2.2	408	445	382	500	555	460	347	591	627	348
	19	HCBR-11-27	2.2	367	309	289	403	329	305	251	463	416	305
	20	HCBR-11-28	3.9	387	533	334	539	655	529	334	519	398	307
	21	HCBR-11-30	1.5	378	299	266	385	226	221	294	559	552	420
Matsumura (1986)	22	KW4-1	2.5	454	353	281	362	279	300	184	319	330	236
	23	KW3-1	2.5	290	254	209	248	212	190	122	213	220	174
	24	KW3S-1	2.5	290	254	209	248	212	190	122	213	220	174
	25	KW2-1	2.5	156	165	138	145	164	81	78	127	130	104
	26	WS2	2.5	299	281	303	348	132	168	152	353	353	286
	27	WS4	2.5	393	346	362	412	304	259	214	435	446	326
	28	WS5	2.5	431	454	421	476	477	351	276	518	538	366
	29	WS9	2.5	474	487	421	476	477	351	276	536	557	383
	30	WS10	2.5	528	660	539	605	822	534	399	701	742	462
	31	WS9-2	2.5	540	490	464	527	541	375	305	571	595	408
	32	WSB21	2.5	516	473	452	513	533	375	299	563	586	399
	33	WSB22	2.5	541	510	484	548	614	416	329	603	631	421
	34	WSB3	2.5	527	488	461	523	556	387	308	577	602	408
	35	WSB4	2.5	559	504	473	538	547	375	309	578	602	415
	36	WSR2-2	3.8	336	326	201	343	130	155	149	355	355	298
	37	WSR4-2	2.6	432	382	258	406	312	250	209	436	444	338
	38	WSR5-2	2.3	471	483	315	469	495	346	270	518	533	378
	39	WSR6-2	1.9	527	641	429	596	861	537	392	680	711	458

Specimens with gray shading were constructed with clay brick

Table A.5(continued): Predicted In-Plane Shear strength (V_n)

Source	Specimen no.	Specimen label	μ_Δ	V_n (kN)									
				Matsumura (1988)	Shing et al. (1990)	Anderson and Priestley (1992)	NEHRP (1997) MSJC (2013)	UBC (1997)	AS3700-2001	CSA S304-14	NZS 4230:2004	Voon and Ingham (2007)	Proposed Equation
Okomoto (1987)	40	WS1	2.5	573	496	399	544	456	546	295	373	399	243
	41	WS4	2.5	403	358	371	424	319	269	221	449	460	335
	42	WS7	2.5	165	178	156	166	247	122	95	137	141	111
	43	WSN1	2.5	475	404	483	535	319	269	284	485	496	359
	44	WSN2	2.5	547	450	595	647	319	269	347	485	496	359
	45	WSR1	2.5	700	570	286	639	517	546	336	424	449	287
	46	WSR4	2.5	348	323	166	324	325	269	163	236	247	193
	47	WSR7	2.5	180	192	104	177	253	122	100	145	148	118
Shing et al. (1990)	48	S-3	2.5	429	423	394	406	256	371	223	405	418	402
	49	S-4	3.2	325	354	165	269	247	371	130	154	167	219
	50	S-5	2.5	354	371	303	314	247	371	173	284	297	294
	51	S-7	2.6	378	392	303	329	256	371	175	285	297	302
	52	S-9	3.4	377	371	266	406	256	371	190	303	316	313
	53	S-13	4.8	448	502	249	489	422	500	264	347	375	327
	54	S-14	2.8	419	406	360	417	261	371	207	366	379	370
	55	S-16	3.3	424	490	340	459	406	500	253	398	426	419
	56	S-21	3.2	433	420	241	422	265	360	196	331	343	346
	57	S-22	3.9	382	385	109	345	265	360	161	151	164	238
Voon and Ingham (2006)	58	A1	2.7	272	246	188	218	151	289	99	127	141	157
	59	A2	2.6	256	218	181	202	114	259	85	109	128	142
	60	A4	2.6	270	236	199	218	147	286	103	134	143	161
	61	A7	2.7	302	265	218	256	155	289	115	175	186	196
	62	A8	2.7	291	259	202	240	155	289	107	150	164	178
	63	A9	2.9	250	376	205	268	207	159	113	170	179	155
	64	A10	1.3	628	492	556	568	356	541	388	582	601	493
Current study	65	W-Ref	4.2	399	453	177	413	295	499	211	262	283	308
	66	W-ρ_h0	3.0	333	324	231	317	123	361	118	238	238	252
	67	W-σ_n0	4.1	343	426	91	328	295	499	172	124	144	256
	68	W-σ_n1.5	3.4	428	466	303	456	295	499	230	363	383	375
	69	W-M/Vd_v1.8	5.2	399	453	177	413	295	499	211	262	283	201
	70	W-90°	3.9	399	453	187	413	295	499	211	269	247	327
	71	W-Str	3.6	399	453	235	413	295	499	211	302	280	343
	72	W-S_v800	3.4	482	410	672	413	295	499	211	483	348	355
	73	W-S_h800	2.3	646	389	2515	413	295	499	251	731	441	391

Specimens with gray shading were constructed with clay brick

Table A.6: Experimental Results vs Predicted In-Plane Shear Strength (V_n)

Source	Specimen no.	Specimen label	μ_Δ	$V_{experimental} / V_{predicted}$									
				Matsumura (1988)	Shing et al. (1990)	Anderson and Priestley (1992)	NEHRP (1997) MSJC (2013)	UBC (1997)	AS3700-2001	CSA S304-14	NZS 4230:2004	Voon and Ingham (2007)	Proposed Equation
Sveinsson et al., (1985)	1	HCBL-11-13	3.8	1.07	1.11	1.69	0.87	0.93	1.05	1.67	0.95	1.19	1.53
	2	HCBL-11-15	2.6	1.18	1.26	1.11	0.94	1.13	1.28	1.63	0.85	1.00	1.33
	3	HCBL-11-17	2.3	1.20	1.21	1.07	0.97	0.94	1.07	1.47	0.91	1.18	1.53
	4	HCBL-11-18	1.9	1.38	1.20	1.01	0.97	0.94	1.07	1.35	0.87	1.10	1.46
	5	HCBL-11-20	2.7	1.27	1.83	1.38	1.13	1.48	1.47	2.07	1.19	1.42	1.83
	6	HCBL-11-21	2.5	1.42	1.72	1.23	1.07	1.41	1.39	1.84	1.09	1.28	1.66
	7	HCBL-11-23	3.1	1.14	1.50	1.50	1.05	1.98	1.62	2.44	1.27	1.30	1.85
	8	HCBL-11-24	2.7	1.26	1.26	1.30	1.08	1.23	1.30	1.87	1.11	1.38	1.77
	9	HCBL-11-25	2.9	1.17	1.63	1.42	1.07	1.24	1.22	2.02	1.02	0.98	1.57
	10	HCBL-11-26	2.3	1.30	1.87	1.29	1.15	1.52	1.50	1.92	1.15	1.10	1.76
	11	HCBR-11-19	2.6	0.89	1.28	1.25	0.82	1.10	1.15	1.51	0.77	0.89	1.17
	12	HCBR-11-20	2.2	0.82	0.75	0.88	0.67	0.60	0.73	0.96	0.57	0.73	0.96
	13	HCBR-11-21	2.7	1.14	1.54	1.62	1.05	1.40	1.47	1.97	0.98	1.12	1.48
	14	HCBR-11-22	2.9	1.12	0.93	1.20	0.84	0.75	0.91	1.37	0.77	1.02	1.29
	15	HCBR-11-23	2.9	1.16	1.40	1.45	0.91	1.21	1.27	1.79	0.88	1.02	1.36
	16	HCBR-11-24	2.8	1.08	0.86	1.09	0.77	0.69	0.83	1.24	0.70	0.92	1.18
	17	HCBR-11-25	2.3	1.06	1.51	1.41	0.98	1.30	1.36	1.65	0.87	0.84	1.30
	18	HCBR-11-26	2.2	0.92	0.84	0.98	0.75	0.67	0.81	1.08	0.63	0.60	1.08
	19	HCBR-11-27	2.2	1.07	1.27	1.36	0.98	1.20	1.29	1.57	0.85	0.95	1.29
	20	HCBR-11-28	3.9	1.03	0.74	1.19	0.74	0.61	0.75	1.19	0.76	1.00	1.29
	21	HCBR-11-30	1.5	1.24	1.57	1.77	1.22	2.08	2.13	1.60	0.84	0.85	1.12
Matsumura (1986)	22	KW4-1	2.5	0.89	1.14	1.44	1.11	1.44	1.34	2.20	1.26	1.22	1.71
	23	KW3-1	2.5	0.91	1.03	1.26	1.06	1.24	1.38	2.17	1.24	1.20	1.52
	24	KW3S-1	2.5	1.00	1.14	1.39	1.17	1.37	1.52	2.39	1.36	1.32	1.67
	25	KW2-1	2.5	1.12	1.05	1.26	1.20	1.06	2.14	2.22	1.36	1.34	1.68
	26	WS2	2.5	1.08	1.15	1.07	0.93	2.46	1.93	2.13	0.92	0.92	1.13
	27	WS4	2.5	1.14	1.29	1.24	1.09	1.47	1.72	2.09	1.03	1.00	1.37
	28	WS5	2.5	1.16	1.11	1.19	1.05	1.05	1.43	1.82	0.97	0.93	1.37
	29	WS9	2.5	1.07	1.04	1.20	1.06	1.06	1.44	1.83	0.94	0.91	1.32
	30	WS10	2.5	1.21	0.97	1.18	1.05	0.77	1.19	1.60	0.91	0.86	1.38
	31	WS9-2	2.5	1.02	1.12	1.18	1.04	1.01	1.46	1.80	0.96	0.92	1.34
	32	WSB21	2.5	0.94	1.03	1.07	0.95	0.91	1.30	1.62	0.86	0.83	1.22
	33	WSB22	2.5	1.10	1.16	1.23	1.08	0.97	1.43	1.80	0.98	0.94	1.41
	34	WSB3	2.5	1.01	1.09	1.16	1.02	0.96	1.38	1.73	0.92	0.89	1.31
	35	WSB4	2.5	1.05	1.16	1.24	1.09	1.07	1.57	1.90	1.01	0.98	1.41
	36	WSR2-2	3.8	1.34	1.38	2.24	1.31	3.48	2.91	3.03	1.27	1.27	1.51
	37	WSR4-2	2.6	1.04	1.17	1.74	1.10	1.43	1.79	2.14	1.03	1.01	1.32
	38	WSR5-2	2.3	1.03	1.00	1.54	1.03	0.98	1.40	1.80	0.94	0.91	1.28
	39	WSR6-2	1.9	0.98	0.81	1.21	0.87	0.60	0.97	1.32	0.76	0.73	1.13

Specimens with gray shading were constructed with clay brick

Table A.6(continued): Experimental Results vs Predicted In-Plane Shear Strength (V_n)

Source	Specimen no.	Specimen label	μ_Δ	$V_{experimental}/V_{predicted}$									
				Matsumura (1988)	Shing et al. (1990)	Anderson and Priestley (1992)	NEHRP (1997) MSJC (2013)	UBC (1997)	AS3700-2001	CSA S304-14	NZS 4230:2004	Voon and Ingham (2007)	Proposed Equation
Okomoto (1987)	40	WS1	2.5	1.78	2.05	2.55	1.87	2.23	1.87	3.45	2.73	2.55	4.19
	41	WS4	2.5	1.11	1.26	1.21	1.06	1.41	1.67	2.03	1.00	0.98	1.34
	42	WS7	2.5	1.88	1.75	1.99	1.87	1.26	2.54	3.25	2.26	2.20	2.80
	43	WSN1	2.5	1.15	1.36	1.14	1.02	1.72	2.04	1.93	1.13	1.10	1.53
	44	WSN2	2.5	1.09	1.32	1.00	0.92	1.87	2.22	1.72	1.23	1.20	1.66
	45	WSR1	2.5	1.70	2.08	4.16	1.86	2.30	2.18	3.54	2.81	2.64	4.14
	46	WSR4	2.5	1.52	1.64	3.18	1.63	1.63	1.97	3.24	2.24	2.14	2.73
	47	WSR7	2.5	1.72	1.62	2.99	1.75	1.23	2.54	3.10	2.14	2.09	2.64
Shing et al. (1990)	48	S-3	2.5	1.06	1.08	1.16	1.12	1.78	1.23	2.04	1.13	1.09	1.13
	49	S-4	3.2	1.09	1.00	2.15	1.32	1.43	0.95	2.72	2.30	2.12	1.61
	50	S-5	2.5	1.09	1.04	1.27	1.23	1.56	1.04	2.22	1.35	1.30	1.31
	51	S-7	2.6	1.14	1.10	1.42	1.31	1.69	1.16	2.46	1.52	1.45	1.43
	52	S-9	3.4	1.13	1.15	1.61	1.05	1.67	1.15	2.24	1.41	1.35	1.36
	53	S-13	4.8	1.12	1.00	2.01	1.02	1.19	1.00	1.90	1.44	1.33	1.53
	54	S-14	2.8	1.11	1.15	1.30	1.12	1.79	1.26	2.25	1.28	1.23	1.26
	55	S-16	3.3	1.26	1.09	1.58	1.17	1.32	1.07	2.12	1.35	1.26	1.28
	56	S-21	3.2	1.08	1.12	1.95	1.11	1.77	1.30	2.40	1.42	1.37	1.35
	57	S-22	3.9	1.07	1.06	3.73	1.18	1.54	1.13	2.53	2.70	2.49	1.71
Voon and Ingham (2006)	58	A1	2.7	0.77	0.85	1.12	0.96	1.39	0.73	2.13	1.65	1.49	1.34
	59	A2	2.6	0.73	0.85	1.03	0.92	1.62	0.72	2.18	1.70	1.46	1.31
	60	A4	2.6	0.79	0.90	1.07	0.97	1.45	0.74	2.05	1.58	1.48	1.32
	61	A7	2.7	0.87	0.99	1.20	1.02	1.69	0.91	2.27	1.50	1.41	1.34
	62	A8	2.7	0.85	0.95	1.22	1.03	1.60	0.86	2.30	1.65	1.49	1.39
	63	A9	2.9	0.82	0.55	1.00	0.77	1.00	1.29	1.83	1.21	1.16	1.32
	64	A10	1.3	0.93	1.19	1.05	1.03	1.64	1.08	1.51	1.01	0.97	1.19
	65	W-Ref	4.2	1.04	0.91	2.34	1.00	1.40	0.83	1.96	1.58	1.46	1.34
	66	W-ρ_h0	3.0	1.10	1.13	1.59	1.16	2.97	1.01	3.11	1.54	1.54	1.45
	67	W-σ_n0	4.1	0.99	0.80	3.72	1.04	1.15	0.68	1.98	2.75	2.36	1.33
	68	W-σ_n1.5	3.4	1.06	0.98	1.50	1.00	1.54	0.91	1.98	1.26	1.19	1.21
	69	W-M/Vd_v1.8	5.2	0.76	0.67	1.71	0.73	1.02	0.61	1.44	1.15	1.07	1.50
	70	W-90°	3.9	1.02	0.90	2.19	0.99	1.38	0.82	1.94	1.52	1.66	1.25
	71	W-Str	3.6	0.98	0.86	1.66	0.94	1.32	0.78	1.85	1.29	1.39	1.14
	72	W-S_v800	3.4	0.79	0.93	0.57	0.92	1.29	0.76	1.81	0.79	1.09	1.07
	73	W-S_h800	2.3	0.55	0.90	0.14	0.85	1.19	0.71	1.40	0.48	0.80	0.90

Specimens with gray shading were constructed with clay brick